Design of advanced multifunctional biomaterial-based biomimetic and pH-responsive hybrid nanocarriers for antibiotic delivery against bacterial infections and sepsis

by

Eman Hussain Elmubarak Elhassan
(M. Pharm –University of Gezira)

Submitted as a fulfilment of the requirements for the degree of
Doctor of Philosophy in Pharmaceutics at the Discipline of Pharmaceutical Sciences of the School of Health Sciences at the University of KwaZulu-Natal

Supervisor: Professor Thirumala Govender
(PhD, University of Nottingham, United Kingdom)

Co-supervisor: Professor Calvin A. Omolo.
(PhD, University of KwaZulu-Natal, South Africa).

Date submitted: 8th December 2023

"What counts in life is not the mere fact that we have lived. It is what difference we have made to the lives of others that will determine the significance of the life we lead."

- Nelson Mandela-

Dedication

"This thesis is dedicated to my beloved parents and husband, the soul of my dear mother-in-law "Saadia", my beloved daughters and son, my sisters and brother, family and friends who have always taught me how to see the vitality in myself, conquer fears, and overcome challenges.

I hope that I have made you proud."

Declaration 1 – Plagiarism

I, **Mrs. Eman Elhassan,** declare that

1. The research data reported in this thesis, except where otherwise indicated, is my own original work.
2. This thesis has not been submitted for any degree or examination to any other university.
3. This thesis does not contain data, pictures, graphs, or other information belonging to other people, unless specifically acknowledged as being sourced from other people.
4. This thesis does not contain any other person's writing, unless specifically acknowledged as being sourced from other researchers, where other written sources have been quoted.
   a. Their words have been rephrased; however, the general information attributed to them has been referenced.
   b. Where their exact words were used, their writing was placed inside quotation marks and referenced.
5. Where I have reproduced a publication of which I am an author, co-author, or editor, I have indicated in detail which part of the publication was written by myself alone and have fully referenced such publications.
6. This thesis does not contain any graphics, text, or tables copied from the Internet unless specifically acknowledged; the source is detailed in the dissertation's reference sections.

Signed: **Date**: 8th December 2023

I, **Professor Thirumala Govender**, as supervisor of the PhD studies, hereby consent to the submission of this PhD thesis.

Signed: **Date**: 8th December 2023

I, Professor Calvin A. Omolo, as a co-supervisor of the PhD studies hereby consent to the submission of this PhD thesis.

Signed: **Date**: 8th December 2023

Declaration 2 – Publications

Mrs. Eman Elhassan contributed to the literature search, evaluation and critical analysis, conceptualization and creating the table of the literature, design of the projects, synthesis and characterization of the novel biomaterials, method modification and optimization, formulations, and characterization of the nanosystems. In addition, **Mrs. Eman Elhassan** was responsible for the analysis and interpretation of all data, wrote the first drafts of the papers, and undertook all revisions. She was also involved in the formulation and characterization of the processes for all nanosystems that were formulated from the synthesized materials in terms of particle size, polydispersity index (PDI), zeta potential (ZP), surface morphology, entrapment efficiency, *in vitro* drug release, differential scanning calorimetry (DSC), *in vitro* antibacterial, antibiofilm, and efflux pump inhibition activities, *in vitro* antioxidant studies, *in vitro* anti-inflammatory studies, and the statistical analysis. Dr. Nikita Devnarain and Dr. Rene Khan assisted in conducting the cytotoxicity studies. Dr. Aimen Aljoundi and Dr. Ghazi Elamin undertook the *in silico* studies. Dr. Usri H. Ibrahim assisted in conducting the *in vitro* anti-inflammatory studies. Prof. Calvin A. Omolo served as co-supervisor/assistant with the project's conceptualization, design, solving technical problems, and supervision of the studies. Prof. Thirumala Govender served as a supervisor and was responsible for project conceptualization, problem solving, paper, abstract editing, and general supervision of the study.

Research output from the thesis

1. First-authored Publications

The following **review article** was published following a literature review of the study-related topics:

1. **Eman Elhassan**, Nikita Devnarain, Mahir Mohammed, Thirumala Govender and Calvin A. Omolo, 2022, Engineering hybrid nanosystems for efficient and targeted delivery against bacterial infections. Journal of Controlled Release, 351, 598-622. (Impact factor 11.467). DOI: https://doi.org/https://doi.org/10.1016/j.jconrel.2022.09.052.

The following **experimental papers** were submitted based on the results generated from the specific objectives in this study. These include:

2. **Eman Elhassan**, Mohammed A. Gafar, Calvin A. Omolo, Usri H. Ibrahim, Rene Khan and Thirumala Govender, Design of multifunctional biomimetic pH-responsive hybrid

nanostructured lipid carriers for targeted delivery of vancomycin against bacterial sepsis. Submitted to the *International Journal of Biological Macromolecules* (Manuscript ID: IJBIOMAC-D-23-18902). (Impact factor: 8.2).

1. **Eman Elhassan**, Calvin A. Omolo, Mohammed A. Gafar, Usri H. Ibrahim, Aimen Aljoundi, Ghazi Elamin, Nikita Devnarain, Mahir Mohammed, Thirumala Govender, Disease-inspired design of a biomimetic tannic acid-based hybrid nanocarriers for targeted delivery of ciprofloxacin against bacterial-induced sepsis. Submitted to the *International Journal of Pharmaceutics* (Manuscript ID: IJPHARM-D-23-03925) (Impact Factor: 5.875).

2. Conference Presentation

The following **conference presentation** was produced from data generated from this study:

1. **Eman Elhassan**, Calvin A. Omolo, Mohammed A. Gafar, Nikita Devnarain, Usri H. Ibrahim, Mahir Mohammed, Thirumala Govender. Disease-inspired design of a biomimetic tannic acid-based hybrid nanocarriers for targeted delivery of ciprofloxacin against bacterial-induced sepsis. The 44th Annual Conference of the South African Academy of Pharmaceutical Sciences, The Capital Zambili Hotel, 31st August – 2nd September 2023, Ballito, South Africa. (Oral presentation).

3. Co-authored publications

The following article is a **co-authored publication** related to the overall objective of this study (enhancing the delivery and efficacy of antibiotics via the development of an advanced novel drug delivery system).

1. Mahir Mohammed, Nikita Devnarain, **Eman Elhassan** and Thirumala Govender, 2022, Exploring the applications of hyaluronic acid-based nanoparticles for diagnosis and treatment of bacterial infections. WIREs Nanomedicine and Nanobiotechnology, 14(4), e1799. DOI: https://doi.org/https://doi.org/10.1002/wnan.1799. (Impact Factor: 9.125).

Abstract

Despite the notable improvements in the management of bacterial infections and sepsis, the mounting threat of antibiotic resistance on a global scale is leading towards a post-antibiotic era. Nano-drug delivery systems have improved the delivery and efficacy of various antibiotics. Biomimicry and stimuli-responsiveness have recently been used to improve the targetability of these nanocarriers, and enhance their localization at infected sites, thus improving overall therapeutic outcomes and reducing toxicity. Strategies such as targeting bacterial biofilms and efflux pumps can further enhance the delivery and effectiveness of antibiotics. Developing smart biomaterials with multifunctional properties to confer biomimetic, stimuli-responsive and antivirulence properties to antibiotic nanocarriers is the focus of ongoing research. Therefore, the general aim of this study was to investigate the potential of various novel multifunctional biomaterial-based hybrid nanocarriers (HNs), including biomimetic and/or pH-responsive HNs in enhancing the targeted delivery of antibiotics and modulating the proinflammatory response against bacterial infections and sepsis. In this study, two biomaterials with multifunctional activities, hyaluronic acid-lysine conjugate (HA-Lys) and tannic acid (TA), were employed to design, formulate, and extensively characterize innovative biomimetic and pH-responsive HNs for efficient and targeted delivery of antibiotics.

The novel HA-Lys was synthesized and fully characterized using proton nuclear magnetic resonance (^{1}H NMR) spectroscopy and Fourier-transform infrared spectroscopy (FT-IR). Then it was successfully employed with tocopherol succinate (TS) and Oleylamine (OLA) to fabricate biomimetic pH-responsive vancomycin-loaded hybrid nanostructured lipid carriers (VCM-HNLCs). The prepared VCM-HNLCs were spherical and had average diameters, zeta potential, polydispersity index, drug encapsulation efficiency and loading capacity of 110.77 ± 1.69 nm, 0.11 ± 0.02, -2.92 ± 0.21 mV, 76.27 ± 1.20 % and 8.36 ± 0.25 %, respectively. Both HA-Lys conjugate and its respective nanoformulations had excellent biosafety profiles (>70 % cell viability and < 1 % hemolytic effect). Possible VCM-HNLCs competitive inhibition activity to toll-like receptors 2 and 4 (TLR2 and TLR4) was demonstrated via microscale thermophoresis (MST) analysis, which showed a 5-times and 16-times lower K_d values than their natural substrates peptidoglycan (PGN) and lipopolysaccharide (LPS), respectively. VCM-HNLCs exhibited a pH-responsive drug release profile under acidic conditions, higher bacterial killing kinetics, enhanced antibacterial, anti-biofilm, and efflux pump inhibition activities over bare VCM. Also, they showed an improved activity in neutralizing reactive oxygen species (ROS) and modulating the inflammatory response induced by LPS.

On the other hand, tannic acid (TA) and Oleylamine (OLA) were successfully employed to formulate biomimetic ciprofloxacin-loaded tannic acid hybrid nanoparticles (CIP-loaded TAH-NPs) to enhance the efficacy of CIP against bacterial infections and sepsis. The prepared HNs had onion-shaped morphology, with average diameters, zeta potential, polydispersity index, drug encapsulation efficiency and loading capacity of 85.65 ± 0.89 nm, 0.126 ± 0.01, +16.3 ± 0.23 mV, 68.73 ± 0.54 % and 6.86 ± 0.09 %, respectively. The hemolysis and MTT assays confirmed the biosafety and non-hemolytic activity of CIP-loaded TAH-NPs formulations (>70 % cell viability and < 1 % hemolytic effect). The results of MST investigations and *in-silico* simulations demonstrated that TA and its nanoformulation (CIP-loaded TAH-NPs) competitively inhibited TLR4 compared to its natural substrate LPS. CIP-loaded TAH-NPs showed a diffusion-based sustained release profile at physiological pH 7.4. Also, in comparison to bare CIP, the hybrid nanovesicles demonstrated improved antibacterial, anti-biofilm and efflux pump inhibition properties, as well as faster bacterial killing kinetics. Moreover, they showed a significant neutralization of ROS and the ability to control the inflammatory responses brought on by LPS.

In summary, VCM-HNLCs and CIP-loaded TAH-NPs were successfully formulated and showed significant improvement in antibiotics efficacy and overall therapeutic outcomes. This study confirmed the potential of biomimetic stimuli-responsive antibiotic hybrid nanocarriers for enhancing antibiotic efficacy against bacterial sepsis and addressing the antimicrobial resistance crisis. The data from this study has resulted in one first-authored review article, two first-authored research publications and one co-authored review article.

Acknowledgments

Firstly, I would like to sincerely thank my supervisor **Prof. Thirumala Govender**, for her continued support during my Ph.D. studies. Her encouragement, inspiration, persistence, and enormous expertise enabled me to write the articles and this thesis at all study times. I will be forever grateful for her endless support. Really, I have not found suitable words that could express my gratitude for what she has done for me.

Special thanks to my co-supervisor, **Prof. Calvin A. Omolo**, for his assistance in the design of this project and his continued guidance and motivation. I will forever be indebted to him for being with me every step of the way, helping to tackle any problem encountered along the way and instilling invaluable skills that will be crucial in my career ahead.

I would like to express my sincere appreciation and thanks to all my colleagues in the NDD unit, and a special mention goes to my dear colleagues, Mr. Mohammed A. Gafar, Mr. Mahir Mohammed, Mr. Abdelrahman Tageldeen, Mr. Usri H. Ibrahim, Melissa Ramtahal and Mr. Leslie Murugan for all their support, technical assistance in the lab and life-long friendship.

My sincere gratitude goes to all the organisations that gave me their invaluable, generous resources, including the UKZN Nanotechnology Platform and the College of Health Sciences at UKZN. Without their support, facilities, and financial help, it would not have been possible for me to pursue and complete this Ph.D. project successfully. My appreciation goes to the Electron Microscope Unit and Biomedical Resource Unit at UKZN for their technical support.

Special thanks and appreciation to my beloved mother and father for their motivation, prayers and more. Your efforts are responsible for creating the person I am today, and I will continue to pursue my dreams, and I hope to make both of you proud. Thank you to my family and friends for their complete support and motivation throughout my studies. Special mention goes to my dear friends, Sara Alfatih and Rayan Abdelrahim. Thanks, Abubaker Mohammed Sharaf (my beloved husband), and my lovely kids, Minna, Mohammed, and Lina for always believing in me and pushing me for greatness. Last, but not least, I give my thanks to the Almighty ALLAH for the gift of life, wisdom, grit, perseverance, health, and humility.

Table of contents

Declaration 1 – Plagiarism iv
Declaration 2 – Publications v
Research output from the thesis v
Abstract vii
Acknowledgments ix
List of abbreviations xii
List of figures xiii
List of schemes xix
List of tables xix
CHAPTER 1. INTRODUCTION 21
1.1 General Introduction 21
1.2. Background 21
1.3 Problem Statement 31
1.4 Aims and Objectives of the Study 32
1.5 The Novelty of the Study 33
1.6 Significance of the Study 34
1.7 Overview of the Thesis 35
References 38
CHAPTER 2. REVIEW PAPER 44
2.1 General Introduction 44
2.2 Author contributions 44
2.4 Published Manuscript 46
CHAPTER 3. FIRST EXPERIMENTAL PAPER 114
3.1 General Introduction 114
3.2 Author contributions 114
3.3 Submitted manuscript 115
Graphical abstract 116
Abstract 117
3.1. Introduction 117
3. 2. Materials and methods 121
3. 3. Results and discussion 132

3. 4. Conclusion 156
3.5. References 157
CHAPTER 4. SECOND EXPERIMENTAL PAPER 167
4.1 General Introduction 167
4.2 Author contributions 167
4.3 Submitted manuscript 168
Graphical abstract 169
Abstract 170
4. 1. Introduction 170
4. 2. Materials and methods 174
4. 3. Results and discussion 187
4. 4. Conclusion 217
4. 5. References 218
CHAPTER 5. CO-AUTHORED PUBLICATIONS 230
5.1 General Introduction 230
5.2.1 Abstract 230
CHAPTER 6. CONCLUSION 231
6.1 General conclusions 231
6.2 Significance of the findings in the study 234
6.3 Limitations of the study 236
6.4 Recommendations for future studies 237
6.4 Conclusion 238
Appendix I 239
Appendix II 242
Appendix III 246
Appendix IV 271

List of abbreviations

^{1}H NMR	Proton Nuclear Magnetic Resonance	MRSA	Methicillin-Resistant *Staphylococcus aureus*
ABS	Absorbance	MST	Microscale Thermophoresis
AMR	Antimicrobial Resistance	PDI	Polydispersity Index
ANOVA	One-Way Analysis of Variance	PEG	Polyethylene Glycol
CDC	Centers for Disease Control and Prevention	PGN	Peptidoglycan
CFU/mL	Colony-Forming Units per mL	PLGA	Poly-D, L-Lactic-co-Glycolic Acid
CIP	Ciprofloxacin	PLX407	Poloxamer 407
CO_2	Carbon Dioxide	PVA	Poly-Vinyl Alcohol
DEMEM	Dulbecco's Modified Eagle Medium	NDDS	Nano Drug Delivery Systems
DL% w/w	Drug Loading Percentage weight per weight	NLCs	Nanostructured Lipid Carriers
DLS	Dynamic Light Scattering	NMR	Nuclear Magnetic Resonance
DMSO	Dimethyl Sulfoxide	NPs	Nanoparticles
DPPH	2,2-Diphenyl-1-Picrylhydrazyl	OD	Optical Density
DSC	Differential Scanning Calorimetry	OLA	Oleylamine
EDC	1-Ethyl-3- (Dimethyl amino propyl) Carbodiimide	PBS	Phosphate Buffer Saline
EE %	Encapsulation Efficiency	RBS	Red Blood Cell
EMEM	Eagle's Minimum Essential Medium for HepG2 cells	RMSE	Root Mean Square Error
FBS	Fetal Bovine Serum	RMSF	Root-Mean-Square Fluctuation
FT-IR	Fourier Transform Infrared	RT	Room Temperature
HA	Hyaluronic Acid	SD	Standard Deviation
HEK-293	Human Embryonic Kidney Cells	SEM	Scanning Electron Microscopy
HepG2	Human Hepatoblastoma	SLN	Solid Lipid Nanoparticles
HIV	Human Immunodeficiency Virus	TA	Tannic Acid
HNs	Hybrid Nanocarriers	TEM	Transmission Electron Microscope
HPLC	High-Performance Liquid Chromatography	TNF-α	Tumor Necrosis Factor Alpha
IL-6	Interleukin 6	TLRs	Toll-Like Receptors
K_d	Dissociation Constant	VCM	Vancomycin
LPS	Lipopolysaccharide	VDW	Van der Waals Force
MCF-7	Michigan Cancer Foundation-7	WHO	The World Health Organization
MD	Molecular Dynamics		

List of figures

Figure	Title	Page
CHAPTER 1. BACKGROUND		
Figure 1	The anticipated worldwide mortality rate from AMR and other causes by 2050	22
Figure 2	Bacterial targets of antibiotics and resistance mechanisms	23
Figure 3	(**A**) The incidence of antimicrobial resistance (AMR) is overshadowing the decreasing availability of antibiotics. (**B**) The rate of antibiotic discovery 1930-2010 and the first incidence of resistance to the same antibiotic	24
Figure 4	Different mechanisms exist by nanocarriers for antimicrobial treatment and control of MDR bacteria	26
Figure 5	Stimuli-responsive nanoparticles as emerging targeted, controlled and triggered drug delivery systems	27
CHAPTER 2. REVIEW ARTICLE		
Figure 1	Scheme illustrating the structural designs of LPHNPs.	50
Figure 2	Scheme representing organic-inorganic hybrid NPs prepared by (a) direct synthesis; (b) grafting-to; and (c) grafting-from approaches of the RAFT technique	53
Figure 3	Scheme illustrating the preparation of MOFs through the co-ordination of metal ions or clusters with organic linkers (adapted with permission from	54
Figure 4	Various synthesis methods of CMCH-NPs	56
Figure 5	**(A):** Confocal laser scanning microscopy (CLSM) images of a) *E. faecalis* and b) *S. aureus* biofilms co-stained by PI encapsulated PLGA-NPs (i) or PLGA-LPHNPs (ii). **(B):** *In vitro* release profiles of different antibiotics from (a) PLGA-NPs and (b) PLGA-LPHNPs in PBS (pH 7.4) for 24 hrs at 37 ± 1°C	60
Figure 6	Scheme illustrating the design of antimicrobial PCL/Cur/GLE-Ag hybrid NPs	73
Figure 7	Scheme illustrating the design and the dual stimuli-responsive	78

	photothermal/pharmacological therapy of vancomycin/ZIF-8@PDA system and its in vivo application	
Figure 8	Scheme represents (**a**) the biomimetic mineralization synthesis process for GO_{χ} / $_{L}$-Arg@ Cu-BDC hybrid NPs; and (**b**) the self-activated double-cascade reaction mechanism for enhanced synergistic bactericidal activity	82
Figure 9	Scheme illustrating the preparation method of vancomycin/chlorogenic acid-loaded RBCM-coated supramolecular GNPs, and their synergistic and infection microenvironment-responsive antibacterial and antibiofilm effectiveness mechanisms to eradicate MRSA infection in mice model	88
Figure 10	Scheme representing the preparation and application of TR-701-PLGA@RBCM NPs in treating MRSA-wound infection	89
Figure 11	Scheme illustrating the preparation of BACA/Cu NPs@Gel-MA hybrid hydrogel and the synergistic antibacterial photothermal therapy via the generation of ROS under NIR irradiation	92
CHAPTER 3. EXPERIMENTAL PAPER ONE		
Figure 1	^{1}H NMR characterization of (**A**) HA, (**B**) Lys and (**C**) HA-Lys conjugate in D_2O. (*HA=Hyaluronic acid, Lys=$_{L}$-Lysine, HA-Lys= Hyaluronic acid-lysine conjugate).	132
Figure 2	FT-IR spectrum of (**A**) HA, (**B**) Lys and (**C**) HA-Lys conjugate. (*HA=Hyaluronic acid, Lys=$_{L}$-Lysine, HA-Lys= Hyaluronic acid-lysine conjugate)	134
Figure 3	The effect of pH change on the surface charge of VCM-HNLCs (*P*-value = 0.0004). Data are presented as mean ± SD (n=3)	137
Figure 4	(**A**) TEM image of VCM-HNLCs and (**B**) A histogram displaying the size distribution of VCM-HNLCs determined by DLS.	137
Figure 5	DSC thermograms of (**A**) Hyaluronic acid (HA); (**B**) $_{L}$-Lysine (Lys); (**C**) HA-Lys conjugate; (**D**) Vancomycin; (**E**) α-Tocopherol succinate; (**F**) physical mixture; (**G**) lyophilized VCM-HNLCs formulation.	138
Figure 6	The Cell viability % of different concentrations of (**A**) HA-Lys conjugate and (**B**) VCM-HNLCs, and controls on HEK293 and HepG2 cell lines. Data are presented as mean ± SD (n = 3).	139
Figure 7	(**A**) and (**B**) Non-hemolytic activity of different concentrations of VCM-	140

	HNLCs (*DW= distilled water, PBS=phosphate buffer saline pH 7.4). Data are presented as mean ± SD (n = 3).	
Figure 8	A Comparison view for different ligands fraction bound to (**A**) TLR2 and (**B**) TLR4. *PGN: Peptidoglycan, LPS: lipopolysaccharide, HA: hyaluronic acid, HA-Lys: hyaluronic acid-lysine conjugate and VCM-HNLCs: vancomycin-loaded hybrid nanostructured lipid carriers. Results represented in mean ± SD (n = 3).	142
Figure 9	*In vitro* drug release profile of bare VCM and VCM-HNLCs at pH 7.4 and pH 6.0. All data represented as mean ± SD (n = 3).	143
Figure 10	Changes in particle size (nm) and ZP (mV) of VCM-HNLCs during 90-days of storage at (**A**) room temperature (RT) and (**B**) 4 °C. All results are presented as mean ± SD (n = 3).	145
Figure 11	Histogram of cell count versus propidium iodide (PI) uptake, where **A** represent untreated MRSA (live cells); **B**, **C** and **D** indicate the proportion of dead cells in the population following incubation with bare VCM at its MIC (7.8 μg/mL), bare VCM in NPs MIC (3.9 μg/mL) and VCM-HNLCs at its MIC (3.9 μg/mL), respectively. The experiment was conducted in triplicate (n = 3).	148
Figure 12	(**A**) Percentage of biofilm growth suppression following the exposure of MRSA biofilms to bare VCM, VCM-HNLCs and controls (PBS pH 7.4 and 6.0). Each result is shown as mean ± SD (n = 3) (*P*-values **** < 0.0001). (**B**) MRSA biofilm growth reduction after exposure to bare VCM and VCM-HNLCs at PBS pH 7.4 and 6.0, as indicated by changes in the crystal violet intensity (* PBS = phosphate buffered saline, VCM = vancomycin, NLCs = nanostructured lipid carriers).	150
Figure 13	Images of the fluorescence microscope assay of MRSA biofilms stained with Syto9 and PI. **1**. Untreated MRSA biofilms **2.** Bare VCM treated biofilms, and **3.** VCM-HNLCs treated biofilms, respectively. (Scale bar =100 μm).	151
Figure 14	Time killing kinetics of MRSA exposed to bare VCM, VCM-HNLCs and (**A**) PBS pH 7.4 and (**B**) pH 6.0 (as controls). Results represented in mean ± SD (n = 3). VCM-HNLCs showed more and significant enhancement of	152

	VCM killing kinetics at pH 6 (*P*-value <0.0001).	
Figure 15	Efflux pump inhibition effect of VCM-HNLCs against MRSA compared to the bare VCM at 0.25×MIC.	153
Figure 16	The antioxidant activity (%) of various concentrations (µg/mL) of TS, Lys, HA-Lys conjugate and VCM-HNLCs according to a DPPH radical scavenging assay in comparison to ascorbic acid (positive control). Data in the graph are presented as mean ± SD (n = 3). (*TS= Tocopherol succinate, Lys= L-Lysine, HA-Lys= hyaluronic acid-lysine conjugate, VCM-HNLCs= vancomycin-loaded hybrid nanostructured lipid carriers, DPPH= 2.2-diphenyl-1-picrylhydrazyl)	154
Figure 17	(**A**) The Cytotoxicity of LPS on HepG2 cells and the protective effects of HA-Lys and VCM-HNLCs as measured by MTT assy, and (**B**) The effect of HA-Lys and VCM-HNLCs on IL-6 expression induced by LPS. (**** *P*-value<0.0001, *** *P*-value = 0.0002, in comparison with the LPS-treated group). Data in the graph are presented as mean ± SD (n =3).	156
CHAPTER 4. EXPERIMENTAL PAPER TWO		
Figure 1	TEM image of CIP-loaded TAH-NPs (*TEM = Transmission Electron Microscope; CIP = Ciprofloxacin; TAH-NPs = Tannic acid hybrid nanoparticles)	189
Figure 2	DSC thermograms of (A) PLX407; (B) CIP; (C) TA; (D) physical mixture; (E) lyophilized CIP-loaded TAH-NPs. (*PLX407 = poloxamer 407, CIP= ciprofloxacin, TA= tannic acid)	190
Figure 3	Cell viability % of different concentrations of (A) blank TAH-NPs and (B) CIP-loaded TAH-NPs, and controls on MCF-7, HEK293 and HepG2 cell lines. Data are presented as mean ± SD (n=3)	191
Figure 4	(A) and (B) Non-hemolytic activity of different concentrations of CIP-loaded TAHNPs (DW= distilled water, PBS=phosphate buffer saline pH 7.4). Data are presented as mean ± SD (n=3)	192
Figure 5	Structures of CIP, TA, OLA and PLX407 at four distinct simulated time points: (**A**) at t = 0 ns; (**B**) at t = 15 ns; (**C**) at t = 50 ns; and (**D**) at t = 90 ns. CIP was represented in a ball-and-stick model, TA (cyan), OLA (blue) and	192

	PLX407 (magenta) are represented in the sphere model. (* CIP = ciprofloxacin, TA = tannic acid, OLA = Oleylamine and PLX407 = poloxamer 407)	
Figure 6	(**A**) The COM distance between TAH-NPs components loaded with CIP with time. (**B**) The interaction energy between the molecules and their nonbonded components as it changes over time.	193
Figure 7	Structural representation of alterations occurring during the binding of LPS (blue), TA (Yellow), OLA (Green), PLX407 (Orange) and CIP (Black) to human TLR4. (A) The Conformational stability, C-α atoms RMSD for human TLR4 bound to LPS, TA, OLA, PLX407 and CIP (B) The time evolution RMSF of each residue of the protein C-α atom over 300 ns for LPS, TA, OLA, PLX407 and CIP bound to human TLR4. (C) Structural representation of changes occurring during solvent accessible surface (SASA) binding of five molecules. (D) A close view for LPS at the binding site of humanTLR4, showing the hydrogen bonds interactions over 300 ns period.	196
Figure 8	The total binding free energies of LPS, TA, OLA, PLX407 and CIP complexes with TLR4. All data are presented as mean ± SD (n-3). *P*-values **** < 0.0001, * = 0.0175, ns = 0.4056 for PLX407 and ns = 0.7992 for CIP (* LPS = lipopolysaccharide, TA = tannic acid, OLA = Oleylamine, PLX407 = poloxamer 407, CIP = ciprofloxacin).	198
Figure 9	Comparison of TLR4 fraction bound to LPS, TA, OLA and CIP-loaded TAH-NPs using MST. Results represented in mean ± SD (n = 3)	199
Figure 10	*In vitro* release profile of bare CIP and CIP-loaded TAH-NPs. All data represented in mean ± STD (n=3).	200
Figure 11	Changes in particle size (nm) and ZP (mV) of CIP-loaded TAH-NPs during 90-days of storage at (A) room temperature (RT) and (B) 4 °C. All results are presented as mean ± SD (n=3).	202
Figure 12	Cell counts versus propidium iodide (PI) uptake histograms, for (i) MRSA and (ii) *P. aeruginosa*, where (i) A, represents untreated MRSA (live cells); B, C and D represents percentage of dead cells in the population after incubation with bare CIP at its MIC (12.5 μg/mL), bare CIP at NPs MIC	207

	(1.56 μg/mL) and CIP-loaded TAH-NPs at its MIC (1.56 μg/mL), respectively. (ii) A represents untreated *P. aeruginosa* (live cells); B, and C represents percentage of dead cells in the population after incubation with bare CIP at its MIC (0.78 μg/mL) and CIP-loaded TAH-NPs at its MIC (0.78 μg/ml), respectively. The experiment was conducted in triplicate (n=3).	
Figure 13	Biofilm inhibition % after exposing (A) MRSA and (B) *P. aeruginosa* biofilms to bare CIP, CIP-loaded TAH-NPs, and control (PBS pH 7.4). All results are presented as mean ± SD (n = 4) (*P*-values *** 0.0006 and **** < 0.0001).	209
Figure 14	The fluorescence microscope assay depicts the images of (A) MRSA and (B) *P. aeruginosa* biofilms stained with Syto9 and PI. 1) Untreated biofilms 2) Biofilms treated with bare CIP, and 3) Biofilms treated with CIP-loaded TAH-NPs, respectively. (Scale bar = 100 μm).	210
Figure 15	Time killing kinetics curve of (A) MRSA and (B) *P. aeruginosa* exposed to CIP, CIP-loaded TAH-NPs, and control (PBS pH 7.4). Results represented in mean ± SD (n = 3). CIP-loaded TAH-NPs showed a significant enhancement of CIP killing kinetics (*P*-value <0.0001).	211
Figure 16	Efflux pump inhibition effect of CIP-loaded TAH-NPs against (A) MRSA and (B) *P. aeruginosa* compared with bare CIP (0.25×MIC).	212
Figure 17	Hemolytic activity (%) of (A) MRSA and (B) *P. aeruginosa* culture supernatants on sheep erythrocytes in the presence of MIC, 0.5 MIC and 0.25 MIC of bare CIP and CIP-loaded TAH-NPs. Values represent mean ± SD (n=3). (*P*-value ****< 0.0001)	214
Figure 18	The antioxidant activity (%) of different concentrations of TA and CIP-loaded TAH-NPs according to a DPPH radical scavenging assay in comparison to ascorbic acid (positive control). Data in the graph are presented as mean ± SD (n=3). (*TA= Tannic acid, CIP= Ciprofloxacin, H-NPs= hybrid nanoparticles, DPPH= 2.2-diphenyl-1-picrylhydrazyl)	215
Figure 19	Cytotoxicity of LPS on HepG2 cells and the protective effects of TA and CIP-loaded TAH-NPs as measured by MTT assay, and (B) Effect of TA and CIP-loaded TAH-NPs on IL-6 expression induced by LPS. (**** P-	217

	value<0.0001, *** *P*-value = 0.0005, in comparison with the LPS-treated cells). Data in the graph are presented as mean ± SD (n = 3)	

List of schemes

Table	Title	Page
CHAPTER 3. EXPERIMENTAL PAPER ONE		
Scheme 1	Synthesis of HA-Lys conjugate	122

List of tables

Table	Title	Page
CHAPTER 2. REVIEW ARTICLE		
Table 1	Different methods of preparation of LPHNPs, including the components of the hybrid nanosystems with their encapsulated drugs, if any.	51
Table 2	Summary of the studies undertaken to date with LPHNPs using PLGA as a polymeric core.	63
Table 3	Reported organic-inorganic hybrid NPs for enhancing antibacterial delivery	74
Table 4	Summary of the reported MOFs and their antibacterial mechanisms.	84
Table 5	Hybrid NP-hydrogels for localized antibacterial delivery.	96
CHAPTER 3. EXPERIMENTAL PAPER ONE		
Table 1	Size, PDI, ZP, EE% and DL% w/w for the different lipid: surfactant, drug: lipid, and lipid: polymer mass ratios used in the optimization of VCM-HNLCs. Results represented as mean ± SD (n = 3).	136
Table 2	Summary of the dissociation constant values (K_d) obtained from the MST analysis for PGN, LPS, individual excipients (HA, Lys and HA-Lys	142

	conjugate), VCM-HNLCs and non-hybrid NLCs components binding to TLR2 and TLR4, respectively. Data are presented as mean ± SD (n = 3).	
Table 3	Drug release kinetics data for the VCN-HNLCs at pH 7.4 and pH 6.	144
Table 4	The *in vitro* antibacterial activity of bare VCM, VCM-HNLCs and blank HNLCs showing MIC (μg/mL) results at pH 7.4 and pH 6.0 against *S. aureus* and MRSA bacteria. The experiment was conducted in triplicate (n = 3).	146
Table 5	∑FIC values against *S. aureus* and MRSA at pH 7.4 and pH 6.0.	147
CHAPTER 4. EXPERIMENTAL PAPER TWO		
Table 1	Size, PDI, ZP, EE % and DL % w/w for the parameters used in the optimization of CIP-loaded TAH-NPs (surfactant % w/v and lipid: polymer mass ratio). Results represented as mean ± SD (n = 3).	189
Table 2	Shows the average binding energy and its constituent parts for the TAH-NPs complex loaded with CIP, as determined by the MM-PBSA calculation. Each set of data is shown as mean ± SD (n = 3).mean ± SD (n=3).	193
Table 3	Shows the RMSD, RMSF, and SASA profile of the LPS, TA, OLA, PLX407 and CIP bound to human TLR4.	195
Table 4	Summary of the dissociation constant values (K_d) of LPS, TA, OLA and CIP-loaded TAH-NPs binding to TLR4 obtained from MST analysis. Data are presented as mean ± SD (n=3).	199
Table 5	Drug release kinetics data for CIP-loaded TAH-NPs	201
Table 6	*In vitro* antibacterial activity of bare CIP, blank-TAH-NPs and CIP-loaded TAH-NPs showing MIC (μg/mL) results against *S. aureus*, MRSA, *E. coli* and *P. aeruginosa*. The experiment was conducted in triplicate (n = 3).	204
Table 7	∑FIC values for *S. aureus*, MRSA, *E. coli* and *P. aeruginosa* at each time interval.	205

CHAPTER 1. INTRODUCTION

1.1 General Introduction

This chapter provides a brief overview of the study, including the current status of bacterial infections and associated sepsis, and emphasizes the various challenges associated with the increasing emergence of resistant bacteria, as well as the limitations of existing antibiotic therapy. This chapter further discusses recent advances in nano-drug delivery systems, including the design of hybrid nanocarriers using bioactive materials and the use of stimuli-responsive and biomimetic approaches to improve the clinical outcomes of antibiotics in treating bacterial infections and sepsis. Highlights of problem identification and justification, the aims and objectives, the novelty and significance of the study, and the overall structure of the thesis are also presented.

1.2 Background

Bacterial infections play a significant role in global morbidity and mortality, particularly in regions with limited access to healthcare resources, such as Sub-Saharan Africa [1]. In 2019, 7.7 million people died from bacterial infections worldwide, accounting for 13.6% of all global deaths, making bacterial infections the second leading cause of mortality [2, 3]. The prevalence of bacterial infections and antimicrobial resistance (AMR) remain public health issues of global concern [4]. According to recent World Health Organization (WHO) publications, AMR ranks among the top 10 global public health and socioeconomic challenges affecting human life [5, 6]. Infections due to AMR bacteria are increasing worldwide, bringing the threat of untreatable infections closer to reality [7]. It is estimated that more than 35,000 people die from AMR infections in the EU/EEA each year, outpacing deaths from influenza, tuberculosis and HIV/AIDS [8]. In sub-Saharan Africa the burden of AMR is largely unclear. Measurement of AMR burden in community and hospital settings; microbiological acquisition of AMR; genotypic development of AMR mechanisms and transmission patterns are among the significant gaps in AMR data in Africa [9]. Additionally, AMR appears to be a low priority in most countries in Sub-Saharan Africa, despite the urgent need for more coordinated measures, as shown by the scant number of implemented national action plans [10]. According to the latest report published by the Lancet Glob Health (2024), there were an estimated 1.05 million deaths associated with bacterial AMR in the WHO African region in 2019 [11], and unless action is taken quickly enough, an additional 10 million people will die worldwide from drug-resistant infections every year by 2050 (**Figure 1**) [12].

On the other hand, sepsis, a fatal complication of impaired immune response to systemic infections, has been identified as a serious threat to the healthcare system [13]. Even with advanced medical care, sepsis carries a significant risk of mortality worldwide [14]. The 2020 Global Burden of Disease Report on sepsis shows that, 48.9 million people were diagnosed with sepsis and 11 million died in 2017, making it a bigger killer than cancer [15]. Most significantly, a Lancet study revealed secondary bacterial infections and severe sepsis as complications in COVID-19 patients, posing further risks to their recovery [16]. Therefore, addressing bacterial infections and sepsis requires urgent attention and should be given a high priority in public health.

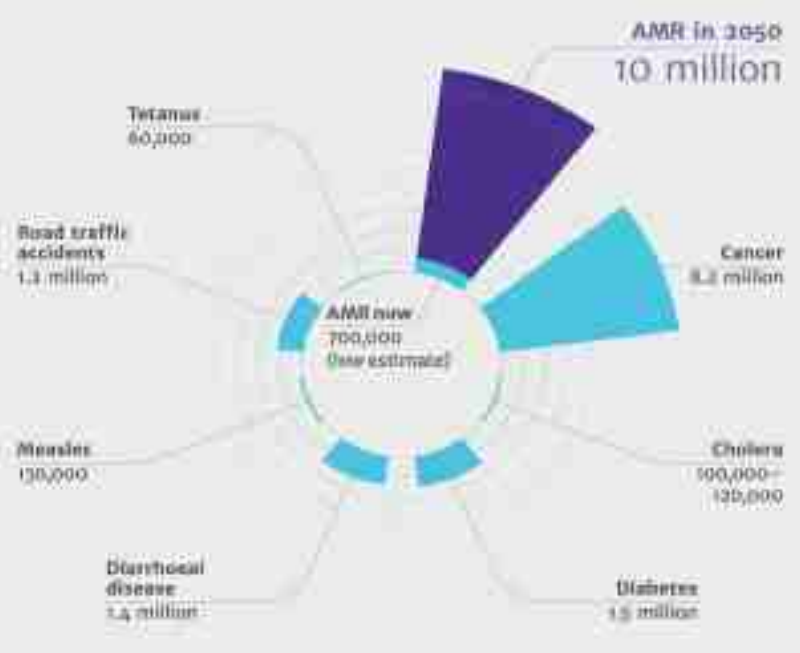

Figure 1. The anticipated worldwide mortality rate from AMR and other causes by 2050 [17].

In the realm of modern medicine, antibiotics stand as formidable weapons against bacterial infections since their discovery in the early 20th century. They have revolutionized the healthcare sector by effectively managing life-threatening diseases like sepsis and greatly improving the safety of surgical procedures, leading to a substantial reduction in mortality rates and saving countless lives [18]. Antibiotics have been currently used in treating both planktonic and biofilm-related infections. [19]. They target bacteria through various mechanisms, depending on the type of antibiotic and the bacterial strain [17]. These mechanisms rely on blocking specific bacterial intracellular targets or inhibiting essential bacterial metabolic pathways, such as inhibition of cell wall synthesis (β-lactams and vancomycin), interference with vital protein synthesis (erythromycin), disruption of cell membrane integrity

(Polymyxin), disruption of folic acid metabolism (sulfonamides), and inhibition of nucleic acid synthesis (ciprofloxacin) (**Figure 2**)[17, 20, 21]. However, resistance to nearly all classes of currently in use antibiotics has evolved, as bacteria develop defense mechanisms to withstand the effects of antibiotics, making these once-effective drugs increasingly ineffective [22]. They are capable of acquiring mutations in their genetic material (DNA) either through natural processes under the effect of external antibiotic pressure (spontaneous mutations) or through horizontal gene transfer within and/or between bacterial populations in biofilms [17]. Other intrinsic mechanisms of antibiotic resistance include enzymatic inactivation, alteration of antibiotic target sites, modification of cell components, efflux pumps expression and biofilm formations [23, 24]. Furthermore, bacteria can simultaneously use multiple resistance mechanisms, rendering them extremely resistant to all antibiotics (superbug) and giving rise to multi-drug resistant (MDR) bacterial strains, which are difficult to eradicate and necessitate multiple and high doses of antibiotics [22].

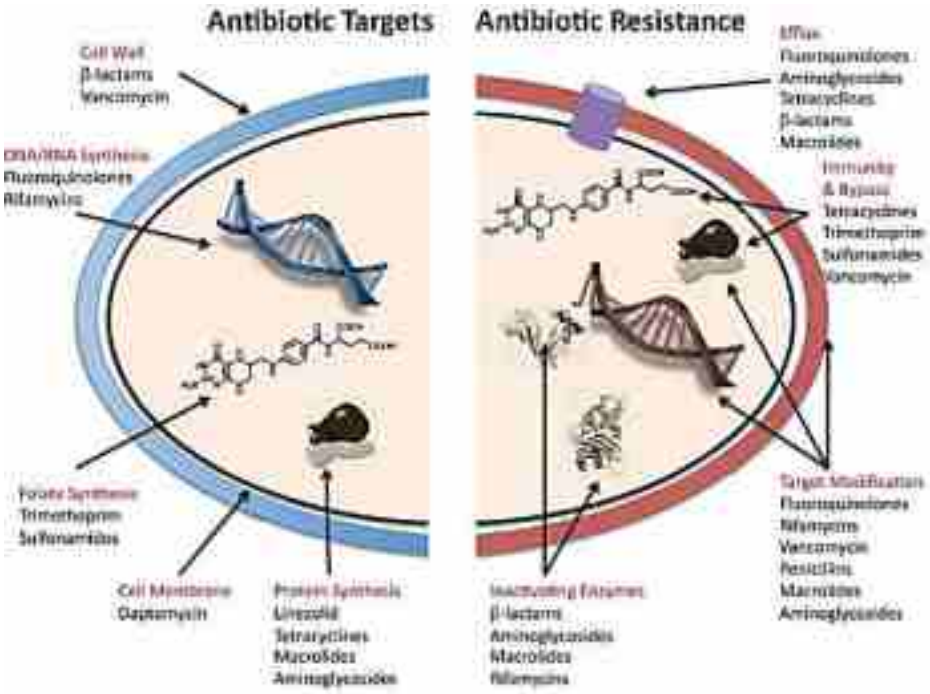

Figure 2. Bacterial targets of antibiotics and resistance mechanisms [21].

The misuse and overuse of antibiotics [25], along with the challenges associated with conventional antibiotic dosage forms such as sub-optimal concentrations, poor pharmacokinetic properties, enzymatic degradation and inadequate targeting, have been widely recognized as significant contributing factors to antimicrobial therapy failure, infection recurrence, and development of AMR [26-28]. Moreover, the

complex molecular pathophysiology of sepsis can significantly impact antibiotic therapy in multiple ways [29]. For instance, the dysregulated systemic inflammatory response to infection which ultimately results in multiorgan failure can lead to increased distribution and clearance of antibiotics from the bloodstream. As a result, higher doses or more frequent administration may be necessary to achieve therapeutic levels [30]. Additionally, changes in blood flow, organ perfusion, drug biodistribution and metabolism in sepsis can affect the drug's pharmacokinetics and its effective concentrations in tissues and compartments [31, 32]. These factors are known to play a substantial role in the breakdown of infection control and increasing healthcare expenditures [33]. Moreover, the prohibitive cost of bringing a new drug to market, the low success rate in clinical trials, the possibility of antibiotic resistance even to new classes of antibiotics, and difficulties in obtaining regulatory approval are the primary reasons for the declining adoption of new antibiotics from the pharmaceutical industry, resulting in the depletion of antibiotics pipeline (**Figure 3**) [28, 34]. For these reasons, more innovative delivery approaches that can be efficiently used for combating bacterial infections and sepsis are urgently required.

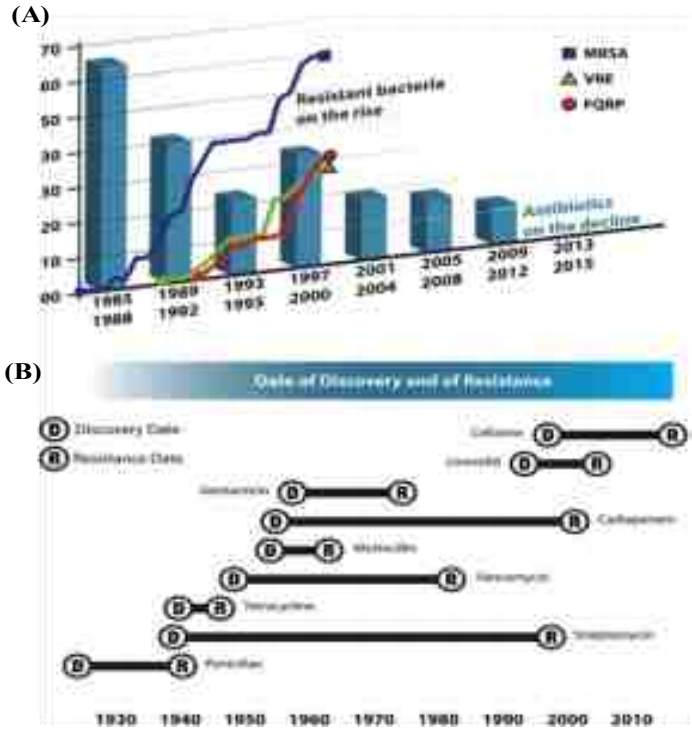

Figure 3. (**A**) The incidence of antimicrobial resistance (AMR) is overshadowing the decreasing availability of antibiotics. (**B**) The rate of antibiotic discovery 1930-2010 and the first incidence of resistance to the same antibiotic [28].

Over the past few decades, the escalating challenge of antibiotic-resistant bacteria has prompted a paradigm shift in medicine, with nanotechnology emerging as a beacon of hope. Antibiotic-delivering nanomedicines provide an opportunity to boost the effectiveness of antibacterial regimen and tackle the obstacles associated with conventional antibiotics [35]. By harnessing the unique properties of nanoparticles, scientists have made significant strides in developing targeted drug delivery systems that enhance the efficacy of antibiotics while minimizing side effects [36]. These nanosystems render numerous advantages over conventional therapies, including higher solubility, enhanced stability and improved bioavailability [37]. In addition, their unique nanoscale size, shape and surface charge allow them to easily pass through the endothelium in an inflammatory region and accumulate effectively in the site of infection, which promotes the targeting of antibiotics to bacteria [38]. Furthermore, the high surface-to-volume ratio of these nanoparticles permits surface functionalization and enhances the drug loading capacity, which together with their strong affinity for bacteria help to produce effective antibacterial activity [39]. Moreover, encapsulating antibiotics into nanoparticles can protect the drugs from enzymatic attack, improve their pharmacokinetic profile and therapeutic index, offer controlled and sustained release profiles and can also decrease the exposure of the drug to normal tissues. These advantages can, in turn, reduce the toxicity and adverse side effects associated with high systemic drug and frequent dosing [40].

Most significantly, nanoparticles-based drug delivery systems have the potential to effectively circumvent the AMR mechanisms through multiple pathways as shown in **Figure 4** [41]. For instance, the targeted delivery of the antibiotic nanocarrier to the site of infection promotes the accumulation and release of higher drug concentrations at the infection site for prolonged period of time. Exposure of bacteria to these high concentrations may prevent the growth and promote the killing of both susceptible and dormant populations without increasing the dose [42]. Similarly, the nanoparticles, owing to their small size, possess the ability to damage bacterial biofilms, thereby permitting drugs to easily penetrate the biofilm and subsequently eradicate the bacteria [43]. They can also be engineered to bypass or inhibit bacterial efflux pumps, enabling the antibiotic to remain within the bacterial cell and exert its bacteriostatic or bactericidal effects [44]. Other strategies that can further enhance the potential of nanoparticles in combating AMR include disrupting bacterial membranes, altering drug-pathogen interactions, and promoting intracellular uptake [45]. By employing these strategies, nanoparticles offer a multifaceted approach to enhance the efficacy of antibiotics and provide new tools in the battle against MD bacterial infections.

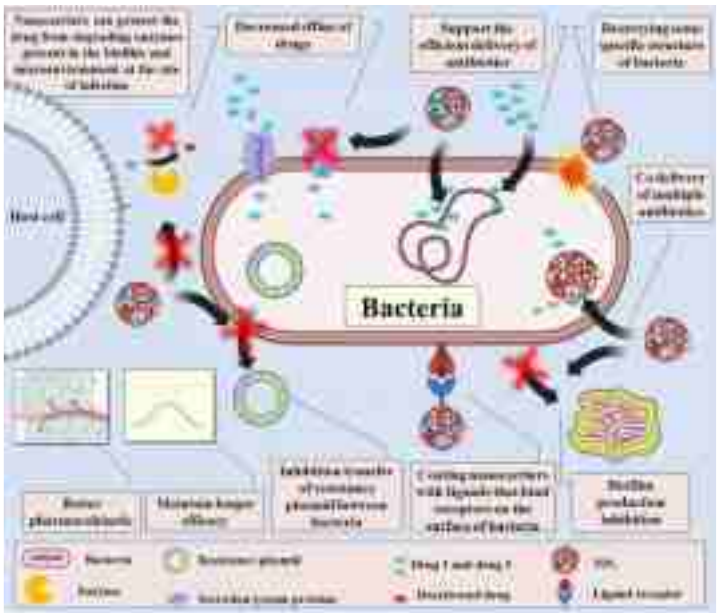

Figure 4. Different mechanisms exist by nanocarriers for antimicrobial treatment and control of MDR bacteria [41]

Numerous nanosystems, including polymeric nanoparticles [46], micelles [47], dendrimers [48], liposomes [49], solid lipid nanoparticles [50] and nanoplexes [51], have been investigated for antibiotic delivery since Alec D. Bangham and his colleagues developed the first nanocarrier, liposomes, in 1965 [52]. One of the promising nanodrug delivery system (NDDS) for antibiotic delivery are hybrid nanocarriers (HNs), which are composed of a variety of biomaterial combinations, at sub-micrometer scales [53]. The use of HNs has proven to be a solution for the difficulties associated with drug delivery and treatments, as they enable the creation of nanosystems that possess the desirable properties of the combination of biomaterials used to create them, while addressing their drawbacks [54]. HNs have demonstrated the ability to overcome the constraints present in non-hybrid nanocarriers, such as poor biocompatibility, premature drug release, rapid elimination, instability in storage, and unacceptable toxicity resulting from long-term exposure [55]. HNs have lately received attention for antibacterial delivery thanks to their numerous advantages, which include good biodegradability and biocompatibility, high loading capacity, robust structural integrity, chemical diversity for targeting and versatility in functionalization [39, 56]. However, challenges still exist for achieving maximum targeting and interaction with bacteria at the infection site. Given the rapid advances in nanotechnology, several strategies have been proposed to maximize the potential of HNs in the treatment of bacterial infections and sepsis, including the design of stimuli-responsive and biomimetic NDDSs.

Recently, the advancement in stimuli-responsive nanosystems has improved the targeted delivery of antibiotics to the site of infection. These nanomaterials can be triggered by various biochemical signals characterizing the bacterial and sepsis microenvironment such as alterations in pH and redox potential, the action of bacterial enzymes and the overproduction of reactive oxygen species (ROS) (**Figure 5**), which enable precise and on-demand release of antibiotics at the site of infection and improved interaction with the targeted bacteria [39, 57]. By taking this approach, the risk of antibiotic leakage can be minimized, and the accumulation of nanocarriers can be particularly concentrated in the infected area, resulting in a higher drug concentration at the infection site [58], which consequently improves bacterial targeting and minimizes toxicity and unfavorable side effects.

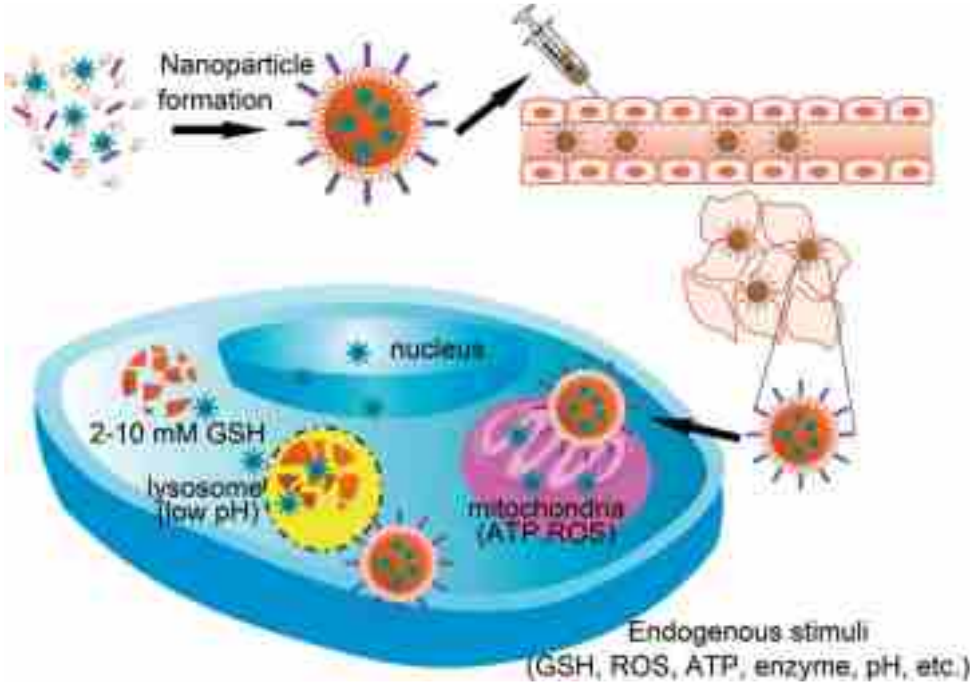

Figure 5. Emerging triggered and controlled drug delivery systems using stimuli-responsive nanoparticles [57].

Among various stimuli responses, pH appears to be an attractive biomarker for targeted antibiotic delivery, as some pathogenic bacteria such as *Staphylococcus aureus* (*S. aureus*) and *Pseudomonas aeruginosa* (*P. aeruginosa*), generate acidic environments at the infection site through their metabolic processes and the host's immune response to infection [59, 60]. Incorporating pH-responsive properties into an NDDS represents an attractive strategy that holds great promise in the fight against bacterial infections and sepsis. The design of pH-responsive nanocarriers involves the use of different

biocompatible materials that ensure stability under physiological conditions while undergoing structural changes in response to pH alterations, triggering drug release at the infection site, and allowing eradication of the bacteria in a highly localized manner [58]. Several pH-sensitive biomaterials, including natural polymers (chitosan and alginate), fatty acids (oleic acid), and fatty amines (Oleylamine (OLA) and stearylamine), have been used to create pH-responsive nanocarriers with improved drug loading and fewer side effects [61-63]. However, there is still a need to expand the scope of pH-responsive nano-delivery of antibiotics to effectively treat bacterial sepsis and combat the growing AMR.

On the other hand, biomimicry is currently being investigated as a potential strategy to improve the advantages of NDDSs by mimicking biological structures or disease-associated cellular communication pathways, which leads to an increased attraction to target cells [64]. Biomimetic nanocarriers offer several advantages that can potentially lead to more effective and personalized treatments. These advantages include enhanced targeting and specificity to the drug action site, improved biodegradability, and greater compatibility with biological systems [65]. In addition, they can be engineered to bypass or overcome various physiological barriers in the body, allowing for more efficient drug delivery [66]. Furthermore, the surface modification of biomimetic nanocarriers can be tailored to specific biomarkers associated with a disease condition, which potentially improves the overall treatment outcomes [67]. Considering these benefits, biomimetic nanocarriers can be engineered to mimic multiple inflammatory pathways in bacterial infections and sepsis with the goal of optimizing their targeting to the infection microenvironment.

Upon infection of the host cell, pattern recognition receptors such as toll-like receptors (TLRs) are activated by structurally conserved microbial toxins, which allows the innate immune system to recognize and identify invading bacteria [68]. The interaction between specific microbial components, such as lipoteichoic acid (LTA), peptidoglycan (PGN), and lipopolysaccharide (LPS) and TLRs leads to the activation of inflammatory responses that helps in eliminating the invading bacteria [69]. Nevertheless, in cases of severe sepsis caused by bacterial infection, excessive and unregulated TLR activation takes place, resulting in overpowering systemic inflammation, oxidative stress, and damage to multiple organs [70]. Clarifying the function of TLR activation in bacterial sepsis is essential for creating therapies that can regulate the immune response and enhance the chances of survival in patients with sepsis. Motivated by this natural process of bacterial recognition and immune activation, recent studies show an interest in developing therapeutic inhibitors of TLRs, with a specific focus on treating sepsis resulting from infections.[71-74]. These studies have revealed that small molecules, such as glycopeptides, steroids, and

antibodies, can competitively bind to TLRs and have demonstrated promising outcomes in reducing TLR signaling activity in several inflammatory conditions [74-76]. As a result, this strategy of minimizing TLR activation by inhibiting their binding to bacterial toxins can be applied as a biomimetic approach to an antibiotic nanocarrier, in order to enhance the overall treatment outcomes of bacterial infections and sepsis. More interestingly, merging this biomimetic principle with the pH-responsive approach in HNs could be a promising approach for potentiating the effectiveness of antibiotics against bacterial sepsis.

Furthermore, bacterial biofilms and efflux pumps can significantly contribute to the development of chronic infections that can progress to sepsis. The extracellular matrix of biofilms provides a protective barrier that prevents the penetration of antimicrobial agents and immune cells, leading to a high level of resistance to treatment for biofilm-associated infections.[77]. Also, efflux pumps are vital for the survival and adaptability of bacteria in their natural habitats. These molecular mechanisms have evolved to actively expel a diverse range of antimicrobial substances from the cell of bacteria, which allows the bacteria to endure and proliferate even when exposed to deadly antibiotic concentrations [78]. Targeting bacterial biofilms and efflux pumps is an additional strategy that can be utilized in NDDSs to enhance the effectiveness of antibiotics to prevent AMR and treat infections associated with sepsis.

In summary, developing an advanced HN integrating the biomimetic principle and pH-responsiveness with biofilm eradication and efflux pump inhibition approach could be a novel antibacterial-immunoregulatory strategy that requires an innovative combination of materials with multifunctional properties to enhance the efficacy and targeted delivery of antibiotics against bacterial sepsis.

A variety of biomaterials have been employed in the creation of nanosystems that demonstrate biocompatibility, extended circulation time, appropriate engagement with targeted pathogens and optimal localization at infection sites. This approach has been shown to be effective in the fabrication of drug delivery systems that potentiate the therapeutic effectiveness of loaded antibiotics [79]. In this regard, natural biomaterials such as hyaluronic acid (HA) and L-lysine (Lys) are gaining popularity as excellent bioactive materials for effective drug delivery, thanks to their anti-inflammatory and antioxidant properties, excellent bio-safety profiles, biocompatibility and ease of fabrication into various nanosystems. Similarly, natural polyphenols like tannic acid (TA) and vitamin derivatives like tocopherol succinate (TS) are increasingly being recognized as outstanding bioactive materials for antibiotic drug delivery, due to their excellent biocompatibility properties, intrinsic antimicrobial activity, anti-inflammatory effects, antioxidant properties, and ability to inhibit bacterial biofilms and efflux pumps. Likewise, fatty amines such as OLA, possess unique properties that can be applied to the development of

drug delivery systems. Their pH-dependent functionality and inherent antimicrobial properties can be leveraged to create nanosystems with controlled drug release and improved therapy for the treatment of infectious diseases. As a result, using such biomaterials to design smart HNs with multifunctional properties that can respond to pH and/or mimic biological processes may enhance the effectiveness and overall clinical performance of existing antibiotics against bacterial infections and associated sepsis.

Therefore, the general aim of this study was to explore the potential of various novel multifunctional biomaterial-based HNs, including biomimetic and/or pH-responsive HNs in enhancing the targeted delivery of antibiotics and suppressing the proinflammatory response against bacterial infections and sepsis.

In this regard, the first aim of this study was to combine biomimicry and stimuli-responsive principles through the design and synthesis of a novel biomimetic hyaluronic acid-lysine conjugate (HA-Lys) and subsequently exploit the attributes of the synthesized polymer with TS and OLA in the formulation of multifunctional biomimetic pH-responsive hybrid nanostructured lipid carriers (HNLCs) loaded with vancomycin (VCM-HNLCs), to combat bacterial-induced sepsis. The creation of a novel HA-Lys conjugate that possesses both TLRs antagonistic properties (due to the HA moiety) and oxidative stress reduction activities (due to the Lys moiety) could potentially offer a therapeutic adjuvant with increased potency and targeting against sepsis-causing bacteria. In our scenario, we anticipated that the modified HA-Lys polymer would impart biomimetic properties to the system by simulating the natural PGN-TLR2 and LPS-TLR4 interactions. This would be accomplished by the direct and competitive binding of the HA-Lys conjugate to the host TLRs, thereby preventing their binding to the bacterial endotoxins (PGN and LPS), which would result in the modulation of host immune response, reduction of oxidative stress, and the control of inflammatory cytokine levels. On the other hand, TS may have the potential to decrease bacterial antibiotic resistance by inhibiting biofilm formation and efflux pumps. Furthermore, the controlled and triggered release of VCM from HNLCs could be enhanced through the pH-sensitive properties of OLA. In general, this innovative multifunctional HN provides multiple mechanisms of action to eliminate MRSA and reduce excessive inflammatory activation for optimal therapeutic outcomes against bacterial infections and sepsis. The data obtained from the synthesis and characterization of HA-Lys conjugate, formulation, and optimization of VCM-HNLCs, *in vitro* characterization, and *in vitro* antibacterial, antioxidants and anti-inflammatory studies are presented in **Chapter 3.**

The second aim of this study was to develop a novel HN integrating the biomimetic principle with biofilm eradication and efflux pump inhibition approaches. In this study, we proposed a HN derived from TA and OLA, to improve the efficacy of ciprofloxacin (CIP-loaded TAH-NPs) against bacterial-induced sepsis through several combined strategies. First, TA could lower bacterial infectivity and resistance mechanisms via its possible actions against bacterial biofilms and efflux pumps. Also, it could confer biomimetic properties to the system by mimicking the natural LPS-TLR4 interaction, which would be achieved by the direct and competitive binding of TA to TLR4 in the host cells, thereby reducing the LPS-induced hyperactivation of TLR4 and the subsequent downstream signal activation. In addition to its ability to neutralize ROS, TA contributes to modulating the host's immune response, controlling inflammatory cytokine levels and reducing oxidative stress. On the other hand, OLA could provide mechanical strength, stability, improved loading capacity, effective permeation into bacterial membrane, and may work synergistically with CIP and TA to combat both Gram-positive and Gram-negative bacteria. Overall, this novel nanosystem could be a fruitful avenue in sepsis research, with the potential to significantly reduce the severity of this fatal disease and enhance treatment outcomes. The data resulting from the formulation of CIP-loaded TAH-NPs, optimization, *in vitro* characterization, *in silico* studies and *in vitro* antibacterial, antioxidant and anti-inflammatory studies are reported in **Chapter 4.**

1.3 Problem Statement

The burden of bacterial infections and sepsis is rising worldwide, particularly in low-income countries. They are considered significant problems in the healthcare sector that require prompt attention. The current global crisis of antibiotic resistance, coupled with the scarcity of new antibiotics has significantly hindered the treatment of patients with bacterial sepsis, resulting in treatment failures, prolonged hospital stays, and ultimately increased morbidity and mortality rates. Additionally, the efficacy of existing antibiotics is reduced due to many factors such as poor pharmacokinetic properties, low bioavailability, poor drug penetration into the infection site and fast degradation, resulting in subtherapeutic concentrations, higher therapeutic dose requirements, and increased risk of toxicity. NDDSs including HNs hold great promise in the fight against sepsis and bacterial infections, thanks to their remarkable advances in antibiotic therapy. However, difficulties for achieving optimal targeting and interaction with bacteria at the infection site still exist. Consequently, more sophisticated stimuli-responsive and biomimetic approaches have been used with the goal of improving the targetability of the nanocarriers and enhancing the localization of antibiotics at the infected sites, thereby increasing the therapeutic outcomes, and reducing adverse toxicity. Furthermore, targeting bacterial biofilms and efflux pumps is an

additional tactic that can further enhance the antibiotics' delivery and activity. Even more interestingly, there is an additional advantage in the development of biomimetic nanocarriers that can modulate the signalling pathways of bacterial sepsis and function as therapeutic agents. The use and/or synthesis of smart biomaterials with multifunctional activity to confer biomimetic, stimuli-responsive, and antivirulence properties to antibiotic nanocarriers remains an active area of research that could provide innovative and promising results in the fight against bacterial infections and associated sepsis.

1.4 Aims and Objectives of the Study

The study was broadly aimed to design, synthesize, and characterize novel biomaterials with multifunctional activities for the development of biomimetic and/or pH-responsive HNs to enhance the targeted delivery of antibiotics and modulate the proinflammatory response against bacterial infections and sepsis. In order to achieve this goal, the study pursues the following specific aims and objectives:

Aim1

The study aimed to synthesize a novel HA-Lys conjugate and to explore its potential with TS and OLA in the formulation of multifunctional biomimetic pH-responsive HNLCs to improve the targeted delivery of vancomycin (VCM-HNLCs) against bacterial infections and sepsis.

In order to achieve this aim, the specific objectives of the study were:

1. To synthesize HA-Lys conjugate using a simple amidation reaction.
2. To characterize the synthesized HA-Lys conjugate by FT-IR and ^{1}H NMR.
3. To confirm the biosafety of HA-Lys by performing cytotoxicity studies.
4. To use the synthesized HA-Lys with TS and OLA in the production and optimization of VCM-HNLCs using a hot homogenization ultra sonication technique
5. To characterize the formulated VCM-HNLCs in terms of average particle size, polydispersity index (PDI), zeta potential (ZP), pH-responsiveness, entrapment efficiency (EE %), drug loading capacity (DL % w/w), surface morphology, thermal profile, pH-responsive *in vitro* drug release, and physical stability studies.
6. To confirm the biosafety of VCM-HNLCs by performing cytotoxicity and hemolysis studies.
7. To determine the binding affinity of HA-Lys and VCM-HNLCs to human TLR2 and TLR4 using microscale thermophoresis (MST).
8. To assess the formulated VCM-HNLCs for their *in vitro* antibacterial, antibiofilm, efflux pump inhibition, antioxidant and anti-inflammatory efficacy.

Aim 2

This study aimed to formulate a novel HN derived from TA and OLA for the biomimetic targeted delivery of CIP against bacterial infections and sepsis

In order to achieve this aim, the detailed objectives of the study were:

1. To formulate and optimize CIP-loaded TA-HNPs using a hot ultrasonic dispersion method.
2. To characterize the formulated CIP-loaded TA-HNPs in terms of average particle size, PDI, ZP, EE %, DL % w/w, nanoparticle morphology, thermal profile, *in vitro* drug release, and physical stability studies.
3. To confirm the biosafety of CIP-loaded TA-HNPs by performing cytotoxicity and hemolysis studies.
4. To determine the binding affinity of TA and CIP-loaded TA-HNPs to TLR4 using *in-silico* investigations and confirm the binding using MST.
5. To assess the formulated CIP-loaded TA-HNPs for their *in vitro* antibacterial, antibiofilm, efflux pump inhibition, antioxidant and anti-inflammatory efficacy.

1.5 The Novelty of the Study

The novelty of the study is presented in two experimental studies.

Aim 1

The novelty of the experimental research, presented in **Chapter 3**, is discussed in the following section:

- This study reports for the first time the synthesis of a modified HA-Lys polymer.
- This study reports the first application of HA-Lys as a targeting adjuvant to treat bacterial sepsis.
- This study reports the first stimuli-responsive HNLCs for the delivery of any class of drug.
- This study also reports the first combined biomimetic and pH-responsive HNLCs to deliver antibiotics against bacterial sepsis.

Aim 2

The novelty of the experimental research presented in **Chapter 4** is discussed in the following section:

- This study reports the first HN formulated using TA and OLA to deliver any class of drug.
- This study reports the first application of a HN that simultaneously combined biomimicry with efflux pump inhibition and biofilm eradication approaches.

- This study reports for the first time the strategy of using TLRs as a pathway for immune regulation in drug delivery.

1.6 Significance of the Study

This study presents groundbreaking and advanced strategies in the treatment of bacterial infections and sepsis. The NDDSs proposed in this study are innovative nanocarriers that specifically target both the site of bacterial infection and the sepsis microenvironment. This allows for efficient delivery of antibiotics to eliminate the causative bacteria, overcome AMR mechanisms, and minimize the overactivation of TLRs that occurs during sepsis. As a result, the proposed strategies exhibit enhanced antibacterial efficacy and improved inflammatory responses, leading to better therapeutic outcomes and patient compliance. The following highlights the significance of this study:

- ***New pharmaceutical products***

The present study introduces unique pharmaceutical products, namely, novel targeting ligands and HNs, which have not been previously reported in the literature. This creative approach has the potential to encourage local pharmaceutical companies to develop more cost-effective products, thereby enhancing their competitiveness in the global pharmaceutical market, which is known to be highly profitable.

- ***Improved patient well-being and disease control***

The advanced HNs presented in this work could potentiate the treatment of patients with severe bacterial infections and sepsis worldwide. They could also benefit individuals suffering from COVID-19 and other illnesses exacerbated by bacterial infections and sepsis, leading to better disease management, improved patient lives, and reduced mortality rates.

- ***Generating new knowledge for the scientific community***

The innovation of this study will open new avenues for research and development worldwide in the field of manufacturing techniques, synthesis strategies, and design approaches for the creation of innovative and intelligent biomaterials and their subsequent use in the production of novel stimuli-responsive and biomimetic NDDSs. It will also shed light on the *in vitro* characteristics of these novel nanocarriers. The study may help scientists whose work is relevant in developing novel NDDS that will improve the potential use of these drugs in medicine.

- ***Conceptualization of new research***

The proposed novel multifunctional biomaterials and their associated nanoformulations (VCM-HNLCs and CIP-loaded TAH-NPs) as strategies to improve antibiotic delivery to infection sites, and their overall therapeutic effect in treating complicated bacterial infections and sepsis, may stimulate further studies on their scalability, clinical evaluation, other potential applications, and the design and synthesis of other novel biomimetic and targeting biomaterials.

1.7 Overview of the Thesis

The research work performed in this thesis is presented in a publication format in accordance with the guidelines of the College of Health Sciences, University of KwaZulu-Natal. It specifies the inclusion of a brief introductory chapter, published/submitted papers and a final concluding chapter. At least three first-authored papers, two of which must be experimental, should come from a Ph.D. study.

CHAPTER ONE: INTRODUCTION

This chapter provides a brief overview of the study, including the current status of bacterial infections and associated sepsis, and emphasizes the various challenges associated with the emergence of resistant bacteria, as well as the limitations of existing antibiotic therapy. This chapter further discusses recent advances in nano-drug delivery systems, including the design of hybrid nanocarriers using bioactive materials and the use of stimuli-responsive and biomimetic approaches to improve the clinical outcomes of antibiotics in treating bacterial infections and sepsis. Highlights of problem identification and justification, the aims and objectives, the novelty and significance of the study, and the overall structure of the thesis are also presented.

CHAPTER TWO: REVIEW PAPER

This chapter focuses mainly on the recent developments, technological advancements, and contributions of the various hybrid nanosystems created for antibacterial delivery. The review first provides a theoretical overview on different hybrid nanosystems, including lipid-polymer hybrid NPs (LPHNPs); organic-inorganic hybrid NPs; metal-organic frameworks (MOFs); cell membrane-coated hybrid NPs (CMCH-NPs); and hybrid NPs-hydrogels, and their design approaches. The significance and limitations of using these novel NDDSs in the treatment of bacterial infections are then critically discussed and evaluated in detail. Finally, this review identifies the future strategies required to optimize the potential of

hybrid nanosystems for treating bacterial infections. This chapter is a first-authored review article published in Q1 ISI International Journal: Journal of Controlled Release (Impact Factor = 11.467).

CHAPTER THREE: EXPERIMENTAL PAPER ONE

This chapter addresses Aim 1, Objectives 1-8, and is a first-authored experimental paper submitted to an ISI International Journal: *International Journal of Biological Macromolecules* (Manuscript ID: IJBIOMAC-D-23-18902). (Impact factor: 8.2). This article highlights the synthesis of a novel HA-Lys conjugate and explores its biomimetic activity to competitively inhibit bacterial-TLRs induced inflammatory responses using *in vitro* investigations. It also highlights the formulation, optimization, and characterization of multifunctional biomimetic pH-responsive VCM-HNLCs, which were prepared from the synthesized HA-Lys, TS, and OLA to enhance VCM delivery. Furthermore, it evaluates the biocompatibility, hemocompatibility, *in vitro* TLR2 and TLR4 binding affinity, *in vitro* antibacterial, antibiofilm, efflux pump inhibition, antioxidant, and anti-inflammatory activities of the prepared VCM-HNLCs.

CHAPTER FOUR: EXPERIMENTAL PAPER TWO

This chapter addresses Aim 2, Objectives 1-5, and is a first-authored experimental paper submitted to an ISI International Journal: *International Journal of Pharmaceutics* (Manuscript ID: IJPHARM-D-23-03925) (Impact Factor: 5.875). This article highlights the formulation, optimization, and characterization of biomimetic CIP-loaded TAH-NPs to enhance CIP delivery. Also, it highlights the *in vitro* cytotoxicity, non-hemolytic activity, TLR4 binding affinity using *in-silico* and *in vitro* tools, *in vitro* antibacterial, antibiofilm, efflux pump inhibition, antioxidant, and anti-inflammatory activities of the prepared CIP-loaded TAH-NPs.

CHAPTER FIVE: CO-AUTHORED PUBLICATIONS

In addition to the first-authored papers presented in Chapters 2, 3, and 4, I have also contributed as a co-author in another paper published by our group during the period of my Ph.D. study. This publication shared the same broad aims of this Ph.D. project to improve the delivery and effectiveness of antibiotics through the development of an advanced novel drug delivery system. As such, it has been included in this thesis. This chapter includes a review paper published in an ISI International Journals: WIREs Nanomedicine and Nanobiotechnology (Impact Factor: 9.125).

CHAPTER SIX: CONCLUSION

This chapter presents the key findings and the overall conclusions of this study. It describes the significance and the limitations of the study and offers suggestions for further research in the field of HNs using stimuli-responsive and biomimetic approaches for antibiotic delivery.

References

1. Rothe, C., C. Schlaich, and S. Thompson, *Healthcare-associated infections in sub-Saharan Africa.* Journal of Hospital Infection, 2013. **85**(4): p. 257-267. https://doi.org/10.1016/j.jhin.2013.09.008
2. Olatunji, Y.A., A.A. Banjo, A. Jarde, R. Salaudeen, M. Ndiaye, L.B. Galega, A. Odutola, I.M. Hossain, C. Osuorah, M.S. Sahito, B.S. Muhammad, N.U. Ikumapayi, M.M. Drammeh, A. Manjang, R.A. Adegbola, B.M. Greenwood, P.C. Hill, and M.A. Grant, *Invasive bacterial disease in young infants in rural Gambia: Population-based surveillance.* Journal of Global Health, 2023. **13**: p. 04106. https://doi.org/10.7189/jogh.13.04106
3. Patel, U. and E.C. Hunt, *Recent Advances in Combating Bacterial Infections by Using Hybrid Nano-Systems.* Journal of Nanotheranostics, 2023. **4**(3): p. 429-462. https://doi.org/10.3390/jnt4030019
4. Majumder, M.A.A., S. Rahman, D. Cohall, A. Bharatha, K. Singh, M. Haque, and M. Gittens-St Hilaire, *Antimicrobial Stewardship: Fighting Antimicrobial Resistance and Protecting Global Public Health.* Infection and Drug Resistance, 2020. **13**: p. 4713-4738. https://doi.org/10.2147/IDR.S290835
5. WHO. *Global antimicrobial resistance and use surveillance system (GLASS) report: 2022*. 2022 09 December 2022 [cited 2023 30 January 2023]; Available from: https://www.who.int/news/item/09-12-2022-report-signals-increasing-resistance-to-antibiotics-in-bacterial-infections-in-humans-and-need-for-better-data.
6. WHO. *Antimicrobial resistance*. 2021 17 November 2021 [cited 2021 30 January 2023]; Available from: https://www.who.int/news-room/fact-sheets/detail/antimicrobial-resistance.
7. Aljeldah, M.M., *Antimicrobial resistance and its spread is a global threat.* Antibiotics, 2022. **11**(8): p. 1082. https://doi.org/10.3390/antibiotics11081082
8. ECDC. *35 000 annual deaths from antimicrobial resistance in the EU/EEA*. 2022 17 November 2022 [cited 2023 30 January 2023]; Available from: https://www.ecdc.europa.eu/en/news-events/eaad-2022-launch.
9. Elton, L., M.J. Thomason, J. Tembo, T.P. Velavan, S.R. Pallerla, L.B. Arruda, F. Vairo, C. Montaldo, F. Ntoumi, M.M. Abdel Hamid, N. Haider, R. Kock, G. Ippolito, A. Zumla, T.D. McHugh, and P.-I.D.N.E.T.c. the, *Antimicrobial resistance preparedness in sub-Saharan African countries.* Antimicrobial Resistance & Infection Control, 2020. **9**(1): p. 145. https://doi.org/10.1186/s13756-020-00800-y
10. Kariuki, S., K. Kering, C. Wairimu, R. Onsare, and C. Mbae, *Antimicrobial Resistance Rates and Surveillance in Sub-Saharan Africa: Where Are We Now?* Infect Drug Resist, 2022. **15**: p. 3589-3609. https://doi.org/10.2147/idr.S342753
11. Antimicrobial Resistance, C., *The burden of bacterial antimicrobial resistance in the WHO African region in 2019: a cross-country systematic analysis.* Lancet Glob Health, 2024. **12**(2): p. e201-e216. https://doi.org/10.1016/S2214-109X(23)00539-9
12. Willyard, C., *The drug-resistant bacteria that pose the greatest health threats.* Nature, 2017. **543**(7643): p. 15. https://doi.org/10.1038/nature.2017.21550
13. WHO. *Improving the prevention, diagnosis and clinical management of sepsis*. 2020 [cited 2023 15 October 2023]; Available from: https://www.who.int/activities/improving-the-prevention-diagnosis-and-clinical-management-of-sepsis.
14. Reinhart, K., R. Daniels, N. Kissoon, F.R. Machado, R.D. Schachter, and S. Finfer, *Recognizing Sepsis as a Global Health Priority - A WHO Resolution.* New England Journal of Medicine, 2017. **377**(5): p. 414-417. https://doi.org/10.1056/NEJMp1707170

15. WHO. *Global report on the epidemiology and burden of sepsis*. 2020 9 September 2020 [cited 2020 05 May 2023]; Available from: https://www.who.int/publications/i/item/9789240010789.
16. Li, H., L. Liu, D. Zhang, J. Xu, H. Dai, N. Tang, X. Su, and B. Cao, *SARS-CoV-2 and viral sepsis: observations and hypotheses.* Lancet, 2020. **395**(10235): p. 1517-1520. https://doi.org/10.1016/s0140-6736(20)30920-x
17. Yu, T., G. Jiang, R. Gao, G. Chen, Y. Ren, J. Liu, H.C. van der Mei, and H.J. Busscher, *Circumventing antimicrobial-resistance and preventing its development in novel, bacterial infection-control strategies.* Expert Opinion on Drug Delivery, 2020. **17**(8): p. 1151-1164. https://doi.org/10.1080/17425247.2020.1779697
18. Lewis, K., *The Science of Antibiotic Discovery.* Cell, 2020. **181**(1): p. 29-45. https://doi.org/10.1016/j.cell.2020.02.056
19. Penesyan, A., M. Gillings, and I.T. Paulsen, *Antibiotic Discovery: Combatting Bacterial Resistance in Cells and in Biofilm Communities.* Molecules, 2015. **20**(4): p. 5286-5298. https://doi.org/10.3390/molecules20045286
20. Makabenta, J.M.V., A. Nabawy, C.H. Li, S. Schmidt-Malan, R. Patel, and V.M. Rotello, *Nanomaterial-based therapeutics for antibiotic-resistant bacterial infections.* Nature Reviews Microbiology, 2021. **19**(1): p. 23-36. https://doi.org/10.1038/s41579-020-0420-1
21. Wright, G.D., *Q&A: Antibiotic resistance: where does it come from and what can we do about it?* BMC Biology, 2010. **8**(1): p. 123. https://doi.org/10.1186/1741-7007-8-123
22. I.K, K., N. Kochhar, A. Ghosh, S. Shrivastava, V. Singh Rawat, S. Mondal Ghorai, K. Kaur Sodhi, A. James, and M. Kumar, *Perspectives on systematic generation of antibiotic resistance with special emphasis on modern antibiotics.* Total Environment Research Themes, 2023. **8**: p. 100068. https://doi.org/10.1016/j.totert.2023.100068
23. Christaki, E., M. Marcou, and A. Tofarides, *Antimicrobial Resistance in Bacteria: Mechanisms, Evolution, and Persistence.* Journal of Molecular Evolution, 2020. **88**(1): p. 26-40. https://doi.org/10.1007/s00239-019-09914-3
24. Gupta, A., S. Mumtaz, C.H. Li, I. Hussain, and V.M. Rotello, *Combatting antibiotic-resistant bacteria using nanomaterials.* Chem. Soc. Rev., 2019. **48**(2): p. 415-427. https://doi.org/10.1039/c7cs00748e
25. English, B.K. and A.H. Gaur, *The use and abuse of antibiotics and the development of antibiotic resistance.* Advances in Experimental Medicine and Biology, 2010. **659**: p. 73-82. https://doi.org/10.1007/978-1-4419-0981-7_6
26. Serwecińska, L., *Antimicrobials and Antibiotic-Resistant Bacteria: A Risk to the Environment and to Public Health.* Water, 2020. **12**(12): p. 3313. https://doi.org/10.3390/w12123313
27. Zhang, L., D. Pornpattananangkul, C.M.J. Hu, and C.M. Huang, *Development of Nanoparticles for Antimicrobial Drug Delivery.* Current Medicinal Chemistry, 2010. **17**(6): p. 585-594. https://doi.org/10.2174/092986710790416290
28. Brooks, B.D. and A.E. Brooks, *Therapeutic strategies to combat antibiotic resistance.* Advanced Drug Delivery Reviews, 2014. **78**: p. 14-27. https://doi.org/10.1016/j.addr.2014.10.027
29. Lazzaro, A., G. De Girolamo, V. Filippi, G.P. Innocenti, L. Santinelli, G. Ceccarelli, E.M. Trecarichi, C. Torti, C.M. Mastroianni, G. d'Ettorre, and A. Russo, *The Interplay between Host Defense, Infection, and Clinical Status in Septic Patients: A Narrative Review.* International Journal of Molecular Sciences, 2022. **23**(2): p. 803. https://doi.org/10.3390/ijms23020803
30. Cohen, J., *The immunopathogenesis of sepsis.* Nature, 2002. **420**(6917): p. 885-891. https://doi.org/10.1038/nature01326

31. Fujii, M., T. Karumai, R. Yamamoto, E. Kobayashi, K. Ogawa, M. Tounai, J. Lipman, and Y. Hayashi, *Pharmacokinetic and pharmacodynamic considerations in antimicrobial therapy for sepsis.* Expert Opinion on Drug Metabolism & Toxicology, 2020. **16**(5): p. 415-430. https://doi.org/10.1080/17425255.2020.1750597
32. Sanz Codina, M. and M. Zeitlinger, *Biomarkers Predicting Tissue Pharmacokinetics of Antimicrobials in Sepsis: A Review.* Clinical Pharmacokinetics, 2022. **61**(5): p. 593-617. https://doi.org/10.1007/s40262-021-01102-1
33. Stewart, S., C. Robertson, S. Kennedy, K. Kavanagh, L. Haahr, S. Manoukian, H. Mason, S. Dancer, B. Cook, and J. Reilly, *Personalized infection prevention and control: identifying patients at risk of healthcare-associated infection.* Journal of Hospital Infection, 2021. **114**: p. 32-42. https://doi.org/10.1016/j.jhin.2021.03.032
34. Ventola, C.L., *The antibiotic resistance crisis: part 1: causes and threats.* Pharmacy and therapeutics, 2015. **40**(4): p. 277-83.
35. Teixeira, M.C., E. Sanchez-Lopez, M. Espina, A.C. Calpena, A.M. Silva, F.J. Veiga, M.L. Garcia, and E.B. Souto, *Chapter 9 - Advances in antibiotic nanotherapy: Overcoming antimicrobial resistance*, in *Emerging Nanotechnologies in Immunology*, R. Shegokar and E.B. Souto, Editors. 2018, Elsevier: Boston. p. 233-259 https://doi.org/10.1016/B978-0-323-40016-9.00009-9
36. Huh, A.J. and Y.J. Kwon, *"Nanoantibiotics": A new paradigm for treating infectious diseases using nanomaterials in the antibiotics resistant era.* J Control Release, 2011. **156**(2): p. 128-145. https://doi.org/10.1016/j.jconrel.2011.07.002
37. Aminu, N., I. Bello, N.M. Umar, N. Tanko, A. Aminu, and M.M. Audu, *The influence of nanoparticulate drug delivery systems in drug therapy.* Journal of Drug Delivery Science and Technology, 2020. **60**: p. 101961. https://doi.org/10.1016/j.jddst.2020.101961
38. Yeh, Y.-C., T.-H. Huang, S.-C. Yang, C.-C. Chen, and J.-Y. Fang, *Nano-Based Drug Delivery or Targeting to Eradicate Bacteria for Infection Mitigation: A Review of Recent Advances.* Frontiers in Chemistry, 2020. **8**: p. 1-22. https://doi.org/10.3389/fchem.2020.00286
39. Colino, C.I., J.M. Lanao, and C. Gutierrez-Millan, *Recent advances in functionalized nanomaterials for the diagnosis and treatment of bacterial infections.* Mater. Sci. Eng. C, 2021. **121**: p. 111843. https://doi.org/10.1016/j.msec.2020.111843
40. Kalhapure, R.S., N. Suleman, C. Mocktar, N. Seedat, and T. Govender, *Nanoengineered Drug Delivery Systems for Enhancing Antibiotic Therapy.* J. Pharm. Sci., 2015. **104**(3): p. 872-905. https://doi.org/10.1002/jps.24298
41. Aflakian, F., F. Mirzavi, H.T. Aiyelabegan, A. Soleimani, J. Gholizadeh Navashenaq, I. Karimi-Sani, A. Rafati Zomorodi, and R. Vakili-Ghartavol, *Nanoparticles-based therapeutics for the management of bacterial infections: A special emphasis on FDA approved products and clinical trials.* European Journal of Pharmaceutical Sciences, 2023. **188**: p. 106515. https://doi.org/10.1016/j.ejps.2023.106515
42. Nazli, A., D.L. He, D. Liao, M.Z.I. Khan, C. Huang, and Y. He, *Strategies and progresses for enhancing targeted antibiotic delivery.* Advanced Drug Delivery Reviews, 2022. **189**: p. 114502. https://doi.org/10.1016/j.addr.2022.114502
43. Al-Wrafy, F.A., A.A. Al-Gheethi, S.K. Ponnusamy, E.A. Noman, and S.A. Fattah, *Nanoparticles approach to eradicate bacterial biofilm-related infections: A critical review.* Chemosphere, 2022. **288**: p. 132603. https://doi.org/10.1016/j.chemosphere.2021.132603

44. Yang, X., W. Ye, Y. Qi, Y. Ying, and Z. Xia, *Overcoming Multidrug Resistance in Bacteria Through Antibiotics Delivery in Surface-Engineered Nano-Cargos: Recent Developments for Future Nano-Antibiotics.* Front. bioeng. biotechnol., 2021. **9**. https://doi.org/10.3389/fbioe.2021.696514
45. Cano, A., M. Ettcheto, M. Espina, A. López-Machado, Y. Cajal, F. Rabanal, E. Sánchez-López, A. Camins, M.L. García, and E.B. Souto, *State-of-the-art polymeric nanoparticles as promising therapeutic tools against human bacterial infections.* Journal of Nanobiotechnology, 2020. **18**(1): p. 156. https://doi.org/10.1186/s12951-020-00714-2
46. Günday, C., S. Anand, H.B. Gencer, S. Munafò, L. Moroni, A. Fusco, G. Donnarumma, C. Ricci, P.C. Hatir, N.G. Türeli, A.E. Türeli, C. Mota, and S. Danti, *Ciprofloxacin-loaded polymeric nanoparticles incorporated electrospun fibers for drug delivery in tissue engineering applications.* Drug Delivery and Translational Research, 2020. **10**(3): p. 706-720. https://doi.org/10.1007/s13346-020-00736-1
47. Guo, R., K. Li, J. Qin, S. Niu, and W. Hong, *Development of polycationic micelles as an efficient delivery system of antibiotics for overcoming the biological barriers to reverse multidrug resistance in Escherichia coli.* Nanoscale, 2020. **12**(20): p. 11251-11266. https://doi.org/10.1039/d0nr01366h
48. Bosnjakovic, A., M.K. Mishra, W. Ren, Y.E. Kurtoglu, T. Shi, D. Fan, and R.M. Kannan, *Poly(amidoamine) dendrimer-erythromycin conjugates for drug delivery to macrophages involved in periprosthetic inflammation.* Nanomedicine: Nanotechnology, Biology and Medicine, 2011. **7**(3): p. 284-294. https://doi.org/10.1016/j.nano.2010.10.008
49. Gottesmann, M., F.M. Goycoolea, T. Steinbacher, T. Menogni, and A. Hensel, *Smart drug delivery against Helicobacter pylori: pectin-coated, mucoadhesive liposomes with antiadhesive activity and antibiotic cargo.* Applied Microbiology and Biotechnology, 2020. **104**(13): p. 5943-5957. https://doi.org/10.1007/s00253-020-10647-3
50. Ho, H.N., H.H. Le, T.G. Le, T.H.A. Duong, V.Q.T. Ngo, C.T. Dang, V.M. Nguyen, T.H. Tran, and C.N. Nguyen, *Formulation and characterization of hydroxyethyl cellulose-based gel containing metronidazole-loaded solid lipid nanoparticles for buccal mucosal drug delivery.* International Journal of Biological Macromolecules, 2022. **194**: p. 1010-1018. https://doi.org/10.1016/j.ijbiomac.2021.11.161
51. Abioye, A., A. Sanyaolu, P. Dudzinska, A.A. Adepoju-Bello, and H.A.B. Coker, *Chitosan-induced Synergy for Extended Antimicrobial Potency and Enhanced In Vitro Drug Release of Free Base Ciprofloxacin Nanoplexes.* Pharmaceutical Nanotechnology, 2020. **8**(1): p. 33-53. https://doi.org/10.2174/2211738507666191021102256
52. Patil, J.S., S.B. Dhadde, and B.N. Chandakavathe, *Chapter 7 - Nanostructure Drug Delivery System Is an Option to Solve Antimicrobial Drug Resistance: Perspective Review*, in *Characterization and Biology of Nanomaterials for Drug Delivery*, S.S. Mohapatra, S. Ranjan, N. Dasgupta, R.K. Mishra, and S. Thomas, Editors. 2019, Elsevier. p. 165-197 https://doi.org/https://doi.org/10.1016/B978-0-12-814031-4.00007-6
53. Seaberg, J., H. Montazerian, M.N. Hossen, R. Bhattacharya, A. Khademhosseini, and P. Mukherjee, *Hybrid Nanosystems for Biomedical Applications.* ACS Nano, 2021. **15**(2): p. 2099-2142. https://doi.org/10.1021/acsnano.0c09382
54. Asadullah, M., T. Nayab, R. Mubashar, R. Ahmed, M. Muhammad Ahmad, K. Muhammad Imran, and K. Prince Muhammad, *Hybrid Nano-carriers for Potential Drug Delivery*, in *Advanced Technology for Delivering Therapeutics*, M. Sabyasachi and S. Kalyan Kumar, Editors. 2017, IntechOpen: Rijeka. p. Ch. 4 https://doi.org/10.5772/66466

55. Dave, R., R. Patel, and M. Patel, *Hybrid lipid-polymer nanoplatform: A systematic review for targeted colorectal cancer therapy.* European Polymer Journal, 2023. **186**: p. 111877. https://doi.org/10.1016/j.eurpolymj.2023.111877
56. Park, W., H. Shin, B. Choi, W.-K. Rhim, K. Na, and D. Keun Han, *Advanced hybrid nanomaterials for biomedical applications.* Progress in Materials Science, 2020. **114**: p. 100686. https://doi.org/10.1016/j.pmatsci.2020.100686
57. Chen, H., D. Liu, and Z. Guo, *Endogenous Stimuli-responsive Nanocarriers for Drug Delivery.* Chemistry Letters, 2016. **45**(3): p. 242-249. https://doi.org/10.1246/cl.151176
58. Huang, Y., L. Zou, J. Wang, Q. Jin, and J. Ji, *Stimuli-responsive nanoplatforms for antibacterial applications.* WIREs Nanomedicine and Nanobiotechnology, 2022. **14**(3): p. e1775. https://doi.org/10.1002/wnan.1775
59. Bjarnsholt, T., M. Whiteley, K.P. Rumbaugh, P.S. Stewart, P.Ø. Jensen, and N. Frimodt-Møller, *The importance of understanding the infectious microenvironment.* The Lancet. Infectious diseases, 2022. **22**(3): p. e88-e92. https://doi.org/10.1016/s1473-3099(21)00122-5
60. Zhang, C.Y., J. Gao, and Z. Wang, *Bioresponsive Nanoparticles Targeted to Infectious Microenvironments for Sepsis Management.* Advanced Materials, 2018. **30**(43): p. 1803618. https://doi.org/10.1002/adma.201803618
61. Bami, M.S., M.A. Raeisi Estabragh, P. Khazaeli, M. Ohadi, and G. Dehghannoudeh, *pH-responsive drug delivery systems as intelligent carriers for targeted drug therapy: Brief history, properties, synthesis, mechanism and application.* Journal of Drug Delivery Science and Technology, 2022. **70**: p. 102987. https://doi.org/10.1016/j.jddst.2021.102987
62. Maji, R., C.A. Omolo, N. Agrawal, K. Maduray, D. Hassan, C. Mokhtar, I. Mackhraj, and T. Govender, *pH-Responsive Lipid–Dendrimer Hybrid Nanoparticles: An Approach To Target and Eliminate Intracellular Pathogens.* Molecular Pharmaceutics, 2019. **16**(11): p. 4594-4609. https://doi.org/10.1021/acs.molpharmaceut.9b00713
63. Zhang, Y., P. Li, R. Su, F. Wen, Z. Jia, Y. Lv, J. Cai, and W. Su, *Curcumin-loaded multifunctional chitosan gold nanoparticles: An enhanced PDT/PTT dual-modal phototherapeutic and pH-responsive antimicrobial agent.* Photodiagnosis and Photodynamic Therapy, 2022. **39**: p. 103011. https://doi.org/10.1016/j.pdpdt.2022.103011
64. Sabu, C., C. Rejo, S. Kotta, and K. Pramod, *Bioinspired and biomimetic systems for advanced drug and gene delivery.* Journal of Controlled Release, 2018. **287**: p. 142-155. https://doi.org/10.1016/j.jconrel.2018.08.033
65. Beh, C.Y., R.P. Prajnamitra, L.L. Chen, and P.C. Hsieh, *Advances in Biomimetic Nanoparticles for Targeted Cancer Therapy and Diagnosis.* Molecules, 2021. **26**(16). https://doi.org/10.3390/molecules26165052
66. Yoo, J.-W., D.J. Irvine, D.E. Discher, and S. Mitragotri, *Bio-inspired, bioengineered and biomimetic drug delivery carriers.* Nature Reviews Drug Discovery, 2011. **10**(7): p. 521-535. https://doi.org/10.1038/nrd3499
67. Chen, L., W. Hong, W. Ren, T. Xu, Z. Qian, and Z. He, *Recent progress in targeted delivery vectors based on biomimetic nanoparticles.* Signal Transduction and Targeted Therapy, 2021. **6**(1): p. 225. https://doi.org/10.1038/s41392-021-00631-2
68. Albiger, B., S. Dahlberg, B. Henriques-Normark, and S. Normark, *Role of the innate immune system in host defence against bacterial infections: focus on the Toll-like receptors.* J. Intern. Med., 2007. **261**(6): p. 511-528. https://doi.org/10.1111/j.1365-2796.2007.01821.x

69. Nguyen, M.T. and F. Götz, *Lipoproteins of Gram-Positive Bacteria: Key Players in the Immune Response and Virulence.* Microbiol. Mol. Biol., 2016. **80**(3): p. 891-903. https://doi.org/doi:10.1128/mmbr.00028-16
70. McBride, M.A., A.M. Owen, C.L. Stothers, A. Hernandez, L. Luan, K.R. Burelbach, T.K. Patil, J.K. Bohannon, E.R. Sherwood, and N.K. Patil, *The Metabolic Basis of Immune Dysfunction Following Sepsis and Trauma.* Frontiers in Immunology, 2020. **11**. https://doi.org/10.3389/fimmu.2020.01043
71. Zhang, Y., Y. Long, J. Wan, S. Liu, A. Shi, D. Li, S. Yu, X. Li, J. Wen, J. Deng, Y. Ma, and N. Li, *Macrophage membrane biomimetic drug delivery system: for inflammation targeted therapy.* J Drug Target, 2023. **31**(3): p. 229-242. https://doi.org/10.1080/1061186X.2022.2071426
72. Deng, Y., M. Ren, P. He, F. Liu, X. Wang, C. Zhou, Y. Li, and S. Yang, *Genetically engineered cell membrane-coated nanoparticles for antibacterial and immunoregulatory dual-function treatment of ligature-induced periodontitis.* Front. bioeng. biotechnol., 2023. **11**. https://doi.org/10.3389/fbioe.2023.1113367
73. Li, Y., H. Zhang, C. Chen, K. Qiao, Z. Li, J. Han, X. Han, K. Li, K. Lai, N. Liu, A. Li, N. Xiao, Y. Zhang, X. Zhao, W. Gao, Y. Zhang, H. Liu, and T. Sun, *Biomimetic Immunosuppressive Exosomes that Inhibit Cytokine Storms Contribute to the Alleviation of Sepsis.* Adv Mater, 2022. **34**(19): p. 2108476. https://doi.org/10.1002/adma.202108476
74. Gao, W., Y. Xiong, Q. Li, and H. Yang, *Inhibition of Toll-Like Receptor Signaling as a Promising Therapy for Inflammatory Diseases: A Journey from Molecular to Nano Therapeutics.* Front. physiol, 2017. **8**. https://doi.org/10.3389/fphys.2017.00508
75. Patra, M.C. and S. Choi, *Recent progress in the development of Toll-like receptor (TLR) antagonists.* Expert Opin. Ther. Pat., 2016. **26**(6): p. 719-730. https://doi.org/10.1080/13543776.2016.1185415
76. Connolly, D.J. and L.A.J. O'Neill, *New developments in Toll-like receptor targeted therapeutics.* Curr Opin Pharmacol., 2012. **12**(4): p. 510-518. https://doi.org/10.1016/j.coph.2012.06.002
77. Bassegoda, A., K. Ivanova, E. Ramon, and T. Tzanov, *Strategies to prevent the occurrence of resistance against antibiotics by using advanced materials.* Appl. Microbiol. Biotechnol., 2018. **102**(5): p. 2075-2089. https://doi.org/10.1007/s00253-018-8776-0
78. Spengler, G., A. Kincses, M. Gajdács, and L. Amaral, *New Roads Leading to Old Destinations: Efflux Pumps as Targets to Reverse Multidrug Resistance in Bacteria.* Molecules, 2017. **22**(3): p. 468. https://doi.org/10.3390/molecules22030468
79. Eleraky, N.E., A. Allam, S.B. Hassan, and M.M. Omar, *Nanomedicine Fight against Antibacterial Resistance: An Overview of the Recent Pharmaceutical Innovations.* Pharmaceutics, 2020. **12**(2): p. 142. https://doi.org/10.3390/pharmaceutics12020142

CHAPTER 2. REVIEW PAPER

2.1 General Introduction

This chapter focuses mainly on the recent developments, technological advancements, and contributions of the various hybrid nanosystems created for antibacterial delivery. The review first provides a theoretical overview on different hybrid nanosystems, including lipid-polymer hybrid NPs (LPHNPs); organic-inorganic hybrid NPs; metal-organic frameworks (MOFs); cell membrane-coated hybrid NPs (CMCH-NPs); and hybrid NPs-hydrogels, and their design approaches. The significance and limitations of using these novel NDDS in the treatment of bacterial infections are then critically discussed and evaluated in detail. Finally, this review identifies the future strategies required to optimize the potential of hybrid nanosystems for treating bacterial infections. This chapter is a first-authored review article published in an ISI International Journal: Journal of Controlled Release (Impact Factor = 11.467).

2.2 Author contributions

Eman Elhassan: Conceptualization (equal); data curation (equal); formal analysis (equal); investigation (equal); methodology (equal); validation (equal); visualization (equal); writing-original draft (equal); writing-review and editing (equal). **Nikita Devnarain**: Data curation (equal); formal analysis (equal); methodology (equal); writing-original draft (equal); project administration (equal); writing-review and editing (equal). **Mahir Mohammed**: Data curation (equal); methodology (equal); writing-original draft (equal); writing-review and editing (equal). **Thirumala Govender**: Conceptualization (equal); funding acquisition (equal); supervision (equal); validation (equal); writing-review and editing (equal). **Calvin A. Omolo**: Conceptualization (equal); supervision (equal); project administration (equal); validation (equal); writing-review and editing (equal)

2.3 Graphical abstract

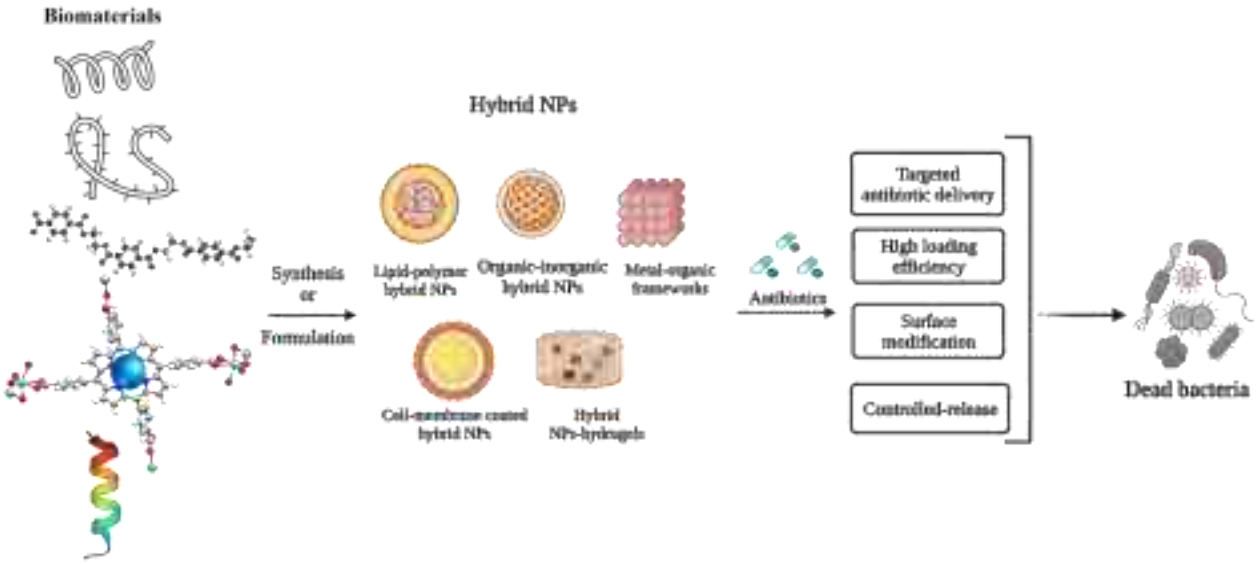

2.4 Published Manuscript

Abstract

Hybrid nanoparticles (NPs) are emerging as superior alternatives to conventional nanocarriers for enhancing the delivery of antibiotics and improving their targeting at the infection site, resulting in the eradication of bacterial infections and overcoming antimicrobial resistance. They can specifically control the release of antibiotics when reaching the targeted site of infection, thus enhancing and prolonging their antimicrobial efficacy. In this review, we provide a comprehensive and an up-to-date overview of the recent advances and contributions of lipid-polymer hybrid NPs; organic-inorganic hybrid NPs; metal-organic frameworks; cell membrane-coated hybrid NPs; hybrid NP-hydrogels; and various others, that have been reported in the literature for antibacterial delivery, with emphasis on their design approaches; the nanomaterials constructed; the mechanisms of drug release; and the enhanced antibacterial efficacy of the reported hybrid nanocarriers. This review also highlights future strategies that can be used to improve the potential of hybrid nanosystems to treat bacterial infections and overcome antibiotic resistance.

Keywords

Hybrid nanosystems, antibacterial, drug delivery, bacterial infections, antibiotic resistance, nanocarriers.

1. Introduction

Bacterial infections and their induced diseases, like sepsis, are major causes of mortality worldwide. They are considered to cause significant public health challenges, especially in low-income countries [80]. In 2017, there were 48.9 million cases of sepsis globally, with nearly 11 million deaths related to sepsis [81]. Moreover, the emergence and prevalence of multidrug-resistant bacteria (MDR) have led to antimicrobial resistance (AMR), which is an increasing threat to human health. [82]. A recent report published by the Centers for Disease Control and Prevention (CDC) stated that antibiotic-resistant bacteria cause more than 2.8 million illnesses each year, with 35,000 deaths, in the United States [83]. Furthermore, the complications resulting from secondary bacterial infections caused by antibiotic-resistant bacteria have increased the rates of morbidity and mortality in patients with coronavirus disease (COVID-19) around the world [84]. As a result, eradicating certain bacterial infections and their associated problems remains a challenge, owing to the complex pathogenic mechanisms involved in the destruction of the host's immune system, as well as the rise in the cost of healthcare services [85]. Hence, more preventative efforts and innovative strategies are urgently required to control and eliminate bacterial infections.

Antibiotics are often used to treat and control bacterial infections [86]. However, there is an increase in resistance across all classes of antibiotics. It is reported that conventional antibiotic dosage forms are one of the major contributing factors to the development of antibiotic resistance, due to their lack of selectivity to attack only specific pathogenic bacteria; inability to enhance solubility; instability; low bioavailability; difficulty in reaching the site of action; high frequency of administration due to fluctuations in plasma drug concentrations resulting in severe side effects; toxicity; and thus, poor patient compliance [87, 88]. Moreover, the problem is compounded by pharmaceutical companies abandoning the production, research, and development of new antibiotics [87, 89]. As a result of these complications, the development of novel drug delivery systems to improve the delivery of current and new antibiotics is recognized as a major priority in research [90].

In the last few decades, pharmaceutical nanotechnology has opened a new era for research in the design and characterization of drug delivery systems [91, 92]. These systems have been reported to enhance the delivery of several antibacterial agents through overcoming the developed bacterial resistance mechanisms that involve drug decomposition by β-lactamase [93]; efflux pumps [94]; biofilm formation [95] and thickening of the bacterial cell wall [92, 96]. Thus, the continued development of the nanomedicine field promises to be critical in combating antimicrobial resistance.

Among the nano drug delivery systems showing promise in antibiotic delivery are hybrid nanosystems, which are formulated from a plethora of inorganic, organic, or a combination of both, materials on a scale of less than one micrometer [97]. These nanosystems are solving challenges in drug delivery and theranostic as they can be utilized to formulate nanosystems with the positive attributes of the blend of biomaterials employed to formulate them, while simultaneously overcoming their shortcomings [98]. Moreover, hybrid nanosystems have been shown to overcome the limitations of conventional, or non-hybrid, nanocarriers such as low stability; premature release of the encapsulated drug before reaching the target tissue; poor biocompatibility; instability during storage; and unacceptable toxicity [99-101]. Intensive research efforts have focused on several hybrid nanosystems, such as lipid-based hybrid systems, polymeric hybrid systems, organic/inorganic hybrid systems, and others, with proposed applications in various biomedical fields such as cancer treatment and drug delivery [102], food supplements [103] and vaccine therapy [104].

Recently, hybrid nanocarriers have been gaining prominence for antibacterial delivery due to several advantages, including excellent biocompatibility and biodegradability; stable structural integrity; chemical diversity that can be employed for targeting [85]; high dual and multiple loading capacity[105];

and flexibility for functionalization to suit specific applications [106]. Besides the aforementioned advantages, the hybridization of organic and inorganic biomaterials that possess intrinsic antibacterial activity, such as metal ions (e.g., silver and gold NPs), antimicrobial peptides and lipids, results in a powerful synergistic antibacterial effect [105].

Based on the advantages of hybrid nanosystems, reviews in the literature have broadly covered the development and applications of different hybrid nanocarriers for cancer therapy[107, 108]; oral drug delivery [109, 110]; skin repair and wound healing [111]; gene delivery [112]; and molecular targeting/imaging [113]. However, despite the current bacterial disease and resistance crises, no review in the literature has focused on the various hybrid nanocarriers that have been reported for antibacterial delivery.

Herein, we present an up-to-date overview of the recent advances, technological progress, and contributions of the different hybrid nanosystems that have been developed for antibacterial delivery. Initially, the review provides a theoretical background about different hybrid nanosystems, including lipid-polymer hybrid NPs (LPHNPs); organic-inorganic hybrid NPs; metal-organic frameworks (MOFs); cell membrane-coated hybrid NPs (CMCH-NPs); and hybrid NPs-hydrogels, and their design approaches. Thereafter, the significance and limitations of applying these novel nano-delivery systems in the treatment of bacterial infections are critically discussed and evaluated in detail. Finally, this review identifies the future strategies required to maximize the potential of hybrid nanosystems in the treatment of bacterial infections.

2. Engineering hybrid nanosystems for antibacterial delivery

The design of hybrid nanosystems strongly mimics natural architectural structures where a complex hierarchical assembly is achieved by employing different complementing materials to produce functional systems [114]. Advances in nanotechnology, synthetic techniques, supramolecular chemistry, and an understanding of the forces involved in self-assembly have led to the development of higher order functional hybrid nanostructures for drug delivery. The manufacturing of hybrid nanosystems involves a myriad of interactions between the building blocks of hybrid nanocarriers, including covalent, non-covalent, or a combination of both, types of interactions. Such nano assemblies use a variety of intermolecular associations, such as electrostatic, hydrophobic, and hydrogen bonding, to create diverse structural designs (for example, LPHNPs; lipid-dendrimer hybrid NPs (LDHNPs); mixed micelles; metal-organic frameworks (MOFs); cell membrane-coated hybrid NPs (CMCH-NPs); hybrid nanogels) with

infinite applications, including drug delivery [115]. Individually, organic and inorganic NPs, such as liposomes; polymeric NPs; metal/metal oxide NPs and mesoporous silica NPs (MSNs) have their own merits and drawbacks. Therefore, combining them in a single hybrid drug delivery platform provides a multifunctional carrier with enhanced biological properties that can improve therapeutic efficacy as well as reduce drug resistance. The following section presents a theoretical background of different hybrid nanosystems, including LPHNPs; organic-inorganic hybrid NPs; MOFs; CMCH-NPs' and hybrid NPs-hydrogels, with a focus on their design principles and synthetic strategies.

2.1 Design of LPHNPs

To combine the unique advantages, and simultaneously address the limitations of polymeric NPs and lipid-based nanovesicles, LPHNPs have been developed [100, 116]. They have been widely investigated in the preclinical phase due to their attractive properties for drug delivery [116]. These unique drug delivery systems can be classified according to their structural design into monolithic matrix lipid polymeric nanoparticles, in which a lipid phase contains a homogeneous polymeric drug complex or a polymeric matrix covered with a lipid phase; core-shell LPHNPs characterized by a polymeric core surrounded by a lipid shell or the other way around; and liposomes decorated with polymeric materials (**Figure 1**) [117]. The lipid layer behaves as a molecular barrier to prevent the loss of the entrapped drug during fabrication and to slow down the degradation rate of the hybrid NPs in any physiological environment, enabling sustained release kinetics of the contained drug [85, 99]. The polymeric NPs and the lipid layer are linked together through different binding forces, such as van der Waals (vdW) forces; hydrophobic interactions; electrostatic interactions; and various noncovalent bonds [118]. A wide variety of therapeutic agents (drugs; peptides and proteins; genes; vaccines; antibiotics; and others) can be either encapsulated, adsorbed, or covalently bonded to the polymeric NPs, the lipid layer, or both, depending on the hydrophobicity of the drug and the construction of the hybrid system [118]. A combination of the biomimetic behavior of the lipid materials and the mechanical advantages linked to the polymeric NPs can give an advanced delivery platform with high encapsulation efficiency; well-defined release kinetics; well-tolerated serum stability; and well-triggered tissue, cellular, and molecular targeting [117, 119].

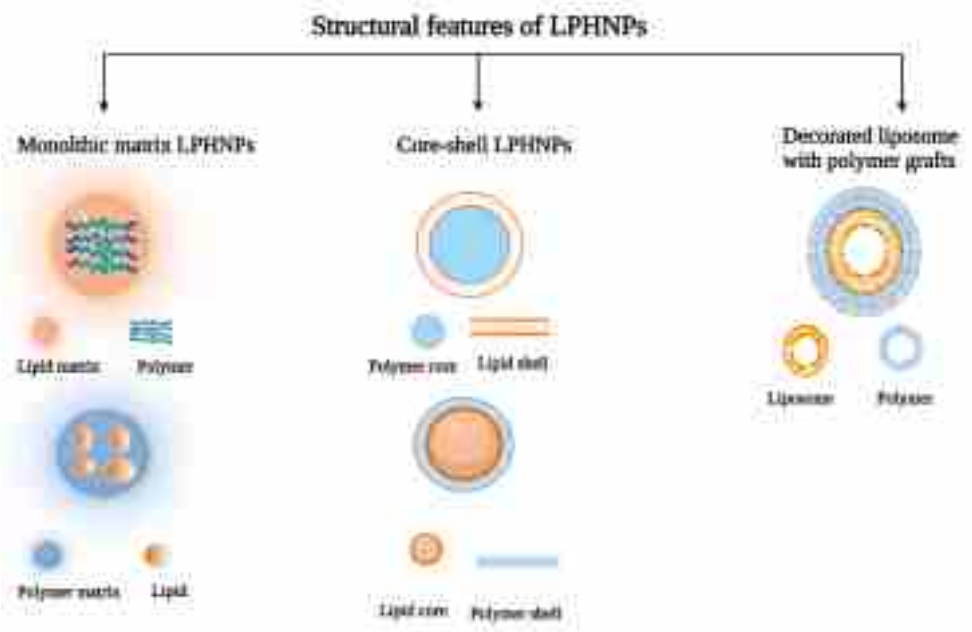

Figure 1: Scheme illustrating the structural designs of LPHNPs.

The primary concern surrounding LPHNPs has been their method of preparation. The various methods of preparing LPHNPs reported in the literature thus far are summarized in **Table 1**. Generally, on a laboratory scale, two broad methods have been applied to manufacture LPHNPs, namely, the two-step preparation and the single-step preparation methods [120]. The conventional two-step preparation method has mainly been employed in the early phases of LPHNP development. A preformulated polymeric NP is added into either a dried lipid film or a preformulated lipid vesicle via vortexing or sonication. Extrusion or homogenization steps are also required after preparation to obtain homogeneous mono-sized hybrid NPs [118, 120]. Recently, non-conventional techniques have been implemented in addition to conventional techniques, including spray drying [121] and soft lithography particle moulding [122]. However, the alternative single-step preparation method is preferred because it is easier, highly scalable, more efficient, and cost-effective [99, 118]. This method involves the simple mixing of a lipid solution and polymeric NPs by nanoprecipitation [123], emulsification solvent evaporation (ESE) [106], or chemical conjugation method [124]; and the polymeric NPs are precipitated with simultaneous self-assembly of the lipid layer around them, or vice versa. Nowadays, microfluidic-based rapid-mixing protocols, and a new advanced herringbone-patterned multi-inlet vortex mixer (MIVM), have been introduced to generate small-sized LPHNPs with uniform size distribution and a shorter mixing time in a scalable, reproducible manner [125]. In addition, other factors such as the aqueous solubility and

lipophilicity of the drug; the type of lipid used; and the lipid/polymer (L/P) ratio have a critical impact on the particle size, drug loading (DL), entrapment efficiency (EE%) and stability of the formulated hybrid system. These parameters have been investigated by Cheow *et al*. (2011) using fluoroquinolone antibiotics as a drug model. They noticed a reduction in particle size with an increase in the L/P ratio. Also, they proved that ionic interactions between the drug and the lipid are crucial in the formulation of LPHNPs by the ESE method [126].

Table 1: Different methods of preparation of LPHNPs, including the components of the hybrid nanosystems with their encapsulated drugs, if any.

Preparation method	Lipid	Polymer	Encapsulated drug	Ref.
Conventional two-step method	POPS	Allylamine plasma polymer	AgNPs	[127]
Non-conventional two-step method (spray drying)	Lecithin	PLGA	Levofloxacin	[121]
Non-conventional two-step method (soft lithography)	DOTAP/DOPE	PLGA	siRNA	[122]
One-step method (nanoprecipitation)	Lecithin	PLGA	N-Acetyl Cysteine	[123]
One-step method (ESE)	Soy lecithin Stearyl amine	PLA	Norfloxacin	[106]

POPs, 1-palmitoyl-2-oleoyl-sn-glycero-3-phospho-L-serine; AgNPs, silver NPs; PLGA, Poly D, L-lactic-*co*-glycolic acid; DOTAP, 1,2-Dioleoyl-3-trimethylammonium-propane; DOPE, 1,2-Dioleoyl-sn-glycero-3-phosphoethanolamine; siRNA, small interfering ribonucleic acid; PLA, polylactic acid; ESE, emulsification solvent evaporation.

2.2 Design of organic-inorganic hybrid NPs

Inorganic NPs such as metal/metal oxide NPs, magnetic NPs and mesoporous silica NPs (MSNs) can be hybridized by surface engineering with a wide variety of organic moieties through different synthesis strategies to provide hybrid nanosystems for various biomedical applications, including diagnosis, therapeutics, imaging and drug delivery [128, 129]. The integration of organic materials and inorganic NPs retains the components and beneficial features of both, resulting in a hybrid system with high colloidal stability; high biocompatibility; biodegradability; and low toxicity [129, 130]. Also, the organic shell of the hybrid NP can be further functionalized with stimuli-responsive materials [129] or targeting moieties such as antibodies, peptides, and aptamers [128] for triggering drug release.

Organic-inorganic hybrid NPs can be classified according to the nature of the interaction between the two components into Class I and Class II hybrid NPs [129, 131]. In Class I, the binding can be achieved by physical interactions through vdW forces, electrostatic interactions, or hydrogen bonds. In contrast, Class II includes different covalent and noncovalent chemical bonds [129]. The organic moieties play an essential role in the stabilization of the hybrid system [120]. They can be divided into chemical organic materials that include polymers (most common), or biological materials such as lipids, proteins, and nucleic acids [132].

There are two main strategies for the synthesis of organic-inorganic hybrid NPs. The first strategy is called the reversible addition-fragmentation chain transfer (RAFT) technique [129], which is based on introducing an anchoring group onto the surface of a pre-formulated inorganic NP. Their role is to enable the organic material to conjugate strongly with the inorganic core; and the organic material can be in the form of a monomer/initiator (grafting-from approach) or a polymer chain (grafting-to approach) [120]. Alternatively, direct synthesis or '*in situ'* synthesis of organic-inorganic hybrid NPs can be applied [131]. In this method, the inorganic NPs are prepared in the presence of the organic material, which acts as a stabilizer. This technique can yield hybrid NPs of high quality, with narrow size dispersity and long-term colloidal stability in biological media [129, 131]. **Figure 2** represents a schematic illustration of the strategies available for the synthesis of organic-inorganic hybrid NPs.

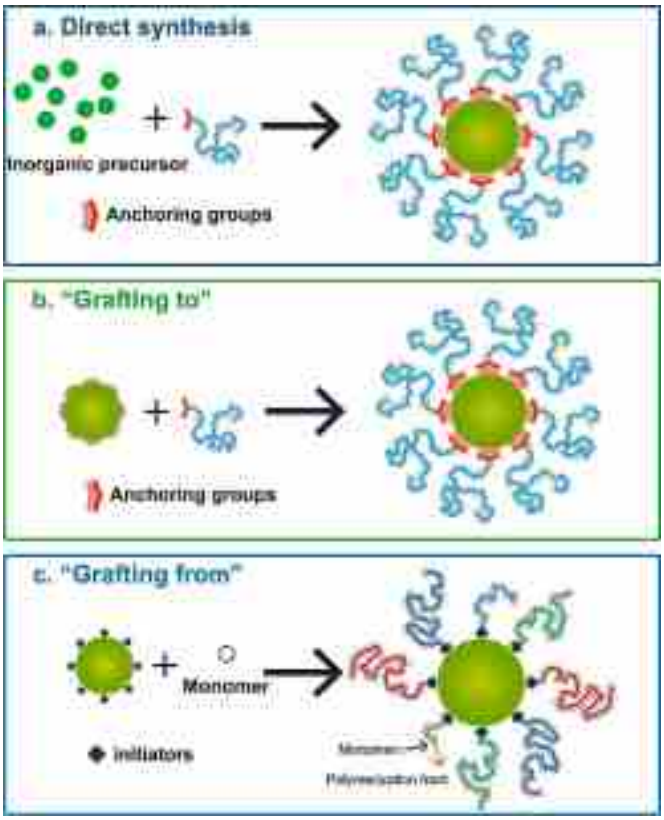

Figure 2: Scheme representing organic-inorganic hybrid NPs prepared by (a) direct synthesis; (b) grafting-to; and (c) grafting-from approaches of the RAFT technique (adapted with permission from [129]).

2.3 Design of metal-organic frameworks (MOFs)

Metal-organic frameworks are novel porous hybrid materials prepared through the co-ordination of metals/metal oxides (ions or clusters) with organic polydentate linkers, forming a three-dimensional structure (**Figure 3**) [133, 134]. Researchers became interested in these hybrid materials in the late 1990s when William and co-workers (1999) formulated a MOF called HKUST-1 by co-ordinating copper-based clusters and benzene tricarboxylate linkers to create a three-dimensional system of channels with a pore size of 1 nm and an accessible porosity of about 40 % [135]. Also, in 1999, a crystalline MOF, known as MOF-5, made from zinc-based groups and benzene carboxylate linkers, was reported by Yaghi *et al.* (1999). They prepared a three-dimensional framework structure with a higher apparent surface area and pore volume than most porous crystalline zeolites and related materials [136].

The main characteristics of MOFs are their high porosity; large internal surface area; biodegradability; high loading capacity; the possibility of functionality through surface modification; and the flexible

architecture of the structure by selecting appropriate metal ions and linkers [105, 137, 138]. The possible functional groups representing the organic linkers are carboxylates; phosphonates; imidazolates; sulphonates; and amines, while the metal ions mainly include transition elements [105, 133]. The building blocks of MOFs can be held together through different binding forces, including hydrogen bonds, electrostatic interactions, and π-π stacking [105].

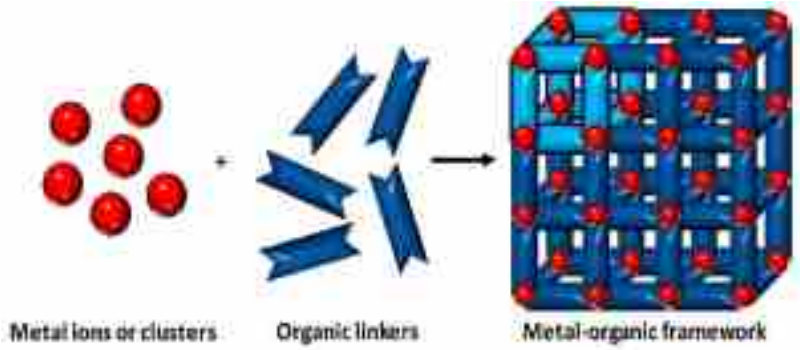

Figure 3: Scheme illustrating the preparation of MOFs through the co-ordination of metal ions or clusters with organic linkers (adapted with permission from [139]).

In the literature, different approaches have been reported for the synthesis of MOFs, ranging from conventional solvothermal/hydrothermal reactions [135, 140] to more convenient procedures, including microfluidic synthesis [141]; microwave synthesis [142]; and mechanochemical [143] and sonochemical techniques [142]. These methods have been described in detail by Stock and Biswas (2012) [144]. A wide range of hydrophilic, hydrophobic, or amphiphilic drugs, can be quickly loaded into MOFs through different loading strategies such as *in situ* (one-step) encapsulation strategy during the synthesis phase of the hybrid framework or via *ex situ* (post-synthesis) encapsulation strategy [133, 134]. The drug can be tethered through biomolecules in the ligand, or encapsulated in the core of the MOFs via covalent or noncovalent interactions [134]. Drug release from MOFs may be through matrix degradation mechanisms; ion exchange; desorption; or free diffusion [133, 134]. The porosity of the hybrid framework is thought to be the rate-governing factor for controlling the release rate of the encapsulated drug [134]. In addition to their large storage capacity and specific drug release properties, the porous nature of MOFs makes them promising candidates for drug delivery [133, 137]. The first MOF used as a drug delivery carrier was achieved by Férey *et al*. (2006), who encapsulated ibuprofen in MIL100 (Fe) and MIL-101 (Fe) [145]. Nowadays, MOFs can be used for the delivery of many therapeutic agents, including anticancer drugs [146], vaccines [147], insulin [148], and antibiotics [149].

2.4 Design of cell membrane-coated hybrid NPs (CMCH-NPs)

Cell membrane-coated hybrid NPs are biomimetic drug delivery systems consisting of organic or inorganic NPs core, coated with membranes derived from natural cells. This hybrid system has recently attracted much interest because it retains more advantages from both domains, including the flexibility of the synthetic NPs, with the functionality and complexity of the natural cell membranes [150]. This technology has been developed to provide a hybrid system with enhanced biocompatibility; deep cell penetration properties; prolonged circulation time; high selectivity; improved pharmacokinetics; immuno-compatibility; and targeting properties [151-153]. Among the cell membrane-coated NPs, red blood cell membrane-coated NPs were the first CMCH-NPs developed as an alternative to polyethylene glycol (PEG) coating due to their high compatibility and low immunogenicity [154]. Currently, several cell membranes derived from macrophages; platelets; leucocytes; cancer cells; and bacterial cells have been utilized [155]. A top-down approach has been commonly used to fabricate CMCH-NPs, which involves three stages: isolation and extraction of the cell-membrane vesicles through hypotonic treatment; synthesis of the core NP; and then fusion of the NP with the vesicle by physical extrusion or electrostatic interactions [152]. The different steps involved in the synthesis of different types of CMCH-NPs are illustrated in **Figure 4**. Due to the biomimetic features and improved distribution of CMCH-NPs, they can be utilized as nanocarriers for enhanced drug delivery through interaction with pathogenic cells using their unique cell surface coating [152]. Once the hybrid system is within the cell, the therapeutic drug can be released slowly by natural diffusion through the membrane after polymer matrix degradation, or rapidly released through external stimuli such as UV-triggered membrane degradation [153].

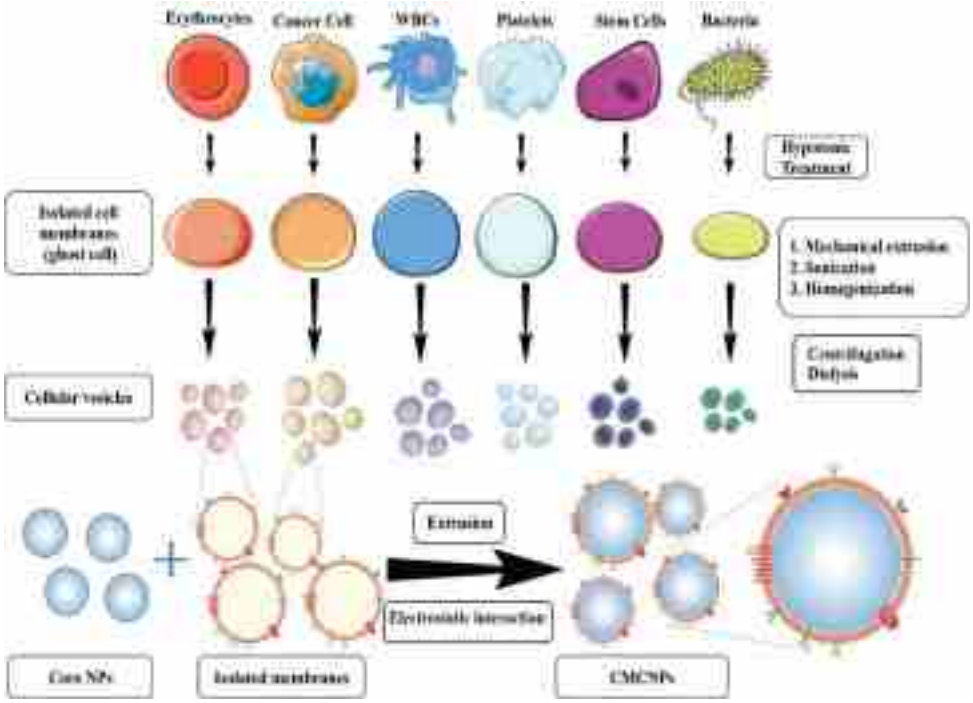

Figure 4: Various synthesis methods of CMCH-NPs (adapted with permission from [151]).

2.5 Design of hybrid NP-hydrogels

Polymeric nanohydrogels (nanogels) have been increasingly combined with NPs to form hybrid complexes with unique physicochemical and biological properties for localized and controlled drug delivery [156]. A wide range of NPs, including carbon-based nanomaterials; lipid-based vesicles; polymeric NPs; inorganic NPs; and metal/metal oxides NPs, can be incorporated within the polymeric network to obtain hybrid NP-hydrogels [157]. This innovative incorporation of the two diverse materials results in a novel hybrid nanosystem with enhanced structural integrity and controllable release rate of the combined NPs preserved by the nanogel network [156, 157]. In addition, they can offer extra engineering flexibility to enhance the overall therapeutic efficacy. The improved properties of the hybrid NP-hydrogels are mainly attributed to the enhanced physical or covalent interactions between the polymer chains of the hydrogel and the NPs [157].

These hybrid NP-hydrogels can be prepared using three approaches: (a) the addition of NPs into a preformulated hydrogel; (b) the addition of NPs to the polymer solution followed by hydrogel network formation; or (c) monomer polymerization in the presence of preformulated NPs [158, 159]. Furthermore, inorganic NPs can be often produced *in situ* within the gel matrix by loading an NP precursor into the gel first, followed by a reduction reaction for the formation of NPs [156]. Generally, drug release from the

hybrid NP-hydrogel system is determined by two steps: first, the NPs are released from the hydrogel through diffusion or swelling, which is controlled by the network dissolution. Secondly, the drug is released from the NPs that are governed by the structure, size and fabrication conditions of the NP system [156].

A variety of hybrid NP-hydrogels have been developed for specific drug targeting to different infectious sites, such as infections in the joints [160], the spinal cord [161], and the skin [162]. These hybrid biomaterials have shown superior capabilities in modifying drug release kinetics facilitating site-specific drug targeting and NP-based detoxification [156].

3. Application of hybrid nanosystems for antibacterial drug delivery

In recent years, hybrid NPs are being developed to improve the therapeutic efficacy of various antibiotics against bacteria and other infectious pathogens. These hybrid nanosystems have superior physicochemical properties that enable them to enhance the regulated delivery of antibiotics to bacterial cells and, therefore, improve their targeting against bacterial infections. In this section, the latest developments and technical advancements in the field of antibacterial delivery of hybrid nanosystems are discussed.

3.1 Lipid polymer hybrid NPs (LPHNPs)

LPHNPs have been explored as one of the promising strategies in antibiotic delivery against bacterial infections. The subcellular size of LPHNPs allows them to effectively penetrate the target site and release the loaded antibiotic locally, improving antibiotic concentration and localization at the infection site [89]. Polymers have a significant impact on the characteristics of LPHNPs. The incorporation of hydrophobic polymers has been shown to improve the loading of poorly water-soluble drugs, while hydrophilic polymers have been shown to coat the lipid core ,which enhances the stability, the loading capacity and the systemic circulation lifetime of hydrophilic drugs [163]. Moreover, some polymers can be modified with specific ligands to impact the targeting of the LPHNPs. Therefore, due to the importance of the polymeric material used to formulate LPHNPs, this section discusses the applications of LPHNPs for their antibiotic delivery based on their polymeric constituents, such as the PLGA-, chitosan- (CHT) and dendrimers employed in formulating them.

3.1.1 PLGA-based LPHNPs

PLGA has primarily been used as a polymeric core in various LPHNP formulations for antibacterial delivery, demonstrating excellent physical properties, biocompatibility, sustained drug release and biodegradability [164]. Due to the versatility and biocompatibility of the polymer, various research groups have explored the potential use of PLGA-based LPHNPs as a drug delivery system for different

routes of administration. The first study in this field was published by Bhardwaj *et al.* (2015), who designed and optimized LPHNPs for combined pulmonary delivery of isoniazid and ciprofloxacin hydrochloride. The spray drying technique was used to create a dry powder inhaler (DPI) form of the drug-loaded hybrid nanosystem. The presence of PLGA had a significant impact on controlling drug release from the LPHNPs. Furthermore, antibiotic-loaded LPHNPs achieved the maximum cellular uptake in alveolar macrophages compared to free antibiotics. *In vivo* studies revealed that maximum internalization efficiency into the lung was achieved by delivering LPHNPs in spray-dried powdered forms via the pulmonary route. Hence, the antibiotic-loaded LPHNPs developed in this study could be beneficial as an antibiotic delivery system to treat bacterial tuberculosis [165]. However, further evaluation of essential parameters such as biocompatibility studies, and *in vitro* and *in vivo* antibacterial activity studies, for the prepared LPHNPs are necessary to confirm the biosafety and antibacterial profile of the nanosystem.

In addition to the pulmonary route, topical application of PLGA-LPHNPs has also been reported for drug delivery. In a subsequent study, Dave and coworkers (2017) designed biodegradable LPHNPs with a sustained-release profile using different ratios of the hydrophobic polymer PLGA to control the release of the antibiotic norfloxacin at the site of infection, and to improve its topical activity to treat burn infections. The optimized norfloxacin-loaded LPHNPs formulation was selected to prepare LPHNPs@Carbopol gel for topical antibiotic delivery. *In vitro* skin permeation results of this formula showed a maximum release profile, due to the higher encapsulation of the drug in NPs, compared to other formulations. Antimicrobial activity against *Staphylococcus aureus (S. aureus)* and *Pseudomonas aeruginosa (P. aeruginosa)* indicated that norfloxacin-loaded LPHNPs are effective against gram-positive and gram-negative bacteria, confirmed by measuring the zone of inhibition. As a result, these norfloxacin-loaded LPHNPs were shown to be safe and efficient for long-term treatment of bacterial infections caused by burn [166].

More recently, Fangary's research group (2022) produced a unique liposome combined with small PLGA- NPs (PLGA NP-Lips) for simultaneous ocular administration of erythromycin and 3c (a novel 5-cyanothiazolyl urea derivative with promising antibacterial activity). This work attempted to overcome antibiotic drug resistance by increasing nanocarrier uptake and antibiotic delivery in bacterial cells while minimizing toxicity toward human cells. The two-step manufacturing approach was used to create erythromycin/3c-loaded PLGA NP-Lips, and the antibacterial activity of these hybrid NPs was assessed against gram-negative *Escherichia coli* (*E. coli*) and *P. aeruginosa*. *In vitro* studies revealed that incorporation of small PLGA NPs into liposomes reduced the NP uptake by HEK293 cells while

enhancing it in gram-negative bacterial cells. Consequently, four-fold and eight-fold improvements in antibiotic selectivity were observed for *E. coli* and *P. aeruginosa*, respectively. Ocular administration of the erythromycin/3c-loaded PLGA NP-Lips in a *P. aeruginosa* keratitis mouse model allowed for potent selective inhibition of bacterial infection and full recovery. Moreover, in comparison to free antibiotics and PLGA NPs, administration of PLGA NP-Lips showed substantial reduction in infection-induced inflammation (tumor necrosis factor-α(TNF-α) and interleukins (IL-6) levels), confirming the cytocompatibility and the therapeutic potential of the developed hybrid nanocarrier [167]. Overall, given the flexibility and biosafety of PLGA, other routes of administration can be explored in future research using PLGA-based LPHNPs.

Besides improving the antibacterial activity of antibiotics, PLGA-LPHNPs are being used to eradicate biofilms. Biofilms are multicellular aggregates of microorganisms embedded in a self-produced polymer matrix consisting of polysaccharides, lipids, proteins and DNA [168]. Bacterial biofilms have been linked to chronic infectious diseases such as staphylococcal infections and chronic *P. aeruginosa* lung infections, due to their increased tolerance to antibiotics, aside from resisting the host's immune system defence mechanisms [169]. To improve the therapeutic efficacy of antibiotics against bacterial biofilm, Baek *et al.* (2018) and Guo *et al*. (2020) have reported the development of self-assembling PLGA-LPHNPs with different lipid components. Both studies examined the effect of PLGA and lipid constituents of the LPHNPs on the release profiles of encapsulated antibiotics. The results showed more extended antibiotic release from PLGA-LPHNPs compared to non-hybrid PLGA-NPs, confirming the impact of the hybrid system on controlling the drug release. Baek *et al.* (2018) investigated the binding affinity of PLGA-NPs and PLGA-LPHNPs to both planktonic cells and bacterial biofilm. Propidium bromide (PI)-encapsulated NPs were prepared and introduced into planktonic cells and biofilms of different gram-positive and gram-negative strains. The increased PI intensity indicated the aggregation of the PLGA-LPHNPs around the bacteria and biofilm with higher affinity than PLGA-NPs (**Figure 5A**). Furthermore, they investigated the release profile of antibiotics with varying degrees of hydrophilicity from PLGA-NPs and PLGA-LPHNPs. The latter had a more sustained release profile for hydrophobic (rifamycin), amphiphilic (ampicillin), and hydrophilic (amoxicillin, kanamycin, D-cycloserine) antibiotics; while PLGA-NPs exhibited a faster release profile for hydrophilic drugs (**Figure 5B**). When comparing the antimicrobial activity of LPHNPs against bacterial biofilms to that of free antibiotics, PLGA-LPHNPs demonstrated a significant increase in biofilm inhibition at concentrations 8 - 32 times lower than that of free antibiotics, confirming the effectiveness of the prepared hybrid NPs in eradicating bacterial biofilm [170].

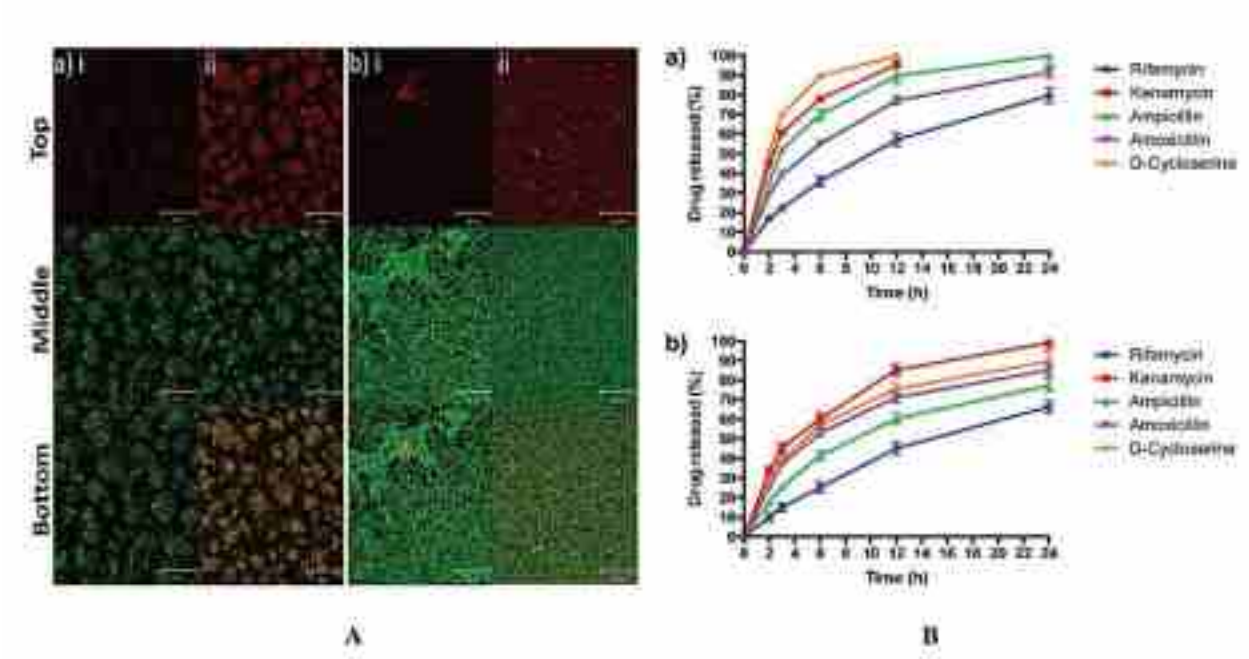

Figure 5: (A): Confocal laser scanning microscopy (CLSM) images of a) *E. faecalis* and b) *S. aureus* biofilms co-stained by PI encapsulated PLGA-NPs (i) or PLGA-LPHNPs (ii). **(B):** *In vitro* release profiles of different antibiotics from (a) PLGA-NPs and (b) PLGA-LPHNPs in PBS (pH 7.4) for 24 hrs at 37 ± 1°C (adapted with permission from [170]).

While the above study focused solely on biofilm eradication, there are emerging studies evaluating combined antibacterial and antibiofilm effectiveness. For instance, Guo *et al*. (2020) created linezolid@PLGA-LPHNPs, aiming to evaluate the antibacterial and antibiofilm activities of the prepared hybrid system against intracellular MRSA residing within osteoblasts and biofilms to treat osteomyelitis. Although the hybrid system attained lower antibacterial activity against planktonic MRSA, it was far more effective against intracellular MRSA embedded inside bone cells than free linezolid. Furthermore, linezolid-loaded LPHNPs showed superior antibiofilm activity to the free antibiotic, and these activities were attributed to the excessive accumulation of the hybrid system inside the infected bone cells and biofilms, which was validated by an *in vivo* biodistribution study (> 4-fold increase in linezolid -bone level was observed when linezolid-LPHNPs was used) [171]. Later, the same research team developed similar hybrid NPs loaded with rifampicin to target intracellular and biofilm-embedded MRSA (2020). Rifampicin-loaded LPHNPs showed moderate but significant antibacterial activity against planktonic osteomyelitis-causing MRSA, with superiority to the free drug. Also, in comparison to free rifampicin, rifampicin-LPHNPs showed improved antibacterial and antibiofilm activity against intracellular MRSA

within osteoblasts and biofilms. Confocal microscopy pictures demonstrated the widespread deposition of antibiotic-loaded LPHNPs inside MRSA-infected bone cells and biofilm matrices [172]. Further studies are needed to improve the bone and biofilm targeting properties of rifampicin-LPHNPs and evaluate their *in vivo* antimicrobial activity and biosafety, in addition to investigating the possibility of using these hybrid NPs for the systemic delivery of antibiotic combinations.

In order to construct successful hybrid nanocarriers for antibacterial delivery, and further enhance the performance of LPHNPs against intracellular bacteria, it is essential to identify correlations between the physicochemical properties of hybrid NPs and their intracellular uptake. An emerging research has been reported by Bose and coworkers (2020), who explored the effect of lipid constituents and lipid-based surface engineering on the biological cell-NP interaction. The research team investigated the effect of surface charge on the physicochemical properties, macrophage uptake, and *in vitro* intracellular killing efficiency of cationic and zwitterionic PLGA-LPHNPs loaded with doxycycline or vancomycin against *S. aureus* and *M. smegmatis*. All tested PLGA-NPs, and cationic LPHNPs, inhibited the intracellular growth of *S. aureus* and *M. smegmatis* effectively, with the latter was more successful. This is due to the synergism between the antibiotics and the cationic hybrid NPs, enhancing the antibacterial activity against intracellular pathogens. However, the authors did not notice a synergistic effect for zwitterionic LPHNPs. In addition, cationic LPHNPs showed higher macrophage recognition and uptake, and thus enhanced *in vitro* intracellular antibacterial activity compared to zwitterionic LPHNPs and non-lipid PLGA-NPs because of strong adhesion of the cationic lipid shell and the negatively charged bacteria [173]. Overall, the data obtained from this research study suggest that LPHNPs containing cationic lipids have the potential to enhance macrophage uptake and thereby improve the intracellular antibacterial efficacy of antibiotics against gram-positive bacterial infections.

Taken together, the findings of these studies encourage the application of PLGA-based LPHNPs as antibacterial delivery systems, because of their ability to enhance stability; biodegradability; controlled drug release; and antibacterial activity, suggesting a promising approach to improve antibiotics efficacy and reduce the development of resistance. Also, the investigations indicated that PLGA-based LPHNPs could remove hard-to-treat infections such as intracellular bacteria, osteomyelitis and biofilms, despite the fact that free antibiotics are not able to reach those infection sites. Most of these hard-to-treat conditions have been reported as a source of chronic infections and antimicrobial resistance [168, 174, 175]. The versatility of PLGA-based LPHNPs has been proved by their ability to be formulated into different dosage forms via spray drying, loading into gels and colloidal systems, and then administered to the body

via different routes such as transdermal, inhalation, ocular and parenteral. **Table 2** summarizes the current state of research on the preparation of LPHNPs using PLGA as a polymeric core, highlighting their lipid constituent; the ratios of poly lactic acid (PLA)/poly glycolic acid (PGA) copolymer used; the antibiotic drug loaded; the method of preparation; and the characterization studies and findings. As shown in the table, only PLGA 50:50 has been used to formulate all PLGA-based LPHNPs. This could be due to its favorable degradation properties compared to the other PLGA types [164], making it an attractive polymeric candidate to fabricate LPHNPs for controlled antibiotic delivery.

Table 2: Summary of the studies undertaken to date with LPHNPs using PLGA as a polymeric core.

Lipid	PLA/PGA copolymer ratio	Antibiotic drug	Method of preparation -	Characterization studies	Characteristic findings -	Ref.
Soy lecithin	50:50	Isoniazid/Ciprofloxacin	DESE	PS, PDI, EE %. Particle flow properties Aerodynamic properties DSC, FT-IR, morphology (SEM)	- Size: 111 and 172nm, PDI: 0.189 and 0.169 and EE %: 63.64% and 68.49 % for isoniazid and ciprofloxacin-loaded LPHNPs, respectively. - DPI had good flow properties. - MMAD < 5 μm with high lung localization.	[165]
Soy lecithin Stearyl amine	50:50	Norfloxacin	ESE -	PS, PDI, ZP Morphology (TEM/ SEM) FT-IR DSC and TGA. Characterization of the LPHNPs loaded gel: - Viscosity - pH - Spreadability - Skin irritation assay.	- Size: 186 - 219 nm - Suitable viscosity, pH and spreadability with decreased skin irritation upon application on burnt skin.	[166]
Soy lecithin Cholesterol	50:50	Erythromycin/3c	ESE/thin film hydration	PS, ZP Morphology (SEM, TEM) EE % Cytotoxicity assay	- Size: 364 nm - ZP: -20 Mv - EE% : 98.4% - Minimum dose-dependent cytotoxicity	[167]
Cationic DOTAP	50:50	Rifamycin Ampicillin	Self-assembly approach	PS, PDI, ZP Morphology (SEM)	- Positive ZP indicating the coating of PLGA surface with the	[170]

		Kanamycin Amoxicillin D-cycloserine		EE %	cationic DOTAP. - High EE% for antibiotics, irrespective of their water solubility.	-
Lecithin DSPE-mPEG-2000 Cholesterol	50:50	Linezolid	Nanoprecipitation	PS, PDI, ZP Morphology (TEM) EE % Dispersion stability Cytotoxicity assay	- Size: 110 - PDI: 0.130 - Controlled drug release. - Enhanced serum stability - Minimum cytotoxicity against osteoblast	[171]
Lecithin DSPE-mPEG-2000 Cholesterol	50:50	Rifampicin	Nanoprecipitation	PS, PDI, ZP Morphology (SEM) EE % Dispersion stability Cytotoxicity assay	- Size: 110 nm and - PDI: 0.142. - Controlled drug release. - Maintained serum stability. - No noticeable toxicity against osteoblast.	- [172]
Cationic DOTAP Zwitterionic PC	50:50	Doxycycline Vancomycin	Modified ESE	PS, PDI, ZP Morphology (SEM, TEM) EE % Cytotoxicity assay	- LPHNPs had significantly less particle size than non-lipid PLGA NPs (p-value < 0.05) - Dose-dependent cytotoxicity for cationic LPHNPs, and no noticeable cytotoxicity for zwitterionic LPHNPs.	- [173]

DESE, double emulsification solvent evaporation; PS, particle size; PDI, polydispersity index; EE%, percentage entrapment efficiency; DSC, differential scanning calorimetry; FT-IR, Fourier transform infra-red; SEM, scanning electron microscope; TEM, transmission electron microscope; DPI, dry powder inhaler; MMAD, mass median aerodynamic diameter; TGA, thermogravimetric analysis; DSPE-mPEG-2000, 1,2-distearoyl-sn-glycero-3 phosphoethanolamine-N-amino(polyethylene glycol)-2000; DOTAP, 1,2-dioleoyl-3-trimethylammonium-propane; PC, phosphatidylcholine.

3.1.2 Chitosan-based LPHNPs

Chitosan (CHT) is a cationic natural polymer with inherent antimicrobial and antifungal properties. It has been widely employed as an antibiotic delivery polymer. This is due to its unique characteristics, such as biocompatibility; biodegradability; non-toxicity; and target specific triggering due to its cationic nature [176]. Recently, the application of CHT in the preparation of antibacterial-loaded hybrid NPs has attracted considerable interest for its use against microbial infections. Therefore, in this subsection, conventional and stimuli-responsive CHT-based LPHNPs with mono-antibiotic therapy and CHT-based LPHNPs with dual-antibiotic therapy will be discussed.

Monotherapy with the use of various antimicrobials, such as antibiotics, is one of the successful strategies to treat different bacterial infections. Two research studies were reported by Thakur and coworkers, describing the use of CHT to fabricate conventional LPHNPs with mono-antibiotic therapy. In the first study, Thakur's research group investigated the possibility of combined lipid NPs and CHT as a therapy for managing and treating wound infections (2018). They developed and optimized LPHNPs loaded with fusidic acid by the hot micro-emulsion method. Administration of fusidic acid-LPHNPs resulted in a five-fold decrease in its MIC against MRSA and other *S. aureus* bacterial strains, accompanied by a longer period of antibacterial activity compared to the free fusidic acid solution. This protracted antibacterial activity is attributed to the incorporation of the drug within the hybrid system, which attempts to prolong the residence time of the drug at the infection site, besides enhancing its penetration into the bacterial cell wall. The optimized formulation of fusidic acid-LPHNPs was selected to prepare LPHNP-loaded carbopol gel for the topical application against burn wound infections. The gel incorporating NPs exhibited good gel strength; extrudability; spreadability and enhanced permeation into mice skin. The comprehensive studies indicated that the developed hybrid system offers possible advantages in prolonged and improved burn wound healing [177]. One year later, the same research group subjected the fusidic acid-LPHNPs gel to *in vivo* pharmacodynamic studies in a murine burn wound model infected with MRSA (2019). The results of the *in vivo* bacterial loads indicated that the fusidic acid-LPHNP gel exhibited significant antibacterial potency against the MRSA that was present in the burn wound, as the animals treated with fusidic acid-LPHNPs gel exhibited significantly higher bacterial count reduction, compared to the conventional fusidic acid topical formulation, during 15 days of treatment [178]. The formulation strategies of these studies show the safety and effectiveness of fusidic acid-encapsulated LPHNPs in inhibiting bacterial infections. They also provide a unique hybrid system for topical application against burn wound infection.

Furthermore, CHT has been introduced to prepare stimuli-responsive LPHNPs with mono-antibiotic therapy. Stimuli-responsive LPHNPs have the potential to improve the therapeutic efficacy of antibiotics, while reducing their side effects, by releasing the encapsulated drug at the site of infection in response to stimuli [179]. Depending on the type of polymer, lipid and functional groups, various

stimuli-responsive LPHNPs, such as pH-responsive LPHNPs, have been developed. To explore the advantages of these pH-responsive LPHNPs, Hassan *et al*. (2020) fabricated novel vancomycin-loaded pH-responsive LPHNPs using CHT and a synthesized oleyl amine based zwitterionic lipid (OLA), produced by ion gelation, to deliver vancomycin against MRSA. The *in vitro* antibacterial activity of the developed hybrid nanosystem against MRSA was higher than bare vancomycin and was also enhanced at pH 6.0, compared to the physiological pH 7.4, indicating that the system was pH-dependent. The overall enhancement in the antibacterial activity of the LPHNPs could be due to the increase in the binding of the system to the negative bacterial membrane and the additive intrinsic antimicrobial activity of the LPHNPs. Assessment of the developed LPHNPs with different *in vitro* antibacterial activity tests, indicated that LPHNPs had the potential to effectively treat MRSA, and resulted in the successful and irrecoverable membrane disruption and biofilm eradication, compared to the free vancomycin. Also, the *in vivo* results obtained by treating mice skin infection revealed the ability of the LPHNPs to reduce and eradicate MRSA colonies (MRSA/CFU) by 95-fold, when compared to bare vancomycin treatment, confirming the effectiveness of the prepared hybrid nanosystem in treating MRSA infections [180]. According to the author's findings in this work, innovative biocompatible vancomycin-loaded pH-responsive LPHNPs can potentially be effective in the pH-responsive targeted delivery of VCM to effectively prevent the development of antimicrobial resistance.

Besides mono-antibiotic therapy, dual-therapy, which combines different antibiotics or antibiotics with adjuncts, has been introduced to improve the efficiency of already-in-use antibiotics through synergistic effects, or to combat antibiotic resistance [181]. Rodenak-Kladniew *et al.* (2019) and Bueloni *et al.* (2020), published two research studies on the use of CHT-based LPHNPs encapsulating an antibiotic-adjunct combination for dual antibacterial therapy. Their strategy aimed to enhance the antibacterial efficacy of the loaded antibiotics against both gram-positive *S. aureus* and gram-negative *P. aeruginosa*. Both research groups employed a hot homogenization/ultrasonication technique, while using different lipid nanocarriers for the development of a CHT-hybrid nanosystem. Rodenak-Kladniew *et al.* (2019), developed hybrid CHT-based solid lipid NPs (CHT/SLNs) incorporating the broad-spectrum antibiotic, ofloxacin, and a natural phenolic compound, eugenol (Eu), into a lipid matrix (ofloxacin-Eu@CHT/SLNs). Characterization of the developed hybrid SLNs by different analytical tools confirmed the presence of spherical NPs composed of a lipid matrix containing an ofloxacin-Eu combination and coated with positively charged CHT. This hybrid ofloxacin-Eu/CHT SLNs showed improved antimicrobial activity against *P. aeruginosa* and *S. aureus*, with MICs that were 6- and 16-fold lower than free ofloxacin, respectively. These findings suggest that CHT and Eu may have an impact on the increased antibacterial activity of the encapsulated antibiotic. Moreover, *in*

vivo investigations using hybrid SLNs delivered via a pulmonary route to mice in the form of DPI showed that the hybrid NPs were nontoxic to human pulmonary cells and can be applied as an inhalable therapeutic system to treat pulmonary infections [182]. Alternatively, Bueloni *et al.* (2020) incorporated nalidixic acid-vanadium complex into myristyl myristate nanostructured lipid carriers (NCL) hybridized with CHT to improve the antibiotic complex's solubility, bioavailability, and antimicrobial activity. Likewise, the results showed a significant antibacterial enhancement for the loaded NCL/CHT against *P. aeruginosa* with a MIC value of 129.3 μM compared to 625 μM of the free nalidixic acid-vanadium antibiotic complex, while the MIC of the loaded NCL/CHT against *S. aureus* was in the same order as the free complex (129.9 μM vs. 125μM). Furthermore, the authors investigated the quorum-sensing inhibition activity of the developed NCL/CHT hybrid NPs, and the results indicated that the formulated hybrid NPs exhibited an inhibitory effect on quorum sensing, observed by reporter strain *Chromobacterium violaceum.* However, further investigations for the developed nalidixic acid-vanadium hybrid NPs, including *in silico* studies and preclinical studies in appropriate animal models, are still required [183]. In summary, the outcomes of these reported studies confirm the influence of CHT on controlling LPHNP drug release and increasing the antibacterial efficacy of the encapsulated antibiotics against both gram-positive and gram-negative bacterial infections.

Accordingly, the overall data illustrate that chitosan-based LPHNPs are actively being studied, as the polymer has an intrinsic, antimicrobial effect that improves the overall antimicrobial activity of the system. Moreover, the polysaccharide polymer has multiple surface amine groups which use covalent modifications, and electrostatic and supramolecular interactions, to formulate stable conventional and stimuli-responsive LPHNPs.

3.1.3 Dendritic-based LPHNPs (LDHNPs)

Dendrimers are synthetic polymers with an especial branching architecture. They possess numerous advantages that make them suitable as drug delivery platforms, such as multivalency; globular architecture; well-defined molecular weight; the ability to encapsulate a variety of therapeutic agents within the internal hydrophobic environment; and the availability of multiple surface functional groups [184, 185]. Therefore, dendrimers with specific properties can be used to improve the performance of lipid dendrimer hybrid NPs (LDHNPs) as a novel type of LPHNP for effective antibiotic delivery. Encapsulation of a dendrimer in a lipid shell as liposomes and SLNs can improve the solubility and the EE percentage of the loaded drug [186]. To date, only two papers using dendrimers have been published by Govender's research group. In the early study, Sonawane *et al.* (2016) developed a system of LPHNPs with a dendrimer for the effective delivery of vancomycin against MRSA infections. They prepared LDHNPs through a hot stirring ultrasonication technique

using the solid lipid Compritol 888 ATO, and a generation 4 poly amidoamine-succinamic acid dendrimer (G4 PAMAM-SA). The formation of LDHNPs with G4 PAMAM-SA entrapped inside the lipid shell, and vancomycin encapsulated within the dendrimer core, were confirmed using DSC and FT-IR studies. *In vitro* antibacterial activity studies confirmed the enhanced antibacterial activity of vancomycin-LDHNPs with MICs of 15.62 μg/ml and 7.81 μg/ml against *S. aureus* and MRSA, respectively. In addition, the formulation exhibited sustained antibacterial activity with an MIC of 62.5 μg/ml against *S. aureus* and 500 μg/ml against MRSA for up to 72 hrs and 54 hrs, respectively [187]. Later, Maji and coworkers (2019) formulated and optimized novel pH-responsive LDHNPs to effectively deliver vancomycin into the site of infection targeting intracellular MRSA. The LDHNPs were formulated by the ESE method using OLA as a lipid and G3 PAMAM-SA dendrimer as a polymer. The antibacterial activity of LDHNPs against MRSA showed an 8-fold lower MIC at pH 6.0 and 7.4, compared to treatment with bare vancomycin. Also, bacterial cell viability study indicated that, despite the lower MIC values, vancomycin-LDHNPs were more effective at killing MRSA than free vancomycin, with complete cell membrane destruction. Likewise, the treatment with vancomycin-LDHNPs showed significant intracellular antibacterial activity, as compared to untreated cells and cells treated with vancomycin only [98]. Although, the same research group had previously conducted two studies on the formulation and development of LDHNPs for antibacterial drug delivery, the latter confirmed that the therapeutic potential of such a hybrid system for improving antibiotic delivery and combating drug resistance could be enhanced by designing it as a pH-responsive system using different lipid and dendrimer components. Therefore, in both studies, further investigation with *in vivo* studies is required to prove their *in vitro* findings of the developed LDHNPs.

As already stated, dendrimers have traits that make them attractive and promising candidates for drug delivery. However, concerns about their toxicity and biocompatibility limit their applications and translational potential [185, 188]. According to the studies discussed, dendrimers have the potential to be used as an effective delivery system for antibiotics, when incorporated into LPHNPs with various polymeric and lipid constituents, because they have the ability to control antibiotic release; improve biocompatibility and stability; and enhance antibacterial efficacy and the formulation of stimuli-responsive systems. However, there is a need for acute and long-term, in-depth toxicological studies to confirm their safety profiles. Moreover, apart from PAMAM dendrimers which are cationic in nature, studies involving anionic dendrimers, which have better biosafety profiles, could result in safer hybrid nanosystems [189].

3.2 Organic-inorganic hybrid NPs

Various combinations of organic and inorganic materials are being used to construct different nanocarriers to treat bacterial infections, including nanofibers, mesoporous silica NPs (MSNs) and nanocomposites. In this sub-section, we describe the incorporation of antibiotics, as well as free radical releasing biomaterials, into organic-inorganic hybrid NPs, to achieve site-specific and controlled-release delivery systems, which offer significant advantages in improving antibacterial efficiency and overcoming therapeutic problems caused by bacteria.[190].

Several classes of antibiotics, such as penicillins; tetracyclines; aminoglycosides; fluoroquinolones; macrolides and polymyxins have been employed to fabricate antibiotic-loaded organic-inorganic hybrid NPs for effective antibacterial delivery. The first report of an organic-inorganic hybrid NP loaded with an antibiotic was by Wang *et al.* (2012), who employed an electrospinning approach to fabricate amoxicillin-loaded laponite (LAP) doped PLGA (amoxicillin-LAP/PLGA) nanofibers for antibacterial application. The authors aimed to provide the nanofiber hybrid system with a sustained release profile and to improve its mechanical durability. The amoxicillin-LAP/PLGA nanofibers showed a biphasic *in vitro* release pattern due to the combination of two different dissociation pathways, leading to a slower release of the antibiotic for up to nine days. Also, the hybrid nanofibers revealed concentration-dependent and long-term antibacterial activity against *S. aureus* in a liquid and a solid medium for 48 hrs. The system showed ≥ 90 % antibacterial inhibition at higher concentrations, with no significant difference compared to the free amoxicillin and amoxicillin-loaded PLGA nanofibers [191]. One year later, the same research group reported two research studies with the same preparation approach to fabricate hybrid nanofibers using the same organic material, PLGA, but with different inorganic materials, namely n-hydroxyapatite(n-HA) and halloysite nanotubes (HNTs), and encapsulated antibiotics, amoxicillin and tetracycline, respectively, to target *S. aureus*. The results were comparable with the previous study as the encapsulation of the antibiotics into the hybrid nanofibers also enabled sustained and controlled release profiles, with effective and prolonged growth inhibition activity of the antibiotics against the gram-positive bacterial strain. Among the reported organic-inorganic hybrid nanofibers, tetracycline-loaded HNTs/PLGA NPs showed the most sustained release for up to 42 days, and thus their antibacterial activity was improved significantly [192, 193]. Cytocompatibility of the formulated hybrid nanofibers in the three studies, together with the improved mechanical durability and antibacterial activity, indicated the potential of such hybrid organic-inorganic NPs for application as antibacterial drug delivery systems in the field of tissue engineering. However, if such research modifications are to have an impact, more investigations, such as preclinical *in vivo* studies, are required.

Another antibiotic that has been explored for loading organic-inorganic hybrid NPs formulations is gentamicin. Vasile *et al.* (2014) and Yang *et al*. (2018) have reported different gentamicin-loaded organic-inorganic hybrid NPs intended for the treatment of extracellular and intracellular bacterial pathogens, respectively. Vasile and coworkers (2014) developed and optimized a gentamicin-loaded zinc oxide-CHT (gentamicin-ZnO/CHT) hybrid nanocomposite to improve the targeting efficacy of gentamicin in treating external bacterial infections. The sustained release characteristics of the prepared gentamicin-ZnO/CHT NPs improved the antibacterial activity of the hybrid nanosystem against *S. aureus* and *P. aeruginosa* in both planktonic and surface-attached conditions, since controlled, synergistic and prolonged antibacterial activity was obtained, with four-fold and two-fold lower MIC values against *S. aureus* and *P. aeruginosa*, respectively, compared to the free gentamicin control [194]. On the other hand, Yang *et al.* (2018) developed a novel gentamicin-loaded MSNs decorated with bacteria toxin-sensitive liposomes immobilized with a targeting peptide ubiquicidin (UB_{I29-41}) to enhance the targeting efficacy and binding affinity of gentamicin to the intracellular *S. aureus*. The antibiotic release from MSNs/LU hybrid NPs was triggered by bacterial toxins which degraded the liposome bilayer, allowing the rapid release of the loaded antibiotic from the hybrid system. *In vitro* and *in vivo* antibacterial activity studies confirmed the superior antibacterial effects of gentamicin-MSNs/LU hybrid NPs against planktonic and intracellular bacterial infection, in comparison to free gentamicin and gentamicin-loaded MSNs. Moreover, the inflammation-related gene expression in infected pre-osteoblasts and macrophages was also reduced extensively after treatment with the gentamicin-MSNs/LU hybrid NPs. Therefore, the cytocompatibility and the microenvironment-responsive antibiotic release of gentamicin-MSNs/LU hybrid NPs confirm their potential to target intracellular pathogens and inflammation associated with intracellular *S. aureus* infections and possibly other gram-positive bacterial infections [195]. In both studies, the therapeutic efficacy of gentamicin against bacteria has been improved significantly; although, in the later work, the authors modified the prepared organic-inorganic hybrid NPs by integrating a bacteria toxin-sensitive liposome and a targeting peptide into the nanosystem. In addition, the prepared NPs were fully characterized, including *in vivo* studies, which allow the clinical translation of such a research study.

Moreover, fluoroquinolone antibiotics, especially ciprofloxacin, have been introduced into various organic-inorganic hybrid NPs to treat infectious diseases caused by gram-positive and gram-negative pathogens. Two research studies reported the delivery of ciprofloxacin via organic-inorganic hybrid NPs for controlled and targeted drug delivery. Murugesan and coworkers (2018) investigated the functionalization of a natural biocompatible organic humic acid (HA) with ZnO for the pH-responsive and site-specific delivery of ciprofloxacin, using a simple ESE method. The prepared ciprofloxacin-

loaded ZnO-HA hybrid NPs showed higher bacterial growth inhibition against *P. aeruginosa* and *B. cereus,* with lower MIC values compared to the blank ZnO-HA hybrid NPs and free ciprofloxacin. In addition, the biofilm formation was suppressed by 75% and 85%, for *B. cereus* and *P. aeruginosa*, respectively, when treated with the drug-loaded hybrid nanocarrier [196]. Later in the same year, Al-Obaidi *et al.* (2018) reported novel hybrid NPs of silica-coated AgNPs embedded into a ciprofloxacin-encapsulated-CHT matrix for effective inhibition of growth and biofilm formation of *P. aeruginosa*. The authors attempted to produce a first inhalable dosage form of ciprofloxacin for treating cystic fibrosis (CF) caused by gram-negative bacteria. They investigated and optimized various parameters, such as Ag^{+} concentration and CHT ratio, to obtain hybrid NPs with an improved particle deposition within the lung. The prepared hybrid NPs were deposited in Stage 2, reaching ~70 % deposition, which is considered essential for the successful delivery of the drug deep inside the lung. *In vitro* antibacterial and antibiofilm formation assays revealed that the formulated hybrid system exhibited 3 - 4 times more growth and biofilm inhibition with a synergistic antibacterial effect against *P. aeruginosa,* compared to free ciprofloxacin [197]. Despite the promising outcomes in these two studies, further development through performing a cytotoxicity investigation, and cellular uptake and *in vivo* studies in suitable animal models, are required to illustrate the advantages of both hybrid nanocarriers.

Tetracyclines were also loaded into organic-inorganic hybrid NPs to improve their targeting efficacy against pathogenic bacteria. Kankala *et al.* (2020) designed a novel pH-responsive trio-hybrid nanocomposite system based on MSNs with the goal of overcoming antibiotic resistance. They developed tetracycline-immobilized Cu-doped MSNs coated with silver-stabilized polyethyleneimine (AgNPs-PEI) through a series of reaction steps. The antibacterial activity was studied against MDR *E. coli* species, and the results indicated that hybridization of tetracycline-encapsulated Cu-MSNs NPs with AgNPs-PEI significantly improved the antibacterial effectiveness of tetracycline against MDR *E. coli* through sensitizing the cell membrane to the ROS generation effect of Ag, thus improving the intracellular availability of the hybrid nanocarrier for the pH-triggered release of the antibiotic associated with high ROS levels due to the Cu-MSNs. Altogether, this biocompatible trio-hybrid nanocomposite with a synergistic effect and pH-responsive delivery of tetracycline is considered a promising approach for efficiently combatting MDR infections [198].

Currently, two research studies published by Iudin *et al*. (2022) and Xiang *et al*. (2022), further improved the performance of organic-inorganic hybrid NPs for efficient antibiotic therapy. First, Iudin *et al*. (2022) developed a novel organic-inorganic hybrid nanocarrier for polymyxins delivery, aimed to optimize their antibacterial properties against various infectious diseases while minimizing their toxic side effects. A hybrid core-shell silver-poly glutamic acid NPs loaded with polymyxins B

and E, respectively, (polymyxin@PGlu-Ag NPs) have been designed and carefully investigated. Cytotoxicity studies were performed to confirm the biosafety, biocompatibility, and minimal macrophage uptake of the prepared hybrid nanocarriers. Then, the synthesized NPs were incorporated into an agarose gel to form a hydrogel nanocomposite delivery system proposed to treat skin wound infections. The antibacterial efficacy of both polymyxin-loaded hybrid NPs and their nanocomposites were assessed against *P. aeruginosa, in vitro*. Both formulations demonstrated a synergistic bacterial growth inhibition against *P. aeruginosa* proved by the lower MICs (1 μg/ml), when compared to free polymyxins, blank hybrid NPs and bare AgNPs. This decreased MIC values could be attributed to the combined activity of the polymyxins and AgNPs in one hybrid nanosystem. In summary, they concluded that polymyxin@PGlu-Ag NPs and their hydrogel composite could eventually enhance the therapeutic potential of polymyxins to treat skin injuries [199].

More recently, Xiang and co-workers (2022) loaded a macrolide antibiotic azithromycin and a photosensitizer methylene blue into zwitterionic pH-responsive MSNs/polypeptide hybrid nanoparticles (azithromycin/MB@MSPNs) for chemo-photodynamic combination therapy against MRSA infections. A pH-triggered and lipase-induced controlled azithromycin release was achieved, and the loaded MB revealed an efficient generation of singlet oxygen ($^1O_2$), which resulted in a facilitated photodynamic action. Also, the prepared azithromycin/MB@MSPNs showed improved biocompatibility towards normal mammalian cells, and a strong antibacterial and antibiofilm activity against MRSA. Moreover, *in vivo* studies were conducted in an MRSA infected mice model, and the hybrid nanocarrier exhibited synergistic and enhanced bactericidal action with a rapid wound healing process for up to 94 % comparing to mono azithromycin therapy. Therefore, the developed azithromycin/MB@MSPNs could be promising candidate for clinical application in combined chemo-photodynamic therapy against MDR bacteria [200].

In addition to antibiotic delivery, different organic-inorganic hybrid nanoparticulate systems have been explored as a free radical release platform against infectious diseases. Free radicals have been known to have significant antibacterial activity against gram-positive and gram-negative bacteria, in addition to multidrug-resistant pathogens. They act by stimulating natural microbial elimination through modulating the host defensive mechanisms. This process results in a high production of reactive oxygen species (ROS), which increases the susceptibility of the immune cells to oxidative stress [168]. Cui *et al.* (2016) and Elsherbiny *et al.* (2016) used different approaches to design organic-inorganic hybrid NPs comprising various organic and inorganic components in an attempt to treat bacterial infections by enhancing the generation of free radicals from NPs. Cui *et al.* (2016) employed an *in situ* reduction method to develop photosensitizer-loaded hybrid NPs synthesized by directly reducing AuNPs onto the surface of polyallylamine/CHT polymeric NPs (PAA/CHT NPs),

followed by the conjugation of a photosensitizer, Rose Bengal (RB), with the PAA/CHT-Au hybrid NPs. The RB-loaded PAA/CHT-Au hybrid NPs exhibited a prolonged lifetime and excellent antibacterial activity against *E. coli;* higher than that of blank PAA/CHT-AuNPs and free RB, due to the excessive and direct *in situ* generation of ROS at the bacterial cell surface, from the RB-loaded hybrid NPs [201]. Instead, Elsherbiny *et al.* (2016) studied the photo-induced green synthesis, antimicrobial activity and free radical formation of poly(ε-caprolactone)/curcumin/grape leaf extract-silver hybrid NPs (PCL/Cur/GLE-Ag NPs) against different strains of gram-positive and gram-negative bacteria, in addition to two fungal strains. The antibacterial activity of the natural antimicrobial curcumin/grape leaf extract was enhanced significantly when combined with AgNPs, compared to the pure curcumin and grape leaf extract, and this could be related to the free radical formation properties of the AgNPs, as well as the high surface area of the PCL/Cur/GLE-Ag hybrid NPs that enables them to be in direct contact with the bacterial cell wall, leading to bacterial cell damage [202]. Finally, the overall findings of the two studies can provide a foundation to promote the use of photosensitizers and natural antimicrobials loaded into hybrid organic-inorganic NPs as alternative strategies against bacterial infections, thus helping to combat bacterial resistance. **Figure 6** illustrates the design of the antimicrobial PCL/Cur/GLE-Ag hybrid NPs.

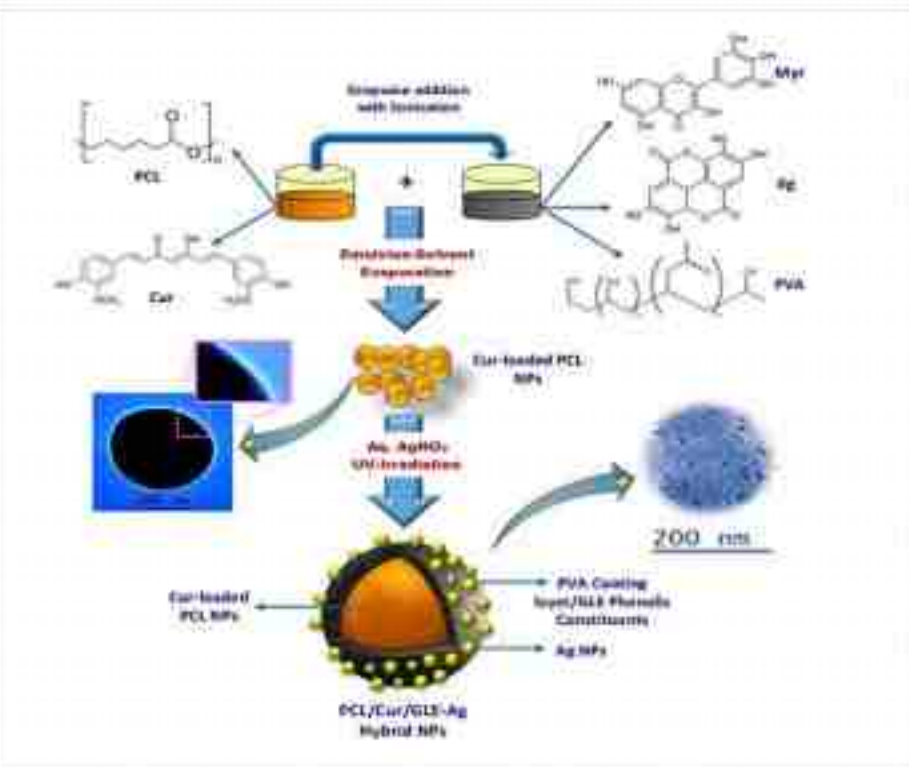

Figure 6: Scheme illustrating the design of antimicrobial PCL/Cur/GLE-Ag hybrid NPs (adapted with permission from [202]).

Overall, organic-inorganic hybrid NPs loaded with various antibacterial agents, such as antibiotics and free radical releasing biomaterials, have been successfully applied to achieve targeted and controlled drug delivery for the effective treatment of gram-positive and gram-negative bacteria, which helps in overcoming antibiotic resistance caused by such pathogens. A summary of organic-inorganic hybrid NPs reported to enhance antibacterial delivery is provided in **Table 3,** highlighting the nanocarrier components; the method of preparation; the loaded antibacterial agent; and the *in vitro* antibacterial assays that have been done for each reported study. So far, the majority of the research has used polymeric NPs as organic materials to formulate various organic-inorganic hybrid nanocarriers for antibacterial delivery, with only one study incorporating liposomes. Therefore, other organic biomaterials such as dendrimers, carbon nanomaterials and polymeric micelles, could also be investigated in the future.

Table 3: Reported organic-inorganic hybrid NPs for enhancing antibacterial delivery

Organic material	Inorganic material	Method of preparation	Loaded antibacterial agent	*In vitro* antibacterial assays	Ref.
PLGA	LAP n-HA HNTs	Electrospinning	Amoxicillin Amoxicillin Tetracycline	- Growth inhibition % in liquid and solid medium	[191-193]
CHT	ZnO NPs	-	Gentamicin	-Qualitative growth inhibition % in planktonic and surface-attached conditions -MICs	[194]
Bacteria toxin-responsive liposomes	MSNs	Co-condensation + thin layer hydration method	Gentamicin	-MICs -Bacterial affinity -Change in bacterial morphology (SEM).	[195]
HA	ZnO NPs	ESE method	Ciprofloxacin	-MICs and MBCs -Time killing assay -Biofilm inhibition -Motility and colony-spreading assay	[196]

CHT	Silica-coated AgNPs	Ion-gelation method	Ciprofloxacin	-MICs and minimal biofilm eradication concentration (MBEC) -Biofilm quantification	[197]
AgNPs-PEI	Cu-MSNs	-	Tetracycline	-CFU Assay -ROS determination -Membrane permeability assay	[198]
PGlu	AgNPs	-	Polymyxin B polymyxin E	- MICs	[199]
Poly peptide	MSNs	Nanoprecipitation method	Azithromycin Methylene blue	-CFU Assay - Biofilm inhibition - Bacterial cell membrane disruption	[200]
CHT/PAA	AuNPs	*In situ* reduction method	Photosensitizer Rose Bengal	-Colony forming unit (CFU) assay -ROS determination -SEM (bacteria-NPs interaction)	[201]
PCL	AgNPs	ESE + photo induced green synthesis	Curcumin Grape leaf extracts	-MICs and growth reduction (IC_{50}) -Minimum bacterial concentration (MBC)	[202]

PLGA, poly D, L-lactic-*co*-glycolic acid; LAP, laponite; n-HA, n-hydroxyapatite; HNTs, halloysite nanotubes; CHT, chitosan; ZnO, zinc oxide; NPs; nanoparticles; MSNs, mesoporous silica NPs; HA, humic acid; AgNPs, silver NPs; CuNPs, copper NPs; PEI, polyethyleneimine; PGlu, polyglutamic acid; AuNPs, gold NPs; PAA, polyallylamine ; PCL, poly ε-caprolactone.

3.3 Metal-organic framework (MOFs)

The advantages of MOFs as potent antimicrobial agents are due to their larger pore size, which allows the storage of antimicrobial molecules; their biocompatibility; and the ability to release antimicrobial metal ions such as Ag^{+}, Au^{+}, Cu^{2+}, Fe^{3+} and Zn^{2+}. Also, the organic linkers used to create the framework may have antimicrobial properties [105]. As a result, the antimicrobial activities of metal ions and linkers could reveal synergistic effects. Therefore, due to their high drug loading capacity and precise drug release, MOFs have been applied as carriers of many active pharmaceutical

substances, including antibiotics [203]. In this section, MOFs comprising various organic linkers such as imidazole, carboxylate and terephthalate linkers are discussed.

3.3.1 Zeolitic imidazole frameworks (ZIFs)

Zeolite imidazole frameworks are a subclass of three-dimensional MOFs that consist of zinc ions (Zn^{2+}) and 2-methylimidazole linkage. These frameworks are considered to be strong pH-responsive nanocarriers that can be used for triggering antibacterial release at the acidic environment of bacterial infections [204]. Among the ZIFs, ZIF-8 crystals have been studied extensively by many research groups. These hybrid NPs were modified and functionalized through direct conjugation or surface coating with various materials to produce a novel nanosystem with synergistic and promising antibacterial effects. In this case, Soomro *et al*. (2019) have encapsulated a natural antimicrobial drug physcion into conventional ZIF-8 crystals using a one-step nanoprecipitation method. The release behavior of physcion from physcion@ZIF-8 NPs was investigated at three pH levels (7.4, 5.4 and 5). The authors observed that, in acidic conditions (pH 5 and 5.4), the release was significantly enhanced as the cumulative drug release was 88.72% and 81.31%, respectively, at the end of 72 hrs. Also, the formulated physcion@ZIF-8 NPs exhibited a maximum growth inhibition activity against gram-positive and gram-negative bacteria strains compared to the pure antimicrobial. Therefore, the findings of this study are promising in improving the antibacterial activity of a natural antimicrobial agent, physcion, against various infections[205].

Also, instead of using conventional ZIFs, direct conjugation of ZIF-8 with a natural polymer has also been done for more effective antibacterial treatment. Zhang *et al.* (2019) developed a modified pH-responsive MOFs/antibiotic system targeting intracellular gram-positive and gram-negative bacteria. They designed a tetracycline-loaded ZIF-8@hyaluronic acid (HA) system (abbreviated as TZH hybrid system) through a simple *in situ* encapsulation approach. Tetracycline showed a faster release profile at pH 5.5 compared to pH 7.4, with approximately 80% and 20% of the drug released from TZH within 3 hrs, respectively. Moreover, the TZH hybrid system demonstrated enhanced and synergistic *in vitro* and *in vivo* antibacterial activity, compared to free tetracycline and free ZIF-8. The overall results suggested that the TZH could be promising for optimizing the efficacy of tetracycline against intracellular bacteria through the combination of a triple effect of HA, ZIF-8 and Zn^{2+} in one drug delivery system, which could result in a potent synergistic antibacterial effect [206].

Furthermore, ZIF-8 nanoparticles have been incorporated into nano-structured polymer scaffolds to deliver different active pharmaceutical ingredients for effective tissue regeneration. For example, Karakeçili and coworkers (2019) used ZIF-8 as a vancomycin carrier to achieve a pH-responsive, controlled drug delivery system. CHT scaffolds loaded with vancomycin-ZIF-8 were prepared by a wet spinning technique to obtain a three-dimensional fiber scaffold to be used as a tissue substitute in

the treatment of bone infections. The swelling behavior and the release profile of the vancomycin-ZIF-8/CHT scaffolds were pH-dependent and exhibited higher effects at pH 5.4 than at pH 7.4, due to the presence of ZIF-8. Also, vancomycin-ZIF-8/CHT scaffolds displayed a stronger antibacterial effect against gram-positive bacteria compared to the free ZIF-8 and CHT scaffolds. This enhanced effect was due to the pH-triggered release of vancomycin, in addition to the combined release of Zn^{2+} from the ZIF-8, which synergize the antibacterial effects of the antibiotic. Besides the enhanced antibacterial properties, the cell culture assay using MC3T3-E1 preosteoblasts showed a high proliferation of osteogenic activity on vancomycin-ZIF-8/CHT scaffolds, confirming the safety and biocompatibility of the prepared hybrid system [207].

Likewise, surface modification is further facilitated by the framework flexibility of ZIF-8. As a result, ZIF-8 crystals can be modified on their surface with magnetic biomaterials to improve the antibacterial efficiency of antibiotics, resulting in a drug with a superior antibacterial effect. A novel MOF was prepared by Esfahanian *et al.* (2019) using ZIF-8 crystals, as they formulated a magnetic framework based on Fe_3O_4-polyacrylic acid (PAA)@ZIF-8 for the delivery of ciprofloxacin. Fe_3O_4 and PAA were added to improve the drug-loading capacity and modify the MOFs for drug delivery. Ciprofloxacin-loaded Fe_3O_4-PAA@ZIF-8 showed a pH-responsive release profile, as rapid degradation of the framework occurred in acidic pH 5, resulting in a faster antibiotic release compared to that at pH 7.4. Furthermore, the antimicrobial activity of ciprofloxacin was enhanced significantly when it was loaded into the modified MOFs compared to the bare drug and Fe_3O_4-PAA@ZIF-8. So, the use of Fe_3O_4-PAA@ZIF-8 as an antibiotic carrier can improve the antibacterial properties of the antibiotics [208].

In another study, Yang *et al*. (2020) developed a novel, carbonized ZIF-8 NP (called C-ZIF) with effective ion releasing properties and photothermal activity for a broad-spectrum antibacterial action. They prepared an AgNPs-doped C-ZIF composite (AgNPs@C-ZIF NPs) with a graphitic-like carbon framework through *in situ* displacement reaction. The formulated AgNPs@C-ZIF NPs were examined for their metal-ion release capability and their photothermal activity. The results revealed that these functionalized MOFs possessed rapid metal-ion release and photothermal conversion properties, which provide the potential of photothermal therapy for synergistic bacterial eradication. Gram-positive and gram-negative bacteria were used as models to investigate the photothermal antibacterial activity of the AgNPs@C-ZIF system. The results illustrated that AgNPs@C-ZIF nanocomposites possess nearly 100% bactericidal ratio against both bacterial strains at extremely low concentrations (0.16 mg/ml). Furthermore, a cytocompatibility study and wound healing evaluation *in vivo* on rabbit skin demonstrated its biosafety and rapid wound healing and disinfection ability. Overall, these novel

carbonized ZIF-8 NPs show high chemical and photothermal antibacterial efficiency and can be applied for broad-spectrum bacterial sterilization [209].

More recently, Xiao and coworkers (2021) exploited the benefits of both ZIF-8 and polydopamine (PDA) to design near infrared (NIR)/pH dual stimuli responsive MOFs for synergistic photothermal/ pharmacological antibacterial therapy. ZIF-8 crystals were used to encapsulate the antibiotic vancomycin first; and then surface modification of the vancomycin/ZIF-8 NPs with PDA was undertaken to improve the structure stability, dispersibility, and biocompatibility of the system. Vancomycin/ZIF-8@PDA displayed an enhanced drug release in response to acidic pH 4.7, compared to the physiological pH 7.4, with a more potent effect under NIR irradiation. The antibacterial activity of the system was examined *in vitro* and *in vivo* against gram-negative strains and a vancomycin-intermediate gram-positive bacteria (called Mu50). All findings indicated that the combination of photothermal/pharmacotherapy of vancomycin/ZIF-8@PDA NPs significantly enhanced the antibacterial activity of vancomycin against both strains, *in vitro* and *in vivo*, and reduced the effective concentration of the antibiotic (MIC was 3.62 μg/ml). This enhanced antibacterial activity resulted in bacterial death and healing of the infected mice's skin. Therefore, a NIR/pH dual stimuli responsive vancomycin/ZIF-8@PDA system could be promising for biomedical application in overcoming antibiotic resistance [210]. **Figure 7** represents a schematic diagram explaining the photothermal/pharmacological therapy of the vancomycin/ZIF-8@PDA system and its *in vivo* application.

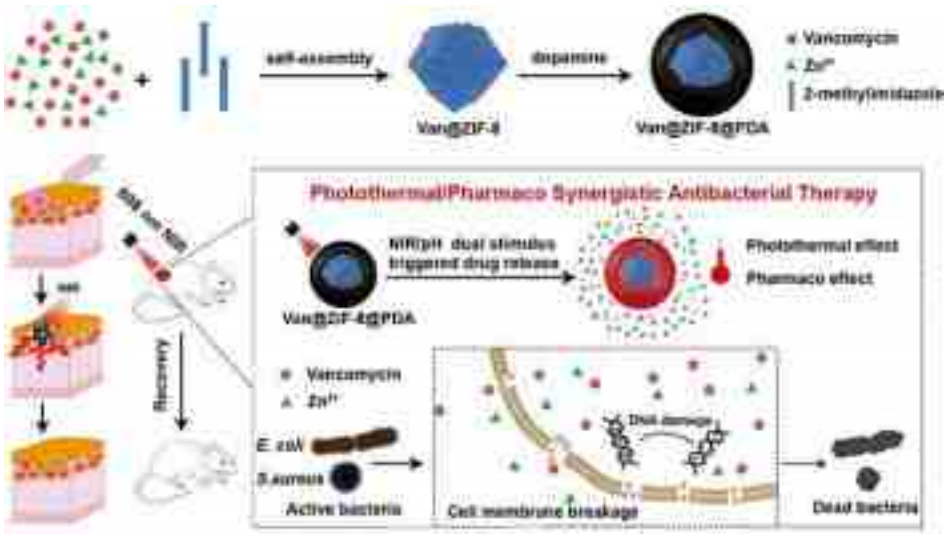

Figure 7: Scheme illustrating the design and the dual stimuli-responsive photothermal/pharmacological therapy of vancomycin/ZIF-8@PDA system and its *in vivo* application (adapted with permission from [210]).

Taken together, the findings of these studies proved the modification and the potential use of ZIF-8 NPs to enhance the delivery and efficacy of various antibacterial agents. Photodynamic antimicrobial therapy (PACT), as a novel strategy, shows potential for treating and overcoming antimicrobial resistance. The application of ZIF-8 hybrid NPs in PACT significantly enhances its antimicrobial activity. In addition, other antimicrobial drugs are being combined with photosensitizers to achieve activity both in dark and in the presence of light. However, as interesting as the ZIF-8 hybrid NPs are, there is a need for additional biocompatibility, stability and *in vivo* antibacterial activity studies, as most reports lack them. It is critical to confirm the biosafety and antibacterial profiles of these modified MOFs in animal experiments, before moving further to clinical application.

3.3.2 Metal-carboxylate frameworks

Metal-carboxylate frameworks are another subclass of MOFs composed of metal ions such as Fe^{3+} and carboxylic acid or carboxylate derivatives. They are among the flexible and highly porous biodegradable and biocompatible MOFs that can adapt their pore diameters during drug adsorption. In addition, these carboxylate-based MOFs exhibit high stability in acidic conditions and, thus, metal-carboxylate frameworks can significantly control the release of drugs, such as antibiotics, under physiological conditions [211].

Three research studies reported the use of carboxylate MOFs for antibacterial drug delivery. Lin *et al*. (2017) designed a carboxylate-iron MOF called MOF-53(Fe) NP as a drug carrier to enhance the antibacterial efficacy of vancomycin against gram-positive bacteria. Vancomycin release from vancomycin-loaded MOF-53(Fe)NPs was sustained with an initial burst release profile at pH 7.4, reaching up to 97% after 36 hrs; while in acidic pH levels of 6.5 and 5.5, vancomycin showed slower release profiles. The authors suggested that the accelerated release rate of vancomycin in neutral pH 7.4 was due to the partial degradation of MOF-53(Fe) NPs; while in acidic conditions, the system showed a smaller degree of degradation, and the release of vancomycin was relatively slow. This property could be beneficial in targeting the local therapy of bacterial infections that require prolonged treatment. Despite the controlled and slower release of vancomycin in an acidic environment, vancomycin-loaded MOF-53(Fe)NPs showed excellent antibacterial activity with a high efficiency of 99.3% [212]. On the other hand, to improve the oral bioavailability and control the release of gentamicin, Unamuno and coworkers (2018) formulated and optimized a gentamicin-loaded (Fe)-carboxylate MOF (gentamicin@MIL-100(Fe)NPs) through a simple impregnation method. *In vitro* drug release studies for gentamicin were conducted using different oral and intravenous simulated physiological conditions. The results indicated that gentamicin-loaded MIL-100(Fe) NPs exhibited superior colloidal, chemical and structural stability under gastrointestinal conditions, with good biocompatibility and enhanced delivery of the antibiotic under intestinal conditions, making

these MOFs highly promising for the oral administration of gentamicin. Furthermore, the *in vitro* antibacterial activity of gentamicin@MIL-100(Fe) NPs was investigated against different strains of gram-positive and gram-negative bacteria, and the results showed that the loaded MOFs exhibited the same antibacterial activity as free gentamicin, confirming that the antimicrobial activity of the antibiotic was maintained after its encapsulation into MIL-100(Fe) NPs [213].

Furthermore, carboxylate MOFs have been modified via saccharide coating to promote their surface contact with bacterial cells. Recently, Haseena *et al*. (2022) designed and evaluated a novel mannose (MNS)-coated Fe-MIL-88NH_2 NPs loaded with vancomycin to improve its efficacy against *S. aureus* and MRSA. The prepared MNS-coated/vancomycin@MOFs exhibited superior antibacterial activity than the un-coated nanocarriers against all gram-positive strains, confirmed by lower MIC values. This improved antibacterial effect could be due to the interaction of MNS coating with lectins on the cell wall of gram-positive bacteria, which ultimately promotes the cellular penetration and increase the bactericidal potential of vancomycin against both susceptible and resistant bacteria. In addition, atomic force microscope (AFM) investigation of all *S. aureus* strains showed total morphological damage upon treatment with MNS-coated/vancomycin@MOFs. Overall, this study suggested that coating of MOFs with MNS could be an effective technique to enhance the bactericidal activity of vancomycin and hence, improve the antibiotic therapy against MDR-associated diseases. [214].

In summary, the previous studies reported the use of carboxylate-iron MOFs to improve the antibacterial efficacy of various classes of antibiotics. Vancomycin revealed a controlled release profile with more enhanced antibacterial effects in the first experiment [212], whereas its killing efficacy against MDR strains was improved significantly with complete bacterial cell damage when loaded into MNS-coated carboxylate MOFs [214] Also, the bioavailability and the oral antibacterial activity of gentamicin could be maintained when encapsulated into carboxylate-iron MOFs [213]. Therefore, to confirm the *in vitro* findings and the applicability of such promising MOFs, stability studies and *in vivo* antibacterial studies for the formulated carboxylate-iron MOFs are required

3.3.3. Metal-terephthalate frameworks

Another generation of MOFs are metal-terephthalate frameworks which contain metal ions such as Zn^{2+}, Cu^{2+}, Ti^{4+}, and others with terephthalic acid or terephthalate derivatives. These MOFs are characterized by their photocatalytic activity when exposed to UV-Vis irradiation [215]. In this regard, three emerging studies reported the use of metal-terephthalate frameworks for treatment of bacterial infections. The first report was by Bhardwaj *et al.* (2018), who investigated the antimicrobial efficiency of three Zn-terephthalate frameworks called IRMOF-3, MOF-5, and Zn-BTC alone, and in combination with ampicillin and kanamycin. Antibacterial activity assessment showed that all

antibiotic-loaded Zn-terephthalate frameworks exhibited superior antimicrobial activity, indicated by lower MIC values against gram-positive and gram-negative strains, compared to the free antibiotics and free MOFs, with synergistic (for kanamycin-loaded IRMOF-3) and additive (for other antibiotic-loaded MOFs) interactions [216]. However, to confirm these *in vitro* antibacterial findings and the potential use of these metal-terephthalate frameworks, additional characterization, including stability studies, *in vitro* drug and metal ions release studies from the MOFs in different physiological environments and *in vivo* antibacterial studies, are also essential.

Metal-terephthalate frameworks have also been explored for the design of antibacterial surface coatings, since bacterial adhesion and growth remain a concern in the design of various medical and surgical devices. Taking this different approach, Arenas-Vivo and coworkers (2019) developed a novel silver NP-loaded photoactive titanium (IV) aminoterephthalate framework (AgNPs@ MIL-125(Ti)NH_2 MOFs) as an antifouling and bactericidal surface coating to act against bacterial biofilm. Silver nanoparticles were efficiently entrapped into the MIL-125 (Ti) MOFs using the impregnation-reduction method. The antibacterial activity investigation indicated that the bactericidal effects of MIL-125(Ti) NPs were significantly enhanced after encapsulation of AgNPs, compared to free AgNPs, MIL-125(Ti)NH2 MOFs, and a physical mixture of both AgNPs and MOFs. This bactericidal activity of the nanocomposite film, in addition to their ability to detach the bacterial biofilm, was further promoted when the hybrid film received UVA irradiation for 2 hrs [217]. Therefore, the promising results of this study can be applied with different antimicrobial agents to prove the potential of this film nanocomposite as a surface coating for biofilm treatment on high-touch surfaces such as surgical devices.

Moreover, MOFs have been proposed as a promising candidate for encapsulating a variety of biomolecules as a biomimetic strategy to combat bacterial infections. Generally, biomimetic strategies have been explored for the development of nano delivery systems, with the goal of either mimicking cellular communication signal pathways or utilizing the activity path of biological structures in living organisms to achieve several advantages, such as biocompatibility and targeting characteristics [88]. Nowadays, this strategy shows the potential for encapsulating nanoparticles/biomolecules into MOFs to construct antibacterial nanosystems with synergistic activity. In a recent study, novel biomimetic multienzyme MOFs with Fenton-like catalytic activity were designed by Cheng *et al.* (2020) to acquire synergistic antibacterial activity against both gram-positive and gram-negative strains. Glucose oxidase (GO_χ) and L-arginine ($_L$-Arg) were simultaneously entrapped within Cu-MOFs (called Cu-BDC) through a biomimetic mineralization growth technique on an enzyme surface. The preparation technique resulted in uniform distribution of the biomolecules (GO_χ and $_L$-Arg) within the Cu-BDC pores, which enhanced the synergistic bactericidal activity by spontaneously activating the

double cascade reaction of ROS and reactive nitrogen species (RNS). The *in vitro* antibacterial activity studies indicated that the bacterial viability of both gram-negative and gram-positive bacteria were significantly reduced when treated with GO_{χ} / $_{L}$-Arg@ Cu-BDC hybrid composite with inactivation rates of 98 % and 97 % for *E. coli* and *S. aureus*, respectively. This was due to the biomimetic structure of the hybrid composite and the synergistic antibacterial activity of GO_{χ}, $_{L}$-Arg and Cu-BDC. In addition, an *in vivo* study was carried out in mice models to confirm the cytocompatibility of the formulated hybrid MOFs and the results revealed that the prepared GO_{χ} / $_{L}$-Arg@ Cu-BDC hybrid composite has good biocompatibility, indicating the *in vivo* potential of such biomimetic multienzyme hybrid MOFs [218]. **Figure 8** represents a schematic diagram of the biomimetic mineralization synthesis process for GO_{χ} / $_{L}$-Arg@ Cu-BDC hybrid NPs and their antibacterial mechanism.

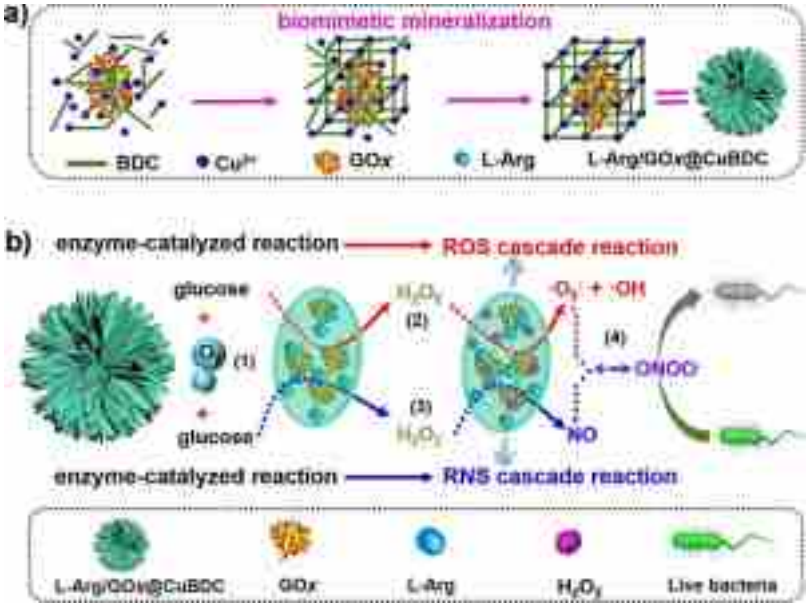

Figure 8: Scheme represents (**a**) the biomimetic mineralization synthesis process for GO_{χ} / $_{L}$-Arg@ Cu-BDC hybrid NPs; and (**b**) the self-activated double-cascade reaction mechanism for enhanced synergistic bactericidal activity (adapted with permission from [218]).

3.3.4 MOFs using other metal ions and organic linkers

In addition to the above-mentioned linkers, some other MOFs that contain different metal ions and linkers can be used as nanocarriers for antibacterial application. André and his coworker (2019) developed a novel BioMOF that consisted of antibiotic nalidixic acid as an organic linker and magnesium (Mg) and manganese (Mn) as metal ions. The system showed improved antimicrobial activity against both gram-positive and gram-negative strains compared to free nalidixic acid, with more efficacy reported against gram-negative bacteria. A significant bacterial growth inhibition effect

was observed with bactericidal action when it was treated with Mg-MOFs, while Mn-MOFs exhibited bacteriostatic actions. However, *in vivo* studies are needed to support the *in vitro* antibacterial activity findings [219].

More recently, Wei's group (2021) designed a γ-cyclodextrin-based MOF using γ-cyclodextrin as an organic ligand co-ordinated with potassium ions to encapsulate the antibiotics, enrofloxacin and florfenicol. The antibiotics were primarily adsorbed into the pores of the γ-cyclodextrin-MOF structure via an impregnation method to achieve small NPs and to improve the stability of the formulated antibiotics@γ-cyclodextrin-MOFs. The formulated MOFs displayed continuous sustained release behavior over a period of 4 hrs at physiological pH 7.4, and the cumulative amount released was 79.85% and 87.50% for florfenicol and enrofloxacin, respectively. The *in vitro* and *in vivo* antibacterial activity results confirmed that the antibiotic loaded γ-cyclodextrin-MOF NPs showed higher and longer inhibition efficacy against gram-positive and gram-negative bacteria, compared to free antibiotics with lower MIC values, and a 90% inhibition rate for both antibacterial agents. Therefore, this study indicated that antibiotics@γ-cyclodextrin-MOF could be an effective, biocompatible carrier for antibiotic therapy with a controlled release profile [220].

Altogether, the outcomes of the abovementioned studies confirm the prospective use of MOFs as promising nanocarriers for the treatment of bacterial infections, and they can be successfully applied to enhance the antibacterial efficacy of antibiotics, thus helping in overcoming resistance. **Table 4** summarizes all the MOFs reported in this review. It provides comprehensive information such as metal ions; loaded antibacterial agent (s); bacteria species; the mechanism of antibacterial actions; and the mode of antibacterial investigation.

Table 4: Summary of the reported MOFs and their antibacterial mechanisms.

MOF	Antibacterial agent	Targeted bacteria	Mechanism of the antibacterial actions	Mode of study	Ref.
ZIF-8	Physcion	*S. aureus* *E. coli* *P. putida*	Binding to cell membrane's protein leading to membrane destruction.	*In vitro*	[205]
ZIF-8/HA	Tetracycline	*S. aureus* *Salmonella*	Binding to CD_{44} antigen receptor by the aid of HA and kill the bacteria intracellularly.	*In vivo*	[206]
ZIF-8/CHT	Vancomycin	*S. aureus*	Inhibition of biofilm formation and affecting the morphology of the bacteria.	*In vitro*	[207]
ZIF-8/Fe_3O_4-PAA	Ciprofloxacin	*S. aureus* *E. coli*	Damage of bacterial cell wall.	*In vitro*	[208]
C-ZIF	AgNPs	*S. aureus* *E. coli*	Release of Ag^+ and irradiation heat destroyed the bacterial cell membrane.	*In vivo*	[209]
ZIF-8/PDA	Vancomycin	*E. coli* *VM- intermediate S. aureus* (Mu50)	Nucleic acid degradation, biofilm inhibition and cell membrane damage.	*In vivo*	[210]
MOF-53 (Fe)	Vancomycin	*S. aureus*	Inhibition of bacterial cell wall synthesis	*In vitro*	[211]
MIL-100(Fe) UiO-66(Zr)	Gentamicin	*S. aureus* *S. epidermidis* *P. aeruginosa*	Not reported	*In vitro*	[212]
MNS-coated/Fe-MIL-88NH_2	Vancomycin	*S. aureus* MRSA	Damage of bacterial cell wall.	*In vitro*	[214]
IRMOF-3 MOF-5 Zn-BTC	Ampicillin Kanamycin	*S. aureus* *S. lentus* *L. monocytogenes* *E. coli*	Sustained release of Zn^{+2} and inhibition of the enzymes and proteins involved in cell wall production which resulted in membrane injury.	*In vitro*	[213]
MIL-125(Ti)	AgNPs	*S. aureus*	Biofilm inhibition and generation of ROS.	*In vitro*	[217]

Cu-BDC	Glucose oxidase and L-arginine	*S. aureus* *E. coli*	Change of bacterial morphology due to the release of free radicals through a double cascade reaction.	*In vivo*	[218]
BioMOFs	Nalidixic acid	*S. aureus* *E. faecalis* *P. aeruginosa* *E. coli*	Not reported	*In vitro*	[219]
γ-cyclodextrin-MOF	Enrofloxacin florfenicol	*S. aureus* *E. coli*	Not reported	*In vivo*	[220]

MOF, metal organic framework; HA, hyaluronic acid; CHT, chitosan; PAA, poly allylamine; PDA, poly dopamine; MNS, mannose; MRSA, methicillin resistant *S. aureus.*

3.4 Cell membrane-coated hybrid NPs (CMCH-NPs)

Coating of NPs with extracted cell membranes is one of the strategies that has been used to improve the pharmacokinetic parameters of various drugs, including antibiotics, which makes CMCH-NPs attractive candidates for targeted and sustained antibacterial drug delivery [152]. In this field, red blood cell membrane-coated hybrid NPs (RBCM/CH-NPs) and CMCH-NPs using other extracted cell membranes, such as gastric epithelial cells, bacterial cell membranes and neutrophils, and their applications in antibacterial delivery are discussed.

Several nanosystems have been modified by coating them with red blood cell membranes (RBCM) to enhance the delivery of antibiotics within the body, reducing its clearance by the immune system and enhancing its blood circulation time [2], which improves the pharmacokinetic properties of the antibiotic nanocarrier. In this regard, three research studies have been reported by Li *et al.* (2014), Lin *et al*. (2019) and Kamal *et al.* (2022) for combating MDR bacteria. They developed a core-shell gelatin NP (GNP) decorated on their surface with RBCM for adaptive and 'on-demand' antibiotic delivery. All hybrid nanosystems were designed for gelatinase-triggered release of antibiotics at the infection site, and the results indicated that the release of all loaded antibacterials was gelatinase concentration/time-dependent, as they showed a higher release profile in the presence of gelatinase and gelatinase-positive bacteria. The authors suggested that the coating of GNPs with RBCM improved their stability and cytocompatibility and enhanced their antihaemolytic activity against bacterial toxins. Li and coworkers (2014) designed vancomycin-loaded RBCM-coated supramolecular GNPs (vancomycin-loaded SGNPs-RBCM) using the desolvation method. The antibacterial activity of the prepared vancomycin-loaded hybrid NPs was examined *in vitro,* and the results revealed higher activity against gelatinase-positive strains, including *S. aureus*, *P. vulgaris* and *P. aeruginosa*, with lower MIC values compared to free vancomycin. This enhanced activity was due to the degradation of gelatin in response to the gelatinase enzyme that is overexpressed in the infection site, which resulted in vancomycin release and bacterial death [221]. Thereafter, Lin *et al*. (2019) developed ruthenium (Ru)-complexes functionalized selenium (Se) NPs loaded into RBCM-GNPs (Ru−Se@GNP-RBCM) for the *in situ* detection and inhibition of MDR bacteria. *In vitro* investigations of the antibacterial activity of the system showed that the Ru−Se@GNP-RBCM had a strong antibacterial effect on MRSA, as the survival rates of the bacteria decreased significantly, indicating a good synergistic antibacterial effect against gelatinase-positive strains. Moreover, an *in vivo* assessment of MRSA-infected mouse models was performed for the evaluation of wound healing ability, and the overall findings confirmed that the prepared Ru−Se@GNP-RBCM could be used to detect bacterial infection *in vivo* and improve the healing of MRSA-infected wounds [222].

More recently, Kamal and co-workers (2022) developed a unique RBCM-coated supramolecular GNPs loaded with vancomycin and chlorogenic acid for combined antibacterial and antibiofilm activity against MRSA infection, both *in vitro* and *in vivo*. The prepared biomimetic hybrid NPs were able to evade the immune system and greatly prolong their systemic circulation for the responsive and sustained release of vancomycin/chlorogenic. The successful *in vitro* time-concentration dependent antibacterial and antibiofilm effects were validated through *in vivo* studies using leg- and skin-infected mice models. Synergistic antibacterial activities of vancomycin and chlorogenic acid in response to the microenvironment of MRSA infection were confirmed by the total eradication of bacteria, as well as the healing of inflammation and wounds. Therefore, these smart on-demand antibiotic delivery platform could be promising in future nanotechnology to treat resistant infectious pathogens [223].

Compared to the first study published by Li [221], both Lin *et al*. (2019) and Kamal *et al.* (2022) reached the *in vivo* stage in their studies, thereby building a solid *in vitro-in vivo* correlation [222, 223]; while Li *et al.* (2014) did not investigate the *in vivo* activity, which is crucial in considering such nanosystems for clinical trials. In summary, the promising results of all reported studies indicated that RBCM-coated GNPs loaded with various antibacterial agents could be used as an alternative to antibiotics for combating MDR bacterial infection. **Figure 9** demonstrated the preparation method of vancomycin/chlorogenic acid-loaded RBCM-coated supramolecular GNPs, and the mechanism of combating MRSA infection in mice models by means of prolonged circulation time, immune escaping ability and responsive on-demand antibiotic delivery.

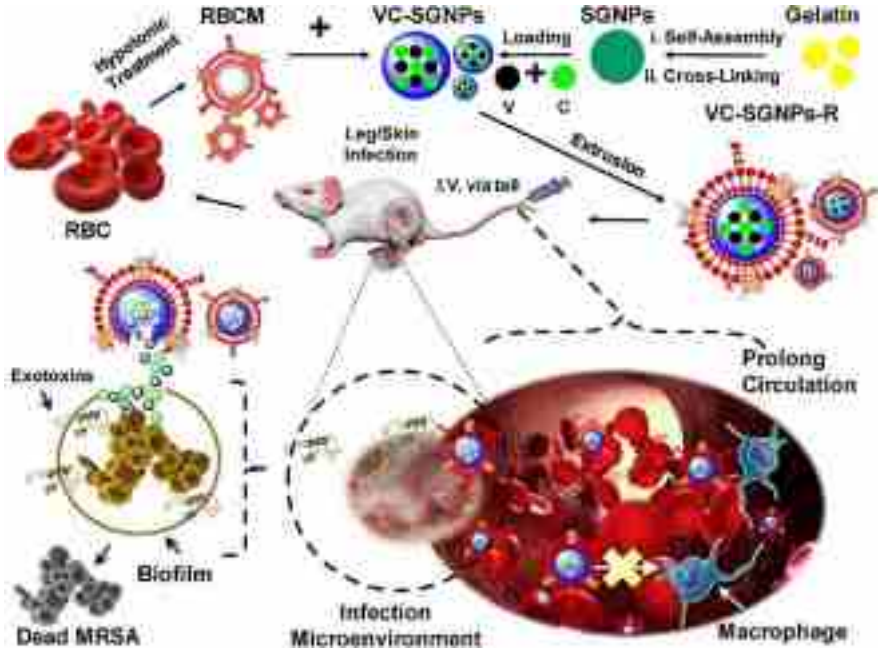

Figure 9: Scheme illustrating the preparation method of vancomycin/chlorogenic acid-loaded RBCM-coated supramolecular GNPs, and their synergistic and infection microenvironment-responsive antibacterial and antibiofilm effectiveness mechanisms to eradicate MRSA infection in mice model (adapted with permission from [223]).

Using the same coating strategy, a cell membrane-coated nanogel system composed of a redox-responsive nanogel core and RBCM shell was reported by Zhang *et al.* (2017) for vancomycin delivery to combat intracellular MRSA. The vancomycin-loaded nanogel core was crosslinked with disulfide bonds to be cleaved in response to the intracellular reducing environment for the on-site release of vancomycin, while the *in situ* gelation method was used to coat the surface of vancomycin-loaded nanogel with RBCM. The RBCM-coated nanogel effectively neutralized MRSA α-toxin, which in turn enhanced the intracellular bacterial uptake. Vancomycin release from the RBCM-nanogels in the presence of reducing agents was significantly increased, reaching a cumulative release of about 95% in 24 hrs, confirming the responsiveness of the system to the intracellular reducing environment. Additionally, the *in vitro* antibacterial activity study revealed that the RBCM-coated/vancomycin-nanogel exhibited improved antibacterial activity against intracellular MRSA with an MIC value of 2.5 μg/ml, while the non-coated vancomycin-loaded nanogel showed less anti-MRSA activity with an MIC value of 5 μg/ml, compared to free vancomycin. These findings suggest that the redox-responsive RBCM-coated nanogel system could be promising for treating intracellular MRSA infection [224].

Finally, in 2021, Wu *et al.* used a simple ultrasound method to prepare RBCM-coated tedizolid phosphate (TR-701)-loaded PLGA NPs (TR-701-PLGA@RBCM NPs) for treating methicillin-sensitive *S. aureus* (MSSA) and MRSA wound infections. The formulated hybrid biomimetic system was evaluated for its *in vitro* and *in vivo* biocompatibility, toxin adsorption capability and antibacterial efficiency. The results showed that TR-701-PLGA@RBCM NPs were safe and highly biocompatible, with significant exotoxin neutralizing ability. The *in vitro* antibacterial activity study indicated that the antibacterial activity of the prepared hybrid system was equivalent to free TR-701 against both MRSA and MSSA. Moreover, the healing rate of the MRSA-infected wound was improved significantly when treated with TR-701-PLGA@RBCM NP, due to its improved growth inhibition of MRSA in the mice skin wound, compared to free TR-701. Accordingly, TR-701-PLGA@RBCM NPs could be promising in treating MRSA-infected wounds due to their high stability, biocompatibility and enhanced antibacterial efficacy *in vitro* and *in vivo* [225]. **Figure 10** presents a schematic illustration of the preparation and application of TR-701-PLGA@RBCM NPs in treating MRSA-wound infection.

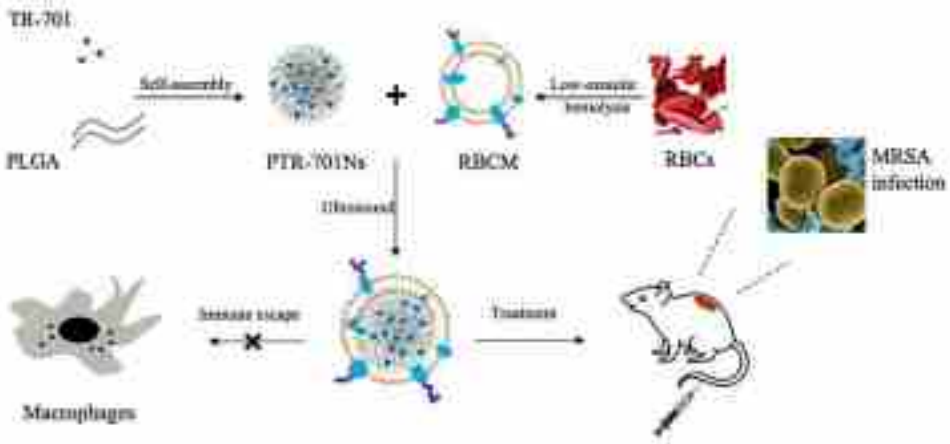

Figure 10: Scheme representing the preparation and application of TR-701-PLGA@RBCM NPs in treating MRSA-wound infection (adapted with permission from [225]).

The coating of NPs with extracted cell membranes can be used also as a pathogen-host adhesion strategy for active targeting of various antibiotics to enhance the drug localization, reduce side effects, and improve their therapeutic effectiveness [226]. Two research studies have reported the coating of PLGA NPs with extracted cell membranes for active targeting and improving antibiotic delivery and localization at the site of infection. A membrane derived from gastric epithelial cells (called AGS cells) has been successfully applied by Angsantikul *et al.* (2018) to enhance the delivery and active bacterial targeting of

clarithromycin. They prepared AGS coated-clarithromycin-loaded PLGA NPs (clarithromycin-PLGA@AGS NPs) to treat *H. pylori* infection. The prepared biomimetic hybrid NPs exhibited enhanced bacterial adhesion with prolonged and controlled antibiotic release, which improved the therapeutic efficacy of clarithromycin. The antibacterial activity of clarithromycin-PLGA@AGS NPs was studied *in vitro* and *in vivo*, and the results indicated that the system had superior *in vitro* antibacterial activity against *H. pylori*, compared with free antibiotic and clarithromycin-loaded PLGA NPs. In addition, the NPs were able to reduce the *H. pylori* burden effectively in an infected mouse model. Therefore, coating of clarithromycin-loaded polymeric NPs with a membrane derived from gastric epithelial cells could be a useful and safe approach for effective, targeted antibiotic delivery to treat *H. pylori* infection. Also, this bacteria-host adhesion approach can be applied to treat other bacterial infections [227]. Continuing the research into the coating of PLGA NPs with extracted cell membranes, Gao and coworkers (2018) used PLGA NPs coated with a membrane of extracellular vesicles (EV) secreted by *S. aureus* (PLGA NPs@EV) as an active targeting carrier to eliminate bacterial infections caused by intracellular *S. aureus*. The prepared PLGA NPs@EV were internalized by *S. aureus*-infected macrophages *in vitro,* with better efficiency compared to PLGA NPs coated with liposomes and *E. coli* outer membrane vesicles, respectively. In addition, the hybrid NPs were loaded with vancomycin and rifampicin and were injected intravenously to intracellular *S. aureus*-infected mouse models. The antibiotic-loaded PLGA NPs@EV exhibited significantly enhanced antibacterial activity as they reduced the pathogen burdens in major organs, especially in the kidneys and lungs. The overall findings of this study suggested that EV-coated hybrid NPs can improve the therapeutic efficiency of loaded antibiotics by providing them with an active targeting capacity, both *in vitro* and *in vivo* [228].

In addition to the previous biological coating materials, the most recent study of CMCH-NPs for the treatment of bacterial infections and inflammation was reported by Wang *et al*. (2020). In this study, PCL-PEG NPs were coated with neutrophil membrane and then loaded with sparfloxacin for specific targeting to inflammatory sites. The prepared neutrophil-coated hybrid NPs demonstrated good biocompatibility, controlled drug release profiles and targeted delivery to pulmonary sites of inflammation. Also, the hybrid NPs showed significantly higher antibacterial activity against MRSA, confirmed by larger zones of inhibition when compared to free antibiotic and PLC-PEG NPs. Finally, the *in vivo* study findings indicated that these neutrophil-coated hybrid NPs could efficiently treat lung inflammation in the mouse pneumonia model [229].

Taken together, the studies discussed in this subsection have confirmed the potential use of CMCH-NPs as biomimetic antibiotic nanocarriers for the effective treatment of bacterial infections. Functionalization of such hybrid nanosystems combines nanotechnology with biomimetic strategies and takes the advantages of biological cell membranes to develop nature-inspired nanomedicines for targeted antibiotic delivery.

3.5 Hybrid NP-hydrogels

In recent years, hybrid NP-hydrogels have garnered more attention as antibacterial drug delivery carriers due to their unique advantages, such as self-healing abilities; injectability; tissue adhesiveness; high drug loading capacity; controlled drug release; and superior biocompatibility. Hybrid NP-hydrogels loaded with different antibiotics can be used for local antibacterial delivery to the site of infection, thereby reducing the development of antibiotic resistance. They can be applied to treat different infectious diseases, including skin wounds and bone infections [230]. Herein, hybrid NP-hydrogels based on the types of the combined NPs are discussed.

3.5.1 Hybrid metal and metal oxide NP-hydrogels

A variety of metal/metal oxide NPs such as AgNPs, AuNPs, CuO NPs and ZnO NPs have been incorporated into hydrogels to form hybrid systems applied in the treatment of bacterial infections. These NPs combined with hydrogels can be used for the controlled release of antibacterial metal ions or encapsulated antibiotics. In this regard, Sattari *et al.* (2018) incorporated Ag, CuO and ZnO NPs into a polyaspartic acid/graphene nanosheets@polyacrylamide-co-acrylic acid hydrogel for pH-responsive and controlled release of a loaded drug, curcumin. The release profile of curcumin from the prepared hybrid NP-hydrogels was sustained and pH-dependent as it showed more drug release at pH 7.4 than at pH 2.1, due to the increased electrostatic repulsion and hydrogel swelling. Hybrid curcumin-loaded AgNP-hydrogel exhibited more curcumin release compared to the hybrid metal oxide-hydrogels. In addition, the prepared curcumin-loaded hybrid hydrogels exhibited enhanced antibacterial activity against *E. coli* and *S. aureus*, compared to the bare curcumin, with the AgNP-hydrogel proving the most successful. This improved antibacterial activity was due to the enhanced curcumin release and more synergistic antibacterial effects of AgNPs, compared to hydrogel embedded with CuO and ZnO NPs. As a result, the prepared metal/metal oxide NP-hydrogel could be useful for wound healing and dressing applications [231]. However, biocompatibility and *in vivo* studies are crucial in motivating such a use.

In addition, hybrid metal NP-hydrogels can be used as an alternative strategy for combined local antibacterial/photothermal therapy. Tao and co-workers (2019) prepared an NP-hydrogel hybrid system

composed of methacrylate modified gelatin (Gel-MA) combined with N, N-bis(acryloyl) cystamine-chelated CuNPs (BACA/Cu NPs) via a radical polymerization technique. The formulated BACA/Cu NPs@Gel-MA was able to convert NIR laser irradiation energy into localized heat for antibacterial photothermal therapy. *In vitro* antibacterial studies indicated that the hybrid hydrogel exhibited superior antibacterial efficacy against both *S. aureus* and *E. coli,* with biofilm inhibition capability. This enhanced antibacterial activity derived from the synergistic effect of photothermal activity and the rapid release Cu^{2+} and ROS under laser irradiation of CuNPs (as shown in **Figure 11**). Moreover, the wound-healing process of an *S. aureus*- infected mice model was significantly accelerated by enhancing neovascularization with a reduced inflammatory response *in vivo*. Overall, the biocompatible CuNPs-hydrogel hybrid system is a promising candidate in photothermal therapy for wound healing applications and skin tissue regeneration [232].

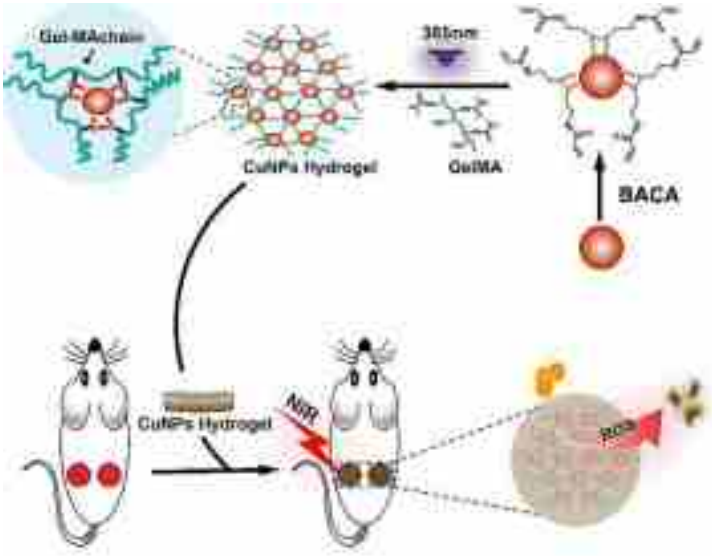

Figure 11: Scheme illustrating the preparation of BACA/Cu NPs@Gel-MA hybrid hydrogel and the synergistic antibacterial photothermal therapy via the generation of ROS under NIR irradiation (adapted with permission from [232]).

Likewise, Lin *et al.* (2020) employed the same synergistic antibacterial photothermal therapy to treat periodontal infections. The research team designed a NIR-activated hybrid hydrogel system, composed of Gel-MA with mesoporous silica-coated AuNPs (SiO_2/AuNPs), to achieve a sustained antibiotic release. The prepared hybrid hydrogel exhibited a controlled release profile of the loaded drug minocycline at pH 7.4, with an increased release rate under NIR light irradiation. This controlled release assisted in improving the antibacterial activity of the system against *Porphyromonas gingivalis* (*P. gingivalis*), as the

prepared SiO_2/AuNP-hydrogel showed enhanced antibacterial efficacy (~90 %) under NIR irradiation, with rapidly eliminated pathogens in the periodontal pocket. In addition, cytotoxicity studies confirmed the cytocompatibility of the formulated hybrid hydrogels [233]. Therefore, the NPs-Gel-MA hybrid hydrogels developed in the two previous studies with synergistic antibiotic release and photothermal therapy show promise for the prolonged treatment of local skin wound infections and periodontal diseases.

3.5.2 Hybrid polymeric NP-hydrogels

Various polymeric NPs embedded in hydrogels, such as PLGA and PCL, have been investigated for controlled and sustained antibiotic release to improve targeted and localized antibacterial drug delivery. Posadowska *et al.* (2016) designed an injectable hybrid hydrogel system composed of vancomycin-loaded PLGA NPs combined with gellan gum (GG) for local treatment of osteomyelitis. Vancomycin was loaded successfully into both polymeric NPs and within the gel matrix and, as a result, the system exhibited a biphasic release profile: an initial burst release at day ten, followed by a sustained prolonged release for up to 40 days. Also, the vancomycin-PLGA NPs@GG hydrogel system showed cytocompatibility with osteoblast-like cells and more enhanced antibacterial activity against osteomyelitis-causing *S. aureus* than bare vancomycin, vancomycin-loaded PLGA NPs, and vancomycin-loaded GG hydrogel, confirmed by a zone of inhibition [160]. Later in the same year, the same research group prepared a hybrid PLGA NPs@GG hydrogel injectable system loaded with gentamicin (2016). The results were comparable with the previous study, as the gentamicin-loaded hydrogel system demonstrated a controlled release profile for up to 90 days and the *in vitro* studies confirmed the antibacterial activity and the cytocompatibility of the prepared hybrid hydrogel system [234]. Hence, the developed hybrid, antibiotic-loaded, polymeric NP-hydrogels displayed good injectability, self-healing ability, adjustable drug release and enhanced antibacterial efficacy, revealing their potential for localized treatment of bone infections. However, both studies required *in vivo* investigations to be applied clinically.

To further improve the performance and activity of hybrid NP-hydrogels at the infection sites, bioadhesive materials can be included into the hydrogel network to form a bioadhesive delivery system. These bioadhesive nanogels combine the extensive swelling ability of the hydrogel with its bioadhesion properties [235]. As a result, they can efficiently adhere to the infected tissue surface and deliver antibiotics locally. In two other studies, Zhang *et al.* (2016) and Salatin *et al.* (2020) reported the design of bioadhesive hybrid NP-hydrogels for localized and sustained topical drug delivery. Zhang and coworkers (2016) constructed a bio-adhesive hybrid PLGA NP-dopamine methacrylamide (DMA) hydrogel to enhance the local delivery of ciprofloxacin under high shear force conditions. Ciprofloxacin

was loaded into PLGA NPs and then combined into a tissue adhesive DMA hydrogel. The prepared hybrid system showed enhanced adhesion and antibiotic retention under high shear stress on bacterial biofilm, mammalian cells, and mouse skin tissue, allowing for a gradual release of ciprofloxacin from the PLGA NP-DMA hydrogel, which continued for up to seven days. In addition, the system effectively inhibited the formation of *E. coli* bacterial biofilm under *in vitro* flow conditions with more enhanced antibacterial activity, compared to the free ciprofloxacin and ciprofloxacin-loaded PLGA NPs. Moreover, the NP-hydrogel was safe and cytocompatible within seven days of treatment on a mouse skin model [236]. On the other hand, Salatin *et al.* (2020) developed a thermosensitive and bio-adhesive cephalexin-loaded PCL NPs@ pluronic F-127(PF-127)/CHT hydrogel for topical antibacterial delivery. The formulated system had good viscosity, suitable spreadability and bioadhesion with an *in situ* thermogelling-forming ability at body temperature. The *in vitro* antibacterial activity results indicated that the drug-loaded NP-hydrogel had superior antibacterial efficacy against *S. aureus*, confirmed by the reduced MIC values when compared to the free drug and the drug-loaded CHT hydrogel. Similarly, the hybrid NP-hydrogel exhibited an enhanced antibacterial activity after six days of treatment on an infected rat skin [162]. Overall, the developed bioadhesive hybrid polymeric NP-hydrogels reported in these two studies can potentially be applied for prolonged and localized delivery of antibiotics to treat various bacterial infections and overcome antibiotic resistance.

3.5.3 Hybrid vesicular NP-hydrogels

Aside from metal/metal oxide and polymeric NPs, numerous vesicular NPs, such as liposomes and nanotransfersomes (NTs), were combined with hydrogels to generate a hybrid hydrogel system with high stability and a controlled release profile [237]. This strategy has also been applied to enhance the antibacterial activity of antibiotics for localized antibacterial delivery. In this case, two research studies have also reported the use of bio-adhesive and/or thermosensitive hybrid vesicular NP-hydrogels for topical delivery of antibiotics to treat skin infections. Gao *et al.* (2014) designed a pH-responsive carboxyl-modified AuNP (C-AuNPs)-stabilized liposomes@polyacrylamide hydrogel for topical antimicrobial delivery. The formulated hybrid hydrogel system maintained the structural integrity of the stabilized liposomes, allowing for controlled release kinetics of the C-AuNPs-liposome. The released stabilized liposomes could fuse with the membrane of *S. aureus* in response to the skin infection environment (pH 4.5), resulting in an enhanced and prolonged bacterial inhibition activity of Au^{+}, confirmed by the liposome-bacterium fusion assay. Finally, a mouse skin model was used to evaluate the toxicity of the prepared C-AuNPs-liposome@hydrogel, and the results confirmed the compatibility of the system within seven days of treatment [238]. A more recent study reporting the use of hybrid vesicular

NP-hydrogels was conducted by Salatin and coworkers (2020), who developed and optimized a thermosensitive and bio-adhesive hybrid NT-CHT hydrogel to enhance the skin bioavailability and the antibacterial activity of cephalexin. The findings were comparable to their previous research study which used polymeric NP-hydrogel [162]. As the optimized hybrid, NT-CHT hydrogel improved cephalexin penetration through the skin pores after eight hours of treatment, and exhibited more enhanced *in vitro* antibacterial activity against *S. aureus* compared to the bare drug, and confirmed by MIC. In addition, the system was cytocompatible and showed superior antibacterial activity when applied to the rat skin for ten days [239]. Therefore, the overall results proved the potential application of the hybrid vesicular NP-hydrogels for prolonged and localized transdermal delivery of antibiotics.

In summary, hybrid NP-hydrogel systems could be an alternative, promising strategy for local antibacterial drug delivery due to their ability to reduce bacterial infections in a controlled manner, decrease side effects, combat bacterial resistance, and improve patient compliance. A summary of the reported hybrid NP-hydrogels for localized antibacterial delivery is provided in **Table 5,** highlighting the advantages and application of such hybrid NP-hydrogels.

Table 5: Hybrid NP-hydrogels for localized antibacterial delivery.

NPs	Hydrogel	Advantages	Application	Ref.
AgNPs CuO NPs ZnO NPs	Polyacrylamide-co-acrylic acid hydrogel	-pH-responsive controlled release. -Synergistic antibacterial activity.	Wound dressing	[231]
CuNPs	Gel-MA hydrogel	-Enhanced antibacterial activity with biofilm inhibition ability. -Combined antibiotic treatment and photothermal therapy.	Wound healing and skin tissue regeneration	[232]
AuNPs	Gel-MA hydrogel	-Controlled release of antibiotic in response to NIR irradiation. -Combined antibiotic treatment and photothermal therapy	Periodontal infections	[233]
PLGA NPs	GG hydrogel	-Improved mechanical properties -Ensured local antibiotic delivery in a controlled manner	Bone infections.	[160, 234]

PLGA NPs	DMA hydrogel	-Enhanced drug permeability through the skin. -Bioadhesion. -Increased stability	Topical antibiotic delivery	[236]
PCL NPs	PF-127/CHT hydrogel	-Thermosensitive gel-forming ability. -Bioadhesion Enhanced permeability through the skin. -Increased stability	Topical antibiotic delivery	[162]
NP-stabilized liposomes	Polyacrylamide hydrogel	-Enhanced permeation through the skin. -Bioadhesion. -pH-responsive and controlled antimicrobial release.	Topical antibiotic delivery	[238]
NTs	CHT hydrogel	-Thermosensitive gel-forming ability. - Bioadhesion - Enhanced permeability through the skin. -Increased stability	Transdermal antibiotic delivery	[239]

Gel-MA, methacrylate modified gelatin; GG, gellan gum; DMA, dopamine methacrylamide; PLGA, Poly D, L-lactic-*co*-glycolic acid; CHT, chitosan; PCL, poly ε-caprolactone; NTs, nanotransfersomes.

3.6 Miscellaneous hybrid NPs.

In addition to all the above-mentioned hybrid nanosystems as promising antibiotic delivery vehicles, researchers have reported on a number of other hybrid NPs for antibacterial application. These nanosystems include hybrid magnetite nanocomplexes, hybrid linear polymer-dendrimer NPs and hybrid self-assembled core-shell polymeric NPs.

In this regard, three research studies reported the design of hybrid magnetite nanocomplexes to enhance the antibacterial delivery of loaded antimicrobial metal ions and/or antibiotics. Tung *et al.* (2016) synthesized hybrid magnetite Fe_3O_4-Ag nanocomplexes by a simple photochemical method to investigate their antibacterial efficacy against MRSA infections. The prepared hybrid NPs had a dimer-like nanostructure confirmed by XRD and TEM. *In vitro* antibacterial activity of the hybrid nanosystem was evaluated using paper-disc diffusion and standard microdilution methods, and the results indicated that the prepared hybrid magnetite Fe_3O_4-Ag NPs were more effective than the bare Fe_3O_4NPs and AgNPs against MRSA. This enhanced activity could be a result of the Ag nanocrystals decorated on the magnetic oxide seeds, in addition to the direct contact of the bacterial cell wall with hybrid NPs, leading to Ag^+ release, membrane rupture, biofilm inhibition and bacterial cell death [240]. On the other hand, Zhang and his research group (2019) examined the biofilm eradication ability of the same Fe_3O_4-Ag hybrid system against gram-negative bacteria. They prepared hybrid, multinucleated Fe_3O_4-Ag seeds with a flower-structured morphology. The results confirmed that the prepared hybrid NPs exhibited superior antibacterial and antibiofilm activity against *E. coli* and *P. aeruginosa* when compared to free AgNPs and Fe_3O_4NPs, and these activities were improved with the application of an external magnetic field, since the nanocomposites could penetrate deep into bacterial biofilms and kill the bacteria within the destroyed biofilm [241]. Similarly, a recent study describing a novel hybrid nanodrug delivery system based on magnetite NPs was reported by Zhang *et al.* (2020), who designed a hybrid core/shell Fe_3O_4-SiO_2 NP coated with a vancomycin-loaded polyvinyl alcohol (PVA) and conjugated with a cell-penetrating peptide (CPP) for the effective treatment of both gram-positive and gram-negative bacterial infections. The prepared complex hybrid NPs demonstrated a controlled release profile of vancomycin due to the swelling and shrinking effect of the PVA coat. Also, the conjugation of the hybrid system with a CPP resulted in enhanced antibacterial activity, with a lower effective dosage of vancomycin against both *S. aureus* and resistant *E. coli*, when compared to bare vancomycin and Fe_3O_4-SiO_2 NPs. The enhanced activity of the hybrid system could be attributed to its ability to be significantly internalized into bacterial cells with aid of CPP [242]. These promising results indicated the potential application of the hybrid magnetite nanocomplexes as efficient antibacterial nanocarriers for rapid targeted-drug delivery process. However, all the above-mentioned studies required more investigations, such as stability studies and *in vivo* examinations in suitable animal models with localized infection, before being clinically applied in the future.

In a different approach, hybrid star polymer NPs (called 3-mPEA,) composed of a linear diblock copolymer methoxy PEG-b-PCL (mPEG-b-PCL) and a poly (ester-amine) dendrimer (G1-PEA), were developed by Omolo *et al.* (2018) for the efficient delivery of vancomycin. Different physicochemical characterization tests confirmed the spontaneous self-aggregation of the prepared hybrid 3-mPEA NPs. Vancomycin release from the hybrid nanocomposite was found to be sustained, with a 65.8% release over a period of 72 hrs. In addition, the system exhibited an enhanced antibacterial activity compared to the bare vancomycin, as it had 8- and 16-fold lower MIC values against *S. aureus* and MRSA, respectively. Also, the flow cytometry study showed 3.9-fold more dead MRSA cells when samples were treated with the vancomycin-loaded hybrid NPs than with the plain vancomycin. Finally, an *in vivo* skin infection mice model was used to confirm the *in vitro* antibacterial activity results, and the vancomycin-loaded hybrid NPs showed a 103- and 20-fold reduction in the MRSA load compared to the untreated and VCM treated mice, respectively. Overall, the formulated 3-mPEA hybrid NPs could be a promising biocompatible nanocarrier against bacterial infections caused by MRSA strains [188].

Another hybrid nanocarrier that has been investigated for its targeted antibacterial delivery is a hybrid self-assembled polymeric NP. A research study reported by Wan *et al.* (2019) demonstrated the formulation of self-assembled PLGA/D-α-tocopheryl polyethylene glycol 1000 succinate (TPGS) hybrid NPs via the microfluidic nanoprecipitation method, for site-specific delivery of azithromycin to bacterial biofilm in the lung. The enzymatically cleavable TPGS shell enables the hybrid NPs to penetrate through the mucus and accumulate within the bacterial biofilms, allowing for a sustained release of azithromycin from the PLGA@TPGS NPs and prolonged exposure of the antibiotic to the bacteria, thereby improving the antibacterial activity of the antibiotic against a biofilm-forming *P. aeruginosa*. The killing efficacy of the azithromycin-loaded hybrid NPs was investigated using confocal laser scanning microscopy (CLSM), and the results demonstrated that hybrid NPs had a ~2.5-times greater killing efficacy than bare antibiotic at six hours. Thus, PLGA@TPGS NPs are an efficient delivery system to improve the treatment of cystic fibrosis-related bacterial biofilm infections [243].

In conclusion, various materials were used for the synthesis of each hybrid nanocarrier for targeting and site-specific delivery of various antibacterial agents, including antimicrobial metal ions and antibiotics; and most of the results showed significant enhanced antibacterial activity. The overall outcomes of the reported studies suggest that hybrid nanosystems have promising potential for antibacterial therapy and overcoming resistance, and the novel synthesized materials may be modified for the treatment of other infectious diseases.

4. Conclusion and future perspectives

Over the last two decades, hybrid nanosystems have been developed extensively in the field of drug delivery. This review highlights and discusses the potential of hybrid nanosystems for improving antibacterial drug delivery and enhancing the treatment of bacterial infections. The encapsulation of antibiotics into various hybrid nanocarriers, including LPHNPs; organic-inorganic hybrid NPs; MOFs; CMCH-NPs; and hybrid NP-hydrogels with high encapsulation efficiency and drug loading capacity was successfully established by these studies. Most of the reported hybrid nanocarriers have demonstrated the potential for improved targeting; controlled drug release profiles; long circulation times; and significantly enhanced antibacterial activity, particularly against intracellular bacterial strains and biofilms. In addition to delivering antibiotics, some hybrid NPs with inorganic metal ions also possess potent antimicrobial activity against various gram-positive and gram-negative bacterial species. Furthermore, combining diagnostic functions, active targeting and therapeutic delivery in antibiotic-loaded hybrid nanocarriers are being explored for intravital imaging and antimicrobial therapy. Such nano-theranostic strategy could provide an interesting research area that will inspire researchers to develop new nanotherapeutics for effective diagnosis and treatment of several pathogenic infections

However, despite the enhanced potential of hybrid nanosystems for bacterial eradication, most of these nanocarriers are still in their infancy and have not been translated clinically. Therefore, further studies are required to overcome challenges associated with their complex constitutions; formulation optimization; scalable production; and development of a cost-effective nanocarriers to achieve regulatory approval. Also, for clinical translation, additional studies using appropriate animal models to assess *in vivo* antibacterial performances; *in vivo* ADME; cytotoxicity; and long-term stability of the hybrid nanocarriers are required to validate their efficacy, pharmacokinetic profiles, biosafety, and shelf-life. Additionally, supplementary molecular dynamic studies are essential to understand the enhanced activity of the reported hybrid nanocarriers and the molecular interactions between their constituents.

Currently, relatively few hybrid nanosystems are being reported for antimicrobial delivery. Even though, their formulation has boundless possibilities due to the combination of different biomaterials, resulting in an infinite number of nano-assemblies with endless bio-nanotechnology applications. Recent technologies such as microfluids; particle-replication in non-wetting templates (PRINT) technology; and double spray drying techniques, have served as promising large-scale methods for the development of well-defined hybrid nanocarriers with acceptable characteristics for industrial upscaling.

As more advances are witnessed in synthetic chemistry and supramolecular chemistry, and with the introduction of more innovative elucidation techniques, smarter hybrid nanosystems for precise targeting, with the ability to overcome antimicrobial resistance at the sub-molecular level, will be developed. Therefore, this review represents a platform for the pharmaceutical industries to understand and scale-up hybrid NPs to develop more effective disease site-targeting drug delivery systems that could be employed to overcome antimicrobial resistance. Future research should identify other multifunctional hybrid nanomaterials that are multi-stimuli responsive, biomimetic and cooperate with *in situ* imaging, to elucidate the mechanism of overcoming antimicrobial resistance and improve antibiotic delivery.

Declaration of Competing Interest

The authors declare no conflicts of interest.

Acknowledgments

The authors wish to acknowledge the University of KwaZulu-Natal (UKZN), the National Research Foundation of South Africa (NRF Grant No. 106040, 129326, and 116652), the United States International University-Africa (USIU-AFRICA) and the Medical Research Council (MRC) of South Africa for the financial support of this work.

References

80. Cao, Z., Y. Luo, Z. Li, L. Tan, X. Liu, C. Li, Y. Zheng, Z. Cui, K.W.K. Yeung, Y. Liang, S. Zhu, and S. Wu, *Antibacterial Hybrid Hydrogels.* Macromol Biosci, 2021. **21**(1): p. e2000252. https://doi.org/10.1002/mabi.202000252
81. WHO. *WHO calls for global action on sepsis - cause of 1 in 5 deaths worldwide*. 2020 Acessed 09 November 2021]; Available from: https://www.who.int/news/item/08-09-2020-who-calls-for-global-action-on-sepsis---cause-of-1-in-5-deaths-worldwide.
82. Aslam, B., W. Wang, M.I. Arshad, M. Khurshid, S. Muzammil, M.H. Rasool, M.A. Nisar, R.F. Alvi, M.A. Aslam, M.U. Qamar, M.K.F. Salamat, and Z. Baloch, *Antibiotic resistance: a rundown of a global crisis.* Infect Drug Resist, 2018. **11**: p. 1645-1658. https://doi.org/10.2147/IDR.S173867
83. CDC. *Antibiotic Resistance Threats in the United States*. 2019 Accessed 09 November 2021]; Available from: https://www.cdc.gov/drugresistance/pdf/threats-report/2019-ar-threats-report-508.pdf.
84. Zhou, F., T. Yu, R. Du, G. Fan, Y. Liu, Z. Liu, J. Xiang, Y. Wang, B. Song, X. Gu, L. Guan, Y. Wei, H. Li, X. Wu, J. Xu, S. Tu, Y. Zhang, H. Chen, and B. Cao, *Clinical course and risk factors for mortality of adult inpatients with COVID-19 in Wuhan, China: a retrospective cohort study.* The Lancet, 2020. **395**(10229): p. 1054-1062. https://doi.org/https://doi.org/10.1016/S0140-6736(20)30566-3
85. Jiang L, Lee HW, and L. SCJ, *Therapeutic lipid-coated hybrid nanoparticles against bacterial infections.* RSC Advances, 2020. **10**(14): p. 8497-8517. https://doi.org/10.1039/C9RA10921H
86. Fischbach, M.A. and C.T. Walsh, *Antibiotics for emerging pathogens.* Science, 2009. **325**(5944): p. 1089-93. https://doi.org/10.1126/science.1176667

87. Parisi, O.I., L. Scrivano, M.S. Sinicropi, and F. Puoci, *Polymeric nanoparticle constructs as devices for antibacterial therapy.* Curr Opin Pharmacol, 2017. **36**: p. 72-77. https://doi.org/10.1016/j.coph.2017.08.004
88. Ibrahim, U.H., N. Devnarain, and T. Govender, *Biomimetic strategies for enhancing synthesis and delivery of antibacterial nanosystems.* Int J Pharm, 2021. **596**: p. 1-15, Article 120276. https://doi.org/10.1016/j.ijpharm.2021.120276
89. Kalhapure, R.S., N. Suleman, C. Mocktar, N. Seedat, and T. Govender, *Nanoengineered drug delivery systems for enhancing antibiotic therapy.* J Pharm Sci, 2015. **104**(3): p. 872-905. https://doi.org/10.1002/jps.24298
90. Eleraky, N.E., A. Allam, S.B. Hassan, and M.M. Omar, *Nanomedicine Fight against Antibacterial Resistance: An Overview of the Recent Pharmaceutical Innovations.* Pharmaceutics, 2020. **12**(2): p. 1-51, Article 142. https://doi.org/10.3390/pharmaceutics12020142
91. Abed, N. and P. Couvreur, *Nanocarriers for antibiotics: a promising solution to treat intracellular bacterial infections.* Int J Antimicrob Agents, 2014. **43**(6): p. 485-96. https://doi.org/10.1016/j.ijantimicag.2014.02.009
92. Khorsandi, K., S. Keyvani-Ghamsari, F. Khatibi Shahidi, R. Hosseinzadeh, and S. Kanwal, *A mechanistic perspective on targeting bacterial drug resistance with nanoparticles.* J Drug Target, 2021: p. 1-19. https://doi.org/10.1080/1061186X.2021.1895818
93. Gad El-Rab, S.M.F., E.M. Halawani, and A. Hassan, *Formulation of Ceftriaxone Conjugated Gold Nanoparticles and Their Medical Applications against Extended-Spectrum β-Lactamase Producing Bacteria and Breast Cancer.* J Microbiol Biotechnol, 2018. **28**(9): p. 1563-1572. https://doi.org/10.4014/jmb.1711.11037
94. Khameneh, B., M. Iranshahy, M. Ghandadi, D. Ghoochi Atashbeyk, B.S. Fazly Bazzaz, and M. Iranshahi, *Investigation of the antibacterial activity and efflux pump inhibitory effect of co-loaded piperine and gentamicin nanoliposomes in methicillin-resistant Staphylococcus aureus.* Drug Dev Ind Pharm, 2015. **41**(6): p. 989-94. https://doi.org/10.3109/03639045.2014.920025
95. Mahamuni-Badiger, P.P., P.M. Patil, M.V. Badiger, P.R. Patel, B.S. Thorat-Gadgil, A. Pandit, and R.A. Bohara, *Biofilm formation to inhibition: Role of zinc oxide-based nanoparticles.* Mater Sci Eng C Mater Biol Appl, 2020. **108**: p. 1-72, Article 110319. https://doi.org/10.1016/j.msec.2019.110319
96. Yin, I.X., J. Zhang, I.S. Zhao, M.L. Mei, Q. Li, and C.H. Chu, *The Antibacterial Mechanism of Silver Nanoparticles and Its Application in Dentistry.* Int J Nanomedicine, 2020. **15**: p. 2555-2562. https://doi.org/10.2147/IJN.S246764
97. Alemán, J.V., A.V. Chadwick, J. He, M. Hess, K. Horie, R.G. Jones, P. Kratochvíl, I. Meisel, I. Mita, G. Moad, S. Penczek, and R.F.T. Stepto, *Definitions of terms relating to the structure and processing of sols, gels, networks, and inorganic-organic hybrid materials (IUPAC Recommendations 2007).* Pure and Applied Chemistry, 2007. **79**(10): p. 1801-1829. https://doi.org/10.1351/pac200779101801
98. Maji, R., C.A. Omolo, N. Agrawal, K. Maduray, D. Hassan, C. Mokhtar, I. Mackhraj, and T. Govender, *pH-Responsive Lipid-Dendrimer Hybrid Nanoparticles: An Approach To Target and Eliminate Intracellular Pathogens.* Mol Pharm, 2019. **16**(11): p. 4594-4609. https://doi.org/10.1021/acs.molphar–aceut.9b00713
99. Hadinoto, K., A. Sundaresan, and W.S. Cheow, *Lipid-polymer hybrid nanoparticles as a new generation therapeutic delivery platform: a review.* Eur J Pharm Biopharm, 2013. **85**(3): p. 427-443. https://doi.org/10.1016/j.ejpb.2013.07.002

100. Mandal, B., H. Bhattacharjee, N. Mittal, H. Sah, P. Balabathula, L.A. Thoma, and G.C. Wood, *Core-shell-type lipid-polymer hybrid nanoparticles as a drug delivery platform.* Nanomedicine, 2013. **9**(4): p. 474-91. https://doi.org/10.1016/j.nano.2012.11.010
101. Obuobi, S. and N. Skalko-Basnet, *Nucleic Acid Hybrids as Advanced Antibacterial Nanocarriers.* Pharmaceutics, 2020. **12**(7): p. 1-25. https://doi.org/10.3390/pharmaceutics12070643
102. AlQahtani, S.A., G.I. Harisa, A.H. Alomrani, F.K. Alanazi, and M.M. Badran, *Improved pharmacokinetic and biodistribution of 5-fluorouracil loaded biomimetic nanoerythrocytes decorated nanocarriers for liver cancer treatment.* Colloids Surf B Biointerfaces, 2021. **197**: p. 111380. https://doi.org/10.1016/j.colsurfb.2020.111380
103. Dalmoro, A., S. Bochicchio, G. Lamberti, P. Bertoncin, B. Janssens, and A.A. Barba, *Micronutrients encapsulation in enhanced nanoliposomal carriers by a novel preparative technology.* RSC Advances, 2019. **9**(34): p. 19800-19812. https://doi.org/10.1039/c9ra03022k
104. Walsh, E.E., R.W. Frenck, Jr., A.R. Falsey, N. Kitchin, J. Absalon, A. Gurtman, S. Lockhart, K. Neuzil, M.J. Mulligan, R. Bailey, K.A. Swanson, P. Li, K. Koury, W. Kalina, D. Cooper, C. Fontes-Garfias, P.Y. Shi, O. Tureci, K.R. Tompkins, K.E. Lyke, V. Raabe, P.R. Dormitzer, K.U. Jansen, U. Sahin, and W.C. Gruber, *Safety and Immunogenicity of Two RNA-Based Covid-19 Vaccine Candidates.* N Engl J Med, 2020. **383**(25): p. 2439-2450. https://doi.org/10.1056/NEJMoa2027906
105. Wyszogrodzka, G., B. Marszalek, B. Gil, and P. Dorozynski, *Metal-organic frameworks: mechanisms of antibacterial action and potential applications.* Drug Discov Today, 2016. **21**(6): p. 1009-1018. https://doi.org/10.1016/j.drudis.2016.04.009
106. Dave, V., R.B. Yadav, K. Kushwaha, S. Yadav, S. Sharma, and U. Agrawal, *Lipid-polymer hybrid nanoparticles: Development & statistical optimization of norfloxacin for topical drug delivery system.* Bioact Mater, 2017. **2**(4): p. 269-280. https://doi.org/10.1016/j.bioactmat.2017.07.002
107. Li, M., Z. Luo, and Y. Zhao, *Hybrid Nanoparticles as Drug Carriers for Controlled Chemotherapy of Cancer.* The Chemical Record, 2016. **16**(4): p. 1833-1851. https://doi.org/10.1002/tcr.201600029
108. Wu, M.X. and Y.W. Yang, *Metal-Organic Framework (MOF)-Based Drug/Cargo Delivery and Cancer Therapy.* Adv Mater, 2017. **29**(23): p. 1-20, Article 1606134. https://doi.org/10.1002/adma.201606134
109. Hallan, S.S., P. Kaur, V. Kaur, N. Mishra, and B. Vaidya, *Lipid polymer hybrid as emerging tool in nanocarriers for oral drug delivery.* Artif Cells Nanomed Biotechnol, 2016. **44**(1): p. 334-49. https://doi.org/10.3109/21691401.2014.951721
110. Maghrebi, S., C.A. Prestidge, and P. Joyce, *An update on polymer-lipid hybrid systems for improving oral drug delivery.* Expert Opin Drug Deliv, 2019. **16**(5): p. 507-524. https://doi.org/10.1080/17425247.2019.1605353
111. Matter, M.T., S. Probst, S. Lauchli, and I.K. Herrmann, *Uniting Drug and Delivery: Metal Oxide Hybrid Nanotherapeutics for Skin Wound Care.* Pharmaceutics, 2020. **12**(8): p. 1-17. https://doi.org/10.3390/pharmaceutics12080780
112. Graczyk, A., R. Pawlowska, D. Jedrzejczyk, and A. Chworos, *Gold Nanoparticles in Conjunction with Nucleic Acids as a Modern Molecular System for Cellular Delivery.* Molecules, 2020. **25**(1): p. 1-27. https://doi.org/10.3390/molecules25010204
113. Liu, X., Q. Zhang, W. Knoll, B. Liedberg, and Y. Wang, *Rational Design of Functional Peptide-Gold Hybrid Nanomaterials for Molecular Interactions.* Adv Mater, 2020. **32**(37): p. 1-37, Article e2000866. https://doi.org/10.1002/adma.202000866

114. Gaspar, V.M., P. Lavrador, J. Borges, M.B. Oliveira, and J.F. Mano, *Advanced Bottom-Up Engineering of Living Architectures.* Adv Mater, 2020. **32**(6): p. e1903975. https://doi.org/10.1002/adma.201903975
115. Mandal, B., H. Bhattacharjee, N. Mittal, H. Sah, P. Balabathula, L.A. Thoma, and G.C. Wood, *Core–shell-type lipid–polymer hybrid nanoparticles as a drug delivery platform.* Nanomedicine: Nanotechnology, Biology and Medicine, 2013. **9**(4): p. 474-491. https://doi.org/10.1016/j.nano.2012.11.010
116. Bose, R.J.C., R. Ravikumar, V. Karuppagounder, D. Bennet, S. Rangasamy, and R.A. Thandavarayan, *Lipid-polymer hybrid nanoparticle-mediated therapeutics delivery: advances and challenges.* Drug Discov Today, 2017. **22**(8): p. 1258-1265. https://doi.org/https://doi.org/10.1016/j.drudis.2017.05.015
117. Bochicchio, S., G. Lamberti, and A.A. Barba, *Polymer-Lipid Pharmaceutical Nanocarriers: Innovations by New Formulations and Production Technologies.* Pharmaceutics, 2021. **13**(2): p. 1-15. https://doi.org/10.3390/pharmaceutics13020198
118. Dave, V., K. Tak, A. Sohgaura, A. Gupta, V. Sadhu, and K.R. Reddy, *Lipid-polymer hybrid nanoparticles: Synthesis strategies and biomedical applications.* J Microbiol Methods, 2019. **160**: p. 130-142. https://doi.org/10.1016/j.mimet.2019.03.017
119. Mukherjee A, Waters A K, K. P, Achrol A S, Kesari S, and Y.V. M, *Lipid–polymer hybrid nanoparticles as a next- generation drug delivery platform: state of the art, emerging technologies, and perspectives.* Int. J. Nanomedicine, 2019. **14**: p. 1937-1952. https://doi.org/10.2147/IJN.S198353
120. Ferreira Soares, D.C., S.C. Domingues, D.B. Viana, and M.L. Tebaldi, *Polymer-hybrid nanoparticles: Current advances in biomedical applications.* Biomed Pharmacother, 2020. **131**: p. 1-13, Article 110695 https://doi.org/10.1016/j.biopha.2020.110695
121. Wang, Y., K. Kho, W.S. Cheow, and K. Hadinoto, *A comparison between spray drying and spray freeze drying for dry powder inhaler formulation of drug-loaded lipid–polymer hybrid nanoparticles.* Int J Pharm, 2012. **424**(1-2): p. 98-106. https://doi.org/10.1016/j.ijpharm.2011.12.045
122. Hasan, W., K. Chu, A. Gullapalli, S.S. Dunn, E.M. Enlow, J.C. Luft, S. Tian, M.E. Napier, P.D. Pohlhaus, J.P. Rolland, and J.M. DeSimone, *Delivery of multiple siRNAs using lipid-coated PLGA nanoparticles for treatment of prostate cancer.* Nano Lett, 2012. **12**(1): p. 287-292. https://doi.org/10.1021/nl2035354
123. Ahmaditabar, P., A.A. Momtazi-Borojeni, A.H. Rezayan, M. Mahmoodi, A. Sahebkar, and M. Mellat, *Enhanced Entrapment and Improved in Vitro Controlled Release of N-Acetyl Cysteine in Hybrid PLGA/Lecithin Nanoparticles Prepared Using a Nanoprecipitation/Self-Assembly Method.* J Cell Biochem, 2017. **118**(12): p. 4203-4209. https://doi.org/10.1002/jcb.26070
124. Luchini, A., C. Irace, R. Santamaria, D. Montesarchio, R.K. Heenan, N. Szekely, A. Flori, L. Menichetti, and L. Paduano, *Phosphocholine-decorated superparamagnetic iron oxide nanoparticles: defining the structure and probing in vivo applications.* Nanoscale, 2016. **8**(19): p. 10078-10086. https://doi.org/10.1039/c5nr08486e
125. Bokare, A., A. Takami, J.H. Kim, A. Dong, A. Chen, R. Valerio, S. Gunn, and F. Erogbogbo, *Herringbone-Patterned 3D-Printed Devices as Alternatives to Microfluidics for Reproducible Production of Lipid Polymer Hybrid Nanoparticles.* ACS Omega, 2019. **4**(3): p. 4650-4657. https://doi.org/10.1021/acsomega.9b00128
126. Cheow, W.S. and K. Hadinoto, *Factors affecting drug encapsulation and stability of lipid-polymer hybrid nanoparticles.* Colloids Surf B Biointerfaces, 2011. **85**(2): p. 214-220. https://doi.org/10.1016/j.colsurfb.2011.02.033

127. Taheri, S., A. Cavallaro, S.N. Christo, P. Majewski, M. Barton, J.D. Hayball, and K. Vasilev, *Antibacterial Plasma Polymer Films Conjugated with Phospholipid Encapsulated Silver Nanoparticles.* ACS Biomater Sci Eng, 2015. **1**(12): p. 1278-1286. https://doi.org/10.1021/acsbiomaterials.5b00338
128. Vivero-Escoto, J.L. and Y.T. Huang, *Inorganic-organic hybrid nanomaterials for therapeutic and diagnostic imaging applications.* Int J Mol Sci, 2011. **12**(6): p. 3888-3927. https://doi.org/10.3390/ijms12063888
129. Huang, X., J. Hu, Y. Li, F. Xin, R. Qiao, and T.P. Davis, *Engineering Organic/Inorganic Nanohybrids through RAFT Polymerization for Biomedical Applications.* Biomac, 2019. **20**(12): p. 4243-4257. https://doi.org/10.1021/acs.biomac.9b01158
130. Aguilar, C.A., A.B. Jimenez, A.R. Silva, N. Kaur, P. Thangarasu, J.M. Ramos, and N. Singh, *Organic-inorganic hybrid nanoparticles for bacterial inhibition: synthesis and characterization of doped and undoped ONPs with Ag/Au NPs.* Molecules, 2015. **20**(4): p. 6002-6021. https://doi.org/10.3390/molecules20046002
131. Adnan, M.M., A.R.M. Dalod, M.H. Balci, J. Glaum, and M.A. Einarsrud, *In Situ Synthesis of Hybrid Inorganic(-)Polymer Nanocomposites.* Polymers (Basel), 2018. **10**(10): p. 1-32. https://doi.org/10.3390/polym10101129
132. Saveleva, M.S., K. Eftekhari, A. Abalymov, T.E.L. Douglas, D. Volodkin, B.V. Parakhonskiy, and A.G. Skirtach, *Hierarchy of Hybrid Materials-The Place of Inorganics-in-Organics in it, Their Composition and Applications.* Front Chem, 2019. **7**: p. 1-21, Article 179. https://doi.org/10.3389/fchem.2019.00179
133. Luo, Z., S. Fan, C. Gu, W. Liu, J. Chen, B. Li, and J. Liu, *Metal-Organic Framework (MOF)-based Nanomaterials for Biomedical Applications.* Curr Med Chem, 2019. **26**(18): p. 3341-3369. https://doi.org/10.2174/0929867325666180214123500
134. Wang, L., M. Zheng, and Z. Xie, *Nanoscale metal-organic frameworks for drug delivery: a conventional platform with new promise.* J Mater Chem B, 2018. **6**(5): p. 707-717. https://doi.org/10.1039/c7tb02970e
135. Chui. S, Samuel M.-F. Lo, Jonathan P. H. Charmant, A. Guy Orpen, and I.D. Williams, *A Chemically Functionalizable Nanoporous Material [Cu3(TMA)2(H2O)3]n.* Science, 1999. **243**(5405): p. 1148-1150. https://doi.org/10.1126/science.283.5405.1148
136. Li, H., M. Eddaoudi, M. O'Keeffe, and O.M. Yaghi, *Design and synthesis of an exceptionally stable and highly porous metal-organic framework.* NATURE, 1999. **402**(6759): p. 276-279. https://doi.org/10.1038/46248
137. Tibbetts, I. and G.E. Kostakis, *Recent Bio-Advances in Metal-Organic Frameworks.* Molecules, 2020. **25**(6): p. 1-32. https://doi.org/10.3390/molecules25061291
138. Giliopoulos, D., A. Zamboulis, D. Giannakoudakis, D. Bikiaris, and K. Triantafyllidis, *Polymer/Metal Organic Framework (MOF) Nanocomposites for Biomedical Applications.* Molecules, 2020. **25**(1): p. 1-28. https://doi.org/10.3390/molecules25010185
139. Carrasco, S., *Metal-Organic Frameworks for the Development of Biosensors: A Current Overview.* Biosensors (Basel), 2018. **8**(4): p. 1-30. https://doi.org/10.3390/bios8040092
140. Pachfule, P., R. Das, P. Poddar, and R. Banerjee, *Solvothermal Synthesis, Structure, and Properties of Metal Organic Framework Isomers Derived from a Partially Fluorinated Link.* Crystal Growth & Design, 2011. **11**(4): p. 1215-1222. https://doi.org/10.1021/cg101414x
141. Pan, Y., Y. Liu, G. Zeng, L. Zhao, and Z. Lai, *Rapid synthesis of zeolitic imidazolate framework-8 (ZIF-8) nanocrystals in an aqueous system.* Chem Commun (Camb), 2011. **47**(7): p. 2071-2073. https://doi.org/10.1039/c0cc05002d
142. Haque, E., N.A. Khan, J.H. Park, and S.H. Jhung, *Synthesis of a metal-organic framework material, iron terephthalate, by ultrasound, microwave, and conventional electric heating: a*

kinetic study. Chemistry, 2010. **16**(3): p. 1046-1052. https://doi.org/10.1002/chem.200902382

143. Klimakow, M., P. Klobes, A.F. Thünemann, K. Rademann, and F. Emmerling, *Mechanochemical Synthesis of Metal–Organic Frameworks: A Fast and Facile Approach toward Quantitative Yields and High Specific Surface Areas.* Chemistry of Materials, 2010. **22**(18): p. 5216-5221. https://doi.org/10.1021/cm1012119
144. Stock, N. and S. Biswas, *Synthesis of metal-organic frameworks (MOFs): routes to various MOF topologies, morphologies, and composites.* Chem Rev, 2012. **112**(2): p. 933-969. https://doi.org/10.1021/cr200304e
145. Horcajada, P., C. Serre, M. Vallet-Regí, M. Sebban, F. Taulelle, and G. Férey, *Metal-organic frameworks as efficient materials for drug delivery.* Angew Chem Int Ed Engl, 2006. **45**(36): p. 5974-8. https://doi.org/10.1002/anie.200601878
146. Yao, J., Y. Liu, J. Wang, Q. Jiang, D. She, H. Guo, N. Sun, Z. Pang, C. Deng, W. Yang, and S. Shen, *On-demand CO release for amplification of chemotherapy by MOF functionalized magnetic carbon nanoparticles with NIR irradiation.* Biomaterials, 2019. **195**: p. 51-62. https://doi.org/10.1016/j.biomaterials.2018.12.029
147. Zhang, Y., F. Wang, E. Ju, Z. Liu, Z. Chen, J. Ren, and X. Qu, *Metal-Organic-Framework-Based Vaccine Platforms for Enhanced Systemic Immune and Memory Response.* Advanced Functional Materials, 2016. **26**(35): p. 6454-6461. https://doi.org/10.1002/adfm.201600650
148. Chen, Y., P. Li, J.A. Modica, R.J. Drout, and O.K. Farha, *Acid-Resistant Mesoporous Metal-Organic Framework toward Oral Insulin Delivery: Protein Encapsulation, Protection, and Release.* J Am Chem Soc, 2018. **140**(17): p. 5678-5681. https://doi.org/10.1021/jacs.8b02089
149. Andre, V., A.R.F. da Silva, A. Fernandes, R. Frade, C. Garcia, P. Rijo, A.M.M. Antunes, J. Rocha, and M.T. Duarte, *Mg- and Mn-MOFs Boost the Antibiotic Activity of Nalidixic Acid.* ACS Appl Bio Mater, 2019. **2**(6): p. 2347-2354. https://doi.org/10.1021/acsabm.9b00046
150. Luk, B.T. and L. Zhang, *Cell membrane-camouflaged nanoparticles for drug delivery.* J Control Release, 2015. **220**(Pt B): p. 1-18. https://doi.org/10.1016/j.jconrel.2015.07.019
151. Narain, A., S. Asawa, V. Chhabria, and Y. Patil-Sen, *Cell membrane coated nanoparticles: next-generation therapeutics.* Nanomedicine (Lond), 2017. **12**(21): p. 2677-2692. https://doi.org/10.2217/nnm-2017-0225
152. Ai, X., M. Hu, Z. Wang, W. Zhang, J. Li, H. Yang, J. Lin, and B. Xing, *Recent Advances of Membrane-Cloaked Nanoplatforms for Biomedical Applications.* Bioconjug Chem, 2018. **29**(4): p. 838-851. https://doi.org/10.1021/acs.bioconjchem.8b00103
153. Kroll, A.V., R.H. Fang, and L. Zhang, *Biointerfacing and Applications of Cell Membrane-Coated Nanoparticles.* Bioconjug Chem, 2017. **28**(1): p. 23-32. https://doi.org/10.1021/acs.bioconjchem.6b00569
154. Hu, C.-M.J., L. Zhang, S. Aryal, C. Cheung, R.H. Fang, and L. Zhang, *Erythrocyte membrane-camouflaged polymeric nanoparticles as a biomimetic delivery platform.* Proceedings of the National Academy of Sciences of the United States of America, 2011. **108**(27): p. 10980-10985. https://doi.org/10.1073/pnas.1106634108
155. Chen, H.Y., J. Deng, Y. Wang, C.Q. Wu, X. Li, and H.W. Dai, *Hybrid cell membrane-coated nanoparticles: A multifunctional biomimetic platform for cancer diagnosis and therapy.* Acta Biomater, 2020. **112**: p. 1-13. https://doi.org/10.1016/j.actbio.2020.05.028
156. Gao, W., Y. Zhang, Q. Zhang, and L. Zhang, *Nanoparticle-Hydrogel: A Hybrid Biomaterial System for Localized Drug Delivery.* Ann Biomed Eng, 2016. **44**(6): p. 2049-2061. https://doi.org/10.1007/s10439-016-1583-9
157. Gaharwar, A.K., N.A. Peppas, and A. Khademhosseini, *Nanocomposite hydrogels for biomedical applications.* Biotechnol Bioeng, 2014. **111**(3): p. 441-453. https://doi.org/10.1002/bit.25160

158. Mandal, M. and M.J. Hindin, *From family to friends: does witnessing interparental violence affect young adults' relationships with friends?* J Adolesc Health, 2013. **53**(2): p. 187-93. https://doi.org/10.1016/j.jadohealth.2013.03.015
159. Maji, R., C.A. Omolo, Y. Jaglal, S. Singh, N. Devnarain, C. Mocktar, and T. Govender, *A transferosome-loaded bigel for enhanced transdermal delivery and antibacterial activity of vancomycin hydrochloride.* Int J Pharm, 2021. **607**: p. 120990. https://doi.org/10.1016/j.ijpharm.2021.120990
160. Posadowska, U., M. Brzychczy-Wloch, and E. Pamula, *Injectable gellan gum-based nanoparticles-loaded system for the local delivery of vancomycin in osteomyelitis treatment.* J Mater Sci Mater Med, 2016. **27**(1): p. 1-9. https://doi.org/10.1007/s10856-015-5604-2
161. Baumann, M.D., C.E. Kang, C.H. Tator, and M.S. Shoichet, *Intrathecal delivery of a polymeric nanocomposite hydrogel after spinal cord injury.* Biomaterials, 2010. **31**(30): p. 7631-9. https://doi.org/10.1016/j.biomaterials.2010.07.004
162. Salatin, S., F. Lotfipour, and M. Jelvehgari, *Preparation and characterization of a novel thermosensitive and bioadhesive cephalexin nanohydrogel: a promising platform for topical antibacterial delivery.* Expert Opin Drug Deliv, 2020. **17**(6): p. 881-893. https://doi.org/10.1080/17425247.2020.1764530
163. Ishak, R.A.H., N.M. Mostafa, and A.O. Kamel, *Stealth lipid polymer hybrid nanoparticles loaded with rutin for effective brain delivery - comparative study with the gold standard (Tween 80): optimization, characterization and biodistribution.* Drug delivery, 2017. **24**(1): p. 1874-1890. https://doi.org/10.1080/10717544.2017.1410263
164. Makadia, H.K. and S.J. Siegel, *Poly Lactic-co-Glycolic Acid (PLGA) as Biodegradable Controlled Drug Delivery Carrier.* Polymers (Basel), 2011. **3**(3): p. 1377-1397. https://doi.org/10.3390/polym3031377
165. Bhardwaj, A., S. Mehta, S. Yadav, S.K. Singh, A. Grobler, A.K. Goyal, and A. Mehta, *Pulmonary delivery of antitubercular drugs using spray-dried lipid-polymer hybrid nanoparticles.* Artif Cells Nanomed Biotechnol, 2016. **44**(6): p. 1544-1555. https://doi.org/10.3109/21691401.2015.1062389
166. Dave, V., K. Kushwaha, R.B. Yadav, and U. Agrawal, *Hybrid nanoparticles for the topical delivery of norfloxacin for the effective treatment of bacterial infection produced after burn.* J Microencapsul, 2017. **34**(4): p. 351-365. https://doi.org/10.1080/02652048.2017.1337249
167. Fangary, S., M. Abdel-Halim, R.K. Fathalla, R. Hassan, N. Farag, M. Engel, S. Mansour, and S.N. Tammam, *Nanoparticle Fraught Liposomes: A Platform for Increased Antibiotic Selectivity in Multidrug Resistant Bacteria.* Mol Pharm, 2022. **19**(9): p. 3163-3177. https://doi.org/10.1021/acs.molpharmaceut.2c00258
168. Fasiku Oluwaseun, V., C.A. Omolo, and T. Govender, *Free radical-releasing systems for targeting biofilms.* J Control Release, 2020. **322**: p. 248-273. https://doi.org/10.1016/j.jconrel.2020.03.031
169. Høiby, N., T. Bjarnsholt, M. Givskov, S. Molin, and O. Ciofu, *Antibiotic resistance of bacterial biofilms.* International Journal of Antimicrobial Agents, 2010. **35**(4): p. 322-332. https://doi.org/10.1016/j.ijantimicag.2009.12.011
170. Baek, J.S., C.H. Tan, N.K.J. Ng, Y.P. Yeo, S.A. Rice, and S.C.J. Loo, *A programmable lipid-polymer hybrid nanoparticle system for localized, sustained antibiotic delivery to Gram-positive and Gram-negative bacterial biofilms.* Nanoscale Horiz, 2018. **3**(3): p. 305-311. https://doi.org/10.1039/c7nh00167c
171. Guo, P., B.A. Buttaro, H.Y. Xue, N.T. Tran, and H.L. Wong, *Lipid-polymer hybrid nanoparticles carrying linezolid improve treatment of methicillin-resistant Staphylococcus aureus (MRSA) harbored inside bone cells and biofilms.* Eur J Pharm Biopharm, 2020. **151**: p. 189-198. https://doi.org/10.1016/j.ejpb.2020.04.010

172. Guo, P., H.Y. Xue, B.A. Buttaro, N.T. Tran, and H.L. Wong, *Enhanced eradication of intracellular and biofilm-residing methicillin-resistant Staphylococcus aureus (MRSA) reservoirs with hybrid nanoparticles delivering rifampicin.* Int J Pharm, 2020. **589**: p. 1-10, Article 119784. https://doi.org/10.1016/j.ijpharm.2020.119784
173. Bose, R.J.C., N. Tharmalingam, Y. Choi, T. Madheswaran, R. Paulmurugan, J.R. McCarthy, S.H. Lee, and H. Park, *Combating Intracellular Pathogens with Nanohybrid-Facilitated Antibiotic Delivery.* Int J Nanomedicine, 2020. **15**: p. 8437-8449. https://doi.org/10.2147/IJN.S271850
174. Lew, D.P. and F.A. Waldvogel, *Osteomyelitis.* The Lancet, 2004. **364**(9431): p. 369-379. https://doi.org/10.1016/S0140-6736(04)16727-5
175. Abed, N. and P. Couvreur, *Nanocarriers for antibiotics: A promising solution to treat intracellular bacterial infections.* International Journal of Antimicrobial Agents, 2014. **43**(6): p. 485-496. https://doi.org/https://doi.org/10.1016/j.ijantimicag.2014.02.009
176. Ali, A. and S. Ahmed, *A review on chitosan and its nanocomposites in drug delivery.* Int J Biol Macromol, 2018. **109**: p. 273-286. https://doi.org/10.1016/j.ijbiomac.2017.12.078
177. Thakur, K., G. Sharma, B. Singh, S. Chhibber, A.B. Patil, and O.P. Katare, *Chitosan-tailored lipidic nanoconstructs of Fusidic acid as promising vehicle for wound infections: An explorative study.* Int J Biol Macromol, 2018. **115**: p. 1012-1025. https://doi.org/10.1016/j.ijbiomac.2018.04.092
178. Thakur, K., G. Sharma, B. Singh, S. Chhibber, and O.P. Katare, *Nano-engineered lipid-polymer hybrid nanoparticles of fusidic acid: an investigative study on dermatokinetics profile and MRSA-infected burn wound model.* Drug Deliv Transl Res, 2019. **9**(4): p. 748-763. https://doi.org/10.1007/s13346-019-00616-3
179. Deok Kong, S., M. Sartor, C.-M. Jack Hu, W. Zhang, L. Zhang, and S. Jin, *Magnetic field activated lipid–polymer hybrid nanoparticles for stimuli-responsive drug release.* Acta biomaterialia, 2013. **9**(3): p. 5447-5452. https://doi.org/https://doi.org/10.1016/j.actbio.2012.11.006
180. Hassan, D., C.A. Omolo, V.O. Fasiku, C. Mocktar, and T. Govender, *Novel chitosan-based pH-responsive lipid-polymer hybrid nanovesicles (OLA-LPHVs) for delivery of vancomycin against methicillin-resistant Staphylococcus aureus infections.* Int J Biol Macromol, 2020. **147**: p. 385-398. https://doi.org/10.1016/j.ijbiomac.2020.01.019
181. Nwabuife, J.C., A.M. Pant, and T. Govender, *Liposomal delivery systems and their applications against Staphylococcus aureus and Methicillin-resistant Staphylococcus aureus.* Advanced Drug Delivery Reviews, 2021. **178**: p. 113861. https://doi.org/10.1016/j.addr.2021.113861
182. Rodenak-Kladniew, B., S. Scioli Montoto, M.L. Sbaraglini, M. Di Ianni, M.E. Ruiz, A. Talevi, V.A. Alvarez, N. Duran, G.R. Castro, and G.A. Islan, *Hybrid Ofloxacin/eugenol co-loaded solid lipid nanoparticles with enhanced and targetable antimicrobial properties.* Int J Pharm, 2019. **569**: p. 1-13, Article 118575. https://doi.org/10.1016/j.ijpharm.2019.118575
183. Bueloni, B., D. Sanna, E. Garribba, G.R. Castro, I.E. Leon, and G.A. Islan, *Design of nalidixic acidvanadium complex loaded into chitosan hybrid nanoparticles as smart strategy to inhibit bacterial growth and quorum sensing.* Int J Biol Macromol, 2020. **161**: p. 1568-1580. https://doi.org/10.1016/j.ijbiomac.2020.07.304
184. Madaan, K., S. Kumar, N. Poonia, V. Lather, and D. Pandita, *Dendrimers in drug delivery and targeting: Drug-dendrimer interactions and toxicity issues.* J Pharm Bioallied Sci, 2014. **6**(3): p. 139-50. https://doi.org/10.4103/0975-7406.130965
185. Chauhan, A.S., *Dendrimers for Drug Delivery.* Molecules, 2018. **23**(4). https://doi.org/10.3390/molecules23040938
186. Kesharwani, P., A. Gothwal, A.K. Iyer, K. Jain, M.K. Chourasia, and U. Gupta, *Dendrimer nanohybrid carrier systems: an expanding horizon for targeted drug and gene delivery.* Drug Discov Today, 2018. **23**(2): p. 300-314. https://doi.org/10.1016/j.drudis.2017.06.009

187. Sonawane, S.J., R.S. Kalhapure, S. Rambharose, C. Mocktar, S.B. Vepuri, M. Soliman, and T. Govender, *Ultra-small lipid-dendrimer hybrid nanoparticles as a promising strategy for antibiotic delivery: In vitro and in silico studies.* Int J Pharm, 2016. **504**(1-2): p. 1-10. https://doi.org/10.1016/j.ijpharm.2016.03.021
188. Omolo, C.A., R.S. Kalhapure, N. Agrawal, M. Jadhav, S. Rambharose, C. Mocktar, and T. Govender, *A hybrid of mPEG-b-PCL and G1-PEA dendrimer for enhancing delivery of antibiotics.* J Control Release, 2018. **290**: p. 112-128. https://doi.org/10.1016/j.jconrel.2018.10.005
189. Araujo, R.V., S.D.S. Santos, E. Igne Ferreira, and J. Giarolla, *New Advances in General Biomedical Applications of PAMAM Dendrimers.* Molecules, 2018. **23**(11). https://doi.org/10.3390/molecules23112849
190. Moorcroft SCT, Jayne DG, Evans SD, and O. ZY., *Stimuli-responsive release of antimicrobials using hybrid inorganic nanoparticle-associated drug-delivery systems.* Macromol Biosci, 2018. **18**(12): p. 1-14. https://doi.org/10.1002/mabi.201800207
191. Wang, S., F. Zheng, Y. Huang, Y. Fang, M. Shen, M. Zhu, and X. Shi, *Encapsulation of amoxicillin within laponite-doped poly(lactic-co-glycolic acid) nanofibers: preparation, characterization, and antibacterial activity.* ACS Appl Mater Interfaces, 2012. **4**(11): p. 6393-6401. https://doi.org/10.1021/am302130b
192. Zheng, F., S. Wang, S. Wen, M. Shen, M. Zhu, and X. Shi, *Characterization and antibacterial activity of amoxicillin-loaded electrospun nano-hydroxyapatite/poly(lactic-co-glycolic acid) composite nanofibers.* Biomaterials, 2013. **34**(4): p. 1402-1412. https://doi.org/10.1016/j.biomaterials.2012.10.071
193. Qi, R., R. Guo, F. Zheng, H. Liu, J. Yu, and X. Shi, *Controlled release and antibacterial activity of antibiotic-loaded electrospun halloysite/poly(lactic-co-glycolic acid) composite nanofibers.* Colloids Surf B Biointerfaces, 2013. **110**: p. 148-55. https://doi.org/10.1016/j.colsurfb.2013.04.036
194. Vasile, B.S., O. Oprea, G. Voicu, A. Ficai, E. Andronescu, A. Teodorescu, and A. Holban, *Synthesis and characterization of a novel controlled release zinc oxide/gentamicin-chitosan composite with potential applications in wounds care.* Int J Pharm, 2014. **463**(2): p. 161-169. https://doi.org/10.1016/j.ijpharm.2013.11.035
195. Yang, S., X. Han, Y. Yang, H. Qiao, Z. Yu, Y. Liu, J. Wang, and T. Tang, *Bacteria-Targeting Nanoparticles with Microenvironment-Responsive Antibiotic Release To Eliminate Intracellular Staphylococcus aureus and Associated Infection.* ACS Appl Mater Interfaces, 2018. **10**(17): p. 14299-14311. https://doi.org/10.1021/acsami.7b15678
196. Murugesan, G., N. Latha, K. Suganya, M. Murugan, M.A. Munusamy, and M. Rajan, *Stimulus-responsive zinc oxide-functionalized macromolecular humic acid nanocarrier for enhancement of antibacterial activity of ciprofloxacin hydrochloride.* Int J Biol Macromol, 2018. **114**: p. 1109-1116. https://doi.org/10.1016/j.ijbiomac.2018.03.120
197. Al-Obaidi, H., R. Kalgudi, and M.G. Zariwala, *Fabrication of inhaled hybrid silver/ciprofloxacin nanoparticles with synergetic effect against Pseudomonas aeruginosa.* Eur J Pharm Biopharm, 2018. **128**: p. 27-35. https://doi.org/10.1016/j.ejpb.2018.04.006
198. Kankala, R.K., W.Z. Lin, and C.H. Lee, *Combating Antibiotic Resistance through the Synergistic Effects of Mesoporous Silica-Based Hierarchical Nanocomposites.* Nanomaterials (Basel), 2020. **10**(3): p. 1-15. https://doi.org/10.3390/nano10030597
199. Iudin, D., M. Vasilieva, E. Knyazeva, V. Korzhikov-Vlakh, E. Demyanova, A. Lavrentieva, Y. Skorik, and E. Korzhikova-Vlakh, *Hybrid Nanoparticles and Composite Hydrogel Systems for Delivery of Peptide Antibiotics.* Int J Mol Sci, 2022. **23**(5). https://doi.org/10.3390/ijms23052771

200. Xiang, Y.L., S.H. Huang, Q.H. Hu, Q.Y. Wang, M.Q. Zhao, Y.C. Jiang, X. Chen, J. Lin, and Q.H. Zhou, *Zwitterionic meso-silica/polypeptide hybrid nanoparticles for efficient azithromycin delivery and photodynamic therapy for synergistic treatment of drug-resistant bacterial infection.* Int J Biol Macromol, 2022. **219**: p. 597-610. https://doi.org/10.1016/j.ijbiomac.2022.08.022
201. Wang, C., Q. Cui, X. Wang, and L. Li, *Preparation of Hybrid Gold/Polymer Nanocomposites and Their Application in a Controlled Antibacterial Assay.* ACS Appl Mater Interfaces, 2016. **8**(42): p. 29101-29109. https://doi.org/10.1021/acsami.6b12487
202. El-Sherbiny, I.M., A. El-Shibiny, and E. Salih, *Photo-induced green synthesis and antimicrobial efficacy of poly (varepsilon-caprolactone)/curcumin/grape leaf extract-silver hybrid nanoparticles.* J Photochem Photobiol B, 2016. **160**: p. 355-363. https://doi.org/10.1016/j.jphotobiol.2016.04.029
203. Rasheed, T., K. Rizwan, M. Bilal, and H.M.N. Iqbal, *Metal-Organic Framework-Based Engineered Materials-Fundamentals and Applications.* Molecules, 2020. **25**(7): p. 1-26. https://doi.org/10.3390/molecules25071598
204. Zhuang, J., C.H. Kuo, L.Y. Chou, D.Y. Liu, E. Weerapana, and C.K. Tsung, *Optimized metal-organic-framework nanospheres for drug delivery: evaluation of small-molecule encapsulation.* ACS nano, 2014. **8**(3): p. 2812-9. https://doi.org/10.1021/nn406590q
205. Soomro, N.A., Q. Wu, S.A. Amur, H. Liang, A.U. Rahman, Q. Yuan, and Y. Wei, *Natural drug physcion encapsulated zeolitic imidazolate framework, and their application as antimicrobial agent.* Colloids Surf B Biointerfaces, 2019. **182**: p. 1-7. https://doi.org/10.1016/j.colsurfb.2019.110364
206. Zhang, X., L. Liu, L. Huang, W. Zhang, R. Wang, T. Yue, J. Sun, G. Li, and J. Wang, *The highly efficient elimination of intracellular bacteria via a metal organic framework (MOF)-based three-in-one delivery system.* Nanoscale, 2019. **11**(19): p. 9468-9477. https://doi.org/10.1039/c9nr01284b
207. Karakecili, A., B. Topuz, S. Korpayev, and M. Erdek, *Metal-organic frameworks for on-demand pH controlled delivery of vancomycin from chitosan scaffolds.* Mater Sci Eng C Mater Biol Appl, 2019. **105**: p. 1-11. https://doi.org/10.1016/j.msec.2019.110098
208. Esfahanian, M., M.A. Ghasemzadeh, and S.M.H. Razavian, *Synthesis, identification and application of the novel metal-organic framework Fe3O4@PAA@ZIF-8 for the drug delivery of ciprofloxacin and investigation of antibacterial activity.* Artif Cells Nanomed Biotechnol, 2019. **47**(1): p. 2024-2030. https://doi.org/10.1080/21691401.2019.1617729
209. Yang, Y., X. Wu, C. He, J. Huang, S. Yin, M. Zhou, L. Ma, W. Zhao, L. Qiu, C. Cheng, and C. Zhao, *Metal-Organic Framework/Ag-Based Hybrid Nanoagents for Rapid and Synergistic Bacterial Eradication.* ACS Appl Mater Interfaces, 2020. **12**(12): p. 13698-13708. https://doi.org/10.1021/acsami.0c01666
210. Xiao, Y., M. Xu, N. Lv, C. Cheng, P. Huang, J. Li, Y. Hu, and M. Sun, *Dual stimuli-responsive metal-organic framework-based nanosystem for synergistic photothermal/pharmacological antibacterial therapy.* Acta Biomater, 2021. **122**: p. 291-305. https://doi.org/10.1016/j.actbio.2020.12.045
211. Giménez-Marqués, M., T. Hidalgo, C. Serre, and P. Horcajada, *Nanostructured metal–organic frameworks and their bio-related applications.* Coord. Chem. Rev, 2016. **307**: p. 342-360. https://doi.org/10.1016/j.ccr.2015.08.008.
212. Lin, S., X. Liu, L. Tan, Z. Cui, X. Yang, K.W.K. Yeung, H. Pan, and S. Wu, *Porous Iron-Carboxylate Metal-Organic Framework: A Novel Bioplatform with Sustained Antibacterial Efficacy and Nontoxicity.* ACS Appl Mater Interfaces, 2017. **9**(22): p. 19248-19257. https://doi.org/10.1021/acsami.7b04810

213. Unamuno, X., E. Imbuluzqueta, F. Salles, P. Horcajada, and M.J. Blanco-Prieto, *Biocompatible porous metal-organic framework nanoparticles based on Fe or Zr for gentamicin vectorization.* Eur J Pharm Biopharm, 2018. **132**: p. 11-18. https://doi.org/10.1016/j.ejpb.2018.08.013
214. Haseena, M. Shah, K. Rehman, A. Khan, A. Farid, C. Marini, A. Di Cerbo, and M.R. Shah, *Characterization and Antibacterial Evaluation of Biodegradable Mannose-Conjugated Fe-MIL-88NH2 Composites Containing Vancomycin against Methicillin-Resistant Staphylococcus aureus Strains.* Polymers (Basel), 2022. **14**(13). https://doi.org/10.3390/polym14132712
215. Mateo, D., A. Santiago-Portillo, J. Albero, S. Navalon, M. Alvaro, and H. Garcia, *Long-Term Photostability in Terephthalate Metal-Organic Frameworks.* Angew Chem Int Ed Engl, 2019. **58**(49): p. 17843-17848. https://doi.org/10.1002/anie.201911600
216. Bhardwaj, N., S.K. Pandey, J. Mehta, S.K. Bhardwaj, K.H. Kim, and A. Deep, *Bioactive nano-metal-organic frameworks as antimicrobials against Gram-positive and Gram-negative bacteria.* Toxicol Res (Camb), 2018. **7**(5): p. 931-941. https://doi.org/10.1039/c8tx00087e
217. Arenas-Vivo, A., G. Amariei, S. Aguado, R. Rosal, and P. Horcajada, *An Ag-loaded photoactive nano-metal organic framework as a promising biofilm treatment.* Acta Biomater, 2019. **97**: p. 490-500. https://doi.org/10.1016/j.actbio.2019.08.011
218. Cheng, X., S. Zhang, H. Liu, H. Chen, J. Zhou, Z. Chen, X. Zhou, Z. Xie, Q. Kuang, and L. Zheng, *Biomimetic Metal-Organic Framework Composite-Mediated Cascade Catalysis for Synergistic Bacteria Killing.* ACS Appl Mater Interfaces, 2020. **12**(33): p. 36996-37005. https://doi.org/10.1021/acsami.0c12159
219. André, V., A.R.F. da Silva, A. Fernandes, R. Frade, C. Garcia, P. Rijo, A.M.M. Antunes, J. Rocha, and M.T. Duarte, *Mg- and Mn-MOFs Boost the Antibiotic Activity of Nalidixic Acid.* ACS Appl. Bio Mater, 2019. **2**(6): p. 2347-2354. https://doi.org/10.1021/acsabm.9b00046
220. Wei, Y., C. Chen, S. Zhai, M. Tan, J. Zhao, X. Zhu, L. Wang, Q. Liu, and T. Dai, *Enrofloxacin/florfenicol loaded cyclodextrin metal-organic-framework for drug delivery and controlled release.* Drug Deliv, 2021. **28**(1): p. 372-379. https://doi.org/10.1080/10717544.2021.1879316
221. Li, L.L., J.H. Xu, G.B. Qi, X. Zhao, F. Yu, and H. Wang, *Core-shell supramolecular gelatin nanoparticles for adaptive and "on-demand" antibiotic delivery.* ACS nano, 2014. **8**(5): p. 4975-4983. https://doi.org/10.1021/nn501040h
222. Lin, A., Y. Liu, X. Zhu, X. Chen, J. Liu, Y. Zhou, X. Qin, and J. Liu, *Bacteria-Responsive Biomimetic Selenium Nanosystem for Multidrug-Resistant Bacterial Infection Detection and Inhibition.* ACS nano, 2019. **13**(12): p. 13965-13984. https://doi.org/doi.org/10.1021/acsnano.9b05766
223. Kamal, Z., J. Su, W. Yuan, F. Raza, L. Jiang, Y. Li, and M. Qiu, *Red blood cell membrane-camouflaged vancomycin and chlorogenic acid-loaded gelatin nanoparticles against multi-drug resistance infection mice model.* Journal of Drug Delivery Science and Technology, 2022: p. 103706. https://doi.org/https://doi.org/10.1016/j.jddst.2022.103706
224. Zhang, Y., J. Zhang, W. Chen, P. Angsantikul, K.A. Spiekermann, R.H. Fang, W. Gao, and L. Zhang, *Erythrocyte membrane-coated nanogel for combinatorial antivirulence and responsive antimicrobial delivery against Staphylococcus aureus infection.* J Control Release, 2017. **263**: p. 185-191. https://doi.org/10.1016/j.jconrel.2017.01.016
225. Wu, X., Y. Li, F. Raza, X. Wang, S. Zhang, R. Rong, M. Qiu, and J. Su, *Red Blood Cell Membrane-Camouflaged Tedizolid Phosphate-Loaded PLGA Nanoparticles for Bacterial-Infection Therapy.* Pharmaceutics, 2021. **13**(1): p. 1-17. https://doi.org/10.3390/pharmaceutics13010099
226. Osman, N., N. Devnarain, C.A. Omolo, V. Fasiku, Y. Jaglal, and T. Govender, *Surface modification of nano-drug delivery systems for enhancing antibiotic delivery and activity.*

Wiley Interdiscip Rev Nanomed Nanobiotechnol, 2021: p. e1758. https://doi.org/10.1002/wnan.1758

227. Angsantikul, P., S. Thamphiwatana, Q. Zhang, K. Spiekermann, J. Zhuang, R.H. Fang, W. Gao, M. Obonyo, and L. Zhang, *Coating nanoparticles with gastric epithelial cell membrane for targeted antibiotic delivery against Helicobacter pylori infection.* Adv Ther (Weinh), 2018. **1**(2). https://doi.org/10.1002/adtp.201800016
228. Gao, F., L. Xu, B. Yang, F. Fan, and L. Yang, *Kill the Real with the Fake: Eliminate Intracellular Staphylococcus aureus Using Nanoparticle Coated with Its Extracellular Vesicle Membrane as Active-Targeting Drug Carrier.* ACS Infect Dis, 2019. **5**(2): p. 218-227. https://doi.org/10.1021/acsinfecdis.8b00212
229. Wang, K., Y. Lei, D. Xia, P. Xu, T. Zhu, Z. Jiang, and Y. Ma, *Neutrophil membranes coated, antibiotic agent loaded nanoparticles targeting to the lung inflammation.* Colloids Surf B Biointerfaces, 2020. **188**: p. 110755. https://doi.org/10.1016/j.colsurfb.2019.110755
230. Cao, Z., Y. Luo, Z. Li, L. Tan, X. Liu, C. Li, Y. Zheng, Z. Cui, K.W.K. Yeung, Y. Liang, S. Zhu, and S. Wu, *Antibacterial Hybrid Hydrogels.* Macromol Biosci, 2021. **21**(1): p. 1-24, Article e2000252. https://doi.org/10.1002/mabi.202000252
231. Sattari, S., A. Dadkhah Tehrani, and M. Adeli, *pH-Responsive Hybrid Hydrogels as Antibacterial and Drug Delivery Systems.* Polymers (Basel), 2018. **10**(6): p. 1-15. https://doi.org/10.3390/polym10060660
232. Tao, B., C. Lin, Y. Deng, Z. Yuan, X. Shen, M. Chen, Y. He, Z. Peng, Y. Hu, and K. Cai, *Copper-nanoparticle-embedded hydrogel for killing bacteria and promoting wound healing with photothermal therapy.* J Mater Chem B, 2019. **7**(15): p. 2534-2548. https://doi.org/10.1039/c8tb03272f
233. Lin, J., Z. He, F. Liu, J. Feng, C. Huang, X. Sun, and H. Deng, *Hybrid Hydrogels for Synergistic Periodontal Antibacterial Treatment with Sustained Drug Release and NIR-Responsive Photothermal Effect.* Int J Nanomedicine, 2020. **15**: p. 5377-5387. https://doi.org/10.2147/IJN.S248538
234. Posadowska, U., M. Brzychczy-Wloch, A. Drozdz, M. Krok-Borkowicz, M. Wlodarczyk-Biegun, P. Dobrzynski, W. Chrzanowski, and E. Pamula, *Injectable hybrid delivery system composed of gellan gum, nanoparticles and gentamicin for the localized treatment of bone infections.* Expert Opin Drug Deliv, 2016. **13**(5): p. 613-620. https://doi.org/10.1517/17425247.2016.1146673
235. Chopra, H., S. Kumar, and I. Singh, *Bioadhesive Hydrogels and Their Applications*, in *Bioadhesives in Drug Delivery*. 2020. p. 147-170 https://doi.org/10.1002/9781119640240.ch6
236. Zhang, Y., J. Zhang, M. Chen, H. Gong, S. Thamphiwatana, L. Eckmann, W. Gao, and L. Zhang, *A Bioadhesive Nanoparticle-Hydrogel Hybrid System for Localized Antimicrobial Drug Delivery.* ACS Appl Mater Interfaces, 2016. **8**(28): p. 18367-18374. https://doi.org/10.1021/acsami.6b04858
237. Tan, C., J. Wang, and B. Sun, *Biopolymer-liposome hybrid systems for controlled delivery of bioactive compounds: Recent advances.* Biotechnol Adv, 2021. **48**: p. 1-22, Article 107727. https://doi.org/10.1016/j.biotechadv.2021.107727
238. Gao, W., D. Vecchio, J. Li, J. Zhu, Q. Zhang, V. Fu, J. Li, S. Thamphiwatana, D. Lu, and L. Zhang, *Hydrogel containing nanoparticle-stabilized liposomes for topical antimicrobial delivery.* ACS nano, 2014. **8**(3): p. 2900-7. https://doi.org/10.1021/nn500110a
239. Salatin, S. and M. Jelvehgari, *Desirability function approach for development of a thermosensitive and bioadhesive nanotransfersome-hydrogel hybrid system for enhanced skin bioavailability and antibacterial activity of cephalexin.* Drug Dev Ind Pharm, 2020. **46**(8): p. 1318-1333. https://doi.org/10.1080/03639045.2020.1788068

240. Tung le, M., N.X. Cong, T. Huy le, N.T. Lan, V.N. Phan, N.Q. Hoa, K. Vinh le, N.V. Thinh, T. Tai le, D.T. Ngo, K. Mølhave, T.Q. Huy, and A.T. Le, *Synthesis, Characterizations of Superparamagnetic Fe3O4-Ag Hybrid Nanoparticles and Their Application for Highly Effective Bacteria Inactivation.* J Nanosci Nanotechnol, 2016. **16**(6): p. 5902-5912. https://doi.org/10.1166/jnn.2016.11029

241. Zhang, C., C. Du, J.Y. Liao, Y. Gu, Y. Gong, J. Pei, H. Gu, D. Yin, L. Gao, and Y. Pan, *Synthesis of magnetite hybrid nanocomplexes to eliminate bacteria and enhance biofilm disruption.* Biomater Sci, 2019. **7**(7): p. 2833-2840. https://doi.org/10.1039/c9bm00057g

242. Zhang, W., R. Taheri-Ledari, Z. Hajizadeh, E. Zolfaghari, M.R. Ahghari, A. Maleki, M.R. Hamblin, and Y. Tian, *Enhanced activity of vancomycin by encapsulation in hybrid magnetic nanoparticles conjugated to a cell-penetrating peptide.* Nanoscale, 2020. **12**(6): p. 3855-3870. https://doi.org/10.1039/c9nr09687f

243. Wan, F., S.S. Bohr, S.N. Kłodzińska, H. Jumaa, Z. Huang, T. Nylander, M.B. Thygesen, K.K. Sørensen, K.J. Jensen, C. Sternberg, N. Hatzakis, and H. Mørck Nielsen, *Ultrasmall TPGS-PLGA Hybrid Nanoparticles for Site-Specific Delivery of Antibiotics into Pseudomonas aeruginosa Biofilms in Lungs.* ACS Appl Mater Interfaces, 2020. **12**(1): p. 380-389. https://doi.org/10.1021/acsami.9b19644

CHAPTER 3. FIRST EXPERIMENTAL PAPER

3.1 General Introduction

This chapter addresses Aim 1, Objectives 1-8, and is a first-authored experimental paper submitted to an ISI International Journal: *International Journal of Biological Macromolecules* (Manuscript ID: IJBIOMAC-D-23-18902) (Impact factor: 8.2). This article highlights the synthesis of a novel HA-Lys conjugate and explores its biomimetic activity to competitively inhibit bacterial-TLRs induced inflammatory responses using *in vitro* investigations. It also highlights the formulation, optimization, and characterization of multifunctional biomimetic pH-responsive VCM-HNLCs, which was prepared from the synthesized HA-Lys, TS, and OLA to enhance VCM delivery. Furthermore, it evaluates the biocompatibility, hemocompatibility, *in vitro* TLR2 and TLR4 binding affinity, *in vitro* antibacterial, antibiofilm, efflux pump inhibition, antioxidant, and anti-inflammatory activities of the prepared VCM-HNLCs.

3.2 Author contributions

In this paper, **Mrs. Eman Elhassan** performed the literature searches that contributed to the conceptualization and the design and execution of this project. These involved the synthesis, preparation, and characterization of the novel biomaterial and hybrid nanocarriers (HNs). The HNs were characterized for physicochemical properties including average particle size, polydispersity index, zeta potential, entrapment efficiency, drug loading capacity, thermal profiles, and surface morphology. Furthermore, **Mrs. Eman Elhassan** contributed towards the characterization of the formulation in terms of *in vitro* antibacterial activity, hemocompatibility studies, *in vitro* drug release study and its mathematical modelling, colloidal stability studies, receptor binding with microscale thermophoresis (MST) technique and *in vitro* antioxidant study. **Mrs. Eman Elhassan** was also responsible for analysis and data collection, as well as writing entire draft version of the first authored article and revised it according to co-authors comments. Mr. Mohammed A. Gafar assisted with the antibacterial and *in vitro* binding affinity studies. Prof. Calvin A. Omolo served as co-supervisor and assisted with the conceptualization, design of the project, solving any technical problems and supervision of the studies. Mr. Usri H. Ibrahim conducted the anti-inflammatory studies. Dr. Rene Khan conducted the cytotoxicity studies. Prof. Thirumala Govender served as supervisor and was responsible for project conceptualization, problem-solving, editing of paper and abstract as well as general supervision of all the experiments.

3.3 Submitted manuscript

Design of multifunctional biomimetic pH-responsive hybrid nanostructured lipid carriers for targeted delivery of vancomycin against bacterial sepsis

Eman Elhassan [1], Mohammed A. Gafar [1,2], Calvin A. Omolo [1,3 *], Usri H. Ibrahim [4], Rene Khan [5], Thirumala Govender [1 *].

[1] Discipline of Pharmaceutical Sciences, College of Health Sciences, University of KwaZulu-Natal, Private Bag X54001, Durban, South Africa.

[2] Department of Pharmaceutics, Faculty of Pharmacy, University of Khartoum, Sudan.

[3] Department of Pharmaceutics and Pharmacy Practice, School of Pharmacy and Health Sciences, United States International University-Africa, P. O. Box 14634-00800, Nairobi, Kenya.

[4] Discipline of Human Physiology, School of Laboratory Medicine and Medical Sciences, College of Health Sciences, University of KwaZulu-Natal, Durban, South Africa.

[5] Discipline of Medical Biochemistry, School of Laboratory Medicine and Medical Science, University of KwaZulu-Natal, Durban, South Africa.

[*] Corresponding authors: comolo@usiu.ac.ke, govenderth@ukzn.ac.za.

Graphical abstract

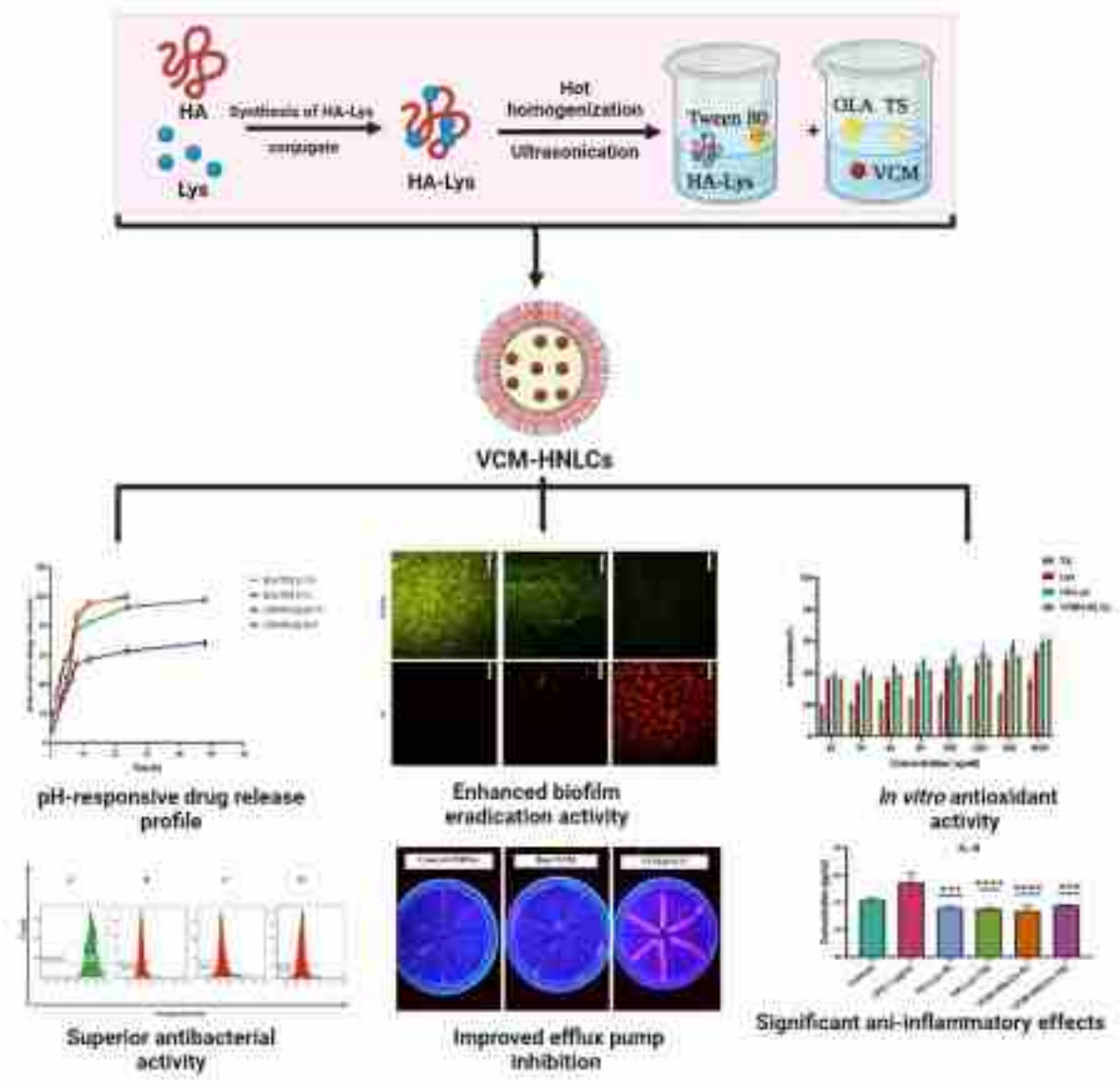

Abstract

Developing innovative drug delivery strategies is crucial for improving the accuracy and efficiency of antibiotics in combating bacterial sepsis. The application of biomimetic and stimuli-responsive nanocarriers displays considerable promise in improving the management of bacterial sepsis and overcoming antimicrobial resistance. In this study, a novel hyaluronic acid-lysine conjugate (HA-Lys) was synthesized for the creation of multifunctional biomimetic pH-responsive vancomycin-loaded hybrid NLCs (VCM-HNLCs) to treat bacterial sepsis. The HA-Lys conjugate was synthesized and analyzed by FTIR, and ^{1}H NMR spectroscopy. The VCM-HNLCs were prepared using the HA-Lys conjugate, tocopherol succinate (TS) and Oleylamine (OLA) by hot homogenization ultrasonication technique, and their particle size, PDI, ZP, EE %, and DL % w/w were measured, with values of 110.77 ± 1.69 nm, 0.11 ± 0.02, -2.92 ± 0.21 mV, 76.27 ± 1.20 % and 8.36 ± 0.25 %, respectively. Studies on *in vitro* biocompatibility proved that VCM-HNLCs are non-hemolytic and biosafe. The strong binding affinity of HA-Lys and VCM-HNLCs to human Toll-like receptor 2 (TLR2) and TLR4 in comparison to their native substrates was validated by *in vitro* microscale thermophoresis (MST) investigations. The VCM-HNLCs demonstrated a more rapid drug release at pH 6.0 than at pH 7.4 and displayed improved and pH-sensitive antibacterial and biofilm eradication activities, with a considerable inhibitory impact against MRSA efflux pumps, compared to bare VCM. Moreover, the prepared hybrid nanosystem showed potential activity in neutralizing ROS and modulating the inflammatory response induced by LPS, as confirmed by *in vitro* DPPH scavenging and anti-inflammatory investigations. In conclusion, the results demonstrate the potential of VCM-HNLCs as novel multifunctional nanocarriers to reduce the spread of AMR-bacteria and improve the outcome of VCM use in sepsis management.

Keywords: Biomimetic; pH-responsive; Hyaluronic acid-lysine; Hybrid nanocarriers; Bacterial Sepsis; Antibiotic delivery.

1. Introduction

Bacterial sepsis is a life-threatening organ dysfunction caused by a dysregulated host immune response to infection [244]. It is a serious disease that can lead to shock and multi-organ failure, accounting for 50 % of sepsis-related deaths [245]. Despite advances in medical care, bacterial sepsis remains a significant public health concern globally with high morbidity and mortality rates. According to the global burden of disease report published by the World Health Organization (WHO), sepsis affects more than 49 million people, with an estimated 11 million deaths annually, accounting for approximately 20 % of all causes of death worldwide [246]. In addition, 30 % of septic patients who survive through the initial inflammatory storm may experience long-term immunosuppressive

dysfunctions and cognitive impairment, worsening the prognosis of sepsis and placing a heavy burden on both individuals and society [245, 247]. The emergence of antimicrobial resistance (AMR) further complicates infection therapy and sepsis management in all settings, especially in high-risk populations, such as infants and patients in intensive care units (ICUs) [5, 246, 248].

The pathophysiology of sepsis involves a complex cascade of events, including the release of pro-inflammatory cytokines, activation of coagulation pathways, overproduction of reactive oxygen species (ROS), endothelial and organ dysfunction, and impaired immune response [249]. This intricate molecular pathophysiology presents numerous potential targets for pharmacological interventions. In general, administration of effective antibiotics to control the infection and adjuvant medicines such as antioxidants and anti-inflammatory agents to regulate the host immune response are the most fundamental strategies for sepsis management [250]. However, persistent infection still occurs in 70 -80 % of sepsis-related deaths, demonstrating the prevalence of AMR that limits the effectiveness of available antimicrobial agents [251]. In addition, the dysregulated immune response in sepsis can lead to immunosuppression, a post-sepsis immune paralysis, that makes patients susceptible to secondary infections, which further worsens the clinical course of sepsis [252, 253]. Therefore, there is an urgent need for more innovative multi-task therapeutic approaches and enhanced antibiotic treatments to reduce the spread of AMR-bacteria and control the prevalence of sepsis.

Nanotechnology has created a new avenue for research, in the last few decades, to enhance the potential of antibiotic therapy. Numerous nano-drug delivery systems (NDDSs) have been investigated to enhance antibiotic treatments and delivery against bacterial infections, featuring the ability to get around the restrictions of current dosage forms of antibiotic and evade existing mechanisms associated with acquired antimicrobial resistance [44, 254]. These nanosystems offer several advantages, including improved solubility, sustained and controlled drug release profiles and enhanced binding to bacterial cells with better cellular internalization [40, 255]. However, challenges for achieving maximum targeting and interaction with bacteria at the infection site still exist and must be overcome.

Bacterial infections often create acidic microenvironments due to the bacteria's metabolic activities and the host's immune response [256]. Advances in NDDSs, therefore, involve the creation of pH-responsive NDDSs that adapt to this unique microenvironment, enabling precise and on-demand antibiotic release at the infection site and improved interaction with the targeted bacteria [257]. In addition, biomimicry is currently being explored as a potential strategy to enhance the benefits of NDDSs by mimicking biological structures or disease-associated cellular communication pathways,

thereby increasing affinity to target cells [258, 259]. The merging of biomimetic principles with the benefits of pH-responsive nanocarriers could be a promising approach to maximize the potential of various nanomedicines in treating infectious diseases. However, only few research have been documented using the combined strategy of pH-responsiveness and biomimetic properties for cancer therapy [260-262] and antibiotic delivery [263]. Therefore, it is of great interest to address the considerable gap in this field to increase the effectiveness of antibiotics against bacterial sepsis and combat AMR.

During infections, pattern recognition receptors in the host cell, such as toll-like receptors (TLRs), are activated by structurally conserved microbial toxins, enabling the innate immune system to identify invasive pathogens such as bacteria [68]. Binding of specific microbial ligands, such as peptidoglycan (PGN) of gram-positive bacteria or lipopolysaccharide (LPS) of gram-negative bacteria to TLRs triggers inflammatory responses that facilitate the control of invading bacteria [69]. However, in severe sepsis associated with bacterial infection, excessive activation of TLR occurs, leading to systemic inflammation and organs damage [264, 265]. Emerging research shows an interest in developing therapeutic TLR activation inhibitors or antagonists, particularly for TLR2 and TLR4, to treat infection-induced sepsis [71-74]. Researchers have identified small drug molecules and antibodies that prevent TLR ligands from binding to the receptor, and they have shown promising results in lowering TLR signaling activity in many inflammatory diseases [74-76]. Therefore, this biomimetic strategy of minimizing TLR activation by inhibiting their binding to bacterial toxins can be applied to an antibiotic nanocarrier to kill the bacteria while enhancing the treatment of sepsis specifically.

Nanostructured lipid carriers (NLCs) have emerged as a promising approach in the field of drug delivery, particularly for treating bacterial infections and related inflammatory disorders [266, 267]. These systems offer numerous advantages, including unique nanosized-dependent properties, tissue-targeted drug delivery, ease of fabrication, cost-efficiency, and practicability of large-scale manufacturing, making these delivery systems more attractive.[268-271]. Recently, hybrid NLCs-based nanosystems (HNLCs) are developed by incorporating different polymeric biomaterials into the NLCs make-up to increase their stability, improve their pharmacokinetic properties and enhance the encapsulation of hydrophilic drugs in a lipid-based nanoformulation [272, 273]. Few research have reported using HNLCs for the delivery of antihypertensive [272], anticancer [274, 275] and antimalarial drugs to date [276]. However, only one study reported the application of chitosan-based HNLCs for antibiotic delivery [277]. As a result, research of this kind is required to progress the area, aid in the management of bacterial sepsis, and help combat AMR. However, there is a need to identify

an innovative combination of materials with multifunctional properties to develop a biomimetic pH-responsive HNLC with enhanced efficacy and targeted antibiotic delivery against bacterial sepsis.

High molecular weight hyaluronic acid (HA) has gained attention as a potential therapeutic agent in managing inflammations due to its well-known anti-inflammatory and immunosuppressive properties [278]. Several studies have reported the ability of HA to reduce the expression of human TLRs in many inflammatory disorders by selectively binding to the receptor and inhibiting their binding to bacterial endotoxins, thereby lowering their infection-induced inflammatory mediators [279-282]. In contrast, L-Lysine (Lys), an essential amino acid, has been found to exhibit antioxidant activity against oxidative stress-induced tissue damage in many disease conditions, including diabetes, chronic kidney disease, lung infections and sepsis [283-285]. The antioxidant activity of Lys plays a beneficial role in scavenging and neutralizing ROS generated during the inflammatory process, thereby reducing oxidative stress and tissue damage, and mitigating the harmful effects of sepsis on the body [286]. The modification of HA with Lys through the synthesis of a novel HA-lysine conjugate (HA-Lys) that exhibits both TLR antagonism and oxidative stress reduction activities could, therefore, be a potential approach that provides a therapeutic adjuvant with increased potency and targeting against sepsis-causing bacteria.

Tocopherol succinate (TS), a vitamin E derivative, has also shown potential in treating various infectious diseases, primarily due to its antioxidant, anti-inflammatory and antimicrobial properties [287, 288]. It has shown promising efflux pump inhibition activities, mainly against NorA and NorB of gram-positive bacteria, allowing for more enhanced intracellular accumulation of antibiotics in the target bacterial cells and restoring the efficacy of existing antibiotics to combat multidrug-resistant (MDR) bacteria [289-291]. Moreover, it has been reported that TS has significant anti-adhesive properties against *Staphylococcus aureus* (*S. aureus*) biofilms. Therefore, it could act synergistically with an antibiotic to affect pathogen adhesion and biofilm formation, making it a suitable pharmaceutical adjuvant for antibiotic therapy [292, 293]. On the other hand, Oleylamine (OLA), a lipid with pH-responsive activity, offers unique properties that can be exploited in the design of drug delivery systems. Its pH-dependent functionality and its intrinsic antimicrobial behavior enable the development of lipid-based nanosystems with controlled drug release and improved therapy for the treatment of infectious diseases [294]. Overall, designing a multifunctional HNLC that combines the benefits of HA-Lys conjugate, TS and OLA could improve the therapeutic index of antibiotics and enhance the overall performance of the drug delivery system against bacterial sepsis.

Therefore, the study aimed to synthesize a novel HA-Lys conjugate and to utilize the attributes of the synthesized HA-Lys with TS and OLA in the formulation of multifunctional biomimetic pH-

responsive HNLCs loaded with vancomycin (VCM-HNLCs), to combat bacterial sepsis. We hypothesize that HA-Lys may directly and competitively bind to host TLR2 or TLR4, therefore, prevents their binding to bacterial toxins, reduces excessive TLR activation, and neutralizes ROS. All of these contribute to modulating host immune response, reducing oxidative stress and controlling inflammatory cytokine levels. Also, TS may potentially reduce bacterial antibiotic resistance via its potential activity against biofilm formation and efflux pumps. In addition, the on-demand release of VCM from the HNLCs could be enhanced through the pH sensitivity of OLA. Altogether, this novel multifunctional NDDS offers multiple mechanisms of action to eradicate bacteria and reduce excessive inflammatory activation for optimal therapeutic outcomes against bacterial infections and sepsis. To our knowledge, this is the first report on synthesizing and using a modified HA-Lys polymer as a targeting adjuvant to treat bacterial sepsis. Also, this study reports the first stimuli-responsive HNLCs for the delivery of any class of drug and the first combined biomimetic and pH-responsive HNLCs to deliver antibiotics against bacterial sepsis. The data obtained from the synthesis and characterization of HA-Lys conjugate, formulation and optimization of VCM-HNLCs, *in vitro* characterizations, *in vitro* antibacterial, antioxidant and anti-inflammatory studies are provided herein.

2. Materials and methods

2.1 Materials

L-Lysine (Lys), tocopherol succinate (TS), Oleylamine (OLA), 1-ethyl-3-(dimethyl amino propyl) carbodiimide (EDC), *N*-hydroxy succinimide (NHS), ethidium bromide, peptidoglycan (PGN) from *Staphylococcus* aureus, lipopolysaccharides (LPS) from *Escherichia coli* (O55:B5) and 2,2-diphenyl-1-picrylhydrazyl (DPPH) were purchased from Sigma-Aldrich (USA). Hyaluronic acid sodium salt (average molecular weight = 10 kDa), *Staphylococcus aureus* (ATCC 25923) and multi-drug resistant *Staphylococcus aureus* (SA Rosenbach ATCC BAA 70699) were obtained from DLD Scientific (South Africa). Vancomycin hydrochloride was procured from Sino-bright Import and Export Co., Ltd (China) and then converted to vancomycin free base (VCM) using a previously described method [295]. Dulbecco's modified Eagle's medium (DMEM), Eagle's Minimum Essential Medium (EMEM), fetal bovine serum, propidium iodide (PI) and Syto9 were obtained from Thermo Fisher (USA). 3(4,5-Dimethylthiazol-2-yl)-2,5-diphenyltetrazolium bromide (MTT), Tween 80, dimethyl sulfoxide (DMSO) and crystal violet were purchased from Merck Chemicals (Germany). Cell lines were purchased from Highveld Biologicals (Johannesburg, South Africa) and cell culture materials were purchased from Whitehead Scientific (Johannesburg, South Africa). Sheep blood used for hemolytic activity evaluations was obtained from United Scientific (South Africa). Mueller-Hinton Broth (MHB), and Mueller- Hinton Agar (MHA) were obtained from Biolab (South Africa). Recombinant human TLR2 (RPA663Hu03) was purchased from Biocom Africa (Centurion, South

Africa). Recombinant human TLR4 (Active ab233665) was obtained from Abcam (Cambridge, UK). Enzyme Linked Immunosorbent Assay (ELISA) kits were purchased from ABclonal Technology (Wuhan, Hubie, China). Microscale thermophoresis (MST) reagents were purchased from Nano Temper Technologies (Germany). A mill-Q water purification system (Millipore corp., USA) was used to obtain a purified milli-Q water. All solvents and reagents used in this study were of analytical grade.

2.2 Synthesis and characterization of HA-Lys conjugate

The HA-Lys conjugate was synthesized via the formation of an amide bond between the primary amino group of Lys and the free carboxylic acid group of HA according to a previously documented EDC/NHS method with minor modifications (**Scheme 1**) [296, 297]. To activate the carboxyl acid groups of HA, 200 mg (0.496 mmol) of HA was dissolved in 50 mL of deionized water. Next, EDC (479.75 mg, 2.5 mmol) and NHS (287.7 mg, 2.5 mmol) were added to the HA solution, and the mixture was continuously stirred at room temperature for 15 min. Afterward, the reaction mixture was mixed with 250 mg of Lys (1.710 mmol), and it was continuously stirred at room temperature for overnight. The resultant conjugate solution was purified by three rounds of dialysis against 0.1 % w/v NaCl solution and finally against distilled water, followed by lyophilization at -40 °C to obtain a white powder with a quantitative yield of 81.12 %. The freeze-dried samples were characterized using FT-IR (Bruker ALPHA II compact FT-IR spectrometer, UK) and ^{1}H NMR (Bruker Advance 400 MHz spectrometer, UK), and then stored at 4 °C for further use. The characterization was as follows: ^{1}H NMR: (400 MHz, D_2O) δ(ppm): HA: δ 1.90 (c), 3.30–3.59 (f, g), and 4.44 (h); Lys: δ 1.18 (a), 1.59–2.30 (b, d), and 2.76 (e), and FT-IR: 3400, 3345.08, 3301.47, 2921.06, 2887.12, 1628.97, 1576.07, 1507, 1400.24, 1388.44, 1035.89 and 656.64 cm^{-1}.

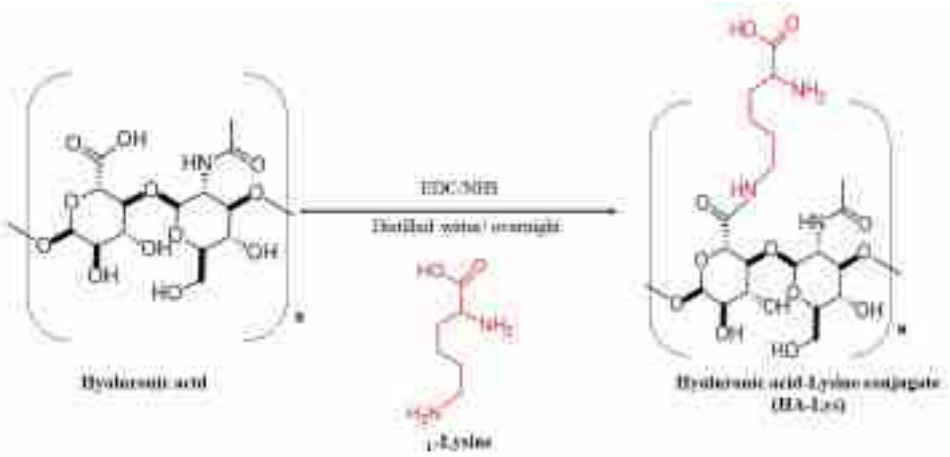

Scheme 1. Synthesis of HA-Lys conjugate using a one-step amidation reaction. (* EDC = 1-ethyl-3-(dimethyl amino propyl) carbodiimide, NHS = *N*-hydroxy succinimide)

2.3 Preparation of the hybrid nanoparticles

The VCM-loaded HNLCs (VCM-HNLCs) were formulated using a hot homogenization/ultrasonication technique that had been previously reported by our group with a slight modification [267]. To create the lipid phase, a specific amount of TS, OLA and VCM free base were dissolved in 2 mL of ethanol, and the mixture was heated at 80 °C for 20 min. To create the aqueous phase, a specific amount of HA-Lys conjugate and an appropriate surfactant were dissolved in 20 mL of milli-Q water, and heated separately at 80 °C for 20 min. Both phases were then mixed and homogenized using an Ultra Turrax T-25 homogenizer (IKA Labortechnik, Germany) at 6000 rpm for 15 min at the same temperature. The resultant emulsion was promptly cooled using an ice bath for 30 min after being further sonicated at 30 % amplitude for 10 min using a probe sonicator (Omni Sonic-Ruptor 400 Ultrasonic Homogenizer, USA). The prepared VCM-HNLCs were stirred overnight to remove the organic solvent, and if required, milli-Q water was used to adjust the final volume to 20 mL. Blank (VCM-free) HNLCs were also prepared using the same procedure. Different types of surfactants (Span 80, polyethylene glycol 400 (PEG 400), poly(*N*-vinylpyrrolidone) (PVP), poloxamer 188 (PLX 188) and Tween 80) were screened to create a stable nanosystem. Thereafter, various parameters including lipid: surfactant, drug: lipid and lipid: polymer mass ratios were evaluated. The optimal formulation with minimum particle size, polydispersity index (PDI), maximum entrapment efficiency percent (EE %) and drug loading capacity (DL % w/w) was selected for further studies. Each batch was prepared in triplicate.

2.4 Physicochemical characterization of VCM-HNLCs

2.4.1 Determination of particle size, polydispersity index (PDI), zeta potential (ZP) and nanoparticle morphology

The mean particle size, size distribution (PDI) and ZP of the fabricated VCM-HNLCs were measured using the dynamic light scattering (DLS) method with a Zetasizer Nano ZS90 (Malvern Instruments Ltd., UK) fitted with a 633 nm laser at 173° detection optics. The samples were appropriately diluted in distilled water, and the measurement was carried out in triplicate at 25 °C. Transmission electron microscopy (TEM) was used to analyze the morphological structure of VCM-HNLCs. On a coated grid surface, a drop of properly diluted VCM-HNLCs formulation was placed. It was then let to dry at room temperature, stained for 30 sec with 2 % phosphtungestic acid and then visualized at an accelerating voltage of 75 kV to obtain TEM images.

2.4.2 Determination of entrapment efficiency percent (EE %) and drug loading capacity (DL % w/w)

A previously described ultrafiltration method was employed to determine the EE % and the DL % w/w of VCM within the HNLCs [267]. Concisely, 2 mL of the formulation was added to an AmiconUltra-4 centrifugal filter tube (Millipore Corp., USA) with a molecular weight cutoff of 10 kDa and centrifuged at 3000 rpm for 30 min in room temperature. The concentration of free VCM in the supernatant was measured by high performance liquid chromatography (HPLC), using an LC-2050C- 3D (Shimadzu HPLC, Japan) with UV detection at 280 nm, 0.1 % aqueous trifluoracetic acid: acetonitrile (15:85) as mobile phases, Gemini® 5µm NX-C18 110 Å (250×4.6 mm) column, 1 mL/min low pressure gradient flow rate, 100 µL injection volume, and 10 min run time, with a linear equation of Y = 18420 (x) – 4555.5 and linearity coefficient (R^2) of 0.9998 (**Figure S1, Appendix I**). The experiment was carried out in triplicate, and the EE % and DL % w/w were calculated using the following equations [298].

$$\text{EE \%} = \frac{\text{Weight of VCM in the HNLCs}}{\text{Total weight of VCM added}} \times 100 \quad (1)$$

$$\text{DL \%} = \frac{\text{Weight of VCM in the HNLCs}}{\text{Total weight of NPs}} \times 100 \quad (2)$$

2.4.3 Thermal profiles

Using a Shimadzu DSC-60 (Japan), differential scanning calorimetry (DSC) analysis was performed to determine the thermograms of HA, Lys, HA-Lys conjugate, TS, VCM, physical mixture and lyophilized VCM-HNLCs. Briefly, a total of 5 mg of each sample was loaded in an aluminum pan, which was then sealed with a crimper and heated under a stream of nitrogen to 330 °C at a steady 10 °C/min. An empty pan served as a reference.

2.5 *In vitro* biosafety studies

2.5.1 Cytotoxicity and cell viability assay

The cytocompatibility of the synthesized HA-Lys conjugate and its nanoformulation (VCM-HNLCs) was assessed using human embryonic kidney 293 (HEK 293) and human hepatocyte carcinoma (HepG2) cells, employing a previously reported MTT assay [299, 300]. Briefly, cells were seeded (2.5 x 10^3 cells/well) in a 96-well plate with 100 µL of DMEM, 10 % fetal bovine serum (FBS), 1 % pen-strep-fungizone and 1 % L-glutamine and incubated at 37 °C for 24 hrs using a CO_2 humidified incubator. Subsequently, the cells were incubated for the next 24 hrs after being exposed to HA-Lys and VCM-HNLCs (diluted with DMEM) at doses of 20, 40, 60, 80, and 100 µg/mL, respectively.

Thereafter, the cells were grown for an extra 4 hrs using new culture medium (100 µL/well) and 20 µL/well of MTT solution (5 mg/mL in PBS). After removing the supernatant, 100 µL of sterile dimethyl sulfoxide (DMSO) was used to solubilize the formazan crystals. The absorbance at 540 nm were then recorded after 1 hr using a microplate spectrophotometer (Spectrostar Nano, Germany). The experiment was carried out in triplicate and the cell viability percent was computed using equation (3):

$$\text{Cell viability } \% = \frac{\text{A540 nm treated cells}}{\text{A540 nm untreated cells}} \times 100 \quad (3)$$

2.5.2 Hemolysis

The non-hemolytic activity of the prepared VCM-HNLCs was assessed using a previously reported method [301, 302]. In summary, three washes of freshly collected sheep blood was performed using 0.1N sterile isotonic PBS (pH 7.4) by centrifugation at 3000 rpm for 10 min. Next, 1.8 mL of six distinct concentrations of VCM-HNLCs formulation in 0.1N sterile PBS (0.05, 0.1, 0.2, 0.3, 0.4 and 0.5 mg/mL), PBS (as negative control) and distilled water (as positive control) were separately mixed and incubated with 0.2 mL of the previously purified red blood cell suspension for 30 min at 37 °C. After incubation, the samples were centrifuged using the ultracentrifuge (Centurion Scientific, UK) at 3000 rpm and 4 °C for 10 min. The supernatants of each sample were then collected into 96-well plates and their hemoglobin absorbances were quantitatively recorded at 540 nm using a microplate reader (SpectraMax M2, USA). The experiment was done in triplicate and the percentage of non-hemolytic activity was calculated using the following equation:

$$\text{Non-hemolytic activity } \% = 100 - \frac{(\text{ABS} - \text{ABS}_0)}{(\text{ABS}_{100} - \text{ABS}_0)} \quad (4)$$

Where ABS_0 and ABS_{100} are the absorbances at 0 % and 100 % hemolysis, respectively.

2.6 *In vitro* binding affinity study

The binding affinity of individual adjuvants (HA, Lys and HA-Lys conjugate), non-hybrid NLCs components and VCM-HNLCs to human TLR2 and TLR4 was determined and compared to their natural substrates, peptidoglycan (PGN) and lipopolysaccharide (LPS), respectively, employing microscale thermophoresis (MST) on a Nano Temper Monolith NT.115 instrument (Nano Temper Technology, Germany) [263].

2.6.1 Determination of *in vitro* binding affinity to TLR2

According to the manufacturer's protocol, recombinant human TLR2 was first adjusted to a concentration of 200 nM, labeled with the Monolith His-Tag labeling kit Red -tris-NTA, incubated for 30 min at room temperature and then centrifuged at 15000 rpm for 10 min at 4 °C. After protein

labeling, serial dilutions of different ligands with varying starting concentrations were prepared using an appropriate MST buffer (0.1 M PBS, 0.05 % Tween 20, pH 7.4). Then, each dilution was mixed with an equivalent volume (10 µL) of the labeled TLR2 in a final concentration of 50 nM and the mixture was incubated for 10 min. Samples were then loaded into Standard Treated MST glass capillaries (Nano Temper Technology, Germany) and MST traces were measured using the Nano Temper Monolith NT.115 instrument at 25 °C and 70 % MST medium power. All experiments were performed in triplicate. The dissociation constant (K_d) for each ligand was adjusted using the Monolith-Affinity analysis program version 2.1.3 (Nano Temper Technologies, Germany).

2.6.2 Determination of *in vitro* binding affinity to TLR4

In the experiment, the concentration of recombinant human TLR4 was first adjusted to 3.6 µM and labeled with the Monolith NT.115 protein labeling kit Blue-NHS according to the manufacturer's protocol using a 1:3 protein-to-dye ratio. The mixture was incubated at room temperature for 15 min, protected from light, and then purified with a gel-filtration column. Following protein labeling, serial dilutions of various ligands were prepared using a suitable MST buffer (0.1 M PBS, 0.05 % Tween 20, pH 7.4) with different starting concentrations. Next, each dilution was supplemented with an equivalent volume of the labeled TLR4 (10 µL) at a final concentration of 20 nM and incubated for 10 min. Finally, the samples were loaded into Standard Treated glass MST capillaries (Nano Temper Technology, Germany) and MST traces were recorded in Nano Temper Monolith NT.115 instrument at 25 °C, blue LED and 80 % MST power. All experiments were performed in triplicate. The dissociation constant (K_d) values were calculated using Monolith-Affinity analysis software version 2.1.3 (Nano Temper Technologies, Germany) for every tested ligand.

2.7. *In vitro* drug release study and linear kinetics

The release behavior of VCM from the VCM-HNLCs in response to different pH values (7.4 and 6.0) was evaluated using a dialysis bag method [263]. Briefly, 2 mL of pure VCM solution (1 mg/mL) and VCM-HNLCs solution (containing 1 mg/mL VCM) were separately placed in cellulose dialysis bags (molecular weight:14,400 Da) and the bags were shaken and dialyzed against 40 mL of the buffer of choice receiver solution (PBS pH 7.4 or 6.0) at 37 °C and 100 rpm. At predetermined time intervals, 2 mL samples were withdrawn from the receiver solution and promptly replaced with an equivalent amount of fresh appropriate buffer (PBS pH 7.4 or 6.0) to maintain sink condition. The amount of VCM released per time was determined by HPLC according to the same analysis method mentioned for EE % evaluation (**2.4.2**). The experiment was performed in triplicate and the cumulative release percentage of VCM was calculated using the following equation:

$$\text{Cumulative release \%} = \frac{Q_t}{Q_v} \times 100 \quad (5)$$

Where Q_t is the amount of VCM released at time t, and Q_v the total amount of VCM previously used in the VCM-HNLCs formulation.

Different mathematical models, including zero-order; first-order, Higuchi, Krosmeyer-Peppas, Hixson-Crowell and Weibull, were then employed to examine the kinetics of VCM release from the VCM-HNLCs using the software program DDSolver [303]. The best-fit model was selected based on the correlation coefficient (R^2) and the root mean square error (RMSE), and the release mechanism was identified using Weibull and Krosmeyer-Peppas models by computing the values of the Weibull exponent parameter (β) and the release exponent (n), respectively.

2.8 Short-term physical stability study

The short-term colloidal stability of the prepared VCM-HNLCs formulation was evaluated at two different conditions: room temperature (25 °C) and cold temperature (4 °C) over 90 days of storage. Using a Zetasizer Nano ZS90 (Malvern Instruments Ltd., UK) equipped with a 633 nm laser with a detection optics of 173°, the mean particle size, PDI and ZP were measured at 0, 30, 60 and 90 days. All experiments were run in triplicate.

2.9 *In vitro* antibacterial activity studies

2.9.1 Determination of Minimum Inhibitory Concentration (MIC) and Fractional Inhibitory Concentration (FIC)

The antibacterial activity (MIC) of bare VCM, blank HNLCs and VCM-HNLCs against *S. aureus* and MRSA at pH 7.4 and 6.0 was investigated using a broth microdilution method, as previously reported [304]. In brief, *S. aureus* and MRSA cultures in Mueller- Hinton broth (MHB) were grown overnight at 37 °C and 100 rpm using a shaking incubator (Labcon, USA). The bacterial suspensions were adjusted to 0.5 McFarland standard (1.5×10^8 colony-forming units (CFU)/mL) using a DEN-1B densitometer (Latvia), and further diluted to a final concentration of 5×10^5 CFU/mL. Then, 135 µL of MHB solution was pipetted into 96-well plates, and the treatments (bare VCM, blank HNLCs and VCM-HNLCs solutions) were added individually and serially diluted to obtain a range of concentrations. Thereafter, 15 µL of the bacterial suspension was added to each well, and the mixture was incubated for 72 hrs in the shaking incubator (Labcon, USA) adjusted at 37 °C and 100 rpm. Following incubation, 5 µL of the sample mixtures were spotted on Mueller- Hinton agar (MHA) plates at specified time intervals (24, 48, and 72 hr) and finally, the MIC values were calculated after 24 hrs of incubation at 37 °C. All experiments were performed in triplicate.

Based on the MIC values obtained from the aforementioned antibacterial activity study, the cumulative FIC was determined, to understand the combined antibacterial activity of the blank HNLCs and VCM in the VCM-HNLCs against *S. aureus* and MRSA at pH 7.4 and 6.0. Equations (6) and (7) were used to calculate the ΣFIC, and the FIC index is shown in **Table S1**.

$$\text{FIC (VCM)} = \frac{\text{(the MIC of VCM in combination with HNLCs)}}{\text{(the MIC of VCM)}} \quad (6)$$

$$\text{FIC (Blank HNLCs)} = \frac{\text{(the MIC of HNLCs in combination with VCM)}}{\text{(the MIC of Blank HNLCs)}} \quad (7)$$

$$\Sigma\text{FIC} = \text{FIC (VCM)} + \text{FIC (Blank HNLCs)}$$

2.9.2 Flow cytometry

The cell viability of MRSA in the population following the treatment with VCM and VCM-HNLCs for 18 hrs was assessed using a flow cytometry method that was previously reported by our group with minor modifications [188]. To prepare the bacterial cultures, MRSA was grown overnight at 37 °C and 100 rpm in a shaking incubator to a concentration of 0.5 McFarland standard (1.5×10^8 CFU/mL) in MHB. The grown bacteria were then collected by centrifugation at 3000 rpm for 30 min and the supernatant was discarded. The pellets were resuspended in PBS and incubated for an additional 4 hrs at 37 °C. Afterward, 15 µL of bacterial suspension at a concentration of 5×10^5 CFU/mL, was added to a 96-well plate each containing 135 µL of bare VCM and VCM-HNLCs formulations at the MIC concentrations of 7.8 µg/mL and 3.9 µg/mL, respectively. The sample mixture was further incubated at 37 °C in a shaking incubator (100 rpm) for 18 hrs. Following incubation, 50 µL of each sample was transferred to the flow cytometry tubes containing 350 µL of sheath fluid and vortexed for 5 min. Then, 5 µL of membrane-impermeable propidium iodide (PI) and membrane-penetrating Syto9 dyes were added to each tube and the mixture was incubated for 30 min in the dark. Samples were analyzed on the flow cytometry device (BECKMAN COULTER DxFLEX, Nyon 1, Switzerland), collecting at least 10,000 cells in triplicate for each sample. Untreated MRSA cells were used as a negative control.

2.9.3 Determination of *in vitro* antibiofilm activity

2.9.3.1 Crystal violet assay

The microtiter dish biofilm formation assay was employed to evaluate the ability of VCM-HNLCs to remove MRSA biofilms [305, 306]. Bacterial suspension in MHB at pH 7.4 and 6.0 (1.5×10^8 CFU/mL) was added to 96-well plates (200 µL/well) and incubated at 37 °C for 7 days to create mature biofilms. Following incubation, the medium was removed from the wells and non-adherent

bacterial cells were eliminated by washing the wells three times with a sterile PBS (pH 7.4 and 6.0). Thereafter, 200 μL of bare VCM solution and VCM-HNLCs formulation at a concentration of 10×MIC were added to the wells and incubated at 37 °C for 24 hrs. The excess treatments and unattached bacteria were then removed by washing the wells three times in sterile PBS (pH 7.4 and 6.0), followed by staining of the biofilms with 0.01 % w/v crystal violet solution for 15 min. Later, excess dye was gently aspirated, thoroughly washed using PBS pH 7.4 and 6.0, and left to dry overnight. To elute crystal violet stain, 30 % acetic acid solution (125 μL) was added to each well and incubated for 10 min. The eluted dye was then transferred to another 96-well plate and imaged for qualitative analysis. Subsequently, the intensity of the crystal violet dye was quantitatively measured at 570 nm using a microplate reader (SpectraMax M2, USA) to investigate the antibiofilm effect of the test samples.

2.9.3.2 Florescence microscope assay

To confirm the ability of VCM-HNLCs to eliminate MRSA biofilms, a florescence microscope assay was conducted using glass microscope coverslips (18 mm × 18 mm) as carriers for biofilm formation. [188]. Coverslips were initially placed at the bottom of 6-well plates, then, 2 mL of bacterial suspension in MHB (1.5×10^8 CFU/mL) was added in each well. The plates were incubated for 7 days at 37 °C to allow biofilms to grow over the coverslips. After developing mature biofilms, non-adherent bacterial cells were removed from the wells by washing them three times with PBS pH 7.4 using a Pasteur pipette. The wells containing biofilms were then treated with 2 mL of PBS pH 7.4 (as a control), and 2 mL of bare VCM and VCM-HNLCs solutions (5×MIC) and incubated for 12 hrs at 37 °C. The treatments and unattached bacteria were removed from the wells by washing them twice with PBS pH 7.4. After that, the coverslips were stained with a solution of Syto9 and propidium iodide (PI) (30 μL diluted with 1 mL of distilled water) for 30 mins in the dark to avoid photobleaching. Following that, the plates were washed with PBS pH 7.4 to remove excess dye, the coverslips were inverted on a glass microscope slide, and the edges were gently glued. Fluorescence microscope images were captured and processed using Nikon Eclipse 80i FM (Japan) to visualize the biofilm eradication effects of bare VCM and VCM-HNLCs.

2.9.4 Time killing assay (TKA)

The time-killing kinetics of the prepared VCM-HNLCs against MRSA were evaluated at pH 7.4 and 6.0 using a previously described colony counting method [307]. In brief, an overnight MRSA culture (0.5 McFarland standard) was diluted into concentrations of 10^5-10^6 CFU/mL using a sterile PBS (pH 7.4 and 6.0). Then, bare VCM and VCM-HNLCs solutions at 5×MIC were added to the diluted bacteria and incubated in the shaking incubator (Labcon, USA) at 100 rpm and 37 °C. Untreated

bacteria in PBS solution (pH 7.4 and 6.0) was used as a control. At specified time intervals (0, 1, 2, 4, 6, 8, 12 and 24 hrs), 0.2 mL of each sample was withdrawn and subjected to serial dilution with sterile PBS (pH 7.4 and 6.0). Subsequently, 0.1 mL of each diluted sample was sub-cultured on MHA plate and incubated for 24 hrs. After incubation, the number of colonies formed in each dilution plate were counted and converted into CFU/mL using equation (8). The TKA of the prepared samples was determined by plotting $\log_{10}$ CFU/mL versus time. The experiment was performed in triplicate.

$$\text{CFU/mL} = \frac{\text{no. of colonies} \times \text{dilution factor}}{\text{Volume of dilution taken}} \quad (8)$$

2.9.5 Efflux Pump Inhibition

The potential of VCM-HNLCs to supress MRSA efflux pumps was evaluated using a simple cartwheel method according to previously reported protocols with minor modifications [308, 309]. Briefly, MHA plates containing 2 µg/mL ethidium bromide (EtBr) were freshly prepared and protected from light on the same day of the experiment. An overnight culture of MRSA (0.5 McFarland standard) was seeded into a 96-well plate and treated with bare VCM and VCM-HNLCs formulation at a concentration of 0.25×MIC values. A group of untreated bacteria was served as a control. The samples were incubated at 37 °C for 1 hr and then streaked on the MHA containing EtBr in a cartwheel form. All plates were incubated in the dark at 37 °C for 24 hrs. The plates were then visualized using a UV trans-illuminator (Uvitec Cambridge, UK.) to observe any residual fluorescence exhibited by the bacteria. The inhibitory effect of the tested samples on the MRSA efflux pumps can be identified from the fluorescence emission under the UV transilluminator.

2.10 *In vitro* antioxidant study

Following a previously described DPPH radical scavenging method with minor modifications, the antioxidant activity of TS, Lys, HA-Lys and VCM-HNLCs through free radical scavenging was investigated [310]. A methanolic solution of DPPH at a concentration of 0.5 mM and various concentrations of the treatments in distilled water (20-1000 µg/mL) were individually prepared. Subsequently, 150 µL of each formulation sample was mixed with an equal volume of DPPH solution in a 96-well plate and left to incubate at 37 °C in the dark. A negative control consisting of a mixture of DPPH and water (150 µL each) was used. The absorbance of the reaction mixture was measured at 517 nm after 1 hr of incubation using a microplate reader (SpectraMax M2, USA). The assay was performed in triplicate and ascorbic acid was used as a positive control. The following equation was used to compute the percentage of antioxidant activity:

$$\text{Antioxidant}\,\% = \frac{\text{A516 nm control} - \text{A516 nm sample}}{\text{A516 nm control}} \times 100 \quad (9)$$

2.11 *In vitro* anti-inflammatory studies

2.11.1 Cytoprotective effect against LPS-induced cytotoxicity

The cytoprotective effect of HA-Lys and VCM-HNLCs against LPS-induced cytotoxicity was assessed *in vitro* using a previously documented methods utilizing an MTT assay and the HepG2 cell line as a model of cells affected by LPS [311-313]. In brief, HepG2 cells were cultured in DMEM supplemented with glutamine, antibiotics, and fetal bovine serum and incubated at 37 °C in a humidified atmosphere containing 5 % carbon dioxide. When the cells reached 80 % confluency, they were plated in a 96-wells plate (20000 cells/well) and left for 24 hrs. The cells were then subjected to a new set of treatments for a further 24 hrs, which included: a) 200 µL of DMEM was used as the control; b) 200 µL of 0.9 mg/mL of LPS was used as the LPS treatment; c) 200 µL of 0.9 mg/mL of LPS and 100 µg/mL of HA-Lys were used as the HA-Lys treatment; d) 200 µL of 0.9 mg/mL of LPS and 100 µg/mL of VCM-HNLCs in DMEM were used as the nanoformulation treatment. Following a 24-hr treatment period, the media were removed and replaced with 100 µL/well of fresh DMEM mixed with 20 µL/well of 5 mg/mL MTT solution. Four hrs later, the media was replaced with 100 µL/well sterile DMSO to solubilize the formazan crystals. Finally, absorbance from each well was measured at 570 nm using a microplate spectrophotometer (Spectrostar Nano, Germany) after 1 hr of adding DMSO. Each treatment was carried out in triplicate, and the percentage of viable cells was determined.

2.11.2 Anti-inflammatory activity against LPS-induced inflammatory responses (measurement of interleukin 6 (IL-6) levels)

The anti-inflammatory activity of HA-Lys and VCM-HNLCs was further examined using an LPS-stimulated HepG2 cells model, as previously described [311]. In this study, IL-6 levels were measured using Enzyme Linked Immunosorbent Assay (ELISA) kits following the stimulation of HepG2 cells with 1µg/mL LPS solution in DMEM for 12 hrs, either with or without treatments. After HepG2 cells were cultured and plated in the manner mentioned in the previous section (**2.11.1**), they were subjected to the following treatments for a duration of 12 hrs: a) Control untreated (200 µL of DMEM); b) LPS-treated (200 µL of 1 µg/mL of LPS in DMEM); c) HA-Lys-treated (200 µL of 1 µg/mL of LPS and 50 µg/mL or 100 µg/mL HA-Lys in DMEM); d) VCM-HNLCs-treated (200 µL of 1 µg/mL of LPS and 50 µg/mL or 100 µg/mL VCM-HNLCs in DMEM). Following treatment, the media were collected to determine the amount of IL-6 in the supernatants using ELISA kits in accordance with the manufacturer's instructions.

2.12 Statistical analysis and figures

The data were statistically analyzed using GraphPad Prism® version 10 (GraphPad Software Inc., USA), which included paired T-tests and one-way analysis of variance (ANOVA). The difference between each compared groups was considered significant if the *P*-value was < 0.05. All results were presented as mean ± standard deviation (SD) and all graphs and figures were generated using GraphPad Prism® 10 and the BioRender website, unless otherwise noted.

3. Results and discussion

3.1 Synthesis and characterization of HA-Lys conjugate

HA-Lys conjugate was successfully synthesized through one-step amidation reaction, purified using intensive dialysis against 0.1 % w/v NaCl solution and distilled water, and subsequently characterized by ^{1}H NMR and FT-IR. The ^{1}H NMR spectrum (**Figure 1**) clearly showed all the signals attributed to the Lys moieties (**1A**) δppm 1.18, 1.59, and 2.76 (CH_2 groups, a, b and d, respectively), and 3.30 (CH groups, e), and to the HA backbone (**1B**) δppm 1.90 (CH_3 groups, **c**),3.59 (CH groups in the tetrahydropyran ring, **f**) and 4.44 (OH groups, **g**). Similar signals of both HA and Lys were observed in the ^{1}H NMR spectrum of HA-Lys conjugate with slight chemical shifts (**1C**). These chemical shifts in particular regions of the ^{1}H NMR spectrum of HA-Lys confirmed the reaction between HA and Lys.

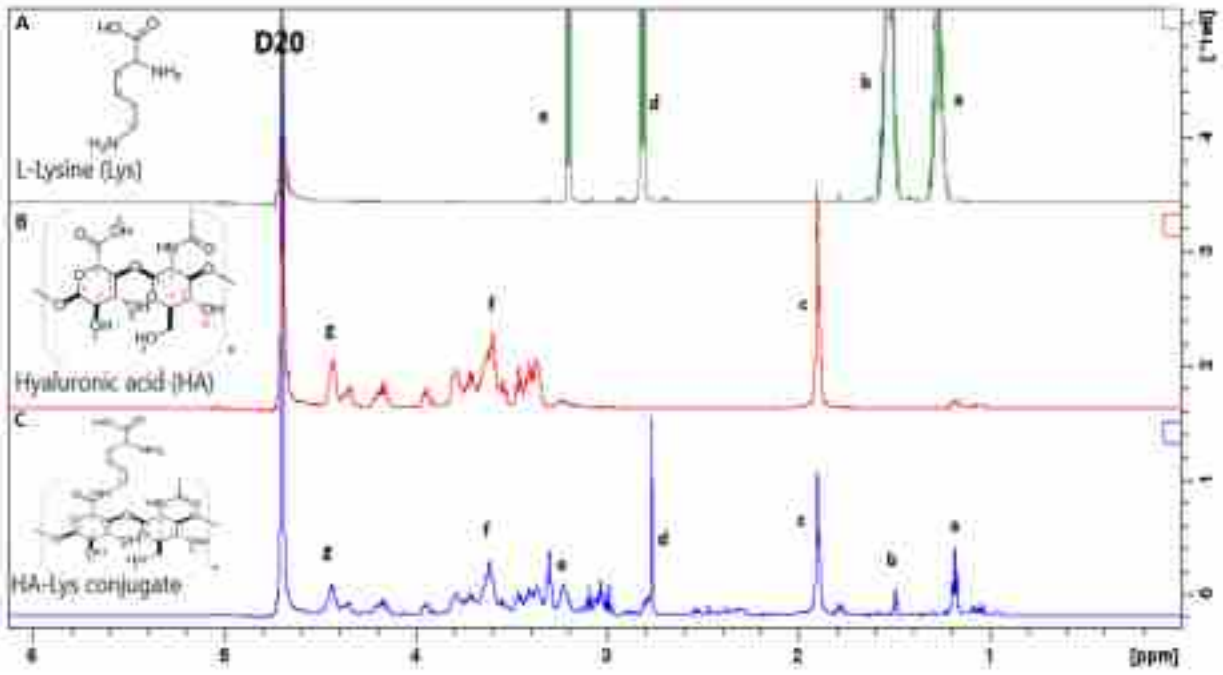

Figure 1. ^{1}H NMR characterization of (**A**) HA, (**B**) Lys and (**C**) HA-Lys conjugate in D_2O.
(*HA=Hyaluronic acid, Lys=$_{L}$-Lysine, HA-Lys= Hyaluronic acid-lysine conjugate).

The FT-IR spectrum (**Figure 2**) revealed a broad stretching band attributed to pure HA (**2A**) at 3400.4 cm^{-1} (due to O-H stretching vibration) and 3301.47 cm^{-1} (due to N-H stretching vibration) in the N-acetyl side chain. Also, other bands were detected at 2887.12 cm^{-1} (due to symmetric methyl C-H stretching in glucuronic acid side chain), 1628.97 cm^{-1} (due to the amide group of C=O carboxyl), 1338.74 cm^{-1} (due to the C-N stretching of primary aromatic amine) and 1035.89 cm^{-1} (due to C-O alcoholic stretching), respectively. The spectrum also displayed the bands associated with pure lysine (**2B**), including those at 3345.08 cm^{-1} (resulting from the overlap of O-H and N-H stretching), 2921.06 cm^{-1} (due to symmetric C-H stretching of the CH_2 group), 2129.12 cm^{-1} (from the overtone and combinational bond), 2816 cm^{-1} (resulting from C-H vibration of the CH group), 1576.07 cm^{-1} (due to the asymmetric stretching of C=O carboxylic group), 1507 cm^{-1} (due to asymmetric scissoring of the NH_2 group), 1400.24 cm^{-1} (resulting from symmetric vibration of C=O carboxyl and C-N group) and 656.64 cm^{-1} (due to C=O carboxyl rocking), respectively. The spectrum of HA-Lys conjugate (**2C**) exhibited all the characteristic bands of both HA and Lys at the same positions. In addition, a prominent and well-defined band with increased intensity was observed at 1628.59 cm^{-1} (shift from 1628.97), which corresponds to the amide group of C=O carboxyl. This intensified band indicates the creation of a new secondary amide bond between the amine group of Lys and the carboxyl group of HA, thus confirming the successful amidation reaction and formation of HA-Lys conjugate.

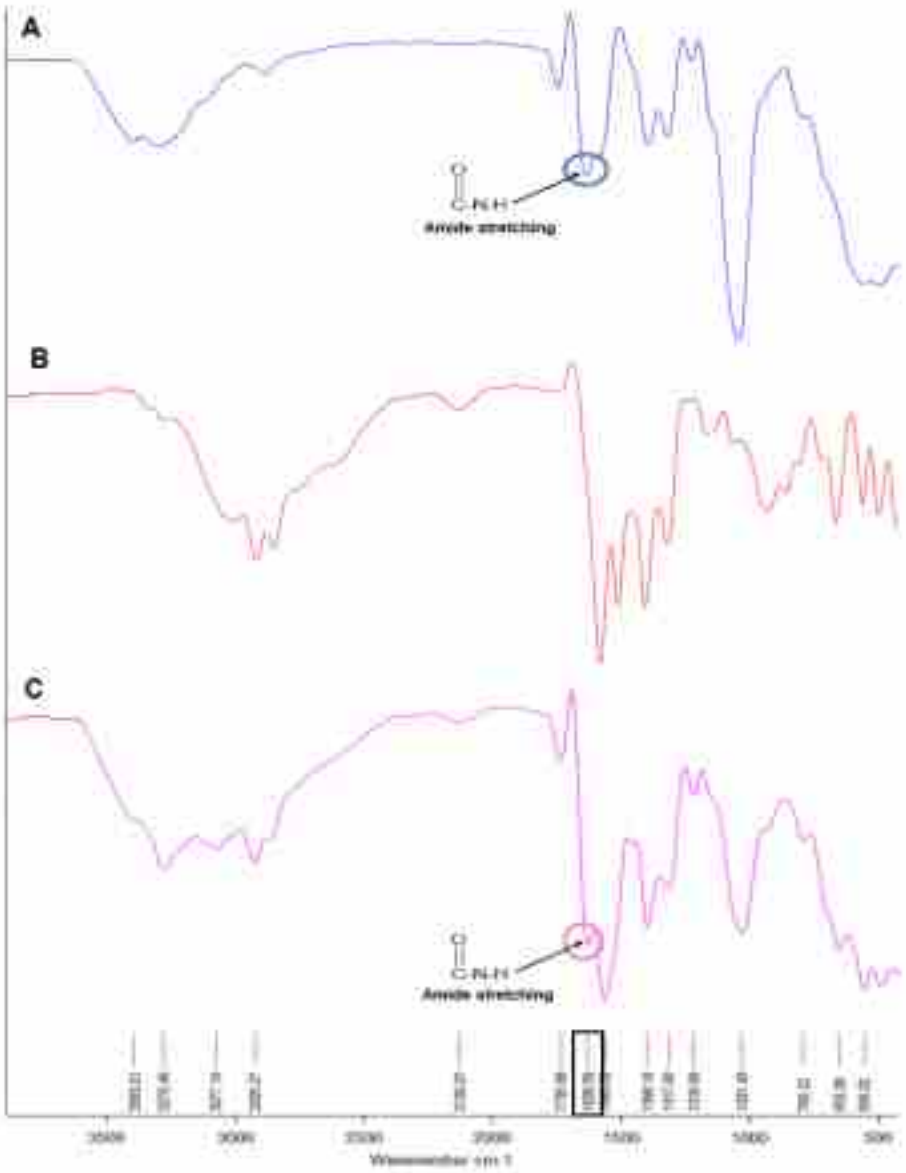

Figure 2. FT-IR spectrum of (**A**) HA, (**B**) Lys and (**C**) HA-Lys conjugate. (*HA=Hyaluronic acid, Lys=$_{L}$-Lysine, HA-Lys= Hyaluronic acid-lysine conjugate)

3.2 Formulation, characterization and optimization of VCM-HNLCs

After the structure of HA-Lys conjugate was validated, its potential for the development of HNLCs was investigated. Both blank HNLCs and VCM-HNLCs were successfully prepared by hot homogenization/ultrasonication technique [267]. The preliminary work involved evaluating different surfactants to select the most suitable one for creating HNLCs with desired particle sizes, smaller PDI, and greater colloidal stability. After screening, Tween 80 was found to be the optimal surfactant, as presented in **Table S2**, which resulted in HNLCs with the best physical properties, including particle size, PDI and ZP.

For the optimization process, various formulation parameters including lipid: surfactant, drug: lipid, and lipid: polymer mass ratios were assessed using a single-factor-at-a time optimization method to obtain the most optimal VCM-HNLCs in terms of particle size, PDI, EE % and DL % w/w, with acceptable charge switch from negative to positive at different pH values. As shown in **Table 1**, it was observed that increasing the lipid: surfactant mass ratio from 1:0.5 to 1:2 while fixing the other optimization parameters (drug: lipid 1:4 and lipid: polymer 1:0.1) resulted in a decrease in the average particle diameter, EE % and DL % w/w from 98.77 to 42.44 nm, 56.18 % to 20.78 % and 7.36 % to 2.07 %, respectively, with an increase in size distribution from 0.156 to 0.233. The drop in particle sizes as the surfactant ratio increases could be attributed to the excess surfactant molecules available to cover and stabilize the lipid-water interfaces created during homogenization, thereby reducing the interfacial tension and producing NPs with smaller particle sizes [314]. Our result is in accordance with other research studies that also reported a reduction in particle size of NLCs at higher surfactant concentrations [315-317]. On the other hand, the decrease in EE % and DL % w/w of the prepared VCM-HNLCs with increasing surfactant content may be due to the high hydrophilicity of the loaded VCM which makes the drug partitioning out of the lipid system into the surrounding aqueous medium [318]. On this basis, the ideal lipid: surfactant ratio of 1:0.5 was chosen for further optimization.

The effect of drug: lipid mass ratio was then evaluated with fixed mass ratios of lipid: surfactant (1:0.5) and lipid: polymer (1:0.1), and the results indicated that increasing the drug: lipid mass ratio from 1:3 to 1:5 led to an increase in EE % and DL % w/w from 45.50 % to 64.77 % and from 5.26 % to 8.28 %, respectively, without significant effects on the size, PDI and ZP. This enhanced EE % could be due to the increase in lipid content, which improves the dispersion of VCM within the lipid matrix while minimizing its leakage from the NPs [267, 319]. Accordingly, optimal lipid: surfactant (1:0.5) and drug: lipid (1:5) mass ratios were used to evaluate the effect of different lipid: polymer mass ratios on the properties of VCM-HNLCs.

It was found that increasing the lipid: polymer mass ratio from 1:0.05 to 1:0.15 resulted in an increase in the EE % from 55.81 % to 72.27 % without significant effects on the other parameters among all the samples tested. This result was comparable to previously published studies, in which increasing the lipid: polymer mass ratio had resulted in an increase in particle size and size distribution of the NPs [320, 321]. Furthermore, all the formulations exhibited negative ZP, ensuring strong electrostatic repulsion and preventing the NPs from coalescence [322]. As a result, VCM-HNLCs with lipid: surfactant mass ratio of 1:0.5, drug: lipid mass ratio of 1:5 and lipid: polymer mass ratio of 1:0.1 were selected as the optimal formulation for further studies. The average particle size, PDI, ZP, EE % and DL % w/w were 110.77 ± 1.69 nm, 0.113 ± 0.02, -2.92 ± 0.21 mV, 76.27 ± 1.20 % and 8.36 ± 0.25 %, respectively.

Table 1. Size, PDI, ZP, EE% and DL% w/w for the different lipid: surfactant, drug: lipid, and lipid: polymer mass ratios used in the optimization of VCM-HNLCs. Results represented as mean ± SD (n = 3).

Optimization parameter	Size (nm)	PDI	ZP (mV)	EE %	DL % w/w
Lipid: surfactant mass ratio	**Fixed drug: lipid (1:4) and lipid: polymer (1:0.1) mass ratios**				
1:0.5	98.77 ± 0.43	0.156 ± 0.01	-2.92 ± 0.33	56.18 ± 3.36	7.36 ±1.58
1:1	62.29 ± 0.44	0.204 ± 0.01	-5.41 ± 0.64	35.70 ± 0.38	5.07 ± 0.05
1:2	42.44 ± 1.15	0.233 ± 0.01	-2.69 ± 0.28	20.78 ± 0.93	2.07 ± 0.09
Drug: lipid mass ratio	**Fixed lipid: surfactant (1:0.5) and lipid: polymer (1:0.1) mass ratios**				
1:3	90.94 ± 0.03	0.151 ± 0.01	-5.59 ± 1.28	45.50 ± 0.02	5.26 ± 0.01
1:4	98.77 ± 0.44	0.156 ± 0.01	-2.92 ± 0.33	56.18 ± 3.40	7.36 ±1.58
1:5	99.39 ± 0.49	0.127 ± 0.01	-2.50 ± 0.06	64.77 ± 0.06	8.28 ± 0.00
Lipid: polymer Mass ratio	**Fixed lipid: surfactant (1:0.5) and drug: lipid (1:5) mass ratios**				
1:0.05	90.58 ± 0.26	0.126 ± 0.00	-2.54 ± 0.26	55.81 ± 0.45	7.38 ± 0.05
1:0.1	99.39 ± 0.49	0.127 ± 0.01	-2.50 ± 0.06	64.77 ± 0.06	8.28 ± 0.00
1:0.15	108.0 ± 0.91	0.136 ± 0.01	-3.16 ± 0.53	72.27 ± 0.28	8.86 ± 0.00

Optimizing the interactions between nanoparticles and bacteria requires an understanding of the physicochemical characteristics of the generated HNLCs as a function of pH [323]. As a result, the impact of pH on VCM-HNLCs was examined at various pH levels (7.4, 6.0 and 4.5). The optimal VCM-HNLCs formulation demonstrated significant pH-responsiveness in terms of charge switching from -2.92 ± 0.21 mV at pH 7.4 (physiological pH) to +1.64 ± 0.17 and +9.97 ± 0.33 mV at pH 6.0 and 4.5 (acidic pH), respectively (**Figure 3**). This charge shift is likely due to protonation of the primary amino group of OLA, which results in positive ZP at low pH values. It is anticipated that this change in surface charge from negative to positive may promote drug release and enhance adherence of VCM-HNLCs to the negatively charged bacterial cell wall, thereby, increasing antibacterial efficacy [324, 325].

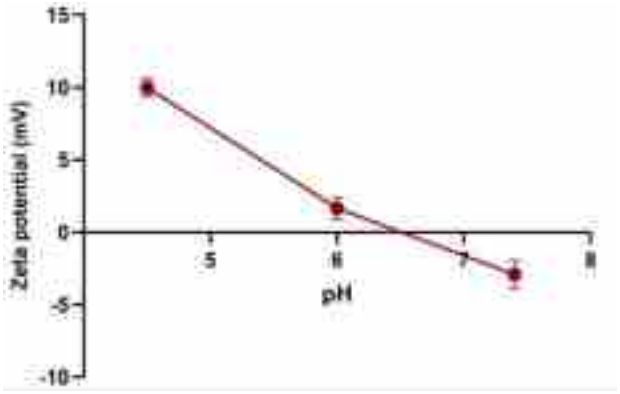

Figure 3. The impact of pH variation on the surface charge of VCM-HNLCs (*P*-value = 0.0004). the data is shown as mean ± SD (n=3)

3.3 Determination of nanoparticle morphology

Transmission electron microscopy (TEM) was used to further investigate the surface morphology of the prepared VCM-HNLCs. The optimized VCM-HNLCs formulation's TEM image showed distinct, spherical-shaped NPs that were consistent to those generated with DLS (**Figure 4**).

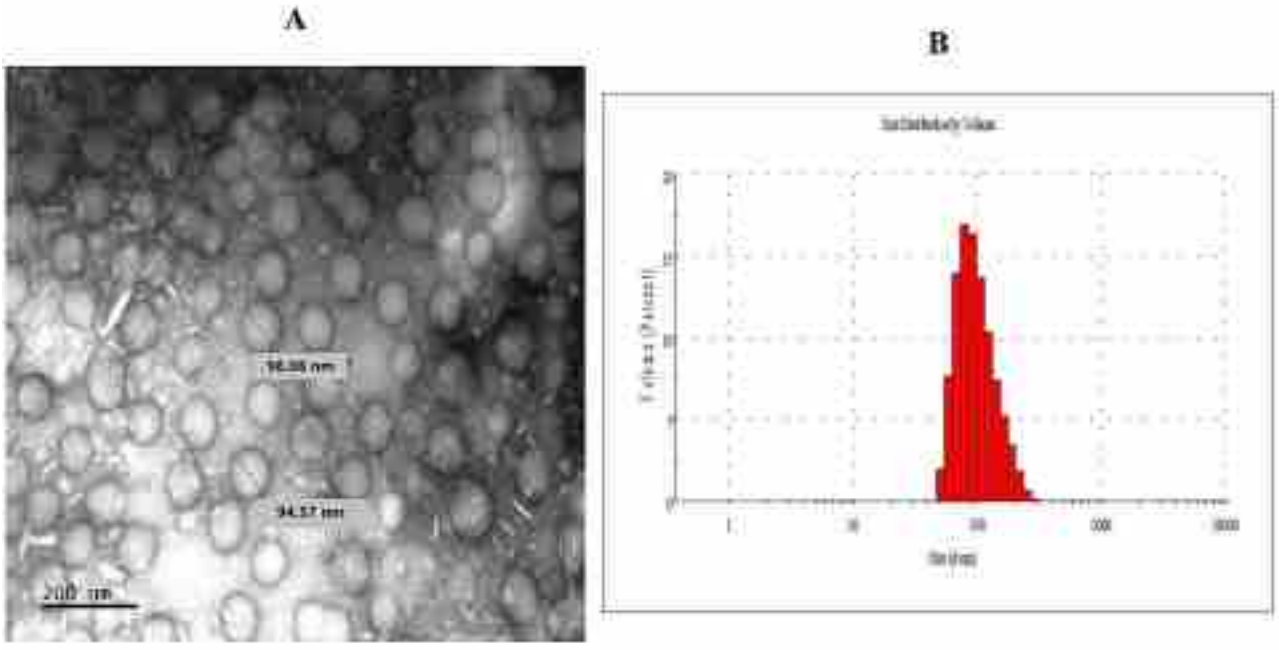

Figure 4. (**A**) TEM image of VCM-HNLCs and (**B**) A histogram displaying the size distribution by volume of VCM-HNLCs determined by DLS.

3.4 Thermal profiles

The thermal profiles of individual excipients, physical mixture, and the lyophilized VCM-HNLCs are shown in **Figure 5**. The results showed that Lys, VCM and TS showed endothermic peaks at 243.5 °C, 109.17 °C and 83.56 °C, respectively, while HA showed an exothermic peak at 233.36 °C. In addition, the thermograms of the HA-Lys conjugate and the physical mixture of VCM-HNLCs excipients showed the same endothermic and exothermic peaks with slight shifts. The successful entrapment of the drug to the prepared NPs in an amorphous form is confirmed by the lack of the characteristic VCM peak in the thermogram of the lyophilized VCM-HNLCs.

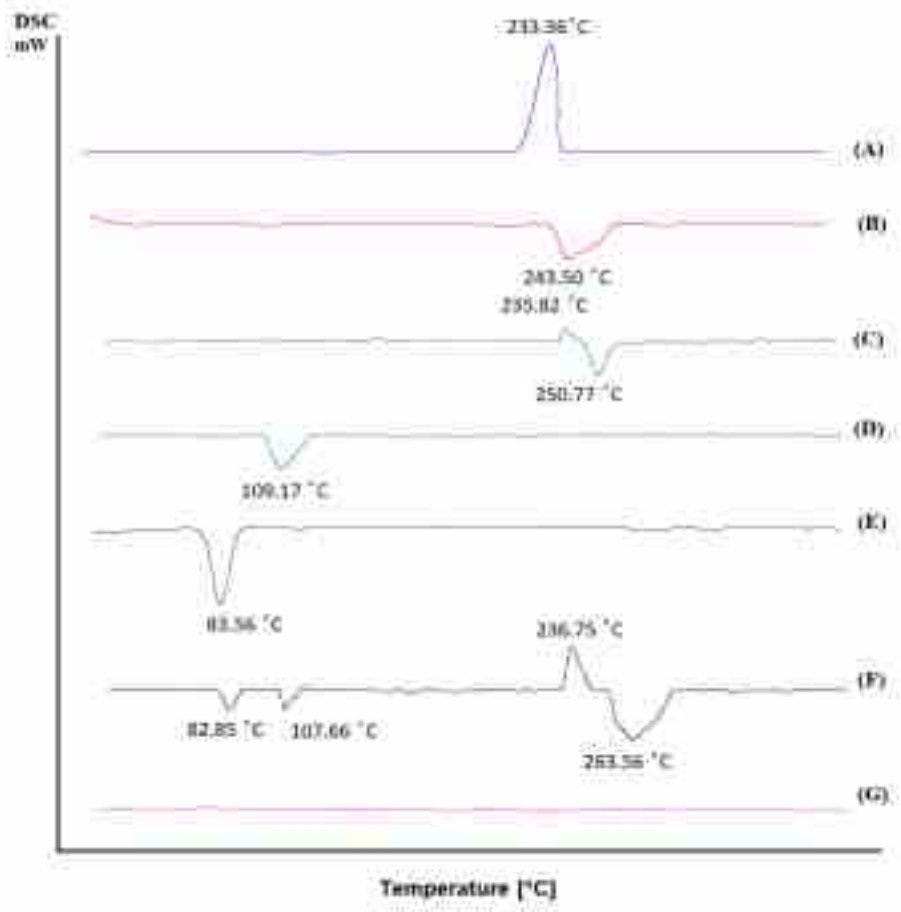

Figure 5. DSC thermograms of (**A**) Hyaluronic acid (HA); (**B**) L-Lysine (Lys); (**C**) HA-Lys conjugate; (**D**) Vancomycin; (**E**) α-Tocopherol succinate; (**F**) physical mixture; (**G**) lyophilized VCM-HNLCs formulation.

3.5 *In vitro* biosafety studies

3.5.1 Cytotoxicity and cell viability assay

The biological safety of a novel biomaterial and/or nanocarrier is a crucial requirement for its application in drug delivery, biomedical, and clinical use [326]. Therefore, we investigated the cytocompatibility of the synthesized HA-Lys conjugate and its nanoformulation (VCM-HNLCs) at different concentration levels (20-100 µg/mL) using a previously described MTT assay on HEK-293 and HepG2 cell lines [299]. As shown in **Figure 6**, all the tested concentrations maintained a cell viability of >70 % across all tested cell lines. The HEK-293 cell line displayed a viability range of 93.52-106.41 % and 73.61-91.92 %, while HepG2 showed a viability range of 80.11-103.88 % and 104.48-106.65 % for HA-Lys and VCM-HNLCs, respectively. Additionally, none of the tested cell lines exhibited concentration-dependent cytotoxicity across the concentration range examined for HA-Lys and VCM-HNLCs. However, in contrast to the control group, the HA-Lys conjugate and VCM-HNLCs formulations demonstrated marginally increased cell viability. This could be attributed to the proliferative action of HA [327], as well as long chain fatty acids derivatives such as OLA [328]. These findings are consistent with the International Standard Organization (ISO) limit for biosafety of biomedical materials (≥70 % cell viability) [329] and support the cytocompatibility and potential use of the prepared VCM-HNLCs for nano antibiotic delivery.

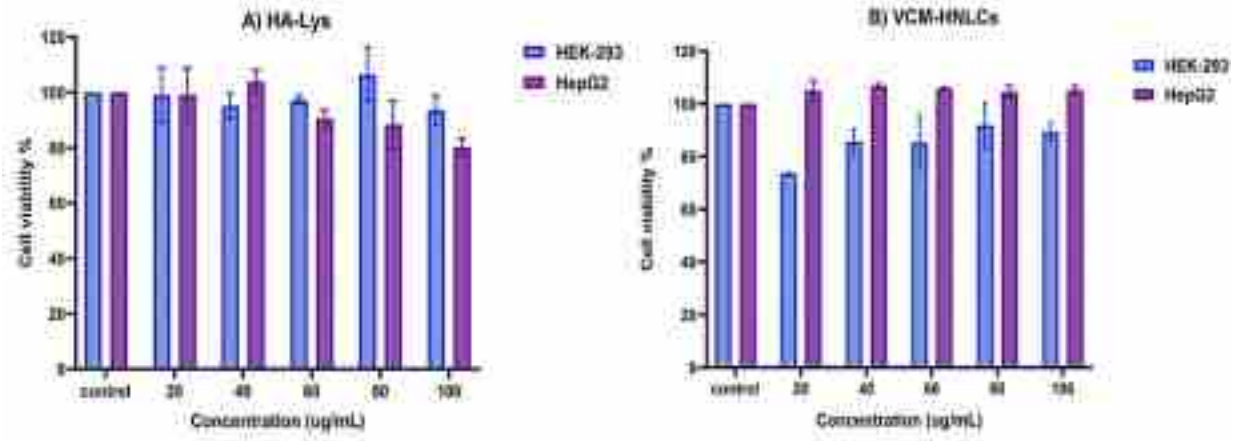

Figure 6. The Cell viability % of different concentrations of (**A**) HA-Lys conjugate and (**B**) VCM-HNLCs, and controls on HEK293 and HepG2 cell lines. Data are presented as mean ± SD (n = 3).

3.5.2 Hemolysis

The hemocompatibility of nanoformulations intended for intravenous administration is an essential prerequisite to ensure their biosafety [330]. Therefore, the impact of the prepared VCM-HNLCs on erythrocytes was investigated using freshly collected and washed sheep blood and the results are shown in **Figure 7.** All concentrations of the VCM-HNLCs showed less than 1 % hemolysis (**Table**

S3), indicating the non-hemolytic activity and favorable biosafety profile of the nanosystem. As a result, VCM-HNLCs could be administered parenterally to treat bacterial infections and sepsis.

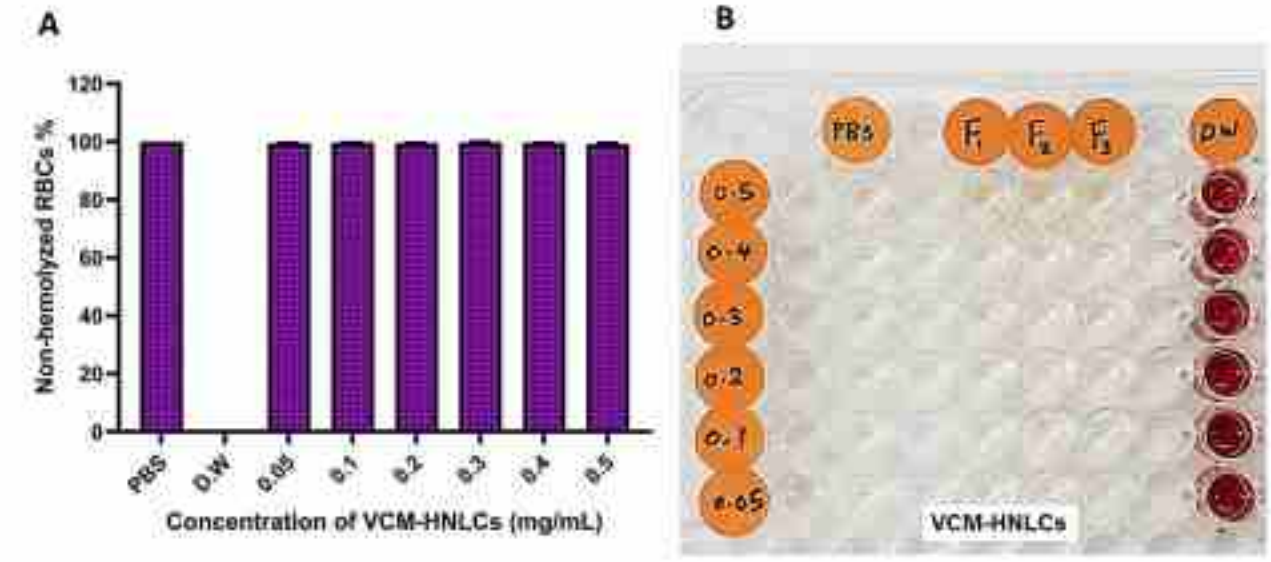

Figure 7. (**A**) and (**B**) Non-hemolytic activity of different concentrations of VCM-HNLCs (*DW= distilled water, PBS=phosphate buffer saline pH 7.4). Data are presented as mean ± SD (n = 3).

3.6 *In vitro* binding affinity study

Activation of TLRs by bacterial endotoxins is a critical step in triggering immune response, which also contributes to the development of chronic and acute inflammatory conditions like sepsis [331]. Therefore, altering TLRs signaling pathways and blocking their binding to their natural substrates in the bacteria, may help in reducing the subsequent downstream signaling molecules activation and could be a potential strategy in treating bacterial sepsis. In this research, for the first time, an MST binding affinity analysis was conducted to evaluate the binding affinity of HA (a known ligand of TLR2 and TLR4), as well as Lys, HA-Lys, and VCM-HNLCs to human TLR2 and TLR4 compared to their natural substrates PGN and LPS, respectively. The affinity of the ligands was determined using the dissociation constant (K_d) values listed in **Table 2,** and the fraction of TLRs bound to each ligand was illustrated in **Figure 8.**

3.6.1 *In vitro* binding affinity to TLR2

The results in **Table 2** and **Figure 8A** demonstrated that HA, Lys and HA-Lys conjugate each had a considerable binding affinity to TLR2 with K_d values of 0.82 ± 0.41, 2.79 ± 0.74 and 0.02 ± 0.85 µM, respectively, compared to the natural substrate PGN that recorded a K_d value of 23.95 ± 0.88 µM (*P*-value < 0.0001). Additionally, VCM-HNLCs had significantly higher binding properties to TLR2

than PGN with a K_d value equal to 4.55 ± 0.49 µM (*P*-value < 0.0001). However, the lowest binding affinity was found for the non-hybrid NLCs components with more than 40-fold and 8-fold higher K_d than VCM-HNLCs and PGN, respectively. Consequently, we can deduce that the inclusion of HA-Lys in the VCM-HNLCs formulation may be responsible for the binding affinity and consequent TLR2 sensitivity. The enhanced binding affinity of the synthesized HA-Lys polymer was due to both HA and Lys, which may act synergistically and enhance the polymer's sensitivity to TLR2. The change in binding affinity of VCM-HNLCs compared to HA-Lys might be attributed to the conformational shift in the HNLCs structure resulting from self-assembly of the nanosystem.

3.6.2 *In vitro* binding affinity to TLR4

We observed a similar trend when examining the binding to TLR4 (**Table 2** and **Figure 8B**). In comparison to the natural substrate LPS, which recorded a K_d value of 38.15 ± 1.44 µM, both HA and HA-Lys conjugate displayed a significant binding affinity to TLR4 (*P*-value < 0.0001), with K_d values of 0.045 ± 0.75 and 0.18 ± 0.73 µM, respectively. The Lys and non-hybrid NLCs components had the lowest binding affinities, with K_d values of 43.53 ± 2.35 and 52.29 ± 2.21 µM, respectively. Therefore, the substantial TLR4 binding of HA-Lys conjugate is mainly attributed to the HA moiety of the synthesized polymer. Additionally, VCM-HNLCs demonstrated much better binding properties to TLR4 in comparison to LPS, with a K_d value equal to 2.44 ± 2.17 µM (*P*-value < 0.0001). This suggests that the inclusion of HA-Lys in the VCM-HNLCs formulation is responsible for the binding affinity and consequent TLR4 sensitivity. Also, the alteration in the binding affinity of VCM-HNLCs relative to HA-Lys might be attributable to the conformational adjustment in the HNLCs structure resulting from the self-assembly process of the nanosystem.

Accordingly, these findings demonstrate a direct and robust binding of HA-Lys and VCM-HNLCs to both human TLR2 and TLR4, which could potentially inhibit the binding of bacterial toxins to their corresponding receptors and suppress the inflammatory response triggered by TLRs. Therefore, HA-Lys and its prepared nanoformulation (VCM-HNLCs) may be suggested as an adjuvant and potential therapeutic nanocarrier for the treatment of sepsis resulted from mixed bacterial infections.

Table 2. The dissociation constant values (K_d) obtained from the MST analysis for PGN, LPS, individual excipients (HA, Lys and HA-Lys conjugate), VCM-HNLCs and non-hybrid NLCs components binding to TLR2 and TLR4, respectively. Data are presented as mean ± SD (n = 3).

Test ligand	Kd (µM)	
	TLR2	**TLR4**
PGN	23.95 ± 0.88	-
LPS	-	38.15 ± 1.44
HA	0.82 ± 0.41	0.05 ± 0.75
Lys	2.79 ± 0.74	43.53 ± 2.35
HA-Lys	0.02 ± 0.85	0.19 ± 0.73
VCM-HNLCs	4.55 ± 0.49	2.44 ± 2.17
Non-hybrid NLCs components	202.10 ± 1.36	52.29 ± 2.21

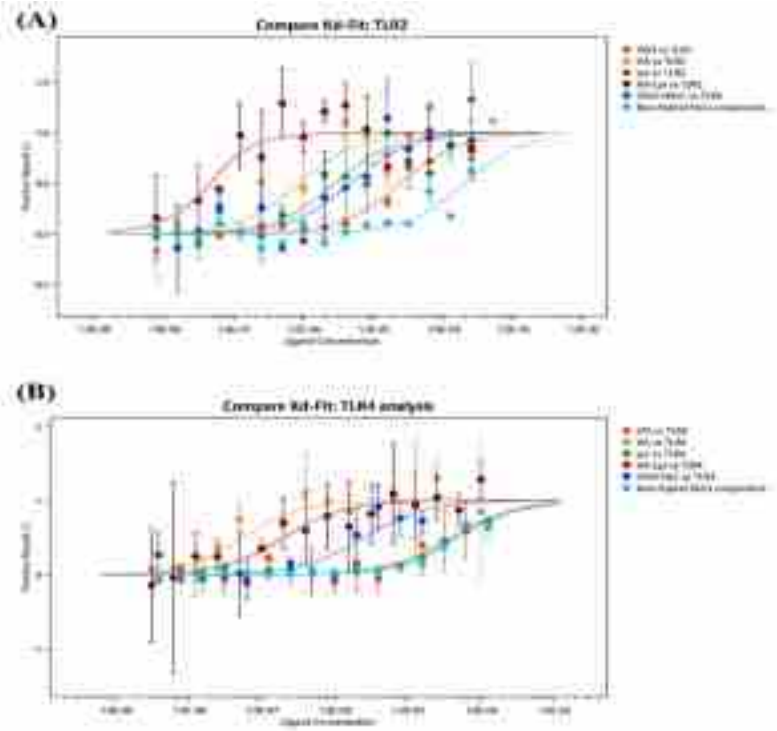

Figure 8. A Comparison view for different ligands fraction bound to (**A**) TLR2 and (**B**) TLR4. *PGN: Peptidoglycan, LPS: lipopolysaccharide, HA: hyaluronic acid, HA-Lys: hyaluronic acid-lysine conjugate and VCM-HNLCs: vancomycin-loaded hybrid nanostructured lipid carriers. Results represented in mean ± SD (n = 3).

3.7 *Invitro* drug release and linear kinetics

The dialysis bag method was used to evaluate the *in vitro* release behavior of bare VCM and VCM-HNLCs at pH 7.4 and pH 6.0. The graph in **Figure 9** reveals that the bare VCM was quickly released at pH 7.4 and had almost completed its release within the first 24 hrs (100.71 %), while VCM-HNLCs formulation showed a slower release rate, with about 62.42 % of VCM released from the hybrid NPs at the same time point. This indicates a sustained release profile for the VCM-HNLCs formulation in contrast to the bare VCM. The delayed release behavior of VCM from the VCM-HNLCs may be caused by the diffusion of the entrapped VCM molecules through the lipid-polymer matrix which retain the antibiotic for a longer period of time [320]. On the other hand, the VCM release from VCM-HNLCs was significantly higher at pH 6.0 compared to pH 7.4 (*P*-value = 0.00014), as 97.48 % of VCM was released from the hybrid NPs at pH 6.0 within 48 hrs, while only 68.23 % of VCM was released at pH 7.4 at the same time, confirming that the release of VCM was pH-responsive. This enhanced drug release at acidic pH is due to the confirmational changes and destabilization of the NP structures as a result of OLA protonation at lower pH values, which accelerates drug release profiles [332]. Our findings are in accordance with previously reported studies, showing that VCM released from pH-responsive nanosystems was greater and occurred more quickly at pH 6.0 than it was at physiological pH 7.4 [267, 323, 333, 334]. This pH-triggered VCM release behavior is essential for better drug protection at the physiological pH and improved localization at the infection sites (acidic pH), which helps in improving the antibacterial activity [335, 336].

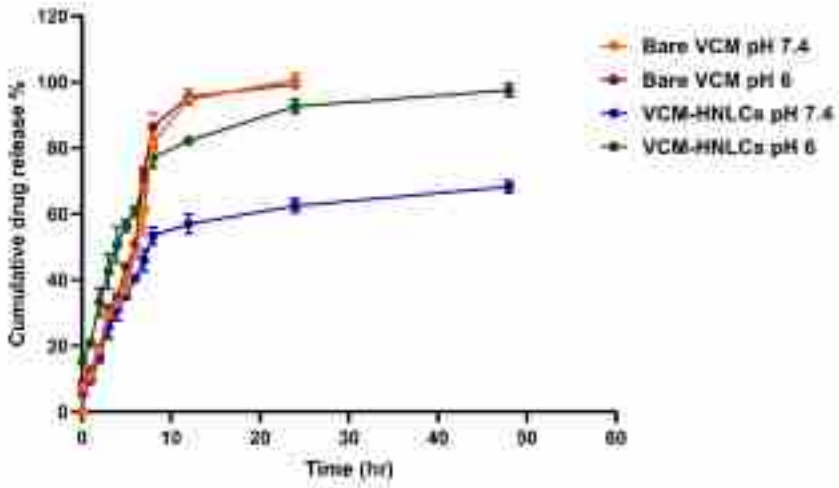

Figure 9. Drug release profile of VCM-HNLCs and bare VCM at pH 7.4 and pH 6.0. All data represented as mean ± SD (n = 3).

To comprehend the release mechanism of VCM from the prepared HNLCs, the cumulative drug release data were fitted into various mathematical models using DDSolver program (**Table 3**). While VCM-HNLCs showed a greater VCM release profile at pH 6.0 in contrast to pH 7.4, the kinetic

behavior remained the same in both circumstances. The Weibull model proved to be the most fit model for VCM release at both pH 7.4 and 6.0. The highest R^2 values were 0.95 and 0.99 and the lowest root means square error (RMSE) values were 5.44 and 3.14 for pH 7.4 and 6.0, respectively. The Weibull exponent parameter (β), which analyzes the transport mechanism of a drug through the lipid-polymer matrix was 0.47 (< 0.75) indicating a Fickian diffusion mechanism of drug release [337]. Likewise, the release exponent value of the Korsmeyer-Peppas model (n) was found to be 0.36 and 0.32 for pH 7.4 and 6.0, respectively (< 0.5), suggesting that Fickian diffusion is the release mechanism of VCM from the HNLCs.

Table 3. Kinetics of drug release data for the VCN-HNLCs at pH 7.4 and pH 6.

Model	Equation	R^2		RMSE		Release exponent (n)		β
		pH 7.4	pH 6	pH 7.4	pH 6	pH 7.4	pH 6	
Zero Order	Q=k*t	-0.17	-0.48	24.27	37.04			
First Order	$Q = Q0. e^{kt}$	0.75	0.98	11.29	4.54			
Higuchi	$Q = k. t^{½}$	0.79	0.74	10.19	15.42			
Korsmeyer- Peppas	$Q = k. t^n$	0.88	0.91	8.04	9.99	0.36	0.32	
Hixson-Crowell	$Q^{⅓} = kt + Q_0^{⅓}$	0.65	0.80	13.28	13.39			
Weibull	Q = 1 exp [-(t)a/b]	0.95	0.99	5.44	3.14			0.47

***R^2** = linear regression coefficient, **RMSE** = Root means square error*

3.8 Short-term physical stability study

The physical colloidal stability of the optimal VCM-HNLCs formulation was evaluated at two distinct storage temperatures (25 °C and 4 °C) over a period of 90 days to monitor any drug leakage or NP aggregation that might occur during storage. There were no appreciable changes in particle size, PDI, or ZP according to the experimental data listed in **Table S4** (*P*-value > 0.05), and no visible signs of instability were observed over the three months of the study when the samples were stored at both 25 °C and 4°C, respectively. These results confirmed the physical stability of the prepared VCM-HNLC as a drug delivery system. **Figure 10** illustrates the effect of RT and 4 °C storage conditions on the physicochemical properties of VCM-HNLCs formulation.

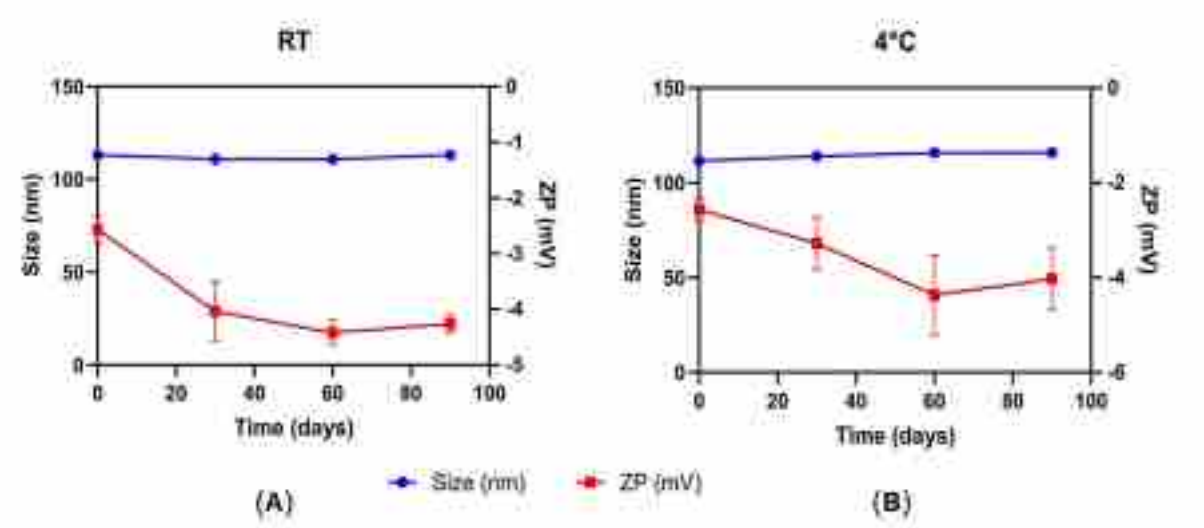

Figure 10. Variations in particle size (nm) and ZP (mV) of VCM-HNLCs during a 90-days storage at (**A**) room temperature (RT) and (**B**) 4 °C. All results are presented as mean ± SD (n = 3).

3.9 *In vitro* antibacterial activity studies

3.9.1 Determination of minimum inhibitory concentration (MIC)

To investigate the pH-dependent antibacterial activity of VCM-HNLCs against *S. aureus* and MRSA, the minimum inhibitory concentration (MIC) was measured using a broth microdilution method [304]. **Table 4** illustrates the MIC values of bare VCM, blank HNLCs and VCM-HNLCs against *S. aureus* and MRSA at pH 7.4 and pH 6.0. At physiological pH, VCM-HNLCs showed higher antibacterial activity with a 2-fold reduction in MIC values compared to the bare VCM against *S. aureus* (1.95 vs 3.9 µg/mL) and MRSA (3.9 vs 7.8 µg/mL) for the first 48 hrs. The bare VCM then steadily lost its activity over the course of 72 hrs, while the antibacterial action of the VCM-HNLCs was persisted for the same time period against both bacteria. This indicates that VCM-HNLCs exhibited sustained antibacterial properties against both *S. aureus* and MRSA compared to bare VCM.

The hybrid NPs also exhibited superior and sustained antibacterial activity compared to bare VCM at pH 6.0, with a 4-fold reduction in MIC values in the first 24 hrs, and an 8-fold reduction in MIC values in the next 48 and 72 hrs against both *S. aureus* and MRSA. On the other hand, the antibacterial activity of VCM-HNLCs was greater at pH 6.0 with a 2-fold decrease in the MICs against both bacteria over 72 hrs of treatment compared to their activity at pH 7.4. These results confirmed the pH-responsive antibacterial activity of VCM-HNLCs against both *S. aureus* and MRSA.

Similarly, it was discovered that the blank HNLCs exhibited some antibacterial activity against *S. aureus* and MRSA, at both pH conditions with MIC values of 16.11 µg/mL and 32.22 µg/mL,

respectively. This could be attributed to the combined and inherent antibacterial properties of Tween 80 [338], OLA [339] and TS [293] against gram-positive bacteria.

The enhanced and sustained antibacterial activity of VCM-HNLCs over the bare VCM under normal conditions may be due to numerous factors include; a) the gradual and extended release profile of VCM from the hybrid NPs resulting in long-lasting antibacterial efficacy [340], b) the smaller particle size of the NPs which facilitates better adsorption and effective cell wall penetration [341], and c) the potential effect as result of the intrinsic antibacterial activity of the nanoformulation components. Furthermore, the improved antimicrobial activity of the prepared VCM-HNLCs at the acidified infection pH may be due to the rapid VCM release from the HNLCs at pH 6.0 and the surface charge switch from negative to positive charge due to the protonation of OLA, which improve the adhesion of VCM-HNLCs to the negatively charged bacterial cell wall leading to superior antibacterial efficacy. The overall enhanced antibacterial activity associated with the antibiotic-loaded hybrid nanocarrier may help in reducing the effective treatment dose without compromising therapeutic outcomes [342]. Moreover, the frequency of VCM administration could be decreased, which reduce the dose-related toxicity and improves patient compliance [343]. A similar trend of enhanced and sustained pH-responsive antibacterial activity was previously reported for VCM-loaded NLCs [267] and VCM-loaded SLNs [263] against both *S. aureus* and MRSA.

Table 4. The minimum inhibitory concentration (MIC) values (μg/mL) for *S. aureus* and MRSA at pH 7.4 and pH 6.0, respectively, for bare VCM, blank HNLCs and VCM-HNLCs. The test was done in triplicate (n = 3).

S. *aureus* (μg/mL)						
Time (hrs)	24	48	72	24	48	72
	pH 7.4			**pH 6.0**		
Bare VCM	3.9	3.9	7.8	3.9	7.8	7.8
Blank HNLCs	16.11	16.11	16.11	16.11	16.11	16.11
VCM-HNLCs	1.95	1.95	1.95	0.98	0.98	0.98
MRSA (μg/mL)						
Time (hrs)	24	48	72	24	48	72
	pH 7.4			**pH 6.0**		
Bare VCM	7.8	7.8	15.62	7.8	15.62	15.62
Blank HNLCs	32.22	32.22	32.22	32.22	32.22	32.22
VCM-HNLCs	3.9	3.9	3.9	1.95	1.95	1.95

*VCM = Vancomycin free base, and HNLCs = hybrid nanostructured lipid carriers.

3.9.2 Determination of Fractional Inhibitory Concentration (FIC)

To further identify the combined antibacterial effect of VCM and blank HNLCs in the VCM-HNLCs against *S. aureus* and MRSA at pH 7.4 and 6.0, the cumulative FIC values were determined for 24, 48 and 72 hrs based on the MIC values acquired from the *in vitro* antibacterial investigation (**Table 5**). At pH 7.4, the calculated ΣFIC for *S. aureus* were found to be 0.62, 0.62 and 0.37, indicating that additive antibacterial effects continued for the first 48 hrs followed by synergistic activity up to 72 hrs, while for MRSA, the ΣFIC values were 0.62, 0.62 and 0.37, indicating additive combination activity. However, the ΣFIC values at pH 6.0 were 0.31, 0.19 and 0.19 for *S. aureus* and 0.31, 0.19 and 0.19 for MRSA, confirming the synergistic interaction for both strains at all time intervals. As a result of this synergistic combination activity, a lower VCM-HNLCs dose could be required to produce the same therapeutic effect as bare VCM, which may potentially increase the antibacterial efficacy while reducing related toxicity and side effects.

Table 5. ∑FIC values against *S. aureus* and MRSA at pH 7.4 and pH 6.0.

FIC against S. *aureus*						
Time (h)	24	48	72	24	48	72
	pH 7.4			pH 6		
FIC (Bare VCM)	0.50	0.50	0.25	0.25	0.13	0.13
FIC (Blank HNLCs)	0.12	0.12	0.12	0.06	0.06	0.06
ΣFIC	**0.62**	**0.62**	**0.37**	**0.31**	**0.19**	**0.19**
Interpretation	Additive	Additive	Synergy	Synergy	Synergy	Synergy
FIC against MRSA						
Time (h)	24	48	72	24	48	72
	pH 7.4			pH 6		
FIC (Bare VCM)	0.50	0.50	0.25	0.25	0.13	0.13
FIC (Blank HNLCs)	0.12	0.12	0.12	0.06	0.06	0.06
ΣFIC	**0.62**	**0.62**	**0.37**	**0.31**	**0.19**	**0.19**
Interpretation	Additive	Additive	Additive	Synergy	Synergy	Synergy

3.9.3 Flow cytometry

Using a previously reported flow cytometry technique with slight modifications, the impact of bare VCM and VCM-HNLCs on the cell viability of MRSA was evaluated [188]. The antibiotics activity on bacteria causes considerable changes in morphology and cell-division cycle that can be detected using specific dyes [344]. Propidium iodide (PI), a non-permeant fluorescent dye, has been employed

to identify damaged bacterial cells whereas Syto9, a green, fluorescent nucleic acid permeant dye has been used to identify live cells in the population. The data acquired from flow cytometry were investigated using the flow cytometer software Kaluza-2.20 (Beckman Coulter, USA), at which two gates were produced to distinguish between viable cells (green) and dead cells (red) in the population. **Figure 11**, which illustrates the cell count versus PI uptake histogram for MRSA, shows that 93.61 ± 0.33% and 97.34 ± 2.71 % of MRSA cell died after incubation with bare VCM (**8B**) and VCM-HNLCs (**8D**) at their respective MICs (7.8 and 3.9 µg/mL, respectively). This indicates that VCM-HNLCs were able to achieve better killing activity than bare VCM at a 2-fold lower inhibitory concentration (*P*-value = 0.003). However, only 79.44 ± 1.13 % of MRSA cells died (**8C**) when treated with bare VCM at the same concentration of VCM-HNLCs (3.9 µg/mL) compared to 97.34 ± 2.71 % in the case of the hybrid NPs formulation (*P*-value <0.0001). These findings further support the potential enhancement in the antibacterial effectiveness of VCM-HNLCs against MRSA, which may also be used to reduce the effective dose of VCM in treating MRSA infections without compromising the overall therapeutic efficacy [345].

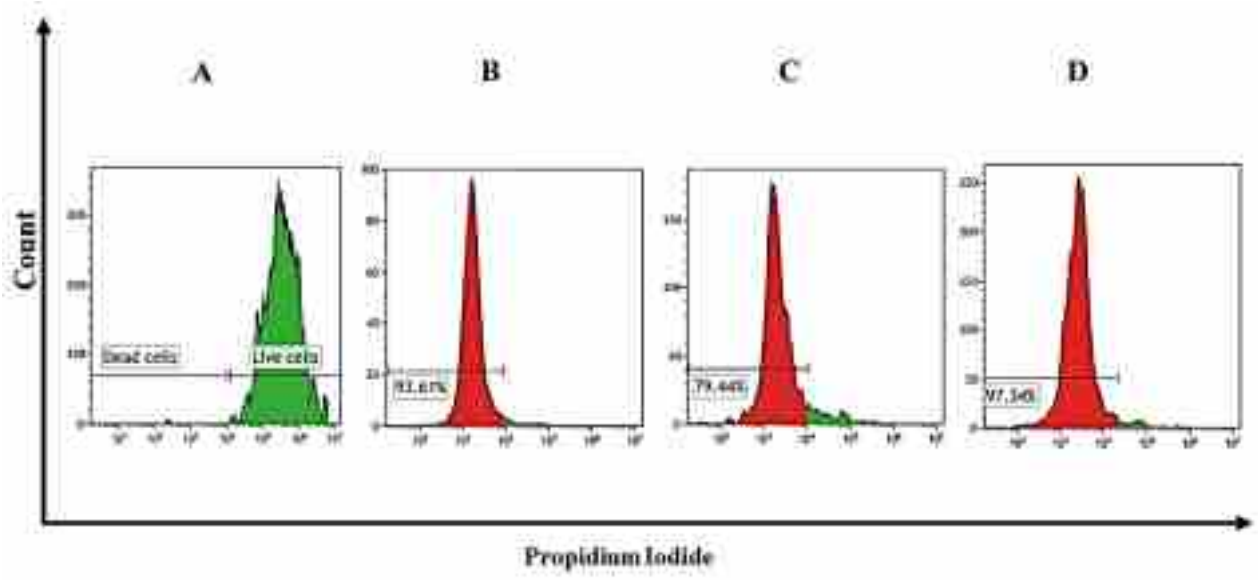

Figure 11. Histogram of cell count versus propidium iodide (PI) uptake. **A** corresponds to the untreated MRSA (live cells); **B**, **C** and **D** indicate the proportion of dead MRSA cells following incubation with bare VCM at its MIC (7.8 µg/mL), bare VCM in NPs MIC (3.9 µg/mL) and VCM-HNLCs at its MIC (3.9 µg/mL), respectively. The experiment was conducted in triplicate (n = 3).

3.9.4 Determination of *in vitro* antibiofilm activity

Biofilms formation is one of the survival strategies of many types of microorganisms, including bacteria. They play a significant role in the pathogenesis of various bacterial infections, particularly

MRSA infections, rendering them more resistant to the host's immune system and antimicrobial treatments [346]. Therefore, it would be beneficial to develop a nano antibiotic delivery system with improved antibacterial activity and has the ability to successfully remove biofilms in order to combat against MDR bacterial infections and sepsis. In this regard, the efficiency of the prepared VCM-HNLCs formulation against MRSA biofilms was explored using the crystal violet staining assay and the florescence microscope assay.

3.9.4.1 Crystal violet assay

Mature MRSA biofilms were exposed to PBS pH 7.4 and 6.0 (as controls), bare VCM solution and VCM-HNLCs formulation for 24 hrs and then stained with crystal violet. The changes in the crystal violet intensity were imaged and the percentage of biofilm growth inhibition was analyzed, and the results are presented in **Figure 12**. VCM-HNLCs displayed higher efficiency in eradication of MRSA biofilms at pH 7.4, as it reduced the biofilm biomass by ~ a 5-fold (68.17 ± 1.83 %) compared to bare VCM that showed only 14.25 ± 2.62 % biofilm elimination activity. At pH 6.0, biofilms treated with VCM-HNLCs showed a reduction in biofilms biomass by ~ a 6-fold compared to bare VCM, as it displayed 93.51 ± 0.83 % while bare VCM showed only 16.41 ± 0.80 % biofilm eradication. Also, VCM-HNLCs exhibited a significant pH-responsive antibiofilm activity against MRSA biofilms with ~ 1.4-fold reduction in MRSA biofilms biomass at pH 6.0 compared to pH 7.4. This improved antibiofilm activity could be due to the combined effects of TS and Tween 80, as well as the pH-responsive property of the nanosystem.

It has been reported that TS has a strong and intrinsic anti-adhesion properties against *S. aureus* biofilms. Therefore, it could act synergistically with VCM to affect pathogen adhesion and biofilm formation, making it a suitable pharmaceutical adjuvant for antibiotic therapy [292, 293, 347]. Furthermore, Tween 80 has been reported to possess potential antibiofilm action against a variety of pathogenic bacteria, including MRSA. It has the ability to reduce bacterial adhesion to surfaces and also facilitate biofilm elimination by disturbing the biofilm matrix and increasing its permeability [322, 348]. On the other hand, the charge reversible property improves the electrostatic attraction between the positively charged VCM-HNLCs with the negatively charged bacterial cell surfaces at the acidic environment inside biofilms, which enhance the binding of the NPs and the transport of the antibiotic to the biofilm barrier, hence improving the efficiency of antibacterial agents in eradicating biofilms and inhibiting biofilms formation [349, 350]. These findings suggest that, in addition to the enhanced antibacterial activity against MRSA, VCM-HNLCs may also be effective in eliminating bacterial biofilms and modulating biofilm formation.

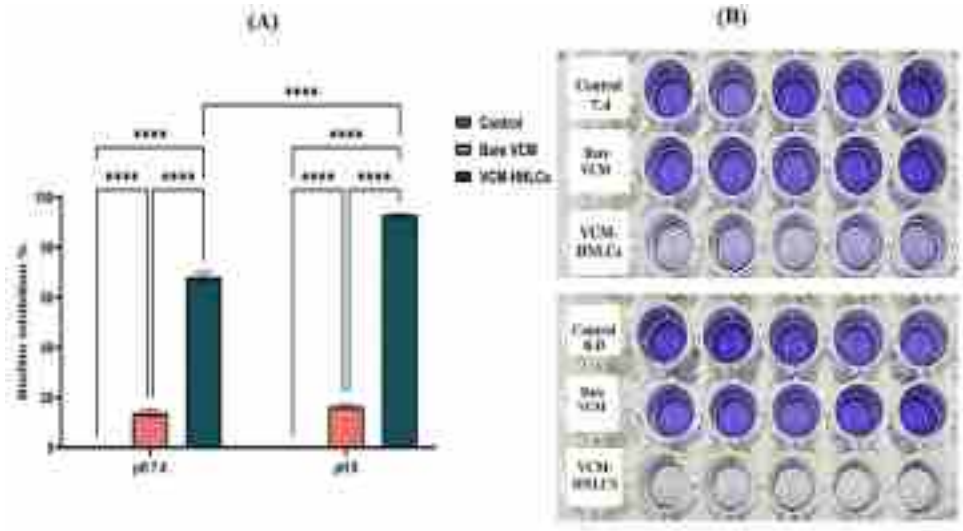

Figure 12. (**A**) Percentage of biofilm growth suppression following the exposure of MRSA biofilms to bare VCM, VCM-HNLCs and controls (PBS pH 7.4 and 6.0). Each result is shown as mean ± SD (n = 3) (*P*-values **** < 0.0001). (**B**) MRSA biofilm growth reduction after exposure to bare VCM and VCM-HNLCs at PBS pH 7.4 and 6.0, as indicated by changes in the crystal violet intensity (* PBS = phosphate buffered saline, VCM = vancomycin, NLCs = nanostructured lipid carriers).

3.9.4.2 Florescence microscope assay

The effectiveness of VCM-HNLCs in removing mature MRSA biofilms was further confirmed using a fluorescence microscope. The mature biofilms were cultured on cover slips and then discolored for 30 min in the dark using Syto9 and PI solutions. After rinsing off the dyes, the cover slips were placed on glass slides, inverted. As shown in **Figure 13**, untreated MRSA biofilms emitted a considerable Syto9 fluorescence over the whole coverslip. (**13A1**), which is caused by the intact membranes of the accumulated bacterial cells on the coverslips [351, 352]. However, there was no significant fluorescence when the untreated MRSA biofilms were treated with PI (**13A2**), since PI cannot enter live cells that have an unbroken cell membrane [353, 354]. MRSA biofilms stained with Syto9 and treated with bare VCM exhibited little reduction in fluorescence when in contrast to untreated biofilms (**13B1**), while those stained with PI displayed a slight fluorescence (**13B2**), indicating that some of the drug had permeated the biofilm and partially killed the bacteria. Interestingly, when the MRSA biofilms were treated with VCM-HNLCs (**13C1**), the Syto9 fluorescence intensity decreased significantly compared to bare VCM treated- or untreated group, suggesting a potential decrease in the number of viable cells on the slide as well as biofilms. Moreover, despite PI's non-cell permeable nature, the biofilms treated with VCM-HNLCs exhibited a remarkably high intensity of PI fluorescence (**13C2**). This intense emission reveals that treatment of MRSA biofilms with VCM-HNLCs led to degradation of MRSA cell membranes and biofilms, allowing for more PI penetration and binding to DNA [353]. As a result, biofilms treated with VCM-HNLCs resulted in a significantly

higher percentage of bacterial death compared to those treated with VCM alone. These results suggest that VCM-HNLCs may be effective in eradicating biofilms, which are responsible for persistent infections and sepsis.

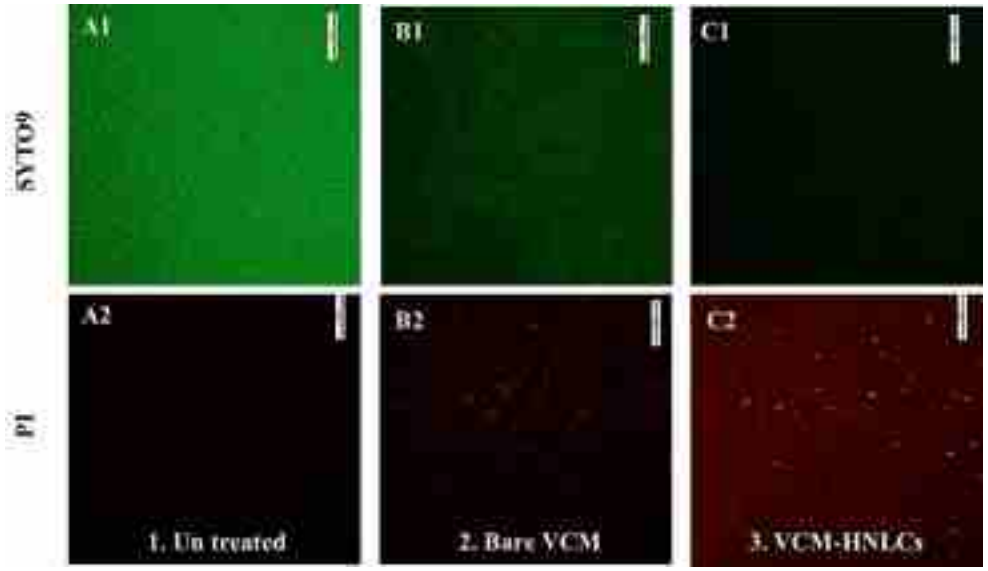

Figure 13. Images of the fluorescence microscope assay of MRSA biofilms stained with Syto9 and PI. **1**. Untreated MRSA biofilms **2.** Bare VCM treated biofilms, and **3.** VCM-HNLCs treated biofilms, respectively. (Scale bar =100 μm).

3.9.5 Time killing assay (TKA)

To determine the rate of bacterial killing after a 24-hrs exposure of MRSA to bare VCM and VCM-HNLCs formulation solution (5×MIC) at pH 7.4 and 6.0, the time killing assay was performed (**Figure 14)**. All antibiotic treatments reduced the number of MRSA colonies under all pH conditions. However, VCM-HNLCs showed superior activity compared to bare VCM as indicated by the total eradication of MRSA bacteria from the first 2 hrs and 1 hr of incubation at pH 7.4 and 6.0, respectively, whereas bare VCM exhibited slower killing kinetics within 24 hrs of incubation at both pHs. Hence, VCM-HNLCs showed a significantly rapid bactericidal effect against MRSA at a 2-fold and 4-fold lower concentration than VCM alone at pH 7.4 and 6.0, respectively (*P*-value <0.0001). The enhanced ability of the VCM-HNLCs to reduce bacterial load at pH 6.0 could also be due to the pH-responsive activity of the nanosystem.

VCM therapy is usually associated with slow and time-dependent antibacterial efficacy, poor penetration into solid organs, and poor pharmacokinetic properties, which contribute to high rates of antimicrobial resistance, treatment failure and toxicity [355]. Therefore, these findings prove that VCM-HNLCs could be an effective nanocarrier for improving the bacterial killing kinetics of

antibiotics with long-term release in the body to obtain a successful therapy with lower dose regimens against MRSA infections and their induced sepsis.

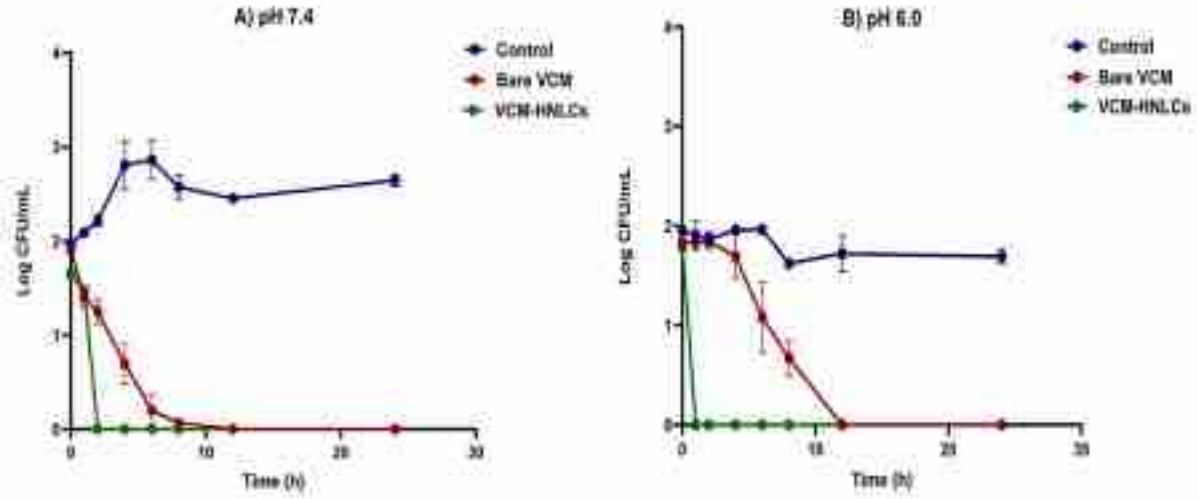

Figure 14. MRSA time killing kinetics when exposed to bare VCM, VCM-HNLCs and (**A**) PBS pH 7.4 and (**B**) pH 6.0 (as controls). The findings are shown as mean ± SD (n = 3). At pH 6, VCM-HNLCs demonstrated more enhancement of VCM killing kinetics (*P*-value <0.0001).

3.9.6 Efflux pump inhibition assay

Recently, bacterial multidrug efflux pumps have gained attention due to their possible association with clinical AMR [356]. For instance, MRSA can develop efflux-mediated resistance to antibiotics through mutations that reduce the bacterial affinity to the antimicrobials [357]. However, the overexpression of bacterial efflux pumps makes it challenging for antibiotics to effectively enter the bacterial cells [358]. Therefore, the ability of the prepared subinhibitory concentrations of VCM-HNLCs (0.25×MIC) to inhibit MRSA-induced efflux pumps overexpression was examined employing EtBr according to a previously described method [309]. EtBr, an efflux pumps substrate, binds to DNA intracellularly and fluoresces inside the bacteria [359]. According to the results presented in **Figure 15**, MRSA treated with VCM-HNLCs displayed higher fluorescence intensity due to the significant EtBr accumulation in the bacterial cells compared to those treated with bare VCM. The presence of TS as a component of the nanocarrier could be responsible for the increased fluorescence intensity observed in the MHA samples treated with VCM-HNLCs, which also supports the reduction in the MIC values and the enhancement of VCM activity when loaded into the HNLCs containing TS. It has been reported in the literature that TS has a promising efflux pump inhibition activity, primarily against NorA and NorB, the chromosomally encoded efflux pumps of gram-positive bacteria [360], which may account for the observed efflux pump inhibition against MRSA [289-291]. Therefore, TS can act synergistically with VCM in the prepared VCM-HNLCs formulation

to combat resistant *S. aureus* and could be employed as an adjuvant for effective antibiotic therapy to overcome antibacterial resistance due to efflux pumps and treat associated conditions like MRSA sepsis.

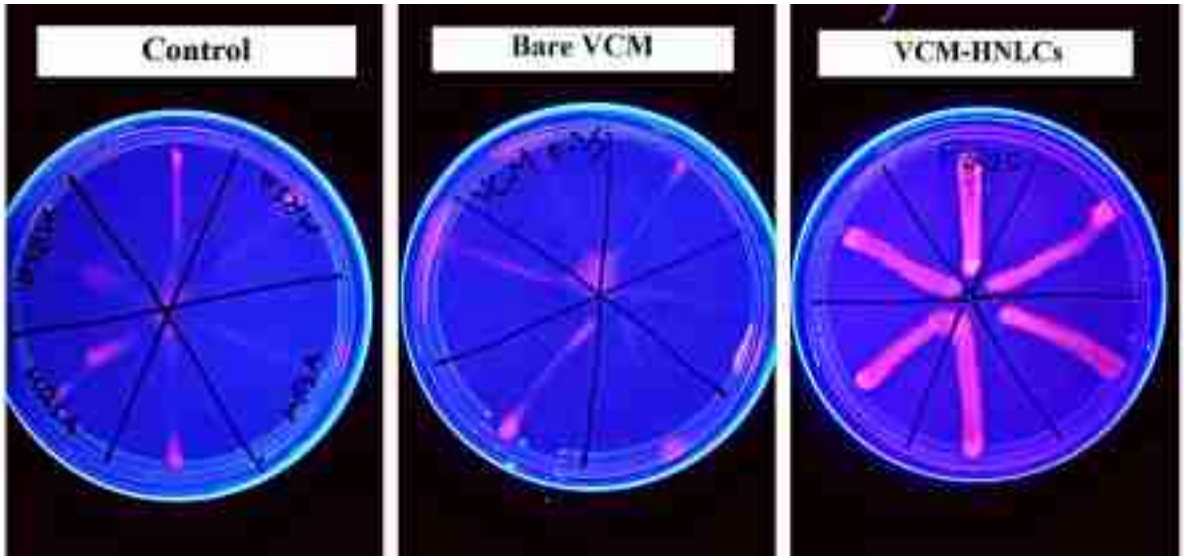

Figure 15. Efflux pump inhibition effect of VCM-HNLCs against MRSA compared to the bare VCM at 0.25×MIC.

3.10 *In vitro* antioxidant study

Excessive reactive oxygen species (ROS) production in response to inflammation, leads to oxidative stress, which is a major contributor to the high mortality rates associated with a number of infectious disorders such as sepsis [361]. Therefore, neutralizing ROS produced during the inflammatory process is of great importance to reduce oxidative stress and alleviate the damaging consequences of sepsis on the body. Therefore, the DPPH radical scavenging method was used to investigate the *in vitro* antioxidant effects of different concentrations of individual excipients (TS, Lys, and HA-Lys conjugate) and the prepared VCM-HNLCs [310]. **Figure 16** shows the antioxidant activity percentage of ascorbic acid (positive control), TS, Lys, HA-Lys conjugate and VCM-HNLCs after being incubated with DPPH solution at 37 °C in the dark. The results indicated that all the examined samples displayed a concentration-dependent ability to scavenge DPPH radicals, with the strongest antioxidant activity observed at a concentration of 1000 µg/mL. Specifically, the activity was found to be 34.98 ± 3.59 %, 53.21 ± 2.30 %, 59.69 ± 4.68 % and 61.08 ± 1.87 % for TS, Lys, HA-Lys conjugate and VCM-HNLCs, respectively. Regarding the individual excipients, we observed that Lys and HA-Lys conjugate demonstrated higher scavenging activity compared to TS at all concentrations. This could be due to the lower hydrogen donor activity of TS compared to the other excipients. Vitamin E derivatives, such as TS, have been reported to have reduced DPPH scavenging activity compared to pure vitamin E (tocopherol), as salts can interfere with DPPH measurements and lower

their antioxidant activity [362, 363]. On the other hand, the enhanced antioxidant activity of pure Lys and the synthesized HA-Lys polymer could be due to the free amino group in Lys units which can donate electrons to stabilize and neutralize DPPH radicals [364, 365]. Additionally, the antioxidant activity of VCM-HNLCs could be attributed to the combined effect of TS and HA-Lys, with the HA-Lys conjugate showing a significant effect over TS. As a result, the protective effect of HA-Lys and its hybrid nanoformulation against DPPH radicals could have potential benefits in inhibiting oxidative stress and lipid peroxidation associated with inflammations and sepsis [283, 286].

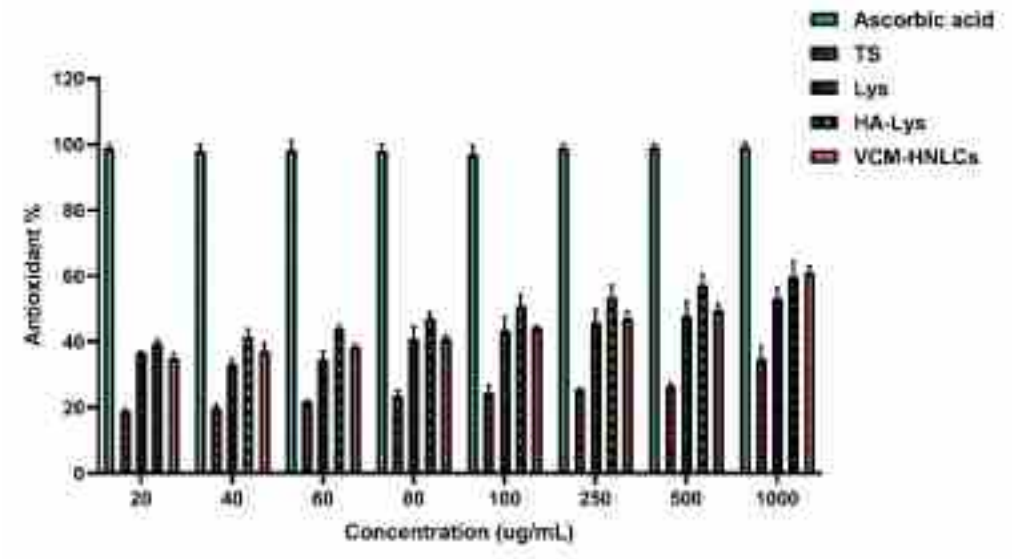

Figure 16. The antioxidant activity (%) of various concentrations (µg/mL) of TS, Lys, HA-Lys conjugate and VCM-HNLCs according to a DPPH radical scavenging assay in comparison to ascorbic acid (positive control). Data in the graph are presented as mean ± SD (n = 3). (*TS= Tocopherol succinate, Lys= L-Lysine, HA-Lys= hyaluronic acid-lysine conjugate, VCM-HNLCs= vancomycin-loaded hybrid nanostructured lipid carriers, DPPH= 2.2-diphenyl-1-picrylhydrazyl)

3.11 *In vitro* anti-inflammatory studies

LPS is one of the most potent bacterial toxins that causes inflammation in a number of illness conditions, including sepsis. It is essential in initiating an immune response that can result in cytotoxicity and multiple organ dysfunction [366]. When LPS triggers an immune response, it can result in the release of several cytokines such as TNF-α, IL-1β, and IL-6 [367]. Additionally, LPS can induce cytotoxic effects in sepsis that can affect different cells and organs [368]. For example, the hyperactivation and malfunction of endothelial and immune cells, as a result of the body's inflammatory response, could harm tissues and organs and affect vascular integrity and permeability.[369, 370]. Therefore, utilizing the HepG2 cell line [300, 311], we investigated the anti-inflammatory effects of HA-Lys and VCM-HNLCs formulations against LPS-induced inflammation

by measuring the cell viability and the IL-6 levels using MTT assay and enzyme-linked immunosorbent assay (ELIZA), respectively.

3.11.1 Cytoprotective effect against LPS-induced cytotoxicity

The cytoprotective effect of HA-Lys and VCM-HNLCs against LPS-stimulated HepG2 was evaluated using a previously reported MTT assay protocol [312]. LPS treatment (0.9 mg/mL) resulted in a substantial decrease in HepG2 cell viability to 36.70 ± 3.30 % compared to the control group, as illustrated in **Figure 17A** (*P*-value<0.0001). However, the addition of HA-Lys or VCM-HNLCs formulations (100 µg/mL) improved cell viability to 100.84 ± 3.91 % and 67.34 ± 1.87 %, respectively, compared to the control. Notably, treatment with HA-Lys and VCM-HNLCs formulations enhanced the cell viability reduced by LPS by 64.14 % (*P*-value<0.0001) and 30.64 % (*P*-value = 0.0002), respectively, compared to the LPS-treated group. The results indicated that HA-Lys and VCM-HNLCs can defend cells from damage caused by LPS. This cytoprotective effect may be due to the antioxidant properties of Lys, which aids in scavenging ROS and reducing oxidative stress, thus lessening cell injury [283, 286]. In addition, HA has been documented to exhibit a protective effect against LPS-induced cell damage [371-373]. As a result, HA-Lys conjugate and its nanoformulation may be considered as potential therapeutic agents for the prevention of cell damage brought on by sepsis.

3.11.2 Anti-inflammatory activity against LPS-induced inflammatory responses (measurement of IL-6 levels).

Sepsis has been associated with altered expression of cytokines, which are crucial for controlling the host immunological response [374]. Interleukin-6 (IL-6) is one of these cytokines that is thought to be important for the development of sepsis, especially as an early marker of inflammation [375]. In cases of severe sepsis and septic shock, the cytokine storm can be exacerbated by an overabundance of IL-6 production, which can cause substantial tissue damage and organ failure. [376, 377]. Therefore, to further verify the anti-inflammatory potential of the synthesized HA-Lys and VCM-HNLCs, we investigated their influence on the expression of the pro-inflammatory cytokine IL-6 in LPS-stimulated HepG2 cells. The levels of IL-6 were found to be significantly elevated when the cells were treated with 1 µg/mL of LPS, as the results shown in **Figure 17B**. Nevertheless, it was observed that the concentration of IL-6 decreased significantly following the treatment with varying concentrations of HA-Lys or VCM-HNLCs formulations (50 and 100 µg/mL), compared to the group treated with LPS alone (*P*-value<0.0001). This indicates that HA-Lys and the hybrid nanocarrier can both regulate the amounts of IL-6 that induced by LPS, which may mitigate tissue damage caused by an excessive immune response. This result confirms the antagonistic action of both HA-Lys and the hybrid NLCs on TLR4, since their enhanced anti-inflammatory effects can be attributed to their strong

and competitive binding to TLR4, which was previously demonstrated in this study through *in vitro* MST investigations. A similar trend of reduction in IL-6 levels was observed in two studies reported by Farajzadeh *et al*. (2018) and Cardoso MSc *et al*. (2022), who revealed the significant anti-inflammatory effects of HA-based NPs and HA-based nanogels against LPS-stimulated inflammatory responses, respectively [378, 379]. Consequently, both HA-Lys and VCM-HNLCs could be a promising candidates for modulating IL-6 levels and controlling the inflammatory response in sepsis.

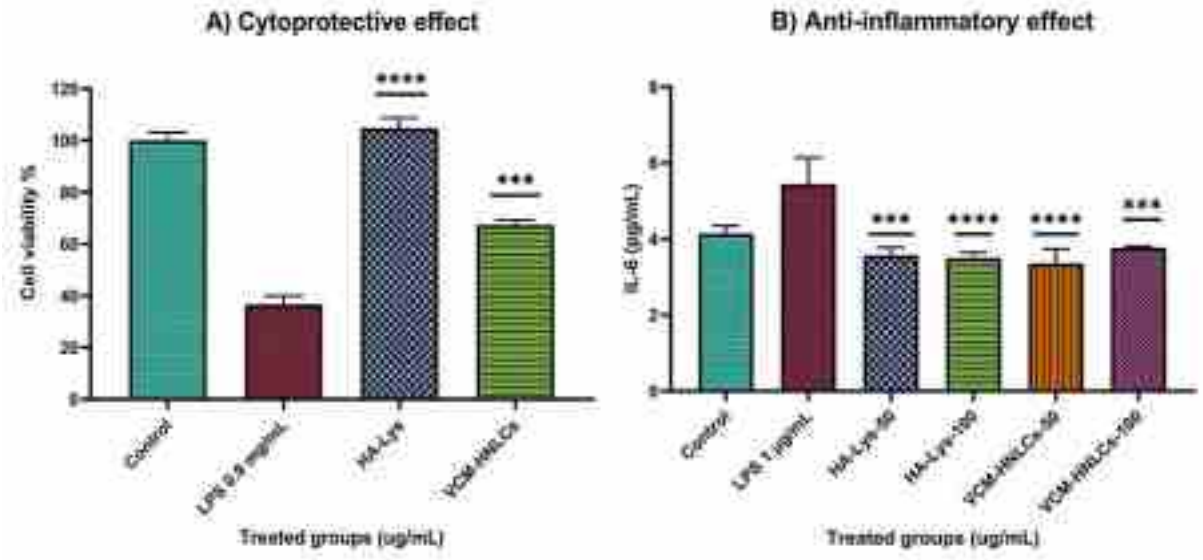

Figure 17. (**A**) The Cytotoxicity of LPS on HepG2 cells and the protective effects of HA-Lys and VCM-HNLCs as measured by MTT assy, and (**B**) The effect of HA-Lys and VCM-HNLCs on IL-6 expression induced by LPS. (**** *P*-value<0.0001, *** *P*-value = 0.0002, in comparison with the LPS-treated group). Data in the graph are presented as mean ± SD (n =3).

4. Conclusion

In recent years, there has been a growing interest in creating advanced, multifunctional biomimetic and stimuli-responsive nanocarriers for effectuve antibiotic delivery against bacterial infections and sepsis. In this study, we aimed to develop a new hyaluronic acid-lysine polymer (HA-Lys) for the creation of biomimetic pH-responsive hybrid nanosctructured lipid carriers (HNLCs) that could improve the delivery of vancomycin to combat bacterial-induced sepsis. The HA-Lys conjugate was successfully synthesized and characterized by FTIR and ^{1}H NMR. The fabrication of VCM-HNLCs using a hot homogenization and ultrasonication technique led to hybrid NPs with an appropriate size, low polydispersity index, acceptable zeta potential, and high encapsulation efficiency and drug loading. The biosafety profiles of HA-Lys and VCM-HNLCs were confirmed by MTT and hemolysis assays. The binding potential of HA-Lys and its VCM-HNLCs to human TLR2 and TLR4 was

demonstrated to be excellent *in vitro*, with higher binding affinity than their natural substrates, PGN and LPS, respectively. This suggests that these compounds may possess the ability to competitively modulate the immune response and potentially reduce the pathogenicity caused by bacterial sepsis. VCM-HNLCs exhibited a pH-triggered drug release profile, superior and pH-sensitive antibacterial and biofilm eradication capabilities, and a significant inhibitory effect against MRSA efflux pumps, as compared to the bare antibiotic. This could improve the anti-virulence efficacy of VCM and enhance sepsis treatment outcomes. The potential of VCM-HNLCs to rapidly kill MRSA was also verified using the time-killing assay and flow cytometry analysis. Moreover, significant free radical scavenging capacities as well as noteworthy cytoprotective and anti-inflammatory effects against LPS-induced inflammation were exhibited by both HA-Lys and VCM-HNLCs. The findings of this research have prompted the creation of a straightforward nanoplatform for treating bacterial sepsis and battling MDR bacteria. Additionally, it contributes to increasing the variety of hybrid NLCs with antivirulence potential and combine both biomimetic and stimui-responsive approaches for improving antibiotics therapy against sepsis-inducing bacteria

References

244. Singer, M., C.S. Deutschman, C.W. Seymour, M. Shankar-Hari, D. Annane, M. Bauer, R. Bellomo, G.R. Bernard, J.-D. Chiche, C.M. Coopersmith, R.S. Hotchkiss, M.M. Levy, J.C. Marshall, G.S. Martin, S.M. Opal, G.D. Rubenfeld, T. van der Poll, J.-L. Vincent, and D.C. Angus, *The Third International Consensus Definitions for Sepsis and Septic Shock (Sepsis-3).* JAMA, 2016. **315**(8): p. 801-810. https://doi.org/10.1001/jama.2016.0287
245. Shi, Y., M.L. Zhu, Q. Wu, Y. Huang, X.L. Xu, and W. Chen, *The Potential of Drug Delivery Nanosystems for Sepsis Treatment.* J. Inflamm. Res., 2021. **14**: p. 7065-7077. https://doi.org/10.2147/jir.S339113
246. WHO. *Global report on the epidemiology and burden of sepsis*. 2020 9 September 2020 [cited 2023 05 May 2023]; Available from: https://www.who.int/publications/i/item/9789240010789.
247. Hotchkiss, R.S., L.L. Moldawer, S.M. Opal, K. Reinhart, I.R. Turnbull, and J.-L. Vincent, *Sepsis and septic shock.* Nat. Rev. Dis. Primers, 2016. **2**(1): p. 16045. https://doi.org/10.1038/nrdp.2016.45
248. Dadgostar, P., *Antimicrobial Resistance: Implications and Costs.* Infect Drug Resist, 2019. **12**: p. 3903-3910. https://doi.org/10.2147/IDR.S234610
249. Wiersinga, W.J., S.J. Leopold, D.R. Cranendonk, and T. van der Poll, *Host innate immune responses to sepsis.* Virulence, 2014. **5**(1): p. 36-44. https://doi.org/10.4161/viru.25436
250. Ko, C.-N., S. Zang, Y. Zhou, Z. Zhong, and C. Yang, *Nanocarriers for effective delivery: modulation of innate immunity for the management of infections and the associated complications.* J. Nanobiotechnology, 2022. **20**(1): p. 380. https://doi.org/10.1186/s12951-022-01582-8
251. Perner, A., A.C. Gordon, D. De Backer, G. Dimopoulos, J.A. Russell, J. Lipman, J.-U. Jensen, J. Myburgh, M. Singer, R. Bellomo, and T. Walsh, *Sepsis: frontiers in diagnosis, resuscitation and antibiotic therapy.* Intensive Care Med . 2016. **42**(12): p. 1958-1969. https://doi.org/10.1007/s00134-016-4577-z

252. Cao, C., M. Yu, and Y. Chai, *Pathological alteration and therapeutic implications of sepsis-induced immune cell apoptosis.* Cell Death Dis., 2019. **10**(10): p. 782. https://doi.org/10.1038/s41419-019-2015-1
253. Salomao, R., M.K. Brunialti, M.M. Rapozo, G.L. Baggio-Zappia, C. Galanos, and M. Freudenberg, *Bacterial sensing, cell signaling, and modulation of the immune response during sepsis.* Shock, 2012. **38**(3): p. 227-42. https://doi.org/10.1097/SHK.0b013e318262c4b0
254. Yeh, Y.-C., T.-H. Huang, S.-C. Yang, C.-C. Chen, and J.-Y. Fang, *Nano-Based Drug Delivery or Targeting to Eradicate Bacteria for Infection Mitigation: A Review of Recent Advances.* Front. Chem., 2020. **8**. https://doi.org/10.3389/fchem.2020.00286
255. Liu, R., C. Luo, Z. Pang, J. Zhang, S. Ruan, M. Wu, L. Wang, T. Sun, N. Li, L. Han, J. Shi, Y. Huang, W. Guo, S. Peng, W. Zhou, and H. Gao, *Advances of nanoparticles as drug delivery systems for disease diagnosis and treatment.* Chin Chem Lett . 2023. **34**(2): p. 107518. https://doi.org/10.1016/j.cclet.2022.05.032
256. Zhao, Z., C. Ding, Y. Wang, H. Tan, and J. Li, *pH-Responsive polymeric nanocarriers for efficient killing of cariogenic bacteria in biofilms.* Biomater. Sci., 2019. **7**(4): p. 1643-1651. https://doi.org/10.1039/C8BM01640B
257. Colilla, M. and M. Vallet-Regí, *Targeted Stimuli-Responsive Mesoporous Silica Nanoparticles for Bacterial Infection Treatment.* Int. J. Mol. Sci., 2020. **21**(22): p. 8605. https://doi.org/10.3390/ijms21228605
258. Santos, R.S., C. Figueiredo, N.F. Azevedo, K. Braeckmans, and S.C. De Smedt, *Nanomaterials and molecular transporters to overcome the bacterial envelope barrier: Towards advanced delivery of antibiotics.* Adv. Drug Deliv. Rev., 2018. **136-137**: p. 28-48. https://doi.org/10.1016/j.addr.2017.12.010
259. Ibrahim, U.H., N. Devnarain, and T. Govender, *Biomimetic strategies for enhancing synthesis and delivery of antibacterial nanosystems.* Int. J. Pharm., 2021. **596**: p. 120276. https://doi.org/10.1016/j.ijpharm.2021.120276
260. Song, Q., Y. Yin, L. Shang, T. Wu, D. Zhang, M. Kong, Y. Zhao, Y. He, S. Tan, Y. Guo, and Z. Zhang, *Tumor Microenvironment Responsive Nanogel for the Combinatorial Antitumor Effect of Chemotherapy and Immunotherapy.* Nano Lett., 2017. **17**(10): p. 6366-6375. https://doi.org/10.1021/acs.nanolett.7b03186
261. Sahu, P., S.K. Kashaw, S. Sau, V. Kushwah, S. Jain, and A.K. Iyer, *Discovering pH triggered charge rebound surface modulated topical nanotherapy against aggressive skin papilloma.* Mater. Sci. Eng. C, 2020. **107**: p. 110263. https://doi.org/10.1016/j.msec.2019.110263
262. Song, X., W. Fu, and U.K. Cheang, *Immunomodulation and delivery of macrophages using nano-smooth drug-loaded magnetic microrobots for dual targeting cancer therapy.* iScience, 2022. **25**(7): p. 104507. https://doi.org/10.1016/j.isci.2022.104507
263. Ibrahim, U.H., N. Devnarain, C.A. Omolo, C. Mocktar, and T. Govender, *Biomimetic pH/lipase dual responsive vitamin-based solid lipid nanoparticles for on-demand delivery of vancomycin.* Int. J. Pharm., 2021. **607**: p. 120960. https://doi.org/10.1016/j.ijpharm.2021.120960
264. Rossaint, J. and A. Zarbock, *Pathogenesis of Multiple Organ Failure in Sepsis.* Crit. Rev. Immunol, 2015. **35**(4): p. 277-91. https://doi.org/10.1615/critrevimmunol.2015015461
265. Kumar, S., J. Saxena, V.K. Srivastava, S. Kaushik, H. Singh, K. Abo-EL-Sooud, M.M. Abdel-Daim, A. Jyoti, and R. Saluja, *The Interplay of Oxidative Stress and ROS Scavenging: Antioxidants as a Therapeutic Potential in Sepsis.* Vaccines, 2022. **10**(10): p. 1575. https://doi.org/10.3390/vaccines10101575
266. Liao, C.C., H.P. Yu, S.C. Yang, A. Alalaiwe, Y.S. Dai, F.C. Liu, and J.Y. Fang, *Multifunctional lipid-based nanocarriers with antibacterial and anti-inflammatory activities for treating MRSA*

bacteremia in mice. J. Nanobiotechnology, 2021. **19**(1): p. 48. https://doi.org/10.1186/s12951-021-00789-5

267. Osman, N., C.A. Omolo, R. Gannimani, A.Y. Waddad, S. Rambharose, C. Mocktar, S. Singh, R. Parboosing, and T. Govender, *Novel fatty acid-based pH-responsive nanostructured lipid carriers for enhancing antibacterial delivery.* J Drug Deliv Sci Technol 2019. **53**: p. 101125. https://doi.org/10.1016/j.jddst.2019.101125
268. Shastri, D.H., *Effective Delivery Routes And Strategies For Solid Lipid Nanoparticles (Sln) And Nanostructured Lipid Carriers (Nlc).* Curr. Pharm. Des., 2017. https://doi.org/10.2174/1381612823666171122111132
269. Khosa, A., S. Reddi, and R.N. Saha, *Nanostructured lipid carriers for site-specific drug delivery.* Biomedicine & Pharmacotherapy, 2018. **103**: p. 598-613. https://doi.org/10.1016/j.biopha.2018.04.055
270. Beloqui, A., M.Á. Solinís, A. Rodríguez-Gascón, A.J. Almeida, and V. Préat, *Nanostructured lipid carriers: Promising drug delivery systems for future clinics.* Nanomed.: Nanotechnol. Biol. Med., 2016. **12**(1): p. 143-161. https://doi.org/10.1016/j.nano.2015.09.004
271. Fang, C.L., S.A. Al-Suwayeh, and J.Y. Fang, *Nanostructured lipid carriers (NLCs) for drug delivery and targeting.* Recent Pat Nanotechnol . 2013. **7**(1): p. 41-55.
272. Khan, A.A., I.M. Abdulbaqi, R. Abou Assi, V. Murugaiyah, and Y. Darwis, *Lyophilized Hybrid Nanostructured Lipid Carriers to Enhance the Cellular Uptake of Verapamil: Statistical Optimization and In Vitro Evaluation.* Nanoscale Res. Lett., 2018. **13**(1): p. 323. https://doi.org/10.1186/s11671-018-2744-6
273. Khalili, L., G. Dehghan, N. Sheibani, and A. Khataee, *Smart active-targeting of lipid-polymer hybrid nanoparticles for therapeutic applications: Recent advances and challenges.* Int. J. Biol. Macromol., 2022. **213**: p. 166-194. https://doi.org/10.1016/j.ijbiomac.2022.05.156
274. Nahak, P., R.L. Gajbhiye, G. Karmakar, P. Guha, B. Roy, S.E. Besra, A.G. Bikov, A.V. Akentiev, B.A. Noskov, K. Nag, P. Jaisankar, and A.K. Panda, *Orcinol Glucoside Loaded Polymer - Lipid Hybrid Nanostructured Lipid Carriers: Potential Cytotoxic Agents against Gastric, Colon and Hepatoma Carcinoma Cell Lines.* Pharm. Res., 2018. **35**(10): p. 198. https://doi.org/10.1007/s11095-018-2469-3
275. Tincu, R., M. Mihaila, M. Bostan, F. Teodorescu, D. Istrati, N. Badea, and I. Lacatusu, *Novel Bovine Serum Albumin-Decorated-Nanostructured Lipid Carriers Able to Modulate Apoptosis and Cell-Cycle Response in Ovarian, Breast, and Colon Tumoral Cells.* Pharmaceutics, 2023. **15**(4). https://doi.org/10.3390/pharmaceutics15041125
276. Kumar, A., T. Behl, T. Uniyal, and S. Chadha, *Synthesis of Nanostructured Lipid Carriers Loaded Chitosan/ Carbopol Hybrid Nanocomposite Gel for Oral Delivery of Artemether and Curcumin.* Pharm. Nanotechnol., 2020. **8**(5): p. 418-432. https://doi.org/10.2174/2211738508666200907110444
277. Bueloni, B., D. Sanna, E. Garribba, G.R. Castro, I.E. León, and G.A. Islan, *Design of nalidixic acid-vanadium complex loaded into chitosan hybrid nanoparticles as smart strategy to inhibit bacterial growth and quorum sensing.* Int. J. Biol. Macromol., 2020. **161**: p. 1568-1580. https://doi.org/10.1016/j.ijbiomac.2020.07.304
278. Zhang, S., J. Dong, R. Pan, Z. Xu, M. Li, and R. Zang, *Structures, Properties, and Bioengineering Applications of Alginates and Hyaluronic Acid.* Polymers, 2023. **15**(9): p. 2149. https://doi.org/10.3390/polym15092149
279. Campo, G.M., A. Avenoso, G. Nastasi, A. Micali, V. Prestipino, M. Vaccaro, A. D'Ascola, A. Calatroni, and S. Campo, *Hyaluronan reduces inflammation in experimental arthritis by modulating TLR-2 and TLR-4 cartilage expression.* Biochim Biophys Acta Mol Basis Dis, 2011. **1812**(9): p. 1170-1181. https://doi.org/10.1016/j.bbadis.2011.06.006

280. Campo, G.M., A. Avenoso, S. Campo, A. D'Ascola, G. Nastasi, and A. Calatroni, *Molecular size hyaluronan differently modulates toll-like receptor-4 in LPS-induced inflammation in mouse chondrocytes.* Biochimie, 2010. **92**(2): p. 204-215. https://doi.org/10.1016/j.biochi.2009.10.006
281. Hashizume, M. and M. Mihara, *High molecular weight hyaluronic acid inhibits IL-6-induced MMP production from human chondrocytes by up-regulating the ERK inhibitor, MKP-1.* Biochemical and Biophysical Research Communications, 2010. **403**(2): p. 184-189. https://doi.org/10.1016/j.bbrc.2010.10.135
282. Altman, R., A. Bedi, A. Manjoo, F. Niazi, P. Shaw, and P. Mease, *Anti-Inflammatory Effects of Intra-Articular Hyaluronic Acid: A Systematic Review.* Cartilage, 2019. **10**(1): p. 43-52. https://doi.org/10.1177/1947603517749919
283. Zhang, Y., W. Yu, D. Han, J. Meng, H. Wang, and G. Cao, *L–lysine ameliorates sepsis-induced acute lung injury in a lipopolysaccharide-induced mouse model.* Biomed. Pharmacother., 2019. **118**: p. 109307. https://doi.org/10.1016/j.biopha.2019.109307
284. O'Grady, K.L., S. Khosla, J.N. Farr, O.P. Bondar, E.J. Atkinson, S.J. Achenbach, B.A. Eckhardt, B.S. Thicke, A.J. Tweed, T.L. Volkman, M.T. Drake, J.M. Hines, and R.J. Singh, *Development and Application of Mass Spectroscopy Assays for Nε-(1-Carboxymethyl)-L-Lysine and Pentosidine in Renal Failure and Diabetes.* J Appl Lab Med., 2020. **5**(3): p. 558-568. https://doi.org/10.1093/jalm/jfaa023
285. Jozi, F., N. Kheiripour, M.A. Taheri, A. Ardjmand, G. Ghavipanjeh, Z. Nasehi, and M.E. Shahaboddin, *L-Lysine Ameliorates Diabetic Nephropathy in Rats with Streptozotocin-Induced Diabetes Mellitus.* Biomed Res. Int., 2022. **2022**: p. 4547312. https://doi.org/10.1155/2022/4547312
286. Zhang., C., Y. He, and Y. Shen, *L-Lysine protects against sepsis-induced chronic lung injury in male albino rats.* Biomed. Pharmacother. , 2019. **117**: p. 109043. https://doi.org/10.1016/j.biopha.2019.109043
287. Hartmann, M.S., S. Mousavi, S. Bereswill, and M.M. Heimesaat, *Vitamin E as promising adjunct treatment option in the combat of infectious diseases caused by bacterial including multi-drug resistant pathogens - Results from a comprehensive literature survey.* Eur. J. Microbiol. Immunol., 2020. **10**(4): p. 193-201. https://doi.org/10.1556/1886.2020.00020
288. Gamna, F. and S. Spriano, *Vitamin E: A Review of Its Application and Methods of Detection When Combined with Implant Biomaterials.* Materials, 2021. **14**(13): p. 3691. https://doi.org/10.3390/ma14133691
289. Davis, S., B.M. Davis, J.L. Richens, K.A. Vere, P.G. Petrov, C.P. Winlove, and P. O'Shea, *α-Tocopherols modify the membrane dipole potential leading to modulation of ligand binding by P-glycoprotein.* J. Lipid Res., 2015. **56**(8): p. 1543-50. https://doi.org/10.1194/jlr.M059519
290. Tintino, S.R., C.D. Morais-Tintino, F.F. Campina, R.L. Pereira, S. Costa Mdo, M.F. Braga, P.W. Limaverde, J.C. Andrade, J.P. Siqueira-Junior, H.D. Coutinho, V.Q. Balbino, T.C. Leal-Balbino, J. Ribeiro-Filho, and L.J. Quintans-Júnior, *Action of cholecalciferol and alpha-tocopherol on Staphylococcus aureus efflux pumps.* Excli j, 2016. **15**: p. 315-22. https://doi.org/10.17179/excli2016-277
291. Oluwole, D.O., L. Coleman, W. Buchanan, T. Chen, R.M. La Ragione, and L.X. Liu, *Antibiotics-Free Compounds for Chronic Wound Healing.* Pharmaceutics, 2022. **14**(5): p. 1021. https://doi.org/10.3390/pharmaceutics14051021
292. Bidossi, A., M. Bortolin, M. Toscano, E. De Vecchi, C.L. Romanò, R. Mattina, and L. Drago, *In vitro comparison between α-tocopheryl acetate and α-tocopheryl phosphate against bacteria responsible of prosthetic and joint infections.* PLOS ONE, 2017. **12**(7): p. e0182323. https://doi.org/10.1371/journal.pone.0182323

293. Salih, M., C.A. Omolo, N. Devnarain, A.A. Elrashedy, C. Mocktar, M.E.S. Soliman, and T. Govender, *Supramolecular self-assembled drug delivery system (SADDs) of vancomycin and tocopherol succinate as an antibacterial agent: in vitro, in silico and in vivo evaluations.* Pharm Dev Technol., 2020. **25**(9): p. 1090-1108. https://doi.org/10.1080/10837450.2020.1797786
294. Andrade, S., M.J. Ramalho, S.B. Santos, L.D.R. Melo, R.S. Santos, N. Guimarães, N.F. Azevedo, J.A. Loureiro, and M.C. Pereira, *Fighting Methicillin-Resistant Staphylococcus aureus with Targeted Nanoparticles.* Int. J. Mol. Sci., 2023. **24**(10): p. 9030. https://doi.org/10.3390/ijms24109030
295. Li, B., K.V. Brown, J.C. Wenke, and S.A. Guelcher, *Sustained release of vancomycin from polyurethane scaffolds inhibits infection of bone wounds in a rat femoral segmental defect model.* J Control Release 2010. **145**(3): p. 221-230. https://doi.org/10.1016/j.jconrel.2010.04.002
296. Li, X., G. Yu, K. Jin, and Z. Yin, *Hyaluronic acid L-cysteine conjugate exhibits controlled-release potential for mucoadhesive drug delivery.* Pharmazie, 2012. **67**(3): p. 224-8. https://doi.org/10.1691/ph.2012.1094
297. Kafedjiiski, K., R.K.R. Jetti, F. Föger, H. Hoyer, M. Werle, M. Hoffer, and A. Bernkop-Schnürch, *Synthesis and in vitro evaluation of thiolated hyaluronic acid for mucoadhesive drug delivery.* Int. J. Pharm., 2007. **343**(1): p. 48-58. https://doi.org/10.1016/j.ijpharm.2007.04.019
298. Liu, N., J. Han, X. Zhang, Y. Yang, Y. Liu, Y. Wang, and G. Wu, *pH-responsive zwitterionic polypeptide as a platform for anti-tumor drug delivery.* Colloids Surf. B, 2016. **145**: p. 401-409. https://doi.org/10.1016/j.colsurfb.2016.05.027
299. Rambharose, S., R.S. Kalhapure, K.G. Akamanchi, and T. Govender, *Novel dendritic derivatives of unsaturated fatty acids as promising transdermal permeation enhancers for tenofovir.* J. Mater. Chem. B, 2015. **3**(32): p. 6662-6675. https://doi.org/10.1039/c5tb00957j
300. Mosmann, T., *Rapid colorimetric assay for cellular growth and survival: Application to proliferation and cytotoxicity assays.* J. Immunol. Methods, 1983. **65**(1): p. 55-63. https://doi.org/10.1016/0022-1759(83)90303-4
301. Neun, B.W. and M.A. Dobrovolskaia, *Method for Analysis of Nanoparticle Hemolytic Properties In Vitro*, in *Characterization of Nanoparticles Intended for Drug Delivery*, S.E. McNeil, Editor. 2011, Humana Press: Totowa, NJ. p. 215-224 https://doi.org/10.1007/978-1-60327-198-1_23
302. Dobrovolskaia, M.A., J.D. Clogston, B.W. Neun, J.B. Hall, A.K. Patri, and S.E. McNeil, *Method for Analysis of Nanoparticle Hemolytic Properties in Vitro.* Nano Lett., 2008. **8**(8): p. 2180-2187. https://doi.org/10.1021/nl0805615
303. Zhang, Y., M. Huo, J. Zhou, A. Zou, W. Li, C. Yao, and S. Xie, *DDSolver: An Add-In Program for Modeling and Comparison of Drug Dissolution Profiles.* AAPS J., 2010. **12**(3): p. 263-271. https://doi.org/10.1208/s12248-010-9185-1
304. Jorgensen, J.H. and J.D. Turnidge, *Susceptibility Test Methods: Dilution and Disk Diffusion Methods*, in *Manual of Clinical Microbiology*. 2015. p. 1253-1273 https://doi.org/10.1128/9781555817381.ch71
305. El-Telbany, M. and A. El-Sharaki, *Antibacterial and anti-biofilm activity of silver nanoparticles on multi-drug resistance pseudomonas aeruginosa isolated from dental-implant.* J Oral Biol Craniofac Res, 2022. **12**(1): p. 199-203. https://doi.org/10.1016/j.jobcr.2021.12.002
306. Au - O'Toole, G.A., *Microtiter Dish Biofilm Formation Assay.* JoVE, 2011(47): p. e2437. https://doi.org/doi:10.3791/2437
307. Mohamed, M.F., M.I. Hamed, A. Panitch, and M.N. Seleem, *Targeting Methicillin-Resistant Staphylococcus aureus with Short Salt-Resistant Synthetic Peptides.* Antimicrob Agents Chemother, 2014. **58**(7): p. 4113-4122. https://doi.org/doi:10.1128/AAC.02578-14

308. Iqbal, G., S. Faisal, S. Khan, D.F. Shams, and A. Nadhman, *Photo-inactivation and efflux pump inhibition of methicillin resistant Staphylococcus aureus using thiolated cobalt doped ZnO nanoparticles.* J Photochem Photobiol B, 2019. **192**: p. 141-146. https://doi.org/10.1016/j.jphotobiol.2019.01.021
309. Martins, M., M.P. McCusker, M. Viveiros, I. Couto, S. Fanning, J.M. Pages, and L. Amaral, *A Simple Method for Assessment of MDR Bacteria for Over-Expressed Efflux Pumps.* Open Microbiol. J., 2013. **7**: p. 72-82. https://doi.org/10.2174/1874285801307010072
310. Oh, H., J.S. Lee, D. Sung, J.M. Lim, and W.I. Choi, *Potential Antioxidant and Wound Healing Effect of Nano-Liposol with High Loading Amount of Astaxanthin.* Int J Nanomedicine, 2020. **15**: p. 9231-9240. https://doi.org/10.2147/IJN.S272650
311. Pierdomenico, M., C. Riccioni, and B. Benassi, *Anti-inflammatory effect of a pomegranate extract on LPS-stimulated HepG2 cells.* Nat. Prod. Res., 2023: p. 1-8. https://doi.org/10.1080/14786419.2023.2196622
312. Nishio, K., M. Horie, Y. Akazawa, M. Shichiri, H. Iwahashi, Y. Hagihara, Y. Yoshida, and E. Niki, *Attenuation of lipopolysaccharide (LPS)-induced cytotoxicity by tocopherols and tocotrienols.* Redox Biol., 2013. **1**(1): p. 97-103. https://doi.org/10.1016/j.redox.2012.10.002
313. Mosmann, T., *Rapid colorimetric assay for cellular growth and survival: application to proliferation and cytotoxicity assays.* J Immunol Methods, 1983. **65**(1-2): p. 55-63. https://doi.org/10.1016/0022-1759(83)90303-4
314. Witayaudom, P. and U. Klinkesorn, *Effect of surfactant concentration and solidification temperature on the characteristics and stability of nanostructured lipid carrier (NLC) prepared from rambutan (Nephelium lappaceum L.) kernel fat.* J. Colloid Interface Sci, 2017. **505**: p. 1082-1092. https://doi.org/10.1016/j.jcis.2017.07.008
315. Zirak, M. and A. Pezeshki, *Effect of Surfactant Concentration on the Particle Size, Stability and Potential Zeta of Beta carotene Nano Lipid Carrier.* Int. j. curr. microbiol. appl. sci. , 2015. **4**(9): p. 924-932
316. Pezeshki, A., B. Ghanbarzadeh, M. Mohammadi, I. Fathollahi, and H. Hamishehkar, *Encapsulation of Vitamin A Palmitate in Nanostructured Lipid Carrier (NLC)-Effect of Surfactant Concentration on the Formulation Properties.* Adv. Pharm. Bull., 2014. **4**(Suppl 2): p. 563-8. https://doi.org/10.5681/apb.2014.083
317. Kaur, P., T. Garg, G. Rath, R.S.R. Murthy, and A.K. Goyal, *Development, optimization and evaluation of surfactant-based pulmonary nanolipid carrier system of paclitaxel for the management of drug resistance lung cancer using Box-Behnken design.* Drug Deliv., 2016. **23**(6): p. 1912-1925. https://doi.org/10.3109/10717544.2014.993486
318. Shinde, U.A., S.J. Parmar, and S. Easwaran, *Metronidazole-loaded nanostructured lipid carriers to improve skin deposition and retention in the treatment of rosacea.* Drug Dev Ind Pharm, 2019. **45**(7): p. 1039-1051. https://doi.org/10.1080/03639045.2019.1569026
319. Sharaf, M., M. Arif, S. Khan, M. Abdalla, S. Shabana, Z. Chi, and C. Liu, *Co-delivery of hesperidin and clarithromycin in a nanostructured lipid carrier for the eradication of Helicobacter pylori in vitro.* Bioorg. Chem., 2021. **112**: p. 104896. https://doi.org/10.1016/j.bioorg.2021.104896
320. Seedat, N., R.S. Kalhapure, C. Mocktar, S. Vepuri, M. Jadhav, M. Soliman, and T. Govender, *Co-encapsulation of multi-lipids and polymers enhances the performance of vancomycin in lipid–polymer hybrid nanoparticles: In vitro and in silico studies.* Mater. Sci. Eng. C, 2016. **61**: p. 616-630. https://doi.org/10.1016/j.msec.2015.12.053
321. Obuobi, S., K. Julin, E.G.A. Fredheim, M. Johannessen, and N. Škalko-Basnet, *Liposomal delivery of antibiotic loaded nucleic acid nanogels with enhanced drug loading and synergistic anti-inflammatory activity against S. aureus intracellular infections.* J Control Release, 2020. **324**: p. 620-632. https://doi.org/10.1016/j.jconrel.2020.06.002

322. Mohammed, M., U.H. Ibrahim, A. Aljoundi, C.A. Omolo, N. Devnarain, M.A. Gafar, C. Mocktar, and T. Govender, *Enzyme-responsive biomimetic solid lipid nanoparticles for antibiotic delivery against hyaluronidase-secreting bacteria.* Int J Pharm, 2023. **640**: p. 122967. https://doi.org/10.1016/j.ijpharm.2023.122967
323. Maji, R., C.A. Omolo, N. Agrawal, K. Maduray, D. Hassan, C. Mokhtar, I. Mackhraj, and T. Govender, *pH-Responsive Lipid-Dendrimer Hybrid Nanoparticles: An Approach To Target and Eliminate Intracellular Pathogens.* Mol. Pharmaceutics, 2019. **16**(11): p. 4594-4609. https://doi.org/10.1021/acs.molpharmaceut.9b00713
324. Radovic-Moreno, A.F., T.K. Lu, V.A. Puscasu, C.J. Yoon, R. Langer, and O.C. Farokhzad, *Surface Charge-Switching Polymeric Nanoparticles for Bacterial Cell Wall-Targeted Delivery of Antibiotics.* ACS Nano, 2012. **6**(5): p. 4279-4287. https://doi.org/10.1021/nn3008383
325. Hasan, N., J. Cao, J. Lee, S.P. Hlaing, M.A. Oshi, M. Naeem, M.-H. Ki, B.L. Lee, Y. Jung, and J.-W. Yoo, *Bacteria-Targeted Clindamycin Loaded Polymeric Nanoparticles: Effect of Surface Charge on Nanoparticle Adhesion to MRSA, Antibacterial Activity, and Wound Healing.* Pharmaceutics, 2019. **11**(5): p. 236. https://doi.org/10.3390/pharmaceutics11050236
326. Su, H., Y. Wang, Y. Gu, L. Bowman, J. Zhao, and M. Ding, *Potential applications and human biosafety of nanomaterials used in nanomedicine.* J Appl Toxicol., 2018. **38**(1): p. 3-24. https://doi.org/10.1002/jat.3476
327. Ehlers, E.M., P. Behrens, L. Wünsch, W. Kühnel, and M. Russlies, *Effects of hyaluronic acid on the morphology and proliferation of human chondrocytes in primary cell culture.* Ann. Anat., 2001. **183**(1): p. 13-17. https://doi.org/10.1016/S0940-9602(01)80007-8
328. Hidalgo, M.A., M.D. Carretta, and R.A. Burgos, *Long Chain Fatty Acids as Modulators of Immune Cells Function: Contribution of FFA1 and FFA4 Receptors.* Front. physiol, 2021. **12**. https://doi.org/10.3389/fphys.2021.668330
329. ISO. *Biological evaluation of medical devices — Part 5: Tests for in vitro cytotoxicity*. 2018 [cited 20 March 2023; Available from: https://www.iso.org/obp/ui/#iso:std:iso:10993:-5:ed-3:v1:en.
330. Peterfreund, R.A. and J.H. Philip, *Critical parameters in drug delivery by intravenous infusion.* Expert Opin Drug Deliv, 2013. **10**(8): p. 1095-1108. https://doi.org/10.1517/17425247.2013.785519
331. Kumar, V., *Toll-like receptors in sepsis-associated cytokine storm and their endogenous negative regulators as future immunomodulatory targets.* Int. Immunopharmacol., 2020. **89**: p. 107087. https://doi.org/https://doi.org/10.1016/j.intimp.2020.107087
332. Kanamala, M., W.R. Wilson, M. Yang, B.D. Palmer, and Z. Wu, *Mechanisms and biomaterials in pH-responsive tumour targeted drug delivery: A review.* Biomaterials, 2016. **85**: p. 152-167. https://doi.org/10.1016/j.biomaterials.2016.01.061
333. Makhathini, S.S., C.A. Omolo, L.W. Kiruri, P. Walvekar, N. Devnarain, C. Mocktar, and T. Govender, *Synthesis of pH-responsive dimethylglycine surface-modified branched lipids for targeted delivery of antibiotics.* Chem. Phys. Lipids, 2022. **249**: p. 105241. https://doi.org/10.1016/j.chemphyslip.2022.105241
334. Jaglal, Y., N. Osman, C.A. Omolo, C. Mocktar, N. Devnarain, and T. Govender, *Formulation of pH-responsive lipid-polymer hybrid nanoparticles for co-delivery and enhancement of the antibacterial activity of vancomycin and 18β-glycyrrhetinic acid.* J Drug Deliv Sci Technol 2021. **64**: p. 102607. https://doi.org/10.1016/j.jddst.2021.102607
335. Omolo, C.A., N.A. Megrab, R.S. Kalhapure, N. Agrawal, M. Jadhav, C. Mocktar, S. Rambharose, K. Maduray, B. Nkambule, and T. Govender, *Liposomes with pH responsive 'on and off' switches for targeted and intracellular delivery of antibiotics.* J. Liposome Res., 2021. **31**(1): p. 45-63. https://doi.org/10.1080/08982104.2019.1686517

336. Devnarain, N., N. Osman, V.O. Fasiku, S. Makhathini, M. Salih, U.H. Ibrahim, and T. Govender, *Intrinsic stimuli-responsive nanocarriers for smart drug delivery of antibacterial agents—An in-depth review of the last two decades.* Wiley Interdiscip Rev Nanomed Nanobiotechnol, 2021. **13**(1): p. e1664. https://doi.org/10.1002/wnan.1664
337. Martín-Camacho, U.d.J., N. Rodríguez-Barajas, J.A. Sánchez-Burgos, and A. Pérez-Larios, *Weibull β value for the discernment of drug release mechanism of PLGA particles.* Int. J. Pharm., 2023. **640**: p. 123017. https://doi.org/10.1016/j.ijpharm.2023.123017
338. Rajendar, V., C.H. Shilpa Chakra, B. Rajitha, K. Venkateswara Rao, M. Chandra Sekhar, B. Purusottam Reddy, and S.-H. Park, *Effect of TWEEN 80 on the morphology and antibacterial properties of ZnO nanoparticles.* J Mater Sci Mater Electron, 2017. **28**(4): p. 3272-3277. https://doi.org/10.1007/s10854-016-5919-x
339. Walvekar, P., R. Gannimani, M. Salih, S. Makhathini, C. Mocktar, and T. Govender, *Self-assembled oleylamine grafted hyaluronic acid polymersomes for delivery of vancomycin against methicillin resistant Staphylococcus aureus (MRSA).* Colloids Surf. B 2019. **182**: p. 110388. https://doi.org/10.1016/j.colsurfb.2019.110388
340. Kalhapure, R.S., M. Jadhav, S. Rambharose, C. Mocktar, S. Singh, J. Renukuntla, and T. Govender, *pH-responsive chitosan nanoparticles from a novel twin-chain anionic amphiphile for controlled and targeted delivery of vancomycin.* Colloids Surf. B 2017. **158**: p. 650-657. https://doi.org/10.1016/j.colsurfb.2017.07.049
341. Díez-Pascual, A.M., *Recent Progress in Antimicrobial Nanomaterials.* Nanomaterials, 2020. **10**(11): p. 2315. https://doi.org/10.3390/nano10112315
342. Wang, S., Y. Gao, Q. Jin, and J. Ji, *Emerging antibacterial nanomedicine for enhanced antibiotic therapy.* Biomater. Sci., 2020. **8**(24): p. 6825-6839. https://doi.org/10.1039/D0BM00974A
343. Imran, M., S.K. Jha, N. Hasan, A. Insaf, J. Shrestha, J. Shrestha, H.P. Devkota, S. Khan, N. Panth, M.E. Warkiani, K. Dua, P.M. Hansbro, K.R. Paudel, and Y. Mohammed, *Overcoming Multidrug Resistance of Antibiotics via Nanodelivery Systems.* Pharmaceutics, 2022. **14**(3). https://doi.org/10.3390/pharmaceutics14030586
344. Fittipaldi, M., A. Nocker, and F. Codony, *Progress in understanding preferential detection of live cells using viability dyes in combination with DNA amplification.* J. Microbiol. Methods, 2012. **91**(2): p. 276-89. https://doi.org/10.1016/j.mimet.2012.08.007
345. Hassan, D., C.A. Omolo, R. Gannimani, A.Y. Waddad, C. Mocktar, S. Rambharose, N. Agrawal, and T. Govender, *Delivery of novel vancomycin nanoplexes for combating methicillin resistant Staphylococcus aureus (MRSA) infections.* International Journal of Pharmaceutics, 2019. **558**: p. 143-156. https://doi.org/10.1016/j.ijpharm.2019.01.010
346. Chen, L. and Y.m. Wen, *The role of bacterial biofilm in persistent infections and control strategies.* Int. J. Oral Sci., 2011. **3**(2): p. 66-73. https://doi.org/10.4248/IJOS11022
347. Caruso, C., A. Porta, A. Tosco, D. Eletto, L. Pacente, S. Bartollino, and C. Costagliola, *A Novel Vitamin E TPGS-Based Formulation Enhances Chlorhexidine Bioavailability in Corneal Layers.* Pharmaceutics, 2020. **12**(7): p. 642. https://doi.org/10.3390/pharmaceutics12070642
348. Nielsen, C.K., J. Kjems, T. Mygind, T. Snabe, and R.L. Meyer, *Effects of Tween 80 on Growth and Biofilm Formation in Laboratory Media.* Front. microbiol., 2016. **7**. https://doi.org/10.3389/fmicb.2016.01878
349. Liu, Y., L. Shi, L. Su, H.C. van der Mei, P.C. Jutte, Y. Ren, and H.J. Busscher, *Nanotechnology-based antimicrobials and delivery systems for biofilm-infection control.* Chem. Soc. Rev., 2019. **48**(2): p. 428-446. https://doi.org/10.1039/c7cs00807d
350. Wang, Y., Y. Jin, W. Chen, J. Wang, H. Chen, L. Sun, X. Li, J. Ji, Q. Yu, L. Shen, and B. Wang, *Construction of nanomaterials with targeting phototherapy properties to inhibit resistant*

bacteria and biofilm infections. J. Chem. Eng., 2019. **358**: p. 74-90. https://doi.org/10.1016/j.cej.2018.10.002

351. Bankier, C., Y. Cheong, S. Mahalingam, M. Edirisinghe, G. Ren, E. Cloutman-Green, and L. Ciric, *A comparison of methods to assess the antimicrobial activity of nanoparticle combinations on bacterial cells.* PLOS ONE, 2018. **13**(2): p. e0192093. https://doi.org/10.1371/journal.pone.0192093
352. Ivanova, A., K. Ivanova, J. Hoyo, T. Heinze, S. Sanchez-Gomez, and T. Tzanov, *Layer-By-Layer Decorated Nanoparticles with Tunable Antibacterial and Antibiofilm Properties against Both Gram-Positive and Gram-Negative Bacteria.* ACS Appl. Mater. Interfaces 2018. **10**(4): p. 3314-3323. https://doi.org/10.1021/acsami.7b16508
353. Rosenberg, M., N.F. Azevedo, and A. Ivask, *Propidium iodide staining underestimates viability of adherent bacterial cells.* Sci. Rep., 2019. **9**(1): p. 6483. https://doi.org/10.1038/s41598-019-42906-3
354. Zhang, Y., T. Yue, W. Gu, A. Liu, M. Cheng, H. Zheng, D. Bao, F. Li, and J.-G. Piao, *pH-responsive hierarchical H2S-releasing nano-disinfectant with deep-penetrating and anti-inflammatory properties for synergistically enhanced eradication of bacterial biofilms and wound infection.* J. Nanobiotechnology, 2022. **20**(1): p. 55. https://doi.org/10.1186/s12951-022-01262-7
355. Roberts, J.A. and J. Lipman, *Antibacterial Dosing in Intensive Care.* Clin. Pharmacokinet., 2006. **45**(8): p. 755-773. https://doi.org/10.2165/00003088-200645080-00001
356. Jang, S., *Multidrug efflux pumps in Staphylococcus aureus and their clinical implications.* J. Microbiol., 2016. **54**(1): p. 1-8. https://doi.org/10.1007/s12275-016-5159-z
357. Vestergaard, M., D. Frees, and H. Ingmer, *Antibiotic Resistance and the MRSA Problem.* Microbiol. Spectr., 2019. **7**(2): p. 1-23. https://doi.org/doi:10.1128/microbiolspec.gpp3-0057-2018
358. Varela, M.F., J. Stephen, D. Bharti, M. Lekshmi, and S. Kumar, *Inhibition of Multidrug Efflux Pumps Belonging to the Major Facilitator Superfamily in Bacterial Pathogens.* Biomedicines, 2023. **11**(5): p. 1448. https://doi.org/10.3390/biomedicines11051448
359. Barfour, A.F., A.Y. Mensah, E. Asante-Kwatia, C.A. Danquah, D. Anokwah, S. Adjei, M.K. Baah, and M.L.K. Mensah, *Antibacterial, Antibiofilm, and Efflux Pump Inhibitory Properties of the Crude Extract and Fractions from Acacia macrostachya Stem Bark.* Sci. World J., 2021. **2021**: p. 5381993. https://doi.org/10.1155/2021/5381993
360. Salih, M., C.A. Omolo, N. Devnarain, A.A. Elrashedy, C. Mocktar, M.E.S. Soliman, and T. Govender, *Supramolecular self-assembled drug delivery system (SADDs) of vancomycin and tocopherol succinate as an antibacterial agent: in vitro, in silico and in vivo evaluations.* Pharm Dev Technol, 2020. **25**(9): p. 1090-1108. https://doi.org/10.1080/10837450.2020.1797786
361. Victor, V.M., M. Rocha, and M. De la Fuente, *Immune cells: free radicals and antioxidants in sepsis.* International Immunopharmacology, 2004. **4**(3): p. 327-347. https://doi.org/10.1016/j.intimp.2004.01.020
362. Mambro, V.M.D., A.E.C.S. Azzolini, Y.M.L. Valim, and M.J.V. Fonseca, *Comparison of antioxidant activities of tocopherols alone and in pharmaceutical formulations.* Int. J. Pharm., 2003. **262**(1): p. 93-99. https://doi.org/10.1016/S0378-5173(03)00333-8
363. Rassu, G., B. Pavan, D. Mandracchia, G. Tripodo, G. Botti, A. Dalpiaz, E. Gavini, and P. Giunchedi, *Polymeric nanomicelles based on inulin D α-tocopherol succinate for the treatment of diabetic retinopathy.* J Drug Deliv Sci Technol, 2021. **61**: p. 102286. https://doi.org/10.1016/j.jddst.2020.102286
364. Sivakanthan, S., S. Rajendran, A. Gamage, T. Madhujith, and S. Mani, *Antioxidant and antimicrobial applications of biopolymers: A review.* Food Res. Int., 2020. **136**: p. 109327. https://doi.org/https://doi.org/10.1016/j.foodres.2020.109327

365. Xu, P., Y. Zheng, X. Zhu, S. Li, and C. Zhou, *L-lysine and L-arginine inhibit the oxidation of lipids and proteins of emulsion sausage by chelating iron ion and scavenging radical.* Asian-australas. J. Anim. Sci., 2018. **31**(6): p. 905-913. https://doi.org/10.5713/ajas.17.0617
366. Nedeva, C., *Inflammation and Cell Death of the Innate and Adaptive Immune System during Sepsis.* Biomolecules, 2021. **11**(7): p. 1011. https://doi.org/10.3390/biom11071011
367. Castellheim, A., O.-L. Brekke, T. Espevik, M. Harboe, and T.E. Mollnes, *Innate Immune Responses to Danger Signals in Systemic Inflammatory Response Syndrome and Sepsis.* Scand. J. Immunol., 2009. **69**(6): p. 479-491. https://doi.org/10.1111/j.1365-3083.2009.02255.x
368. Rossol, M., H. Heine, U. Meusch, D. Quandt, C. Klein, M.J. Sweet, and S. Hauschildt, *LPS-induced cytokine production in human monocytes and macrophages.* Crit. Rev. Immunol, 2011. **31**(5): p. 379-446. https://doi.org/10.1615/critrevimmunol.v31.i5.20
369. Liu, D., S.-Y. Huang, J.-H. Sun, H.-C. Zhang, Q.-L. Cai, C. Gao, L. Li, J. Cao, F. Xu, Y. Zhou, C.-X. Guan, S.-W. Jin, J. Deng, X.-M. Fang, J.-X. Jiang, and L. Zeng, *Sepsis-induced immunosuppression: mechanisms, diagnosis and current treatment options.* Mil. Med. Res, 2022. **9**(1): p. 56. https://doi.org/10.1186/s40779-022-00422-y
370. Maneta, E., E. Aivalioti, S. Tual-Chalot, B. Emini Veseli, A. Gatsiou, K. Stamatelopoulos, and K. Stellos, *Endothelial dysfunction and immunothrombosis in sepsis.* Front. immunol., 2023. **14**. https://doi.org/10.3389/fimmu.2023.1144229
371. Lee, J.H., A. Liu, J.H. Park, H. Kato, Q. Hao, X. Zhang, L. Zhou, and J.W. Lee, *Therapeutic Effects of Hyaluronic Acid in Peritonitis-Induced Sepsis in Mice.* Shock, 2020. **54**(4): p. 488-497. https://doi.org/10.1097/shk.0000000000001512
372. Muto, J., K. Yamasaki, K.R. Taylor, and R.L. Gallo, *Engagement of CD44 by hyaluronan suppresses TLR4 signaling and the septic response to LPS.* Mol. Immunol., 2009. **47**(2): p. 449-456. https://doi.org/10.1016/j.molimm.2009.08.026
373. Huang, H., X. Ding, D. Xing, J. Lin, Z. Li, and J. Lin, *Hyaluronic Acid Oligosaccharide Derivatives Alleviate Lipopolysaccharide-Induced Inflammation in ATDC5 Cells by Multiple Mechanisms.* Molecules, 2022. **27**(17): p. 5619. https://doi.org/10.3390/molecules27175619
374. Schulte, W., J. Bernhagen, and R. Bucala, *Cytokines in Sepsis: Potent Immunoregulators and Potential Therapeutic Targets—An Updated View.* Mediators Inflamm., 2013. **2013**: p. 165974. https://doi.org/10.1155/2013/165974
375. Eichberger, J. and B. Resch, *Reliability of Interleukin-6 Alone and in Combination for Diagnosis of Early Onset Neonatal Sepsis: Systematic Review.* Front Pediatr, 2022. **10**. https://doi.org/10.3389/fped.2022.840778
376. Copaescu, A., O. Smibert, A. Gibson, E.J. Phillips, and J.A. Trubiano, *The role of IL-6 and other mediators in the cytokine storm associated with SARS-CoV-2 infection.* J. Allergy Clin. Immunol., 2020. **146**(3): p. 518-534.e1. https://doi.org/10.1016/j.jaci.2020.07.001
377. Tanaka, T., M. Narazaki, and T. Kishimoto, *Immunotherapeutic implications of IL-6 blockade for cytokine storm.* Immunotherapy, 2016. **8**(8): p. 959-970. https://doi.org/10.2217/imt-2016-0020
378. Cardoso, M., V.M. Gaspar, C. Ferreira, R. Silvestre, I.F. Duarte, and J.F. Mano, *Macrophage-targeted shikonin-loaded nanogels for modulation of inflammasome activation.* Nanomed.: Nanotechnol. Biol. Med., 2022. **42**: p. 102548. https://doi.org/10.1016/j.nano.2022.102548
379. Farajzadeh, R., N. Zarghami, H. Serati-Nouri, Z. Momeni-Javid, T. Farajzadeh, S. Jalilzadeh-Tabrizi, S. Sadeghi-Soureh, N. Naseri, and Y. Pilehvar-Soltanahmadi, *Macrophage repolarization using CD44-targeting hyaluronic acid–polylactide nanoparticles containing curcumin.* Artif Cells Nanomed Biotechnol 2018. **46**(8): p. 2013-2021. https://doi.org/10.1080/21691401.2017.1408116

CHAPTER 4. SECOND EXPERIMENTAL PAPER

4.1 General Introduction

This chapter addresses Aim 2, Objectives 1-5, and is a first-authored experimental paper submitted to an ISI International Journal: *International Journal of Pharmaceutics* (Manuscript ID: IJPHARM-D-23-03925) (Impact Factor: 5.875). This article highlights the formulation, optimization, and characterization of biomimetic CIP-loaded TAH-NPs to enhance CIP delivery. Also, it highlights the *in vitro* cytotoxicity, non-hemolytic activity, TLR4 binding affinity using *in-silico* and *in vitro* tools, *in vitro* antibacterial, antibiofilm, efflux pump inhibition, antioxidant, and anti-inflammatory activities of the prepared CIP-loaded TAH-NPs.

4.2 Author contributions

In this paper, **Mrs. Eman Elhassan** performed the literature searches that contributed to the conceptualization and the design and execution of this project. These involved the preparation and characterization of the novel hybrid nanocarriers (HNs). The HNs were characterized for physicochemical properties including average particle size, polydispersity index, zeta potential, entrapment efficiency, drug loading capacity, thermal profiles, and surface morphology. Furthermore, **Mrs. Eman Elhassan** contributed towards the characterization of the formulation in terms of *in vitro* antibacterial activity, hemocompatibility studies, *in vitro* drug release study and its mathematical modelling, colloidal stability studies, receptor binding with Microscale Thermophoresis (MST) technique and *in vitro* antioxidant study. **Mrs. Eman Elhassan** was also responsible for analysis and data collection, as well as writing entire draft version of the first authored article and revised it according to co-authors comments. Prof. Calvin A. Omolo served as co-supervisor and assisted with the conceptualization, design of the project, solving any technical problems and supervision of the studies. Mr. Mohammed Ali Gafar assisted with the antibacterial and *in vitro* binding affinity studies. Mr. Usri H. Ibrahim conducted the anti-inflammatory studies. Dr. Aimen Aljoundi and Dr. Ghazi Elamin undertook the *in-silico* studies. Dr. Nikita Devnarain conducted the cytotoxicity studies. Mr. Mahir Mohammed assisted with the biosafety studies. Prof. Thirumala Govender served as supervisor and was responsible for project conceptualization, problem-solving, editing of paper and abstract as well as general supervision of all the experiments.

4.3 Submitted manuscript

Disease-inspired design of a biomimetic tannic acid-based hybrid nanocarriers for targeted delivery of ciprofloxacin against bacterial-induced sepsis

Eman Elhassan [1], Calvin A. Omolo [1,2*], Mohammed A. Gafar [1,3], Usri H. Ibrahim [4], Aimen Aljoundi [5], Ghazi Elamin [6], Nikita Devnarain [1], Mahir Mohammed [1,7], Thirumala Govender [1]

[1] Discipline of Pharmaceutical Sciences, College of Health Sciences, University of KwaZulu-Natal, Private Bag X54001, Durban, South Africa.

[2] Department of Pharmaceutics and Pharmacy Practice, School of Pharmacy and Health Sciences, United States International University-Africa, P. O. Box 14634-00800, Nairobi, Kenya.

[3] Department of Pharmaceutics, Faculty of Pharmacy, University of Khartoum, Sudan.

[4] Discipline of Human Physiology, School of Laboratory Medicine and Medical Sciences, College of Health Sciences, University pf KwaZulu-Natal, Durban, South Africa.

[5] Department of Pharmaceutical Chemistry, Collage of Pharmacy, University of Attahadi, Tripoli, V567-7M8, Libya.

[6] Department of Pharmaceutical Chemistry, Collage of Pharmacy, Karary University, Khartoum P.O. Box 11111, Sudan

[7] Department of Pharmacology, Faculty of Pharmacy, University of Khartoum, Sudan.

[*] Corresponding authors: comolo@usiu.ac.ke, govenderth@ukzn.ac.za.

Graphical abstract

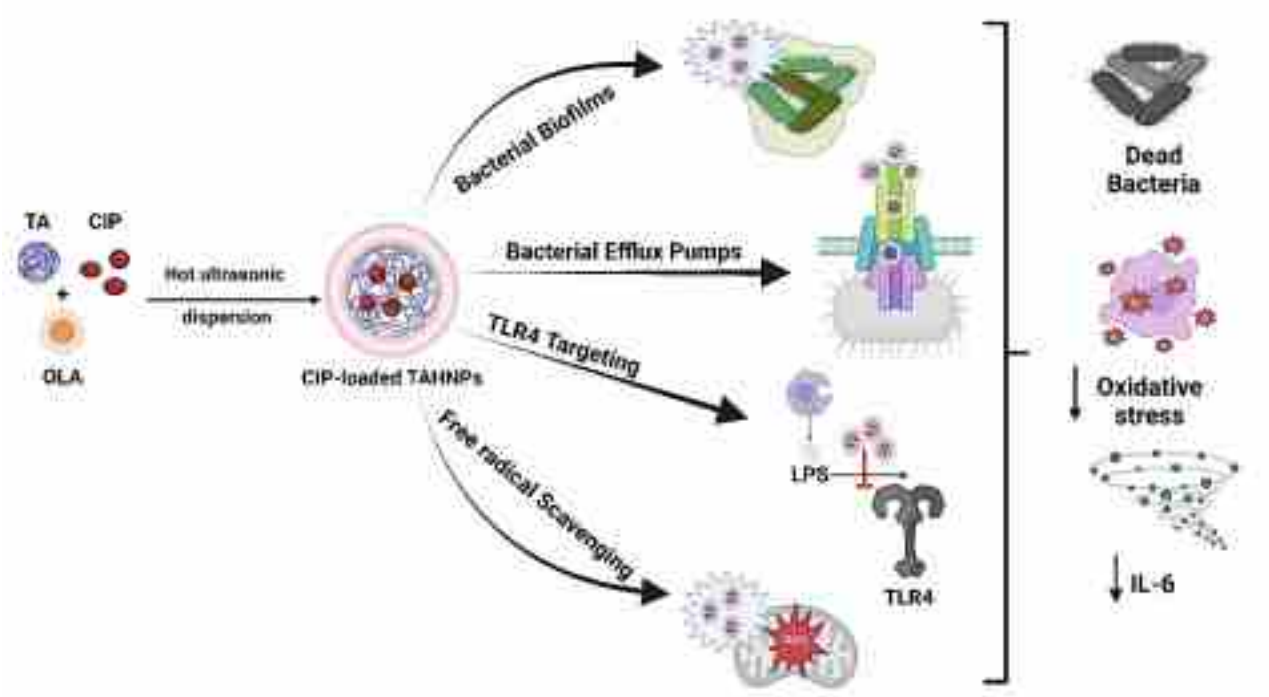

Abstract

To combat bacterial infections and sepsis effectively, innovative approaches that can improve the targeting and potency of antibiotics are required. The implementation of disease-inspired hybrid nano-drug delivery systems has the potential to significantly enhance antibiotic therapy and treat bacterial sepsis. In this study, a novel hybrid nanocarriers (HNs) derived from tannic acid (TA) and Oleylamine (OLA) for targeted delivery of ciprofloxacin (CIP) against bacterial-induced sepsis was successfully formulated and characterized. The prepared CIP-loaded TAH-NPs had an average size, PDI, surface charge, entrapment efficiency and drug loading capacity of 85.65 ± 0.89 nm, 0.13 ± 0.01, +16.3 ± 0.23 mV, 68.73 ± 0.54 % and 6.86 ± 0.09 % respectively. The *in vitro* biosafety studies revealed that CIP-loaded TAH-NPs were biocompatible and non-hemolytic. The *in-silico* simulations and MST analysis proved the strong binding affinity of TA and/or its nanoformulation to the human Toll-like receptor 4 (TLR4) compared to its natural substrate lipopolysaccharide (LPS), indicating that TA and CIP-loaded TAH-NPs could competitively inhibit the virulence effect of bacterial LPS and halting sepsis progression. The release of CIP from TAH-NPs was found to be sustained for 72 hrs. The *in vitro* assays against MRSA and *P. aeruginosa* revealed that CIP-loaded TAH-NPs exhibited enhanced and significant antibacterial and efflux pump inhibition activity and displayed a 3-fold and a 2-fold increase in biofilm eradication activity against MRSA and *P. aeruginosa*, respectively, compared to bare CIP. The time killing assay findings showed 100 % bacterial clearance within 8 hrs of treatment with CIP-loaded TAH-NPs. The *in vitro* DPPH scavenging and anti-inflammatory investigations confirmed the potential activity of the prepared hybrid nanosystem in neutralizing ROS and modulating the LPS-induced inflammatory response. Collectively, the results suggest that CIP-loaded TAH-NPs may serve as an innovative nanocarrier for the effective and targeted delivery of antibiotics against bacterial-induced sepsis.

Keywords: Biomimetic, Tannic acid, Hybrid nanocarriers, Bacterial infections, Sepsis, TLR4 antagonism, Antibiotic delivery.

1. Introduction

Sepsis, a life-threatening disorder characterized by an impaired systemic immune response to infection, is a critical public health problem of global concern, affecting millions of people around the world each year [380, 381]. According to the World Health Organization (WHO), sepsis is responsible for an estimated 11 million deaths annually, making it the leading cause of death from infection [382]. In the United State alone, more than 1.7 million cases of sepsis are reported each year, resulting in nearly 270,000 deaths [383, 384]. The incidence of morbidity and mortality due to sepsis have been further exacerbated by the current global crisis of antimicrobial resistance (AMR) and a decline in the introduction of new antibiotics [5, 385]. The emergence of the COVID-19 pandemic has

also impacted the host's innate and adaptive defenses against bacteria, increasing the prevalence of secondary bacterial infections and severe sepsis caused by multidrug-resistant (MDR) bacteria, leading to worse outcomes and fatal complications [386, 387]. Therefore, early diagnosis and treatment of bacterial infections and associated sepsis are essential for survival and should be given a high priority in public health.

The current strategies for sepsis management focus primarily on the prompt administration of effective intravenous antibiotics to control the infection, in addition to the administration of various anti-inflammatory drugs, antioxidants and immunomodulators to reduce inflammatory responses, as well as supportive care to help stabilize vital organs and systems [380, 388]. However, there are several drawbacks associated with the current dosage forms of sepsis medications, including side effects due to non-specific drug biodistribution and localization, sub-therapeutic levels of the drugs at the infection sites, increased frequency of drug administration due to their rapid elimination, and emergence of AMR [42, 389]. Accordingly, to address these limitations and prevent treatment failure, the development of novel and innovative therapeutic and targeting strategies for effective antibiotic therapy is urgently required.

The use of novel nano-drug delivery systems (NDDSs) has significant potential for meeting the challenges of AMR and improving antibiotic therapy against bacterial infections. Antibiotic-loaded NDDSs offer several advantages over the current antibiotic dosage forms, including enhanced drug targeting and concentration at the infection site, reduced required dose and frequency of drug administration, thereby minimizing the risk of side effects and improving patient compliance [390, 391]. With rapid advances in nanotechnology, researchers are developing multiple strategies to maximize the potential of nanocarriers while also addressing their existing drawbacks [392]. Co-delivery of antibiotics with other therapeutic agents and the development of bio-inspired and stimuli-responsive nanocarriers are some examples of these innovative approaches [393-396].

Biomimicry is a cutting-edge approach in biomedical research that aims to provide more effective and targeted interventions against infectious diseases [397]. In drug delivery, biomimetic strategies are employed to mimic normal cellular processes and increase their affinity for target cells [258]. While this approach has been widely reported in cancer therapy, it is still in its infancy for bacterial infections, necessitating the need for such novel strategy to enhance the efficacy of antibiotics against bacterial sepsis.

During bacterial infection, Toll-like receptors (TLRs) on the host cell recognize microbial toxins such as lipoteichoic acid (LTA) and lipopolysaccharide (LPS) on the Gram-positive and Gram-negative bacterial cell walls, respectively, and this association stimulates the inflammatory process and

immune system response [398]. While TLR activation triggers an immune response to fight infection, excessive TLR activation during sepsis results in overwhelming systemic inflammation, oxidative stress, and multiple organ injury [264, 265]. Understanding the role of TLR activation in bacterial sepsis is crucial for the development of targeted therapies to modulate the immune response and improve outcomes in patients with sepsis. Inspired by this natural pathway of bacterial recognition and immune activation, emerging research has shown interest in the use of TLRs for the development of antagonists/inhibitors, specifically TLR2 and TLR4, to treat infection-associated sepsis [71-74]. Preventing the binding of TLR ligands to the receptor is one approach being reported for TLR inhibition [399]. Researchers have discovered small drug molecules and antibodies that hinder the interactions between ligands and TLRs, and their effects in lowering TLR signaling activity in various inflammatory conditions have demonstrated encouraging results [74-76]. Therefore, a similar strategy of minimizing TLRs activation by inhibiting their binding to bacterial toxins can be applied to an antibiotic nanocarrier to specifically kill bacteria and simultaneously potentiate the treatment of sepsis.

Furthermore, bacterial biofilms and efflux pumps, which are persistent and difficult to eradicate, have been identified as major contributors to AMR infections. The protective nature of the biofilm extracellular matrix serves as a physical barrier that hinders the penetration of antimicrobial agents and immune cells, making biofilm-associated infections highly resistant to treatment [77]. In addition, efflux pumps play a pivotal role in the survival and adaptability of bacteria to their natural environments. These molecular devices have evolved to actively expel a wide variety of antimicrobial compounds, including antibiotics, from the bacterial cells. By conferring resistance to antibiotics, efflux pumps allow bacteria to survive and grow even in the presence of lethal antibiotic doses [78]. Targeting bacterial biofilms and efflux pumps is an alternative approach that can enhance the uptake and performance of antibacterial dugs. As a result, developing a novel nano drug delivery system integrating the biomimetic principle with biofilm eradication and efflux pump inhibition approach could be a novel antibacterial immunoregulatory strategy to simultaneously treat bacterial sepsis and overcome antimicrobial resistance.

Among the promising nano drug delivery systems in antibiotic therapy are hybrid nanocarriers (HNs). They are nanoscale structures made of a variety of excipients, such as polymers, lipids, metals, or inorganic nanoparticles, with the intention of leveraging the attractive traits and excluding the limitations of biomaterials in the combination [400]. Their multifunctionality and tunable properties make them attractive candidates with improved efficacy and biosafety, high drug loading efficiency, membrane permeability, better drug release profiles, enhanced pharmacokinetics and pharmacodynamic characteristics, well-tolerated serum stability, and reduced drug concentrations

required for treatment, thus leading to lower costs and fewer side effects [117, 273, 401]. By combining different biomaterials, researchers take advantage of their unique characteristics to achieve the desired features in nanocarrier systems. For this reason, HNs are widely applied in targeted drug delivery, gene therapy, imaging, and diagnostics of various diseases [402, 403]. However, there have been no reports on the use of HNs for antibiotic delivery to specifically treat bacterial sepsis.

Developing a biomimetic HN with multifunctional activity against bacterial sepsis requires a combination of bioactive excipients with the desired traits. Tannic acid (TA) is an emerging biomaterial used in nanoparticle formulations. It is a natural polyphenolic compound that has been reported to possess antioxidant, anti-inflammatory, antitumor, and antimicrobial activities [404]. The anti-inflammatory effects of TA against various inflammation-induced organ dysfunctions have been investigated in many research studies [405]. It is proposed that TA functions by inhibiting the activity of pro-inflammatory enzymes, such as cyclooxygenase (COX) and lipoxygenase (LOX)) which are responsible for producing several inflammatory cytokines and associated mediators such as prostaglandins and leukotrienes [406, 407]. In addition, TA has been reported to competitively prevent LPS binding to human TLR4, thereby attenuating the expression of the LPS-induced TLR4 signaling pathway and blocking subsequent signal transduction [408, 409]. Furthermore, TA has been shown to have a protective effect against oxidative stress-induced tissue damage and multiorgan failure in many inflammatory conditions by scavenging free radicals and neutralizing ROS generated during the inflammatory process, thereby attenuating the harmful effects of sepsis on the body [410]. Besides its well-established anti-inflammatory and antioxidant activities, TA has significant antibacterial, antibiofilm, and efflux-pump inhibition activities against several pathogens, including *Staphylococcus aureus* (*S. aureus*) and *Escherichia coli* (*E. coli*) [411-414]. Recently, Li *et al*. (2023) reported the synthesis of TA-containing nanoparticles to mitigate cytokine storms for the treatment of bacterial induced- acute lung injury [415]. Therefore, the development of an antibiotic-loaded HN using TA as a multifunctional biomaterial with TLR4 antagonistic action, antioxidant, antibiofilm, and efflux-pump inhibition properties may hold immense potential for precise and targeted treatment of bacterial sepsis.

On the other hand, Oleylamine (OLA) is one of the most popular long-chain fatty amines that has been discovered to possess inherent antibacterial activity against both gram-positive and gram-negative strains [416-418]. It has also been reported to enhance the effectiveness of various antimicrobial agents, including metal NPs [419]. Few studies have been conducted on the use of OLA to create innovative nano drug delivery systems to treat bacterial infections [339, 418, 420]. Therefore, targeting bacterial and sepsis microenvironments using TA and OLA in a novel hybrid NDDS could be effective in advancing the treatment of bacterial sepsis.

In this study, we proposed a novel HN derived from OLA and TA to improve the efficacy of ciprofloxacin (CIP) against bacterial-induced sepsis through several combined strategies. TA can reduce bacterial infectivity and resistance mechanisms through its potential activity against biofilm formation and efflux pumps. In addition, it can hold promise as a targeting moiety by facilitating the direct binding of the nanocarrier with TLR4 in host cells, thereby successfully preventing LPS-induced hyperactivation of TLR4 and subsequent downstream signal activation. Along with its ability to neutralize ROS, TA helps in modulating the host immune response, reducing oxidative stress, and controlling inflammatory cytokine levels. On the other hand, OLA offers stability, mechanical strength, improved loading capacity, effective binding, and permeation to bacterial membranes, and works synergistically with CIP and TA to fight against bacteria. Overall, this novel nanosystem could be a promising avenue in sepsis research with the potential to significantly reduce the severity of this life-threatening condition and improve patient outcomes. To the best of our knowledge, this study reports the first HN formulated using TA and OLA to deliver any class of drug. Also, the application of a HN that simultaneously combines biomimicry with efflux pump inhibition and biofilm eradication approaches has not been previously reported for any bacterial infection. In addition, the use of TLR as a pathway for bacterial recognition and immune regulation in drug delivery has not been reported as a biomimetic strategy. The data obtained from the formulation of CIP-loaded TAH-NPs, optimization, *in vitro* characterization, *in silico* studies, and *in vitro* antibacterial and anti-inflammatory studies are reported herein.

2. Materials and methods

2.1 Materials

Tannic acid (TA), poloxamer407 (PLX407), Oleylamine (OLA), ethidium bromide, 2,2-diphenyl-1-picrylhydrazyl (DPPH) and lipopolysaccharides (LPS) from *Escherichia coli* (O55:B5) were purchased from Sigma-Aldrich (USA). Dulbecco's modified Eagle's medium (DMEM), Eagle's Minimum Essential Medium (EMEM), fetal bovine serum, propidium iodide (PI) and Syto9 were obtained from Thermo Fisher (USA). 3(4,5-Dimethylthiazol-2-yl)-2,5-diphenyltetrazolium bromide (MTT), dimethyl sulfoxide (DMSO) and crystal violet were purchased from Merck Chemicals (Germany). Cell lines were purchased from Highveld Biologicals (Johannesburg, South Africa) and cell culture materials were purchased from Whitehead Scientific (Johannesburg, South Africa). Sheep blood used for assessment of hemolytic activity was purchased from United Scientific (South Africa). Nutrient Broth, Mueller-Hinton Broth (MHB), and Mueller- Hinton Agar (MHA) were obtained from Biolab (South Africa). Ciprofloxacin hydrochloride (CIP), *Staphylococcus aureus* (ATCC 25923), *Escherichia coli* (ATCC 25422), Multi-drug resistant *Staphylococcus aureus* (SA Rosenbach ATCC BAA 70699) and *Pseudomonas aeruginosa* (ATCC 27853) were obtained from DLD Scientific

(South Africa). Recombinant human TLR4 (Active ab233665) was purchased from Abcam (Cambridge, UK). Immunosorbent Assay (ELISA) kits were purchased from ABclonal Technology (Wuhan, Hubie, China). Microscale thermophoresis (MST) reagents were purchased from Nano Temper Technologies (Germany). A mill-Q water purification system (Millipore corp., USA) was used to obtain a purified milli-Q water. All solvents and reagents used in this study were of analytical grade.

2.2 Preparation of the hybrid nanoparticles

CIP-loaded TAH-NPs were prepared using hot ultrasonic dispersion method with a slight modification [421]. Briefly, a specific amount of OLA was dissolved in 3 mL ethanol, and the mixture was heated to 80 °C with continuous stirring at 600 rpm for 20 min. For the aqueous phase, a specified amount of TA, CIP and a suitable surfactant were dissolved in 10 mL milli-Q water, and heated separately to 80 °C with continuous stirring at the same speed for 20 min. Thereafter, the lipid phase was added dropwise into the aqueous phase within 15 min under continuous stirring. Then, the resultant emulsion was sonicated at the same temperature (80 °C) for 5 min at 30% amplitude using a probe sonicator (Omni Sonic-Ruptor 400 Ultrasonic Homogenizer, USA), followed by immediate cooling to 20 °C using an ice bath. The prepared NPs were then stirred overnight to remove the organic solvent, and if necessary, the final volume was adjusted to 10 mL using milli-Q water. Blank (CIP-free) TAH-NPs were also prepared using the same procedure. Various parameters such as surfactant type, surfactant concentration, and lipid: polymer mass ratio were evaluated. The optimum formulation with the minimum particle size (PS), polydispersity index (PDI), maximum entrapment efficiency percent (EE %) and drug loading capacity (DL % w/w) was selected for further studies. Each formulation was prepared in triplicate (n=3).

2.3 Physicochemical characterization of the prepared NPs

2.3.1 Determination of particle size, polydispersity index (PDI) and zeta potential (ZP)

Dynamic light scattering (DLS) method with a Zetasizer Nano ZS90 (Malvern Instruments Ltd., UK) equipped with a 633 nm laser at 173° detection optics was used to determine the average particle size, size distribution and ZP of the prepared CIP-loaded TAH-NPs. Before the measurement, appropriate dilutions of the formula in distilled water were done and the experiment was carried out in triplicate at 25 °C (n=3).

2.3.2 Determination of nanoparticle morphology

The morphological structure of TAH-NPs was determined by transmission electron microscopy (TEM) (Jeol, JEM-1010, Tokyo, Japan). To obtain TEM images, a drop of appropriately diluted CIP-

loaded TAH-NPs dispersion was placed on a surface of coated copper grid, allowed to dry at room temperature, then stained with 2 % phosphtungestic acid for 30 sec. and visualized at an accelerating voltage of 75 kV.

2.3.3 Determination of entrapment efficiency percent (EE %) and drug loading percent (DL% w/w)

The percentage of CIP within TAH-NPs was determined by measuring the EE % and the DL % (w/w) using the previously reported ultrafiltration method [263]. In brief, 2 mL of the formulation was placed in AmiconUltra-4 centrifugal filter tube (Millipore Corp., USA) of 10 kDa molecular weight cutoff and centrifuged at 3000 rpm at 25 °C for 30 min. Free CIP in the supernatant was appropriately diluted with distilled water and its concentration was determined using UV spectrophotometer (Shimadzu UV 1601, Japan) at 276 nm and a regression equation of Y= 0.0962 (x)-0.0062 and linearity coefficient (R^2) of 0.9994 (**Figure S1, Appendix II**). The experiment was performed in triplicate (n=3). The EE % and DL % w/w were calculated using the following equations.

$$\text{EE \%} = \frac{\text{Weight of CIP in the TAH–NPs}}{\text{Total weight of CIP added}} \times 100 \quad (1)$$

$$\text{DL \% w/w} = \frac{\text{Weight of CIP in the TAH–NPs}}{\text{Total weight of NPs}} \times 100 \quad (2)$$

2.3.4 Thermal profiles

Differential scanning calorimetry (DSC) (Shimadzu DSC-60, Japan) was used to assess the thermograms of TA, CIP, PLX407, physical mixture and lyophilized CIP-loaded TAH-NPs. The samples were weighed out at around 5 mg each and then individually placed in an aluminum pan. The pan was then sealed with a crimper and heated to 33 °C under a flow of nitrogen, with the temperature increasing at a constant rate of 10 °C/min. An empty pan was used as a reference.

2.4 *In vitro* biosafety profiles

2.4.1 Cytotoxicity and cell viability assay

To investigate the cytocompatibility of the blank and CIP-loaded TAH-NPs, a previously reported MTT assay method was applied on three different cell lines (Michigan Cancer Foundation-7 (MCF-7) breast cancer, human embryonic kidney 293 (HEK 293) and human hepatocyte carcinoma (HepG2) cells [299]. Concisely, Cells were seeded into a 96-well plate containing 100 µL DMEM (for HEK 293 and MCF-7) or EMEM (for HepG2 cells), 10 % fetal bovine serum (FBS), 1 % pen-strep-fungizone and 1 % L-glutamine at a concentration of 2.5 x 10^3 cells/well. The cell mixture was incubated for 24 hrs at 37 °C in a CO_2 humidified incubator. Then, the cells were treated with 20, 40, 60, 80 and 100 µg/mL of blank and CIP-loaded TAH-NPs formulations (diluted with suitable cell

culture medium) and incubated for the next 24 hrs. After 24 hrs incubation period, the media were replaced with fresh culture media (100 µL/well) and 20 µL/well of MTT solution (5 mg/ml in PBS) and incubated for 4 hrs. The supernatant was then removed, and formazan crystals were solubilized using 100 µL of sterile dimethyl sulfoxide (DMSO). After 1 hr, absorbances were read at 540 nm using a microplate spectrophotometer (Spectrostar Nano, Germany). The experiment was performed in triplicate and the following equation (3) was used to calculate the percentage cell viability:

$$\text{Cell viability \%} = \frac{\text{A540 nm treated cells}}{\text{A540 nm untreated cells}} \times 100 \quad (3)$$

2.4.2 Hemolysis

The hemocompatibility profile of the prepared CIP-loaded TAH-NPs was evaluated according to a previously described procedure [301]. In brief, sheep blood was freshly collected and washed three times with sterile isotonic PBS (pH 7.4) by centrifugation at 3000 rpm for 10 min. Subsequently, 0.2 mL of the purified red blood cell suspension was separately mixed with 1.8 mL of six different concentrations of CIP-loaded TAH-NPs formulations in sterile PBS (20-200 µg/mL), PBS (as a negative control) and distilled water (as a positive control), and incubated at 37 °C for 30 min. After incubation, the samples were centrifuged for 10 min at 3000 rpm and 4 °C using the ultracentrifuge (Centurion Scientific, UK). The supernatants of each sample were then collected in 96-well plates and their hemoglobin absorbance was quantified at 540 nm using a Microplate Reader (SpectraMax M2, USA). The experiment was performed in triplicate, and the following formula was used to determine the percentage of non-hemolytic activity:

$$\text{Non-hemolytic activity \%} = 100\text{-} \frac{(ABS - ABS_0)}{(ABS_{100} - ABS_0)} \quad (4)$$

Where ABS_0 and ABS_{100} are the absorbances at 0 % and 100 % hemolysis, respectively.

2.5 Molecular dynamic simulation studies

2.5.1 Determination of CIP-loaded TAH-NPs complex self-assembly

2.5.1.1 Chemical structures Preparations

All the chemical structures (CIP, TA, OLA and PLX407) were downloaded from the PubChem website as either 2D or 3D structures [422]. The four chemical structures were energy minimized using the universal force field (UFF)[1] employing steepest descents minimization in Avogadro [423].

2.5.1.2 Molecular Dynamics simulation

To get insights on the self-assembly of CIP, TA, OLA and PLX407 molecules, all-atom molecular dynamic (MD) simulations was performed. The topology of the four molecules were parametrized using the CHARMM general force field (CGenFF) [424]. Solvation was done using the cubic box

together with TIP3P water model [425]. Both NVT and NPT equilibration were performed prior to MD simulations to check the temperature and pressure stability, respectively. The canonical ensemble (NVT) energy minimization was done at 300 K using the velocity-rescale thermostat with a time-constant of 0.1 ps. The NPT equilibration used the Parrinello-Rahman barostat [426] at an isotropic pressure of 1 bar for 500 ps followed by the MD production of 100 ns. The MD simulation was performed using GROMACS 2018 software package [427]. The Particle-Mesh Ewald (PME) [428] method was employed for efficient long-range electrostatic interactions. A cutoff of 1.2 nm was used for Lennard-Jones interactions while a real-space cutoff of 1.2 nm was used for electrostatic interactions. All bonds were constrained using the LINCS algorithm and a time step of 2 fs was used for the Verlet integrator. The trajectory analyses were performed using *gmx* built-in tool in GROMACS. The distance was measured from the centers of mass (COM) of the four molecules using an in-house Tcl script. Visualization was done using VMD [429] and Chimera [422] Software.

2.5.1.3 Binding energy calculations

The binding energies calculations were performed using the molecular mechanics Poisson-Boltzmann Surface Area (MM-PBSA) method as implemented in GROMACS. MM-PBSA is an efficient method for the calculations of free energies of diverse molecular systems. ("AmberMDrun: A Scripting Tool for Running Amber MD in an Easy Way - MDPI") The self-assembled particle was extracted from the MD simulation from 50 – 60 ns window, for the calculations with 10 ns trajectory. Although a more extensive explanation of MMPBSA can be found in the original work [430], we provide a brief summary here:

$$\Delta G_{MMPBSA} = \langle G_{complex} - G_{protein} - G_{ligand} \rangle_{comlex} \qquad (5)$$

$$G_x = E_{MM} - T\langle S_{MM} \rangle + \Delta G_{solv} \qquad (6)$$

$$E_{MM} = E_{bonded} + E_{coul} + E_{LJ} \qquad (7)$$

$$\Delta G_{solv} = G_{polar} + G_{nonpolar} \qquad (8)$$

where G_x is the free energy of system *x*, that being the ligand, the protein (in this case; TA, OLA and PLX407) or the complex; E_{MM} is the potential energy in vacuum as defined by the molecular mechanics (*MM*) model, which is composed of the bonded energy terms (E_{bonded}) and nonbonded Coulombic (E_{coul}) and Lennard-Jones (E_{LJ}) terms; S_{MM} is the entropy; ΔG_{solv} is the free energy of solvation, composed by a polar (G_{polar}) and nonpolar ($G_{nonpolar}$) term; T is the temperature and angle brackets represent an ensemble average.

2.5.2 *In silico* analysis of the binding affinity to TLR4

2.5.2.1 System Preparation

The X-ray crystal structures of human toll-like receptor 4 (TLR4) was attained from RSCB Protein Data Bank (PDB code: 3FXI, with a resolution of 3.10 Å by x-ray diffraction) [431, 432]. Chain A of the complex being a TLR4 protein was separated and saved for molecular docking. The crystal structure of lipopolysaccharide (LPS), a natural ligand of TLR4, was obtained from RSCB Protein Data Bank (PDB code: 6S8N) [432, 433] and its unique ligand (lipid A) was obtained using the UCSF Chimera program [422, 434]. The 2D structures of TA, OLA, PLX407 and CIP were retrieved from PubChem database [435] and subsequently converted into 3D structures using ChemDraw 3D software [436] To prepare these structures for molecular dynamics simulation and to ensure that the proper angels and hybridization states of ligands were displayed, Molegro Molecular Viewer (MMV) [437, 438], and UCSF Chimera software package [422], were employed. All missing residues from molecules were added by a structural refinement tool known as Modeller [422].

2.5.2.2 Molecular Docking and Molecular Dynamics Simulation

Preceding docking, UCSF Chimera was used to eliminate all co-factors, non-standard residues such as Cl-, Na+, etc. as well as water molecules surrounding the protein structure [422]. The ligands (LPS, TA, OLA, PLX407 and CIP) were then charged and hydrogenated. The AutoDock Tools GUI was used to estimate ligand docking and partial Gasteiger charge addition [422, 439]. Overall, systems consisting of human TLR4 bound to LPS, TA, OLA, PLX407 and CIP were run at 300 ns MD simulation using the AMBER20 CPU and GPU packages [440, 441] and the PMEMD engine. An atomic partial charge was generated for the five ligands using the AMBER FF14SB of the ANTECHAMBER program [442, 443]. The Leap module of Amber 20 enabled the addition of hydrogen atoms, sodium (Na+), or chloride (Cl-) counter ions to the systems for neutralization. The systems were initially minimized for 2500 steps with 500 kcal/mol Å2 restraint potential, and a total minimization step of 5000 steps was further carried out without restraint using the conjugate algorithm. Thereafter, the system underwent gradual heating from 0 to 300 K for 50 ps using a Langevin thermostat in a canonical assemblage (NVT) [444, 445]. Following heating, equilibration was undertaken at a temperature of 300 K, excluding all restraints, and a maintained atmospheric pressure of 1 bar using the Berendsen barostat until all systems reached equilibrium [446-448]. The complexes were then subjected to a 300 ns MD simulation using the SHAKE algorithm to constrict all hydrogen atoms [449]. The co-ordinates of the human TLR4- LPS, TA, OLA, PLX407 and CIP complexes were saved after the 300 ns production period at every 1ps intervals. The generated trajectories of each system were analyzed using the PTRAJ and CPPTRAJ modules [450]. The

generated data and subsequent complexes were further visualized using Microcal Origin analytical software (www.originlab.com) [451, 452] and UCSF Chimera [422].

2.5.2.3 Post-molecular Dynamics Simulation Analysis

The bound complexes were saved after every 1ps, and their resultant trajectories were analysed using the AMBER 20 integrated CPPTRAJ module. Post analysis for the systems MD simulation included protein stability (RMSD), flexibility (RMSF) and solvent accessible surface area (SASA). Binding free energy is computed by employing Molecular Mechanics/Generalized Born Surface Area (MM/GBSA) technique.

2.5.2.4 Thermodynamics (free binding energy) computations

To estimate the binding interactions of human TLR4 bound to LPS, TA, OLA, PLX407 and CIP, the binding free energy was calculated using the Molecular Mechanics/Generalized Born Surface Area (MM/GBSA) approach [453, 454]. Binding free energy (ΔG_{bind}) is a reliable tool extensively used to measure the binding energies involved in the formation of protein– ligand complexes, and is calculated using the following equation:

$$\Delta G_{bind} = G_{complex} - G_{protein} - G_{inhibitor} \quad (9)$$

$$\Delta G_{bind} = E_{gas} + G_{sol} - TS \quad (10)$$

The ΔG_{bind} is the sum of the gas and solvent energy minus entropy (TS).

$$E_{gas} = E_{int} + E_{vdw} + E_{ele} \quad (11)$$

Where E_{gas} represents the addition of the internal energy terms of the AMBER force fields, which includes E_{int} representing angles, torsions, and bonds, E_{vdw} representing covalent van der Waals energy, and E_{elec} representing the electrostatic energy components that are non-bonded. The following equation is representative of the solvent energy calculation:

$$G_{sol} = G_{GB} + G_{SA} \quad (12)$$

$$G_{SA} = \gamma SASA \quad (13)$$

G_{GB} is representative of the polar solvation impact and G_{SA} is representative of the non-polar solvation impact which is calculated using the solvent accessible surface area (SASA). This is attained by using a water probe radius of 1.4 A°. A surface tension constant (c) was represented by a measure of 0.0072 kcal/mol and (b) by a measure of 0 kcal/mol [422, 455].

2.6 Determination of *in vitro* binding affinity to TLR4

To investigate the biomimetic approach of TA and CIP-loaded TAH-NPs, their binding affinity to TLR4 was determined and compared to the natural substrate (LPS) using microscale thermophoresis (MST) on a Nano Temper Monolith NT.115 instrument (Nano Temper Technology, Germany) [263]. In the study, recombinant human TLR4 was firstly adjusted to a concentration of 10 µM and then

labeled with the Monolith NT.115 protein labelling kit RED-NHS according to manufacturer's protocol using 1:3 protein: dye ratio, incubated at room temperature for 15 min, protected from light and then purified with a gel-filtration column. After protein labeling, serial dilutions of different ligands (LPS, TA, OLA and CIP-loaded TAH-NPs) were prepared with different starting concentrations using suitable MST buffer (0.1 M PBS, 0.05% Tween 20, pH 7.4). Following that, an equivalent volume of the labeled TLR4 (10 µL) in a final concentration of 10 nM was added to each dilution and incubated for 10 min. Finally, the samples were loaded into Standard Treated glass MST capillaries (Nano Temper Technology, Germany) and MST traces were measured in Nano Temper Monolith NT.115 instrument at red LED, 25°C and 40% MST power. All experiments were done in triplicate (n=3). The dissociation constant (K_d) values were fitted for each test ligands using Monolith-Affinity analysis software version 2.1.3 (Nano Temper Technologies, Germany).

2.7 *In vitro* drug release and linear kinetics

The dialysis bag method was employed to investigate the release behavior of CIP from CIP-loaded TAH-NPs [267]. Briefly, 2 mL of bare CIP and CIP-loaded TAH-NPs solutions were placed individually in cellulose dialysis bags with an average molecular weight of 14,400 Da. The bags were shaken at 37 °C and 100 rpm while dialyzing against 40 mL PBS pH 7.4 receiver solution. At predetermined time intervals, 3 mL of samples were taken out from the receiver solution and promptly replaced with an equivalent volume of fresh PBS pH 7.4 solution to maintain sink condition. After an appropriate dilution, the amount of CIP released per time was determined using a UV spectrophotometer by measuring the absorbance at 276 nm, and a regression equation of Y= 0.0962 (x)-0.0062 (R^2 = 0.9994) (**Figure S1, Appendix II**) using blank TAH-NPs solution as a reference. The experiment was conducted in triplicate, and the following equation was used to compute the cumulative release percentage of CIP:

$$\text{Cumulative release \%} = \frac{Q_t}{Q_v} \times 100 \qquad (14)$$

Where Q_t is the amount of CIP released at time t, and Q_v the total amount of CIP previously used in the CIP-loaded TAH-NPs formulation.

The DDSolver software program [303] was then utilized to analyze the kinetics of CIP release from CIP-loaded TAH-NPs using different mathematical models, including zero-order; first-order, Higuchi, Krosmeyer-Peppas, Hixson-Crowell and Weibull . The correlation coefficient (R^2) and the root means square error (RMSE) were calculated to determine the best-fit model, while the Weibull and Krosmeyer-Peppas models were used to determine the release mechanism by calculating the values of the Weibull exponent parameter (β) and the release exponent (n), respectively.

2.8 Short-term physical stability study

The colloidal stability of the prepared CIP-loaded TAH-NPs formulation was studied over three months at room temperature (25 °C) and cold temperature (4 °C). Physical appearance, and other physico-chemical parameters (particle size, PDI and ZP) were quantified at 0, 30, 60 and 90 days using a Zetasizer Nano ZS90 (Malvern Instruments Ltd., UK) equipped with a 633 nm laser with a detection optics of 173°. All experiments were performed in triplicate (n=3).

2.9 *In vitro* antibacterial activity studies

2.9.1 Determination of minimum inhibitory concentration (MIC)

The broad-spectrum activity of bare CIP, blank TAH-NPs, and CIP-loaded TAH-NPs against gram-positive *S. aureus* and MRSA, and gram-negative *E. coli* and *P. aeruginosa* was investigated using a previously described broth microdilution method [304]. Bacterial culture in Mueller- Hinton broth (MHB) was allowed to grow overnight in a shaking incubator at 37 °C and 100 rpm. The incubated bacteria were then adjusted to 0.5 McFarland standard (1.5×10^8 colony-forming units (CFU)/mL) using DEN-1B densitometer (Latvia). Further dilution was done to obtain a final concentration of 5×10^5 CFU/mL. In a 96-well plate, 135 µL of MHB solution was pipetted in each well, and an equal volume of bare CIP, blank TAH-NPs and CIP-loaded TAH-NPs solutions were added and then serially diluted to achieve a range of concentrations. 15 µL of the diluted bacterial suspension were added in each well containing the serially diluted samples and incubated for 24 hrs in the shaking incubator adjusted at 37 °C and 100 rpm. After incubation, 5 µL of the sample mixtures were spotted on Mueller- Hinton agar (MHA) plates and, the MIC values were determined after incubation for 24 hrs at 37 °C. All experiments were conducted in triplicate.

2.9.2 Determination of Fractional Inhibitory Concentration (FIC)

Fractional Inhibitory Concentration (FIC) is defined by the European Committee of Antimicrobial Susceptibility Testing (EUCAST) as a mathematical expression of the combinatorial effect of antibacterial agents [456]. To better understand the combined antibacterial effect of the blank TAH-NPs and CIP in the CIP-loaded TAH-NPs against *S. aureus*, *E. coli*, MRSA and *P. aeruginosa*, the cumulative FIC was determined based on the MIC values obtained from the *in vitro* antibacterial study. Equations (15) and (16) were used to calculate the ΣFIC, and the FIC index is shown in **Table S1 (Appendix II)**.

$$\text{FIC (CIP)} = \frac{\text{(the MIC of CIP in combination with TAH-NPs)}}{\text{(the MIC of CIP)}} \quad (15)$$

$$\text{FIC (Blank TAH-NPs)} = \frac{\text{(the MIC of TAH-NPs in combination with CIP)}}{\text{(the MIC of Blank TAH-NPs)}} \quad (16)$$

$$\Sigma\text{FIC} = \text{FIC (CIP)} + \text{FIC (Blank TAH-NPs)}$$

2.9.3 Flow cytometry

Flow cytometry is a powerful tool used for determining bacterial cell viability, allowing for rapid analysis of the percentage of live and dead bacterial cells in a sample [457]. The information gathered from flow cytometry data can be used to assess the effectiveness of various nano antibiotic formulations on bacterial populations. Viable MRSA and *P. aeruginosa* cells in the population after treatment with CIP and CIP-loaded TAH-NPs for 18 hrs was determined using a flow cytometry method previously reported by our group with a slight modification [188]. Briefly, bacterial cultures in MHB at a concentration of 0.5 McFarland standard (1.5×10^8 CFU/mL) were prepared and allowed to grow for overnight in a shaking incubator at 37 °C/100 rpm. Then, the grown bacteria were harvested by centrifugation at 3000 rpm for 30 min, the supernatant was discharged, and the pellets were resuspended with PBS and incubated at warm room (37 °C) for another 4 hrs. Then, 15 µL of bacterial suspension, which was further diluted into 5×10^5 CFU/mL, was added to a 96 well plate each containing 135 µL of bare CIP and CIP-loaded TAH-NPs formulation at the MIC concentrations of 12.5 µg/mL and 0.78 µg/mL for bare CIP and CIP-loaded TAH-NPs, respectively, for MRSA treatment and 0.78 µg/mL of both formulations for *P. aeruginosa* treatment. The sample mixture was further incubated at 37 °C in a shaking incubator (100 rpm) for 18 hrs. Thereafter, 50 µL of each sample were transferred to the flow cytometry tubes each containing 350 µL of sheath fluid and vortexed for 5 min. 5 µL of membrane impermeant propidium iodide (PI) and membrane permeant Syto9 dyes were added to each tube and the mixture was incubated for 30 min in the dark. Untreated MRSA and *P. aeruginosa* cells were used as negative controls. The samples were analyzed on the flow cytometry instrument (BECKMAN COULTER DxFLEX, Nyon 1, Switzerland) with at least 10,000 cells collected for each sample in triplicate (n=3).

2.9.4 Determination of *in vitro* antibiofilm activity

2.9.4.1 Crystal violet assay

The ability of CIP-loaded TAH-NPs to clear MRSA and *P.aeruginosa* biofilms was assessed using the Microtiter Dish Biofilm Formation Assay [305]. Briefly, 200 µL of bacterial suspension (1.5×10^8 CFU/mL) in MHB was transferred to a 96-well plate and incubated at 37 °C for 7 days to form a mature biofilm. Before treatment, the medium was removed from the wells and the wells were washed three times with PBS pH 7.4 to remove non-adherent bacterial cells. Specifically, 200 µL of bare CIP solution and CIP-loaded TAH-NPs formulation at a concentration of 10×MIC were added to the wells and incubated at 37 °C for 24 hrs. Thereafter, sterile PBS was used to wash each well (three times) to remove excess treatment. 0.01 % w/v crystal violet solution was used to stain the biofilms for approximately 15 min and gently aspirated from each well. Excess crystal violet staining was removed by gentle and thorough washing with PBS and allowed to dry overnight. Finally, 125 µL of

30 % aqueous acetic acid solution was added to each well for 10 min to elute crystal violet. The eluted dye was then carefully transferred to another 96-well plate and photographed for qualitative evaluation. The intensity of the crystal violet dye was then measured quantitatively at 570 nm using a microplate spectrophotometer (Spectrostar Nano, Germany) to determine the antibiofilm effect of the test samples.

2.9.4.2 Florescence microscope assay

To verify the antibiofilm efficacy of CIP-loaded TAH-NPs against MRSA and *P. aeruginosa*, glass microscope coverslips measuring 18 mm ×18 mm were employed as biofilm carriers in a fluorescence microscopy experiment [188]. Initially, the coverslips were inserted into at the bottom of 6-well plates, and each well was pipetted with 2 mL of bacterial solution in MHB (1.5×10^8 CFU/mL). The plates were kept at 37 °C for 7 days in order to promote the growth of biofilms over the coverslips. Following the development of mature biofilms, non-adherent bacterial cells were removed from the wells using PBS pH 7.4 three times before treatment. Subsequently, 2 mL of bare CIP and CIP-loaded TAH-NPs solutions at 5×MIC, as well as 2 mL of PBS pH 7.4 as a control, were added to the biofilm-containing wells, and they were then incubated for 12 hrs at 37 °C. The treatments and unattached bacteria were removed from the wells by washing them twice with PBS pH 7.4. The coverslips were then stained with Syto9 and PI for 30 mins and imaged using a fluorescence microscope. The biofilm eradication effects of bare CIP and CIP-loaded TAH-NPs were visualized by capturing and processing the images using a Nikon Eclipse 80i FM (Japan).

2.9.5 Time killing assay (TKA)

A previously reported plate colony counting method was used to investigate the time killing kinetics of the prepared CIP-loaded TAH-NPs against MRSA and *P. aeruginosa* [307]. Bacterial suspension from an overnight MHB culture (0.5 McFarland standard) was diluted with sterile PBS to obtain concentrations of 10^5-10^6 CFU/mL. Then, the prepared test samples (bare CIP and CIP-loaded TAH-NPs solutions) were added to the diluted bacteria at a 5×MIC and incubated in the shaking incubator at 100 rpm and 37 °C. PBS containing the bacteria only (10^5-10^6 CFU/mL) was used as a control. Then, 0.2 mL was taken from each sample at specified time intervals (0, 1, 2, 4, 6, 8, 12 and 24 hrs) followed by a serial dilution with sterile PBS. Thereafter, 0.1 mL of each diluted samples were sub-cultured on MHA plate and incubated for 24 hrs. After incubation, the number of colonies grown in each dilution plate were counted and converted into CFU/mL using equation (17), and then further converted into $\log_{10}$ values. To determine the TKA of the prepared samples, $\log_{10}$ CFU/mL was plotted versus time. The experiment was performed in triplicate (n=3).

$$\text{CFU/mL} = \frac{\text{no. of colonies} \times \text{dilution factor}}{\text{Volume of dilution taken}} \quad (17)$$

2.9.6 Efflux Pump Inhibition assay

The ability of the prepared CIP-loaded TAH-NPs to inhibit the over-expression of MRSA and *P. aeruginosa* efflux pumps was investigated using a simple cartwheel method according to previously reported protocols with little modifications [308, 309]. Briefly, fresh Mueller- Hinton Agar (MHA) plates containing 2 µg/mL of ethidium bromide (EtBr) were prepared at the same day of the experiment and protected from light. Mueller- Hinton broth (MHB) was used to grow the bacterial culture overnight in a shaking incubator at 37 ℃ and 100 rpm. The overnight grown cultures were further adjusted to a concentration of 0.5 McFarland standard (1.5×10^8 CFU/mL) using MHB, seeded into a 96 well plate and treated with bare CIP and CIP-loaded TAH-NPs formulation at a concentration of 0.25×MIC values, while a group of untreated bacteria was left as a control. The samples were then incubated at 37 °C for one hour and subsequently swabbed on the MHA containing the EtBr in a cartwheel shape. All tested plates were kept in the dark with an overnight incubation at 37 °C for 24 hrs. Thereafter, the plates were visualized under the UV light using a UV trans-illuminator (Uvitec Cambridge, UK.) for the observation of any residual fluorescence exhibited by the bacteria. Efflux pump inhibiting effect can be detected when the fluorescent emission is shown under the UV transilluminator.

2.9.7 Bacterial-induced hemolysis inhibition assay

The hemolysis of sheep erythrocytes caused by MRSA and *P. aeruginosa* in the presence or absence of bare CIP and CIP-loaded TAH-NPs was investigated according to a previously described method with slight modifications [458, 459]. Concisely, different concentrations of bare CIP and CIP-loaded TAH-NPs formulation were incubated with an overnight culture of MRSA and *P. aeruginosa* (1×10^9 CFU/mL) at 37 °C and 100 rpm in a shaking incubator. The bacterial culture was centrifuged for 10 min at 3000 rpm and 4 °C to obtain the culture supernatant after 16 hrs of incubation. 100 µL of the culture supernatant was diluted to 1 mL with sterile PBS, and 25 µL of the purified sheep erythrocytes were added to each sample and incubated at 37°C for 30 min. All samples were then centrifuged (3000 rpm and 4 °C) for 10 min, the supernatants were collected, and the optical density (OD) was measured at 543 nm using a microplate reader (SpectraMax M2, USA). The supernatant of the control culture (untreated bacteria) represented 100 % hemolysis, and the percent hemolysis of the treatments was calculated by comparing it to the control culture. The experiment was performed in triplicate (n=3).

2.10 *In vitro* antioxidant study

The antioxidant activity of TA and CIP-loaded TAH-NPs was investigated using a DPPH radical scavenging method [310]. Different concentrations of TA and CIP-loaded TAH-NPs formulation in distilled water (20-1000 µg/mL) and a methanolic solution of DPPH in a concentration of 0.5 mM were prepared individually. Thereafter, 150 µL of each formulation sample was mixed with an equal

volume of DPPH solution in a 96-well plate and incubated at 37 ℃ in darkness. A mixture of DPPH and water (150 µL each) was prepared as a negative control. After 1 hr of incubation, the absorbance of the reaction mixture was measured at 517 nm in a microplate reader (SpectraMax M2, USA). The test was carried out in triplicate (n3) and ascorbic acid was used as a positive control. The antioxidant activity percent was calculated using the following equation:

$$\text{Antioxidant } \% = \frac{\text{A517 nm control} - \text{A517 nm sample}}{\text{A517 nm control}} \times 100 \qquad (18)$$

2.11 *In vitro* anti-inflammatory studies

2.11.1 Cytoprotective effect against LPS-induced cytotoxicity

The *in vitro* cytoprotective activity of TA and CIP-loaded TAH-NPs against LPS-induced cytotoxicity was evaluated using a previously reported methods that involved an MTT assay and Hepatocellular carcinoma cell, HepG2 cell line, (as a model of cells that affected by LPS) [311-313]. Briefly, DMEM supplemented with glutamine, antibiotic, and fetal bovine serum was used to culture HepG2 cells incubated in a humidified atmosphere of 5 % carbon dioxide at 37 ℃. After 80% confluency, cells were plated in a 96-wells plate (20000 cells/well) for 24 hrs, then treated for another 24 hrs with different set of treatments as follows: a) Control untreated (200 µL of DMEM); b) LPS-treated (200 µL of 0.9 mg/mL of LPS in DMEM); c) TA-treated (200 µL of 0.9 mg/mL of LPS and 100 µg/mL TA in DMEM); d) CIP-loaded TAH-NPs-treated (200 µL of 0.9 mg/mL of LPS and 100 µg/mL CIP-loaded TAH-NPs in DMEM). After 24 hrs of treatment, the media were aspirated and then 100 µL/well of fresh DMEM mixed with 20 µL/well of 5 mg/mL MTT solution were added. To solubilize formazan crystals, the media was replaced with 100 µL/well sterile DMSO, 4 hrs later. Finally, a microplate spectrophotometer (Spectrostar Nano, Germany) was used to record absorbance from each well at 570 nm after 1 hr of adding DMSO. All treatments in this study were done in triplicate and cell viability % was calculated.

2.11.2 Anti-inflammatory activity against LPS-induced inflammatory responses (measurement of IL-6 levels)

The anti-inflammatory activity of TA and CIP-loaded TAH-NPs was further investigated using an LPS-stimulated-HepG2 cells model as previously described [311]. In brief, Enzyme Linked Immunosorbent Assay (ELISA) kits were used to determine IL-6 levels after stimulation of HepG2 cells with 1µg/mL LPS solution in DMEM for 12 hrs, either with or without treatments. HepG2 cells were cultured and plated as described in the previous section (**2.11.1**) and then treated for 12 hrs using different treatments as follow: a) Control untreated (200 µL of DMEM); b) LPS-treated (200 µL of 1 µg/mL LPS in DMEM); c) TA-treated (200 µL of 1 µg/mL of LPS and 50 µg/mL or 100 µg/mL TA in DMEM); d) CIP-loaded TAH-NPs-treated (200 µL of 1 µg/mL LPS and 50 µg/mL or 100 µg/mL

CIP-loaded TAH-NPs in DMEM). After treatment, media were collected to determine the levels of IL-6 in the supernatant using ELISA kits as per manufacturer's recommendations.

2.12 Statistical analysis and figures

Statistical analysis of the findings was carried out using GraphPad Prism® version 10 (GraphPad Software Inc., USA), which included paired T-tests and one-way analysis of variance (ANOVA). The difference between individual groups that were compared was considered significant when the *P*-value was less than 0.05, and all findings were represented as a mean ± standard deviation (SD). Unless otherwise stated, all graphs and figures were created using GraphPad Prism 10 and the BioRender website.

3. Results and discussion

3.1 Preparation, characterization and optimization of TAH-NPs

In this study, blank and CIP-loaded TAH-NPs were effectively formulated by hot ultrasonic dispersion method [421]. In the preliminary work, various types of surfactants were screened to investigate their effect on the average particle size, PDI and ZP. Small particle sizes with a low PDI and a stable ZP are required to achieve hybrid nanoformulations with uniform dispersion and greater stability. Taking this into consideration, PLX407 was selected as the surfactant of choice to formulate TAH-NPs since it provided the prepared hybrid nanosystem with the best physicochemical properties as shown in **Table S2, Appendix II**.

To investigate the impact of different formulation variables on the average particle size, PDI, ZP, EE% and DL% w/w of the prepared CIP-loaded TAH-NPs, a single-factor-at-a-time optimization strategy was employed. The effects of varying surfactant concentration (% w/v) and OLA: TA mass ratios were examined. Initially, a fixed OLA: TA mass ratio of 0.3:1 was used with different concentrations of PLX407 (0.15, 0.3, and 0.45 % w/v) to study the effect of surfactant concentration on the CIP-loaded TAH-NPs properties. Next, the optimal surfactant concentration and varied OLA: TA mass ratios (0.1:1, 0.3:1, and 0.5:1) were used to investigate the effect of OLA: TA mass ratio on the CIP-loaded TAH-NPs properties (**Table 1**).

The results demonstrated that increasing the surfactant concentration from 0.15 % to 0.45 % w/v resulted in a significant increase in particle size, from 83.39 to 169.50 nm, and PDI, from 0.15 to 0.45 (*P*- value < 0.0001). However, no significant effect on ZP, EE %, and DL % w/w was observed (*P*-value > 0.05). The increased particle size and size distribution at higher surfactant concentration could be due to the accumulation and adhesion of free surfactant molecules that fused with the NPs and increased their average particle size [460]. The EE % and DL % w/w were found to be varying from 63.87 % to 65.14 % and 5.73 % to 6.01 %, respectively. These results were consistent with a

previously reported CIP-loaded lipid-polymer hybrid NPs (LPHNPs) [461], as in both studies, loading of CIP into hybrid nanosystems resulted in a higher EE %. Accordingly, the ideal surfactant concentration of 0.15 % w/v was selected for further optimization.

The effect of different OLA: TA mass ratios on CIP-loaded TAH-NPs properties was then evaluated with a fixed PLX407 concentration (0.15 % w/v), and the results revealed that an increase in OLA: TA mass ratio had no significant effect on the average size (slight increase in particle size), PDI, ZP and DL % w/w, while the EE % increased from 57.11 % to 73.41 % as OLA: TA mass ratio increased from 0.1:1 to 0.5:1, respectively. This increase in the EE % could be attributed to the increase in lipid content that may serve as a physical barrier and reduce drug leakage from the NPs [462]. Our results were comparable to previous studies in which the increase in lipid concentration had a negative impact on the EE % of the drugs loaded in the reported hybrid NPs [460, 463, 464].

The zeta potential (ZP) is also a crucial parameter for determining surface charge and potential stability of the nanocarriers [465]. As presented in **Table 1**, all the prepared nanoformulations had positive ZP, which is essential for maintaining NPs dispersion stability and promoting their adhesion to the negatively charged membranes of bacteria. Therefore, the CIP-loaded TAH-NPs with a surfactant concentration of 0.15 % w/v and an OLA: TA mass ratio of 0.5: 1 was selected as the formula of choice for further characterization studies. The size, PDI, ZP, EE% and DL% w/w were 85.65 ± 0.89 nm, 0.13 ± 0.01, +16.30 ± 0.23 mV, 68.73 ± 0.54 % and 6.86 ± 0.09 %, respectively. The surface morphology of the prepared CIP-loaded TAH-NPs was further observed using transmission electron microscopy (TEM). The TEM image (**Figure 1)** of the optimized CIP-loaded TAH-NPs formulation revealed distinct, spherical onion-shaped NPs that were consistent to those obtained using DLS.

Table 1: Size, PDI, ZP, EE % and DL % w/w for the parameters used in the optimization of CIP-loaded TAH-NPs (surfactant % w/v and OLA: TA mass ratio). Results represented as mean ± SD (n = 3).

Optimization parameter	Size (nm)	PDI	ZP (mV)	EE %	DL % w/w
Surfactant % (w/v)	**Fixed lipid: OLA: TA ratio 0.3: 1**				
0.15	83.39 ± 0.41	0.15 ± 0.01	+16.50 ± 0.14	63.87 ± 3.41	5.73 ± 0.29
0.3	109.40 ± 0.27	0.15 ± 0.01	+13.80 ± 0.35	60.43 ± 1.13	5.52 ± 0.04
0.45	169.50 ±1.96	0.45 ± 0.01	+13.30 ±0.21	65.14 ± 1.38	6.01 ± 0.09
(OLA: TA) w/w	**Fixed surfactant 0.15 % w/v**				
0.1:1	80.11 ± 0.71	0.14 ± 0.03	+15.10 ± 0.52	57.11 ± 0.75	5.16 ± 0.06
0.3:1	83.39 ± 0.41	0.15 ± 0.01	+16.50 ± 0.14	63.87 ± 3.41	5.73 ± 0.29
0.5:1	88.33 ± 0.26	0.10 ± 0.01	+18.30 ± 1.44	73.41 ± 1.56	6.46 ± 1.15

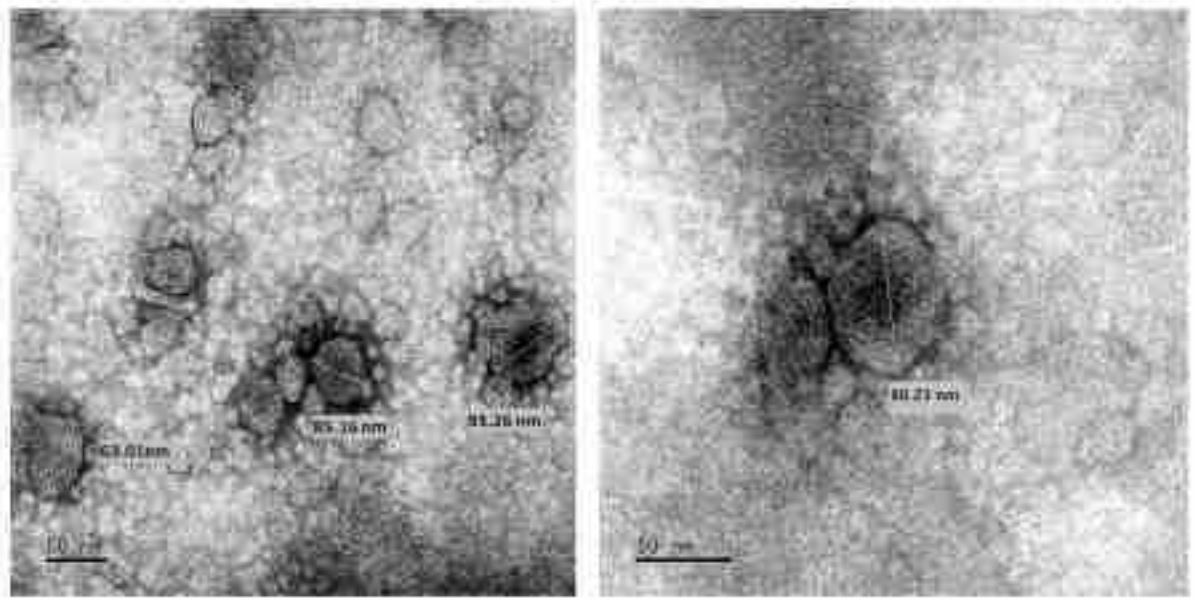

Figure 1. TEM image of CIP-loaded TAH-NPs (*TEM = Transmission Electron Microscope; CIP = Ciprofloxacin; TAH-NPs = Tannic acid hybrid nanoparticles)

3.2 Thermal profiles

Thermal analysis study using DSC is a commonly used tool in the field of nanomedicine to examine the melting and crystallization properties of all formulation excipients and NPs [421]. Hence, it helps

in confirming the drug encapsulation into TAH-NPs. The thermal profiles of PLX407, CIP, TA, physical mixture and the lyophilized CIP-loaded TAH-NPs are illustrated in **Figure 2**. The results indicated that PLX407 (**2A**), CIP (**2B**) and TA (**2C**) exhibited endothermic peaks at 61.46 °C, 160.66 °C, 230.77 °C and 308.88 °C, respectively. Additionally, the thermogram of the physical mixture of formulation excipients (**2D**) showed the same endothermic peaks with slight shifts to lower values for PLX407 and TA (58.10 °C, 211.60 °C and 258.14°C, respectively) and higher value for CIP (168.75 °C). The absence of the characteristic peak of CIP in the thermogram of the lyophilized CIP-loaded TAH-NPs (**2E**) suggests the successful entrapment of CIP within the prepared TAH-NPs in an amorphous state.

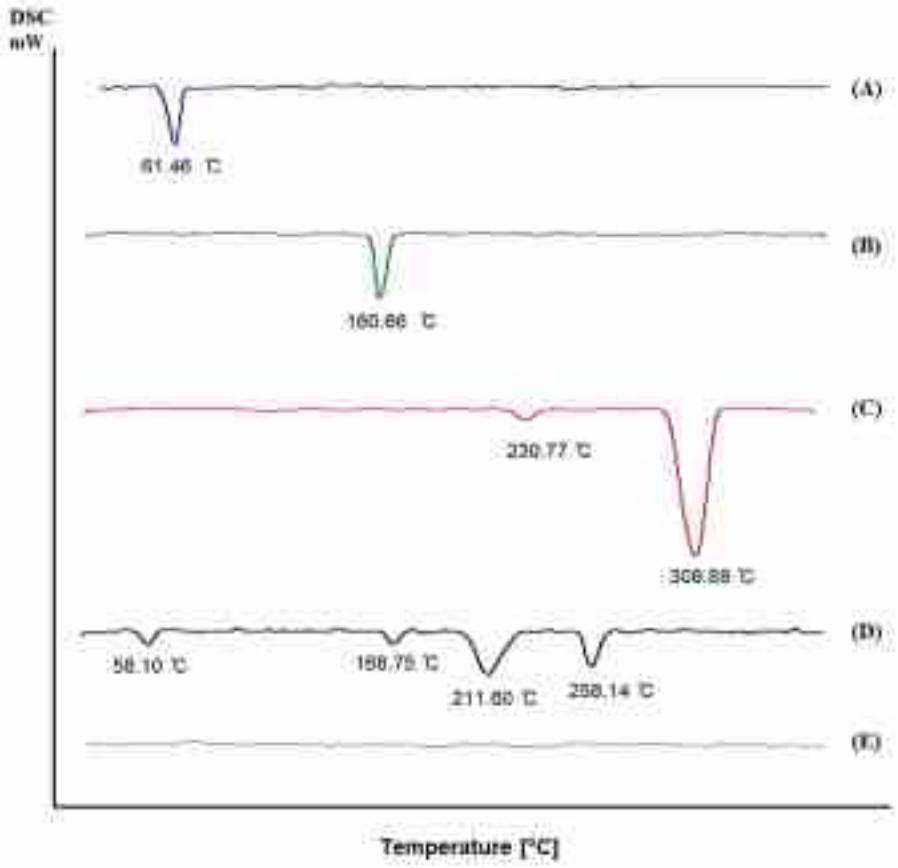

Figure 2. DSC thermograms of (**A**) PLX407; (**B**) CIP; (**C**) TA; (**D**) physical mixture; (**E**) lyophilized CIP-loaded TAH-NPs. (*PLX407 = poloxamer 407, CIP= ciprofloxacin, TA= tannic acid)

3.3 *In vitro* biosafety studies

3.3.1 Cytotoxicity and cell viability assay

The biosafety of a newly developed nanocarrier is an essential requirement for its application in drug delivery, as well as biomedical and clinical use. To investigate the cytocompatibility of the blank and

CIP-loaded TAH-NPs at different concentration ranges (20 - 100 µg/mL), a previously reported MTT assay method was performed using three different cell lines MCF-7, HEK 293 and HepG2 cells [299]. The percentage of cell viability data illustrated in **Figure 3** indicates that all tested concentrations maintained ≥70 % cell viability across the three cell lines tested. MCF-7 showed a viability range of 72.40-89.20 % and 70.01-82.48 %, HEK-293 had a viability range of 80.87-93.55 % and 77.84-96.84 %, while HepG2 showed a viability range of 71.65-100.49 % and 71.65-101.50 % for the blank and CIP-loaded TAH-NPs, respectively. Also, none of the three cell lines within the concentration range examined for both blank and CIP-loaded TAH-NPs showed any signs of concentration-dependent cytotoxicity. However, compared to the control group, the blank and CIP-loaded TAH-NPs formulations exhibited a slightly increased cell viability, which was likely due to the antioxidant and proliferative effects of TA [466, 467]. These results were consistent with the new biosafety level for biomedical materials set by the International Standard Organization (ISO) (≥70 % cell viability). [329], and confirmed the cytocompatibility and suitability of the prepared TAH-NPs for nano antibiotic delivery.

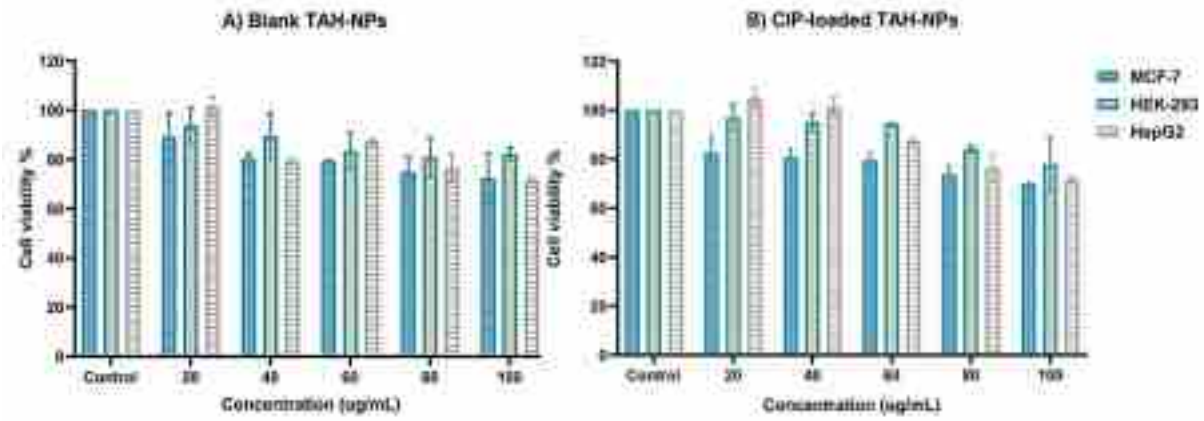

Figure 3. Cell viability % on MCF-7, HEK293 and HepG2 cell lines at varying concentrations of (**A**) blank TAH-NPs and (**B**) CIP-loaded TAH-NPs, and controls. Data are presented as mean ± SD (n=3)

3.3.2 Hemolysis

The compatibility of parenteral nanoformulations with erythrocytes is an essential requirement for their prospective application [330]. Therefore, the non-hemolytic activity of the prepared CIP-loaded TAHNPs was evaluated on freshly collected and washed sheep blood, and the results are displayed in **Figure 4.** All concentrations of CIP-loaded TAH-NPs tested showed less than 1 % hemolysis (**Table S3, Appendix II**), indicating the non-hemolytic activity and suitability of the prepared hybrid nanoformulation for intravenous administration.

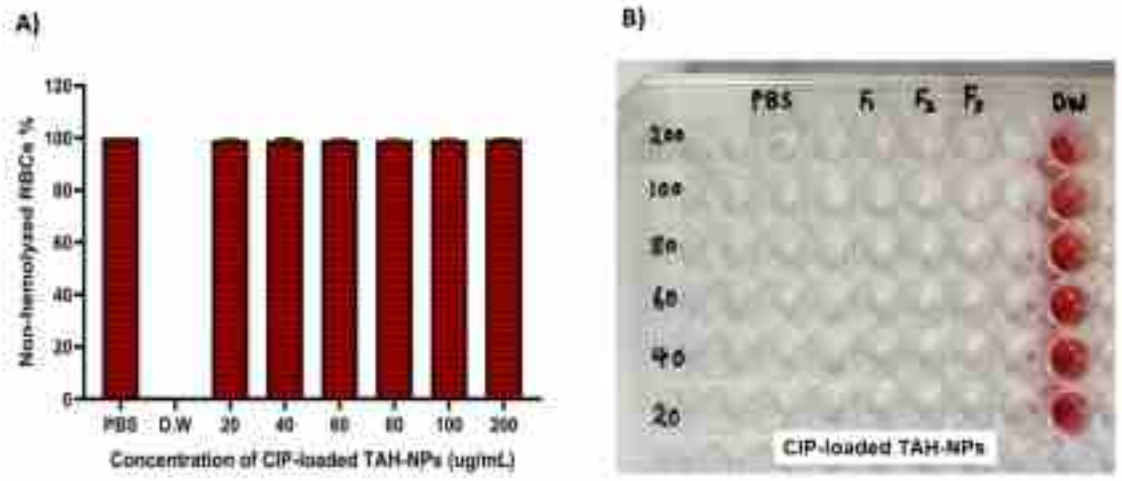

Figure 4. (**A**) and (**B**) Non-hemolytic activity of different concentrations of CIP-loaded TAHNPs (DW= distilled water, PBS=phosphate buffer saline pH 7.4). Data are presented as mean ± SD (n=3)

3.4 Molecular dynamic simulation studies

3.4.1 Determination of CIP-loaded TAH-NPs complex self-assembly

In order to comprehend the binding, interaction, and binding energies of the designed TAH-NPs to administer CIP against bacterial-induced sepsis, we present all-atom MD simulation. **Figure 5** shows the interaction of CIP, TA, OLA and PLX407 at different time points.

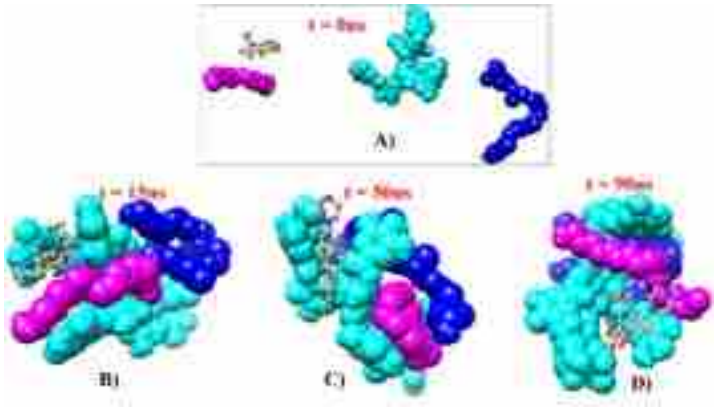

Figure 5. Structures of CIP, TA, OLA and PLX407 at four distinct simulated time points: (**A**) at t = 0 ns; (**B**) at t = 15 ns; (**C**) at t = 50 ns; and (**D**) at t = 90 ns. CIP was represented in a ball-and-stick model, TA (cyan), OLA (blue) and PLX407 (magenta) are represented in the sphere model. (* CIP = ciprofloxacin, TA = tannic acid, OLA = Oleylamine and PLX407 = poloxamer 407)

According to our modeling results, the four molecules (PLX407, TA, OLA, and CIP) spontaneously bound together over the course of 100 ns (**Figure 6A**). The average interaction energy was computed

to be -80.0 kJ/mol, and the average COM distance between them was determined to be around 1.5 nm. Van der Waals (vdW) interactions were a major factor in the spontaneous binding of CIP, TA, OLA, and PLX407, as shown in **Figure 6B**. Using the MM-PBSA, the binding energy (ΔG_{total}) was computed from frames 50 ns to 60 when the interactions between the three molecules were at their closest to determine the observed binding between the four particles. The interactions between CIP, TA, OLA, and PLX407 were influenced by both van der Waals and electrostatic interactions, with ΔE_{vdW} being the most significant, as illustrated in **Table 2**. A value of -42.500 ± 14.179 kJ/mol was determined for the total binding energy (ΔG_{total}). These strong binding energies observed between CIP and the other excipients used in the fabrication of the drug-loaded HNs (TA, OLA and PLX407) appear to correlate computationally with the high experimental EE % and DL % w/w reported previously in this study [468]

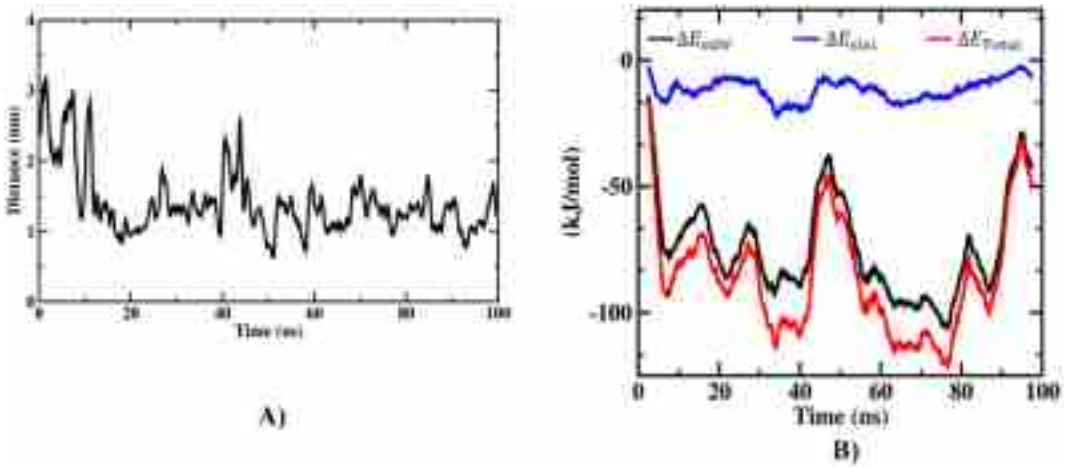

Figure 6. (**A**) The COM distance between TAH-NPs components loaded with CIP with time. (**B**) The dynamic interaction energy as a function of time between the molecules and their unbonded components.

Table 2. Shows the average binding energy and its constituent parts for the TAH-NPs complex loaded with CIP, as determined by the MM-PBSA calculation. Each set of data is shown as mean ± SD (n = 3).

Contribution	Energy (kJ/mol)
ΔE_{vdW}	-65.970 ± 15.80
ΔE_{elec}	-3.182 ± 9.26
ΔG_{polar}	34.158 ± 7.54
$\Delta G_{nonpolar}$	-7.506 ± 1.36
ΔG_{total}	-42.500 ± 14.18

3.4.2 *In-silico* analysis of the binding to TLR4

Activation of TLR4 signal pathway by bacterial endotoxins is critical for starting the innate immune response and causing both acute and chronic inflammatory disorders like sepsis [469]. Alteration of the TLR4 pathway by inhibiting its binding to bacterial endotoxins such as LPS could be a promising approach to specifically target bacterial sepsis. TA has been reported in the literature as a TLR4 inhibitor that can competitively prevent LPS binding to human TLR4, leading to downregulation of TLR4 and subsequent downstream signaling molecules [470]. Therefore, TA could attenuate LPS-induced inflammation and could be a potential therapeutic adjuvant for treating bacterial sepsis [471]. Accordingly, to explore the proposed inhibitory activity and interactions of TA with TLR4, molecular dynamics studies were carried out. Structural stability, flexibility, binding free energy calculations, MD simulations and binding affinity studies were performed to allow an estimation of the binding energies and forces contributing to this binding.

3.4.2.1 Structural Stability, flexibility, and Solvent Accessible Surface Area (SASA) analysis of LPS, TA, OLA, PLX407 and CIP against human TLR4

This experiment employed mmolecular ddynamic simulations to predict the interactions of the potential ligands (LPS, TA, OLA, PLX407 and CIP) with TLR4. The bound protein complexes' stability and fflexibility were ccalculated from the average root mean square deviation (RMSD), root mean square fluctuation (RMSF) and solvent accessible surface area aanalysis (SASA) (**Table 3**). To ensure the accuracy of the simulation and eliminate any potential artifacts, validation of system stability is necessary. Therefore, we evaluated the stability of the five ligands within the active sites of human TLR4, as this could affect the ligand-TLR4 interaction dynamics [472, 473]. It is also important to consider the ligand orientation within the binding site, as this can impact ligand stability [474-476]. Additionally, the stability of a small molecule in the binding area of a target protein determines its therapeutic impact [477].

To evaluate the stability of the systems during the 300 ns simulations, the root-mean-square deviation (RMSD) was calculated. RMSD measures backbone divergence of a protein from its starting structural conformation to its end location. The recorded RMSD for LPS, TA, OLA, PLX407 and CIP were 1.50 Å, 1.57 Å, 1.72 Å, 1.77 Å, and 1.62 Å, respectively. These results suggested that all molecules, including the natural substrate LPS and the nanoformulation components (TA, OLA, PLX407 and CIP) adopted a relatively high stable conformation throughout the 0 to 300 ns simulation period (**Figure 7A**).

Additionally, the analysis of individual residual conformations in response to ligand binding is essential for understanding the performance of the residues and their interaction with the ligand

during molecular dynamics simulation. This analysis is used to measure the nature of fluctuations exhibited by each residue, which ultimately contributes to the therapeutic efficacy of the protein. Therefore, the residual fluctuations of the TLR4-ligand complexes were investigated using the root-mean-square fluctuation (RMSF) algorithm over a 300 ns simulation period. An elevated RMSF value indicates that the backbone structure is more flexible, while a lower RMSF value denotes a less flexible structure, which is usually associated with reduced fluctuations [422]. The RMSF values for LPS, TA, OLA, PLX407 and CIP were 2.25 Å, 2.49 Å, 2.86 Å, 2.09 Å and 1.93 Å, respectively, suggesting that the LPS, TA, OLA and PLX407 systems exhibited higher residue fluctuations compared to the CIP system (**Figure 7B**). This indicates that binding of CIP to TLR4 reduces the overall flexibility of the protein structure more than the other ligands.

The hydrophobic core amino acids near the pocket site of proteins promote their folding, which is essential for their functional characteristics [478]. The amount of surface area exposed to the environment determines how much an amino acid interacts with the solvent and the pocket's contents [479]. Thus, by further measuring the solvent-accessible surface area (SASA) to get the differential conformational changes of studied systems, the displacement and reorientation of the surface protein residues in the five systems were analyzed [480]. As shown in **Table 3**, the computed SASA for LPS, TA, OLA, PLX407 and CIP were 27074.26 Å, 26866.47 Å, 26690.21 Å, 27165.87 Å and 26657.57 Å, respectively, indicating the conformational flexibility of the protein (**Figure 7C**).

Table 3: Shows the RMSD, RMSF, and SASA profile of the LPS, TA, OLA, PLX407 and CIP bound to human TLR4.

Systems	**Estimated averages (Å)**		
	RMSD	**RMSF**	**SASA**
LPS	2.25	1.50	27074.26
TA	2.49	1.57	26866.47
OLA	2.86	1.72	26690.21
PLX407	2.09	1.77	27165.87
CIP	1.93	1.62	26657.57

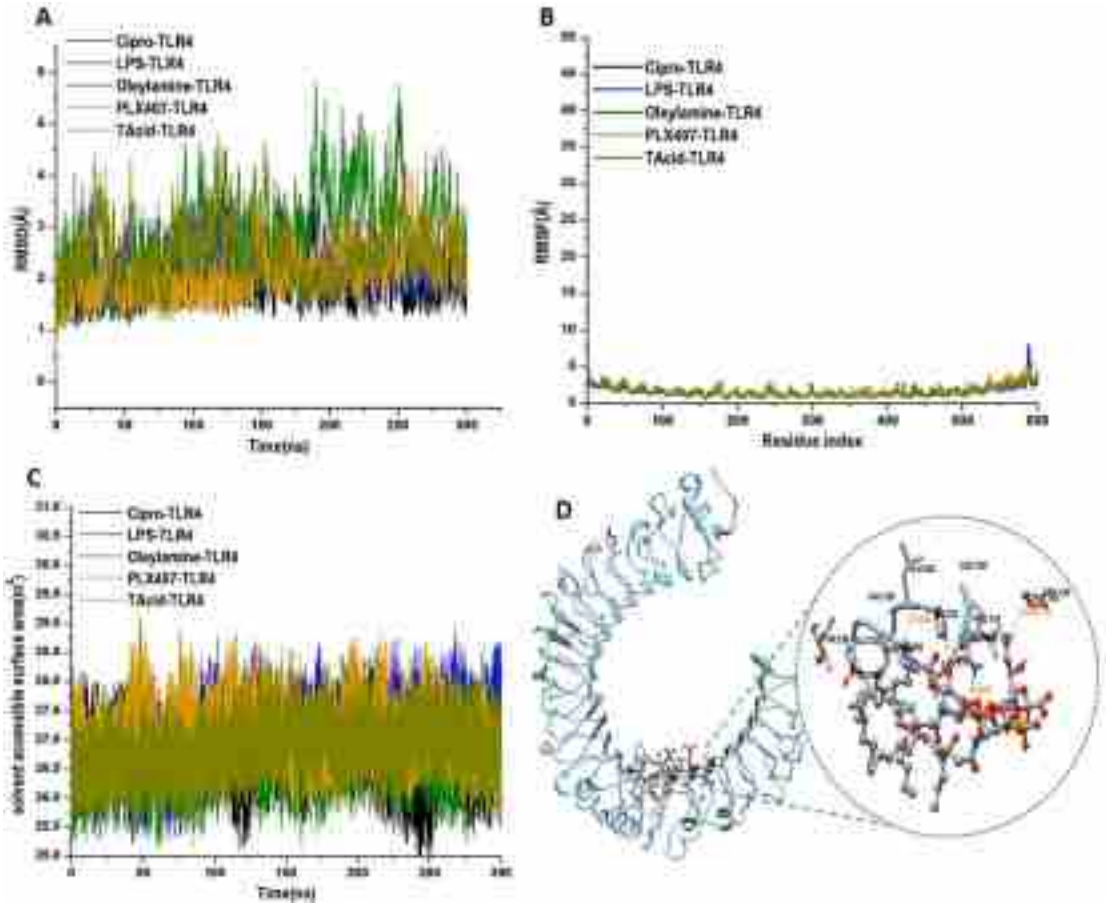

Figure 7: Changes in structure that happen when LPS (blue), TA (yellow), OLA (green), PLX407 (orange), and CIP (black) bind to human TLR4. **(A)** The C-α atoms RMSD (conformational stability) of human TLR4 bound to LPS, TA, OLA, PLX407 and CIP **(B)** The RMSF time evolution of each protein C-α atom residue during 300 ns for LPS, TA, OLA, PLX407 and CIP bound to human TLR4. **(C)** Structural representation of changes occurring during solvent accessible surface (SASA) binding of five molecules. **(D)** A close view for LPS at the binding site of humanTLR4, showing the hydrogen bonds interactions over 300 ns period.

3.4.2.2 Binding free energy calculations of the of LPS, TA, OLA, PLX407 and CIP binding to human TLR4

The therapeutic effects produced by a medication is largely contingent upon a protein's binding site and the subsequent activities that take place when binding ensues. Therefore, the Molecular Mechanics/Generalized Born Surface Area (MM/GBSA) approach was used to analyze the binding free energy in order to obtain insight into the molecular basis of the selectivity and binding of LPS, TA, OLA, PLX407, and CIP to TLR4 [481]. **Table S4** presents the aggregate binding energy of five chemicals in complexes that were predicted using this technique. The extensive molecular evidence

provided by these computed energies can aid in the development of drugs with enhanced ligand binding. Additionally, ligand stability, selectivity, and binding affinity are significantly influenced by the inter-molecular interactions with residues in the catalytic binding site [482].

As shown in **Figure 8**, the highest significant binding free energy calculated after 300 ns simulation time was observed in TA complexes with a ΔG_{bind} value of -67.97 kcal/mol (*P*-value < 0.0001), followed by OLA complexes with a ΔG_{bind} value of -16.56 kcal/mol (*P*-value = 0.0175), compared to the natural substrate LPS which had a ΔG_{bind} value of -7.04 kcal/mol. Both PLX407 and CIP showed non-significant alterations in binding free energy when compared to LPS, with ΔG_{bind} values of -9.35 (*P*-value = 0.4056) kcal/mol and -8.72 kcal/mol (*P*-value = 0.7992), respectively. Thus, TA bound favourably with the strongest binding affinity towards TLR4 than the other ligands including LPS. The difference in binding energy between TA and LPS was -60.93 kcal/mol, which is high enough for the competitive binding and inhibition of TLR4 by TA.

Furthermore, the TA complex displayed the highest van der Waals binding energy (ΔE_{vdW}), with a value of -79.43 kcal/mol, compared to the other ligands, which had ΔE_{vdW} of -10.50 kcal/mol, -21.77 kcal/mol, -15.84 kcal/mol, -12.93 kcal/mol for LPS, OLA, PLX407 and CIP, respectively (**Table S4)**. Additionally, TA had the highest electrostatic binding energy, with a value of -87.89 kcal/mol compared to LPS (ΔE_{ele} = -14.30 kcal/mol), OLA (ΔE_{ele} = -2.03 kcal/mol), PLX407 (ΔE_{ele} = -8.52 kcal/mol) and CIP (ΔE_{ele} = 125.92 kcal/mol). In terms of gas-phase energy (ΔGgas), TA had a value of -167.32 kcal/mol, which was significantly higher than the values of the other ligands, which had a ΔG_{gas} value of ~ -24 kcal/mol (**Table S4, Appendix II)**. The overall differences in van der Waals energy (ΔE_{vdW}), Electrostatic energy (ΔE_{ele}) and gas-phase energy (ΔG_{gas}) between TA and LPS were -68.93 kcal/mol, -73.59 kcal/mol and -142.52 kcal/mol, respectively, which are also high enough for the competitive inhibition of TLR4. The solvation energy (ΔG_{sol}) was the only energy showing a positive values of 17.76 kcal/mol, 99.35 kcal/mol, 7.23 kcal/mol and 15.03 kcal/mol in LPS, TA, OLA and PLX407 complexes, respectively, except for CIP, which had a negative value of -121.71 kcal/mol (**Table S4, Appendix II)**.

The *in-silico* findings indicate that both TA and OLA can bind to TLR4 more favourably than LPS. Furthermore, TA has the ability to strongly compete with and inhibit the activation of LPS-TLR4 complex, which can ultimately reduce the inflammatory response triggered by TLR4 in sepsis. The results obtained in our study are consistent with the findings of Sivanantham *et al* (2019), who performed an *in-silico* work to investigate the mechanism of TA's activity in preventing LPS-induced pro-fibrotic responses in macrophage cells. They suggested that the suppressive effect of TA on the

LPS-induced inflammatory response might be due to its direct and competitive binding to TLR4 [483]. Accordingly, we carried out an *in vitro* study to validate our hypothesis.

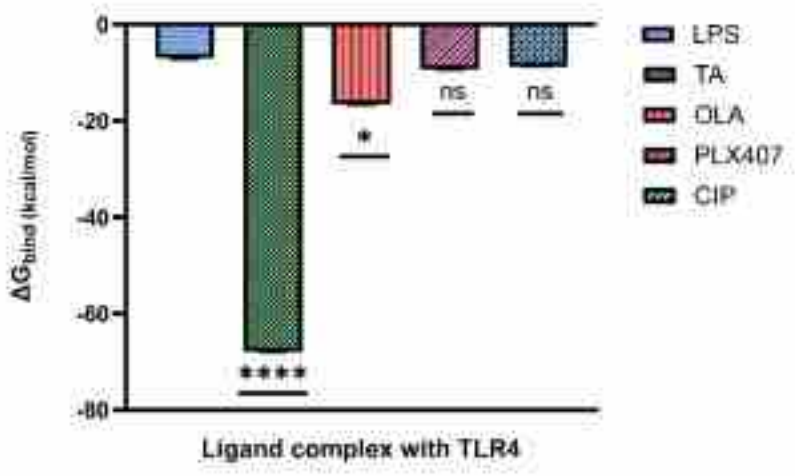

Figure 8. The total binding free energies of LPS, TA, OLA, PLX407 and CIP complexes with TLR4. All data are presented as mean ± SD (n-3). *P*-values **** < 0.0001, * = 0.0175, ^{ns} = 0.4056 for PLX407 and ^{ns} = 0.7992 for CIP (* LPS = lipopolysaccharide, TA = tannic acid, OLA = Oleylamine, PLX407 = poloxamer 407, CIP = ciprofloxacin).

3.5 Determination of *in vitro* binding affinity to TLR4

Subsequently, an MST binding affinity study was performed for the first time to further confirm the binding affinity of TA (a known TLR4 antagonist), OLA and CIP-loaded TAH-NPs to human TLR4 compared to its natural substrate LPS, as predicted by *in-silico* analysis. Recording of dissociation constant (K_d) values (**Table 4**) and quantification of TLR4 fraction bounds (**Figure 9**) obtained from the MST experiments were used to investigate the strength of binding. The results showed that both TA and CIP-loaded TAH-NPs had significantly (*P*-value < 0.0001) higher binding properties to TLR4 with K_d values equal to 0.009 ± 0.46 and 0.068 ± 0.25µM, respectively, compared to the natural substrate LPS, which had the highest K_d value of 10.36 ±0.35 µM. Also, OLA showed a relatively higher binding affinity than LPS with a K_d value of 0.32 ± 0.29 µM. This could be attributed to the structural similarity between OLA and lipid A, the active binding site of LPS that contains a number of fatty acyl chains [484]. These findings are consistent with the previously mentioned *in-silico* work, which suggest that both TA and OLA may strongly bind to TLR4 even in the presence of LPS. The findings also show the ability of CIP-loaded TAH-NPs to bind directly and competitively to human TLR4, which may be useful in suppressing the binding of LPS to TLR4 and inhibiting the subsequent

activation of downstream signaling molecules. Therefore, the results of the MST experiment revealed that TA and its prepared nanoformulation (CIP-loaded TAH-NPs) could be recommended as potential drug candidates for the treatment of bacterial-induced sepsis.

Table 4. Summary of the dissociation constant values (K_d) of LPS, TA, OLA and CIP-loaded TAH-NPs binding to TLR4 obtained from MST analysis. Data are presented as mean ± SD (n=3).

Test ligand	K_d (µM)
LPS	10.36 ± 0.35
TA	0.009 ± 0.47
OLA	0.32 ± 0.29
CIP-loaded TAH-NPs	0.068 ± 0.25

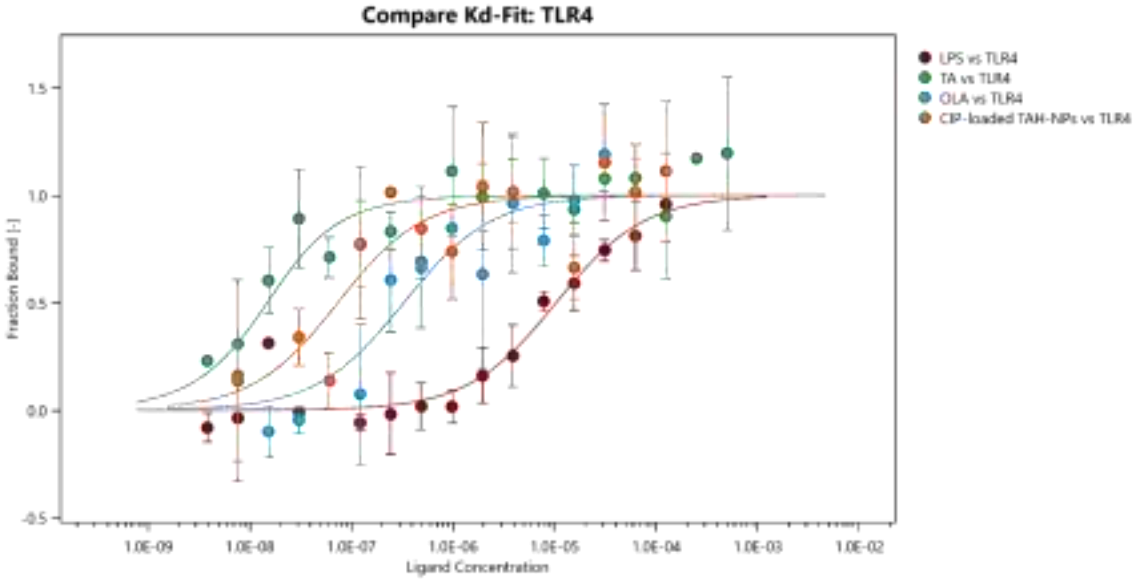

Figure 9. Comparison of TLR4 fraction bound to LPS, TA, OLA and CIP-loaded TAH-NPs using MST. Results represented in mean ± SD (n = 3)

3.6 *In vitro* drug release and linear kinetics

The release profile of bare CIP and CIP-loaded TAH-NPs was investigated *in vitro* using a dialysis bag method at physiological pH 7.4. **Figure 10** illustrates the release profile of bare CIP and CIP-loaded TAH-NPs over 72 hrs. The results showed that the release of CIP from the hybrid NPs was

sustained over a period of 72 hrs with an initial burst release followed by a slower release phase. In contrast, bare CIP exhibited a fast release profile with almost all the drug (100.42 ± 0.362 %) being released within the first 4 hrs compared to 53.45 ± 0.94 % release of CIP from the CIP-loaded TAH-NPs at the same time. After 72 hrs, the release of CIP from the NPs was 68.91 ± 2.99 % indicating controlled release profile (**Figure 10)**. The initial burst release of CIP may be attributed to the drug molecules adsorbed on the surface of the NPs while the slower release phase may be due to the diffusion of entrapped drug molecules through the lipid-polymer matrix [485, 486]. Additionally, the long carbon chain length of OLA may have slowed down the rate of drug diffusion, resulting in slower release rate [334, 418]. This controlled release of the entrapped antibiotic is useful and might be crucial for prolonged antibacterial activity.

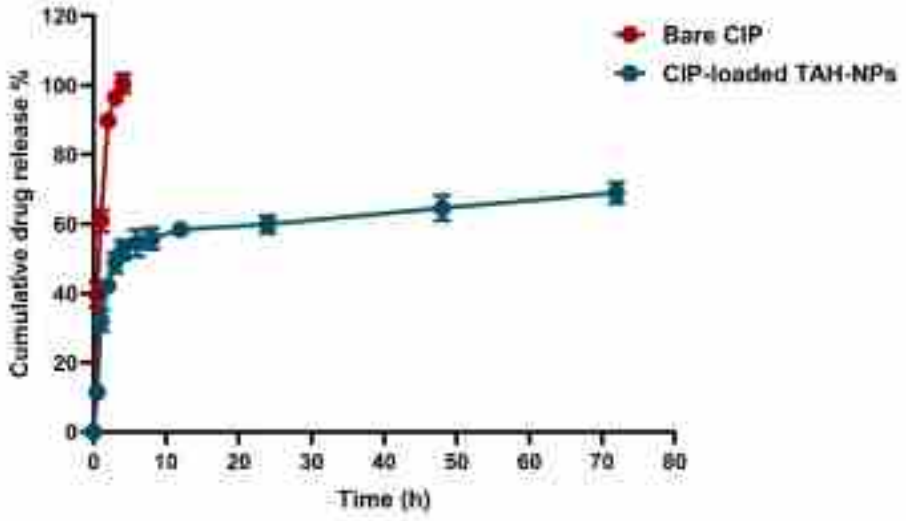

Figure 10. Release profiles of bare CIP and CIP-loaded TAH-NPs. Every data point is shown as mean ± SD (n=3).

To clarify the mechanism of release kinetics of CIP from the prepared CIP-loaded TAH-NPs, the obtained release data were fitted into various mathematical kinetic models as shown in **Table 5,** using a software program DDSolver which compares drug release profiles using model-dependent approaches [303]. Weibull model, which had the highest R^2 value of 0.99 and the lowest root means square error (RMSE) value of 2.60 was found to be the best fit model. The value of Weibull exponent parameter (β) was used as an indicator of the mechanism of transport of a drug through the lipid-polymer matrix with $\beta \leq 0.75$ indicating a Fickian diffusion mechanism, $0.75 < \beta < 1$ suggesting a hybrid mechanism (Fickian diffusion and Case II transport) and $\beta > 1$ indicating a complex release mechanism [487]. The release kinetics investigation revealed that the CIP-loaded TAH-NPs had an exponent parameter value (β) of 0.20, which suggests a Fickian diffusion release mechanism. In

addition, the Korsmeyer-Peppas model's (n) value was 0.19 (< 0.5), which further confirms that Fickian diffusion is the release mechanism of CIP from the CIP-loaded TAH-NPs [488].

Table 5. Data on drug release kinetics for CIP-loaded TAH-NPs

Model	Equation	R^2	RMSE	Release exponent (n)	β
Zero Order	Q=k*t	-1.70	35.28		
First Order	$Q = Q0. e^{kt}$	0.13	19.99		
Higuchi	$Q = k. t^{½}$	0.127	20.05		
Korsmeyer- Peppas	$Q = k. t^{n}$	0.87	8.05	0.19	
Hixson-Crowell	$Q^{⅓} = kt + Q_0^{⅓}$	-0.21	23.61		
Weibull	Q = 1 exp [-(t)a/b]	0.99	2.60		0.20

R^2 = linear regression coefficient, RMSE = Root means square error

3.7 Short-term physical stability study.

The physical colloidal stability of the optimal CIP-loaded TAH-NPs formulation was studied over a period of three months. Data collected during the 90-day storage period at RT (25 °C) and 4 °C is presented in **Table S5 (Appendix II)**. Results showed that the particle size, PDI, and ZP of the hybrid nanoformulation remained stable at RT throughout the three months (*P*-value > 0.05). However, when the samples were stored at 4 °C, they showed a slight increase in the mean particle size (from 85.65 ± 0.89 to 115.30 ± 6.90 nm), PDI (from 0.13 ± 0.01 to 0.30 ± 0.04) and ZP (from +16.30 ± 0.23 to +28.10 ± 1.33 mV) with time (*P*-value = 0.0012). Therefore, these findings suggest that RT is a more suitable storage condition than 4 °C for CIP-loaded TAH-NPs. **Figure 11** illustrates the effect of RT and 4 °C storage conditions on the physicochemical properties of CIP-loaded TAH-NPs.

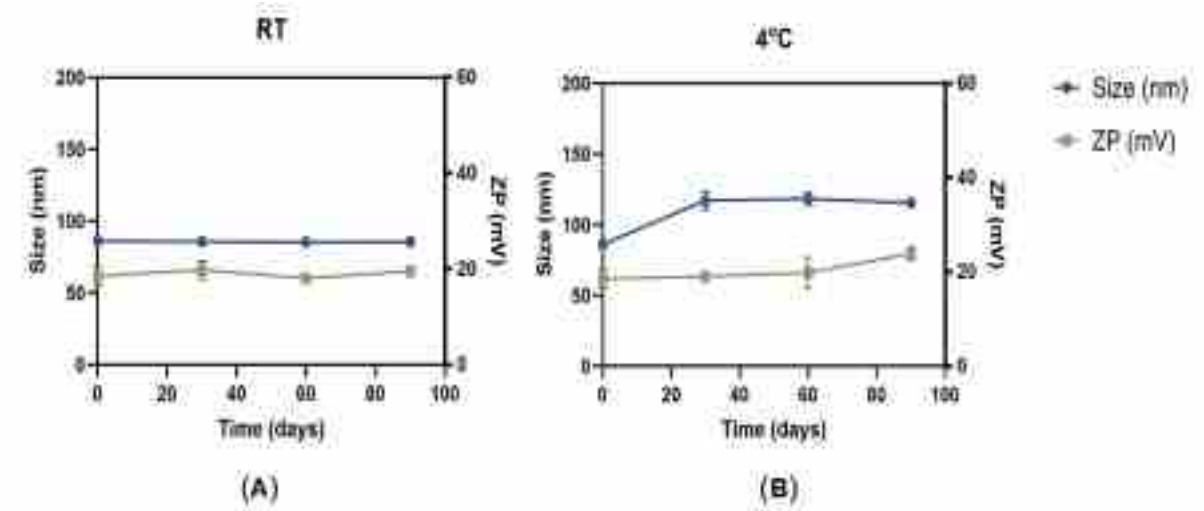

Figure 11. Variations in particle size (nm) and ZP (mV) of CIP-loaded TAH-NPs during their storage for 90-days (**A**) room temperature (RT) and (**B**) 4 °C. All results are presented as mean ± SD (n=3).

3.8 *In vitro* antibacterial activity studies

3.8.1 Determination of minimum inhibitory concentration (MIC)

Broth microdilution technique was carried out to measure the MIC of bare CIP, blank TAH-NPs and CIP-loaded TAH-NPs, against gram-positive *S. aureus* and MRSA, and gram-negative *E. coli* and *P. aeruginosa*, in order to evaluate their antibacterial activity potential. The MIC results recorded after 24, 48, and 72 hrs are presented in **Table 6**. CIP-loaded TAH-NPs displayed similar activity to bare CIP against *S. aureus* for the first 24 hrs, as indicated by an equal MIC value of 0.78 µg/mL. Between 48 and 72 hrs, CIP gradually lost its antibacterial activity while the hybrid NPs retained theirs. In the case of MRSA, the antibiotic-loaded hybrid NPs showed higher activity compared to the bare drug with an 8-fold and a 32-fold lower MIC values (1.56 and 12.50 µg/mL at 24 and 48 hrs and 1.56 and 50 µg/mL at 72 hrs for the hybrid NPs and bare CIP, respectively). CIP is known for its differential activity against both gram-positive and gram-negative bacteria [489]. However, its use against MRSA is limited due to resistance [490]. In our study, CIP-loaded TAH-NPs was found to be 8-fold more effective against MRSA compared to bare CIP within the first 24 hrs. Hence, encapsulating CIP into TAH-NPs could potentially enhance its therapeutic efficacy against MRSA bacterial infections.

In the case of gram-negative strains, the MIC of bare CIP against *E. coli* and *P. aeruginosa* was shown to be 0.31 and 0.78 µg/mL, respectively. Meanwhile, the MICs for CIP-loaded TAH-NPs against the same pathogens were found to be 0.16 and 0.78 µg/mL, respectively. These results indicated that encapsulation of CIP into TAH-NPs resulted in a 2-fold reduction in the MIC value against sensitive *E. coli*, while similar activity to bare CIP was observed against *P. aeruginosa* for the first 24 hrs. However, further incubation of the treatments for 48 and 72 hrs resulted in a 2-fold and 4-fold reduction in the MIC values of the CIP-loaded TAH-NPs against *E. coli*, and 4-fold reduction in

the MIC values against *P. aeruginosa* compared to the bare antibiotic. Accordingly, the antibacterial activity of CIP-loaded TAH-NPs against all organisms were found to be maintained for up to 3 days, while the activity of bare CIP gradually decreased over the course of 72 hrs.

Additionally, it was observed that the blank TAH-NPs formulation had some action against all of the bacteria that were examined, with MIC values of 10.24 and 82.03 μg/mL in the first 24 hours of treatment, and 20.50 and 164.06 μg/mL in 72 hrs against *S. aureus* and MRSA, respectively. The same trend was shown against *E. coli* and *P. aeruginosa* with MICs of 40.02 μg/mL against *E. coli* and 164.06 μg/mL against *P. aeruginosa* throughout the study period. These findings imply that the blank TAH-NPs have inherent antibacterial activity, likely due to the combined activity of TA and OLA, which was also confirmed by previous studies [339, 491].

Generally, the enhanced and prolonged antibacterial activity of CIP-loaded TAH-NPs as compared to the bare CIP may be attributed to several factors. These include the slow release of CIP from the hybrid NPs resulting in long-lasting antibacterial efficacy [461], and the smaller particle size of the NPs that possess a high surface area to volume ratio which enables well adsorption and more effective penetration to the cell wall [341, 492]. Furthermore, the inherent antibacterial activity of OLA, in addition to its ability to contact and disrupt the negatively charged bacterial cell walls, may have potentiated the antibacterial effectiveness of CIP-loaded TAH-NPs compared to the bare antibiotic [417]. The lower MIC values and the extended antibacterial activity associated with the hybrid nanocarrier may result in reducing the effective dose of treatment without compromising the therapeutic outcomes. Additionally, the frequency of CIP administration could be decreased, which helps in reducing the dose-dependent side effects and improves patient compliance [493, 494].

Table 6: The minimum inhibitory concentration (MIC) values (μg/mL) against *S. aureus*, MRSA, *E. coli* and *P. aeruginosa*, for bare CIP, blank-TAH-NPs and CIP-loaded TAH-NPs. The test was done in triplicate (n = 3).

	***S. aureus* (μg/mL)**			**MRSA (μg/mL)**		
Time (hr)	**24**	**48**	**72**	**24**	**48**	**72**
Bare CIP	0.78	1.56	3.13	12.50	12.50	50.00
Blank TAH-NPs	10.25	10.25	20.50	82.03	164.06	164.06
CIP-loaded TAH-NPs	0.78	0.78	0.78	1.56	1.56	1.56
	***E. coli* (μg/mL)**			***P. aeruginosa* (μg/mL)**		
Time (hr)	**24**	**48**	**72**	**24**	**48**	**72**
Bare CIP	0.313	0.313	0.63	0.78	3.13	3.13
Blank TAH-NPs	40.02	40.02	40.02	164.06	164.06	164.06
CIP-loaded TAH-NPs	0.16	0.16	0.16	0.78	0.78	0.78

* CIP = Ciprofloxacin hydrochloride, and TAH-NPs = Tannic acid hybrid nanoparticles.

3.8.2 Determination of Fractional Inhibitory Concentration (FIC)

To comprehend the combined antibacterial activity of the blank TAH-NPs and bare CIP in the CIP-loaded TAH-NPs against *S. aureus*, *E. coli*, MRSA and *P. aeruginosa*, the cumulative FIC was calculated for each time interval (24, 48 and 72 hrs) used the MIC values acquired from the antibacterial investigation (**Table 7**). The calculated ΣFIC values for *S. aureus* were 1.0761, 0.5761 and 0.3257, indicating indifference activity for the first 24 hrs, followed by additive and synergistic effects at 48 and 72 hrs, respectively. On the other hand, the ΣFIC values for *E. coli* were found to be 0.50, 0.50 and 0.25, indicating that additive effects continued for the first 48 hrs followed by synergistic activity up to 72 hrs. Notably, the ΣFIC values for MRSA were found to be 0.14, 0.13 and 0.04, confirming the synergistic activity throughout the 72 hrs, unlike *P. aeruginosa* ΣFIC values that indicated indifference activity for the first 24 hrs (1.00), followed by synergistic activity up to 72 hrs (0.2544). This result further confirms the superior antibacterial activity of CIP-loaded TAH-NPs against MRSA compared to *P. aeruginosa* in the first 24 hrs.

The synergistic effects observed suggest that a reduced concentration of CIP-loaded TAH-NPs is necessary to achieve the same antibacterial effect as bare CIP. This reduction in concentration could enhance the antibacterial efficacy while decreasing toxicity, which is a promising outcome [495-497].

This synergistic action of bare CIP and blank TAH-NPs on the bacteria is likely due to the inherent antibacterial properties of TA and OLA present in the hybrid nanoformulation, which may act via different mechanisms in combination with CIP, resulting in improved antibacterial activity compared to bare CIP.

Table 7: ∑FIC values for *S. aureus*, MRSA, *E. coli* and *P. aeruginosa* at each time interval.

Time (hrs)	**FIC (Bare CIP)**	**FIC (Blank TAH-NPs)**	**ΣFIC (Bare CIP+ Blank TAH-NPs)**	**Interpretation**
S. aureus				
24	1.00	0.08	1.08	Indifference
48	0.50	0.08	0.58	Additive
72	0.25	0.08	0.33	Synergy
MRSA				
24	0.12	0.02	0.14	Synergy
48	0.12	0.01	0.13	Synergy
72	0.03	0.01	0.04	Synergy
E. coli				
24	0.50	0.004	0.50	Additive
48	0.50	0.004	0.50	Additive
72	0.25	0.004	0.25	Synergy
P. aeruginosa				
24	1.00	0.01	1.05	Indifference
48	0.25	0.01	0.25	Synergy
72	0.25	0.01	0.25	Synergy

3.8.3 Flow cytometry

The rapid cell viability of MRSA and *P. aeruginosa* cells after incubation with bare CIP and CIP-loaded TAH-NPs for 18 hrs was investigated using a previously reported flow cytometry method [188]. Incubation of bacteria in the presence of antibiotics causes changes in cell-division cycle and morphology that can be measured using special dyes [344]. Syto9, a green, fluorescent nucleic acid dye, penetrates both viable and dead cells, and was used to detect live cells in the population, while propidium iodide (PI), a non-permeant fluorescent dye, was used to detect only damaged cells in the population. Kaluza-2.20 flow cytometer software (Beckman Coulter, USA) was used to analyze the data captured from flow cytometry whereby two gates were created representing viable cells (green)

and dead cells (red) in the population. **Figure 12** represents the cell count versus PI uptake histogram for MRSA **(i)** and *P. aeruginosa* **(ii)**. The shift in PI fluorescence, which is caused by the intercalation of bacterial DNA with PI stain, was considered an indicator of bacterial cell death and increased cell wall damage.

As shown in **Figure 12(i),** after incubation of MRSA with bare CIP (**iB**) and CIP-loaded TAH-NPs (**iD**) at their respective MICs (12.5 and 1.56 μg/mL, respectively), 93.51 ± 2.33 % and 99.92 ± 1.71 % death was observed. However, for the MRSA cells treated with bare CIP at the same concentration as the CIP-loaded TAH-NPs (1.56 μg/mL), there were only 87.48 ± 1.03 % dead cells (**iC**) compared to 99.92 % of the hybrid NPs formulation (*P*-value = 0.00082). The killing activity of CIP-encapsulated TAH-NPs was similar to that of the bare CIP but at an 8-fold lower concentration (*P*-value = 0.0041). These results further supported the significant improvement in the efficacy of CIP-loaded hybrid NPs against MRSA and could be applied for reducing the effective dose of CIP in treatment of MRSA infections without affecting the overall therapeutic outcomes. In the case of *P. aeruginosa* (**Figure 12(ii)**), incubation of the bacteria with bare CIP (**iiB**) and CIP-loaded TAH-NPs (**iiC**) at their respective MICs (0.78 μg/mL for both treatments) resulted in 83.81 ± 2.6 % and 99.82±1.49 % cell death, respectively. These results showed that the killing properties of CIP was enhanced when loaded into TAH-NPs as indicated by ~1.2-fold increase in dead cells of *P. aeruginosa* in the population when samples were treated with the drug loaded nanoformulation than the bare CIP at the same concentration 0.78 μg/mL (*P*-value <0.0001). From the overall findings we can conclude that the combined effect of OLA and TA as a component of the hybrid nanocarrier helps in enhancing the antibacterial activity of CIP against both MRSA and *P. aeruginosa*. These findings may potentially result in reducing the dose required for treatment, which would decrease the likelihood of CIP's dose-dependent side effects such as tendon rupture, nerve damage, and central nervous system changes [498].

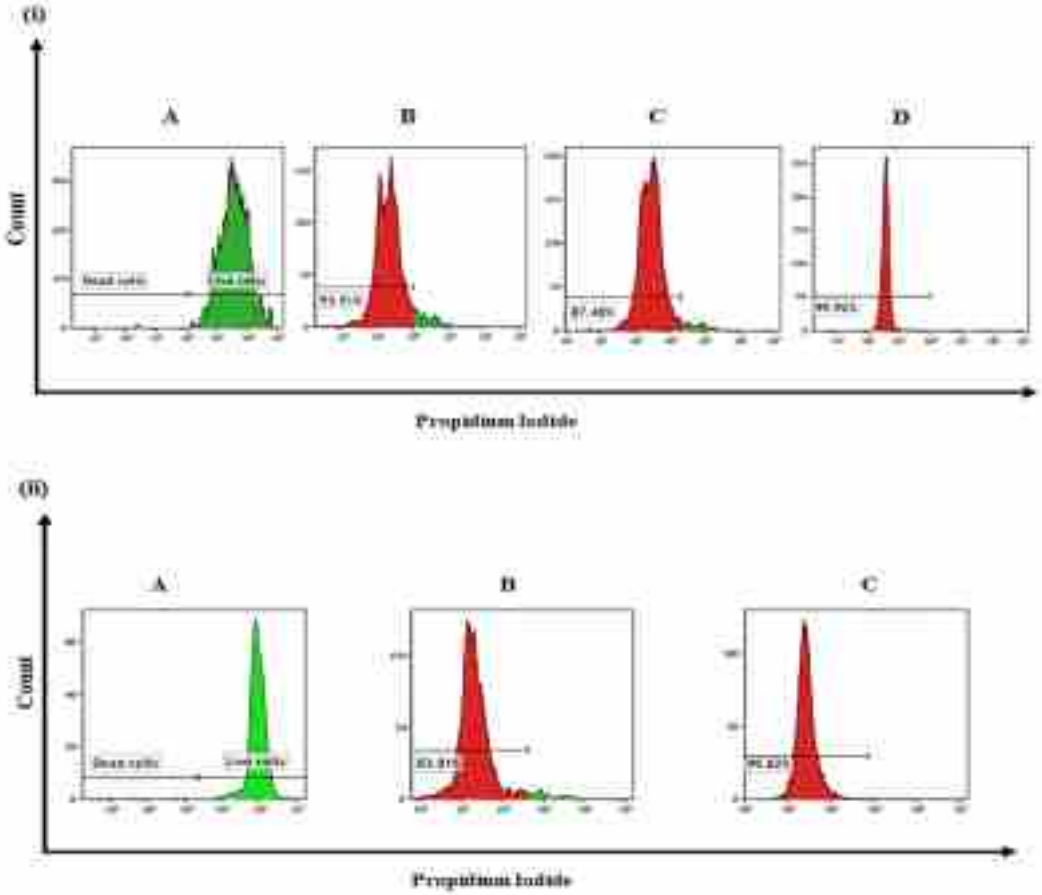

Figure 12. The propidium iodide (PI) uptake histograms for (**i**) MRSA and (**ii**) *P. aeruginosa*, where **(i) A**, denotes untreated MRSA (live cells); **B**, **C** and **D** shows the proportion of dead cells following incubation with bare CIP at its MIC (12.5 µg/mL), bare CIP at NPs MIC (1.56 µg/mL) and CIP-loaded TAH-NPs at its MIC (1.56 µg/mL), respectively. **(ii) A** stands for untreated *P. aeruginosa* (live cells); **B, and C** presents the proportion of dead cells following incubation with bare CIP at its MIC (0.78 µg/mL) and CIP-loaded TAH-NPs at its MIC (0.78 µg/ml), respectively. The experiment was conducted in triplicate (n=3).

3.8.4 Determination of *in vitro* antibiofilm activity

3.8.4.1 Crystal violet assay

Bacterial biofilms have been associated with chronic infectious diseases. Besides their resistance to host immunity, they have been identified as major contributors to antibiotic resistance due to increased tolerability of bacterial cells to antibiotic therapy within the biofilms [499, 500]. Therefore, developing a nano delivery system with enhanced antibacterial activity and ability to effectively eliminate biofilms would be useful in fighting bacterial infections and related complications like sepsis. In this regard, the efficacy of the formulated CIP-loaded TAH-NPs against MRSA and *P.*

aeruginosa biofilms was investigated qualitatively and quantitatively using the Microtiter Dish Biofilm Formation Assay (crystal violet staining assay), where mature biofilms grown in a 96-well plate were exposed to PBS (as a control), bare CIP solution and CIP-loaded TAH-NPs formulation for 24 hrs. **Figure 13** illustrates the percentage of biofilm growth inhibition following the exposure of MRSA and *P. aeruginosa* biofilms to bare CIP and CIP-loaded TAH-NPs. CIP-loaded TAH-NPs displayed higher efficiency in eradication of MRSA biofilms compared to bare CIP, reducing biofilm by 52.98 ± 2.65 % compared to 18.49 ± 4.07 % of biofilm eliminated by bare CIP. Therefore, the prepared hybrid nanocarrier showed ~ a 3-fold more antibiofilm activity than the bare drug (*P*-values< 0.0001). On the other hand, against *P. aeruginosa*, bare CIP exhibited 55.77 ± 0.64 % biofilm inhibition, while the CIP-loaded TAH-NPs formulation cleared 88.34 ± 0.73 % of *P. aeruginosa* biofilms, showing ~ a 1.6-fold greater biofilm inhibition activity than bare drug (*P*-values< 0.0001).
The improved antibiofilm activity of the CIP-loaded TAH-NPs against both strains may be attributed to the incorporation of TA as a component of the hybrid nanosystem. The antioxidant activity of TA may enhance the elimination of MRSA biofilms due to the presence of the hydroxyl groups and carboxylic acid groups, which enable TA to reduce the biofilm activity of the bacterial cells by inhibiting enzymes involved in biofilm formation [501]. A study reported by Payne *et al.* (2013) also found that TA increases extracellular IsaA (immunodominant staphylococcal antigen A) levels, which aid in the inhibition of *S. aureus* biofilms [502]. In addition, biofilm formation can also be inhibited by disturbing the production of quorum-sensing (QS) molecules, and TA is a well-known potent QS inhibitor of both gram-positive and gram-negative strains [503]. These findings indicate that besides the enhanced antibacterial activity against MRSA and *P. aeruginosa*, CIP-loaded TAH-NPs may also be effective in eradicating bacterial biofilms and modulate biofilm formation.

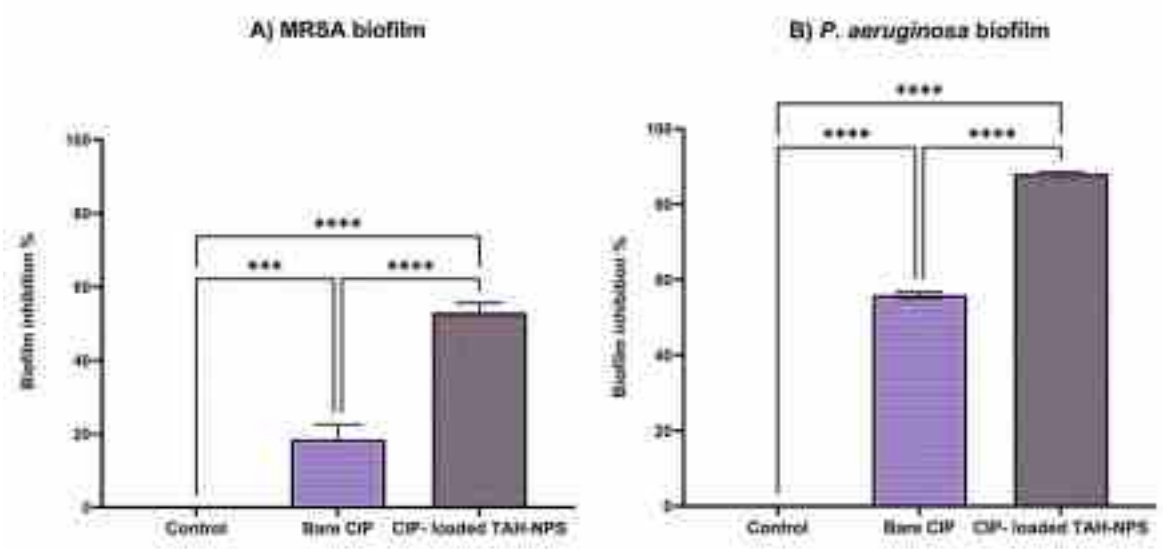

Figure 13. Biofilm inhibition % after exposing (**A)** MRSA and **(B)** *P. aeruginosa* biofilms to bare CIP, CIP-loaded TAH-NPs, and control (PBS pH 7.4). All results are presented as mean ± SD (n = 4) (*P*-values *** 0.0006 and **** < 0.0001).

3.8.4.2 Florescence microscope assay

Using a fluorescence microscope, the efficacy of CIP-loaded TAH-NPs in eradicating MRSA and *P. aeruginosa* biofilms was further validated. To culture the mature biofilms, cover slips were incubated with the bacteria, followed by a 30-minute dark staining process using Syto9 and PI solutions. After that, the dyes were rinsed off, and the cover slips were placed inverted on glass slides. As demonstrated in **Figure 14**, untreated biofilms of MRSA (**Fig. 14A**) and *P. aeruginosa* (**Fig. 14B**) both exhibited a strong Syto9 fluorescence emission spanning the entire coverslips (**14A1**), which is noticeably caused by the undamaged membranes of the bacterial cells that have accumulated on the coverslips [351, 352]. However, there was no discernible fluorescence when the untreated bacterial biofilms were dyed with PI (**14A2**), as PI cannot enter through the intact membrane of live cells [353, 354]. On the other hand, bacterial biofilms treated with bare CIP and dyed with Syto9 showed a marginal decrease in fluorescence compared to untreated biofilms (**14B1**), while those stained with PI showed a slight fluorescence (**14B2**), indicating that portion of the drug had permeated the biofilm and partially eliminated the bacteria. Interestingly, compared to those treated with bare CIP or left untreated, the Syto9 fluorescence intensity dropped sharply when biofilms treated with CIP-loaded TAH-NPs (**14C1**) suggesting a possible decrease in biofilms and the number of viable cells on the slide. Moreover, despite PI's non-cell permeable nature, the biofilms treated with CIP-loaded TAH-NPs exhibited a notably strong PI fluorescence (**14C2**). This indicates that treatment of MRSA and *P. aeruginosa* biofilms with the antibiotic-loaded hybrid NPs resulted in degradation of bacterial cell membranes and biofilms, increasing the amount of PI that could penetrate and bind to DNA [353].

Therefore, biofilms treated with CIP-loaded TAH-NPs had a significantly higher proportion of bacterial mortality compared to those treated with CIP alone. These results suggest that CIP-loaded TAH-NPs could be promising in eliminating biofilms, which cause sepsis and recurrent infections.

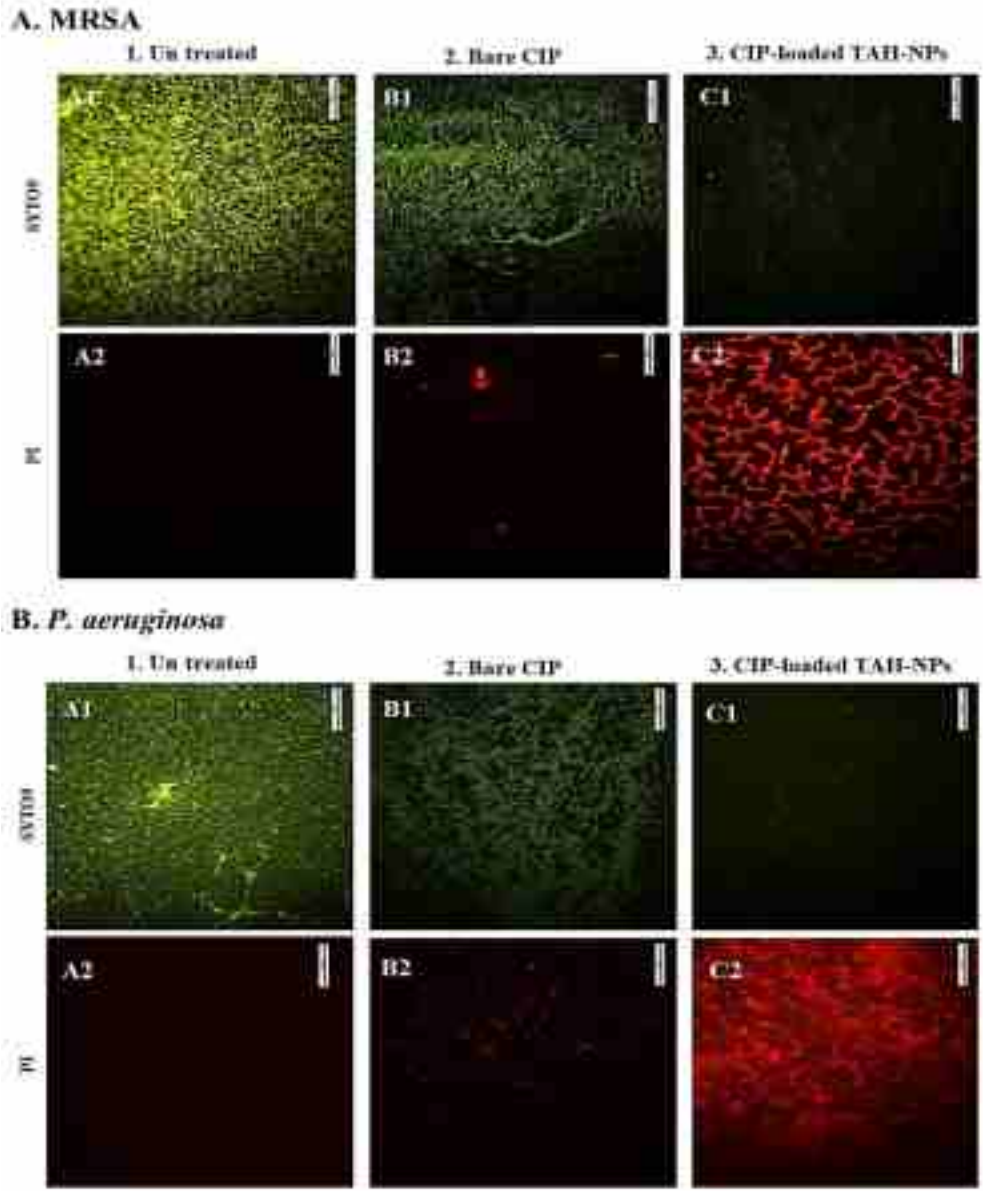

Figure 14. The fluorescence microscope assay depicts the images of (**A)** MRSA and (**B**) *P. aeruginosa* biofilms stained with Syto9 and PI. **1**) Untreated biofilms **2**) Biofilms treated with bare CIP, and **3**) Biofilms treated with CIP-loaded TAH-NPs, respectively. (Scale bar = 100 μm).

3.8.5 Time killing assay (TKA)

The TKA was performed on MRSA and *P. aeruginosa* to determine the rate of bacterial killing following a 24-hour exposure to bare CIP and the prepared CIP-loaded TAH-NPs at 5 times MIC (**Figure 15)**. Both bare CIP and CIP-loaded TAH-NPs reduced the number of MRSA and *P. aeruginosa* CFUs. However, CIP-loaded TAH-NPs demonstrated superior activity compared to bare CIP, as they completely eradicated both bacteria within 8 hrs of incubation, while bare CIP showed slower killing efficacy within 24 hrs of incubation. Hence, CIP-loaded TAH-NPs exhibited a significantly rapid bactericidal effect at an 8-fold lower concentration against MRSA and a concentration comparable to the bare CIP against *P. aeruginosa* (*P*-value <0.0001). These results demonstrate that CIP-loaded TAH-NPs could be an efficient nanocarrier for rapid lowering of bacterial burden in the body, thereby enabling a successful therapy with reduced dose regimens against gram-positive and gram-negative infections and their induced sepsis.

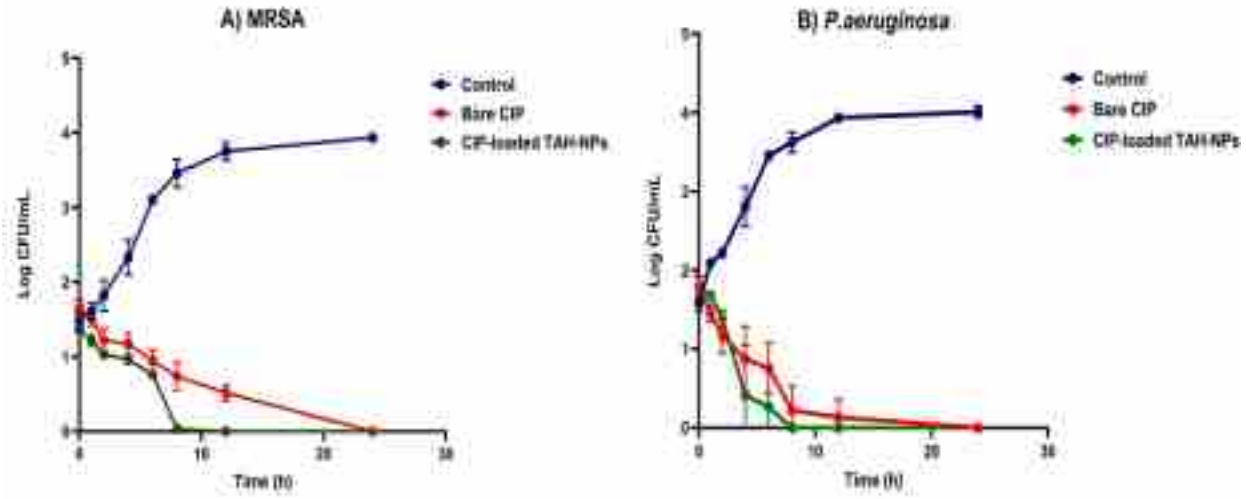

Figure 15. Time killing kinetics curve of **(A)** MRSA and (**B**) *P. aeruginosa* exposed to CIP, CIP-loaded TAH-NPs, and control (PBS pH 7.4). Results represented in mean ± SD (n = 3). The CIP killing kinetics were significantly enhanced by CIP-loaded TAH-NPs (*P*-value <0.0001).

3.8.6 Efflux pump inhibition assay

MRSA and *P. aeruginosa* develop efflux-mediated resistance to fluoroquinolone antibiotics through mutations that reduce the bacterial affinity to the drugs [504]. CIP is known to exert its antibacterial action on both gram-positive and gram-negative bacteria by preventing bacterial DNA replication via inhibition of DNA topoisomerase and DNA gyrase [505]. However, the over-expression of bacterial efflux pumps makes it difficult for CIP to specifically target the DNA of the bacterial cells. Therefore, the ability of the prepared CIP-loaded TAH-NPs to inhibit the increase in expression of efflux pumps caused by MRSA and *P. aeruginosa* was explored using EtBr according to a previously reported

method [309]. EtBr, an efflux pumps substrate, binds intracellularly to DNA and fluoresces when inside the bacteria [359]. According to the results, MRSA and *P. aeruginosa* treated with CIP-loaded hybrid NPs exhibited a greater fluorescence intensity than those treated with bare CIP, owing to the significant accumulation of EtBr in the bacterial cells which was noticed in the MHA used for the experiment (**Figure 16**). The presence of TA as a component of the nanocarrier's make-up may be responsible for the increased fluorescence intensity seen in the MHA samples treated with the nanoformulation. TA has been known to cause an inhibition of efflux pumps of gram-positive and gram-negative pathogens [506, 507]. It has been reported to cause the inhibition of NorA efflux pumps of gram-positive bacteria due to its ability to chelate metal ions that are necessary for the function of bacterial membrane protein, which could account for the observed efflux pump inhibition in MRSA [413]. Also, the ability of TA to inhibit QS might be related to its efflux pump inhibitory actions against both MRSA and *P. aeruginosa* [508, 509]. Studies have shown a direct correlation between the QS signaling system and the regulation of the genes responsible for active efflux systems [510-512]. Therefore, TA, that has the potential to block efflux pumps, can act synergistically with CIP in the prepared CIP-loaded TAH-NPs formulation to combat MRSA and *P. aeruginosa,* and could serve as an effective antivirulence therapy to treat associated conditions like sepsis.

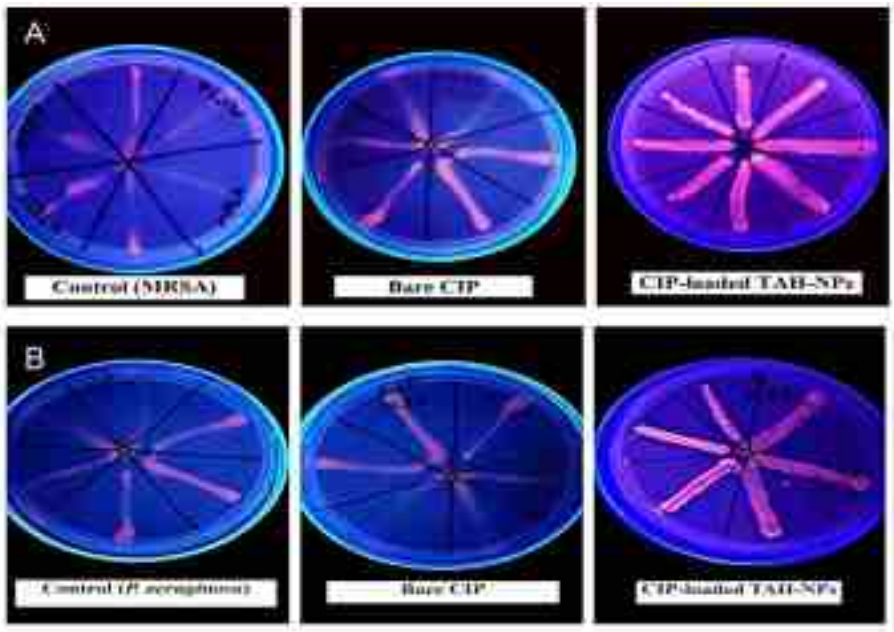

Figure 16. Efflux pump inhibition effect of CIP-loaded TAH-NPs against **(A)** MRSA and **(B)** *P. aeruginosa* compared with bare CIP (0.25×MIC).

3.8.7 Bacterial-induced hemolysis inhibition assay

Bacterial species such as *S. aureus* and *P. aeruginosa* are known to produce a variety of virulence factors that contribute significantly to sepsis [513, 514]. One of the most significant bacterial virulence factors are membrane- disrupting exotoxins such as α, β, δ, and γ hemolysins generated by *S. aureus*, and proteases, exotoxin A, phospholipase C and hemolysin produced by *P. aeruginosa* [515, 516]. These toxins have the potential to compromise the integrity of the host cell membranes such as RBCs membranes, which can result in hemoglobin leakage, cell death, and a breakdown of the host's defense mechanisms against sepsis and other inflammatory disorders [517-520]. Therefore, the impact of MRSA and *P. aeruginosa* on sheep erythrocyte integrity in the presence or absence of different concentrations of bare CIP and CIP-loaded TAH-NPs was evaluated using previously published methods [458, 459]. The exposure of erythrocytes to MRSA resulted in 89.75 ± 3.4 % hemolysis, while *P. aeruginosa* resulted in 80.28 ± 1.13 % hemolysis. These values were considered as 100% hemolysis throughout the entire experiment. **Figure 17 (A)** shows that the hemolytic activity of MRSA culture supernatant in the presence of MIC, 0.5MIC and 0.25MIC of bare CIP and CIP-loaded TAH-NPs were found to be 51.08 ± 4.35 %, 40.89 ± 5.74 % and 29.01 ± 7.46 % for the bare drug, and 6.68 ± 0.22 %, 6.86 ± 1.13 % and 5.89 ± 0.72 % for CIP-loaded TAH-NPs compared to the untreated MRSA culture (100 %). It can be noticed that bare CIP exhibited a dose-dependent antihemolytic activity, with the lowest concentration (0.25MIC) inhibited the hemolytic activity of MRSA by 70.99 % versus control. In contrast, all concentrations of CIP-loaded TAH-NPs displayed a remarkable antihemolytic effect, with the lowest concentration (0.25MIC) inhibited the hemolytic activity of MRSA by 94.11 % compared to the control. Therefore, the antihemolytic activity of CIP was significantly enhanced when loaded into TAH-NPs (*P*- value < 0.0001). The same trend was observed in the case of *P. aeruginosa* when exposed to bare CIP, as it demonstrated dose-dependent antihemolytic activity, which was found to be 36.97 ± 2.20 %, 22.09 ± 4.10 % and 18.33 ± 2.31 % at the MIC, 0.5MIC and 0.25MIC, respectively. However, when CIP was loaded into TAH-NPs, the antihemolytic activity against *P. aeruginosa* was found to be 5.04 ± 0.65 %, 4.39 ± 0.67 % and 5.82 ± 1.2 % at the MIC, 0.5MIC and 0.25MIC, respectively (**Figure 16 (B)**). Notably, at a concentration of 0.5MIC, CIP-loaded TAH-NPs displayed the highest effectiveness in inhibiting the hemolytic activity of *P. aeruginosa* by 95.61 % as opposed to 77.91 % inhibition displayed by bare CIP at the same concentration (*P*- value < 0.0001). These results indicate that subinhibitory concentrations of CIP-loaded TAH-NPs effectively inhibited the hemolytic activity of both MRSA and *P. aeruginosa* supernatants.

This enhanced antihemolytic activity could be attributed to the presence of TA, which has been reported to have an inhibition activity against the production and/or secretion of toxins [521]. Additionally, polyphenols, such as TA, have the ability to interact directly with released toxins,

changing their structure and activity, which restricts toxins interaction with erythrocyte membranes [522, 523]. Moreover, the antibacterial, QS inhibition and antibiofilm activities of TA could may also contribute to the enhanced protective action of CIP-loaded TAH-NPs against hemolysis caused by bacteria, since these factors are involved in the virulence activities of bacterial exotoxins in many disease conditions, including bacterial sepsis [524, 525]. Overall, CIP-loaded TAH-NPs may be useful as an ani-virulence therapy in combating pathogenic bacteria and can help prevent and cure sepsis and other life-threatening infections

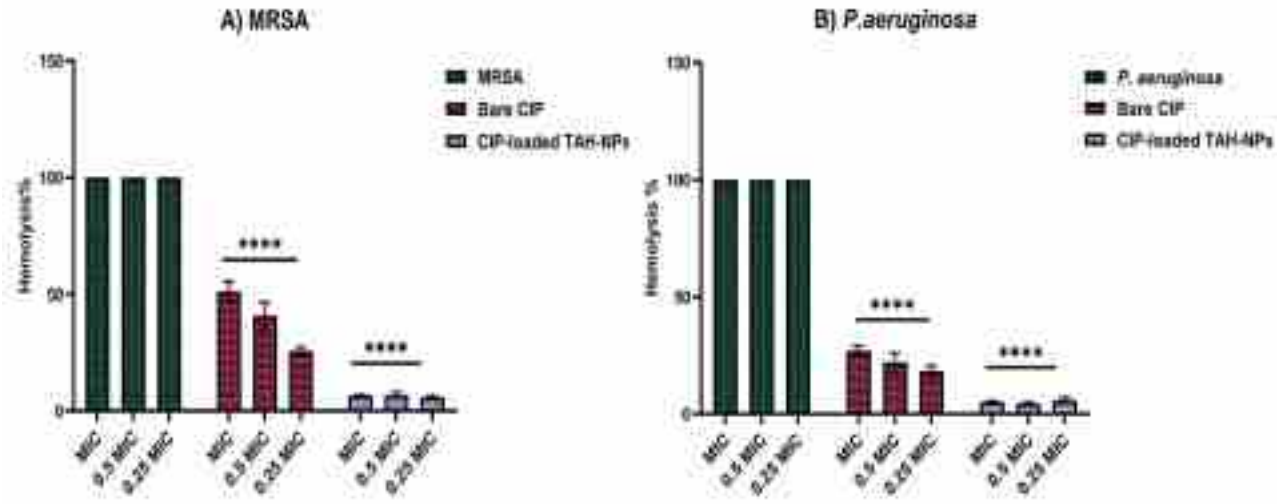

Figure 17. Hemolytic activity (%) of (**A**) MRSA and (**B**) *P. aeruginosa* culture supernatants on sheep erythrocytes in the presence of MIC, 0.5 MIC and 0.25 MIC of bare CIP and CIP-loaded TAH-NPs. Values represent mean ± SD (n=3). (*P*- value ****< 0.0001)

3.9 *In vitro* antioxidant study

The overproduction of reactive oxygen species (ROS) in response to inflammation can result in oxidative stress, which is a primary cause of the high mortality rates linked to several infectious diseases, including sepsis [361]. Neutralizing ROS generated during the inflammatory response is crucial in reducing oxidative stress and mitigating the harmful effects of sepsis on the body. Therefore, the DPPH radical scavenging method was utilized to evaluate the antioxidant behavior of varied concentrations of TA and the prepared CIP-loaded TAH-NPs (20-1000 µg/mL) [310]. DPPH is a free radical that is stable and has a prominent absorption band at 517 nm. However, it transforms into non- absorbent diphenyl-picryl-hydrazine, in the presence of hydrogen donors or free radical scavengers [526]. **Figure 18** shows the antioxidant activity percentage of ascorbic acid (positive control), TA and CIP-loaded TAH-NPs after being incubated with DPPH alcoholic solution at 37 °C in the dark. The results indicated that all concentrations of TA and CIP-loaded TAH-NPs displayed a strong antioxidant activity by scavenging DPPH radicals, with the highest activity observed at a concentration of 1000 µg/mL. At this concentration, TA showed 68.75 ± 4.31 % antioxidant activity,

while CIP-loaded TAH-NPs demonstrated 61.75 ± 4.04 % activity. Previous research have reported on the antioxidant activity of free TA. These studies found that TA was effective in neutralizing DPPH radicals [527-530], thanks to its strong hydrogen- and electron- donating capacities, which are attributed to the galloyl and ortho-hydroxyl groups of TA [528, 531]. More interestingly, the presence of TA in the hybrid nanocarrier enhanced the ability of CIP-loaded TAH-NPs to convert DPPH into its reduced form. However, free TA exhibited higher antioxidant activity than the hybrid NPs formulation in all the concentrations investigated. The improved reactivity of TA toward the DPPH radical compared to its hybrid formulation may be due to the free molecule's reaction sites being more exposed and hence more accessible for DPPH interactions [527]. Our results are consistent with a study reported by Pucci *et al*. (2022), who revealed the significant *in vitro* antioxidant and scavenging activity of TA-based NPs against oxidative stress [527]. Consequently, the protective effect of CIP-loaded TAH-NPs against DPPH radicals could have potential benefits in combating and preventing oxidative and lipid peroxidation-related diseases such as sepsis [283, 286]

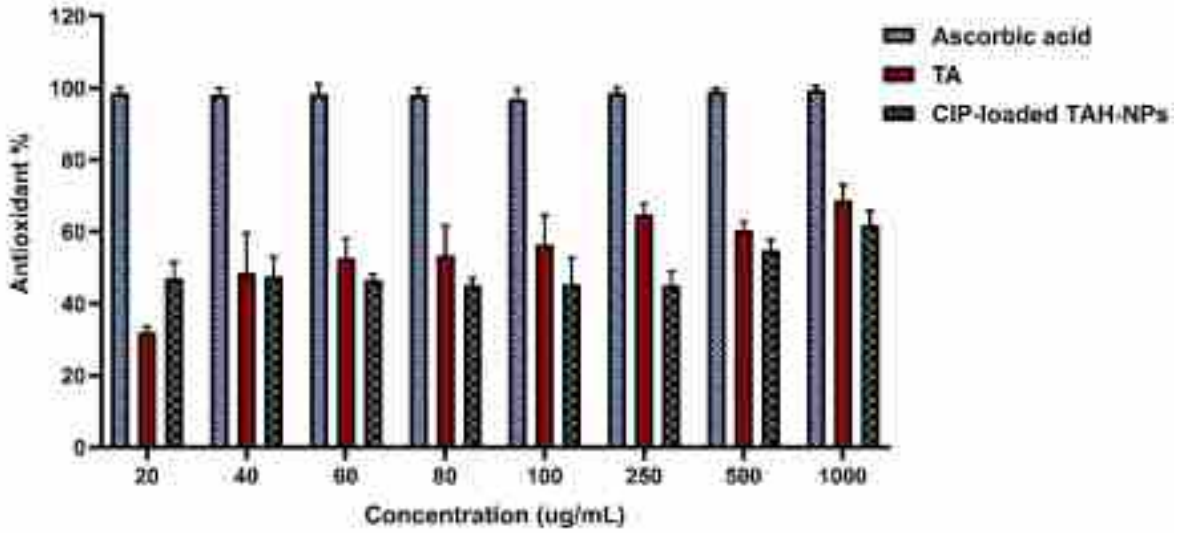

Figure 18. illustrates The antioxidant activity (%) of different concentrations of TA and CIP-loaded TAH-NPs according to a DPPH radical scavenging assay in comparison to ascorbic acid (positive control). Data in the graph are presented as mean ± SD (n=3). (*TA= Tannic acid, CIP= Ciprofloxacin, H-NPs= hybrid nanoparticles, DPPH= 2.2-diphenyl-1-picrylhydrazyl)

3.10 *In vitro* anti-inflammatory studies

LPS is responsible for triggering inflammatory responses in a variety of disease states such as sepsis. It plays a pivotal role in initiating an immune response that can lead to cytotoxicity and multiple organ dysfunction [366]. The activation of immune response by LPS can result in the production of various cytokines such as TNF-α, IL-1β, and IL-6. Furthermore, the cytotoxic effects induced by higher concentrations LPS can affect various cell types and organs [368]. For instance, endothelial cells may

become activated and dysfunctional due to the inflammatory response, leading to impaired vascular integrity and increased permeability [370]. Moreover, immune cells such as macrophages and neutrophils, can become hyperactivated in response to LPS, releasing excessive ROS and other cytotoxic molecules, which can also damage healthy tissues and exacerbate organ dysfunction in sepsis [369]. Therefore, to evaluate the anti-inflammatory effects of TA and CIP-loaded TAH-NPs formulations against LPS-triggered inflammation, we conducted cell viability and cytokine levels assays using HepG2 cells [311, 532].

3.10.1 Cytoprotective effect against LPS-induced cytotoxicity

The effect of TA and CIP-loaded TAH-NPs on LPS-induced cytotoxicity was evaluated on HepG2 cell lines using a previously reported MTT assay protocol [312]. As shown in **Figure 19A**, LPS treatment (0.9 mg/mL) significantly reduced HepG2 cell viability to 36.70 ± 3.30 % compared to the control group (*P*-value<0.0001). However, the addition of free TA or CIP-loaded TAH-NPs formulations (100 µg/mL) improved cell viability to 90.03 ± 6.76 % and 76.11 ± 4.64 %, respectively, compared to the control. Notably, treatment with TA and CIP-loaded TAH-NPs formulations increased cell viability diminished by LPS by 53.3 % (*P*-value<0.0001) and 39.41 % (*P*-value = 0.0005), respectively, compared to the LPS-treated group. This result indicated that TA and CIP-loaded TAH-NPs are capable of protecting cells from LPS-induced cell death. This cytoprotective effect is likely due to the antioxidant activity of TA, which helps in scavenging ROS and reducing oxidative stress, thereby mitigating cell injury [528]. Other studies have also demonstrated the cytoprotective effect of TA against LPS-induced cell death [471, 533]. Therefore, TA and its nanoformulation may be considered as potential therapeutic agents for the prevention of sepsis-induced cell damages.

3.10.2 Anti-inflammatory activity against LPS-induced inflammatory responses (measurement of IL-6 levels)

Cytokines play a crucial role in regulating the host immune response, and altered expression of cytokines has been implicated in the development of sepsis [374]. Among these cytokines, IL-6 is considered to have a significant role in the progression of sepsis, particularly as an early indicator of the inflammatory state [375]. When immune cells are excessively activated by LPS via TLR4, they release IL-6 as part of the inflammatory response. Elevated levels of IL-6 are commonly observed in septic patients and are associated with the severity of the condition [534]. Additionally, excessive production of IL-6 contributes to the cytokine storm, leading to widespread tissue damage and organ dysfunction in severe sepsis and septic shock [376, 377]. Consequently, the anti-inflammatory effect

of TA and CIP-loaded TAH-NPs were investigated further by measuring the IL-6 concentration in LPS-induced HepG2 cells using ELISA kits. The results in **Figure 19B** showed significant elevation in the levels of IL-6 when the cells were treated with 1 µg/mL of LPS. In converse, when the inflamed cells were treated with different concentrations of TA or CIP-loaded TAH-NPs formulations (50 and 100 µg/mL) the levels of IL-6 suppressed greatly compared to LPS alone (*P*-value<0.0001). This indicates that both free TA and the hybrid nanocarrier have the ability to control the levels of IL-6 induced by LPS, which could mitigate tissue damage and prevent organ dysfunction caused by the overwhelming immune response. This result confirms the antagonistic action of TA and the hybrid NPs on TLR4, since their enhanced anti-inflammatory effects may be attributed to their strong and competitive binding to TLR4, which was previously demonstrated in this study by *in-silico* and *in vitro* investigations. Therefore, CIP-loaded TAH-NPs could be a promising candidate for modulating IL-6 levels and managing the inflammatory response in sepsis.

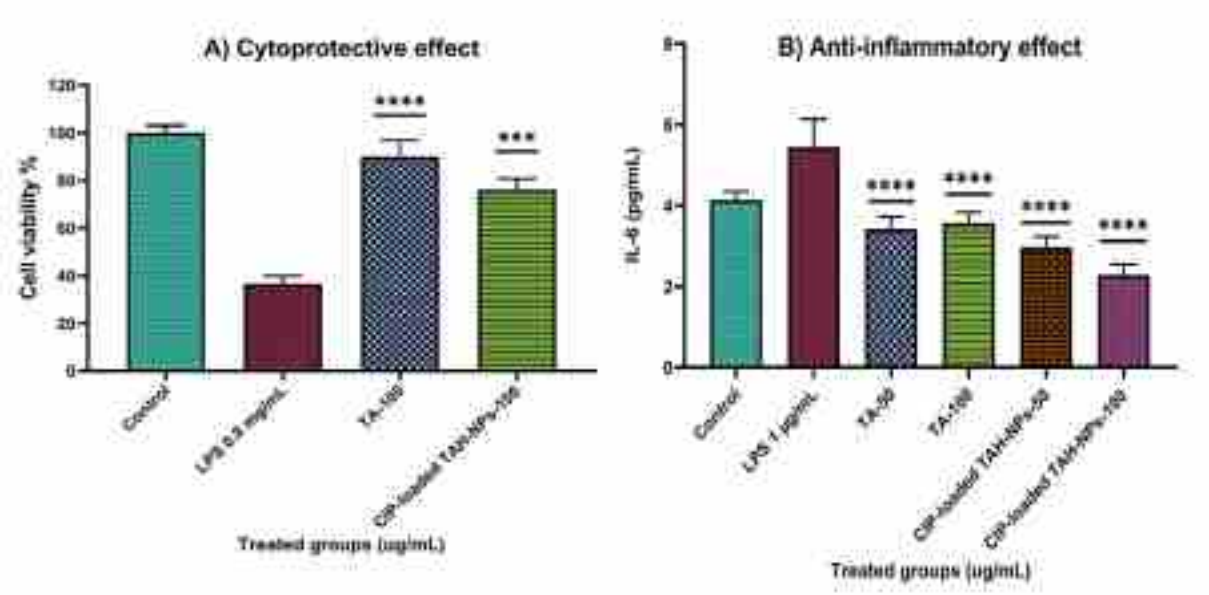

Figure 19. (**A**) Cytotoxicity of LPS on HepG2 cells and the protective effects of TA and CIP-loaded TAH-NPs as measured by MTT assy, and (**B**) Effect of TA and CIP-loaded TAH-NPs on IL-6 expression induced by LPS. (**** *P*-value<0.0001, *** *P*-value = 0.0005, in comparison with the LPS-treated cells). Data in the graph are presented as mean ± SD (n =3)

4. Conclusion

The creation of intelligent and effective multifunctional drug nanocarriers for antibiotic delivery against sepsis-causing bacteria has attracted a lot of interest. Herein, we aimed to develop a novel biomimetic TAH-NPs that could enhance the delivery of ciprofloxacin to combat bacterial-induced sepsis. The successful formulation of CIP-loaded TAH-NPs using a hot ultrasonic dispersion method

resulted in hybrid NPs with a good morphology, suitable size, low polydispersity index, acceptable zeta potential, and high encapsulation efficiency and drug loading. The biocompatibility of the prepared CIP-loaded TAH-NPs was confirmed by MTT and hemolysis assays. TA and its CIP-loaded NPs showed excellent *in-silico* and *in vitro* binding potential to human TLR4 with higher binding affinity than its natural substrate, LPS, indicating possible competitive inhibition activity to modulate the host immune response and reduce LPS -induced sepsis pathogenicity and organ dysfunction. *In vitro* drug release profile of the loaded CIP was found to be sustained over a period of 72 hrs. CIP-loaded TAH-NPs demonstrated excellent and sustained antibacterial, antibiofilm and efflux pump inhibition activities on both MRSA and *P.aeruginosa*. This could lead to effectively combat the well-known antimicrobial resistance mechanisms, while also improving CIP delivery and achieving better sepsis treatment outcomes. Also, the time-killing assay and flow cytometry analysis revealed the potential of CIP-loaded TAH-NPs to kill both MRSA and *P.aeruginosa*. Furthermore, CIP-loaded TAH-NPs demonstrated considerable free radical scavenging capabilities, as well as notable cytoprotective and anti-inflammatory efficacy against LPS-triggered inflammation. Accordingly, our research findings provides a simple and reliable nanoplatform to fight MDR bacteria and treat bacterial sepsis. It also helps to expand the pool of hybrid NPs available for delivering antibiotics along with a natural biomimetic and synergistic adjuvant against sepsis-inducing pathogens.

References

380. Pant, A., I. Mackraj, and T. Govender, *Advances in sepsis diagnosis and management: a paradigm shift towards nanotechnology.* J. Biomed. Sci., 2021. **28**(1): p. 6. https://doi.org/10.1186/s12929-020-00702-6
381. Duan, C., Y. Wang, Q. Wang, J. Li, J. Xie, S. Liu, J. Yang, Y. Huang, W. Zhao, and W. Yin, *Gram negative bacterial infection causes aggravated innate immune response in sepsis: Studies from clinical study and cellular models.* Biochem Biophys Res Commun, 2023. https://doi.org/10.1016/j.bbrc.2023.01.048
382. WHO. *WHO calls for global action on sepsis - cause of 1 in 5 deaths worldwide*. 2020 08 September 2020 [cited 2020 03 February 2023]; Available from: https://www.who.int/news/item/08-09-2020-who-calls-for-global-action-on-sepsis---cause-of-1-in-5-deaths-worldwide.
383. Rafiei, A., A. Rezaee, F. Hajati, S. Gheisari, and M. Golzan, *SSP: Early prediction of sepsis using fully connected LSTM-CNN model.* Comput. Biol. Med., 2021. **128**: p. 104110. https://doi.org/10.1016/j.compbiomed.2020.104110
384. CDC. *What is Sepsis*. 2022 09 August 2022 [cited 2022 05 February 2023]; Available from: https://www.cdc.gov/sepsis/what-is-sepsis.html.
385. Mohsen, N., K.S.I. Christopher J. L. M., Fablina Sharara, , G.R.A. Lucien Swetschinski, and C.M. Authia Gray, Christiane Dolecek., *Global burden of bacterial antimicrobial resistance in 2019: a systematic analysis.* Lancet, 2022. **399**(10325): p. 629-655. https://doi.org/10.1016/s0140-6736(21)02724-0

386. Lai, C.-C., S.-Y. Chen, W.-C. Ko, and P.-R. Hsueh, *Increased antimicrobial resistance during the COVID-19 pandemic.* Int. J. Antimicrob. Agents, 2021. **57**(4): p. 106324. https://doi.org/https://doi.org/10.1016/j.ijantimicag.2021.106324
387. Ghosh, S., C. Bornman, and M.M. Zafer, *Antimicrobial Resistance Threats in the emerging COVID-19 pandemic: Where do we stand?* J. Infect. Public Health, 2021. **14**(5): p. 555-560. https://doi.org/10.1016/j.jiph.2021.02.011
388. Zhao, Y., M. Pu, J. Zhang, Y. Wang, X. Yan, L. Yu, and Z. He, *Recent advancements of nanomaterial-based therapeutic strategies toward sepsis: bacterial eradication, anti-inflammation, and immunomodulation.* Nanoscale, 2021. **13**(24): p. 10726-10747. https://doi.org/10.1039/d1nr02706a
389. Alam, M.S., K.K. Pillai, S.A.H. Abdi, P. Kapur, P.K. Pillai, and K. Nagarajan, *Adverse drug reaction monitoring during antimicrobial therapy for septicemia patients at a university hospital in New Delhi.* Korean J. Intern. Med., 2018. **33**(6): p. 1203-1209. https://doi.org/10.3904/kjim.2016.001
390. Hetta, H.F., Y.N. Ramadan, A.I. Al-Harbi, E. A. Ahmed, B. Battah, N.H. Abd Ellah, S. Zanetti, and M.G. Donadu, *Nanotechnology as a Promising Approach to Combat Multidrug Resistant Bacteria: A Comprehensive Review and Future Perspectives.* Biomedicines, 2023. **11**(2): p. 413. https://doi.org/10.3390/biomedicines11020413
391. Van Giau, V., S.S.A. An, and J. Hulme, *Recent advances in the treatment of pathogenic infections using antibiotics and nano-drug delivery vehicles.* Drug Des. Devel. Ther., 2019. **13**: p. 327-343. https://doi.org/10.2147/DDDT.S190577
392. Patra, J.K., G. Das, L.F. Fraceto, E.V.R. Campos, M.d.P. Rodriguez-Torres, L.S. Acosta-Torres, L.A. Diaz-Torres, R. Grillo, M.K. Swamy, S. Sharma, S. Habtemariam, and H.-S. Shin, *Nano based drug delivery systems: recent developments and future prospects.* J. Nanobiotechnology, 2018. **16**(1): p. 71. https://doi.org/10.1186/s12951-018-0392-8
393. Zazo, H., C.I. Colino, and J.M. Lanao, *Current applications of nanoparticles in infectious diseases.* J Control Release, 2016. **224**: p. 86-102. https://doi.org/10.1016/j.jconrel.2016.01.008
394. Tu, Y., F. Peng, A. Adawy, Y. Men, L.K.E.A. Abdelmohsen, and D.A. Wilson, *Mimicking the Cell: Bio-Inspired Functions of Supramolecular Assemblies.* Chem. Rev., 2016. **116**(4): p. 2023-2078. https://doi.org/10.1021/acs.chemrev.5b00344
395. Naziris, N., N. Pippa, S. Pispas, and C. Demetzos, *Stimuli-responsive Drug Delivery Nanosystems: From Bench to Clinic.* Recent Pat Nanomed, 2016. **6**(3): p. 166-185.
396. Li, X., B. Wu, H. Chen, K. Nan, Y. Jin, L. Sun, and B. Wang, *Recent developments in smart antibacterial surfaces to inhibit biofilm formation and bacterial infections.* J. Mater. Chem. B, 2018. **6**(26): p. 4274-4292. https://doi.org/10.1039/c8tb01245h
397. Yu, H., M. Wu, S. Chen, M. Song, and Y. Yue, *Biomimetic nanoparticles for tumor immunotherapy.* Front. bioeng. biotechnol., 2022. **10**. https://doi.org/10.3389/fbioe.2022.989881
398. Kumar, S., H. Ingle, D.V.R. Prasad, and H. Kumar, *Recognition of bacterial infection by innate immune sensors.* Crit. Rev. Microbiol., 2013. **39**(3): p. 229-246. https://doi.org/10.3109/1040841X.2012.706249
399. Anwar, M.A., S. Basith, and S. Choi, *Negative regulatory approaches to the attenuation of Toll-like receptor signaling.* Exp. Mol. Med, 2013. **45**(2): p. e11-e11. https://doi.org/10.1038/emm.2013.28
400. Mehta, S., A. Suresh, Y. Nayak, R. Narayan, and U.Y. Nayak, *Hybrid nanostructures: Versatile systems for biomedical applications.* Coord. Chem. Rev., 2022. **460**: p. 214482. https://doi.org/10.1016/j.ccr.2022.214482

401. Mukherjee, A., A.K. Waters, P. Kalyan, A.S. Achrol, S. Kesari, and V.M. Yenugonda, *Lipid-polymer hybrid nanoparticles as a next-generation drug delivery platform: state of the art, emerging technologies, and perspectives.* Int J Nanomedicine, 2019. **14**: p. 1937-1952. https://doi.org/10.2147/ijn.S198353
402. Liang, X., K. Cao, W. Li, X. Li, D.J. McClements, and K. Hu, *Tannic acid-fortified zein-pectin nanoparticles: Stability, properties, antioxidant activity, and in vitro digestion.* Food Res Int, 2021. **145**: p. 110425. https://doi.org/10.1016/j.foodres.2021.110425
403. Nguyen, K.T. and Y. Zhao, *Engineered Hybrid Nanoparticles for On-Demand Diagnostics and Therapeutics.* Acc. Chem. Res., 2015. **48**(12): p. 3016-3025. https://doi.org/10.1021/acs.accounts.5b00316
404. Bigham, A., V. Rahimkhoei, P. Abasian, M. Delfi, J. Naderi, M. Ghomi, F. Dabbagh Moghaddam, T. Waqar, Y. Nuri Ertas, S. Sharifi, N. Rabiee, S. Ersoy, A. Maleki, E. Nazarzadeh Zare, E. Sharifi, E. Jabbari, P. Makvandi, and A. Akbari, *Advances in tannic acid-incorporated biomaterials: Infection treatment, regenerative medicine, cancer therapy, and biosensing.* J. Chem. Eng., 2022. **432**: p. 134146. https://doi.org/10.1016/j.cej.2021.134146
405. Hussain, T., B. Tan, Y. Yin, F. Blachier, M.C.B. Tossou, and N. Rahu, *Oxidative Stress and Inflammation: What Polyphenols Can Do for Us?* Oxid Med Cell Longev, 2016. **2016**: p. 7432797. https://doi.org/10.1155/2016/7432797
406. Adebayo, S.A., J.P. Dzoyem, L.J. Shai, and J.N. Eloff, *The anti-inflammatory and antioxidant activity of 25 plant species used traditionally to treat pain in southern African.* BMC Complement Altern. Med., 2015. **15**(1): p. 159. https://doi.org/10.1186/s12906-015-0669-5
407. Song, D., J. Zhao, W. Deng, Y. Liao, X. Hong, and J. Hou, *Tannic acid inhibits NLRP3 inflammasome-mediated IL-1β production via blocking NF-κB signaling in macrophages.* Biochem Biophys Res Commun, 2018. **503**(4): p. 3078-3085. https://doi.org/10.1016/j.bbrc.2018.08.096
408. Sivanantham, A., D. Pattarayan, R. Bethunaickan, A. Kar, S.K. Mahapatra, R.K. Thimmulappa, R. Palanichamy, and S. Rajasekaran, *Tannic acid protects against experimental acute lung injury through downregulation of TLR4 and MAPK.* Journal of Cellular Physiology, 2019. **234**(5): p. 6463-6476. https://doi.org/https://doi.org/10.1002/jcp.27383
409. Sameer, A.S. and S. Nissar, *Toll-Like Receptors (TLRs): Structure, Functions, Signaling, and Role of Their Polymorphisms in Colorectal Cancer Susceptibility.* Biomed Res. Int., 2021. **2021**: p. 1157023. https://doi.org/10.1155/2021/1157023
410. Ranjbaran, M., F. Kianian, G. Ashabi, K. Lorian, and F. Azizi, *Beneficial effects of tannic acid on comorbid anxiety in cecal ligation and puncture-induced sepsis in rats and potential underlying mechanisms.* Naunyn Schmiedebergs Arch. Pharmacol., 2023. **396**(5): p. 1019-1030. https://doi.org/10.1007/s00210-022-02374-5
411. Dong, G., H. Liu, X. Yu, X. Zhang, H. Lu, T. Zhou, and J. Cao, *Antimicrobial and anti-biofilm activity of tannic acid against Staphylococcus aureus.* Nat. Prod. Res., 2018. **32**(18): p. 2225-2228. https://doi.org/10.1080/14786419.2017.1366485
412. Tintino, S.R., C.D. Morais-Tintino, F.F. Campina, M.D.S. Costa, I.R.A. Menezes, Y. de Matos, J.T. Calixto-Júnior, P.S. Pereira, J.P. Siqueira-Junior, T.C. Leal-Balbino, H.D.M. Coutinho, and V.Q. Balbino, *Tannic acid affects the phenotype of Staphylococcus aureus resistant to tetracycline and erythromycin by inhibition of efflux pumps.* Bioorg. Chem. , 2017. **74**: p. 197-200. https://doi.org/10.1016/j.bioorg.2017.08.004
413. Tintino, S.R., C.D.M. Oliveira-Tintino, F.F. Campina, R.L.P. Silva, M.d.S. Costa, I.R.A. Menezes, J.T. Calixto-Júnior, J.P. Siqueira-Junior, H.D.M. Coutinho, T.C. Leal-Balbino, and V.Q. Balbino, *Evaluation of the tannic acid inhibitory effect against the NorA efflux pump of Staphylococcus aureus.* Microb. Pathog., 2016. **97**: p. 9-13. https://doi.org/https://doi.org/10.1016/j.micpath.2016.04.003

414. Villanueva, X., L. Zhen, J.N. Ares, T. Vackier, H. Lange, C. Crestini, and H.P. Steenackers, *Effect of chemical modifications of tannins on their antimicrobial and antibiofilm effect against Gram-negative and Gram-positive bacteria.* Front. microbiol., 2022. **13**: p. 987164. https://doi.org/10.3389/fmicb.2022.987164
415. Li, Z., Y. Feng, S. Zhang, T. Li, H. Li, D. Wang, K. Hao, C. He, H. Tian, and X. Chen, *A Multifunctional Nanoparticle Mitigating Cytokine Storm by Scavenging Multiple Inflammatory Mediators of Sepsis.* ACS Nano, 2023. **17**(9): p. 8551-8563. https://doi.org/10.1021/acsnano.3c00906
416. Kitahara, T., N. Koyama, J. Matsuda, Y. Aoyama, Y. Hirakata, S. Kamihira, S. Kohno, M. Nakashima, and H. Sasaki, *Antimicrobial activity of saturated fatty acids and fatty amines against methicillin-resistant Staphylococcus aureus.* Biol. Pharm. Bull., 2004. **27**(9): p. 1321-6. https://doi.org/10.1248/bpb.27.1321
417. Hassan, D., C.A. Omolo, V.O. Fasiku, C. Mocktar, and T. Govender, *Novel chitosan-based pH-responsive lipid-polymer hybrid nanovesicles (OLA-LPHVs) for delivery of vancomycin against methicillin-resistant Staphylococcus aureus infections.* Int. J. Biol. Macromol., 2020. **147**: p. 385-398. https://doi.org/10.1016/j.ijbiomac.2020.01.019
418. Salih, M., C.A. Omolo, N. Agrawal, P. Walvekar, A.Y. Waddad, C. Mocktar, C. Ramdhin, and T. Govender, *Supramolecular amphiphiles of Beta-cyclodextrin and Oleylamine for enhancement of vancomycin delivery.* Int. J. Pharm., 2020. **574**: p. 118881. https://doi.org/10.1016/j.ijpharm.2019.118881
419. Desbois, A.P. and K.C. Lawlor, *Antibacterial Activity of Long-Chain Polyunsaturated Fatty Acids against Propionibacterium acnes and Staphylococcus aureus.* Marine drugs, 2013. **11**(11): p. 4544-4557.
420. Khurana, C., A.K. Vala, N. Andhariya, O.P. Pandey, and B. Chudasama, *Antibacterial activity of silver: the role of hydrodynamic particle size at nanoscale.* J Biomed Mater Res A 2014. **102**(10): p. 3361-8. https://doi.org/10.1002/jbm.a.35005
421. Sonawane, S.J., R.S. Kalhapure, S. Rambharose, C. Mocktar, S.B. Vepuri, M. Soliman, and T. Govender, *Ultra-small lipid-dendrimer hybrid nanoparticles as a promising strategy for antibiotic delivery: In vitro and in silico studies.* Int. J. Pharm., 2016. **504**(1-2): p. 1-10. https://doi.org/10.1016/j.ijpharm.2016.03.021
422. Pettersen, E.F., T.D. Goddard, C.C. Huang, G.S. Couch, D.M. Greenblatt, E.C. Meng, and T.E. Ferrin, *UCSF Chimera—A visualization system for exploratory research and analysis.* J. Comput. Chem., 2004. **25**(13): p. 1605-1612. https://doi.org/10.1002/jcc.20084
423. Rajendran, P., R. Rathinasabapathy, S. Chandra Kishore, and S. Bellucci, *Computational-Simulation-Based Behavioral Analysis of Chemical Compounds.* J. Compos. Sci., 2023. **7**(5): p. 196. https://doi.org/10.3390/jcs7050196
424. Vanommeslaeghe, K., E. Hatcher, C. Acharya, S. Kundu, S. Zhong, J. Shim, E. Darian, O. Guvench, P. Lopes, I. Vorobyov, and A.D. Mackerell Jr., *CHARMM general force field: A force field for drug-like molecules compatible with the CHARMM all-atom additive biological force fields.* J. Comput. Chem., 2010. **31**(4): p. 671-690. https://doi.org/10.1002/jcc.21367
425. Mark, P. and L. Nilsson, *Structure and Dynamics of the TIP3P, SPC, and SPC/E Water Models at 298 K.* J. Phys. Chem. A, 2001. **105**(43): p. 9954-9960. https://doi.org/10.1021/jp003020w
426. Parrinello, M. and A. Rahman, *Polymorphic transitions in single crystals: A new molecular dynamics method.* 1981. **52**: p. 7182-7190. https://doi.org/10.1063/1.328693
427. Abraham, M., D. Van Der Spoel, E. Lindahl, and B. Hess, *the GROMACS development team, GROMACS User Manual version 2018*. 2018.
428. Darden, T., D. York, and L. Pedersen, *Particle mesh Ewald: An Nślog(N) method for Ewald sums in large systems.* 1993. **98**: p. 10089-10092. https://doi.org/10.1063/1.464397

429. Humphrey, W., A. Dalke, and K.J.J.o.m.g. Schulten, *VMD: visual molecular dynamics.* 1996. **14**(1): p. 33-38.
430. Kumari, R., R. Kumar, and A. Lynn, *g_mmpbsa—A GROMACS Tool for High-Throughput MM-PBSA Calculations.* J. Chem. Inf. Model, 2014. **54**(7): p. 1951-1962. https://doi.org/10.1021/ci500020m
431. Park, B.S., D.H. Song, H.M. Kim, and J.-O. Lee. *Crystal structure of the human TLR4-human MD-2-E.coli LPS Ra complex*. 2009 03 March 2009 [cited 2023 11 November 2023]; Available from: https://www.rcsb.org/structure/3FXI.
432. Berman, H.M., T. Battistuz, T.N. Bhat, W.F. Bluhm, P.E. Bourne, K. Burkhardt, Z. Feng, G.L. Gilliland, L. Iype, S. Jain, P. Fagan, J. Marvin, D. Padilla, V. Ravichandran, B. Schneider, N. Thanki, H. Weissig, J.D. Westbrook, and C. Zardecki, *The Protein Data Bank.* Acta Crystallogr. D: Struct. Biol., 2002. **58**(6-1): p. 899-907. https://doi.org/10.1107/S0907444902003451
433. Tang, X.D., S.H. Chang, Q.H. Luo, Z.Y. Zhang, and H.H. Dong. *Cryo-EM structure of LptB2FGC in complex with lipopolysaccharide*. 2019 25 September 2019 [cited 2023 11 November 2023]; Available from: https://www.rcsb.org/structure/6s8n.
434. Park, B.S., D.H. Song, H.M. Kim, B.-S. Choi, H. Lee, and J.-O. Lee, *The structural basis of lipopolysaccharide recognition by the TLR4–MD-2 complex.* Nature, 2009. **458**(7242): p. 1191-1195. https://doi.org/10.1038/nature07830
435. Kim, S., J. Chen, T. Cheng, A. Gindulyte, J. He, S. He, Q. Li, B.A. Shoemaker, P.A. Thiessen, B. Yu, L. Zaslavsky, J. Zhang, and E.E. Bolton, *PubChem 2019 update: improved access to chemical data.* Nucleic Acids Res., 2018. **47**(D1): p. D1102-D1109. https://doi.org/10.1093/nar/gky1033
436. Kerwin, S.M., *ChemBioOffice Ultra 2010 Suite.* J. Am. Chem. Soc., 2010. **132**(7): p. 2466-2467. https://doi.org/10.1021/ja1005306
437. Kusumaningrum, S. and E.B. , Soleh Kosela, Wahono Sumaryono, Fifit Juniarti, *The molecular docking of 1,4-naphthoquinone derivatives as inhibitors of Polo-like kinase 1 using Molegro Virtual Docker*. Vol. Volume: 4;. 2014: ssue: 11. 047-053.
438. Thomsen, R. and M.H. Christensen, *MolDock: A New Technique for High-Accuracy Molecular Docking.* J. Med. Chem., 2006. **49**(11): p. 3315-3321. https://doi.org/10.1021/jm051197e
439. Salifu, E.Y., A.R. Issahaku, C. Agoni, M.A.A. Ibrahim, N. Manimbulu, and M.E.S. Soliman, *Prioritizing the Catalytic Gatekeepers through Pan- Inhibitory Mechanism of Entrectinib against ALK, ROS1 and TRKA Tyrosine Kinases.* Cell Biochem Biophys, 2022. **80**(1): p. 11-21. https://doi.org/10.1007/s12013-021-01052-2
440. Trott, O. and A.J. Olson, *AutoDock Vina: Improving the speed and accuracy of docking with a new scoring function, efficient optimization, and multithreading.* J. Comput. Chem., 2010. **31**(2): p. 455-461. https://doi.org/10.1002/jcc.21334
441. Eberhardt, J., D. Santos-Martins, A.F. Tillack, and S. Forli, *AutoDock Vina 1.2.0: New Docking Methods, Expanded Force Field, and Python Bindings.* J Chem Inf Model, 2021. **61**(8): p. 3891-3898. https://doi.org/10.1021/acs.jcim.1c00203
442. Ben-Shalom, I.Y., C. Lin, T. Kurtzman, R.C. Walker, and M.K. Gilson, *Simulating Water Exchange to Buried Binding Sites.* J. Chem. Theory Comput., 2019. **15**(4): p. 2684-2691. https://doi.org/10.1021/acs.jctc.8b01284
443. Salomon-Ferrer, R., D.A. Case, and R.C. Walker, *An overview of the Amber biomolecular simulation package.* Wiley Interdiscip. Rev. Comput. Mol. Sci., 2013. **3**(2): p. 198-210. https://doi.org/10.1002/wcms.1121
444. Ponder, J.W. and D.A. Case, *Force Fields for Protein Simulations*, in *Adv. Protein Chem.* 2003, Academic Press. p. 27-85 https://doi.org/10.1016/S0065-3233(03)66002-X

445. Wang, J., R.M. Wolf, J.W. Caldwell, P.A. Kollman, and D.A. Case, *Development and testing of a general amber force field.* J. Comput. Chem., 2004. **25**(9): p. 1157-1174. https://doi.org/10.1002/jcc.20035
446. Grest, G.S. and K. Kremer, *Molecular dynamics simulation for polymers in the presence of a heat bath.* Phys. Rev. A, 1986. **33**(5): p. 3628-3631. https://doi.org/10.1103/PhysRevA.33.3628
447. Hanwell, M.D., D.E. Curtis, D.C. Lonie, T. Vandermeersch, E. Zurek, and G.R. Hutchison, *Avogadro: an advanced semantic chemical editor, visualization, and analysis platform.* J. Cheminformatics, 2012. **4**(1): p. 17. https://doi.org/10.1186/1758-2946-4-17
448. Berendsen, H.J.C., J.P.M. Postma, W.F. van Gunsteren, A. DiNola, and J.R. Haak, *Molecular dynamics with coupling to an external bath.* J. Chem. Phys., 1984. **81**(8): p. 3684-3690. https://doi.org/10.1063/1.448118
449. Ryckaert, J.-P., G. Ciccotti, and H.J.C. Berendsen, *Numerical integration of the cartesian equations of motion of a system with constraints: molecular dynamics of n-alkanes.* J. Comput. Phys., 1977. **23**(3): p. 327-341. https://doi.org/10.1016/0021-9991(77)90098-5
450. Roe, D.R. and T.E. Cheatham, III, *PTRAJ and CPPTRAJ: Software for Processing and Analysis of Molecular Dynamics Trajectory Data.* J. Chem. Theory Comput., 2013. **9**(7): p. 3084-3095. https://doi.org/10.1021/ct400341p
451. Seifert, E., *OriginPro 9.1: Scientific Data Analysis and Graphing Software—Software Review.* J. Chem. Inf. Model., 2014. **54**(5): p. 1552-1552. https://doi.org/10.1021/ci500161d
452. Hess, B., H. Bekker, H.J.C. Berendsen, and J.G.E.M. Fraaije, *LINCS: A linear constraint solver for molecular simulations.* J. Comput. Chem., 1997. **18**(12): p. 1463-1472. https://doi.org/10.1002/(SICI)1096-987X(199709)18:12<1463::AID-JCC4>3.0.CO;2-H
453. Hou, T., J. Wang, Y. Li, and W. Wang, *Assessing the performance of the molecular mechanics/Poisson Boltzmann surface area and molecular mechanics/generalized Born surface area methods. II. The accuracy of ranking poses generated from docking.* J. Comput. Chem., 2011. **32**(5): p. 866-877. https://doi.org/10.1002/jcc.21666
454. Dong, L., X. Qu, Y. Zhao, and B. Wang, *Prediction of Binding Free Energy of Protein–Ligand Complexes with a Hybrid Molecular Mechanics/Generalized Born Surface Area and Machine Learning Method.* ACS Omega, 2021. **6**(48): p. 32938-32947. https://doi.org/10.1021/acsomega.1c04996
455. Hou, T., J. Wang, Y. Li, and W. Wang, *Assessing the Performance of the MM/PBSA and MM/GBSA Methods. 1. The Accuracy of Binding Free Energy Calculations Based on Molecular Dynamics Simulations.* Journal of Chemical Information and Modeling, 2011. **51**(1): p. 69-82. https://doi.org/10.1021/ci100275a
456. EUCAST, E.C.f.S., *Terminology relating to methods for the determination of susceptibility of bacteria to antimicrobial agents.* Clin. Microbiol. Infect, 2000. **6**(9): p. 503-508. https://doi.org/https://doi.org/10.1046/j.1469-0691.2000.00149.x
457. McKinnon, K.M., *Flow Cytometry: An Overview.* Curr Protoc Immunol 2018. **120**: p. 5.1.1-5.1.11. https://doi.org/10.1002/cpim.40
458. Khan, F., P. Manivasagan, D.T.N. Pham, J. Oh, S.K. Kim, and Y.M. Kim, *Antibiofilm and antivirulence properties of chitosan-polypyrrole nanocomposites to Pseudomonas aeruginosa.* Microb. Pathog., 2019. **128**: p. 363-373. https://doi.org/10.1016/j.micpath.2019.01.033
459. Olchowik-Grabarek, E., S. Sekowski, M. Bitiucki, I. Dobrzynska, V. Shlyonsky, M. Ionov, P. Burzynski, A. Roszkowska, I. Swiecicka, N. Abdulladjanova, and M. Zamaraeva, *Inhibition of interaction between Staphylococcus aureus alpha-hemolysin and erythrocytes membrane by hydrolysable tannins: structure-related activity study.* Sci. Rep., 2020. **10**(1): p. 11168. https://doi.org/10.1038/s41598-020-68030-1

460. Tahir, N., A. Madni, V. Balasubramanian, M. Rehman, A. Correia, P.M. Kashif, E. Makila, J. Salonen, and H.A. Santos, *Development and optimization of methotrexate-loaded lipid-polymer hybrid nanoparticles for controlled drug delivery applications.* Int. J. Pharm., 2017. **533**(1): p. 156-168. https://doi.org/10.1016/j.ijpharm.2017.09.061
461. Omer, M.E., M. Halwani, R.M. Alenazi, O. Alharbi, S. Aljihani, S. Massadeh, M. Al Ghoribi, M. Al Aamery, and A.E. Yassin, *Novel Self-Assembled Polycaprolactone-Lipid Hybrid Nanoparticles Enhance the Antibacterial Activity of Ciprofloxacin.* SLAS Technol, 2020. **25**(6): p. 598-607. https://doi.org/10.1177/2472630320943126
462. Cheow, W.S. and K. Hadinoto, *Factors affecting drug encapsulation and stability of lipid-polymer hybrid nanoparticles.* Colloids Surf. B, 2011. **85**(2): p. 214-20. https://doi.org/10.1016/j.colsurfb.2011.02.033
463. Santhanes, D., A. Wilkins, H. Zhang, R. John Aitken, and M. Liang, *Microfluidic formulation of lipid/polymer hybrid nanoparticles for plasmid DNA (pDNA) delivery.* Int. J. Pharm., 2022. **627**: p. 122223. https://doi.org/10.1016/j.ijpharm.2022.122223
464. Godara, S., V. Lather, S.V. Kirthanashri, R. Awasthi, and D. Pandita, *Lipid-PLGA hybrid nanoparticles of paclitaxel: Preparation, characterization, in vitro and in vivo evaluation.* Mater. Sci. Eng. C, 2020. **109**: p. 110576. https://doi.org/10.1016/j.msec.2019.110576
465. Nwabuife, J.C., D. Hassan, A. Madhaorao Pant, N. Devnarain, M.A. Gafar, N. Osman, S. Rambharose, and T. Govender, *Novel vancomycin free base – Sterosomes for combating diseases caused by Staphylococcus aureus and Methicillin-resistant Staphylococcus aureus infections (S. Aureus and MRSA).* J Drug Deliv Sci Technol 2023. **79**: p. 104089. https://doi.org/10.1016/j.jddst.2022.104089
466. Perumal, P.O., P. Mhlanga, A.M. Somboro, D.G. Amoako, H.M. Khumalo, and R.M. Khan, *Cytoproliferative and Anti-Oxidant Effects Induced by Tannic Acid in Human Embryonic Kidney (Hek-293) Cells.* Biomolecules, 2019. **9**(12): p. 767. https://doi.org/10.3390/biom9120767
467. Hapidin, H., N.A.A. Romli, and H. Abdullah, *Proliferation study and microscopy evaluation on the effects of tannic acid in human fetal osteoblast cell line (hFOB 1.19).* Microsc. Res. Tech., 2019. **82**(11): p. 1928-1940. https://doi.org/10.1002/jemt.23361
468. Gayathri, N.K., V. Aparna, S. Maya, R. Biswas, R. Jayakumar, and C.G. Mohan, *Preparation, characterization, drug release and computational modelling studies of antibiotics loaded amorphous chitin nanoparticles.* Carbohydr. Polym., 2017. **177**: p. 67-76. https://doi.org/10.1016/j.carbpol.2017.08.112
469. Kuzmich, N.N., K.V. Sivak, V.N. Chubarev, Y.B. Porozov, T.N. Savateeva-Lyubimova, and F. Peri, *TLR4 Signaling Pathway Modulators as Potential Therapeutics in Inflammation and Sepsis.* Vaccines, 2017. **5**(4): p. 34. https://doi.org/10.3390/vaccines5040034
470. Sivanantham, A., D. Pattarayan, R. Bethunaickan, A. Kar, S.K. Mahapatra, R.K. Thimmulappa, R. Palanichamy, and S. Rajasekaran, *Tannic acid protects against experimental acute lung injury through downregulation of TLR4 and MAPK.* J. Cell. Physiol., 2019. **234**(5): p. 6463-6476. https://doi.org/10.1002/jcp.27383
471. Zhang, R., M. Dang, S. Qiu, H. Gu, P. He, G. Guo, and T. Zhang, *Ameliorative effects of tannic acid on lipopolysaccharide-induced sepsis and acute lung injury in mice.* Pharmacogn. Mag., 2019. **15**(61): p. 238-243. https://doi.org/10.4103/pm.pm_364_18
472. Liu, K., E. Watanabe, and H. Kokubo, *Exploring the stability of ligand binding modes to proteins by molecular dynamics simulations.* J. Comput. Aided Mol. Des. , 2017. **31**(2): p. 201-211. https://doi.org/10.1007/s10822-016-0005-2
473. Anwar, M.A., S. Panneerselvam, M. Shah, and S. Choi, *Insights into the species-specific TLR4 signaling mechanism in response to Rhodobacter sphaeroides lipid A detection.* Sci. Rep., 2015. **5**(1): p. 7657. https://doi.org/10.1038/srep07657

474. Ma, B., M. Shatsky, H.J. Wolfson, and R. Nussinov, *Multiple diverse ligands binding at a single protein site: A matter of pre-existing populations.* Protein Sci., 2002. **11**(2): p. 184-197. https://doi.org/10.1110/ps.21302
475. Carlson, H.A. and J.A. McCammon, *Accommodating Protein Flexibility in Computational Drug Design* Mol. Pharmacol.

, 2000. **57**(2): p. 213-218.
476. Yang, C.-Y., R. Wang, and S. Wang, *A Systematic Analysis of the Effect of Small-Molecule Binding on Protein Flexibility of the Ligand-Binding Sites.* J. Med. Chem., 2005. **48**(18): p. 5648-5650. https://doi.org/10.1021/jm050276n
477. Gonzalez-Ruiz, D. and H. Gohlke, *Targeting Protein-Protein Interactions with Small Molecules: Challenges and Perspectives for omputational Binding Epitope Detection and Ligand Finding.* Curr. Med. Chem., 2006. **13**(22): p. 2607-2625. https://doi.org/10.2174/092986706778201530
478. Nicholls, A., K.A. Sharp, and B. Honig, *Protein folding and association: Insights from the interfacial and thermodynamic properties of hydrocarbons.* Proteins: Structure, Function, and Bioinformatics, 1991. **11**(4): p. 281-296. https://doi.org/10.1002/prot.340110407
479. Zhou, H.-X. and X. Pang, *Electrostatic Interactions in Protein Structure, Folding, Binding, and Condensation.* Chem. Rev., 2018. **118**(4): p. 1691-1741. https://doi.org/10.1021/acs.chemrev.7b00305
480. Ausaf Ali, S., M. Imtaiyaz Hassan, A. Islam, and F. Ahmad, *A Review of Methods Available to Estimate Solvent-Accessible Surface Areas of Soluble Proteins in the Folded and Unfolded States.* Curr. Protein Pept. Sci., 2014. **15**(5): p. 456-476.
481. Joseph, M.H. and A. Georgios, *MM-GB(PB)SA Calculations of Protein-Ligand Binding Free Energies*, in *Molecular Dynamics*, W. Lichang, Editor. 2012, IntechOpen: Rijeka. p. Ch. 9 https://doi.org/10.5772/37107
482. De Vivo, M., M. Masetti, G. Bottegoni, and A. Cavalli, *Role of Molecular Dynamics and Related Methods in Drug Discovery.* J. Med. Chem., 2016. **59**(9): p. 4035-4061. https://doi.org/10.1021/acs.jmedchem.5b01684
483. Sivanantham, A., D. Pattarayan, N. Rajasekar, A. Kannan, L. Loganathan, R. Bethunaickan, S.K. Mahapatra, R. Palanichamy, K. Muthusamy, and S. Rajasekaran, *Tannic acid prevents macrophage-induced pro-fibrotic response in lung epithelial cells via suppressing TLR4-mediated macrophage polarization.* Inflamm. Res., 2019. **68**(12): p. 1011-1024. https://doi.org/10.1007/s00011-019-01282-4
484. Moran, A.P., B. Lindner, and E.J. Walsh, *Structural characterization of the lipid A component of Helicobacter pylori rough- and smooth-form lipopolysaccharides.* J. Bacteriol., 1997. **179**(20): p. 6453-6463. https://doi.org/doi:10.1128/jb.179.20.6453-6463.1997
485. Cheow, W.S. and K. Hadinoto, *Lipid-polymer hybrid nanoparticles with rhamnolipid-triggered release capabilities as anti-biofilm drug delivery vehicles.* Particuology, 2012. **10**(3): p. 327-333. https://doi.org/10.1016/j.partic.2011.08.007
486. Bhardwaj, A., S. Mehta, S. Yadav, S.K. Singh, A. Grobler, A.K. Goyal, and A. Mehta, *Pulmonary delivery of antitubercular drugs using spray-dried lipid-polymer hybrid nanoparticles.* Artif Cells Nanomed Biotechnol 2016. **44**(6): p. 1544-55. https://doi.org/10.3109/21691401.2015.1062389
487. Papadopoulou, V., K. Kosmidis, M. Vlachou, and P. Macheras, *On the use of the Weibull function for the discernment of drug release mechanisms.* Int. J. Pharm., 2006. **309**(1-2): p. 44-50. https://doi.org/10.1016/j.ijpharm.2005.10.044

488. Salih, M., C.A. Omolo, N. Agrawal, P. Walvekar, A.Y. Waddad, C. Mocktar, C. Ramdhin, and T. Govender, *Supramolecular amphiphiles of beta-cyclodextrin and oleylamine for enhancement of vancomycin delivery.* International Journal of Pharmaceutics, 2020. **574**: p. 118881.
489. Masadeh, M.M., K.H. Alzoubi, W.S. Ahmed, and A.S. Magaji, *In Vitro Comparison of Antibacterial and Antibiofilm Activities of Selected Fluoroquinolones against Pseudomonas aeruginosa and Methicillin-Resistant Staphylococcus aureus.* Pathogens, 2019. **8**(1). https://doi.org/10.3390/pathogens8010012
490. Jubeh, B., Z. Breijyeh, and R. Karaman, *Resistance of Gram-Positive Bacteria to Current Antibacterial Agents and Overcoming Approaches.* Molecules, 2020. **25**(12): p. 2888. https://doi.org/10.3390/molecules25122888
491. Kaczmarek, B., *Tannic Acid with Antiviral and Antibacterial Activity as A Promising Component of Biomaterials-A Minireview.* Materials (Basel), 2020. **13**(14). https://doi.org/10.3390/ma13143224
492. Lallo da Silva, B., M.P. Abuçafy, E. Berbel Manaia, J.A. Oshiro Junior, B.G. Chiari-Andréo, R.C.L.R. Pietro, and L.A. Chiavacci, *Relationship Between Structure And Antimicrobial Activity Of Zinc Oxide Nanoparticles: An Overview.* Int J Nanomedicine, 2019. **14**: p. 9395-9410. https://doi.org/10.2147/IJN.S216204
493. Sarkar, K., M. Kumar, A. Jha, K. Bharti, M. Das, and B. Mishra, *Nanocarriers for tuberculosis therapy: Design of safe and effective drug delivery strategies to overcome the therapeutic challenges.* J Drug Deliv Sci Technol, 2022. **67**: p. 102850. https://doi.org/10.1016/j.jddst.2021.102850
494. Ferreira, M., M. Ogren, J.N.R. Dias, M. Silva, S. Gil, L. Tavares, F. Aires-da-Silva, M.M. Gaspar, and S.I. Aguiar, *Liposomes as Antibiotic Delivery Systems: A Promising Nanotechnological Strategy against Antimicrobial Resistance.* Molecules, 2021. **26**(7): p. 2047.
495. Lambert, R.J.W. and R. Lambert, *A model for the efficacy of combined inhibitors.* J. Appl. Microbiol., 2003. **95**(4): p. 734-743. https://doi.org/10.1046/j.1365-2672.2003.02039.x
496. Odds, F.C., *Synergy, antagonism, and what the chequerboard puts between them.* Journal of Antimicrobial Chemotherapy, 2003. **52**(1): p. 1-1. https://doi.org/10.1093/jac/dkg301
497. Meletiadis, J., S. Pournaras, E. Roilides, and T.J. Walsh, *Defining Fractional Inhibitory Concentration Index Cutoffs for Additive Interactions Based on Self-Drug Additive Combinations, Monte Carlo Simulation Analysis, and In Vitro/In Vivo Correlation Data for Antifungal Drug Combinations against Aspergillus fumigatus.* Antimicrob Agents Chemother, 2010. **54**(2): p. 602-609. https://doi.org/doi:10.1128/AAC.00999-09
498. Baggio, D. and M.R. Ananda-Rajah, *Fluoroquinolone antibiotics and adverse events.* Aust. Prescr., 2021. **44**(5): p. 161-164. https://doi.org/10.18773/austprescr.2021.035
499. Uruén, C., G. Chopo-Escuin, J. Tommassen, R.C. Mainar-Jaime, and J. Arenas, *Biofilms as Promoters of Bacterial Antibiotic Resistance and Tolerance.* Antibiotics (Basel), 2020. **10**(1). https://doi.org/10.3390/antibiotics10010003
500. Khan, J., S.M. Tarar, I. Gul, U. Nawaz, and M. Arshad, *Challenges of antibiotic resistance biofilms and potential combating strategies: a review.* 3 Biotech, 2021. **11**(4): p. 169. https://doi.org/10.1007/s13205-021-02707-w
501. Sendamangalam, V., O.K. Choi, D. Kim, and Y. Seo, *The anti-biofouling effect of polyphenols against Streptococcus mutans.* Biofouling, 2011. **27**(1): p. 13-9. https://doi.org/10.1080/08927014.2010.535897
502. Payne, D.E., N.R. Martin, K.R. Parzych, A.H. Rickard, A. Underwood, and B.R. Boles, *Tannic acid inhibits Staphylococcus aureus surface colonization in an IsaA-dependent manner.* Infect Immun, 2013. **81**(2): p. 496-504. https://doi.org/10.1128/IAI.00877-12

503. Liu, L., C. Ge, Y. Zhang, W. Ma, X. Su, L. Chen, S. Li, L. Wang, X. Mu, and Y. Xu, *Tannic acid-modified silver nanoparticles for enhancing anti-biofilm activities and modulating biofilm formation.* Biomater. Sci., 2020. **8**(17): p. 4852-4860. https://doi.org/10.1039/d0bm00648c
504. Guardabassi, L. and P. Courvalin, *Modes of Antimicrobial Action and Mechanisms of Bacterial Resistance*, in *Antimicrobial Resistance in Bacteria of Animal Origin*, F.M. Aarestrup, Editor. 2005. p. 1-18 https://doi.org/10.1128/9781555817534.ch1
505. Redgrave, L.S., S.B. Sutton, M.A. Webber, and L.J.V. Piddock, *Fluoroquinolone resistance: mechanisms, impact on bacteria, and role in evolutionary success.* Trends Microbiol., 2014. **22**(8): p. 438-445. https://doi.org/10.1016/j.tim.2014.04.007
506. Srichaiyapol, O., S. Thammawithan, P. Siritongsuk, S. Nasompag, S. Daduang, S. Klaynongsruang, S. Kulchat, and R. Patramanon, *Tannic Acid-Stabilized Silver Nanoparticles Used in Biomedical Application as an Effective Antimelioidosis and Prolonged Efflux Pump Inhibitor against Melioidosis Causative Pathogen.* Molecules, 2021. **26**(4): p. 1004. https://doi.org/10.3390/molecules26041004
507. Baldwin, A. and B.W. Booth, *Biomedical applications of tannic acid.* J. Biomater. Appl, 2022. **36**(8): p. 1503-1523. https://doi.org/10.1177/08853282211058099
508. Seukep, A.J., V. Kuete, L. Nahar, S.D. Sarker, and M. Guo, *Plant-derived secondary metabolites as the main source of efflux pump inhibitors and methods for identification.* J. Pharm. Anal., 2020. **10**(4): p. 277-290. https://doi.org/10.1016/j.jpha.2019.11.002
509. Simoes, M., R.N. Bennett, and E.A. Rosa, *Understanding antimicrobial activities of phytochemicals against multidrug resistant bacteria and biofilms.* Nat. Prod. Rep., 2009. **26**(6): p. 746-57. https://doi.org/10.1039/b821648g
510. Rezaie, P., M. Pourhajibagher, N. Chiniforush, N. Hosseini, and A. Bahador, *The Effect of Quorum-Sensing and Efflux Pumps Interactions in Pseudomonas aeruginosa Against Photooxidative Stress.* J Lasers Med Sci, 2018. **9**(3): p. 161-167. https://doi.org/10.15171/jlms.2018.30
511. Soto, S.M., *Role of efflux pumps in the antibiotic resistance of bacteria embedded in a biofilm.* Virulence, 2013. **4**(3): p. 223-229. https://doi.org/10.4161/viru.23724
512. Rasamiravaka, T. and M. El Jaziri, *Quorum-Sensing Mechanisms and Bacterial Response to Antibiotics in P. aeruginosa.* Curr. Microbiol., 2016. **73**(5): p. 747-753. https://doi.org/10.1007/s00284-016-1101-1
513. Khan, F., P. Manivasagan, D.T.N. Pham, J. Oh, S.-K. Kim, and Y.-M. Kim, *Antibiofilm and antivirulence properties of chitosan-polypyrrole nanocomposites to Pseudomonas aeruginosa.* Microb. Pathog., 2019. **128**: p. 363-373. https://doi.org/10.1016/j.micpath.2019.01.033
514. Watkins, R.R., M.Z. David, and R.A. Salata, *Current concepts on the virulence mechanisms of meticillin-resistant Staphylococcus aureus.* J Med Microbiol Infect Dis 2012. **61**(Pt 9): p. 1179-1193. https://doi.org/10.1099/jmm.0.043513-0
515. Tun, T.N., P.J. Cameron, and A.T.A. Jenkins, *Sensing of pathogenic bacteria based on their interaction with supported bilayer membranes studied by impedance spectroscopy and surface plasmon resonance.* Biosens. Bioelectron., 2011. **28**(1): p. 227-231. https://doi.org/10.1016/j.bios.2011.07.023
516. Vasil, M.L., R.W. Prince, and V.D. Shortridge, *Exoproducts: Pseudomonas exotoxin A and phospholipase C*, in *Pseudomonas aeruginosa the opportunist: pathogenesis and disease. .* J. Robert B. Fick, Editor. 1992, CRC Press, Inc., Boca Raton, Fla J Bacteriol: London. p. 59-77
517. Ramachandran, G., *Gram-positive and gram-negative bacterial toxins in sepsis.* Virulence, 2014. **5**(1): p. 213-218. https://doi.org/10.4161/viru.27024
518. Sonnen, A.F.P. and P. Henneke, *Role of Pore-Forming Toxins in Neonatal Sepsis.* Clin Dev Immunol, 2013. **2013**: p. 608456. https://doi.org/10.1155/2013/608456

519. Minasyan, H., *Sepsis and septic shock: Pathogenesis and treatment perspectives.* J. Crit. Care, 2017. **40**: p. 229-242. https://doi.org/10.1016/j.jcrc.2017.04.015
520. Effenberger-Neidnicht, K. and M. Hartmann, *Mechanisms of Hemolysis During Sepsis.* Inflammation, 2018. **41**(5): p. 1569-1581. https://doi.org/10.1007/s10753-018-0810-y
521. Olchowik-Grabarek, E., S. Sekowski, M. Bitiucki, I. Dobrzynska, V. Shlyonsky, M. Ionov, P. Burzynski, A. Roszkowska, I. Swiecicka, N. Abdulladjanova, and M. Zamaraeva, *Inhibition of interaction between Staphylococcus aureus α-hemolysin and erythrocytes membrane by hydrolysable tannins: structure-related activity study.* Sci. Rep., 2020. **10**(1): p. 11168. https://doi.org/10.1038/s41598-020-68030-1
522. Veiko, A.G., E. Olchowik-Grabarek, S. Sekowski, A. Roszkowska, E.A. Lapshina, I. Dobrzynska, M. Zamaraeva, and I.B. Zavodnik, *Antimicrobial Activity of Quercetin, Naringenin and Catechin: Flavonoids Inhibit Staphylococcus aureus-Induced Hemolysis and Modify Membranes of Bacteria and Erythrocytes.* Molecules, 2023. **28**(3): p. 1252. https://doi.org/10.3390/molecules28031252
523. Olchowik-Grabarek, E., S. Sekowski, F. Mies, M. Bitiucki, I. Swiecicka, N. Abdulladjanova, V. Shlyonsky, and M. Zamaraeva, *Electrophysiological and spectroscopic investigation of hydrolysable tannins interaction with α-hemolysin of S. aureus.* Bioelectrochemistry, 2023. **150**: p. 108318. https://doi.org/10.1016/j.bioelechem.2022.108318
524. Hemati, S., F. Azizi-Jalilian, I. Pakzad, M. Taherikalani, A. Maleki, S. Karimi, A. Monjezei, Z. Mahdavi, M.R. Fadavi, K. Sayehmiri, and N. Sadeghifard, *The correlation between the presence of quorum sensing, toxin-antitoxin system genes and MIC values with ability of biofilm formation in clinical isolates of Pseudomonas aeruginosa.* Iran. J. Microbiol., 2014. **6**(3): p. 133-9.
525. Fleitas Martínez, O., M.H. Cardoso, S.M. Ribeiro, and O.L. Franco, *Recent Advances in Anti-virulence Therapeutic Strategies With a Focus on Dismantling Bacterial Membrane Microdomains, Toxin Neutralization, Quorum-Sensing Interference and Biofilm Inhibition.* Front Cell Infect Microbiol 2019. **9**. https://doi.org/10.3389/fcimb.2019.00074
526. Gulcin, İ. and S.H. Alwasel, *DPPH Radical Scavenging Assay.* Processes, 2023. **11**(8): p. 2248. https://doi.org/10.3390/pr11082248
527. Pucci, C., C. Martinelli, D. De Pasquale, M. Battaglini, N. di Leo, A. Degl'Innocenti, M. Belenli Gümüş, F. Drago, and G. Ciofani, *Tannic Acid–Iron Complex-Based Nanoparticles as a Novel Tool against Oxidative Stress.* ACS Appl. Mater. Interfaces, 2022. **14**(14): p. 15927-15941. https://doi.org/10.1021/acsami.1c24576
528. Choi, J.-M., J. Han, B.-S. Yoon, J.-H. Chung, D.-B. Shin, S.-K. Lee, J.-K. Hwang, and R. Ryang, *Antioxidant properties of tannic acid and its inhibitory effects on paraquat-induced oxidative stress in mice.* Food Sci. Biotechnol, 2006. **15**(5): p. 728-734.
529. Jing, Y., Y. Diao, and X. Yu, *Free radical-mediated conjugation of chitosan with tannic acid: Characterization and antioxidant capacity.* React. Funct. Polym, 2019. **135**: p. 16-22. https://doi.org/10.1016/j.reactfunctpolym.2018.12.005
530. Gülçin, İ., Z. Huyut, M. Elmastaş, and H.Y. Aboul-Enein, *Radical scavenging and antioxidant activity of tannic acid.* Arab. J. Chem., 2010. **3**(1): p. 43-53. https://doi.org/10.1016/j.arabjc.2009.12.008
531. Lou, W., Y. Chen, H. Ma, G. Liang, and B. Liu, *Antioxidant and α-amylase inhibitory activities of tannic acid.* J. Food Sci. Technol., 2018. **55**(9): p. 3640-3646. https://doi.org/10.1007/s13197-018-3292-x
532. Chen, J., Y. Liu, H. Luo, G. Chen, Z. Zheng, T. Wang, X. Hu, Y. Zhao, J. Tang, C. Su, and L. Zha, *Inflammation Induced by Lipopolysaccharide and Palmitic Acid Increases Cholesterol Accumulation via Enhancing Myeloid Differentiation Factor 88 Expression in HepG2 Cells.* Pharmaceuticals (Basel), 2022. **15**(7). https://doi.org/10.3390/ph15070813

533. Yang, Y.-P., J.-Q. Zhao, H.-B. Gao, J.-J. Li, X.-L. Li, X.-L. Niu, Y.-H. Lei, and X. Li, *Tannic acid alleviates lipopolysaccharide-induced H9C2 cell apoptosis by suppressing reactive oxygen species-mediated endoplasmic reticulum stress.* Mol. Med. Rep., 2021. **24**(1): p. 535. https://doi.org/10.3892/mmr.2021.12174
534. Srisangthong, P., A. Wongsa, P. Kittiworawitkul, and A. Wattanathum, *Early IL-6 response in sepsis is correlated with mortality and severity score.* Crit Care, 2013. **17**(2): p. P34. https://doi.org/10.1186/cc11972

CHAPTER 5. CO-AUTHORED PUBLICATIONS

5.1 General Introduction

In addition to the first-authored papers presented in Chapters 2, 3, and 4, I have also contributed as a co-author in another paper published by our group during the period of my Ph.D. study. This publication shared the same broad aims of this Ph.D. project to improve the delivery and effectiveness of antibiotics through the development of an advanced novel drug delivery system. As such, it has been included in this thesis. This chapter includes a review paper published in an ISI International Journals: WIREs Nanomedicine and Nanobiotechnology (Impact Factor: 9.125). In this paper, **Eman Elhassan** contributed towards the data curation; methodology; writing-original draft; writing-review and editing.

5.2 Co-authored paper 1

Exploring the applications of hyaluronic acid-based nanoparticles for diagnosis and treatment of bacterial infections.

Mahir Mohammed, Nikita Devnarain, **Eman Elhassan** and Thirumala Govender. (2022). WIREs Nanomedicine and Nanobiotechnology, 14(4), e1799. DOI: https://doi.org/https://doi.org/10.1002/wnan.1799. (Appendix III).

5.2.1 Abstract

Hyaluronic acid (HA) has become a topic of significant interest in drug delivery research due to its excellent properties, including biosafety, biodegradability, and non-immunogenicity. Moreover, due to its ease of modification, HA can be used to prepare several HA-based nanosystems using various approaches. These approaches involve conjugating/grafting of hydrophobic moieties, polyelectrolytes complexation with cationic polymers, or surface modification of various nanoparticles using HA. These nanoparticles are able to selectively deliver antibacterial drugs or diagnostic molecules into the site of infections. In addition, HA can bind with overexpressed cluster of differentiation 44 (CD44) receptors in macrophages and also can be degraded by a family of enzymes called hyaluronidase (HAase) to release drugs or molecules. By binding with these receptors or being degraded at the infection site by HAase, HA-based nanoparticles allow enhanced and targeted antibacterial delivery. Herein, we present a comprehensive and up-to-date review that highlights various techniques of preparation of HA-based nanoparticles that have been reported in the literature. Furthermore, we also discuss and critically analyze numerous types of HA-based nanoparticles that have been employed in antibacterial delivery to date. This article offers a critical overview of the potential of HA-based nanoparticles to overcome the challenges of conventional antibiotics in the treatment of bacterial infections. Moreover, this review identifies further avenues of research for developing multifunctional and biomimetic HA-based nanoparticles for the treatment, prevention and/or detection of pathogenic bacteria.

CHAPTER 6. CONCLUSION

6.1 General conclusions

The global attempts to mitigate the consequences of bacterial infections and sepsis are being undermined by the rise in drug-resistant bacteria, exorbitant treatment costs and the co-occurrence of other infectious diseases. Therefore, it is imperative to create innovative approaches that can decrease the emergence of resistant bacteria, minimize treatment costs, and enhance the effectiveness of antibiotics. Developing creative nanotechnology-based formulations with enhanced targeting capability, multifunctional activities to combat various resistance mechanisms, and synergistic antibacterial actions could be a cost-effective solution to address this issue and restore the effectiveness of existing antibiotics, as effective antibiotic delivery is a critical component in resolving this problem. Research on the integration of smart biomaterials with multifaceted functions to confer biomimetic, stimuli-responsive, and antivirulence properties to antibiotic nanocarriers is an ongoing area of interest that holds great promise in the development of novel solutions for combating bacterial infections and associated sepsis. Therefore, the general aim of this study was to create and utilize novel biomaterials with multifunctional activities for the development of biomimetic and/or pH-responsive hybrid nanocarriers (HNs) to enhance the targeted delivery of antibiotics and modulate the proinflammatory response against bacterial infections and sepsis. The specific research aims of this study were, to synthesize a novel hyaluronic acid-lysine conjugate (HA-Lys) and to explore its potential with tocopherol succinate (TS) and Oleylamine (OLA) in the formulation of multifunctional biomimetic and pH-responsive hybrid NLCs to improve the targeted delivery of vancomycin; and to formulate a novel HN derived from tannic acid (TA) and OLA for the biomimetic targeted delivery of ciprofloxacin (CIP) against bacterial infections and sepsis.

The main conclusions generated from the research data are summarized below:

Aim1

- The novel HA-Lys conjugate was successfully synthesized, and the characterization using FT-IR and ^{1}H NMR spectroscopic analysis confirmed the successful synthesis and clarified the chemical structure of the modified polymer.
- The cytotoxicity of HA-Lys conjugate was tested using the MTT assay on two mammalian cell lines, human embryonic kidney cells 293 (HEK 293) and liver hepatocellular carcinoma (HepG 2), and the results indicated that the cell viability of both cell lines was found to be more than 70 %, confirming the biosafety of the novel HA-Lys.
- HA-Lys conjugate was used with TS and OLA to formulate smooth spherical vancomycin-loaded hybrid NLCs (VCM-HNLCs), which exhibited average particle size, PDI, ZP, EE %

and DL % (w/w) of 110.77 ± 1.69 nm, 0.11 ± 0.02 and -2.92 ± 0.21 mV, 76.27 ± 1.20 % and 8.36 ± 0.25 %, respectively. The surface charge of VCM-HNLCs switched from -2.92 ± 0.21 mV at pH 7.4 to +1.64 ± 0.17 and +9.97 ± 0.33 mV at pH 6.0 and 4.5, respectively, confirming the pH-responsiveness of the nanosystem. The thermal profile analysis revealed disappearance of the endothermic peak corresponding to VCM in the DSC thermogram of VCM-HNLCs, which demonstrated the successful encapsulation of VCM within the HNs in an amorphous state.

- The release behaviour of VCM from the HN was sustained and pH-responsive over 48 hrs. The stability of VCM-HNLCs formulations was evaluated over a three-month period, and the results indicated that the optimal formulations remained stable with no significant changes on particle sizes, PDI and ZP at both room temperature (25 °C) and cold temperature (4 °C).
- The biosafety profiles of VCM-HNLCs were found to be excellent, as demonstrated by the cell viability studies performed using the MTT assay on two mammalian cell lines, HEK 293 and HepG 2, as well as the hemolysis assay.
- The MST binding affinity study confirmed the TLR2 and TLR4 sensitivity of HA, HA-Lys conjugate and the prepared hybrid NLCs compared to PGN and LPS, respectively. This demonstrates their potential inhibitory effect on the inflammatory responses resulting from the interaction between TLRs and bacterial toxins.
- The *in vitro* antibacterial activity study (MIC) of VCM-HNLCs against *S. aureus* and MRSA at different pH values (pH 7.4 and 6.0) demonstrated enhanced, pH- dependent and sustained antibacterial activity in comparison to the bare antibiotic. The potential of VCM-HNLCs to rapidly kill MRSA compared to bare VCM was verified using the time-killing assay and flow cytometry analysis. The VCM-HNLCs also exhibited a remarkable and potent biofilm inhibition activity compared to the bare VCM at both pH 7.4 and 6.0, with superior performance at pH 6.0.
- The performance of VCM-HNLCs in inhibiting the overexpression of MRSA efflux pumps was assessed using the ethidium bromide (EtBr) method. The results showed that MRSA treated with VCM-HNLCs exhibited greater fluorescence intensity than those treated with bare VCM, indicating the superior activity of the hybrid NPs against bacterial efflux pumps. This could improve anti-virulence efficacy of VCM and enhance sepsis treatment outcomes.
- The HA-Lys conjugate and VCM-HNLCs demonstrated substantial *in vitro* antioxidant activity, cytoprotective and anti-inflammatory activities against LPS-induced inflammation. This was shown by their ability to scavenge free radicals, improve cell viability, and modulate

IL-6 levels, all of which could help reduce oxidative stress, cell damage, and inflammatory responses in sepsis.

Aim2

- A distinct, spherical onion-shaped CIP-loaded TA-HNPs were successfully formulated with an optimal formulation showing an average particle size, PDI, ZP, EE % and DL % (w/w) of 85.65 ± 0.89 nm, 0.126 ± 0.01, +16.30 ± 0.23 mV, 68.73 ± 0.54 % and 6.86 ± 0.09 % respectively. The thermal profile analysis showed that the endothermic peak associated with CIP was no longer present in the DSC thermogram of CIP-loaded TA-HNPs, indicating that CIP had been successfully encapsulated within the HNs in an amorphous form.
- Cytotoxicity studies performed using an MTT assay on three distinct mammalian cell lines, MCF-7, HEK293 and HepG2 showed that CIP-loaded TA-HNPs were biosafe. In addition, the non-hemolytic activity of the NPs was assessed and among all the concentrations used in the assay, the highest concentration of CIP-loaded TAH-NPs (0.2 mg/mL) resulted in a hemolysis rate of <1%, confirming the hemocompatibility of the prepared hybrid nanosystem.
- The *in vitro* release study of CIP-loaded TAH-NPs showed a sustained CIP release pattern that lasted for 72 hrs. The stability of CIP-loaded TAH-NPs formulations was evaluated over a three-month period, and the results demonstrated that the optimal formulations maintained their stability without any significant changes in particle size, PDI, and ZP at room temperature (25°C) compared to cold temperature (4°C).
- The *in-silico* simulations and MST binding affinity studies showed that TA and its nanoformulation (CIP-loaded TAH-NPs) had a strong binding affinity for human Toll-like receptor 4 (TLR4), which was greater than that of its natural substrate lipopolysaccharide (LPS). This suggests that TA and CIP-loaded TAH-NPs can compete with LPS to inhibit its effect, thereby preventing the progression of sepsis.
- CIP-loaded TAH-NPs showed more enhanced and sustained antibacterial activity compared to bare CIP against gram-negative *E. coli* and *P. aeruginosa,* and gram-positive *S. aureus* and MRSA. The time killing assay findings showed 100 % bacterial clearance within 8 hrs of treatment with CIP-loaded TAH-NPs, while in the case of bare CIP total killing occurred after 24 hrs of treatment. The ability of CIP-loaded TAH-NPs to effectively eliminate MRSA and *P. aeruginosa* was further demonstrated using the flow cytometry analysis, showing faster killing efficacy at lower concentrations compared to bare CIP.
- CIP-loaded TAH-NPs demonstrated superior performance in reducing the expression of MRSA and *P. aeruginosa* efflux pumps at subinhibitory concentrations. Additionally, the HN displayed heightened protective effects against bacterial-induced hemolysis. This could

potentially help overcome antimicrobial resistance mechanisms, improve CIP delivery, and enhance sepsis treatment outcomes.

- Significant *in vitro* antioxidant activity, cytoprotective and anti-inflammatory properties were shown by TA and CIP-loaded TAH-NPs against LPS-induced inflammation. This was revealed by their ability to scavenge free radicals, enhance cell viability, and regulate IL-6 levels, which may aid in lowering sepsis-related oxidative stress, cell damage, and inflammatory responses.

Therefore, the findings of this research study validated the potential of VCM-HNLCs and CIP-loaded TAH-NPs as better antibiotic nanocarriers than bare drugs, by leveraging biomimicry and/or pH-responsive principles with enhanced targeting ability, biosafety, and overall therapeutic outcomes.

6.2 Significance of the findings in the study

The newly synthesized HA-Lys conjugate, and the nano-drug delivery systems proposed in this study, namely VCM-HNLCs and CIP-loaded TAH-NPs were successfully designed and employed to specifically target both the bacterial infection site and sepsis milieu. This targeted approach enables the efficient delivery of antibiotics, thereby eliminating the causative bacteria, defeating the mechanisms of antibiotic resistance, and minimizing the overactivation of TLRs that happens during sepsis. Consequently, the proposed strategies demonstrated enhanced antibacterial efficacy and improved inflammatory responses, which could result in better therapeutic outcomes and increased patient compliance.

The following highlights the significance of the findings in this study:

New pharmaceutical products

This study has introduced unique pharmaceutical biomaterials, viz: HA-Lys conjugate and TA to be utilized as multifunctional adjuvants and targeting ligands in HNs for antibiotic delivery. These smart biomaterials have the potential to expand the range of advanced pharmaceutical excipients, enabling the development of new medicines that are more efficient and cost-effective. As a result, local pharmaceutical companies can enhance their competitiveness in the highly profitable global pharmaceutical market.

Improved patient well-being and disease control

The advanced VCM-HNLCs and CIP-loaded TAH-NPs presented in this work were confirmed to have better antibacterial potential and overall therapeutic effects when compared

to bare drugs. These novel HNs demonstrate the potential to effectively control bacterial infections and sepsis through various approaches such as targeted delivery to infection sites, reduced healthy site exposure to antibiotics, enhanced bacterial uptake, reduced bacterial resistance, and modulation of inflammatory responses. This could improve the treatment of patients with severe bacterial infections and sepsis worldwide by minimizing undesirable side effects, reducing the required dose, and lowering overall treatment costs, ultimately leading to better disease management, improved patient outcomes, and reduced mortality rates.

Generating new knowledge for the scientific community

The results obtained from the analysis of the review articles and experimental research papers featured in this study have significantly added to the pharmaceutical sciences knowledge database in various ways. Among them are the following:

- New insights into the potential of combining biomimicry and intrinsic stimuli-responsive principles for improving antibacterial delivery, anti-inflammatory activity and combating bacterial resistance were gained, along with new knowledge about the synthesis, formulation processes, characterization, and toxicity profiles of HA-Lys, VCM-HNLCs and CIP-loaded TAH-NPs. The physicochemical and *in vitro* properties of the formulated VCM-HNLCs and CIP-loaded TAH-NPs were also identified using various experimental techniques.
- The molecular dynamics simulation identified the atomistic mechanism of interactions and binding capacity of TA to human TLR4 at the molecular level, revealing its potential competitive inhibitory effect on TLR4 compared to LPS (natural ligand of TLR4).
- New knowledge on the *in vitro* binding affinity of HA-Lys, TA and their corresponding nanoformulations (VCM-HNLCs and CIP-loaded TAH-NPs) to human TLRs using MST were identified, and this was found to be successfully correlated with the superior anti-inflammatory potential of the developed nanosystems.
- The in-depth antimicrobial testing conducted by MIC determination, time-killing assay, antibiofilm and efflux pump inhibition evaluation has effectively identified the superiority of the nanoformulations when compared to the bare antibiotics.

Conceptualization of new research

The research findings from the development of the novel multifunctional biomaterials and their associated nanoformulations (VCM-HNLCs and CIP-loaded TAH-NPs) can stimulate new research areas, including the following:

- The newly synthesized HA-Lys conjugate can be used for active targeting in other disease microenvironments and for delivering other drugs to treat various disease conditions, including cancer, diabetes, brain disorders, and metabolic diseases. Furthermore, it may inspire the development and synthesis of other novel biomimetic and targeting biomaterials for various biomedical applications.
- The successful formulation and *in vitro* characterization of the HNs reported in this study could inspire future research into the creation of other nano-drug delivery systems for different drug classes to treat other diseases.
- The superior properties of these multifunctional HNs, which combine biomimetic and stimuli-responsive approaches, and exhibit antivirulence, antibacterial, and anti-inflammatory properties, could open new avenues and inspire the use of this strategy in the development of other multifunctional nano drug delivery systems with robust antibacterial and anti-inflammatory effects.

6.3 Limitations of the study

This study demonstrates the benefits of employing innovative biomaterials with multifunctional activities for the creation of antibiotic-loaded biomimetic and/or pH-responsive hybrid nanocarriers (HNs) to eradicate bacterial infections and sepsis. Nevertheless, a number of restrictions reduced the knowledge output of the study to some extent and opened the door for more research. These restrictions include:

- Molecular dynamic simulation section in this study was limited and further investigations could be done to explore the mechanistic properties of nanosystem self-assembly and their binding to their respective targets.
- Lack of *in vivo* antibacterial and anti-inflammatory studies to support the *in vitro* findings and further confirm our theory.
- Lack of long-term physicochemical and stress stability studies of our developed formulation due to time limitation.
- Lack of long term *in vivo* biocompatibility and pharmacokinetics studies that are required to progress to clinical trials.

6.4 Recommendations for future studies

Although these strategies have shown promise for VCM-HNLCs and CIP-loaded TAH-NPs as innovative, multifunctional biomimetic and/or pH-responsive nano-drug delivery systems to enhance treatment options for severe bacterial infections and sepsis, and to overcome resistance issues, additional research is necessary to optimize these formulations and secure eventual regulatory clearance for clinical application. The following studies are therefore recommended:

- The development of VCM-HNLCs necessitates the use of course-grain molecular dynamics (MD) simulations to create a system that can fully self-assemble into drug-loaded nanovesicles and simulate the drug release from the nanosystem. Additionally, MD simulations could be performed to show the *in-silico* binding affinity of the novel HA-Lys conjugate and VCM-HNLCs to human TLRs.
- The successfully developed HNLCs and TAH-NPs for antibiotic delivery can be loaded with a variety of antibiotics, and their synergism and advantages against different bacteria should be investigated. In addition, there is a need for more research on the simultaneous delivery of multiple antibiotics from these hybrid nanovesicles, and their ability to achieve enhanced and synergistic activities, target multiple modes of action and potentially reduce the likelihood of antibacterial resistance.
- It is recommended to conduct further research on the intracellular antimicrobial properties of the developed VCM-HNLCs and CIP-loaded TAH-NPs, as well as the extraction and assessment of various bacterial toxins.
- The potential antioxidant and TLRs inhibition properties of VCM-HNLCs and CIP-loaded TAH-NPs can be tested at the cellular level by examining various cell lines, including macrophage cells (RAW 264.7), human embryonic kidney cells 293 (HEK 293), and lung carcinoma epithelial cells (A549). To further validate their anti-inflammatory effects, specific proteins and nucleic acids can be quantitatively determined using methods such as western blot and PCR, while the expression of additional pro-inflammatory cytokines like TNF-α, NF-κB, IL-10, and IL-1β can also be investigated.
- *In vivo* antibacterial and ani-inflammatory studies in mice bacterial sepsis model should be conducted to further evaluate the effectiveness of the developed hybrid nanovesicles.
- Long-term stability studies to assess the physical and chemical stability parameters of optimized formulations must be conducted in accordance with the international conference of harmonization (ICH) guidelines to confirm their shelf life.

- Investigation of the acute, intermediate, and long-term *in vivo* toxicity of the materials and hybrid nanosystems presented in this study is necessary to create comprehensive toxicological profiles for them.
- *In vivo* pharmacokinetic and bioavailability studies followed by clinical trials are necessary to gain approval for commercializing our developed nanosystems, which can then be introduced into the market.
- Validated large-scale production procedures of the hybrid nano-systems described in this thesis could be established to promote their use in pharmaceutical industries.

6.4 Conclusion

The findings of this study highlight the promising potential of the newly designed VCM-HNLCs and the CIP-loaded TAH-NPs as innovative, multifunctional biomimetic and/or stimuli-responsive antibiotic nanocarriers with inherent antibacterial activity, synergistic anti-virulence properties, and targeted drug delivery potential, for enhancing the management of bacterial infections and sepsis. This research contributes to the development of biomimetic pH-responsive nano-based approaches, to address the limitations of the currently available antibiotic nanocarriers. Additionally, it involves the design and synthesis of innovative smart biomaterials to create multifunctional nano-systems for treating bacterial sepsis. Multidisciplinary collaborative research efforts will be necessary to gain a thorough understanding of the significance of applying nanotechnology, biomimicry, and stimuli-responsive principles in the design and synthesis of novel smart biomaterials to combat the current global antibiotic-resistant crisis. The use of such strategies will strengthen human empowerment against the swiftly expanding risks of resistance, enhance the efficacy of current treatments for sepsis and complicated bacterial infections, and lessen their significant influence on world health.

APPENDICES

Appendix I

Supplementary Material for Experimental Paper One

Design of multifunctional biomimetic pH-responsive hybrid nanostructured lipid carriers for targeted delivery of vancomycin against bacterial sepsis

Eman Elhassan[1], Mohammed A. Gafar[1,2], Calvin A. Omolo[1,3 *], Usri H. Ibrahim[4], Rene Khan[5], Thirumala Govender[1 *].

[1] Discipline of Pharmaceutical Sciences, College of Health Sciences, University of KwaZulu-Natal, Private Bag X54001, Durban, South Africa.

[2] Department of Pharmaceutics, Faculty of Pharmacy, University of Khartoum, Sudan.

[3] Department of Pharmaceutics and Pharmacy Practice, School of Pharmacy and Health Sciences, United States International University-Africa, P. O. Box 14634-00800, Nairobi, Kenya.

[4] Discipline of Human Physiology, School of Laboratory Medicine and Medical Sciences, College of Health Sciences, University of KwaZulu-Natal, Durban, South Africa.

[5] Discipline of Medical Biochemistry, School of Laboratory Medicine and Medical Science, University of KwaZulu-Natal, Durban, South Africa

[*] Corresponding authors: comolo@usiu.ac.ke, govenderth@ukzn.ac.za.

Keywords: Biomimetic; pH-responsive; Hyaluronic acid-lysine; Hybrid nanocarriers; Bacterial Sepsis; Antibiotic delivery.

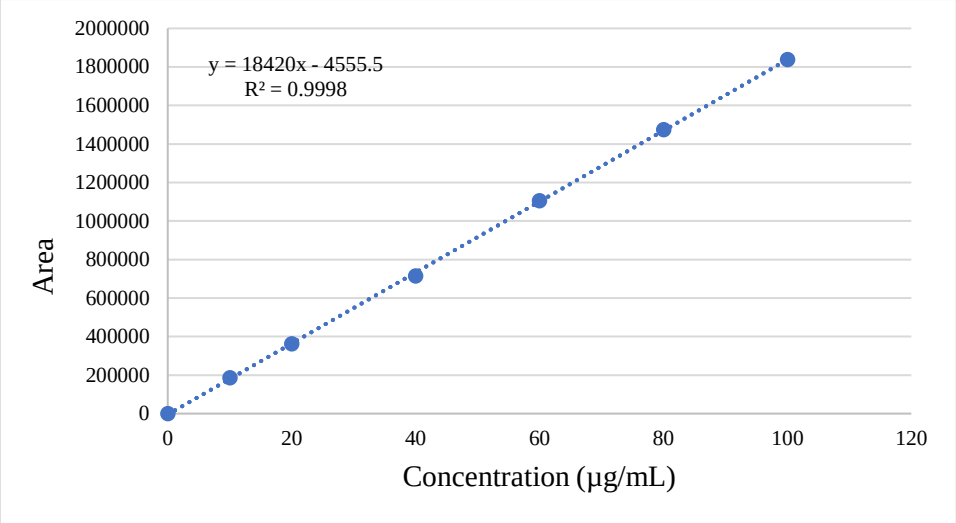

Figure 1. Vancomycin calibration curve

Table 1. The FIC Index

FIC index	Interpretation
≤0.5	Synergy
>0.5 to 1	Additive
>1 to <2	Indifference
≥2	Antagonism

Table 2. Shows the effect of surfactant type on size, PDI and ZP of different HNLCs formulations (blank HNLCs) Data are presented as mean ± SD (n = 3).

Surfactant	Size(nm)	PDI	ZP (mV)
Span 80	3162.00 ± 533.30	1.00 ± 0.00	-5.55 ± 0.22
PEG 400	980.70 ± 86.75	0.63 ± 0.06	-5.74 ± 0.46
PVP	510.10 ± 6.44	0.14 ± 0.03	-5.57 ± 1.38
PLX (P 188)	2082 ± 54.64	1.00 ± 0.00	-6.22 ± 0.62
Tween 80	65.44 ± 0.44	0.26 ± 0.01	-4.07 ± 0.52

Table 3. Hemolysis (%) for different concentrations of VCM-HNLCs, PBS (pH 7.4) and distilled water (D.W). Data are presented as mean ± SD (n = 3).

VCM-HNLCs (mg/ml)	Hemolysis %
0.5	0.39 ± 0.31
0.1	0.19 ± 0.03
0.2	0.33 ± 0.11
0.3	0.44 ± 0.28
0.4	0.38 ± 0.18
0.5	0.63 ± 0.77
PBS	0
D.W	100

Table 4. The results of particle size, PDI and ZP of VCM-HNLCs under different storage durations. Data are presented as mean ± SD (n = 3).

Day	RT			4° C		
	Size (nm)	PDI	ZP (mV)	Size (nm)	PDI	ZP (mV)
0	110.70±1.69	0.11±0.02	-2.92±0.21	110.70±1.69	0.11± 0.02	-2.92± 0.21
30	110.30±1.16	0.09±0.01	-4.04±1.17	114.00±1.23	0.10±0.02	-3.28±0.98
60	110.80±1.21	0.09±0.02	-4.42±0.43	115.80±1.90	0.11±0.03	-4.37±1.48
90	113.30±1.18	0.11±0.02	-4.72±0.86	115.60±1.28	0.10±0.01	-4.10±0.69

**RT*= *room temperature*

Appendix II

Supplementary Material for Experimental Paper Two

Disease-inspired design of a biomimetic tannic acid-based hybrid nanocarriers for targeted delivery of ciprofloxacin against bacterial-induced sepsis

Eman Elhassan[1], Calvin A. Omolo[1,2 *], Mohammed A. Gafar[1,3], Usri H. Ibrahim[4], Nikita Devnarain[1], Aimen Aljoundi[5], Ghazi Elamin[6], Mahir Mohammed[1,7], Thirumala Govender[1 *].

[1] Discipline of Pharmaceutical Sciences, College of Health Sciences, University of KwaZulu-Natal, Private Bag X54001, Durban, South Africa.

[2] Department of Pharmaceutics and Pharmacy Practice, School of Pharmacy and Health Sciences, United States International University-Africa, P. O. Box 14634-00800, Nairobi, Kenya.

[3] Department of Pharmaceutics, Faculty of Pharmacy, University of Khartoum, Sudan.

[4] Discipline of Human Physiology, School of Laboratory Medicine and Medical Sciences, College of Health Sciences, University pf KwaZulu-Natal, Durban, South Africa.

[5] Department of Pharmaceutical Chemistry, Collage of Pharmacy, University of Attahadi, Tripoli, V567-7M8, Libya.

[6] Department of Pharmaceutical Chemistry, Collage of Pharmacy, Karary University, Khartoum P.O. Box 11111, Sudan

[7] Department of Pharmacology, Faculty of Pharmacy, University of Khartoum, Sudan.

[*] Corresponding authors: comolo@usiu.ac.ke, govenderth@ukzn.ac.za.

Keywords: Biomimetic, Tannic acid, Hybrid nanocarriers, Bacterial infections, Sepsis, TLR4 antagonism, Antibiotic delivery.

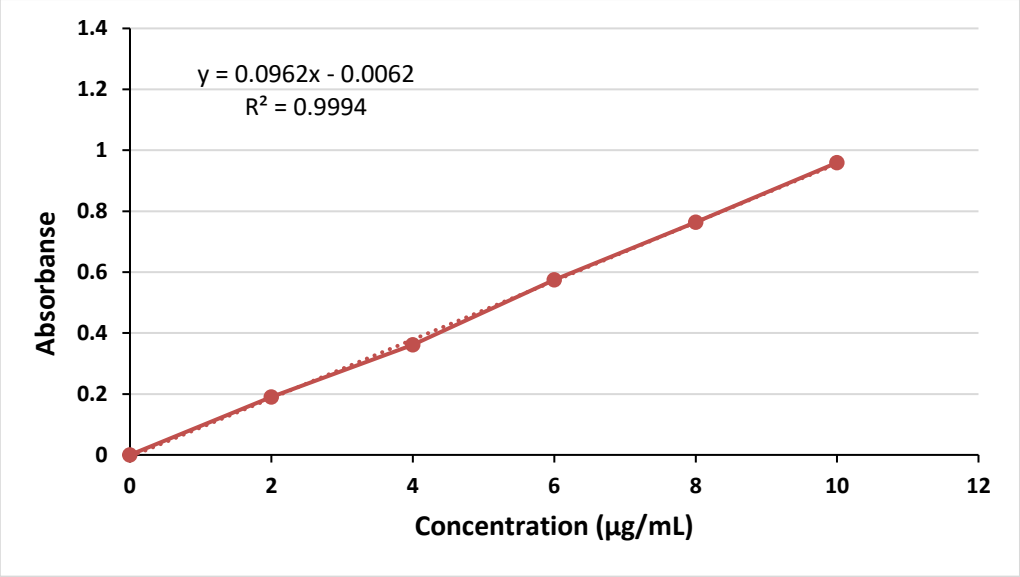

Figure 1. Ciprofloxacin hydrochloride (CIP) calibration curve

Table 1. The FIC Index

FIC index	Interpretation
≤0.5	Synergy
>0.5 to 1	Additive
>1 to <2	Indifference
≥2	Antagonism

Table 2. The effect of surfactant type on size, PDI and ZP of different TAH-NPs formulations (blank TAH-NPs). Data are presented as mean ± SD (n=3).

Surfactant	Size(nm)	PDI	ZP (mV)
PVP	284.40 ± 3.05	0.39 ± 0.03	+2.46 ± 0.23
Poloxamer 407	161.50 ± 1.09	0.10 ± 0.00	+18.3 ± 0.71
Tween 80	222.10 ± 0.44	0.42 ± 0.00	+1.54 ± 0.36
Span 80	817.20 ± 55.10	0.26 ± 0.03	+9.66 ± 0.57
Brij® 58	205.50 ± 5.07	0.23 ± 0.00	+2.41 ± 0.34

Table 3. Hemolysis (%) for different concentrations of CIP-loaded TAH-NPs, PBS (pH 7.4) and distilled water (D.W). Data are presented as mean ± SD (n=3).

Conc (µg/ml)	Hemolysis %.
20	0.30 ± 0.10
40	0.42 ± 0.01
60	0.33 ± 0.09
80	0.45 ± 1.13
100	0.26 ± 0.12
200	0.61 ± 0.64
PBS	0
D.W	100

Table 4: MM/GBSA-based binding free energy profile of LPS, TA, OLA, PLX407 and CIP when bound to human TLR4. Data are presented as mean ± SD (n=3).

Systems	Energy components (kcal/mol)				
	ΔE_{vdw}	ΔE_{ele}	ΔG_{gas}	ΔG_{sol}	ΔG_{bind}
LPS	-10.50 ± 0.20	-14.30 ± 0.32	-24.80 ± 0.47	17.76 ± 0.33	-7.04 ± 0.16
TA	-79.43 ± 0.16	-87.89 ± 0.49	- 167.32 ± 0.52	99.35 ± 0.36	-67.98 ± 0.22
OLA	-21.77 ± 0.23	-2.03 ± 0.08	-23.80 ± 0.27	7.23 ± 0.09	-16.56 ± 0.19
PLX407	-15.84 ± 0.30	-8.54 ± 0.22	-24.38 ± 0.49	15.03 ± 0.29	-9.35 ± 0.22
CIP	-12.93 ± 0.19	125.92 ± 0.56	-24.80 ± 0.47	-121.71 ± 0.52	-8.72 ± 0.15

All energies are in kcal/mol**.**
ΔE_{ele} = electrostatic energy; ΔE_{vdw} = van der Waals energy; ΔG_{bind} = total binding free energy; ΔG_{sol} = solvation free energy; ΔG_{gas} = gas phase free energy.

Table 5. The results of particle size (nm), PDI and ZP (mV) of CIP-loaded TAH-NPs under different storage durations, represented as mean ± SD (n=3).

Day	RT			4°C		
	Size (nm)	**PDI**	**ZP (mV)**	**Size (nm)**	**PDI**	**ZP (mV)**
0	85.65 ± 0.89	0.13 ± 0.01	+16.30 ± 0.23	85.65 ± 0.894	0.13 ± 0.01	+16.3 ± 0.23
30	85.17 ± 1.97	0.14 ± 0.026	+19.80 ± 1.89	119.10 ± 6.16	0.29 ± 0.07	+18.8 ± 1.19
60	85.07 ± 0.99	0.14 ± 0.010	+18.30 ± 1.88	114.30 ± 3.31	0.23 ± 0.04	+19.4 ± 2.67
90	85.66 ± 1.60	0.15 ± 0.020	+19.80 ± 0.07	115.30 ± 6.90	0.30 ± 0.04	+28.1 ± 1.33

Appendix III

Published manuscript (review article 1)

Journal of Controlled Release 361 (2023) 846–877

Contents lists available at ScienceDirect

Journal of Controlled Release

journal homepage: www.elsevier.com/locate/jconrel

Review article

Engineering hybrid nanosystems for efficient and targeted delivery against bacterial infections

Eman Elhassan [a], Nikita Devnarain [a], Mahir Mohammed [a,*], Thirumala Govender [a,**], Calvin A. Omolo [a,b,c]

[a] Discipline of Pharmaceutical Sciences, College of Health Sciences, University of KwaZulu-Natal, Private Bag, Durban X54001, Durban 4000, South Africa
[b] Department of Pharmaceutics and Pharmacy Practice, School of Pharmacy and Health Sciences, United States International University-Africa, P. O. Box 14634-00800, Nairobi, Kenya
[c] Faculty of Pharmacy, University of Khartoum, Sudan

ARTICLE INFO

Keywords:
Hybrid nanosystems
Antibacterial
Drug delivery
Bacterial infection
Antibiotic resistance
Nanocarriers

ABSTRACT

Hybrid nanoparticles (NPs) are emerging as superior alternatives to conventional nanocarriers for enhancing the delivery of antibiotics and improving their targeting at the infection site, resulting in the eradication of bacterial infections and overcoming antimicrobial resistance. They can specifically control the release of antibiotic when reaching the targeted site of infection, thus enhancing and prolonging their antimicrobial efficacy. In this review, we provide a comprehensive and an up-to-date overview of the recent advances and contributions of lipid-polymer hybrid NPs; organic-inorganic hybrid NPs; metal-organic frameworks; cell membrane-coated hybrid NPs; hybrid NP-hydrogels; and various others, that have been reported in the literature for antibacterial delivery, with emphasis on their design approaches; the nanomaterials constituted; the mechanisms of drug release; and the enhanced antibacterial efficacy of the reported hybrid nanocarriers. This review also highlights future strategies that can be used to improve the potential of hybrid nanosystems to treat bacterial infections and overcome antibiotic resistance.

1. Introduction

Bacterial infections and their induced diseases, like sepsis, are major causes of mortality worldwide. They are considered to cause significant public health challenges, especially in low-income countries [1]. In 2017, there were 48.9 million cases of sepsis globally, with nearly 11 million deaths related to sepsis [2]. Moreover, the emergence and prevalence of multidrug-resistant bacteria (MDR) have led to antimicrobial resistance (AMR), which is an increasing threat to human health. [3]. A recent report published by the Centers for Disease Control and Prevention (CDC) stated that antibiotic-resistant bacteria cause >2.8 million illnesses each year, with 35,000 deaths, in the United States [4]. Furthermore, the complications resulting from secondary bacterial infections caused by antibiotic-resistant bacteria have increased the rates of morbidity and mortality in patients with coronavirus disease (COVID-19) around the world [5]. As a result, eradicating certain bacterial infections and their associated problems remains a challenge, owing to the complex pathogenic mechanisms involved in the destruction of the host's immune system, as well as the rise in the cost of healthcare services [6]. Hence, more preventative efforts and innovative strategies are urgently required to control and eliminate bacterial infections.

Antibiotics are often used to treat and control bacterial infections [7]. However, there is an increase in resistance across all classes of antibiotics. It is reported that conventional antibiotic dosage forms are one of the major contributing factors to the development of antibiotic resistance, due to their lack of selectivity to attack only specific pathogenic bacteria; inability to enhance solubility; instability; low bioavailability; difficulty in reaching the site of action; high frequency of administration due to fluctuations in plasma drug concentrations resulting in severe side effects; toxicity; and thus, poor patient compliance [8,9]. Moreover, the problem is compounded by pharmaceutical companies abandoning the production, research, and development of new antibiotics [8,10]. As a result of these complications, the development of novel drug delivery systems to improve the delivery of current

* Corresponding author at: Discipline of Pharmaceutical Sciences, College of Health Sciences, University of KwaZulu-Natal, Private Bag, Durban X54001, Durban 4000, South Africa.
** Corresponding author.
E-mail addresses: govenderth@ukzn.ac.za (T. Govender), omolo@uniis.ac.ke (C.A. Omolo).

https://doi.org/10.1016/j.jconrel.2023.09.022
Received 31 July 2023; Received in revised form 28 September 2023; Accepted 29 September 2023
Available online 6 October 2023
0168-3659/© 2023 Elsevier B.V. All rights reserved.

and new antibiotics is recognized as a major priority in research [11].

In the last few decades, pharmaceutical nanotechnology has opened a new era for research in the design and characterization of drug delivery systems [12,13]. These systems have been reported to enhance the delivery of several antibacterial agents through overcoming the developed bacterial resistance mechanisms that involve drug decomposition by β-lactamase [14]; efflux pumps [15]; biofilm formation [16] and thickening of the bacterial cell wall [13,17]. Thus, the continued development of the nanomedicine field promises to be critical in combating antimicrobial resistance.

Among the nano drug delivery systems showing promise in antibiotic delivery are hybrid nanosystems, which are formulated from a plethora of inorganic, organic, or a combination of both, materials on a scale of less than one micrometer [18]. These nanosystems are solving challenges in drug delivery and theranostic as they can be utilized to formulate nanosystems with the positive attributes of the blend of biomaterials employed to formulate them, while simultaneously overcoming their shortcomings [19]. Moreover, hybrid nanosystems have been shown to overcome the limitations of conventional, or non-hybrid, nanocarriers such as low stability; premature release of the encapsulated drug before reaching the target tissue; poor biocompatibility; instability during storage; and unacceptable toxicity [20–22]. Intensive research efforts have focused on several hybrid nanosystems, such as lipid-based hybrid systems, polymeric hybrid systems, organic/inorganic hybrid systems, and others, with proposed applications in various biomedical fields such as cancer treatment and drug delivery [23], food supplements [24] and vaccine therapy [25].

Recently, hybrid nanocarriers have been gaining prominence for antibacterial delivery due to several advantages, including excellent biocompatibility and biodegradability; stable structural integrity; chemical diversity that can be employed for targeting [6]; high dual and multiple loading capacity [26]; and flexibility for functionalization to suit specific applications [27]. Besides the aforementioned advantages, the hybridization of organic and inorganic biomaterials that possess intrinsic antibacterial activity, such as metal ions (e.g., silver and gold NPs), antimicrobial peptides and lipids, results in a powerful synergistic antibacterial effect [26].

Based on the advantages of hybrid nanosystems, reviews in the literature have broadly covered the development and applications of different hybrid nanocarriers for cancer therapy [28,29]; oral drug delivery [30,31]; skin repair and wound healing [32]; gene delivery [33]; and molecular targeting/imaging [34]. However, despite the current bacterial disease and resistance crises, no review in the literature has focused on the various hybrid nanocarriers that have been reported for antibacterial delivery.

Herein, we present an up-to-date overview of the recent advances, technological progress, and contributions of the different hybrid nanosystems that have been developed for antibacterial delivery. Initially, the review provides a theoretical background about different hybrid nanosystems, including lipid-polymer hybrid NPs (LPHNPs); organic-inorganic hybrid NPs; metal-organic frameworks (MOFs); cell membrane-coated hybrid NPs (CMCH-NPs); and hybrid NPs-hydrogels, and their design approaches. Thereafter, the significance and limitations of applying these novel nano-delivery systems in the treatment of bacterial infections are critically discussed and evaluated in detail. Finally, this review identifies the future strategies required to maximize the potential of hybrid nanosystems in the treatment of bacterial infections.

2. Engineering hybrid nanosystems for antibacterial delivery

The design of hybrid nanosystems strongly mimics natural architectural structures where a complex hierarchical assembly is achieved by employing different complementing materials to produce functional systems [35]. Advances in nanotechnology, synthetic techniques, supramolecular chemistry, and an understanding of the forces involved in self-assembly have led to the development of higher order functional hybrid nanostructures for drug delivery. The manufacturing of hybrid nanosystems involves a myriad of interactions between the building blocks of hybrid nanocarriers, including covalent, non-covalent, or a combination of both, types of interactions. Such nano assemblies use a variety of intermolecular associations, such as electrostatic, hydrophobic, and hydrogen bonding, to create diverse structural designs (for example, LPHNPs; lipid-dendrimer hybrid NPs (LDHNPs); mixed micelles; metal-organic frameworks (MOFs); cell membrane-coated hybrid NPs (CMCH-NPs); hybrid nanogels) with infinite applications, including drug delivery [36]. Individually, organic and inorganic NPs, such as liposomes; polymeric NPs; metal/metal oxide NPs and mesoporous silica NPs (MSNs) have their own merits and drawbacks. Therefore, combining them in a single hybrid drug delivery platform provides a multifunctional carrier with enhanced biological properties that can improve therapeutic efficacy as well as reduce drug resistance. The following section presents a theoretical background of different hybrid nanosystems, including LPHNPs; organic-inorganic hybrid NPs; MOFs; CMCH-NPs' and hybrid NPs hydrogels, with a focus on their design principles and synthetic strategies.

2.1. Design of LPHNPs

To combine the unique advantages, and simultaneously address the limitations of polymeric NPs and lipid-based nanovesicles, LPHNPs have been developed [21,37]. They have been widely investigated in the preclinical phase due to their attractive properties for drug delivery [37]. These unique drug delivery systems can be classified according to their structural design into monolithic matrix lipid polymeric nanoparticles, in which a lipid phase contains a homogeneous polymeric drug complex or a polymeric matrix covered with a lipid phase; core-shell LPHNPs characterized by a polymeric core surrounded by a lipid shell or the other way around; and lipocomes decorated with polymeric materials (Fig. 1) [20]. The lipid layer behaves as a molecular barrier to prevent the loss of the entrapped drug during fabrication and to slow down the degradation rate of the hybrid NPs in any physiological environment, enabling sustained release kinetics of the contained drug [6,20]. The polymeric NPs and the lipid layer are linked together through different binding forces, such as van der Waals (vdW) forces; hydrophobic interactions; electrostatic interactions; and various non-covalent bonds [20]. A wide variety of therapeutic agents (drugs; peptides and proteins; genes; vaccines; antibiotics; and others) can be either encapsulated, adsorbed, or covalently bonded to the polymeric NPs, the lipid layer, or both, depending on the hydrophobicity of the drug and the construction of the hybrid system [20]. A combination of the biomimetic behavior of the lipid materials and the mechanical advantages linked to the polymeric NPs can give an advanced delivery platform with high encapsulation efficiency; well-defined release kinetics; well-tolerated serum stability; and well-triggered tissue, cellular, and molecular targeting [38,40].

The primary concern surrounding LPHNPs has been their method of preparation. The various methods of preparing LPHNPs reported in the literature thus far are summarized in Table 1. Generally, on a laboratory scale, two broad methods have been applied to manufacture LPHNPs, namely, the two-step preparation and the single-step preparation methods [41]. The conventional two-step preparation method has mainly been employed in the early phases of LPHNP development. A preformulated polymeric NP is added into either a dried lipid film or a preformulated lipid vesicle via vortexing or sonication. Extrusion or homogenization steps are also required after preparation to obtain homogeneous nano-sized hybrid NPs [39,41]. Recently, non-conventional techniques have been implemented in addition to conventional techniques, including spray drying [42] and soft lithography particle moulding [43]. However, the alternative single-step preparation method is preferred because it is easier, highly scalable, more efficient, and cost-effective [20,39]. This method involves the single mixing of a

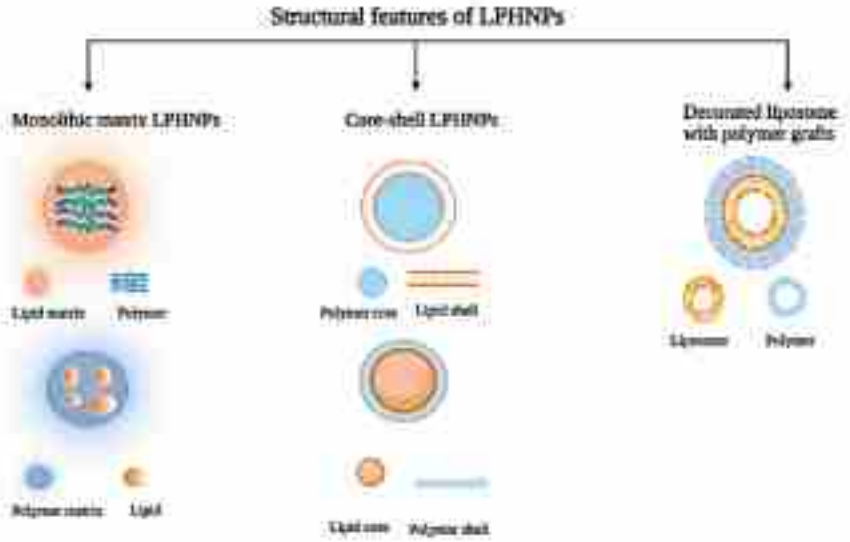

Fig. 1. Scheme illustrating the structural designs of LPHNPs.

Table 1
Different methods of preparation of LPHNPs, including the components of the hybrid nanosystems with their encapsulated drugs, if any.

Preparation method	Lipid	Polymer	Encapsulated drug	Ref.
Conventional two-step method	POPS	Alkylamine-plasma polymer	AgNPs	[42]
Non-conventional two-step method (spray drying)	Lecithin	PLGA	Levofloxacin	[43]
Non-conventional two-step method (soft lithography)	DOTAP/DOPE	PLGA	siRNA	[44]
One-step method (nanoprecipitation)	Lecithin	PLGA	N-Acetyl Cysteine	[45]
One-step method (ESE)	Soy lecithin Glyceryl stearate	PLA	Norfloxacin	[27]

POPs, 1-palmitoyl-2-oleoyl-sn-glycero-3-phospho-L-serine; AgNPs, silver NPs; PLGA, Poly (L-lactic-co-glycolic acid; DOTAP, 1,2-Dioleoyl-3-trimethylammonium-propane; DOPE, 1,2-Dioleoyl-sn-glycero-3-phosphoethanolamine; siRNA, small interfering ribonucleic acid; PLA, polylactic acid; ESE, emulsification solvent evaporation.

lipid solution and polymeric NPs by nanoprecipitation [44], emulsification solvent evaporation (ESE) [27], or chemical conjugation method [45]; and the polymeric NPs are precipitated with simultaneous self-assembly of the lipid layer around them, or *vice versa*. Nowadays, microfluidic-based rapid-mixing protocols, and a new advanced herringbone-patterned multi-inlet vortex mixer (MIVM), have been introduced to generate small-sized LPHNPs with uniform size distribution and a shorter mixing time in a scalable, reproducible manner [46]. In addition, other factors such as the aqueous solubility and lipophilicity of the drug; the type of lipid used; and the lipid/polymer (L/P) ratio have a critical impact on the particle size, drug loading (DL), entrapment efficiency (EE%) and stability of the formulated hybrid system. These parameters have been investigated by Chiesa et al. (2011) using fluoroquinolone antibiotics as a drug model. They noticed a reduction in particle size with an increase in the L/P ratio. Also, they proved that ionic interactions between the drug and the lipid are crucial in the formulation of LPHNPs by the ESE method [47].

2.2. Design of organic-inorganic hybrid NPs

Inorganic NPs such as metal/metal oxide NPs, magnetic NPs and mesoporous silica NPs (MSNs) can be hybridized by surface engineering with a wide variety of organic moieties through different synthesis strategies to provide hybrid nanosystems for various biomedical applications, including diagnosis, therapeutics, imaging and drug delivery [49,50]. The integration of organic materials and inorganic NPs retains the components and beneficial features of both, resulting in a hybrid system with high colloidal stability, high biocompatibility, biodegradability, and low toxicity [50,51]. Also, the organic shell of the hybrid NP can be further functionalized with stimuli-responsive materials [50] or targeting moieties such as antibodies, peptides, and aptamers [49] for triggering drug release.

Organic-inorganic hybrid NPs can be classified according to the nature of the interaction between the two components into Class I and Class II hybrid NPs [50,52]. In Class I, the binding can be achieved by physical interactions through vdW forces, electrostatic interactions, or hydrogen bonds. In contrast, Class II includes different covalent and non-covalent chemical bonds [50]. The organic moieties play an essential role in the stabilization of the hybrid system [41]. They can be divided into chemical organic materials that include polymers (most common), or biological materials such as lipids, proteins, and nucleic acids [53].

There are two main strategies for the synthesis of organic-inorganic hybrid NPs. The first strategy is called the reversible addition-fragmentation chain transfer (RAFT) technique [50], which is based on introducing an anchoring group onto the surface of a pre-formulated inorganic NP. Their role is to enable the organic material to conjugate strongly with the inorganic core; and the organic material can be in the form of a monomer/initiator (grafting-from approach) or a polymer chain (grafting-to approach) [41]. Alternatively, direct synthesis or 'in situ' synthesis of organic-inorganic hybrid NPs can be applied [52]. In this method, the inorganic NPs are prepared in the presence of the organic material, which acts as a stabilizer. This technique can yield hybrid NPs of high quality, with narrow size dispersity and long-term colloidal stability in biological media [50,52]. Fig. 2 represents a schematic illustration of the strategies available for the synthesis of organic-inorganic hybrid NPs.

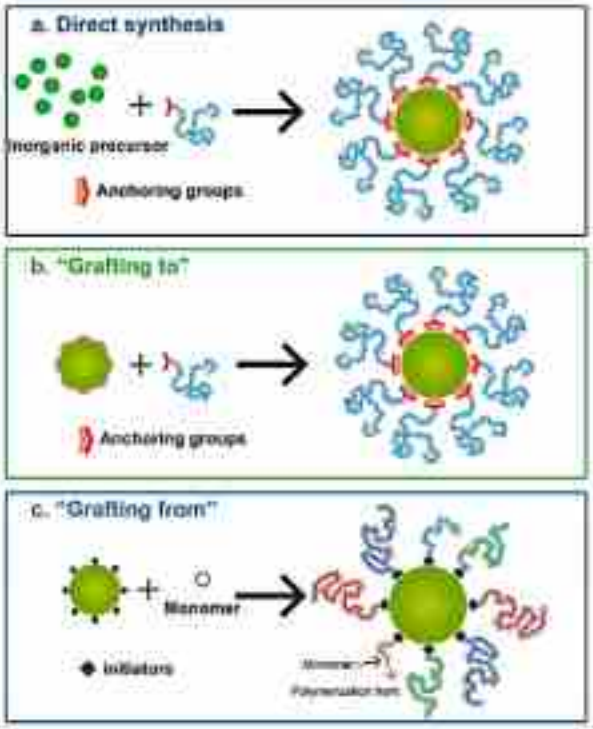

Fig. 3. Scheme representing organic-inorganic hybrid NPs prepared by (a) direct synthesis; (b) grafting-to; and (c) grafting-from approaches of the RAFT technique (adapted with permission from [50]).

2.3. Design of metal organic frameworks (MOFs)

Metal-organic frameworks are novel porous hybrid materials prepared through the co-ordination of metals/metal oxides (ions or clusters) with organic polydentate linkers, forming a three-dimensional structure (Fig. 5) [54,55]. Researchers became interested in these hybrid materials in the late 1990s when Williams and co-workers (1999) formulated a MOF called HKUST-1 by co-ordinating copper-based clusters and benzene tricarboxylate linkers to create a three-dimensional system of channels with a pore size of 1 nm and an accessible porosity of about 40% [56]. Also, in 1999, a crystalline MOF, known as MOF-5, made from zinc-based groups and benzene carboxylate linkers, was reported by Yaghi et al. (1999). They prepared a three-dimensional framework structure with a higher apparent surface area and pore volume than most porous crystalline zeolites and related materials [57].

The main characteristics of MOFs are their high porosity; large internal surface area; biodegradability; high loading capacity; the possibility of functionality through surface modification; and the flexible architecture of the structure by selecting appropriate metal ions and linkers [58,59,56]. The possible functional groups representing the organic linkers are carboxylates; phosphonates; imidazolates; sulphonates; and amines, while the metal ions mainly include transition elements [56,54]. The building blocks of MOFs can be held together through different binding forces, including hydrogen bonds, electrostatic interactions, and π-π stacking [58].

In the literature, different approaches have been reported for the synthesis of MOFs, ranging from conventional solvothermal/hydrothermal reactions [56,61] to more convenient procedures, including microfluidic synthesis [62]; microwave synthesis [63]; and mechanochemical [64] and sonochemical techniques [65]. These methods have been described in detail by Tarek and Biswas (2012) [65]. A wide range of hydrophilic, hydrophobic, or amphiphilic drugs, can be quickly loaded into MOFs through different loading strategies such as *in situ* (one-step) encapsulation strategy during the synthesis phase of the hybrid framework or *via ex situ* (post-synthesis) encapsulation strategy [54,55]. The drug can be tethered through biomolecules in the ligand, or encapsulated in the core of the MOFs *via* covalent or noncovalent interactions [55]. Drug release from MOFs may be through matrix degradation mechanisms; ion exchange; desorption; or free diffusion [54,55]. The porosity of the hybrid framework is thought to be the rate-governing factor for controlling the release rate of the encapsulated drug [55]. In addition to their large storage capacity and specific drug release properties, the porous nature of MOFs makes them promising candidates for drug delivery [54,58]. The first MOF used as a drug delivery carrier was achieved by Férey et al. (2006), who encapsulated ibuprofen in MIL-100 (Fe) and MIL-101 (Fe) [66]. Nowadays, MOFs can be used for the delivery of many therapeutic agents, including anticancer drugs [67], vaccines [68], insulin [69], and antibiotics [70].

2.4. Design of cell membrane-coated hybrid NPs (CMCH-NPs)

Cell membrane-coated hybrid NPs are biomimetic drug delivery systems consisting of organic or inorganic NPs core, coated with membranes derived from natural cells. This hybrid system has recently attracted much interest because it retains more advantages from both domains, including the flexibility of the synthetic NPs, with the functionality and complexity of the natural cell membranes [71]. This technology has been developed to provide a hybrid system with enhanced biocompatibility; deep cell penetration properties; prolonged circulation time; high selectivity; improved pharmacokinetics; immunocompatibility; and targeting properties [72–74]. Among the cell membrane-coated NPs, red blood cell membrane-coated NPs were the first CMCH-NPs developed as an alternative to polyethylene glycol

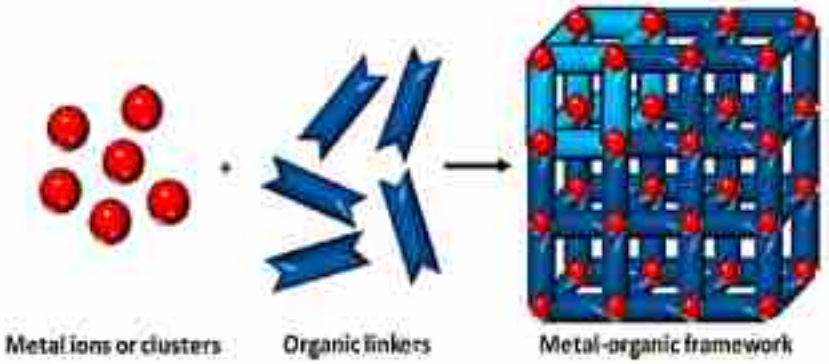

Fig. 5. Scheme illustrating the preparation of MOFs through the co-ordination of metal ions or clusters with organic linkers (adapted with permission from [61]).

(PEG) coating due to their high compatibility and low immunogenicity [73]. Currently, several cell membranes derived from macrophages; platelets; leucocytes; cancer cells; and bacterial cells have been utilized [76]. A top-down approach has been commonly used to fabricate CMCH-NPs, which involves three stages: isolation and extraction of the cell-membrane vesicles through hypotonic treatment; synthesis of the core NP; and then fusion of the NP with the vesicle by physical extrusion or electrostatic interactions [73]. The different steps involved in the synthesis of different types of CMCH-NPs are illustrated in Fig. 4. Due to the biomimetic features and improved distribution of CMCH-NPs, they can be utilized as nanocarriers for enhanced drug delivery through interaction with pathogenic cells using their unique cell surface coating [73]. Once the hybrid system is within the cell, the therapeutic drug can be released slowly by natural diffusion through the membrane after polymer matrix degradation, or rapidly released through external stimuli such as UV-triggered membrane degradation [74].

2.5. Design of hybrid NP-hydrogels

Polymeric nanohydrogels (nanogels) have been increasingly combined with NPs to form hybrid complexes with unique physicochemical and biological properties for localized and controlled drug delivery [77]. A wide range of NPs, including carbon-based nanomaterials; lipid-based vesicles; polymeric NPs; inorganic NPs; and metal-/metal oxides NPs, can be incorporated within the polymeric network to obtain hybrid NP-hydrogels [78]. This innovative incorporation of the two diverse materials results in a novel hybrid nanosystem with enhanced structural integrity and controllable release rate of the combined NPs preserved by the nanogel network [77,78]. In addition, they can offer extra engineering flexibility to enhance the overall therapeutic efficacy. The improved properties of the hybrid NP-hydrogels are mainly attributed to the enhanced physical or covalent interactions between the polymer chains of the hydrogel and the NPs [78].

These hybrid NP-hydrogels can be prepared using three approaches: (a) the addition of NPs into a preformulated hydrogel; (b) the addition of NPs to the polymer solution followed by hydrogel network formation; or (c) monomer polymerization in the presence of preformulated NPs [79,80]. Furthermore, inorganic NPs can be often produced *in situ* within the gel matrix by loading an NP precursor into the gel first, followed by a reduction reaction for the formation of NPs [77]. Generally, drug release from the hybrid NP-hydrogel system is determined by two steps: first, the NPs are released from the hydrogel through diffusion or swelling, which is controlled by the network dissolution. Secondly, the drug is released from the NPs that are governed by the structure, size and fabrication conditions of the NP system [77].

A variety of hybrid NP-hydrogels have been developed for specific drug targeting to different infection sites, such as infections in the joints [81], the spinal cord [82], and the skin [83]. These hybrid biomaterials have shown superior capabilities in modifying drug release kinetics facilitating site-specific drug targeting and NP-based detoxification [77].

3. Application of hybrid nanosystems for antibacterial drug delivery

In recent years, hybrid NPs are being developed to improve the therapeutic efficacy of various antibiotics against bacteria and other infectious pathogens. These hybrid nanosystems have superior physicochemical properties that enable them to enhance the regulated delivery of antibiotics to bacterial cells and, therefore, improve their targeting against bacterial infections. In this section, the latest developments and technical advancements in the field of antibacterial delivery of hybrid nanosystems are discussed.

3.1. Lipid polymer hybrid NPs (LPHNPs)

LPHNPs have been explored as one of the promising strategies in antibiotic delivery against bacterial infections. The subcellular size of LPHNPs allows them to effectively penetrate the target site and release the loaded antibiotic locally, improving antibiotic concentration and localization at the infection site [10]. Polymers have a significant impact on the characteristics of LPHNPs. The incorporation of hydrophobic polymers has been shown to improve the loading of poorly water-soluble drugs, while hydrophilic polymers have been shown to coat the lipid core,which enhances the stability, the loading capacity and the systemic circulation lifetime of hydrophilic drugs [84]. Moreover, some polymers can be modified with specific ligands to impact the targeting of the LPHNPs. Therefore, due to the importance of the polymeric material

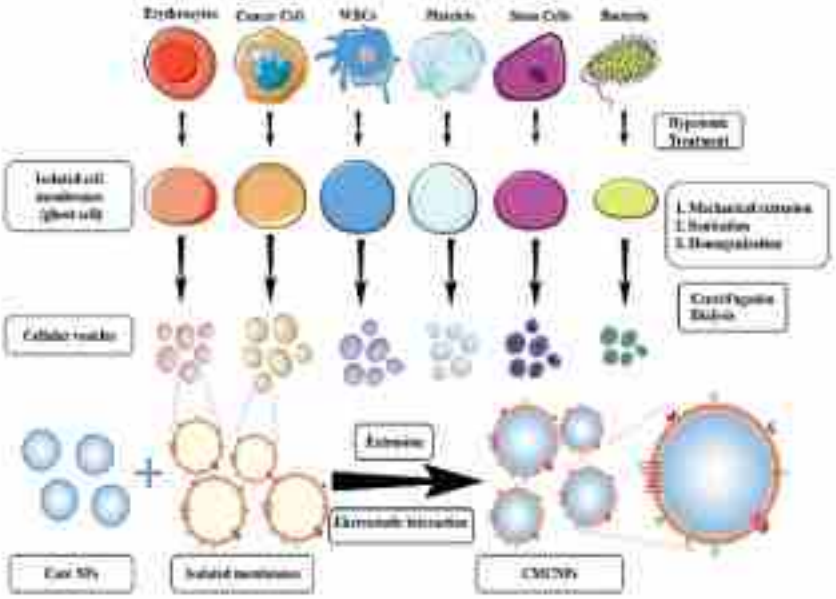

Fig. 4. Various synthesis methods of CMCH-NPs (adapted with permission from [73]).

used to formulate LPHNPs, this section discusses the applications of LPHNPs for their antibiotic delivery based on their polymeric constituents, such as the PLGA-, chitosan- (CHT) and dendrimers employed in formulating them.

3.2.1. PLGA-based LPHNPs

PLGA has primarily been used as a polymeric core in various LPHNP formulations for antibacterial delivery, demonstrating excellent physical properties, biocompatibility, sustained drug release and biodegradability [85]. Due to the versatility and biocompatibility of the polymer, various research groups have explored the potential use of PLGA-based LPHNPs as a drug delivery system for different routes of administration. The first study in this field was published by Bhardwaj et al. (2015), who designed and optimized LPHNPs for combined pulmonary delivery of isoniazid and ciprofloxacin hydrochloride. The spray drying technique was used to create a dry powder inhaler (DPI) form of the drug loaded hybrid nanosystems. The presence of PLGA had a significant impact on controlling drug release from the LPHNPs. Furthermore, antibiotic-loaded LPHNPs achieved the maximum cellular uptake in alveolar macrophages compared to free antibiotics. *In vivo* studies revealed that maximum internalization efficiency into the lung was achieved by delivering LPHNPs in spray-dried powdered forms *via* the pulmonary route. Hence, the antibiotic-loaded LPHNPs developed in this study could be beneficial as an antibiotic delivery system to treat bacterial tuberculosis [86]. However, further evaluation of essential parameters such as biocompatibility studies, and *in vitro* and *in vivo* antibacterial activity studies, for the prepared LPHNPs are necessary to confirm the biosafety and antibacterial profile of the nanosystems.

In addition to the pulmonary route, topical application of PLGA-LPHNPs has also been reported for drug delivery. In a subsequent study, Dave and coworkers (2017) designed biodegradable LPHNPs with a sustained-release profile using different ratios of the hydrophobic polymer PLGA to control the release of the antibiotic norfloxacin at the site of infection, and to improve its topical activity to treat burn infections. The optimized norfloxacin-loaded LPHNPs formulation was selected to prepare LPHNPs@Carbopol gel for topical antibiotic delivery. *In vitro* skin permeation results of this formula showed a maximum release profile, due to the higher encapsulation of the drug in NPs, compared to other formulations. Antimicrobial activity against *Staphylococcus aureus (S. aureus)* and *Pseudomonas aeruginosa (P. aeruginosa)* indicated that norfloxacin-loaded LPHNPs are effective against gram-positive and gram-negative bacteria, confirmed by measuring the zone of inhibition. As a result, these norfloxacin-loaded LPHNPs were shown to be safe and efficient for long-term treatment of bacterial infections caused by burn [87].

More recently, Fangary's research group (2022) produced a unique liposome combined with small PLGA- NPs (PLGA NP-Lips) for simultaneous ocular administration of erythromycin and 3c (a novel 5-cyanothiazolyl urea derivative with promising antibacterial activity). This work attempted to overcome antibiotic drug resistance by increasing nanocarrier uptake and antibiotic delivery in bacterial cells while minimizing toxicity toward human cells. The two-step manufacturing approach was used to create erythromycin/3c-loaded PLGA NP-Lips, and the antibacterial activity of these hybrid NPs was assessed against gram-negative *Escherichia coli* (*E. coli*) and *P. aeruginosa*. *In vitro* studies revealed that incorporation of small PLGA NPs into liposomes reduced the NP uptake by HEK293 cells while enhancing it in gram-negative bacterial cells. Consequently, four-fold and eight-fold improvements in antibiotic selectivity were observed for *E. coli* and *P. aeruginosa*, respectively. Ocular administration of the erythromycin/3c-loaded PLGA NP-Lips in a *P. aeruginosa* keratitis mouse model allowed for potent selective inhibition of bacterial infection and full recovery. Moreover, in comparison to free antibiotics and PLGA NPs, administration of PLGA NP-Lips showed substantial reduction in infection-induced inflammation (tumor necrosis factor-α(TNF-α) and interleukin (IL-6) levels), confirming the cytocompatibility and the therapeutic potential of the developed hybrid nanocarrier [88]. Overall, given the flexibility and biosafety of PLGA, other routes of administration can be explored in future research using PLGA-based LPHNPs.

Besides improving the antibacterial activity of antibiotics, PLGA-LPHNPs are being used to eradicate biofilms. Biofilms are multicellular aggregates of microorganisms embedded in a self-produced polymer matrix consisting of polysaccharides, lipids, proteins and DNA [89]. Bacterial biofilms have been linked to chronic infectious diseases such as staphylococcal infections and chronic *P. aeruginosa* lung infections, due to their increased tolerance to antibiotics, aside from resisting the host's immune system defence mechanisms [90]. To improve the therapeutic efficacy of antibiotics against bacterial biofilm, Baek et al. (2018) and Guo et al. (2020) have reported the development of self-assembling PLGA-LPHNPs with different lipid components. Both studies examined the effect of PLGA and lipid constituents of the LPHNPs on the release profiles of encapsulated antibiotics. The results showed more extended antibiotic release from PLGA-LPHNPs compared to non-hybrid PLGA-NPs, confirming the impact of the hybrid system on controlling the drug release. Baek et al. (2018) investigated the binding affinity of PLGA-NPs and PLGA-LPHNPs to both planktonic cells and bacterial biofilm. Propidium bromide (PI)-encapsulated NPs were prepared and introduced into planktonic cells and biofilms of different gram-positive and gram-negative strains. The increased PI intensity indicated the aggregation of the PLGA-LPHNPs around the bacteria and biofilm with higher affinity than PLGA-NPs (Fig. 5A). Furthermore, they investigated the release profile of antibiotics with varying degrees of hydrophilicity from PLGA-NPs and PLGA-LPHNPs. The latter had a more sustained release profile for hydrophobic (rifamycin), amphiphilic (ampicillin), and hydrophilic (amoxicillin, kanamycin, D-cycloserine) antibiotics; while PLGA-NPs exhibited a faster release profile for hydrophilic drugs (Fig. 5B). When comparing the antimicrobial activity of LPHNPs against bacterial biofilms to that of free antibiotics, PLGA-LPHNPs demonstrated a significant increase in biofilm inhibition at concentrations 8–32 times lower than that of free antibiotics, confirming the effectiveness of the prepared hybrid NPs in eradicating bacterial biofilm [91].

While the above study focused solely on biofilm eradication, there are emerging studies evaluating combined antibacterial and antibiofilm effectiveness. For instance, Guo et al. (2020) created linezolid@PLGA-LPHNPs, aiming to evaluate the antibacterial and antibiofilm activities of the prepared hybrid system against intracellular MRSA residing within osteoblasts and biofilms to treat osteomyelitis. Although the hybrid system attained lower antibacterial activity against planktonic MRSA, it was far more effective against intracellular MRSA embedded inside bone cells than free linezolid. Furthermore, linezolid-loaded LPHNPs showed superior antibiofilm activity to the free antibiotic, and these activities were attributed to the excessive accumulation of the hybrid system inside the infected bone cells and biofilms, which was validated by an *in vivo* biodistribution study (> 4-fold increase in linezolid -bone level was observed when linezolid-LPHNPs was used) [92]. Later, the same research team developed similar hybrid NPs loaded with rifampicin to target intracellular and biofilm embedded MRSA (2020). Rifampicin-loaded LPHNPs showed moderate but significant antibacterial activity against planktonic osteomyelitis-causing MRSA, with superiority to the free drug. Also, in comparison to free rifampicin, rifampicin-LPHNPs showed improved antibacterial and antibiofilm activity against intracellular MRSA within osteoblasts and biofilms. Confocal microscopy pictures demonstrated the widespread deposition of antibiotic-loaded LPHNPs inside MRSA-infected bone cells and biofilm matrices [93]. Further studies are needed to improve the bone and biofilm targeting properties of rifampicin-LPHNPs and evaluate their *in vivo* antimicrobial activity and biosafety, in addition to investigating the possibility of using these hybrid NPs for the systemic delivery of antibiotic combinations.

In order to construct successful hybrid nanocarriers for antibacterial delivery, and further enhance the performance of LPHNPs against intracellular bacteria, it is essential to identify correlations between the

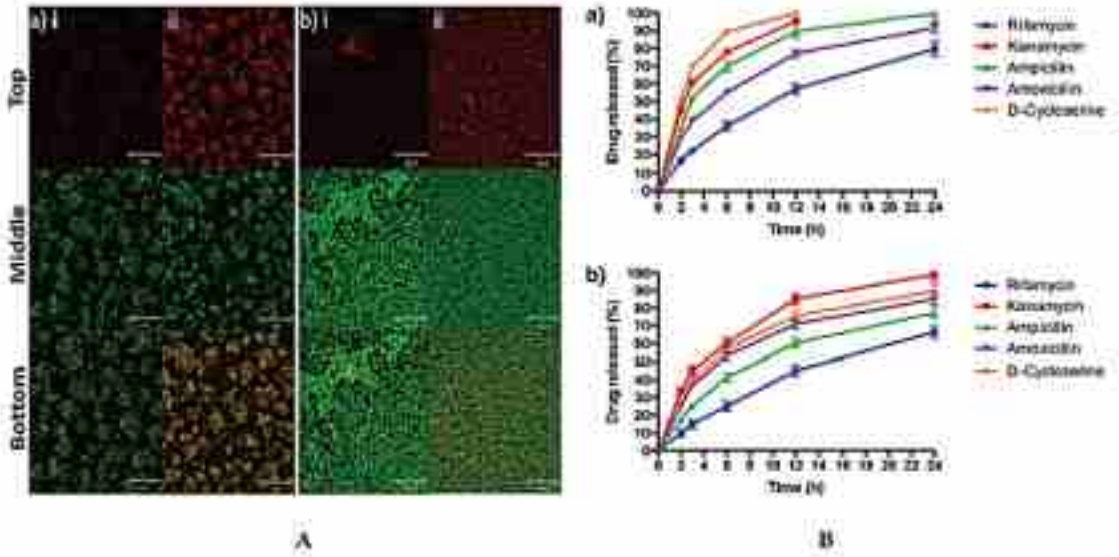

Fig. 5. (A): Confocal laser scanning microscopy (CLSM) images of a) *E. faecalis* and b) *S. aureus* biofilms co-stained by PI encapsulated PLGA-NPs (i) or PLGA-LPHNPs (ii). (B): *In vitro* release profiles of different antibiotics from (a) PLGA-NPs and (b) PLGA-LPHNPs in PBS (pH 7.4) for 24 h at 37 ± 1 °C (adapted with permission from [91]).

physicochemical properties of hybrid NPs and their intracellular uptake. An emerging research has been reported by these and coworkers (2020), who explored the effect of lipid constituents and lipid-based surface engineering on the biological cell-NP interaction. The research team investigated the effect of surface charge on the physicochemical properties, macrophage uptake, and *in vitro* intracellular killing efficiency of cationic and zwitterionic PLGA-LPHNPs loaded with doxycycline or vancomycin against *S. aureus* and *M. smegmatis*. All tested PLGA-NPs, and cationic LPHNPs, inhibited the intracellular growth of *S. aureus* and *M. smegmatis* effectively, with the latter was more successful. This is due to the synergism between the antibiotics and the cationic hybrid NPs, enhancing the antibacterial activity against intracellular pathogens. However, the authors did not notice a synergistic effect for zwitterionic LPHNPs. In addition, cationic LPHNPs showed higher macrophage recognition and uptake, and thus enhanced *in vitro* intracellular antibacterial activity compared to zwitterionic LPHNPs and non-lipid PLGA-NPs because of strong adhesion of the cationic lipid shell and the negatively charged bacteria [94]. Overall, the data obtained from this research study suggest that LPHNPs containing cationic lipids have the potential to enhance macrophage uptake and thereby improve the intracellular antibacterial efficacy of antibiotics against gram-positive bacterial infections.

Taken together, the findings of these studies encourage the application of PLGA-based LPHNPs as antibacterial delivery systems, because of their ability to enhance stability; biodegradability; controlled drug release; and antibacterial activity, suggesting a promising approach to improve antibiotics efficacy and reduce the development of resistance. Also, the investigations indicated that PLGA-based LPHNPs could remove hard-to-treat infections such as intracellular bacteria, osteomyelitis and biofilms, despite the fact that free antibiotics are not able to reach these infection sites. Most of these hard-to-treat conditions have been reported as a source of chronic infections and antimicrobial resistance [90,95,96]. The versatility of PLGA-based LPHNPs has been proved by their ability to be formulated into different dosage forms via spray drying, loading into gels and colloidal systems, and then administered to the body via different routes such as transdermal, inhalation, ocular and parenteral. Table 2 summarizes the current state of research on the preparation of LPHNPs using PLGA as a polymeric core, highlighting their lipid constituent; the ratios of poly lactic acid (PLA)/poly glycolic acid (PGA) copolymer used; the antibiotic drug loaded; the method of preparation; and the characterization studies and findings. As shown in the table, only PLGA 50:50 has been used to formulate all PLGA-based LPHNPs. This could be due to its favorable degradation properties compared to the other PLGA types [88], making it an attractive polymeric candidate to fabricate LPHNPs for controlled antibiotic delivery.

3.1.2. Chitosan-based *LPHNPs*

Chitosan (CHT) is a cationic natural polymer with inherent antimicrobial and antifungal properties. It has been widely employed as an antibiotic delivery polymer. This is due to its unique characteristics, such as biocompatibility; biodegradability; non-toxicity; and target specific triggering due to its cationic nature [97]. Recently, the application of CHT in the preparation of antibacterial-loaded hybrid NPs has attracted considerable interest for its use against microbial infections. Therefore, in this subsection, conventional and stimuli-responsive CHT-based LPHNPs with mono-antibiotic therapy and CHT-based LPHNPs with dual-antibiotic therapy will be discussed.

Monotherapy with the use of various antimicrobials, such as antibiotics, is one of the successful strategies to treat different bacterial infections. Two research studies were reported by Thakur and coworkers, describing the use of CHT to fabricate conventional LPHNPs with mono-antibiotic therapy. In the first study, Thakur's research group investigated the possibility of combined lipid NPs and CHT as a therapy for managing and treating wound infections (2018). They developed and optimized LPHNPs loaded with fusidic acid by the hot micro-emulsion method. Administration of fusidic acid-LPHNPs resulted in a five-fold decrease in its MIC against MRSA and other *S. aureus* bacterial strains, accompanied by a longer period of antibacterial activity compared to the free fusidic acid solution. This protracted antibacterial activity is attributed to the incorporation of the drug within the hybrid system, which attempts to prolong the residence time of the drug at the infection site, besides enhancing its penetration into the bacterial cell wall. The optimized formulation of fusidic acid-LPHNPs was selected to prepare LPHNP-loaded carbopol gel for the topical application against burn wound infections. The gel incorporating NPs exhibited good gel strength; extrudability; spreadability and enhanced permeation into mice skin. The comprehensive studies indicated that the developed

Table 2
Summary of the studies undertaken to date with LPHNPs using PLGA as a polymeric core.

Lipid	PLA/PGA copolymer ratio	Antibiotic drug	Method of preparation	Characterization studies	Characteristic findings	Ref.
Soy lecithin	50:50	Isoniazid/ Ciprofloxacin	DESE	PS, PDI, EE % Particle flow properties Aerodynamic properties DSC, FT-IR, morphology (SEM)	- Size: 111 and 172 nm, PDI: 0.189 and 0.168 and EE %: 82.84% and 88.48% for isoniazid and ciprofloxacin loaded LPHNPs, respectively - DPI had good flow properties - MMAD <3 μm with high lung localization	[96]
Soy lecithin (benzyl amine	50:50	Norfloxacin	RSE	PS, PDI, ZP Morphology (TEM/ SEM) FT-IR DSC and TGA Characterization of the LPHNPs loaded gel - Viscosity - pH - Spreadability - Skin irritation assay	- Size: 109–219 nm - Suitable viscosity, pH and spreadability with decreased skin irritation upon application on burnt skin.	[97]
Soy lecithin Cholesterol	50:50	Erythromycin Tc	RSE/thin film hydration	PS, ZP Morphology (SEM, TEM) EE % Cytotoxicity assay	- Size: 364 nm - ZP: – 20 Mv - EE%: 85.4% - Minimum dose-dependent cytotoxicity	[98]
Cationic DOTAP	50:50	Rifampicin Ampicillin Vancomycin Amoxicillin D-cycloserine	Self-assembly approach	PS, PDI, ZP Morphology (TEM)	- Positive ZP indicating the coating of PLGA surface with the cationic DOTAP. - High EE% for antibiotics, irrespective of their water solubility	[91]
Lecithin DSPE-mPEG-2000 Cholesterol	50:50	Linezolid	Nanoprecipitation	PS, PDI, ZP Morphology (TEM) EE % Dispersion stability Cytotoxicity assay	- Size: 110 - PDI: 0.120 - Controlled drug release. - Enhanced serum stability - Minimum cytotoxicity against osteoblast	[92]
Lecithin DSPE-mPEG-2000 Cholesterol	50:50	Rifampicin	Nanoprecipitation	PS, PDI, ZP Morphology (SEM) EE % Dispersion stability Cytotoxicity assay	- Size: 110 nm and - PDI: 0.141. - Controlled drug release. - Maximized serum stability - No noticeable toxicity against osteoblast	[94]
Cationic DOTAP Zwitterionic PC	50:50	Doxycycline Vancomycin	Modified RSE	PS, PDI, ZP Morphology (SEM, TEM) EE % Cytotoxicity assay	- LPHNPs had significantly less particle size than non-lipid PLGA NPs (p-value <0.05) - Dose-dependent cytotoxicity for cationic LPHNPs, and no noticeable cytotoxicity for zwitterionic LPHNPs.	[34]

DESE, double emulsification solvent evaporation; PS, particle size; PDI, polydispersity index; EE%, percentage entrapment efficiency; DSC, differential scanning calorimetry; FT-IR, Fourier transform infra-red; SEM, scanning electron microscope; TEM, transmission electron microscope; DPI, dry powder inhaler; MMAD, mass median aerodynamic diameter; TGA, thermogravimetric analysis; DSPE-mPEG-2000, 1,2-distearoyl-sn-glycero-3 phosphoethanolamine-N-amino(polyethylene glycol)-2000; DOTAP, 1,2-dioleoyl-3-trimethylammonium-propane; PC, phosphatidylcholine.

hybrid system offer possible advantages in prolonged and improved burn wound healing [95]. One year later, the same research group subjected the fusidic acid-LPHNPs gel to *in vivo* pharmacodynamic studies in a murine burn wound model infected with MRSA (2019). The results of the *in vivo* bacterial loads indicated that the fusidic acid-LPHNP gel exhibited significant antibacterial potency against the MRSA that was present in the burn wound, as the animals treated with fusidic acid-LPHNPs gel exhibited significantly higher bacterial count reduction, compared to the conventional fusidic acid topical formulation, during 15 days of treatment [96]. The formulation strategies of these studies show the safety and effectiveness of fusidic acid-encapsulated LPHNPs in inhibiting bacterial infections. They also provide a unique hybrid system for topical application against burn wound infection.

Furthermore, CHT has been introduced to prepare stimuli-responsive LPHNPs with mono-antibiotic therapy. Stimuli-responsive LPHNPs have the potential to improve the therapeutic efficacy of antibiotics, while reducing their side effects, by releasing the encapsulated drug at the site of infection in response to stimuli [100]. Depending on the type of polymer, lipid and functional groups, various stimuli-responsive LPHNPs, such as pH-responsive LPHNPs, have been developed. To explore the advantages of these pH-responsive LPHNPs, Hasnain et al. (2020) fabricated novel vancomycin-loaded pH-responsive LPHNPs using CHT and a synthesized oleyl amine based zwitterionic lipid (OLA), produced by ion gelation, to deliver vancomycin against MRSA. The *in vitro* antibacterial activity of the developed hybrid nanosystem against MRSA was higher than bare vancomycin and was also enhanced at pH 6.0, compared to the physiological pH 7.4, indicating that the system was pH-dependent. The overall enhancement in the antibacterial activity of the LPHNPs could be due to the increase in the binding of the system to the negative bacterial membrane and the additive intrinsic antimicrobial activity of the LPHNPs. Assessment of the developed LPHNPs with different *in vitro* antibacterial activity tests, indicated that LPHNPs had the potential to effectively treat MRSA, and resulted in the successful and irreversible membrane disruption and biofilm eradication, compared to the free vancomycin. Also, the *in vivo* results obtained by treating mice skin infection revealed the ability of the LPHNPs to reduce and eradicate MRSA colonies (MRSA/CFU) by 95-fold, when compared to bare vancomycin treatment, confirming the effectiveness of the prepared hybrid nanosystem in treating MRSA infections [101]. According to the author's findings in this work, innovative biocompatible vancomycin-loaded pH-responsive LPHNPs can potentially be effective in the pH-responsive targeted delivery of VCM to effectively prevent the development of antimicrobial resistance.

Besides mono-antibiotic therapy, dual-therapy, which combines different antibiotics or antibiotics with adjuncts, has been introduced to

improve the efficiency of already-in-use antibiotics through synergistic effects, or to combat antibiotic resistance [102]. Rodenak-Kladniew et al. (2019) and Bselani et al. (2020), published two research studies on the use of CHT-based LPHNPs encapsulating an antibiotic-adjunct combination for dual antibacterial therapy. Their strategy aimed to enhance the antibacterial efficacy of the loaded antibiotics against both gram-positive *S. aureus* and gram-negative *P. aeruginosa*. Both research groups employed a hot homogenization/ultrasonication technique, while using different lipid nanocarriers for the development of a CHT-hybrid nanosystem. Rodenak-Kladniew et al. (2019), developed hybrid CHT-based solid lipid NPs (CHT/SLNs) incorporating the broad-spectrum antibiotic, ofloxacin, and a natural phenolic compound, eugenol (Eu), into a lipid matrix (ofloxacin-Eu@CHT/SLNs). Characterization of the developed hybrid SLNs by different analytical tools confirmed the presence of spherical NPs composed of a lipid matrix containing an ofloxacin-Eu combination and coated with positively charged CHT. This hybrid ofloxacin-Eu/CHT SLNs showed improved antimicrobial activity against *P. aeruginosa* and *S. aureus*, with MICs that were 4- and 16-fold lower than free ofloxacin, respectively. These findings suggest that CHT and Eu may have an impact on the increased antibacterial activity of the encapsulated antibiotic. Moreover, *in vivo* investigations using hybrid SLNs delivered *via* a pulmonary route to mice in the form of DPI showed that the hybrid NPs were nontoxic to human pulmonary cells and can be applied as an inhalable therapeutic system to treat pulmonary infections [103]. Alternatively, Bselani et al. (2020) incorporated nalidixic acid-vanadium complex into myristyl myristate nanostructured lipid carriers (NCL) hybridized with CHT to improve the antibiotic complex's solubility, bioavailability, and antimicrobial activity. Likewise, the results showed a significant antibacterial enhancement for the loaded NCL/CHT against *P. aeruginosa* with a MIC value of 129.3 μM compared to 625 μM of the free nalidixic acid-vanadium antibiotic complex, while the MIC of the loaded NCL/CHT against *S. aureus* was in the same order as the free complex (129.9 μM vs. 125 μM). Furthermore, the authors investigated the quorum sensing inhibition activity of the developed NCL/CHT hybrid NPs, and the results indicated that the formulated hybrid NPs exhibited an inhibitory effect on quorum sensing, observed by reporter strain *Chromobacterium violaceum*. However, further investigations for the developed nalidixic acid-vanadium hybrid NPs, including *in silico* studies and preclinical studies in appropriate animal models, are still required [104]. In summary, the outcomes of these reported studies confirm the influence of CHT on controlling LPHNP drug release and increasing the antibacterial efficacy of the encapsulated antibiotics against both gram-positive and gram-negative bacterial infections.

Accordingly, the overall data illustrate that chitosan-based LPHNPs are actively being studied, as the polymer has an intrinsic, antimicrobial effect that improves the overall antimicrobial activity of the system. Moreover, the polysaccharide polymer has multiple surface amine groups which use covalent modifications, and electrostatic and supramolecular interactions, to formulate stable conventional and stimuli-responsive LPHNPs.

3.1.3. Dendritic-based LPHNPs (LDHNPs)

Dendrimers are synthetic polymers with an especial branching architecture. They possess numerous advantages that make them suitable as drug delivery platforms, such as multivalency; globular architecture; well-defined molecular weight; the ability to encapsulate a variety of therapeutic agents within the internal hydrophobic environment; and the availability of multiple surface functional groups [105,106]. Therefore, dendrimers with specific properties can be used to improve the performance of lipid dendrimer hybrid NPs (LDHNPs) as a novel type of LPHNP for effective antibiotic delivery. Encapsulation of a dendrimer in a lipid shell as liposomes and SLNs can improve the solubility and the EE percentage of the loaded drug [107]. To date, only two papers using dendrimers have been published by Govender's research group. In the early study, Sonawane et al. (2016) developed a system of LPHNPs with a dendrimer for the effective delivery of vancomycin against MRSA infections. They prepared LDHNPs through a hot stirring ultrasonication technique using the solid lipid Compritol 888 ATO, and a generation 4 poly amidoamine-succinamic acid dendrimer (G4 PAMAM-SA). The formation of LDHNPs with G4 PAMAM-SA entrapped inside the lipid shell, and vancomycin encapsulated within the dendrimer core, were confirmed using DSC and FT-IR studies. *In vitro* antibacterial activity studies confirmed the enhanced antibacterial activity of vancomycin-LDHNPs with MICs of 15.62 μg/ml and 7.81 μg/ml against *S. aureus* and MRSA, respectively. In addition, the formulation exhibited sustained antibacterial activity with an MIC of 62.5 μg/ml against *S. aureus* and 500 μg/ml against MRSA for up to 72 h and 54 h, respectively [108]. Later, Moji and coworkers (2019) formulated and optimized novel pH-responsive LDHNPs to effectively deliver vancomycin into the site of infection targeting intracellular MRSA. The LDHSDPs were formulated by the ESE method using OLA as a lipid and G3 PAMAM-SA dendrimer as a polymer. The antibacterial activity of LDHNPs against MRSA showed an 8-fold lower MIC at pH 6.0 and 7.4, compared to treatment with bare vancomycin. Also, bacterial cell viability study indicated that, despite the lower MIC values, vancomycin-LDHSPs were more effective at killing MRSA than free vancomycin, with complete cell membrane destruction. Likewise, the treatment with vancomycin-LDHNPs showed significant intracellular antibacterial activity, as compared to untreated cells and cells treated with vancomycin only [10]. Although, the same research group had previously conducted two studies on the formulation and development of LDHNPs for antibacterial drug delivery, the latter confirmed that the therapeutic potential of such a hybrid system for improving antibiotic delivery and combating drug resistance could be enhanced by designing it as a pH-responsive system using different lipid and dendrimer components. Therefore, in both studies, further investigation with *in vivo* studies is required to prove their *in vitro* findings of the developed LDHNPs.

As already stated, dendrimers have traits that make them attractive and promising candidates for drug delivery. However, concerns about their toxicity and biocompatibility limit their applications and translational potential [106,109]. According to the studies discussed, dendrimers have the potential to be used as an effective delivery system for antibiotics, when incorporated into LPHNPs with various polymeric and lipid constituents, because they have the ability to control antibiotic release; improve biocompatibility and stability; and enhance antibacterial efficacy and the formulation of stimuli-responsive systems. However, there is a need for acute and long-term, in-depth toxicological studies to confirm their safety profiles. Moreover, apart from PAMAM dendrimers which are cationic in nature, studies involving anionic dendrimers, which have better biosafety profiles, could result in safer hybrid nanosystems [110].

3.2. Organic-inorganic hybrid NPs

Various combinations of organic and inorganic materials are being used to construct different nanocarriers to treat bacterial infections, including nanofibers, mesoporous silica NPs (MSNs) and nanocomposites. In this sub-section, we describe the incorporation of antibiotics, as well as free radical releasing biomaterials, into organic-inorganic hybrid NPs, to achieve site-specific and controlled-release delivery systems, which offer significant advantages in improving antibacterial efficiency and overcoming therapeutic problems caused by bacteria. [111].

Several classes of antibiotics, such as penicillins; tetracyclines; aminoglycosides; fluoroquinolones; macrolides and polymyxins have been employed to fabricate antibiotic-loaded organic-inorganic hybrid NPs for effective antibacterial delivery. The first report of an organic-inorganic hybrid NP loaded with an antibiotic was by Wang et al. (2013), who employed an electrospinning approach to fabricate amoxicillin-loaded laponite (LAP)-doped PLGA (amoxicillin-LAP/PLGA) nanofibers for antibacterial application. The authors aimed to provide

the nanofiber hybrid system with a sustained release profile and to improve its mechanical durability. The amoxicillin LAE/PLGA nanofibers showed a biphasic *in vitro* release pattern due to the combination of two different dissociation pathways, leading to a slower release of the antibiotic for up to nine days. Also, the hybrid nanofibers revealed concentration-dependent and long-term antibacterial activity against *S. aureus* in a liquid and a solid medium for 40 h. The system showed ≥90% antibacterial inhibition at higher concentrations, with no significant difference compared to the free amoxicillin and amoxicillin-loaded PLGA nanofibers [112]. One year later, the same research group reported two research studies with the same preparation approach to fabricate hybrid nanofibers using the same organic material, PLGA, but with different inorganic materials, namely n-hydroxyapatite(n-HA) and halloysite nanotubes (HNTs), and encapsulated antibiotics, amoxicillin and tetracycline, respectively, to target *S. aureus*. The results were comparable with the previous study as the encapsulation of the antibiotics into the hybrid nanofibers also enabled sustained and controlled release profiles, with effective and prolonged growth inhibition activity of the antibiotics against the gram-positive bacterial strain. Among the reported organic-inorganic hybrid nanofibers, tetracycline-loaded HNTs/PLGA NPs showed the most sustained release for up to 42 days, and thus their antibacterial activity was improved significantly [113,114]. Cytocompatibility of the formulated hybrid nanofibers in the three studies, together with the improved mechanical durability and antibacterial activity, indicated the potential of such hybrid organic-inorganic NPs for application as antibacterial drug delivery systems in the field of tissue engineering. However, if such research modifications are to have an impact, more investigations, such as preclinical *in vivo* studies, are required.

Another antibiotic that has been explored for loading organic-inorganic hybrid NPs formulations is gentamicin. Vasile et al. (2014) and Yang et al. (2018) have reported different gentamicin-loaded organic-inorganic hybrid NPs intended for the treatment of extracellular and intracellular bacterial pathogens, respectively. Vasile and co-workers (2014) developed and optimized a gentamicin-loaded zinc oxide-CHT (gentamicin-ZnO/CHT) hybrid nanocomposite to improve the targeting efficacy of gentamicin in treating external bacterial infections. The sustained release characteristics of the prepared gentamicin-ZnO/CHT NPs improved the antibacterial activity of the hybrid nanosystem against *S. aureus* and *P. aeruginosa* in both planktonic and surface-attached conditions. Since controlled, synergistic and prolonged antibacterial activity was obtained, with four-fold and two-fold lower MIC values against *S. aureus* and *P. aeruginosa*, respectively, compared to the free gentamicin control [115]. On the other hand, Yang et al. (2018) developed a novel gentamicin-loaded MSNs decorated with bacteria toxin-sensitive liposomes immobilized with a targeting peptide ubiquicidin (UBI_{29-41}) to enhance the targeting efficacy and binding affinity of gentamicin to the intracellular *S. aureus*. The antibiotic release from MSNs/LU hybrid NPs was triggered by bacterial toxins which degraded the liposome bilayer, allowing the rapid release of the loaded antibiotic from the hybrid system. *In vitro* and *in vivo* antibacterial activity studies confirmed the superior antibacterial effects of gentamicin-MSNs/LU hybrid NPs against planktonic and intracellular bacterial infection, in comparison to free gentamicin and gentamicin-loaded MSNs. Moreover, the inflammation-related gene expression in infected pre-osteoblasts and macrophages was also reduced extensively after treatment with the gentamicin-MSNs/LU hybrid NPs. Therefore, the cytocompatibility and the microenvironment-responsive antibiotic release of gentamicin-MSNs/LU hybrid NPs confirm their potential to target intracellular pathogens and inflammation associated with intracellular *S. aureus* infections and possibly other gram-positive bacterial infections [116]. In both studies, the therapeutic efficacy of gentamicin against bacteria has been improved significantly; although, in the later work, the authors modified the prepared organic-inorganic hybrid NPs by integrating a bacteria toxin-sensitive liposome and a targeting peptide into the nanosystem. In addition, the prepared NPs were fully characterized, including *in vivo* studies, which allow the clinical translation of such a research study.

Moreover, fluoroquinolone antibiotics, especially ciprofloxacin, have been introduced into various organic-inorganic hybrid NPs to treat infectious diseases caused by gram-positive and gram-negative pathogens. Two research studies reported the delivery of ciprofloxacin via organic-inorganic hybrid NPs for controlled and targeted drug delivery. Murugesan and coworkers (2018) investigated the functionalization of a natural biocompatible organic humic acid (HA) with ZnO for the pH-responsive and site-specific delivery of ciprofloxacin, using a simple ESE method. The prepared ciprofloxacin-loaded ZnO-HA hybrid NPs showed higher bacterial growth inhibition against *P. aeruginosa* and *B. cereus*, with lower MIC values compared to the blank ZnO-HA hybrid NPs and free ciprofloxacin. In addition, the biofilm formation was suppressed by 75% and 85%, for *B. cereus* and *P. aeruginosa*, respectively, when treated with the drug-loaded hybrid nanocarrier [117]. Later in the same year, Al-Obaidi et al. (2018) reported novel hybrid NPs of silica-coated AgNPs embedded into a ciprofloxacin-encapsulated CHT matrix for effective inhibition of growth and biofilm formation of *P. aeruginosa*. The authors attempted to produce a first inhalable dosage form of ciprofloxacin for treating cystic fibrosis (CF) caused by gram-negative bacteria. They investigated and optimized various parameters, such as Ag^+ concentration and CHT ratio, to obtain hybrid NPs with an improved particle deposition within the lung. The prepared hybrid NPs were deposited in Stage 2, reaching ~70% deposition, which is considered essential for the successful delivery of the drug deep inside the lung. *In vitro* antibacterial and antibiofilm formation assays revealed that the formulated hybrid system exhibited 3–4 times more growth and biofilm inhibition with a synergistic antibacterial effect against *P. aeruginosa*, compared to free ciprofloxacin [118]. Despite the promising outcomes in these two studies, further development through performing a cytotoxicity investigation, and cellular uptake and *in vivo* studies in suitable animal models, are required to illustrate the advantages of both hybrid nanocarriers.

Tetracyclines were also loaded into organic-inorganic hybrid NPs to improve their targeting efficacy against pathogenic bacteria. Kaushik et al. (2020) designed a novel pH-responsive trio-hybrid nanocomposite system based on MSNs with the goal of overcoming antibiotic resistance. They developed tetracycline immobilized Cu-doped MSNs reacted with silver-stabilized polyethyleneimine (AgNPs-PEI) through a series of reaction steps. The antibacterial activity was studied against MDR *E. coli* species, and the results indicated that hybridization of tetracycline-encapsulated Cu-MSNs NPs with AgNPs-PEI significantly improved the antibacterial effectiveness of tetracycline against MDR *E. coli* through sensitizing the cell membrane to the ROS generation effect of Ag, thus improving the intracellular availability of the hybrid nanocarrier for the pH-triggered release of the antibiotic associated with high ROS levels due to the Cu-MSNs. Altogether, this biocompatible trio-hybrid nanocomposite with a synergistic effect and pH-responsive delivery of tetracycline is considered a promising approach for efficiently combatting MDR infections [119].

Currently, two research studies published by Inalis et al. (2022) and Xiang et al. (2022), further improved the performance of organic-inorganic hybrid NPs for efficient antibiotic therapy. First, Inalis et al. (2022) developed a novel organic-inorganic hybrid nanocarrier for polymyxin delivery, aimed to optimize their antibacterial properties against various infectious diseases while minimizing their toxic side effects. A hybrid core-shell silver-poly glutamic acid NPs loaded with polymyxin B and E, respectively, (polymyxin@PGlu-Ag NPs) have been designed and carefully investigated. Cytotoxicity studies were performed to confirm the biosafety, biocompatibility, and minimal macrophage uptake of the prepared hybrid nanocarriers. Then, the synthesized NPs were incorporated into an agarose gel to form a hydrogel nanocomposite delivery system proposed to treat skin wound infections. The antibacterial efficacy of both polymyxin-loaded hybrid NPs and their nanocomposites were assessed against *P. aeruginosa*, in

vitro. Both formulations demonstrated a synergistic bacterial growth inhibition against *P. aeruginosa* proved by the lower MICs (1 μg/ml), when compared to free polymyxin, blank hybrid NPs and bare AgNPs. This decreased MIC values could be attributed to the combined activity of the polymyxins and AgNPs in one hybrid nanosystem. In summary, they concluded that polymyxin@PGlu-Ag NPs and their hydrogel composite could eventually enhance the therapeutic potential of polymyxins to treat skin injuries [120].

More recently, Xiang and co-workers (2022) loaded a macrolide antibiotic azithromycin and a photosensitizer methylene blue into zwitterionic pH-responsive MSNs/polypeptide hybrid nanoparticles (azithromycin/MB@MSPNs) for chemo-photodynamic combination therapy against MRSA infections. A pH-triggered and lipase-induced controlled azithromycin release was achieved, and the loaded MB revealed an efficient generation of singlet oxygen ($^1O_2$), which resulted in a facilitated photodynamic action. Also, the prepared azithromycin/MB@MSPNs showed improved biocompatibility toward normal mammalian cells, and a strong antibacterial and antibiofilm activity against MRSA. Moreover, *in vivo* studies were conducted in an MRSA infected mice model, and the hybrid nanocarrier exhibited synergistic and enhanced bactericidal action with a rapid wound healing process for up to 94% comparing to mono azithromycin therapy. Therefore, the developed azithromycin/MB@MSPNs could be promising candidate for clinical application in combined chemo-photodynamic therapy against MDR bacteria [121].

In addition to antibiotic delivery, different organic-inorganic hybrid nanoparticulate systems have been explored as a free radical release platform against infectious diseases. Free radicals have been known to have significant antibacterial activity against gram-positive and gram-negative bacteria, in addition to multidrug-resistant pathogens. They act by stimulating natural microbial elimination through modulating the host defensive mechanisms. This process results in a high production of reactive oxygen species (ROS), which increases the susceptibility of the immune cells to oxidative stress [99]. Cui et al. (2016) and Elsherbiny et al. (2016) used different approaches to design organic-inorganic hybrid NPs comprising various organic and inorganic components in an attempt to treat bacterial infections by enhancing the generation of free radicals from NPs. Cui et al. (2016) employed an *in situ* reduction method to develop photosensitizer-loaded hybrid NPs synthesized by directly reducing AuNPs onto the surface of polyallylamine/CHT polymeric NPs (PAA/CHT NPs), followed by the conjugation of a photosensitizer, Rose Bengal (RB), with the PAA/CHT-Au hybrid NPs. The RB-loaded PAA/CHT-Au hybrid NPs exhibited a prolonged lifetime and excellent antibacterial activity against *E. coli* higher than that of blank PAA/CHT-AuNPs and free RB, due to the excessive and direct *in situ* generation of ROS at the bacterial cell surface, from the RB-loaded hybrid NPs [122]. Instead, Elsherbiny et al. (2016) studied the photo-induced green synthesis, antimicrobial activity and free radical formation of poly(ε-caprolactone)/curcumin/grape leaf extract-silver hybrid NPs (PCL/Cur/GLE-Ag NPs) against different strains of gram-positive and gram-negative bacteria, in addition to two fungal strains. The antibacterial activity of the natural antimicrobial curcumin/grape leaf extract was enhanced significantly when combined with AgNPs, compared to the pure curcumin and grape leaf extract, and this could be related to the free radical formation properties of the AgNPs, as well as the high surface area of the PCL/Cur/GLE-Ag hybrid NPs that enables them to be in direct contact with the bacterial cell wall, leading to bacterial cell damage [123]. Finally, the overall findings of the two studies can provide a foundation to promote the use of photosensitizers and natural antimicrobials loaded into hybrid organic-inorganic NPs as alternative strategies against bacterial infections, thus helping to combat bacterial resistance. Fig. 6 illustrates the design of the antimicrobial PCL/Cur/GLE-Ag hybrid NPs.

Overall, organic-inorganic hybrid NPs loaded with various antibacterial agents, such as antibiotics and free radical releasing biomaterials, have been successfully applied to achieve targeted and controlled drug

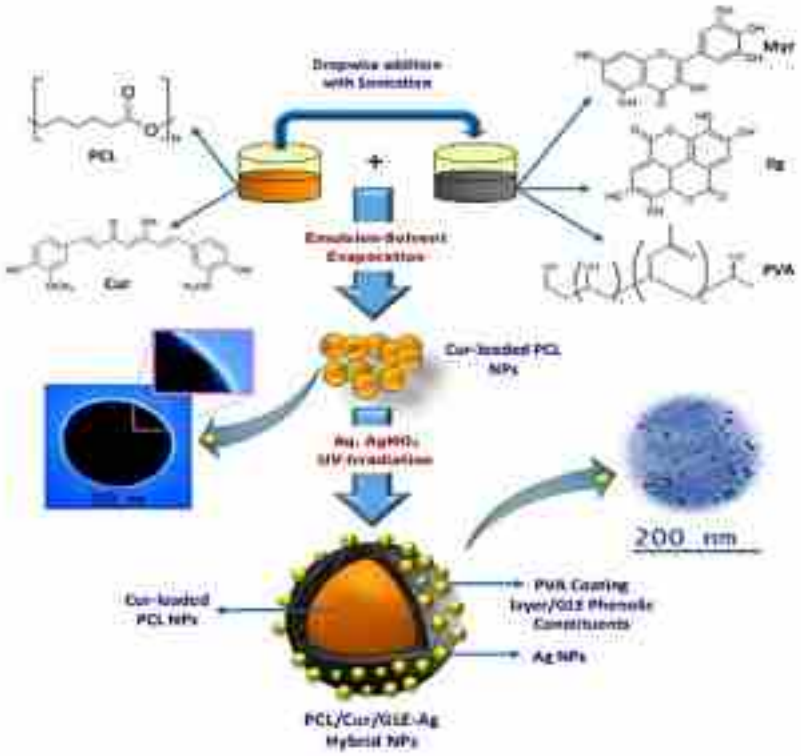

Fig. 6. Scheme illustrating the design of antimicrobial PCL/Cur/GLE-Ag hybrid NPs (adapted with permission from [123]).

delivery for the effective treatment of gram-positive and gram-negative bacteria, which helps in overcoming antibiotic resistance caused by such pathogens. A summary of organic-inorganic hybrid NPs reported to enhance antibacterial delivery is provided in Table 3, highlighting the nanocarrier components; the method of preparation; the loaded antibacterial agent; and the *in vitro* antibacterial assays that have been done for each reported study. So far, the majority of the research has used polymeric NPs as organic materials to formulate various organic-inorganic hybrid nanocarriers for antibacterial delivery, with only one study incorporating liposomes. Therefore, other organic biomaterials such as dendrimers, carbon nanomaterials and polymeric micelles, could also be investigated in the future.

3.3. Metal-organic *framework (MOFs)*

The advantages of MOFs as potent antimicrobial agents are due to their larger pore size, which allows the storage of antimicrobial molecules; their biocompatibility; and the ability to release antimicrobial metal ions such as Ag^{+}, Au^{+}, Cu^{2+}, Fe^{2+} and Zn^{2+}. Also, the organic linkers used to create the framework may have antimicrobial properties [126]. As a result, the antimicrobial activities of metal ions and linkers could reveal synergistic effects. Therefore, due to their high drug loading capacity and precise drug release, MOFs have been applied as carriers of many active pharmaceutical substances, including antibiotics [124]. In this section, MOFs comprising various organic linkers such as imidazole, carboxylate and terephthalate linkers are discussed.

3.3.1. *Zeolitic imidazole frameworks (ZIFs)*

Zeolite imidazole frameworks are a subclass of three-dimensional MOFs that consist of zinc ions (Zn^{2+}) and 2-methylimidazole linkage. These frameworks are considered to be strong pH-responsive nanocarriers that can be used for triggering antibacterial release at the acidic environment of bacterial infections [125]. Among the ZIFs, ZIF-8 crystals have been studied extensively by many research groups. These hybrid NPs were modified and functionalized through direct conjugation or surface coating with various materials to produce a novel nanosystem with synergistic and promising antibacterial effects. In this case, Soonsoo et al. (2019) have encapsulated a natural antimicrobial drug physcion into conventional ZIF-8 crystals using a one-step nanoprecipitation method. The release behavior of physcion from physcion@ZIF-8 NPs was investigated at three pH levels (7.4, 5.4 and 5). The authors observed that, in acidic conditions (pH 5 and 5.4), the release was significantly enhanced as the cumulative drug release was 86.72% and 61.31%, respectively, at the end of 72 h. Also, the formulated physcion@ZIF-8 NPs exhibited a maximum growth inhibition activity against gram-positive and gram-negative bacteria strains compared to the pure antimicrobial. Therefore, the findings of this study are promising in improving the antibacterial activity of a natural antimicrobial agent, physcion, against various infections [126].

Also, instead of using conventional ZIFs, direct conjugation of ZIF-8 with a natural polymer has also been done for more effective antibacterial treatment. Zhang et al. (2019) developed a modified pH-responsive MOFs/antibiotic system targeting intracellular gram-positive and gram-negative bacteria. They designed a tetracycline-loaded ZIF-8@hyaluronic acid (HA) system (abbreviated as TZH hybrid system) through a single *in situ* encapsulation approach. Tetracycline showed a faster release profile at pH 5.5 compared to pH 7.4, with approximately 50% and 20% of the drug released from TZH within 5 h, respectively. Moreover, the TZH hybrid system demonstrated enhanced and synergistic *in vitro* and *in vivo* antibacterial activity, compared to free tetracycline and free ZIF-8. The overall results suggested that the TZH could be promising for optimizing the efficacy of tetracycline against intracellular bacteria through the combination of a triple effect of HA, ZIF-8 and Zn^{2+} in one drug delivery system, which could result in a potent synergistic antibacterial effect [127].

Furthermore, ZIF-8 nanoparticles have been incorporated into nano-

Table 3
Reported organic-inorganic hybrid NPs for enhancing antibacterial delivery.

Organic material	Inorganic material	Method of preparation	Loaded antibacterial agent	*In vitro* antibacterial assays	Ref.
PLGA	LAP n-HA HNTs	Electrospinning	Amoxicillin Ammonillin Tetracycline	- Growth inhibition % in liquid and solid medium	[122–124]
CHT	ZnO NPs	–	Gentamicin	-Qualitative growth inhibition % in planktonic and surface attached conditions -MICs	[116]
Bacteria ionic responsive liposomes	MSNs	Co-condensation + thin layer hydration method	Gentamicin	-MICs -Bacterial affinity -Change in bacterial morphology (SEM)	[118]
HA	ZnO NPs	RSR method	Ciprofloxacin	-MICs and MBCs -Time killing assay -Biofilm inhibition -Motility and colony spreading assay	[119]
CHT	Silica-coated AgNPs	Sol-gel reflux method	Ciprofloxacin	-MICs and minimal biofilm eradication concentration (MBEC) -Biofilm quantification	[120]
AgNPs-PEI	Cu-MOFs	–	Tetracycline	-CFU Assay -ROS determination -Membrane permeability assay	[130]
PGlu	AgNPs	–	Rifampicin & polymyxin B	- MICs	[130]
Poly peptide	MSNs	Nanoprecipitation method	Azithromycin Methylene blue	-CFU Assay - Biofilm inhibition - Bacterial cell membrane disruption	[131]
CHT/PAA	AuNPs	In situ reduction method	Fluorescein Rose Bengal	-Colony forming unit (CFU) assay -ROS determination -DRM (bacteria-NPs interaction)	[132]
PEI	AgNPs	RSR + photo induced green synthesis	Curcumin Grape leaf extracts	-MICs and growth reduction (IC_{50}) -Minimum bactericidal concentration (MBC)	[133]

PLGA, poly (L-lactic-co-glycolic acid); LAP, laponite; n-HA, n-hydroxyapatite; HNTs, halloysite nanotubes; CHT, chitosan; ZnO, zinc oxide NPs; nanoparticles; MSNs, mesoporous silica NPs; HA, humic acid; AgNPs, silver NPs; CuNPs, copper NPs; PEI, polyethylenimine; PGlu, polyglutamic acid; AuNPs, gold NPs; PAA, polyallylamine; PCL, poly ε-caprolactone.

structured polymer scaffolds to deliver different active pharmaceutical ingredients for effective tissue regeneration. For example, Karakurtli and coworkers (2019) used ZIF-8 as a vancomycin carrier to achieve a pH-responsive, controlled drug delivery system. CHT scaffolds loaded with vancomycin-ZIF-8 were prepared by a wet spinning technique to obtain a three-dimensional fiber scaffold to be used as a tissue substitute in the treatment of bone infections. The swelling behavior and the release profile of the vancomycin-ZIF-8/CHT scaffolds were pH-dependent and exhibited higher effects at pH ≤ 4 than at pH 7.4, due to the presence of ZIF-8. Also, vancomycin-ZIF-8/CHT scaffolds displayed a stronger antibacterial effect against gram-positive bacteria compared to the free ZIF-8 and CHT scaffolds. This enhanced effect was due to the pH-triggered release of vancomycin, in addition to the combined release of Zn^{2+} from the ZIF-8, which synergize the antibacterial effects of the antibiotic. Besides the enhanced antibacterial properties, the cell culture assay using MC3T3-E1 preosteoblasts showed a high proliferation of osteogenic activity on vancomycin-ZIF-8/CHT scaffolds, confirming the safety and biocompatibility of the prepared hybrid system [120].

Likewise, surface modification is further facilitated by the framework flexibility of ZIF-8. As a result, ZIF-8 crystals can be modified on their surface with magnetic biomaterials to improve the antibacterial efficiency of antibiotics, resulting in a drug with a superior antibacterial effect. A novel MOF was prepared by Esfahanian et al. (2019) using ZIF-8 crystals, as they formulated a magnetic framework based on Fe_3O_4-polyacrylic acid (PAA)@ZIF-8 for the delivery of ciprofloxacin. Fe_3O_4 and PAA were added to improve the drug-loading capacity and modify the MOFs for drug delivery. Ciprofloxacin-loaded Fe_3O_4-PAA@ZIF-8 showed a pH-responsive release profile, as rapid degradation of the framework occurred in acidic pH 5, resulting in a faster antibiotic release compared to that at pH 7.4. Furthermore, the antimicrobial activity of ciprofloxacin was enhanced significantly when it was loaded into the modified MOFs compared to the bare drug and Fe_3O_4-PAA@ZIF-8. So, the use of Fe_3O_4-PAA@ZIF-8 as an antibiotic carrier can improve the antibacterial properties of the antibiotics [129].

In another study, Yang et al. (2020) developed a novel, carbonized ZIF-8 NP (called C-ZIF) with effective ion releasing properties and photothermal activity for a broad-spectrum antibacterial action. They prepared an AgNPs-doped C-ZIF composite (AgNPs@C-ZIF NPs) with a graphitic-like carbon framework through in situ displacement reaction. The formulated AgNPs@C-ZIF NPs were examined for their metal-ion release capability and their photothermal activity. The results revealed that these functionalized MOFs possessed rapid metal-ion release and photothermal conversion properties, which provide the potential of photothermal therapy for synergistic bacterial eradication. Gram-positive and gram-negative bacteria were used as models to investigate the photothermal antibacterial activity of the AgNPs@C-ZIF system. The results illustrated that AgNPs@C-ZIF nanocomposites possess nearly 100% bactericidal ratio against both bacterial strains at extremely low concentrations (0.16 mg/ml). Furthermore, a cytocompatibility study and wound healing evaluation in vivo on rabbit skin demonstrated its biosafety and rapid wound healing and disinfection ability. Overall, these novel carbonized ZIF-8 NPs show high chemical and photothermal antibacterial efficiency and can be applied for broad-spectrum bacterial sterilization [130].

More recently, Xiao and coworkers (2021) exploited the benefits of both ZIF-8 and polydopamine (PDA) to design near infrared (NIR)/pH dual stimuli responsive MOFs for synergistic photothermal/ pharmacological antibacterial therapy. ZIF-8 crystals were used to encapsulate the antibiotic vancomycin first; and then surface modification of the vancomycin/ZIF-8 NPs with PDA was undertaken to improve the structure stability, dispersibility, and biocompatibility of the system. Vancomycin/ZIF-8@PDA displayed an enhanced drug release in response to acidic pH 4.7, compared to the physiological pH 7.4, with a mere potent effect under NIR irradiation. The antibacterial activity of the system was examined in vitro and in vivo against gram-negative strains and a vancomycin-intermediate gram-positive bacteria (called Mu50). All findings indicated that the combination of photothermal/ pharmacotherapy of vancomycin/ZIF-8@PDA NPs significantly enhanced the antibacterial activity of vancomycin against both strains, in vitro and in vivo, and reduced the effective concentration of the antibiotic (MIC was 3.62 μg/ml). This enhanced antibacterial activity resulted in bacterial death and healing of the infected mice's skin. Therefore, a NIR/pH dual stimuli responsive vancomycin/ZIF-8@PDA system could be promising for biomedical application in overcoming antibiotic resistance [131]. Fig. 7 represents a schematic diagram explaining the photothermal/pharmacological therapy of the vancomycin/ZIF-8@PDA system and its in vivo application.

Taken together, the findings of these studies proved the modification and the potential use of ZIF-8 NPs to enhance the delivery and efficacy of various antibacterial agents. Photodynamic antimicrobial therapy (PACT), as a novel strategy, shows potential for treating and overcoming antimicrobial resistance. The application of ZIF-8 hybrid NPs in PACT significantly enhances its antimicrobial activity. In addition, other antimicrobial drugs are being combined with photosensitizers to achieve activity both in dark and in the presence of light. However, as interesting as the ZIF-8 hybrid NPs are, there is a need for additional biocompatibility, stability and in vivo antibacterial activity studies, as most reports lack them. It is critical to confirm the biosafety and antibacterial profiles of these modified MOFs in animal experiments, before moving further to clinical application.

3.2.2. Metal-carboxylate frameworks

Metal-carboxylate frameworks are another subclass of MOFs composed of metal ions such as Fe^{3+} and carboxylic acid or carboxylate derivatives. They are among the flexible and highly porous biodegradable and biocompatible MOFs that can adapt their pore diameters during drug adsorption. In addition, these carboxylate-based MOFs exhibit high stability in acidic conditions and, thus, metal-carboxylate frameworks can significantly control the release of drugs, such as antibiotics, under physiological conditions [132].

Three research studies reported the use of carboxylate MOFs for antibacterial drug delivery. Liu et al. (2017) designed a carboxylate-Iron MOF called MOF-53(Fe) NP as a drug carrier to enhance the antibacterial efficacy of vancomycin against gram-positive bacteria. Vancomycin release from vancomycin-loaded MOF-53(Fe)NPs was sustained with an initial burst release profile at pH 7.4, reaching up to 97% after 36 h; while in acidic pH levels of 6.5 and 5.5, vancomycin showed slower release profiles. The authors suggested that the accelerated release rate of vancomycin in neutral pH 7.4 was due to the partial degradation of MOF-53(Fe) NPs; while in acidic conditions, the system showed a smaller degree of degradation, and the release of vancomycin was relatively slow. This property could be beneficial in targeting the local therapy of bacterial infections that require prolonged treatment. Despite the controlled and slower release of vancomycin in an acidic environment, vancomycin-loaded MOF-53(Fe)NPs showed excellent antibacterial activity with a high efficiency of 99.3% [133]. On the other hand, to improve the oral bioavailability and control the release of gentamicin, Unamuno and coworkers (2018) formulated and optimized a gentamicin-loaded (Fe)-carboxylate MOF (gentamicin@MIL-100(Fe) NPs) through a simple impregnation method. In vitro drug release studies for gentamicin were conducted using different oral and intravenous simulated physiological conditions. The results indicated that gentamicin-loaded MIL-100(Fe) NPs exhibited superior colloidal, chemical and structural stability under gastrointestinal conditions, with good biocompatibility and enhanced delivery of the antibiotic under intestinal conditions, making these MOFs highly promising for the oral administration of gentamicin. Furthermore, the in vitro antibacterial activity of gentamicin@MIL-100(Fe) NPs was investigated against different strains of gram-positive and gram-negative bacteria, and the results showed that the loaded MOFs exhibited the same antibacterial activity as free gentamicin, confirming that the antimicrobial activity of

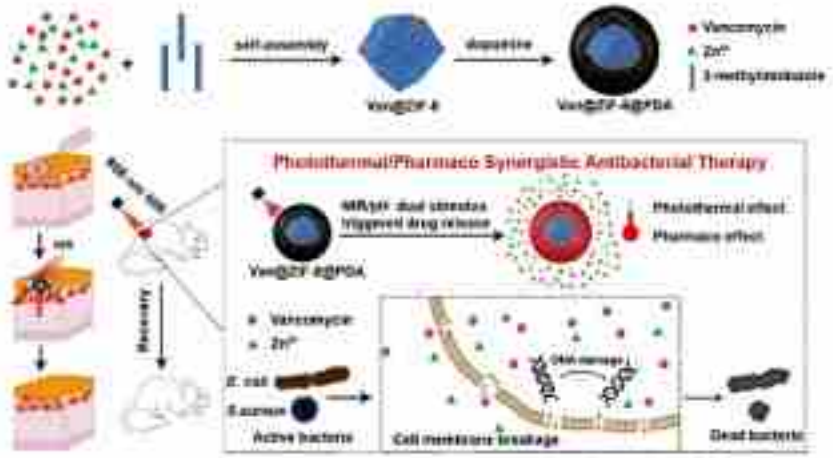

Fig. 7. Scheme illustrating the design and the dual stimuli responsive photothermal/pharmacological therapy of vancomycin/ZIF-8@PDA system and its in vivo application (adapted with permission from [131]).

the antibiotic was maintained after its encapsulation into MIL-100(Fe) NPs [134].

Furthermore, carboxylate MOFs have been modified via saccharide coating to promote their surface contact with bacterial cells. Recently, Hamrena et al. (2022) designed and evaluated a novel mannose (MNS)-coated Fe-MIL-88NH$_2$ NPs loaded with vancomycin to improve its efficacy against *S. aureus* and MRSA. The prepared MNS-coated/vancomycin@MOFs exhibited superior antibacterial activity than the un-coated nanocarriers against all gram-positive strains, confirmed by lower MIC values. This improved antibacterial effect could be due to the interaction of MNS coating with lectin on the cell wall of gram-positive bacteria, which ultimately promotes the cellular penetration and increase the bactericidal potential of vancomycin against both susceptible and resistant bacteria. In addition, atomic force microscope (AFM) investigation of all *S. aureus* strains showed total morphological damage upon treatment with MNS-coated/vancomycin@MOPs. Overall, this study suggested that coating of MOFs with MNS could be an effective technique to enhance the bactericidal activity of vancomycin and hence, improve the antibiotic therapy against MDR-associated diseases [135].

In summary, the previous studies reported the use of carboxylate-ions MOFs to improve the antibacterial efficacy of various classes of antibiotics. Vancomycin revealed a controlled release profile with more enhanced antibacterial effects in the first experiment [130], whereas its killing efficacy against MDR strains was improved significantly with complete bacterial cell damage when loaded into MNS-coated carboxylate MOFs [135] Also, the bioavailability and the oral antibacterial activity of gentamicin could be maintained when encapsulated into carboxylate-ions MOFs [134]. Therefore, to confirm the *in vitro* findings and the applicability of such promising MOFs, stability studies and *in vivo* antibacterial studies for the formulated carboxylate-ions MOFs are required.

2.3.3. Metal-terephthalate frameworks

Another generation of MOFs are metal-terephthalate frameworks which contain metal ions such as Zn^{2+}, Cu^{2+}, Ti^{4+}, and others with terephthalic acid or terephthalate derivatives. These MOFs are characterized by their photocatalytic activity when exposed to UV–Vis irradiation [136]. In this regard, three emerging studies reported the use of metal-terephthalate frameworks for treatment of bacterial infections. The first report was by Bhardwaj et al. (2018), who investigated the antimicrobial efficiency of three Zn-terephthalate frameworks called IRMOF-3, MOF-5, and Zn-BTC alone, and in combination with ampicillin and kanamycin. Antibacterial activity assessment showed that all antibiotic-loaded Zn-terephthalate frameworks exhibited superior antimicrobial activity, indicated by lower MIC values against gram-positive and gram-negative strains, compared to the free antibiotics and free MOFs, with synergistic (for kanamycin-loaded IRMOF-3) and additive (for other antibiotic-loaded MOFs) interactions [137]. However, to confirm these *in vitro* antibacterial findings and the potential use of these metal-terephthalate frameworks, additional characterization, including stability studies, *in vitro* drug and metal ions release studies from the MOFs in different physiological environments and *in vivo* antibacterial studies, are also essential.

Metal-terephthalate frameworks have also been explored for the design of antibacterial surface coatings, since bacterial adhesion and growth remain a concern in the design of various medical and surgical devices. Taking this different approach, Arenas-Vivo and coworkers (2019) developed a novel silver NP-loaded photoactive titanium (IV) aminoterephthalate framework (AgNPs@ MIL-125(Ti)NH$_2$ MOFs) as an antifouling and bactericidal surface coating to act against bacterial biofilm. Silver nanoparticles were efficiently entrapped into the MIL-125 (Ti) MOFs using the impregnation-reduction method. The antibacterial activity investigation indicated that the bactericidal effects of MIL-125 (Ti) NPs were significantly enhanced after encapsulation of AgNPs, compared to free AgNPs, MIL-125(Ti)NH2 MOFs, and a physical mixture of both AgNPs and MOPs. This bactericidal activity of the nanocomposite film, in addition to their ability to detach the bacterial biofilm, was further promoted when the hybrid film received UVA irradiation for 2 h [138]. Therefore, the promising results of this study can be applied with different antimicrobial agents to prove the potential of this film nanocomposite as a surface coating for biofilm treatment on high-touch surfaces such as surgical devices.

Moreover, MOFs have been proposed as a promising candidate for encapsulating a variety of biomolecules as a biomimetic strategy to combat bacterial infections. Generally, biomimetic strategies have been explored for the development of nano delivery systems, with the goal of either mimicking cellular communication signal pathways or utilizing the activity path of biological structures in living organisms to achieve several advantages, such as biocompatibility and targeting characteristics [9]. Nowadays, this strategy shows the potential for encapsulating nanoparticles/biomolecules into MOFs to construct antibacterial nanosystems with synergistic activity. In a recent study, novel biomimetic multienzyme MOFs with Fenton-like catalytic activity were designed by Cheng et al. (2020) to acquire synergistic antibacterial activity against both gram positive and gram-negative strains. Glucose oxidase (GO_x) and L-arginine (L-Arg) were simultaneously entrapped within Cu-MOFs

(called Cu-BDC) through a biomimetic mineralization growth technique on an enzyme surface. The preparation technique resulted in uniform distribution of the biomolecules (GO_x and L-Arg) within the Cu-BDC pores, which enhanced the synergistic bactericidal activity by spontaneously activating the double cascade reaction of ROS and reactive nitrogen species (RNS). The *in vitro* antibacterial activity studies indicated that the bacterial viability of both gram-negative and gram-positive bacteria were significantly reduced when treated with GO_x / L-Arg@ Cu-BDC hybrid composite with inactivation rates of 98% and 97% for *E. coli* and *S. aureus*, respectively. This was due to the biomimetic structure of the hybrid composite and the synergistic antibacterial activity of GO_x, L-Arg and Cu-BDC. In addition, an *in vivo* study was carried out in mice models to confirm the cytocompatibility of the formulated hybrid MOFs and the results revealed that the prepared GO_x / L-Arg@ Cu-BDC hybrid composite has good biocompatibility, indicating the *in vivo* potential of such biomimetic multienzyme hybrid MOFs [139]. Fig. 8 represents a schematic diagram of the biomimetic mineralization synthesis process for GO_x / L-Arg@ Cu-BDC hybrid NPs and their antibacterial mechanism.

2.3.4. MOFs using other metal ion and organic linkers

In addition to the above-mentioned linkers, some other MOFs that contain different metal ion and linkers can be used as nanocarriers for antibacterial application. André and his coworker (2019) developed a novel BioMOF that consisted of antibiotic nalidixic acid as an organic linker and magnesium (Mg) and manganese (Mn) as metal ion. The system showed improved antimicrobial activity against both gram-positive and gram-negative strains compared to free nalidixic acid, with more efficacy reported against gram-negative bacteria. A significant bacterial growth inhibition effect was observed with bactericidal action when it was treated with Mg-MOFs, while Mn-MOFs exhibited bacteriostatic actions. However, *in vivo* studies are needed to support the *in vitro* antibacterial activity findings [140].

More recently, Wei's group (2021) designed a γ-cyclodextrin-based MOF using γ-cyclodextrin as an organic ligand co-ordinated with potassium ions to encapsulate the antibiotics, norfloxacin and florfenicol. The antibiotics were primarily adsorbed into the pores of the γ-cyclodextrin-MOF structure via an impregnation method to achieve small NPs and to improve the stability of the formulated antibiotics@γ-cyclodextrin-MOFs. The formulated MOFs displayed continuous sustained release behavior over a period of 4 h at physiological pH 7.4, and the cumulative amount released was 79.85% and 67.50% for florfenicol and norfloxacin, respectively. The *in vitro* and *in vivo* antibacterial activity results confirmed that the antibiotic loaded γ-cyclodextrin-MOF NPs showed higher and longer inhibition efficacy against gram-positive and gram-negative bacteria, compared to free antibiotics with lower MIC values, and a 90% inhibition rate for both antibacterial agents. Therefore, this study indicated that antibiotics@γ-cyclodextrin-MOF could be an effective, biocompatible carrier for antibiotic therapy with a controlled release profile [141].

Altogether, the outcomes of the abovementioned studies confirm the prospective use of MOFs as promising nanocarriers for the treatment of bacterial infections, and they can be successfully applied to enhance the antibacterial efficacy of antibiotics, thus helping in overcoming resistance. Table 4 summarizes all the MOFs reported in this review. It provides comprehensive information such as metal ions, loaded antibacterial agent (s), bacteria species, the mechanism of antibacterial actions, and the mode of antibacterial investigation.

3.4. Cell membrane-coated hybrid NPs (CMCH-NPs)

Coating of NPs with extracted cell membranes is one of the strategies that has been used to improve the pharmacokinetic parameters of various drugs, including antibiotics, which makes CMCH-NPs attractive candidates for targeted and sustained antibacterial drug delivery [73]. In this field, red blood cell membrane-coated hybrid NPs (RBCM/CH-NPs) and CMCH-NPs using other extracted cell membranes, such as gastric epithelial cells, bacterial cell membranes and neutrophils, and their applications in antibacterial delivery are discussed.

Several nanosystems have been modified by coating them with red blood cell membranes (RBCM) to enhance the delivery of antibiotics within the body, reducing its clearance by the immune system and enhancing its blood circulation time [73], which improves the pharmacokinetic properties of the antibiotic nanocarrier. In this regard, three

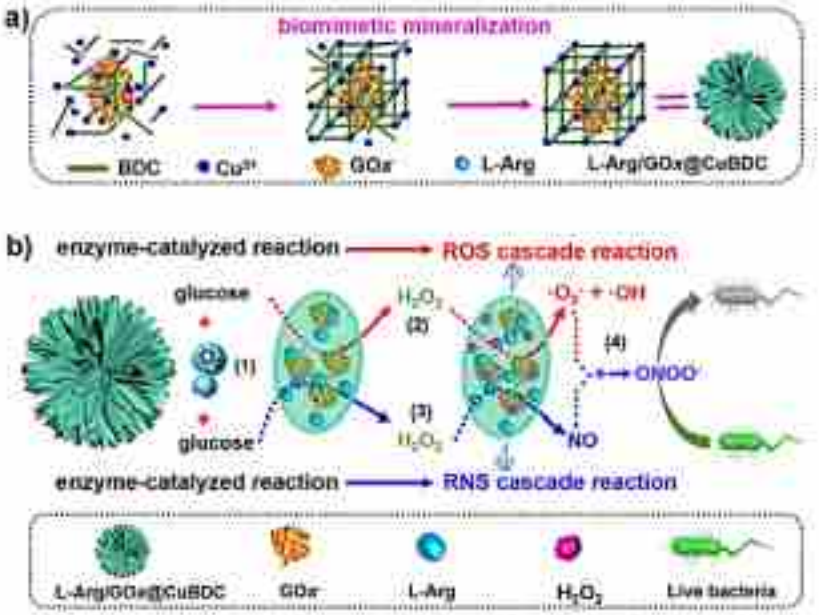

Fig. 8. Scheme represents (a) the biomimetic mineralization synthesis process for GO_x / L-Arg@ Cu-BDC hybrid NPs; and (b) the self-activated double-cascade reaction mechanism for enhanced synergistic bactericidal activity (adapted with permission from [139]).

Table 4
Summary of the reported MOFs and their antibacterial mechanisms.

MOF	Antibacterial agent	Targeted bacteria	Mechanism of the antibacterial actions	Mode of study	Ref.
ZIF-8	Fluvirax	*S. aureus* *E. coli* *P. putida*	Binding to cell membrane's protein leading to membrane destruction.	*In vitro*	[126]
ZIF-8/HA	Tetracycline	*S. aureus* *Salmonella*	Binding to CD_{44} antigen receptor by the aid of HA and kill the bacteria extracellularly.	*In vitro*	[127]
ZIF-8/CMT	Vancomycin	*S. aureus*	Inhibition of biofilm formation and affecting the morphology of the bacteria.	*In vitro*	[128]
ZIF-8/Fe$_3$O$_4$ PAA	Ciprofloxacin	*S. aureus* *E. coli*	Damage of bacterial cell wall	*In vitro*	[129]
C-ZIF	AgNPs	*S. aureus* *E. coli*	Release of Ag^+ and oxidative heat destroyed the bacterial cell membrane	*In vitro*	[130]
ZIF-8/PDA	Vancomycin	*E. coli* SM (intracellular *S. aureus* (SAM))	Nucleic acid degradation, biofilm inhibition and cell membrane damage.	*In vitro*	[131]
MOF-53 (Fe)	Vancomycin	*S. aureus*	Inhibition of bacterial cell wall synthesis	*In vitro*	[132]
MIL-100(Fe) UiO-66(Zr)	Gentamicin	*S. aureus* *S. epidermidis* *P. aeruginosa*	Not reported	*In vitro*	[133]
MNS coated Fe-MIL-101(Al)	Vancomycin	*S. aureus* MRSA	Damage of bacterial cell wall.	*In vitro*	[134]
BMOP-3 MOF-5 Zn-BTC	Ampicillin Kanamycin	*S. aureus* *S. lentus* *L. monocytogenes* *E. coli*	Sustained release of Zn^{+2} and inhibition of the enzymes and proteins involved in cell wall production which resulted in membrane injury	*In vitro*	[135]
MIL-125(Ti)	AgNPs	*S. aureus*	Biofilm inhibition and generation of ROS.	*In vitro*	[136]
Zn-BDC	Glucose oxidase and L-arginine	*S. aureus* *E. coli*	Change of bacterial morphology due to the release of free radicals through a double cascade reaction.	*In vitro*	[124]
BioMOFs	Salicylic acid	*S. aureus* *B. subtilis* *P. aeruginosa* *K. coli*	Not reported	*In vitro*	[140]
γ-cyclodextrin-MOF	Ranolazine dihydrochl	*S. aureus* *E. coli*	Not reported	*In vitro*	[141]

MOF, metal organic framework; HA, hyaluronic acid; CMT, chitosan; PAA, poly allylamine; PDA, poly dopamine; MNS, nanozyme; MRSA, methicillin resistant *S. aureus*.

research studies have been reported by Li et al. (2014), Lin et al. (2019) and Kamal et al. (2022) for combating MDR bacteria. They developed a core-shell gelatin NP (GNP) decorated on their surface with RBCM for adaptive and 'on-demand' antibiotic delivery. All hybrid nanosystems were designed for gelatinase-triggered release of antibiotics at the infection site, and the results indicated that the release of all loaded antibacterials was gelatinase concentration/time-dependent, as they showed a higher release profile in the presence of gelatinase and gelatinase-positive bacteria. The authors suggested that the coating of GNPs with RBCM improved their stability and cytocompatibility, and enhanced their antihemolytic activity against bacterial toxins. Li and coworkers (2014) designed vancomycin-loaded RBCM-coated supramolecular GNPs (vancomycin-loaded GGNPs-RBCM) using the desolvation method. The antibacterial activity of the prepared vancomycin-loaded hybrid NPs was examined *in vitro*, and the results revealed higher activity against gelatinase-positive strains, including *S. aureus*, *P. vulgaris* and *P. aeruginosa*, with lower MIC values compared to free vancomycin. This enhanced activity was due to the degradation of gelatin in response to the gelatinase enzyme that is overexpressed in the infection site, which resulted in vancomycin release and bacterial death [142]. Thereafter, Lin et al. (2019) developed ruthenium (Ru)-complexes functionalized selenium (Se) NPs loaded into RBCM-GNPs (Ru – Se@GNP-RBCM) for the *in situ* detection and inhibition of MDR bacteria. *In vitro* investigations of the antibacterial activity of the system showed that the Ru – Se@GNP-RBCM had a strong antibacterial effect on MRSA, as the survival rates of the bacteria decreased significantly, indicating a good synergistic antibacterial effect against gelatinase-positive strains. Moreover, an *in vivo* assessment of MRSA-infected mouse models was performed for the evaluation of wound healing ability, and the overall findings confirmed that the prepared Ru – Se@GNP-RBCM could be used to detect bacterial infection *in vivo* and improve the healing of MRSA-infected wounds [143]. More recently, Kamal and co-workers (2022) developed a unique RBCM-coated supramolecular GNPs loaded with vancomycin and chlorogenic acid for combined antibacterial and antibiofilm activity against MRSA infection, both *in vitro* and *in vivo*. The prepared biomimetic hybrid NPs were able to evade the immune system and greatly prolong their systemic circulation for the responsive and sustained release of vancomycin/chlorogenic. The successful *in vitro* time-concentration dependent antibacterial and antibiofilm effects were validated through *in vivo* studies using leg- and skin-infected mice models. Synergistic antibacterial activities of vancomycin and chlorogenic acid in response to the microenvironment of MRSA infection were confirmed by the total eradication of bacteria, as well as the healing of inflammation and wounds. Therefore, these smart on-demand antibiotic delivery platform could be promising in future nanotechnology to treat resistant infectious pathogens [144].

Compared to the first study published by Li [142], both Lin et al. (2019) and Kamal et al. (2022) reached the *in vivo* stage in their studies, thereby building a solid *in vitro-in vivo* correlation [143,144]; while Li et al. (2014) did not investigate the *in vivo* activity, which is crucial in considering such nanosystems for clinical trials. In summary, the promising results of all reported studies indicated that RBCM-coated GNPs loaded with various antibacterial agents could be used as an alternative to antibiotics for combating MDR bacterial infection. Fig. 9 demonstrated the preparation method of vancomycin/chlorogenic acid-loaded RBCM-coated supramolecular GNPs, and the mechanism of combating MRSA infection in mice models by means of prolonged circulation time, immune escaping ability and responsive on-demand antibiotic delivery.

Using the same coating strategy, a cell membrane-coated nanogel system composed of a redox-responsive nanogel core and RBCM shell was reported by Zhang et al. (2017) for vancomycin delivery to combat intracellular MRSA. The vancomycin-loaded nanogel core was cross-linked with disulfide bonds to be cleaved in response to the intracellular

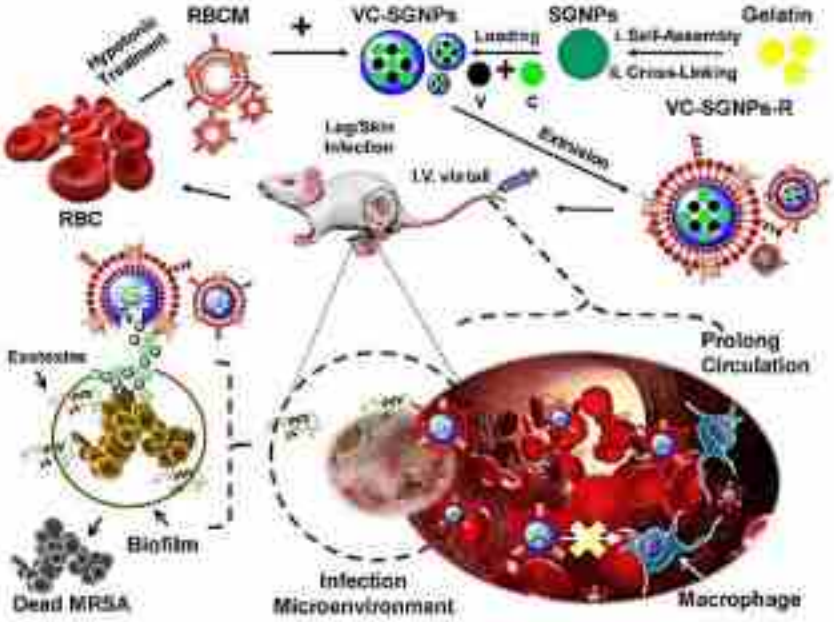

Fig. 9. Scheme illustrating the preparation method of vancomycin/chitosogenic acid-loaded RBCM-coated supramolecular GNPs, and their synergistic and infection microenvironment-responsive antibacterial and antibiofilm effectiveness mechanisms to eradicate MRSA infection in mice model (adapted with permission from [144]).

reducing environment for the on-site release of vancomycin, while the in situ gelation method was used to coat the surface of vancomycin-loaded nanogel with RBCM. The RBCM-coated nanogel effectively neutralized MRSA α-toxin, which in turn enhanced the intracellular bacterial uptake. Vancomycin release from the RBCM-nanogels in the presence of reducing agents was significantly increased, reaching a cumulative release of about 95% in 24 h, confirming the responsiveness of the system to the intracellular reducing environment. Additionally, the in vitro antibacterial activity study revealed that the RBCM-coated/vancomycin-nanogel exhibited improved antibacterial activity against intracellular MRSA with an MIC value of 2.5 μg/mL, while the non-coated vancomycin-loaded nanogel showed less anti-MRSA activity with an MIC value of 5 μg/mL compared to free vancomycin. These findings suggest that the redox-responsive RBCM-coated nanogel system could be promising for treating intracellular MRSA infection [143].

Finally, in 2021, Wu et al. used a simple ultrasound method to prepare RBCM-coated tedizolid phosphate (TR-701)-loaded PLGA NPs (TR-701-PLGA@RBCM NPs) for treating methicillin-sensitive S. aureus (MSSA) and MRSA wound infections. The formulated hybrid biomimetic system was evaluated for its in vitro and in vivo biocompatibility, toxin adsorption capability and antibacterial efficiency. The results showed that TR-701-PLGA@RBCM NPs were safe and highly biocompatible, with significant exotoxin neutralizing ability. The in vitro antibacterial activity study indicated that the antibacterial activity of the prepared hybrid system was equivalent to free TR-701 against both MRSA and MSSA. Moreover, the healing rate of the MRSA-infected wound was improved significantly when treated with TR-701-PLGA@RBCM NP, due to its improved growth inhibition of MRSA in the mice skin wound, compared to free TR-701. Accordingly, TR-701-PLGA@RBCM NPs could be promising in treating MRSA-infected wounds due to their high stability, biocompatibility and enhanced antibacterial efficacy in vitro and in vivo [146]. Fig. 10 presents a schematic illustration of the preparation and application of TR-701-PLGA@RBCM NPs in treating MRSA-wound infection.

The coating of NPs with extracted cell membranes can be used also as a pathogen-host adhesion strategy for active targeting of various

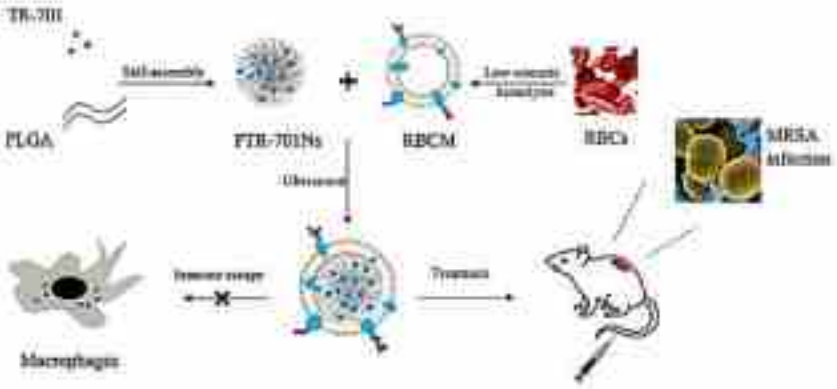

Fig. 10. Scheme representing the preparation and application of TR-701-PLGA@RBCM NPs in treating MRSA-wound infection (adapted with permission from [146]).

antibiotics to enhance the drug localization, reduce side effects, and improve their therapeutic effectiveness [147]. Two research studies have reported the coating of PLGA NPs with extracted cell membranes for active targeting and improving antibiotic delivery and localization at the site of infection. A membrane derived from gastric epithelial cells (called AGS cells) has been successfully applied by Angsantikul et al. (2018) to enhance the delivery and active bacterial targeting of clarithromycin. They prepared AGS coated-clarithromycin loaded PLGA NPs (clarithromycin-PLGA@AGS NPs) to treat *H. pylori* infection. The prepared biomimetic hybrid NPs exhibited enhanced bacterial adhesion with prolonged and controlled antibiotic release, which improved the therapeutic efficacy of clarithromycin. The antibacterial activity of clarithromycin-PLGA@AGS NPs was studied *in vitro* and *in vivo*, and the results indicated that the system had superior *in vitro* antibacterial activity against *H. pylori*, compared with free antibiotic and clarithromycin-loaded PLGA NPs. In addition, the NPs were able to reduce the *H. pylori* burden effectively in an infected mouse model. Therefore, coating of clarithromycin-loaded polymeric NPs with a membrane derived from gastric epithelial cells could be a useful and safe approach for effective, targeted antibiotic delivery to treat *H. pylori* infection. Also, this bacteria-host adhesion approach can be applied to treat other bacterial infections [148]. Continuing the research into the coating of PLGA NPs with extracted cell membranes, Gao and coworkers (2016) used PLGA NPs coated with a membrane of extracellular vesicles (EV) secreted by *S. aureus* (PLGA NPs@EV) as an active targeting carrier to eliminate bacterial infections caused by intracellular *S. aureus*. The prepared PLGA NPs@EV were internalized by *S. aureus*-infected macrophages *in vitro*, with better efficiency compared to PLGA NPs coated with liposomes and *E. coli* outer membrane vesicles, respectively. In addition, the hybrid NPs were loaded with vancomycin and rifampicin and were injected intravenously to intracellular *S. aureus*-infected mouse models. The antibiotic-loaded PLGA NPs@EV exhibited significantly enhanced antibacterial activity as they reduced the pathogen burdens in major organs, especially in the kidneys and lungs. The overall findings of this study suggested that EV-coated hybrid NPs can improve the therapeutic efficiency of loaded antibiotics by providing them with an active targeting capacity, both *in vitro* and *in vivo* [149].

In addition to the previous biological coating materials, the most recent study of CMCH-NPs for the treatment of bacterial infections and inflammation was reported by Wang et al. (2020). In this study, PCL-PEG NPs were coated with neutrophil membrane and then loaded with sparfloxacin for specific targeting to inflammatory sites. The prepared neutrophil-coated hybrid NPs demonstrated good biocompatibility, controlled drug release profiles and targeted delivery to pulmonary sites of inflammation. Also, the hybrid NPs showed significantly higher antibacterial activity against MRSA, confirmed by larger zones of inhibition when compared to free antibiotic and PLC-PEG NPs. Finally, the *in vivo* study findings indicated that these neutrophil-coated hybrid NPs could efficiently treat lung inflammation in the mouse pneumonia model [150].

Taken together, the studies discussed in this subsection have confirmed the potential use of CMCH-NPs as biomimetic antibiotic nanocarriers for the effective treatment of bacterial infections. Functionalization of such hybrid nanosystems combines nanotechnology with biomimetic strategies and takes the advantages of biological cell membranes to develop nature-inspired nanomedicines for targeted antibiotic delivery.

3.5. Hybrid NP-hydrogels

In recent years, hybrid NP-hydrogels have garnered more attention as antibacterial drug delivery carriers due to their unique advantages, such as self-healing abilities; injectability; tissue adhesiveness; high drug loading capacity; controlled drug release; and superior biocompatibility. Hybrid NP-hydrogels loaded with different antibiotics can be used for local antibacterial delivery to the site of infection, thereby reducing the development of antibiotic resistance. They can be applied to treat different infectious diseases, including skin wounds and bone infections [151]. Herein, hybrid NP-hydrogels based on the types of the combined NPs are discussed.

3.5.1. Hybrid metal and metal oxide NP-hydrogels

A variety of metal/metal oxide NPs such as AgNPs, AuNPs, CuO NPs and ZnO NPs have been incorporated into hydrogels to form hybrid systems applied in the treatment of bacterial infections. These NPs combined with hydrogels can be used for the controlled release of antibacterial metal ions or encapsulated antibiotics. In this regard, Sattari et al. (2018) incorporated Ag, CuO and ZnO NPs into a polyaspartic acid/graphene nanosheets@polyacrylamide-co-acrylic acid hydrogel for pH-responsive and controlled release of a loaded drug, curcumin. The release profile of curcumin from the prepared hybrid NP-hydrogels was sustained and pH-dependent as it showed more drug release at pH 7.4 than at pH 2.1, due to the increased electrostatic repulsion and hydrogel swelling. Hybrid curcumin-loaded AgNP-hydrogel exhibited more curcumin release compared to the hybrid metal oxide hydrogels. In addition, the prepared curcumin-loaded hybrid hydrogels exhibited enhanced antibacterial activity against *E. coli* and *S. aureus*, compared to the bare curcumin, with the AgNP-hydrogel proving the most successful. This improved antibacterial activity was due to the enhanced curcumin release and more synergistic antibacterial effects of AgNPs, compared to hydrogel embedded with CuO and ZnO NPs. As a result, the prepared metal/metal oxide NP-hydrogel could be useful for wound healing and dressing applications [152]. However, biocompatibility and *in vivo* studies are crucial to motivating such a use.

In addition, hybrid metal NP hydrogels can be used as an alternative strategy for combined local antibacterial/photothermal therapy. Tao and co-workers (2019) prepared an NP-hydrogel hybrid system composed of methacrylate modified gelatin (Gel-MA) combined with *N, N*-bis(acryloyl) cystamine-chelated CuNPs (BACA/Cu NPs) via a radical polymerization technique. The formulated BACA/Cu NPs@Gel-MA was able to convert NIR laser irradiation energy into localized heat for antibacterial photothermal therapy. *In vitro* antibacterial studies indicated that the hybrid hydrogel exhibited superior antibacterial efficacy against both *S. aureus* and *E. coli*, with biofilm inhibition capability. This enhanced antibacterial activity derived from the synergistic effect of photothermal activity and the rapid release Cu^{2+} and ROS under laser irradiation of CuNPs (as shown in Fig. 11). Moreover, the wound-healing process of an *S. aureus*-infected mice model was significantly accelerated by enhancing neovascularization with a reduced inflammatory

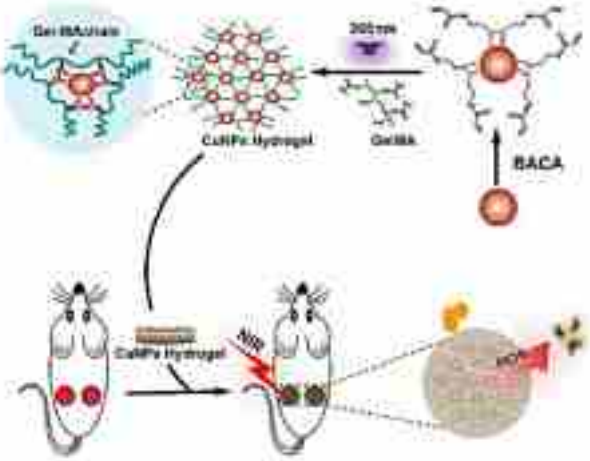

Fig. 11. Scheme illustrating the preparation of BACA/Cu NPs@Gel-MA hybrid hydrogel and the synergistic antibacterial photothermal therapy via the generation of ROS under NIR irradiation (adapted with permission from [152]).

response in vivo. Overall, the biocompatible CuNPs-hydrogel hybrid system is a promising candidate in photothermal therapy for wound healing applications and skin tissue regeneration [153].

Likewise, Lin et al. (2020) employed the same synergistic antibacterial photothermal therapy to treat periodontal infections. The research team designed a NIR activated hybrid hydrogel system, composed of Gel-MA with mesoporous silica coated AuNPs (SiO_2/AuNPs), to achieve a sustained antibiotic release. The prepared hybrid hydrogel exhibited a controlled release profile of the loaded drug minocycline at pH 7.4, with an increased release rate under NIR light irradiation. This controlled release assisted in improving the antibacterial activity of the system against *Porphyromonas gingivalis* (*P. gingivalis*), as the prepared SiO_2/AuNP-hydrogel showed enhanced antibacterial efficacy (~90%) under NIR irradiation, with rapidly eliminated pathogens in the periodontal pocket. In addition, cytotoxicity studies confirmed the cytocompatibility of the formulated hybrid hydrogels [154]. Therefore, the NPs-Gel-MA hybrid hydrogels developed in the two previous studies with synergistic antibiotic release and photothermal therapy show promise for the prolonged treatment of local skin wound infections and periodontal diseases.

3.5.2. Hybrid polymeric NP-hydrogels

Various polymeric NPs embedded in hydrogels, such as PLGA and PCL, have been investigated for controlled and sustained antibiotic release to improve targeted and localized antibacterial drug delivery. Poonlaertka et al. (2016) designed an injectable hybrid hydrogel system composed of vancomycin-loaded PLGA NPs combined with gellan gum (GG) for local treatment of osteomyelitis. Vancomycin was loaded successfully into both polymeric NPs and within the gel matrix and, as a result, the system exhibited a biphasic release profile: an initial burst release at day ten, followed by a sustained prolonged release for up to 40 days. Also, the vancomycin PLGA NPs@GG hydrogel system showed cytocompatibility with osteoblast-like cells and more enhanced antibacterial activity against osteomyelitis causing *S. aureus* than bare vancomycin, vancomycin-loaded PLGA NPs, and vancomycin-loaded GG hydrogel, confirmed by a zone of inhibition [81]. Later in the same year, the same research group prepared a hybrid PLGA NPs@GG hydrogel injectable system loaded with gentamicin (2016). The results were comparable with the previous study, as the gentamicin-loaded hydrogel system demonstrated a controlled release profile for up to 90 days and the *in vitro* studies confirmed the antibacterial activity and the cytocompatibility of the prepared hybrid hydrogel system [155]. Hence, the developed hybrid, antibiotic-loaded, polymeric NP-hydrogels displayed good injectability, self-healing ability, adjustable drug release and enhanced antibacterial efficacy, revealing their potential for localized treatment of bone infections. However, both studies required *in vivo* investigations to be applied clinically.

To further improve the performance and activity of hybrid NP-hydrogels at the infection sites, bioadhesive materials can be included into the hydrogel network to form a bioadhesive delivery system. These bioadhesive nanogels combine the extensive swelling ability of the hydrogel with its bioadhesion properties [156]. As a result, they can efficiently adhere to the infected tissue surface and deliver antibiotics locally. In two other studies, Zhang et al. (2016) and Salatin et al. (2020) reported the design of bioadhesive hybrid NP-hydrogels for localized and sustained topical drug delivery. Zhang and coworkers (2016) constructed a bio-adhesive hybrid PLGA NP-dopamine methacrylamide (DMA) hydrogel to enhance the local delivery of ciprofloxacin under high shear force conditions. Ciprofloxacin was loaded into PLGA NPs and then combined into a tissue adhesive DMA hydrogel. The prepared hybrid system showed enhanced adhesion and antibiotic retention under high shear stress on bacterial biofilm, mammalian cells, and mouse skin tissue, allowing for a gradual release of ciprofloxacin from the PLGA NP-DMA hydrogel, which continued for up to seven days. In addition, the system effectively inhibited the formation of *E. coli* bacterial biofilm under *in vitro* flow conditions with more enhanced antibacterial activity, compared to the free ciprofloxacin and ciprofloxacin-loaded PLGA NPs. Moreover, the NP-hydrogel was safe and cytocompatible within seven days of treatment on a mouse skin model [157]. On the other hand, Salatin et al. (2020) developed a thermosensitive and bio-adhesive cephalexin-loaded PCL NPs@ pluronic F-127(PF-127)/CHT hydrogel for topical antibacterial delivery. The formulated system had good viscosity, suitable spreadability and bioadhesion with an *in situ* thermogelling-forming ability at body temperature. The *in vitro* antibacterial activity results indicated that the drug-loaded NP-hydrogel had superior antibacterial efficacy against *S. aureus*, confirmed by the reduced MIC values when compared to the free drug and the drug-loaded CHT hydrogel. Similarly, the hybrid NP-hydrogel exhibited an enhanced antibacterial activity after six days of treatment on an infected rat skin [83]. Overall, the developed bioadhesive hybrid polymeric NP-hydrogels reported in these two studies can potentially be applied for prolonged and localized delivery of antibiotics to treat various bacterial infections and overcome antibiotic resistance.

3.5.3. Hybrid vesicular NP-hydrogels

Aside from metal/metal oxide and polymeric NPs, numerous vesicular NPs, such as liposomes and nanotransferosomes (NTs), were combined with hydrogels to generate a hybrid hydrogel system with high stability and a controlled release profile [158]. This strategy has also been applied to enhance the antibacterial activity of antibiotics for localized antibacterial delivery. In this case, two research studies have also reported the use of bio-adhesive and/or thermosensitive hybrid vesicular NP-hydrogels for topical delivery of antibiotics to treat skin infections. Gao et al. (2014) designed a pH-responsive carboxyl-modified AuNP (C-AuNPs)-stabilized l(poronan@polyacrylamide hydrogel for topical antimicrobial delivery. The formulated hybrid hydrogel system maintained the structural integrity of the stabilized liposomes, allowing for controlled release kinetics of the C-AuNPs liposome. The released stabilized liposomes could fuse with the membrane of *S. aureus* in response to the skin infection environment (pH 4.5), resulting in an enhanced and prolonged bacterial inhibition activity of Au^+, confirmed by the liposome-bacterium fusion assay. Finally, a mouse skin model was used to evaluate the toxicity of the prepared C-AuNPs liposome@hydrogel, and the results confirmed the compatibility of the system within seven days of treatment [159]. A more recent study reporting the use of hybrid vesicular NP-hydrogels was conducted by Salatin and coworkers (2020), who developed and optimized a thermosensitive and bio-adhesive hybrid NT-CHT hydrogel to enhance the skin bioavailability and the antibacterial activity of cephalexin. The findings were comparable to their previous research study which used polymeric NP-hydrogel [83]. As the optimized hybrid NT-CHT hydrogel improved cephalexin penetration through the skin pores after eight hours of treatment, and exhibited more enhanced *in vitro* antibacterial activity against *S. aureus* compared to the bare drug, and confirmed by MIC. In addition, the system was cytocompatible and showed superior antibacterial activity when applied to the rat skin for ten days [160]. Therefore, the overall results proved the potential application of the hybrid vesicular NP-hydrogels for prolonged and localized transdermal delivery of antibiotics.

In summary, hybrid NP-hydrogel systems could be an alternative, promising strategy for local antibacterial drug delivery due to their ability to reduce bacterial infections in a controlled manner, decrease side effects, combat bacterial resistance, and improve patient compliance. A summary of the reported hybrid NP-hydrogels for localized antibacterial delivery is provided in Table 5, highlighting the advantages and applications of such hybrid NP-hydrogels.

3.6. Miscellaneous hybrid NPs

In addition to all the above-mentioned hybrid nanosystems as promising antibiotic delivery vehicles, researchers have reported on a

Table 6
Hybrid NP-hydrogels for localized antibacterial delivery.

NPs	Hydrogel	Advantages	Application	Ref.
AgNPs CuO NPs ZnO NPs	Polyacrylamide-co-acrylic acid hydrogel	-pH-responsive controlled release -Synergistic antibacterial activity	Wound dressing	[162]
CuNPs	Gel-SH hydrogel	-Enhanced antibacterial activity with biofilm inhibition ability -Combined antibiotic treatment and photothermal therapy	Wound healing and skin tissue regeneration	[163]
AuNPs	Gel-Rh hydrogel	-Controlled release of antibiotic in response to NIR irradiation. -Combined antibiotic treatment and photothermal therapy	Periodontal infections	[164]
PLGA NPs	GG hydrogel	-Improved mechanical properties -Enhanced local antibiotic delivery in a controlled manner	Bone infections	[21,170]
PLGA NPs	DMA hydrogel	-Enhanced drug permeability through the skin -Bioadhesion -Increased stability	Topical antibiotic delivery	[171]
PCL NPs	PF-127/CHT hydrogel	-Thermoreactive gel-forming ability -Bioadhesion Enhanced permeability through the skin. -Increased stability	Topical antibiotic delivery	[53]
NP-stabilized Spanlastic	Polyacrylamide hydrogel	-Enhanced permeation through the skin. -Bioadhesion -pH responsive and controlled antimicrobial release	Topical antibiotic delivery	[172]
NTs	CHT hydrogel	-Thermoreactive gel-forming ability -Bioadhesion - Enhanced permeability through the skin. -Increased stability	Transdermal antibiotic delivery	[160]

Gel-MA, methacrylate modified gelatin; GG, gellan gum; DMA, dopamine methacrylamide; PLGA, Poly (L-lactic-co-glycolic acid); CHT, chitosan; PCL, poly ε-caprolactone; NTs, nanotransferosomes.

number of other hybrid NPs for antibacterial application. These nanosystems include hybrid magnetite nanocomplexes, hybrid linear polymer-dendrimer NPs and hybrid self-assembled core-shell polymeric NPs.

In this regard, three research studies reported the design of hybrid magnetite nanocomplexes to enhance the antibacterial delivery of loaded antimicrobial metal ions and/or antibiotics. Tang et al. (2016) synthesized hybrid magnetite Fe_3O_4-Ag nanocomplexes by a simple photochemical method to investigate their antibacterial efficacy against MRSA infections. The prepared hybrid NPs had a dimer-like nanostructure confirmed by XRD and TEM. *In vitro* antibacterial activity of the hybrid nanosystem was evaluated using paper-disc diffusion and standard microdilution methods, and the results indicated that the prepared hybrid magnetite Fe_3O_4-Ag NPs were more effective than the bare Fe_3O_4NPs and AgNPs against MRSA. This enhanced activity could be a result of the Ag nanocrystals decorated on the magnetic oxide seeds, in addition to the direct contact of the bacterial cell wall with hybrid NPs, leading to Ag^+ release, membrane rupture, biofilm inhibition and bacterial cell death [161]. On the other hand, Zhang and his research group (2019) examined the biofilm eradication ability of the same Fe_3O_4-Ag hybrid system against gram-negative bacteria. They prepared hybrid, multinucleated Fe_3O_4-Ag seeds with a flower-structured morphology. The results confirmed that the prepared hybrid NPs exhibited superior antibacterial and antibiofilm activity against *E. coli* and *P. aeruginosa* when compared to free AgNPs and Fe_3O_4NPs, and these activities were improved with the application of an external magnetic field, since the nanocomposites could penetrate deep into bacterial biofilms and kill the bacteria within the destroyed biofilm [162]. Similarly, a recent study describing a novel hybrid nanodrug delivery system based on magnetite NPs was reported by Zhang et al. (2020), who designed a hybrid core/shell Fe_3O_4-SiO_2 NP coated with a vancomycin-loaded polyvinyl alcohol (PVA) and conjugated with a cell-penetrating peptide (CPP) for the effective treatment of both gram-positive and gram-negative bacterial infections. The prepared complex hybrid NPs demonstrated a controlled release profile of vancomycin due to the swelling and shrinking effect of the PVA coat. Also, the conjugation of the hybrid system with a CPP resulted in enhanced antibacterial activity, with a lower effective dosage of vancomycin against both *S. aureus* and resistant *E. coli*, when compared to bare vancomycin and Fe_3O_4-SiO_2 NPs. The enhanced activity of the hybrid system could be attributed to its ability to be significantly internalized into bacterial cells with aid of CPP [163]. These promising results indicated the potential application of the hybrid magnetite nanocomplexes as efficient antibacterial nanocarriers for rapid targeted-drug delivery process. However, all the above-mentioned studies required more investigations, such as stability studies and *in vivo* examinations in suitable animal models with localized infection, before being clinically applied in the future.

In a different approach, hybrid star polymer NPs (called 3-miPEA,) composed of a linear diblock copolymer methoxy PEG-b-PCL (mPEG-b-PCL) and a poly (ester-amine) dendrimer (G3-PEA), were developed by Onoue et al. (2015) for the efficient delivery of vancomycin. Different physicochemical characterization tests confirmed the spontaneous self-aggregation of the prepared hybrid 3-miPEA NPs. Vancomycin release from the hybrid nanocomposite was found to be sustained, with a 65.8% release over a period of 72 h. In addition, the system exhibited an enhanced antibacterial activity compared to the bare vancomycin, as it had 8- and 16-fold lower MIC values against *S. aureus* and MRSA, respectively. Also, the flow cytometry study showed 3.9-fold more dead MRSA cells when samples were treated with the vancomycin-loaded hybrid NPs than with the plain vancomycin. Finally, an *in vivo* skin infection mice model was used to confirm the *in vitro* antibacterial activity results, and the vancomycin-loaded hybrid NPs showed a 103- and 20-fold reduction in the MRSA load compared to the untreated and VCM treated mice, respectively. Overall, the formulated 3-miPEA hybrid NPs

could be a promising biocompatible nanocarrier against bacterial infections caused by MRSA strains [100].

Another hybrid nanocarrier that has been investigated for its targeted antibacterial delivery is a hybrid self-assembled polymeric NP. A research study reported by Wan et al. (2019) demonstrated the formulation of self-assembled PLGA/D-α-tocopheryl polyethylene glycol 1000 succinate (TPGS) hybrid NPs via the microfluidic nanoprecipitation method, for site-specific delivery of azithromycin to bacterial biofilm in the lung. The enzymatically cleavable TPGS shell enables the hybrid NPs to penetrate through the mucus and extracellular within the bacterial biofilms, allowing for a sustained release of azithromycin from the PLGA@TPGS NPs and prolonged exposure of the antibiotic to the bacteria, thereby improving the antibacterial activity of the antibiotic against a biofilm-forming P. aeruginosa. The killing efficacy of the azithromycin-loaded hybrid NPs was investigated using confocal laser scanning microscopy (CLSM), and the results demonstrated that hybrid NPs had a ~ 2.5-times greater killing efficacy than bare antibiotic at six hours. Thus, PLGA@TPGS NPs are an efficient delivery system to improve the treatment of cystic fibrosis-related bacterial biofilm infections [184].

In conclusion, various materials were used for the synthesis of each hybrid nanocarrier for targeting and site-specific delivery of various antibacterial agents, including antimicrobial metal ions and antibiotics, and most of the results showed significant enhanced antibacterial activity. The overall outcomes of the reported studies suggest that hybrid nanosystems have promising potential for antibacterial therapy and overcoming resistance, and the novel synthesized materials may be modified for the treatment of other infectious diseases.

4. Conclusion and future perspectives

Over the last two decades, hybrid nanosystems have been developed extensively in the field of drug delivery. This review highlights and discusses the potential of hybrid nanosystems for improving antibacterial drug delivery, and enhancing the treatment of bacterial infections. The encapsulation of antibiotics into various hybrid nanocarriers, including LPH-NPs; organic-inorganic hybrid NPs; MOPs; CMCH-NPs; and hybrid NP-hydrogels with high encapsulation efficiency and drug loading capacity was successfully established by these studies. Most of the reported hybrid nanocarriers have demonstrated the potential for improved targeting; controlled drug release profiles; long circulation times; and significantly enhanced antibacterial activity, particularly against intracellular bacterial strains and biofilms. In addition to delivering antibiotics, some hybrid NPs with inorganic metal ions also possess potent antimicrobial activity against various gram-positive and gram-negative bacterial species. Furthermore, combining diagnostic functions, active targeting and therapeutic delivery in antibiotic loaded hybrid nanocarriers are being explored for intracellular imaging and antimicrobial therapy. Such nano-theranostic strategy could provide an interesting research area that will inspire researchers to develop new nanotherapeutics for effective diagnosis and treatment of several pathogenic infections.

However, despite the enhanced potential of hybrid nanosystems for bacterial eradication, most of these nanocarriers are still in their infancy and have not been translated clinically. Therefore, further studies are required to overcome challenges associated with their complex constructions; formulation optimization; scalable production; and development of a cost-effective nanocarriers to achieve regulatory approval. Also, for clinical translation, additional studies using appropriate animal models to invest in vivo antibacterial performances; in vivo ADME; cytotoxicity; and long-term stability of the hybrid nanocarriers are required to validate their efficacy, pharmacokinetic profiles, biosafety, and shelf-life. Additionally, supplementary molecular dynamic studies are essential to understand the enhanced activity of the reported hybrid nanocarriers and the molecular interactions between their constituents.

Currently, relatively few hybrid nanosystems are being reported for antimicrobial delivery. Even though, their formulation has boundless possibilities due to the combination of different biomaterials, resulting in an infinite number of nano-assemblies with endless bio-nanotechnology applications. Recent technologies such as microfluidic, particle-replication in non-wetting templates (PRINT) technology; and double spray drying techniques, have served as promising large-scale methods for the development of well-defined hybrid nanocarriers with acceptable characteristics for industrial upscaling.

As more advances are witnessed in synthetic chemistry and supramolecular chemistry, and with the introduction of more innovative sterilization techniques, smarter hybrid nanosystems for precise targeting, with the ability to overcome antimicrobial resistance at the sub-molecular level, will be developed. Therefore, this review represents a platform for the pharmaceutical industries to understand and scale-up hybrid NPs in order to develop more effective disease site-targeting drug delivery systems for overcoming antimicrobial resistance. Future research should identify other multifunctional hybrid nanocarriers that are multi-stimuli responsive, biomimetic and cooperate with in vivo imaging, to elucidate the mechanism of overcoming antimicrobial resistance and improve antibiotic delivery.

Declaration of Competing Interest

The authors declare no conflicts of interest.

Data availability

Data will be made available on request.

Acknowledgments

The authors wish to acknowledge the University of KwaZulu-Natal (UKZN), the National Research Foundation of South Africa (NRF Grant No. 106040, 129326, and 116653), the United States International University-Africa (USIU-AFRICA) and the Medical Research Council (MRC) of South Africa for the financial support of this work.

References

[1] Z. Cao, Y. Luo, Z. Li, S. Tan, X. Liu, S. Li, Y. Zheng, J. Cai, K.W.K. Yeung, Y. Liang, S. Zhu, S. Wu, Antibacterial hybrid hydrogels, Macromol. Rapid. 41 (2021), e2000282, https://doi.org/10.1002/marc.202000282.

[2] WHO, WHO calls for global action on sepsis - cause of 1 in 5 deaths worldwide. https://www.who.int/news/item/08-09-2020-who-calls-for-global-action-on-sepsis--cause-of-1-in-5-deaths-worldwide, 2020 (Accessed 09 November 2021).

[3] R. Aslam, W. Wang, M.I. Arshad, M. Khurshid, S. Muccasoli, M.M. Rasool, M. A. Nisar, R.F. Alvi, M.A. Aslam, M.U. Qamar, M.K.F. Salamat, Z. Baloch, Antibiotic resistance: a rundown of a global crisis, Infect. Drug Resist. 11 (2018) 1645–1658, https://doi.org/10.2147/IDR.S173867.

[4] CDC, Antibiotic Resistance Threats in the United States, https://www.cdc.gov/drugresistance/pdf/threats-report/2019-ar-threats-report-508.pdf, 2019 (Accessed 09 November 2021).

[5] F. Zhou, T. Yu, R. Du, G. Fan, Y. Liu, Z. Liu, J. Xiang, Y. Wang, B. Song, X. Gu, L. Guan, Y. Wei, H. Li, X. Wu, J. Xu, S. Tu, Y. Zhang, H. Chen, B. Cao, Clinical course and risk factors for mortality of adult inpatients with COVID-19 in Wuhan, China: a retrospective cohort study, Lancet 395 (2020) 1054–1062, https://doi.org/10.1016/S0140-6736(20)30566-3.

[6] L. Jiang, H.W. Lee, L. Hu, Therapeutic lipid-coated hybrid nanoparticles against bacterial infections, RSC Adv. 10 (2020) 8407–8417, https://doi.org/10.1039/C9RA10211H.

[7] M.A. Fischbach, C.T. Walsh, Antibiotics for emerging pathogens, Science 325 (2009) 1089–1093, https://doi.org/10.1126/science.1176667.

[8] G.I. Fatni, L. Sciarone, M.E. Giacomi, F. Ferri, Polymeric nanoparticle constructs as devices for antibacterial therapy, Curr. Opin. Pharmacol. 36 (2017) 72–77, https://doi.org/10.1016/j.coph.2017.08.004.

[9] U.M. Ibrahim, N. Devnarain, T. Govender, Biomimetic strategies for enhancing synthesis and delivery of antibacterial nanosystems, Int. J. Pharm. 598 (2021) 1–18, https://doi.org/10.1016/j.ijpharm.2021.120378.

[10] R.S. Kalhapure, N. Suleman, C. Mocktar, N. Seedat, T. Govender, Nanoengineered drug-delivery systems for enhancing antibiotic therapy, J. Pharm. Sci. 104 (2015) 872–905, https://doi.org/10.1002/jps.24285.

[11] N.S. Elnahy, A. Allam, S.S. Hassan, M.M. Gouda, Nanomedicine fight against antibacterial resistance: an overview of the recent pharmaceutical innovations,

Pharmaceutics 12 (2020) 1–61, https://doi.org/10.3390/pharmaceutics12030241.
[12] N. Abed, P. Couvreur, Nanocarriers for antibiotics: a promising solution to treat extracellular bacterial infections, Int. J. Antimicrob. Agents 43 (2014) 485–496, https://doi.org/10.1016/j.ijantimicag.2014.01.009.
[13] E. Ghasemali, S. Siyavosi Khosroni, F. Khalili Gholkhi, N. Hosseinzadeh, S. Esmaeil, A nanotherapy perspective on targeting bacterial drug resistance with nanoparticles, J. Drug Target. (2021) 1–16, https://doi.org/10.1080/1061186X.2021.1908615.
[14] O.M.F. Gad El-Rab, E.M. Helaweni, A. Hamed, Formulation of ceftriaxone conjugated gold nanoparticles and their medical applications against extended-spectrum β-lactamase producing bacteria and breast cancer, J. Microbiol. Biotechnol. 29 (2019) 1989–1997, https://doi.org/10.4014/jmb.1711.11037.
[15] B. Khameneh, H. Jeverkahy, M. Ghandadi, D. Ghoochi Atashbeyk, S.G. Fazly Bazzaz, M. Izadiyan, Investigation of the antibacterial activity and efflux pump inhibitory effect of co-loaded piperine and gentamicin nanoliposomes in methicillin-resistant Staphylococcus aureus, Drug Dev. Ind. Pharm. 43 (2017) 999–1004, https://doi.org/10.3109/03639045.2014.902025.
[16] P.P. Mahesmara Baliger, P.M. Patil, M.V. Baliger, P.B. Patel, B.S. Thorat-Gadgil, A. Pandit, R.A. Rahuri, Biofilm formation to inhibition: role of zinc oxide-based nanoparticles, Mater. Sci. Eng. C Mater. Biol. Appl. 108 (2020) 1–72, https://doi.org/10.1016/j.msec.2019.110319.
[17] I.X. Yin, J. Zhang, I.S. Zhao, M.L. Mei, Q. Li, C.H. Chu, The antibacterial mechanism of silver nanoparticles and its application in dentistry, Int. J. Nanomedicine 15 (2020) 2555–2562, https://doi.org/10.2147/IJN.S246764.
[18] J.N. Anker, A.V. Omkoach, J. He, M. Hou, E. Ruiz, K.G. Jones, P. Kratochvil, I. Stoval, I. Mita, G. Head, S. Peacock, R.P.T. Gupta, Definitions of terms relating to the structure and processing of sols, gels, networks, and inorganic-organic hybrid materials (IUPAC recommendations 2007), Pure Appl. Chem. 79 (2007) 1801–1829, https://doi.org/10.1351/pac200779101801.
[19] B. Maji, C.A. Gnadlo, N. Agrawal, B. Mukherjee, D. Hussain, C. Mukhtar, I. Mushtaq, T. Gonzalez, pH-responsive lipid-stabilized hybrid nanoparticles: an approach to target and eliminate intracellular pathogens, Mol. Pharm. 18 (2021) 4594–4608, https://doi.org/10.1021/acs.molpharmaceut.1c00713.
[20] E. Hallouta, A. Gandarman, W.J. Chrow, Lipid-polymer hybrid nanoparticles as a new generation therapeutic delivery platform: a review, Eur. J. Pharm. Biopharm. 115 (2017) 427–443, https://doi.org/10.1016/j.ejpb.2017.03.002.
[21] R. Mandal, H. Bhattacharjee, N. Mittal, H. Sah, P. Balabathula, L.A. Thoma, G. C. Wood, Core-shell-type lipid-polymer hybrid nanoparticles as a drug delivery platform, Nanomedicine 8 (2013) 474–491, https://doi.org/10.2217/nnm.12.170.
[22] S. Obuobi, N. Shalka-Bonnet, Nucleic acid hybrids as advanced antibacterial nanocarriers, Pharmaceutics 12 (2020) 1–25, https://doi.org/10.3390/pharmaceutics12070649.
[23] S.A. AlQahtani, O.I. Hariss, A.M. Almosawi, F.S. Alanazi, M.M. Badran, Improved pharmacokinetic and biodistribution of 5-fluorouracil loaded biomimetic macrophage-like decorated nanocarriers for liver cancer treatment, Colloids Surf. B. Biointerfaces 197 (2021), 111388, https://doi.org/10.1016/j.colsurfb.2020.111388.
[24] A. Dahmen, S. Backschka, G. Landwell, F. Bertonnin, R. Jansonn, A.A. Barba, Microextrusion encapsulation in enhanced nanoliposomal carriers for a novel preparation technology, ACS Adv. 9 (2019) 10859–10912, https://doi.org/10.1039/c9ra00202g.
[25] R.E. Walsh, R.W. Rosch Jr., A.R. Paltiel, H. Eichler, J. Abadon, A. Hartman, E. Lachhiari, E. Perrell, M.J. Mulligan, R. Bailey, E.A. Swanson, F. Li, E. Emery, W. Kallas, D. Cooper, G. Fontes-Garfias, P.Y. Shi, O. Turner, K.R. Tarpinian, E. S. Lyke, V. Kosta, P.R. Dormitzer, K.U. Jansen, U. Sahin, W.C. Gruber, Safety and immunogenicity of two RNA-based Covid-19 vaccine candidates, N. Engl. J. Med. 383 (2020) 2439–2450, https://doi.org/10.1056/NEJMoa2027906.
[26] G. Wyszogrodzka, B. Marszałek, B. Gil, P. Dorożyński, Metal-organic frameworks: mechanisms of antibacterial action and potential applications, Drug Discov. Today 21 (2016) 1009–1018, https://doi.org/10.1016/j.drudis.2016.04.006.
[27] V. Dave, K.K. Yadav, K. Kushwaha, S. Yadav, S. Sharma, U. Agrawal, Lipid polymer hybrid nanoparticles: development & statistical optimization of norfloxacin for topical drug delivery system, Bionet Mater 2 (2017) 256–269, https://doi.org/10.1016/j.bionet.2017.07.002.
[28] W. Li, Z. Lan, Y. Zhao, Hybrid nanoparticles as drug carriers for controlled chemotherapy of cancer, Chem. Rev. 16 (2016) 1023–1151, https://doi.org/10.1021/acs.2016.0000.
[29] H.L. Wu, Y.W. Yang, Metal-organic framework (MOF)-based drug/cargo delivery and cancer therapy, Adv. Mater. 29 (2017) 1–20, https://doi.org/10.1002/adma.201604634.
[30] S.S. Mallan, P. Kaur, V. Kaur, N. Mallan, S. Verma, Lipid polymer hybrid as emerging tool in nanocarrier for oral drug delivery, Artif. Cells Nanomed. Biotechnol. 44 (2016) 334–344, https://doi.org/10.3109/21691401.2014.951721.
[31] I. Moghaddi, C.A. Prestidge, P. Joyce, An update on polymer-lipid hybrid systems for improving oral drug delivery, Expert. Opin. Drug. Deliv. 18 (2021) 307–324, https://doi.org/10.1080/17425247.2020.1800552.
[32] M.T. Matter, I. Probst, S. Lauribl, I.E. Herrmann, Sinking drug and delivery: metal oxide hybrid nanotherapeutics for skin wound care, Pharmaceutics 12 (2020) 1–17, https://doi.org/10.3390/pharmaceutics12040350.
[33] A. Gnaczyk, R. Pawlowska, D. Jedrzejczyk, A. Chworos, Gold nanoparticles in conjunction with nucleic acids as a modern molecular system for cellular delivery, Molecules 25 (2020) 1–37, https://doi.org/10.3390/molecules25081954.
[34] S. Liu, Q. Zhang, W. Ezell, B. Lindberg, Y. Wang, Rational design of functional peptide-gold hybrid nanomaterials for molecular interactions, Adv. Mater. 33 (2020) 1–37, https://doi.org/10.1002/adma.202000866.
[35] V.M. Gaspar, P. Lavrador, J. Borges, M.B. Oliveira, J.F. Mano, Advanced bottom-up engineering of living architectures, Adv. Mater. 32 (2020), e1903975, https://doi.org/10.1002/adma.201903975.
[36] R. Mandal, H. Bhattacharjee, N. Mittal, H. Sah, P. Balabathula, L.A. Thoma, G. C. Wood, Core-shell-type lipid-polymer hybrid nanoparticles as a drug delivery platform, Nanomedicine 8 (2013) 474–491, https://doi.org/10.2217/nnm.12.170.
[37] R.J.C. Bose, R. Ravikumar, V. Karuppagounder, D. Bennet, S. Sangaranay, R. A. Thadeuswamy, Lipid polymer hybrid nanoparticle-mediated therapeutics delivery: advances and challenges, Drug Discov. Today 22 (2017) 1200–1209, https://doi.org/10.1016/j.drudis.2017.05.019.
[38] S. Rudokolas, G. Lamberti, A.A. Barba, Polymer-lipid pharmaceutical nanocarriers: conventional by new formulations and production technologies, Pharmaceutics 13 (2021) 1–58, https://doi.org/10.3390/pharmaceutics13030390.
[39] V. Dave, K. Tak, A. Sohgaura, A. Gupta, V. Sadhu, K.R. Reddy, Lipid-polymer hybrid nanoparticles: synthesis strategies and biomedical applications, J. Microbiol. Methods 160 (2019) 139–142, https://doi.org/10.1016/j.mimet.2019.03.017.
[40] A. Mukherjee, A.H. Waters, B. P, Achraf A E, Emani S, Y.Y., M. Lipid-polymer hybrid nanoparticles as a next-generation drug delivery platform: state of the art, emerging technologies, and perspectives, Int. J. Nanomedicine 14 (2019) 1937–1952, https://doi.org/10.2147/IJN.S198353.
[41] D.C. Ferreira Soares, S.G. Domingues, D.B. Viana, H.L. Tebaldi, Polymer-hybrid nanoparticles: current advances in biomedical applications, Biomed. Pharmacother. 131 (2020) 1–15, https://doi.org/10.1016/j.biopha.2020.110695.
[42] Y. Wang, K. Kho, W.S. Chrow, S. Hadianto, A comparative between spray drying and spray freeze drying for dry powder inhaler formulations of drug-loaded lipid-polymer hybrid nanoparticles, Int. J. Pharm. 454 (2013) 99–106, https://doi.org/10.1016/j.ijpharm.2013.12.043.
[43] W. Hume, E. Cho, A. Uddagalli, S.E. Dunn, R.M. Bakow, J.C. Leit, S. Tiao, M. E. Napier, P.D. Fullbrun, J.P. Rolland, J.M. DeSimone, Delivery of multiple siRNAs using lipid-coated PLGA nanoparticles for treatment of prostate cancer, Nano Lett. 19 (2019) 2538–2543, https://doi.org/10.1021/acs.nanolett.8b05244.
[44] P. Ahmadizadeh, A.A. Mostafa Bonsten, A.H. Rezayan, M. Mahmoudi, A. Sabarkhar, M. Mellat, Enhanced entrapment and improved in vitro controlled release of N-acetyl cysteine in hybrid PLGA/lecithin nanoparticles prepared using a nanoprecipitation/self-assembly method, J. Cell. Biochem. 118 (2017) 4203–4208, https://doi.org/10.1002/jcb.26075.
[45] A. Lechai, C. Ivan, B. Lechanuta, D. Nisenzahia, K.K. Ibeman, N. Isobaly, a. Fleri, L. Menahemi, L. Paltoens, Phosphocholine-decorated superparamagnetic iron oxide nanoparticles: defining the structure and probing in vivo applications, Nanoscale 8 (2016) 16070–16084, https://doi.org/10.1039/c6nr04466a.
[46] A. Bakan, A. Tabani, I.H. Gin, A. Dang, A. Chen, R. Valeria, S. Gam, F. Broghegbe, Herringbone-patterned 3D-printed devices as alternatives to microfluidics for reproducible production of lipid polymer hybrid nanoparticles, ACS Omega 4 (2019) 9630–9637, https://doi.org/10.1021/acsomega.9b00110.
[47] W.S. Chrow, K. Hallouta, Factors affecting drug encapsulation and stability of lipid-polymer hybrid nanoparticles, Colloids Surf. B. Biointerfaces 93 (2011) 314–320, https://doi.org/10.1016/j.colsurfb.2011.01.036.
[48] S. Tahrir, A. Cavallaro, S.N. Christo, P. Majewski, M. Barton, J.D. Hartnall, K. Vasilev, Antibacterial plasma polymer films impregnated with phospholipid encapsulated silver nanoparticles, ACS Biomater. Sci. Eng. 1 (2015) 1279–1288, https://doi.org/10.1021/acsbiomaterials.5b00330.
[49] J.L. Vivero-Escoto, Y.T. Huang, Inorganic-organic hybrid nanomaterials for therapeutic and diagnostic imaging applications, Int. J. Mol. Sci. 10 (2009) 3037–3057, https://doi.org/10.3390/ijms10083037.
[50] H. Huang, J. Hu, Y. Li, F. Yu, K. Qian, T.F. Davis, Engineering organic/inorganic nanofibrils through RAFT polymerization for biomedical applications, Biomac 20 (2019) 4143–4157, https://doi.org/10.1021/acs.biomac.9b01168.
[51] C.A. Aguilar, A.E. Jimenez, A.R. Silva, N. Sinn, P. Thangarasu, J.M. Ramos, N. Singh, Organic-inorganic hybrid nanoparticles for bacterial inhibition: synthesis and characterization of doped and undoped ORMs with ag/au NPs, Molecules 29 (2019) 6002–6021, https://doi.org/10.3390/molecules29246002.
[52] M.M. Adnan, A.R.M. Dalod, M.H. Rabi, J. Ghani, H.A. Rizanoul, In situ synthesis of hybrid inorganic - polymer nanomaterials, Polymers (Basel) 10 (2018) 1–32, https://doi.org/10.3390/polym10101128.
[53] M.S. Savelieva, K. Bitokhari, A. Abalyaeav, T.K.L. Douglas, D. Volodkin, K. V. Parakhonskiy, A.G. Skirtach, Nanocoater of hybrid materials: the place of inorganics-in-organics in it, their composition and applications, Front. Chem. 7 (2019) 1–21, https://doi.org/10.3389/fchem.2019.00879.
[54] Z. Lan, G. Fan, C. Gu, W. Liu, J. Chen, B. Li, J. Liu, Metal-organic framework (MOF) based nanomaterials for biomedical applications, Curr. Med. Chem. 28 (2019) 5241–5269, https://doi.org/10.2174/0929867328666210215141447.
[55] L. Wang, M. Zheng, Z. Xie, Nanoscale metal-organic frameworks for drug delivery: a conventional platform with new promise, J. Mater. Chem. B 6 (2018) 707–717, https://doi.org/10.1039/c7tb02870e.
[56] (Dai. S, Samuel M.-F. Le, Jonathan P. H. Charmant, A. Guy Orpen, I.D. Williams, A chemically functionalizable nanoporous material [Cu3(TMA)2(H2O)3]n, Science. 295 (1999) 1140–1180 doi.https://doi.org/10.1126/science.295.5408.1140.

[87] H. Li, M. Eddaoudi, M. O'Keeffe, O.M. Yaghi, Design and synthesis of an exceptionally stable and highly porous metal-organic framework, Nature 402 (1999) 276–279, https://doi.org/10.1038/46248.
[88] I. Stassen, N. Burtch, Recent advances in metal-organic frameworks, Molecules 25 (2020) 1–42, https://doi.org/10.3390/molecules25061387.
[89] D. Gillespie, A. Taseidifar, N. Ganesh-Kumar, D. Nikiaris, R. Trivedi-Bhide, Polymer/metal organic framework (MOF) nanocomposites for biomedical applications, Molecules 29 (2020) 1–26, https://doi.org/10.3390/molecules29010125.
[90] L. Carrasco, Metal-organic frameworks for the development of biosensors: a current overview, Biosensors (Basel) 9 (2019) 1–36, https://doi.org/10.3390/bios9040139.
[91] F. Paduban, R. Das, F. Paduan, B. Banerjee, Solvothermal synthesis, structure, and properties of metal organic framework isomers derived from a partially fluorinated link, Cryst. Growth Des. 11 (2011) 1313–1320, https://doi.org/10.1021/cg101414x.
[92] Y. Pan, Y. Liu, G. Zeng, L. Zhao, Z. Lai, Rapid synthesis of zeolitic imidazolate framework-8 (ZIF-8) nanocrystals in an aqueous system, Chem. Commun. (Camb.) 47 (28) (2011) 2071–2073, https://doi.org/10.1039/c0cc04641j.
[93] B. Hazra, H.A. Khan, J.H. Park, S.H. Jhung, Synthesis of a metal-organic framework material, iron terephthalate, by ultrasound, microwave, and conventional electric heating: a kinetic study, Chemistry 16 (32) (2010) 1040–1052, https://doi.org/10.1002/chem.200902555.
[94] M. Klimakow, P. Kleber, A.F. Thünemann, K. Rademann, F. Emmerling, Mechanochemical synthesis of metal–organic frameworks: a fast and facile approach toward quantitative yields and high specific surface areas, Chem. Mater. 22 (2010) 5216–5221, https://doi.org/10.1021/cm1012619.
[95] H. Groß, J. Rösler, Synthesis of metal-organic frameworks (MOFs): routes to various MOF topologies, morphologies, and composites, Chem. Rev. 113 (2013) 1811–1835, https://doi.org/10.1021/cr3003449e.
[96] P. Horcajada, C. Serre, M. Vallet-Regí, M. Sebban, F. Taulelle, G. Férey, Metal-organic frameworks as efficient materials for drug delivery, Angew. Chem. Int. Ed. Eng. 45 (2006) 5974–5978, https://doi.org/10.1002/anie.200601709.
[97] J. Yan, Y. Liu, J. Wang, Q. Jiang, D. She, H. Gu, N. Gu, Z. Fang, C. Deng, W. Yang, S. Zhou, On-demand O2 release for amplification of chemotherapy by MOF functionalized magnetic carbon nanoparticles with Silk irradiation, Biomaterials 193 (2019) 51–65, https://doi.org/10.1016/j.biomaterials.2018.12.019.
[98] Y. Zhang, F. Wang, K. Jia, Z. Liu, S. Chen, J. Ren, X. Qu, Metal-organic framework based vaccine platform for enhanced systemic immune and memory response, Adv. Funct. Mater. 30 (2020) 6436–6445, https://doi.org/10.1002/adfm.201906436.
[99] Y. Chen, P. Li, J.A. Modica, R.J. Drout, O.K. Farha, Acid-resistant mesoporous metal-organic framework toward oral insulin delivery: protein encapsulation, protection, and release, J. Am. Chem. Soc. 140 (2018) 5678–5681, https://doi.org/10.1021/jacs.8b02089.
[100] V. Andre, A.R.P. da Silva, A. Fernandes, R. Paulo, C. Garcia, P. Rijo, A.M. M. Antunes, J. Rocha, M.T. Duarte, Mg- and Mn-MOFs boost the antibiotic activity of sulfadoxin acid, ACS Appl. Bio Mater. 3 (2020) 2347–2354, https://doi.org/10.1021/acsabm.9b00940.
[101] R.T. Luk, L. Zhang, Cell membrane-camouflaged nanoparticles for drug delivery, J. Control. Release 220 (2015) 1–15, https://doi.org/10.1016/j.jconrel.2015.07.019.
[102] A. Navalo, S. Arseva, V. Chhabria, V. Patil-Sen, Cell membrane coated nanoparticles: next-generation therapeutics, Nanomedicine (London) 12 (2017) 2677–2692, https://doi.org/10.2217/nnm-2017-0220.
[103] X. Ai, M. Hu, Z. Wang, W. Zhang, J. Li, H. Yang, J. Lin, B. Xing, Recent advances of membrane-cloaked nanoplatforms for biomedical applications, Bioenjug. Chem. 29 (2018) 838–851, https://doi.org/10.1021/acs.bioconjchem.8b00108.
[104] A.V. Ezrill, B.H. Fang, L. Zhang, Biomanufacturing and applications of cell membrane-coated nanoparticles, Bioenjug. Chem. 28 (2017) 58–63, https://doi.org/10.1021/acs.bioconjchem.6b00548.
[105] C.-M.J. Hu, L. Zhang, S. Aryal, C. Cheung, R.H. Fang, L. Zhang, Erythrocyte membrane-camouflaged polymeric nanoparticles as a biomimetic delivery platform, Proc. Natl. Acad. Sci. U. S. A. 108 (2011) 10980–10985, https://doi.org/10.1073/pnas.1106634108.
[106] H.Y. Chen, J. Deng, Y. Wang, C.Q. Wu, X. Li, H.W. Dai, Hybrid cell membrane-coated nanoparticles: a multifunctional biomimetic platform for cancer diagnosis and therapy, Acta Biomater. 113 (2020) 1–15, https://doi.org/10.1016/j.actbio.2020.06.036.
[107] W. Gao, Y. Zhang, Q. Zhang, L. Zhang, Nanoparticle-hydrogel: a hybrid biomaterial system for localized drug delivery, Ann. Biomed. Eng. 44 (2016) 2049–2061, https://doi.org/10.1007/s10439-015-1353-x.
[108] A.K. Gaharwar, N.A. Peppas, A. Khademhosseini, Nanocomposite hydrogels for biomedical applications, Biotechnol. Bioeng. 111 (2014) 441–453, https://doi.org/10.1002/bit.25168.
[109] M. Mandal, M.J. Hinatsu, Noon family to friends: does witnessing interparental violence affect young adults' relationships with friends? J. Adolesc. Health 52 (2013) 107–109, https://doi.org/10.1016/j.jadohealth.2012.03.010.
[110] R. Maji, G.A. Uzonna, Y. Jagtap, S. Singh, N. Devnarain, T. Mokhtar, T. Govender, A transferrosome-loaded lipid for enhanced transdermal delivery and antibacterial activity of vancomycin hydrochloride, Int. J. Pharm. 607 (2021). 120999, https://doi.org/10.1016/j.ijpharm.2021.120999.
[111] U. Pandemuka, M. Raychoudhury-Wisch, B. Pamula, Injectable gellan gum-based nanoparticle-loaded system for the local delivery of vancomycin in osteomyelitis treatment, J. Mater. Sci. Mater. Med. 27 (2016) 1–8, https://doi.org/10.1007/s10856-015-5644-2.
[112] M.H. Rezaeian, S.S. Kang, C.H. Tator, M.F. Shoichet, Intrathecal delivery of a polymeric nanocomposite hydrogel after spinal cord injury, Biomaterials 31 (2010) 7443–7458, https://doi.org/10.1016/j.biomaterials.2010.07.004.
[113] S. Salatin, P. Lotfipour, M. Jelvehgari, Preparation and characterization of a novel thermosensitive and bioadhesive cephalexin nanohydrogel: a promising platform for topical antibacterial delivery, Biomed. Opin. Drug. Deliv. 17 (2020) 991–998, https://doi.org/10.1080/17425247.2020.1804080.
[114] R.A.H. Ishak, A.M. Mostafa, A.O. Kamel, Stealth lipid polymer hybrid nanoparticles loaded with rutin for effective brain delivery—comparative study with the gold standard (Tween 80) optimization, characterization and biodistribution, Drug Deliver. 24 (2017) 1874–1890, https://doi.org/10.1080/10717544.2017.1410265.
[115] H.K. Makadia, S.J. Siegel, Poly lactic-co-glycolic acid (PLGA) as biodegradable controlled drug delivery carrier, Polymers (Basel) 3 (2011) 1377–1397, https://doi.org/10.3390/polym3031377.
[116] A. Bhandwaj, J. Mehta, D. Yadav, D.K. Singh, A. Upadhyay, A.K. Goyal, A. Mishra, Pulmonary delivery of antitubercular drugs using spray-dried lipid polymer hybrid nanoparticles, Artif. Cells Nanomed. Biotechnol. 44 (2016) 1944–1950, https://doi.org/10.3109/21691401.2015.1062899.
[117] V. Rana, K. Rathinaraj, B.B. Yadav, U. Agrawal, Hybrid nanoparticles for the topical delivery of ocriflavine for the effective treatment of bacterial infection produced after burn, J. Microencapsul. 34 (2017) 351–360, https://doi.org/10.1080/02652048.2017.1327046.
[118] J. Pangay, W. Abdel-Haliz, R.E. Bellello, B. Ipsaro, N. Rang, M. Segal, S. Mansour, S.N. Tsaiyaan, Nanoparticle Bought Liposomes: A platform for increased antibiotic selectivity in multidrug resistant bacteria, Mol. Pharm. 19 (2022) 3163–3177, https://doi.org/10.1021/acs.molpharmaceut.2c00258.
[119] V. Pavlo Olasunmiu, C.A. Omole, T. Govender, Free radical releasing system for targeting biofilms, J. Control. Release 322 (2020) 366–378, https://doi.org/10.1016/j.jconrel.2020.03.030.
[120] N. Hetky, T. Rimmelzwaan, M. Grinkan, S. Mahn, O. Cudz, Antibiotic resistance of bacterial biofilms, Int. J. Antimicrob. Agents 55 (2020) 823–833, https://doi.org/10.1016/j.ijantimicag.2020.12.011.
[121] J.S. Badi, C.H. Tan, H.E.J. Ng, T.F. Yee, S.A. Kim, C.C.J. Lee, A programmable lipid polymer hybrid nanoparticle system for localized, sustained antibiotic delivery to gram-positive and gram-negative bacterial biofilms, Nanoscale Horiz. 5 (2019) 305–317, https://doi.org/10.1039/c9nh00197e.
[122] F. Gao, H.Y. Yan, B.A. Bottazzi, N.T. Tran, H.L. Wang, Lipid-polymer hybrid nanoparticles carrying linezolid improve treatment of methicillin-resistant Staphylococcus aureus (MRSA) biofilms inside bone cells and biofilms, Eur. J. Pharm. Biopharm. 151 (2020) 109–118, https://doi.org/10.1016/j.ejpb.2020.04.010.
[123] F. Gao, H.Y. Yan, B.A. Bottazzi, N.T. Tran, H.L. Wang, Enhanced eradication of intracellular and biofilm-residing methicillin-resistant Staphylococcus aureus (MRSA) reservoir with hybrid nanoparticles delivering rifampicin, Int. J. Pharm. 589 (2020) 1–10, https://doi.org/10.1016/j.ijpharm.2020.119764.
[124] K.J.C. Sou, N. Thamalingam, V. Chee, T. Muthuswamy, R. Pandurangan, J. B. McCarthy, G.H. Lee, H. Park, Combating intracellular pathogens with nanolipid facilitated antibiotic delivery, Int. J. Nanomedicine 15 (2020) 9427–9448, https://doi.org/10.2147/IJN.S271888.
[125] D.F. Lee, P.A. Wahlvogel, Osteomyelitis, Lancet 364 (2004) 369–379, https://doi.org/10.1016/S0140-6736(04)16727-5.
[126] N. Abed, F. Couvreur, Nanozymes for antibiotics: A promising solution to treat intracellular bacterial infections, Int. J. Antimicrob. Agents 43 (2014) 405–414, https://doi.org/10.1016/j.ijantimicag.2014.02.009.
[127] A. Ali, Z. Ahmed, A review on chitosan and its nanocomposites as drug delivery, Int. J. Biol. Macromol. 109 (2018) 273–286, https://doi.org/10.1016/j.ijbiomac.2017.12.078.
[128] K. Thakur, G. Sharma, B. Singh, S. Chhibber, A.K. Patil, O.P. Katare, Chitosan-tailored lipidic nanocarriers of fusidic acid as promising vehicle for wound infections: an explorative study, Int. J. Biol. Macromol. 115 (2018) 1015–1025, https://doi.org/10.1016/j.ijbiomac.2018.04.092.
[129] K. Thakur, G. Sharma, B. Singh, S. Chhibber, O.P. Katare, Nano-engineered lipid-polymer hybrid nanoparticles of fusidic acid: an investigative study on dermotoxicative profile and MRSA infected burn wound model, Drug Deliv. Transl. Res. 8 (2018) 748–760, https://doi.org/10.1007/s13346-018-00515-5.
[130] S. Deshkar, M. Jadav, C.-M. Jack Hu, W. Zhang, L. Zhang, S. Jia, Magnetic field activated lipid-polymer hybrid nanoparticles for stimuli-responsive drug release, Acta Biomater. 8 (2012) 3447–3452, https://doi.org/10.1016/j.actbio.2012.11.008.
[131] D. Hasan, C.A. Omole, U.O. Paliko, C. Nkolisa, T. Govender, Novel chitosan-based pH-responsive lipid polymer hybrid nanovesicles (OSA-LPHVs) for delivery of vancomycin against methicillin-resistant Staphylococcus aureus infections, Int. J. Biol. Macromol. 147 (2020) 885–895, https://doi.org/10.1016/j.ijbiomac.2020.01.019.
[132] J.C. Newbold, A.N. Patel, T. Govender, Liposomal delivery systems and their applications against Staphylococcus aureus and methicillin-resistant Staphylococcus aureus, Adv. Drug Deliv. Rev. 179 (2021). 113865, https://doi.org/10.1016/j.addr.2021.113865.
[133] R. Rahmati-Yamchi, S. Tohidi Moorani, M.L. Shoaeiyan, M. Di Sanni, M.E. Ruiz, A. Tajeri, V.A. Akopov, N. Barati, K.R. Gasiev, G.A. Silina, Hybrid silkworm/eggnog co-loaded solid lipid nanoparticles with enhanced and targetable antimicrobial properties, Int. J. Pharm. 589 (2020) 1–15, https://doi.org/10.1016/j.ijpharm.2020.119879.

[104] B. Barbosa, D. Costa, E. Custódio, G.R. Castro, I.F. Lyra, G.A. Islan, Design of salicylic acid/vancomycin complex loaded into chitosan hybrid nanoparticles as smart strategy to inhibit bacterial growth and quorum sensing, Int. J. Biol. Macromol. 181 (2020) 1266–1280, https://doi.org/10.1016/j.ijbiomac.2020.07.204.

[105] R. Shehata, S. Nasser, M. Pawula, Y. Lalloz, H. Paolini, Detoxifiers in drug delivery and targeting: drug-detoxifier interactions and toxicity issues, J. Pharm. Biomed. Sci. 6 (2016) 139–156, https://doi.org/10.4103/0975-7406.113965.

[106] A.S. Chauhan, Dendrimers for drug delivery, Molecules 23 (2018), https://doi.org/10.3390/molecules23040938.

[107] P. Eatharasan, A. Gothandi, A.K. Iyer, K. Jain, M.K. Chaurasia, U. Gupta, Dendrimer nanohybrid carrier systems: an expanding horizon for targeted drug and gene delivery, Drug Discov. Today 23 (2018) 830–844, https://doi.org/10.1016/j.drudis.2017.06.009.

[108] S.J. Soenen, R.N. Rajagopal, S. Rahikkanen, C. Markkar, S.B. Yepuri, M. Soliman, T. Gavrunkin, Ultra small lipid-dendrimer hybrid nanoparticles as a promising strategy for antibiotic d-penyc in vitro and in silico studies, Int. J. Pharm. 554 (2018) 1–12, https://doi.org/10.1016/j.ijpharm.2018.10.071.

[109] C.S. Omole, R.G. Kalhapure, N. Agrawal, M. Jadhav, S. Rambharose, C. Mocktar, T. Govender, A hybrid of mPEG-b-PCL and G1-FRA dendrimer for enhancing delivery of antibiotics, J. Control. Release 290 (2018) 113–128, https://doi.org/10.1016/j.jconrel.2018.10.008.

[110] R.V. Araújo, S.H.S. Santos, E. Igne Ferreira, J. Giarolla, New advances in general biomedical applications of PAMAM dendrimers, Molecules 23 (2018), https://doi.org/10.3390/molecules23112849.

[111] S.C.Y. Moorcroft, D.O. Jayne, S.D. Evans, O. Ey, Stimuli-responsive release of antimicrobials using hybrid inorganic nanoparticle-associated drug-delivery systems, Nanomed. Nanot. 18 (2018) 1–14, https://doi.org/10.1002/wnan.2018.e1992.

[112] S. Wang, P. Zheng, Y. Huang, T. Fang, M. Chen, M. Zhu, X. Shi, Encapsulation of amoxicillin within ligandin-doped poly(lactic-co-glycolic acid) nanofibers: preparation, characterization, and antibacterial activity, ACS Appl. Mater. Interfaces 4 (2012) 6360–6451, https://doi.org/10.1021/am3021406.

[113] P. Zheng, L. Wang, J. Wen, M. Chen, M. Zhu, X. Shi, Characterization and antibacterial activity of amoxicillin-loaded electrospun nano-hydroxyapatite/poly (lactic-co-glycolic acid) composite nanofibers, Nanomedicine 9 (2013) 1402–1413, https://doi.org/10.2217/nnm.13.112.

[114] R. Qi, R. Guo, P. Zheng, H. Liu, J. Yu, X. Shi, Controlled release and antibacterial activity of antibiotic-loaded electrospun halloysite/poly(lactic-co-glycolic acid) composite nanofibers, Colloids Surf. B. Biointerfaces 110 (2013) 140–146, https://doi.org/10.1016/j.colsurfb.2013.04.026.

[115] R.S. Vasile, D. Ogren, O. Voiers, A. Firat, E. Stefanescu, A. Tewksbury, A. Hoffan, Synthesis and characterization of a novel controlled release zinc oxide/gentamicin-chitosan composite with potential applications in wounds care, Int. J. Pharm. 463 (2014) 165–169, https://doi.org/10.1016/j.ijpharm.2013.11.035.

[116] S. Yang, X. Ren, Y. Yang, H. Qiao, S. Yu, Y. Liu, J. Wang, T. Tang, Bacteria-targeting nanoparticles with microenvironment-responsive antibiotic release to eliminate intracellular Staphylococcus aureus and associated infection, ACS Appl. Mater. Interfaces 10 (2018) 14299–14311, https://doi.org/10.1021/acsami.7b19057.

[117] U. Sharipova, N. Laha, E. Jagneya, M. Murugan, M.A. Mansoorar, M. Rizwa, Stimulus-responsive zinc oxide-functionalized macromolecular hemin and nanocarrier for enhancement of antibacterial activity of ciprofloxacin hydrochloride, Int. J. Biol. Macromol. 114 (2018) 1109–1118, https://doi.org/10.1016/j.ijbiomac.2018.03.120.

[118] H. Al-Obaidi, R. Kalgudi, M.G. Zaitoun, Fabrication of inhaled hybrid silver-ciprofloxacin nanoparticles with synergistic effect against Pseudomonas aeruginosa, Eur. J. Pharm. Biopharm. 128 (2018) 37–50, https://doi.org/10.1016/j.ejpb.2018.04.026.

[119] E.E. Kashaba, W.Z. Lin, C.H. Lee, Combating antibiotic resistance through the synergistic effects of nanoporous silica based interfacial nanocomposites, Nanomaterials (Basel) 10 (2020) 1–15, https://doi.org/10.3390/nano10050957.

[120] H. Salis, M. Vasilieva, E. Kovaeva, V. Barykina-Vlakh, K. Demyanova, A. Lisovskaya, Y. Skorik, E. Barykina-Vlakh, Hybrid nanoparticles and composite hydrogel systems for delivery of peptide antibiotics, Int. J. Mol. Sci. 23 (2022), https://doi.org/10.3390/ijms23084277.

[121] Y.L. Xiang, S.H. Huang, Q.H. Hu, Q.Y. Wang, M.Q. Zhao, Y.C. Jiang, X. Chen, J. Liu, Q.H. Zhou, Zwitterionic nano-silica/polypeptide hybrid nanoparticles for efficient azithromycin delivery and photodynamic therapy for synergistic treatment of drug-resistant bacterial infection, Int. J. Biol. Macromol. 219 (2022) 397–410, https://doi.org/10.1016/j.ijbiomac.2022.08.202.

[122] C. Wang, Q. Cai, X. Wang, L. Li, Preparation of hybrid gold/polymer nanocomposites and their application in a controlled antibacterial assay, ACS Appl. Mater. Interfaces 5 (2013) 20181–20188, https://doi.org/10.1021/am4041407.

[123] I.M. El-Sherbiny, A. El-Gharbay, K. Salih, Photo-induced green synthesis and antimicrobial efficacy of poly (vancomycin-caprolactone)/curcumin/grape leaf extract-silver hybrid nanoparticles, J. Photochem. Photobiol. B 160 (2016) 255–263, https://doi.org/10.1016/j.jphotobiol.2016.04.024.

[124] T. Rashwal, K. Rizwan, M. Bilal, H.M.N. Iqbal, Metal-organic framework-based engineered materials-fundamentals and applications, Molecules 25 (2020) 1–28, https://doi.org/10.3390/molecules25071595.

[125] J. Zhuang, C.H. Kuo, L.Y. Chou, D.Y. Liu, E. Weerapana, C.K. Tsung, Optimized metal-organic-framework nanospheres for drug delivery: evaluation of small-molecule encapsulation, ACS Nano 8 (2014) 2812–2819, https://doi.org/10.1021/nn406085g.

[126] N.A. Swamy, Q. Wu, S.A. Awan, N. Liang, A.U. Rahman, Q. Yuan, Y. Wei, Natural drug physician encapsulated zeolitic imidazolate framework, and their application as antimicrobial agent, Colloids Surf. B. Biointerfaces 182 (2019) 1–7, https://doi.org/10.1016/j.colsurfb.2019.110384.

[127] S. Zhang, L. Liu, L. Huang, W. Zhang, R. Wang, T. Tse, J. Sun, G. Li, J. Wang, The highly efficient elimination of intracellular bacteria via a metal organic framework (MOF)-based theranostic drug delivery system, Nanoscale 11 (2019) 9469–9477, https://doi.org/10.1039/c9nr01736b.

[128] A. Kandemirli, B. Tuğcan, Z. Karpuzov, M. Bildik, Metal-organic frameworks for on-demand pH controlled delivery of nanoscopic from chitosan scaffolds, Mater. Sci. Eng. C Mater. Biol. Appl. 105 (2019) 1–11, https://doi.org/10.1016/j.msec.2019.110062.

[129] M. Esfahanian, M.A. Ghasemzadeh, S.M.H. Razavian, Synthesis, identification and application of the novel metal-organic framework Pr3O4(FAA)8(2IP)2 for the drug delivery of ciprofloxacin and investigation of antibacterial activity, Artif. Cells. Nanomed. Biotechnol. 47 (2019) 3824–3836, https://doi.org/10.1080/21691401.2019.1647726.

[130] Y. Yang, X. Wu, C. He, J. Huang, Z. Yin, H. Zhou, L. Xia, W. Zhou, L. Qiu, C. Cheng, C. Zhou, Metal-organic framework/sp based hybrid nanogenes for rapid and synergistic bacterial eradication, ACS Appl. Mater. Interfaces 13 (2020) 12648–12708, https://doi.org/10.1021/acsami.0c21660.

[131] Y. Xiao, M. Xu, N. Lv, C. Cheng, F. Wang, J. Li, Y. Hu, M. Gan, Dual stimuli-responsive metal-organic framework-based nanosystem for synergistic photothermal/pharmacological antibacterial therapy, Acta Biomater. 123 (2021) 291–305, https://doi.org/10.1016/j.actbio.2020.12.045.

[132] M. Giménez-Marqués, T. Hidalgo, C. Serre, P. Horcajada, Nanostructured metal-organic frameworks and their bio-related applications, Coord. Chem. Rev. 307 (2016) 342–360, https://doi.org/10.1016/j.ccr.2015.08.001.

[133] S. Liu, F. Liu, L. Tan, Z. Cui, X. Yang, K.W.K. Yeung, H. Pan, S. Wu, Porous bone-molecular metal-organic frameworks: A novel biplatform with sustained antibacterial efficacy and osseointegration, ACS Appl. Mater. Interfaces 9 (2017) 18148–18157, https://doi.org/10.1021/acsami.7b04816.

[134] S. Tamames, R. Imbelcaperta, F. Jalhe, P. Horcajada, M.J. Blanco-Prieto, Biocompatible porous metal-organic framework nanoparticles based on Fe or Zr for protonizer sterilization, Eur. J. Pharm. Biopharm. 132 (2018) 11–18, https://doi.org/10.1016/j.ejpb.2018.08.014.

[135] M. Haseena, K. Shah, A. Rehman, A. Khan, C. Farid, A. Di Muzio, M.R. Ovche, Shah, characterization and antibacterial evaluation of biodegradable mannose conjugated Fe-BTC-ESO12 composites containing vancomycin against methicillin-resistant Staphylococcus aureus strain, Polymer (Basel) 14 (2022), https://doi.org/10.3390/polym14122712.

[136] D. Rivero, A. Santiago-Portilla, J. Albero, D. Navalon, M. Alvaro, H. Garcia, Long-term photostability in terephthalate metal-organic frameworks, Angew. Chem. Int. Ed. Eng. 58 (2019) 17649–17648, https://doi.org/10.1002/anie.201911406.

[137] N. Bhardwaj, S.K. Pandey, J. Mehta, S.K. Bhardwaj, K.H. Kim, A. Deep, Reactive cuno-metal-organic frameworks as antimicrobials against Gram-positive and Gram-negative bacteria, Toxicol. Res. (Camb) 7 (2018) 431–441, https://doi.org/10.1039/c8tx00067e.

[138] A. Arenas-Vivo, G. Amariei, S. Aguado, R. Rosal, P. Horcajada, An ag loaded photoactive nano metal organic framework as a promising biofilm treatment, Acta Biomater. 97 (2019) 496–506, https://doi.org/10.1016/j.actbio.2019.08.013.

[139] S. Cheng, C. Zhang, H. Liu, H. Chen, J. Chen, J. Chen, S. Chen, Z. Su, G. Zhang, L. Zhang, Biomimetic metal-organic framework composite-mediated cascade catalysis for synergistic bacteria killing, ACS Appl. Mater. Interfaces 12 (2020) 36960–37000, https://doi.org/10.1021/acsami.0c12156.

[140] V. André, A.R.P. da Silva, A. Fernandes, B. Prado, C. Garcia, P. Rijo, A.M. M. Antunes, J. Rocha, M.T. Duarte, Mg- and Mn-MOFs boost the antibiotic activity of nalidixic acid, ACS Appl. Bio. Mater. 2 (2019) 2247–2254, https://doi.org/10.1021/acsabm.9b00048.

[141] F. Wu, C. Chen, S. Zhu, M. Tan, J. Zhou, X. Zhu, L. Wang, Q. Liu, T. Du, Ruralfloxacin/fluvastatin loaded cyclodextrin metal-organic framework for drug delivery and controlled release, Drug Deliv. 28 (2021) 873–879, https://doi.org/10.1080/10717544.2021.1870918.

[142] L.L. Li, J.H. Yu, G.R. Qi, X. Zhao, F. Yu, H. Wang, Core-shell supramolecular gelatin nanoparticles for adaptive and "on-demand" antibiotic delivery, ACS Nano 8 (2014) 4975–4983, https://doi.org/10.1021/nn501040n.

[143] A. Lin, Y. Liu, X. Zhu, X. Chen, J. Liu, Y. Zhou, K. Qin, J. Liu, Bacteria-responsive biomimetic antimicrobial nanosystem for multidrug-resistant bacterial infection detection and inhibition, ACS Nano 13 (2019) 13805–13814, https://doi.org/10.1021/acsnano.9b07356.

[144] Z. Kamal, J. Ju, W. Yuan, F. Rana, L. Jiang, Y. Li, M. Qiu, Red blood cell membrane-camouflaged nanozymic acid chitosanic acid-loaded gelatin nanoparticles against multi-drug resistance infection mice model, J. Drug Delivery Sci. Technol. (2021), 102706, https://doi.org/10.1016/j.jddst.2021.102706.

[145] Y. Zhang, J. Zhang, W. Chen, P. Angsantikul, R.A. Spiekermann, R.H. Fang, W. Gao, L. Zhang, Erythrocyte membrane-coated nanogel for combinatorial antimicrobial and responsive antimicrobial delivery against Staphylococcus aureus infection, J. Control. Release 302 (2017) 105–101, https://doi.org/10.1016/j.jconrel.2019.01.018.

[146] S. Wu, Y. Li, F. Rana, X. Wang, L. Zhang, R. Rang, M. Qiu, J. Ju, Red blood cell membrane-camouflaged tellurium phosphate loaded Pt-Ni4 nanoparticles for bacterial infection therapy, Pharmaceutics 13 (2021) 1–17, https://doi.org/10.3390/pharmaceutics13010095.

[147] N. Osman, N. Devnarain, G.A. Omolo, V. Fasiku, T. Jaglal, T. Govender, Surface modification of nano-drug delivery systems for enhancing antibiotic delivery and activity, Wiley Interdiscip. Rev. Nanomed. Nanobiotechnol. (2021), e1758, https://doi.org/10.1002/wnan.1720.

[148] P. Angsantikul, S. Thamphiwatana, Q. Zhang, K. Spiekermann, J. Zhuang, R. H. Fang, W. Gao, M. Obonyo, L. Zhang, Coating nanoparticles with gastric epithelial cell membrane for targeted antibiotic delivery against Helicobacter pylori infection, Adv. Ther. (Weinh). 1 (2018), https://doi.org/10.1002/adtp.201800016.

[149] F. Gao, L. Xu, B. Yang, F. Fan, L. Yang, Kill the real with the fake: eliminate intracellular Staphylococcus aureus using nanoparticle coated with its extracellular vesicle membrane as active-targeting drug carrier, ACS Infect. Dis. 5 (2019) 219–227, https://doi.org/10.1021/acsinfecdis.8b00315.

[150] K. Wang, Y. Lei, D. Xia, P. Xu, T. Zhu, Z. Jiang, Y. Ma, Neutrophil membrane coated, antibiotic agent loaded nanoparticles targeting to the lung inflammation, Colloids Surf. B. Biointerfaces 180 (2019), 110355, https://doi.org/10.1016/j.colsurfb.2019.110355.

[151] Z. Cao, F. Luo, Z. Li, L. Tan, S. Liu, C. Li, Y. Zheng, C. Cai, E.W.K. Yeung, Y. Liang, S. Zhu, S. Wu, Antibacterial hybrid hydrogels, Macromol. Biosci. 21 (2021) 1–34, https://doi.org/10.1002/mabi.202000322.

[152] S. Sattari, A. Dadkhah Tehrani, M., Adeli, pH-responsive hybrid hydrogels as antibacterial and drug delivery systems, Polymers (Basel). 10 (2018) 1–15, https://doi.org/10.3390/polym10060666.

[153] B. Tao, C. Lin, Y. Deng, Z. Yuan, X. Shen, M. Chen, Y. He, Z. Peng, Y. Hu, K. Cai, Copper nanoparticle-embedded hydrogel for killing bacteria and promoting wound healing with photothermal therapy, J. Mater. Chem. B 7 (2019) 2534–2545, https://doi.org/10.1039/c8tb03213f.

[154] J. Lu, T. He, P. Liu, J. Peng, C. Huang, Y. Sun, H. Deng, Hybrid hydrogels for synergistic periodontal antibacterial treatment with sustained drug release and NIR-responsive photothermal effect, Int. J. Nanomedicine 15 (2020) 5377–5387, https://doi.org/10.2147/IJN.S249538.

[155] U. Posadowska, M. Brzeziński-Wlazło, A. Domski, M. Kroll-Rotkowicz, M. Wiadarczyk-Bieguś, P. Dobrzyński, W. Chrzanowski, K. Pamuła, Injectable hybrid delivery system composed of gellan gum, nanoparticles and gentamicin for the localized treatment of bone infections, Expert. Opin. Drug. Deliv. 13 (2016) 619–630, https://doi.org/10.1517/17425247.2016.1146873.

[156] N. Chopra, S. Kumar, S. Singh, Bioadhesive hydrogels and their applications, in: Bioadhesives in Drug Delivery, 2020, pp. 147–176.

[157] Y. Zhang, J. Zhang, M. Chen, H. Gong, S. Thamphiwatana, L. Eckmann, W. Gao, L. Zhang, A bioadhesive nanoparticle-hydrogel hybrid system for localized antimicrobial drug delivery, ACS Appl. Mater. Interfaces 8 (2016) 10367–10374, https://doi.org/10.1021/acsami.6b00439.

[158] C. Tao, J. Wang, B. Sun, Biopolymer-liposome hybrid systems for controlled delivery of bioactive compounds: recent advances, Biotechnol. Adv. 40 (2021) 1–22, https://doi.org/10.1016/j.biotechadv.2021.107727.

[159] W. Gao, D. Vasilyev, J. Li, J. Zhu, Q. Zhang, Y. Fu, J. Li, S. Thamphiwatana, D. Lu, L. Zhang, Hydrogel containing nanoparticle-stabilized liposomes for topical antimicrobial delivery, ACS Nano 8 (2014) 2900–2907, https://doi.org/10.1021/nn500611k.

[160] S. Salatin, M. Jelvehgari, Emulsifier barrier approach for development of a thermoreversible and bioadhesive nanotransferosome-hydrogel hybrid system for enhanced skin bioavailability and antibacterial activity of cephadroxil, Drug Dev. Ind. Pharm. 46 (2020) 1310–1322, https://doi.org/10.1080/03639045.2020.1784588.

[161] M. Tung Le, N.S. Cang, T. Hoa Le, N.T. Lan, V.N. Phan, N.Q. Hoa, K. Vinh Le, N. V. Thinh, T. Tai Le, D.T. Ngo, E. Mullaney, T.Q. Huy, A.T. Le, Synthesis, characterizations of superparamagnetic Fe3O4-4g hybrid nanoparticles and their application for highly effective bacteria inactivation, J. Nanosci. Nanotechnol. 19 (2019) 3903–3913, https://doi.org/10.1166/jnn.2019.16329.

[162] C. Zhang, C. Du, J.Y. Lim, Y. Gu, Y. Hong, J. Pei, M. Gu, D. Yin, L. Gao, Y. Fan, Synthesis of magnetic hybrid nanocomplexes to eliminate bacteria and enhance biofilm disruption, Biomater. Sci. 7 (2019) 2033–2040, https://doi.org/10.1039/c8bm01557g.

[163] W. Zhang, B. Tabarzadeh, Z. Raymaleh, K. Zolfaghari, M.E. Abghari, A. Malekic, M.R. Hamblin, Y. Tian, Enhanced activity of vancomycin by encapsulation in hybrid magnetic nanoparticles conjugated to a cell-penetrating peptide, Nanoscale 12 (2020) 3659–3670, https://doi.org/10.1039/c9nr09037f.

[164] F. Wan, S.S. Bohr, S.N. Khodnitcha, M. Jensen, S. Huang, T. Hylander, M. B. Thygesen, S.B. Sørensen, E.J. Jensen, C. Stensberg, H. Hatunic, H., Marsh Hallen, Ultrasmall TPGS-PLGA hybrid nanoparticles for site-specific delivery of antibiotics into Pseudomonas aeruginosa biofilms in lungs, ACS Appl. Mater. Interfaces 12 (2020) 389–398, https://doi.org/10.1021/acsami.9b16444.

Appendix IV

Co-authored paper (review article 2)

Received: 11 November 2021 | Revised: 21 March 2022 | Accepted: 24 March 2022

DOI: 10.1002/wnan.1799

ADVANCED REVIEW

WILEY

Exploring the applications of hyaluronic acid-based nanoparticles for diagnosis and treatment of bacterial infections

Mahir Mohammed[1,2] | **Nikita Devnarain**[1] | **Eman Elhassan**[1] | **Thirumala Govender**[1]

[1]Discipline of Pharmaceutical Sciences, College of Health Sciences, University of KwaZulu-Natal, Durban, South Africa

[2]Faculty of Pharmacy, University of Khartoum, Khartoum, Sudan

Correspondence
Thirumala Govender, Discipline of Pharmaceutical Sciences, College of Health Sciences, University of KwaZulu-Natal, Private Bag, Durban X54001, Durban 4000, South Africa.
Email: govenderth@ukzn.ac.za

Funding information
National Research Foundation, Grant/Award Numbers: 103664, 106040, 129326, 116652; Medical Research Council (MRC) of South Africa

Edited by: Chun Li, Associate Editor and Nils G. Walter, Co Editor-in-Chief

Abstract

Hyaluronic acid (HA) has become a topic of significant interest in drug delivery research due to its excellent properties, including biosafety, biodegradability, and nonimmunogenicity. Moreover, due to its ease of modification, HA can be used to prepare several HA-based nanosystems using various approaches. These approaches involve conjugating/grafting of hydrophobic moieties, polyelectrolytes complexation with cationic polymers, or surface modification of various nanoparticles using HA. These nanoparticles are able to selectively deliver antibacterial drugs or diagnostic molecules into the site of infections. In addition, HA can bind with overexpressed cluster of differentiation 44 (CD44) receptors in macrophages and also can be degraded by a family of enzymes called hyaluronidase (HAase) to release drugs or molecules by binding with these receptors or being degraded at the infection site by HAase. HA-based nanoparticles allow enhanced and targeted antibacterial delivery. Herein, we present a comprehensive and up-to-date review that highlights various techniques of preparation of HA-based nanoparticles that have been reported in the literature. Furthermore, we also discuss and critically analyze numerous types of HA-based nanoparticles that have been employed in antibacterial delivery to date. This article offers a critical overview of the potential of HA-based nanoparticles to overcome the challenges of conventional antibiotics in the treatment of bacterial infections. Moreover, this review identifies further avenues of research for developing multifunctional and biomimetic HA-based nanoparticles for the treatment, prevention, and/or detection of pathogenic bacteria.

This article is categorized under:

Therapeutic Approaches and Drug Discovery > Nanomedicine for Infectious Disease

Nanotechnology Approaches to Biology > Nanoscale Systems in Biology

Therapeutic Approaches and Drug Discovery > Emerging Technologies

This is an open access article under the terms of the Creative Commons Attribution License, which permits use, distribution and reproduction in any medium, provided the original work is properly cited.
© 2022 The Authors. *WIREs Nanomedicine and Nanobiotechnology* published by Wiley Periodicals LLC.

KEYWORDS
bacterial infection, drug conjugate, hyaluronic acid, surface modification, targeted nano-drug delivery

1 | INTRODUCTION

The treatment of infectious diseases continues to be a significant priority for healthcare workers globally, as they are both a leading cause of death and have a negative impact on quality of life (Bloom & Cadarette, 2019; McArthur, 2019). Among these infectious illnesses, bacterial infections have emerged as a severe threat due to their high risk of causing premature death (Guo et al., 2020; Gupta et al., 2019; McArthur, 2019). Bacterial infections can range from mild (cutaneous) to life-threatening illnesses, including sepsis, pneumonia, tuberculosis (TB), and others (Xiong et al., 2014). Sepsis, which is associated with bacterial infections, has significantly emerged as a bigger killer than cancer and diabetes, especially in African countries (World Health Organization, 2020b). Furthermore, the COVID-19 research highlights that bacterial infections and its complications are more common in lethal cases than in recovered cases (Farrell et al., 2021; Shafran et al., 2021). Thus, it is essential to find effective therapy for such patients, in order to suppress bacterial infection-related death.

Following the advent of antibiotics in 1928, it was expected that bacterial infections would be effortlessly managed (Venuga & Gnoth, 2016); however, practitioners have been challenged with newly emerging infectious diseases since the 1950s, posing significant health and economic concerns (McArthur, 2019). Despite their early success since their market release in 1945, conventional dosage forms of antibiotics have had many well-documented limitations that are unrelated to antibiotic ineffectiveness and is widely acknowledged as a major contributing factor to the emergence of antimicrobial resistance (AMR). These limitations include a lack of selective targeting of the pathological site of action, poor pharmacokinetic profiles, premature drug release, insufficient tissue penetration, and rapid clearance from the blood circulation (Canaparo et al., 2019; N. Y. Lee et al., 2019). Furthermore, larger and frequent doses of antibiotics are necessary to eliminate bacterial infections, resulting in poor patient compliance and increased toxicity (A. Sharma et al., 2012). Together with widespread antibiotic misuse, these limitations have been highlighted as significant contributors to the development and spread of AMR, leading to shortening the interval between introducing antibiotics and the development of resistance (Singer et al., 2020). Multidrug-resistant bacterial strains have rapidly exploded and become a critical worldwide problem, threatening the ability to cure infections such as TB (Singh et al., 2020), sepsis (Pant et al., 2021), and methicillin-resistant *Staphylococcus aureus* (MRSA) infections (Nguyen & Graber, 2009), resulting in extended suffering and premature mortality. According to WHO, AMR is among the most serious international health challenges threatening humanity. Moreover, they estimated that 700,000 people would die each year globally, with the number rising to 10 million by 2050 if no fruitful efforts are made to address AMR (WHO, 2020a). For these collective reasons, discovering innovative methods that reduce toxicity to normal cells, enhance antibacterial efficacy, and slow down the progression of bacterial resistance is becoming increasingly popular in research.

Nanomedicine, which refers to the use of nanoscale materials to diagnose and treat diseases, offers a solution to address this urgent crisis (Soares et al., 2018). Nanomedicine has transformed medical technology to an advanced level, where many diseases such as cancer, AIDS, inflammation, hypertension, and bacterial infections may be treated with minor adverse effects compared to conventional dosage forms of medicines (Misra et al., 2010; Yetisgin et al., 2020). Nano-sized drug delivery systems of antibiotics have proven to be a promising tool for overcoming the current challenges associated with current antibiotic therapy (Kalhapure et al., 2015; Muzammil et al., 2018). This could be due to several advantages of nanoantibiotics over conventional dosage forms, which include (i) selective targeting to site of infections; (ii) improved drug solubility, bioavailability, and tissue distribution; (iii) broadening the therapeutic index of drugs; (iv) sustained drug release, and (v) enhanced cellular uptake. Furthermore, nanoantibiotics enhance both pharmacokinetic and pharmacodynamic profiles of the encapsulated drug, which significantly reduces the required dose to eradicate bacterial infections (Devnarain et al., 2021; Ibrahim et al., 2021). Interestingly, in addition to improving antibacterial activity, nanoantibiotics have a substantial influence on addressing various resistance mechanisms, such as drug degradation by β-lactamases, efflux pumps, biofilm development, and bacterial cell wall thickening (N. Y. Lee et al., 2019). However, compared to other medical diseases such as cardiovascular disease and cancer, the use of nanomedicine for the treatment of bacterial infections is still in its infancy (Misra et al., 2010; Wang et al., 2021).

To date, several types of nanodrug delivery systems, including liposomes, polymersomes, micelles, solid lipid nanoparticles (SLNs), and others, using various types of organic and inorganic materials such as polymers, lipids, or hybrid systems, have been reported in the literature for their enhanced antibacterial potential (Kalhapure et al., 2015; Muzammil et al., 2018; A. Sharma et al., 2012). Owing to their biocompatibility, ease of surface and chemical modifications, high drug loading capacity, and microenvironment responsiveness, polymer-based NPs have gained significant attention in antibacterial applications (Arora et al., 2016; Rao et al., 2020). An interesting natural polymer that has generated increasing interest as a component of antibacterial nanodrug delivery systems over the last two decades is hyaluronic acid (HA; Arshad, Tabish, Naseem, et al., 2021; Gamarra et al., 2018; P. D. Kłodzińska, Rahanjam, et al., 2019; Öztekin-raman et al., 2021). Hyaluronic acid is a linear, naturally occurring mucopolysaccharide composed of alternating N-acetyl glucosamine and D-glucuronic acid units, which is synthesized in the plasma membrane by hyaluronan synthases (Hynes & Walton, 2000). It is also a versatile material for nanodrug delivery systems as it exists in a wide range of molecular weights starting from 6.1 kDa up to 107 kDa (Kolar et al., 2015). Additionally, it plays a crucial role in the configuration and organization of extracellular matrix, wound healing, cell adhesion control, the elasticity of connective tissue, and inflammatory modulation. Very importantly, HA is considered harmless and is rapidly degraded by hyaluronidase enzymes (HAase), making it an ideal polymer for targeted drug delivery systems (Hun et al., 2015). Furthermore, the favorable characteristics of HA, such as biodegradability, nonimmunogenicity, water-retaining activity, and selectivity toward specific receptors, have contributed to its popular use in drug delivery systems (Montanari et al., 2016). The cluster of differentiation, or CD proteins, is a group of glycoproteins that are abundant throughout the body and are considered the primary HA receptors (Dosio et al., 2016). Normally, these receptors (like CD44) are responsible for various cellular actions, including inflammation and cellular adhesion responses. In contrast, it was found to be overexpressed on several cancer cells; this phenomenon captivated the interest of researchers working on anticancer medicine. Consequently, several cancers, including ovarian, colon, breast, and squamous cancer have been extensively studied using HA nanoparticles (HA-NPs; J. H. Kim et al., 2018; Misra et al., 2010).

Nanodrug delivery systems that consist of HA as a component have also exhibited activity against bacteria due to their intrinsic antibiofilm and bacteriostatic activity against certain bacteria (Drago et al., 2014; Pirnazar et al., 1999). Recently, CD44 receptors have been revealed to be overexpressed on human macrophages and could therefore be selectively targeted by HA-NPs to eliminate intracellular bacterial infections (Montanari et al., 2016). Moreover, wound healing and tissue regeneration properties of HA may aid in the treatment of cutaneous infections and enable rapid recovery (Zhu et al., 2018). These exceptional abilities of HA have led to the growing interest in the formulation and development of HA-NPs to target bacterial infections.

There have been reviews that cover in-depth the use of HA-based nanomaterials in the treatment of cancer, inflammatory diseases, and nucleic acids delivery (Dosio et al., 2016; J. H. Kim et al., 2018; Rao et al., 2020; Sakurai & Harashima, 2019). To the best of our knowledge, this is the first review that highlights and discusses all reported nanosystems in the literature that incorporate HA using different approaches for enhanced delivery of antibiotics to prevent, detect, and/or eradicate bacterial infections. Herein, we present an in-depth and up-to-date review that highlights different techniques of preparation of HA-NPs that have been reported in the literature. Furthermore, after an extensive analytical search of several scientific databases, we discuss and critically analyze numerous types of HA-NPs that have been employed in antibacterial delivery to date. We have systematically categorized these HA-NPs according to their approach for application: (i) HA-based NPs; (ii) HA-capped NPs; (iii) Drug-Conjugated HA-NPs. The benefits and limitations of these nanomaterials in the treatment of bacterial infections are thoroughly discussed and assessed. Finally, this review highlights the gaps, challenges, and future perspectives of HA-NPs for antibacterial drug delivery.

2 | HYALURONIC ACID AND ITS APPLICATIONS

Hyaluronic acid, conjointly termed hyaluronan, is a linear natural, polyanionic, and FDA-approved biocompatible polymer (Figure 1), synthesized in mammals by three hyaluronan synthases (HAS1, HAS2, and HAS3; Lapčík et al., 1998). These enzymes elongate the HA backbone by repeatedly adding glucuronic acid and N-acetyl-D-glucosamine groups to the growing sugar, resulting in the formation of HA with a range of molecular weights (2×10^5–2×10^6 Da) (Itano & Kimata, 2002). The estimated quantity of HA in the human body is 15 g, of which one-third is replenished daily, with an average half-life varying from 2.3 to 5.5 min. Approximately 7–8 g of this HA is found in the skin; moreover, HA is also located in connective tissue, vitreous humor, synovial fluids, and others (Necas et al., 2008). Hydrolysis of HA is

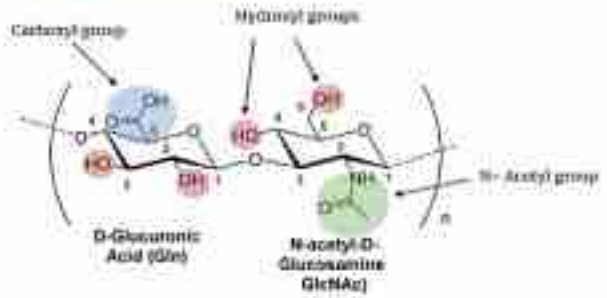

FIGURE 1 The structure of HA as well as potential locations for chemical modification of the polymer

predominantly by the HAase family, which may be categorized based on the producing organism into (i) mammalian HAases, which cleave the β1–4 glycosidic linkage; (ii) leech HAases, which target the β1–3 glycosidic bond; and (iii) bacterial HAase (B-HAase), also known as hyaluronan lyase, which targets β1–4 bond like mammalian enzyme; however, the end product here is unsaturated disaccharides (Hynes & Walton, 2000). For biomedical applications, HA has been historically obtained by isolation from rooster combs; however, due to the overuse of animal rooster combs in the production of biomaterials, microbial fermentation, particularly from Streptococci species, has arisen as a new source of HA (L. Liu et al., 2011). Hyaluronic acid has attracted increased interest in the development of various drug delivery systems; however, owing to its short blood circulation time and poor enzymatic stability, several HA conjugates are prepared to overcome these limitations without affecting the value inherent characteristics of HA (Tiwari & Bahadur, 2019).

The backbone of HA consists of several carboxyl, hydroxyl, and N-acetyl groups (Figure 1), which can be easily modified, resulting in a variety of HA derivatives. The primary approaches for modifying HA include the creation of ester and amide bonds at the carboxyl groups of the polymer in the presence of condensing agents, as well as the formation of ester and ether bonds at the hydroxyl groups of the polymer (Schanté et al., 2011). The resultant conjugates can be used to construct HA-based delivery systems with enhanced physicochemical characteristics, including increased enzymatic stability, altered viscoelastic behavior, or controlled release (Khunmanee et al., 2017). Additionally, they are suitable for drug delivery applications by exploiting the inherent targeting characteristics of HA, minimizing immune recognition, or prolonging drug circulation (Prajapati & Maheriya, 2019).

Hyaluronic acid and its conjugates have been used to formulate several types of nanocarriers, which can be prepared using three main strategies (J. H. Kim et al., 2018; Sakurai & Harashima, 2019), as shown in Figure 2. The first strategy involves conjugating/crosslinking hydrophobic moieties (including drugs) to the HA backbone, which results in the formation of amphiphilic derivatives that can be employed to formulate various types of NPs, including nanogels (Silva et al., 2016), polymersomes (Walvekar et al., 2019), micelles (Gao et al., 2014), and others (J. H. Kim et al., 2018). Owing to the anionic nature of HA, the second strategy is via ionotropic gelation with cationic polymers; this method accounts for approximately 30% of formulated HA-based NPs (Sakurai & Harashima, 2019). Finally, the third strategy involves surface modification of various nano-delivery systems, which is achieved by depositing an auxiliary layer(s) on the surface of the nanocarriers, which alters the properties of the nanocarrier with or without the formation of covalent bonds (K. Kim et al., 2019). The produced HA-based NPs exhibit several desirable features, including non-immunogenicity, biosafety, and anti-inflammatory activity (Choi et al., 2012). HA-based NPs have been thoroughly investigated in the field of drug delivery to enhance the biocompatibility of the material and facilitate drug delivery via passive and active targeting. Recently, the number of published articles on "hyaluronic acid" and "nanoparticles" have grown remarkably (Figure 3) (Sakurai & Harashima, 2019); interestingly, the number of published articles has reached 2019 and 3095 in PubMed and Scopus, respectively, as of the date of this review. However, compared to anticancer delivery, the application of HA in the nano delivery of antibiotics is still in its infancy.

The application of HA to develop nanomaterials for antibacterial delivery may demonstrate enhanced and synergistic activity owing to its intrinsic bacteriostatic and antibiofilm properties against certain bacterial strains (Drago et al., 2014; Pirnazar et al., 1999). Hyaluronic acid is also known to have wound healing, tissue regeneration, and anti-inflammatory characteristics, which may aid in treating cutaneous infections and promoting rapid recovery (Zhu et al., 2018). Furthermore, numerous human macrophages have been shown to overexpress CD44 receptors, suggesting that HA-NPs might be used to target and destroy intracellular bacterial infections selectively (Almalik et al., 2013).

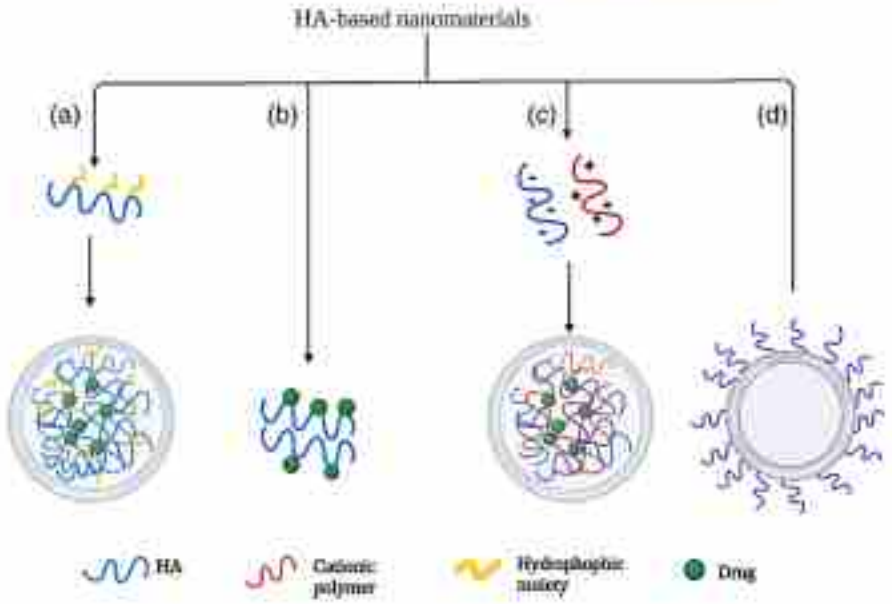

FIGURE 2 Nano-delivery systems based on HA. Both (a) and (b) illustrate conjugation of HA with a hydrophobic moiety or drug, which self-assemble into NPs, (c) ionic gelation of HA with cationic polymer, and (d) HA-coated NP

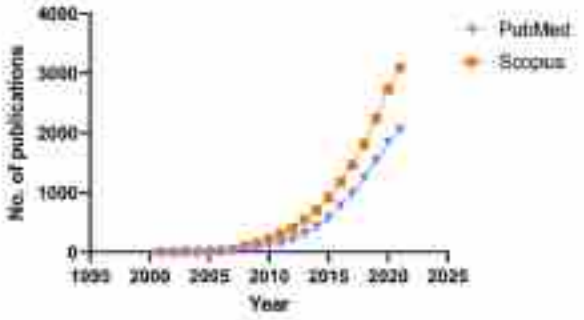

FIGURE 3 The total number of publications on HA-based NPs. When the terms "hyaluronic acid" and "nanoparticles" were entered in PubMed (https://www.ncbi.nlm.nih.gov/pubmed/) and Scopus (https://www.scopus.com/search), the number of publications that appeared year after year was graphed

It has been reported that polycarboxylic acids like HA are found to reduce the pH of infection sites, thereby generating an environment where bacteria find it hard to survive (Walvekar et al., 2019). Additionally, the concept of developing HAase-responsive antibiotic-loaded NPs has been employed to enable on-demand release of the encapsulated antibiotics, resulting in safe and effective antibiotic delivery (Baier et al., 2013). All these benefits make HA-based nanomaterials an excellent candidate for eradicating both extracellular and intracellular bacteria.

The following sections review in detail HA-based nanomaterials that have been used for antibacterial drug delivery. Herein, we systematically classified these nanomaterials into three broad groups based on the rationale behind the use of HA: (i) HA-based nanocarriers that are conjugated, crosslinked, or ionically complexed with other molecules (fatty acids, polymers, etc.); (ii) HA-coated NPs, where HA is utilized to modify the surface of NPs; and (iii) HA-drug conjugate, which contains a variety of antibiotics covalently bonded to HA.

3 | HYALURONIC ACID-BASED NANOCARRIERS

Hyaluronic acid and its conjugates have been used to formulate various types of nanocarriers. These nanocarriers exhibited enhanced biological activity, including anticancer (Han et al., 2015), anti-inflammatory (Rao et al., 2020), and most importantly, antimicrobial activity (Ahire & Dicks, 2016). As it is an ideal biopolymer, HA has been widely used to develop HA-NPs as targeted antibacterial nano delivery systems (Ekdziñska et al., 2018; Montanari et al., 2018, 2020; Walvekar et al., 2019). Therefore, this section will highlight and critically analyze all previously reported HA-based nanocarriers used for antibacterial delivery to date.

3.1 | Nanogels

Nanogels (NGs) are spherical nanosized networks produced when polymers are chemically or physically crosslinked. They exhibit the distinct properties of both hydrogels and NPs. Nanogels can be prepared using a wide variety of polymers. At the top of the list is HA, owing to its simple conjugation methods, excellent mechanical properties, and biosafety (H. Zhang, Zhai, et al., 2016). The review on NGs shows that various HA-NGs have been formulated with as well as without drug loading to target specific objectives (P. D. Ekdziñska, Rahamjam, et al., 2019; Montanari et al., 2020).

Various antibiotics have been encapsulated into HA-based NGs (HA-NGs) to eliminate bacterial infections (S. N. Ekdziñska, Wan, et al., 2019; Yuda Liu et al., 2021; Montanari et al., 2014, 2018). In this regard, Montanari et al. reported two studies on HA-NGs encapsulated with levofloxacin (LVF) and gentamycin (GM). The HA-NGs in these studies were prepared using the nanoprecipitation technique of cholesterol-conjugated HA. In the first study, Montanari et al. (2014) formulated LVF-loaded self-assembled HA-NGs (LVF-NGs) targeting intracellular bacteria (Figure 4). Levofloxacin was loaded into the NGs with a drug loading efficiency of 5% and average size of 155 nm. The antibacterial studies assessed both extracellular and intracellular activity against *Staphylococcus aureus*, MRSA, and *Pseudomonas aeruginosa*. The extracellular in vitro results showed no improvement in the minimum inhibitory concentration (MIC) values of LVF-NGs compared with the free LVF. While the intracellular studies on the human ovarian cancer cell line (HeLa) showed that LVF-NGs significantly killed intracellular bacteria as compared to free LVF (which exhibited no activity). Interestingly, this study represents the first-ever report of antibiotic-loaded self-assembled NGs (Montanari et al., 2014). In their second study, they explored the use of HA-NGs to specifically target infected human keratinocytes. The NGs were preloaded with either GM or LVF. The mean diameters of GM-loaded HA-NGs (GM-NGs) and LVF-NGs were 250 and 350 nm, respectively, with a drug loading efficiency of 40% and 11.4%, respectively. Moreover, the antibacterial studies showed that both formulations had the same MIC and minimum bactericidal concentration (MBC) values as free antibiotics against extracellular *S. aureus*. However, intracellularly, NGs significantly enhanced the antibacterial activity of LVF, while GM and GM-NGs showed comparable activity. This was explained by the ability of HA-NGs to shift the intracellular fate of LVF from the cytosol to the lysosomes, therefore enhancing their activity. In contrast, GM, an antibiotic mainly accumulates in lysosomes, exhibits considerable intracellular activity even without loading into NGs (Montanari et al., 2018). Although the drug loading efficiency in the first study was lower than in the second, both studies demonstrated a substantial improvement in intracellular antibacterial activity

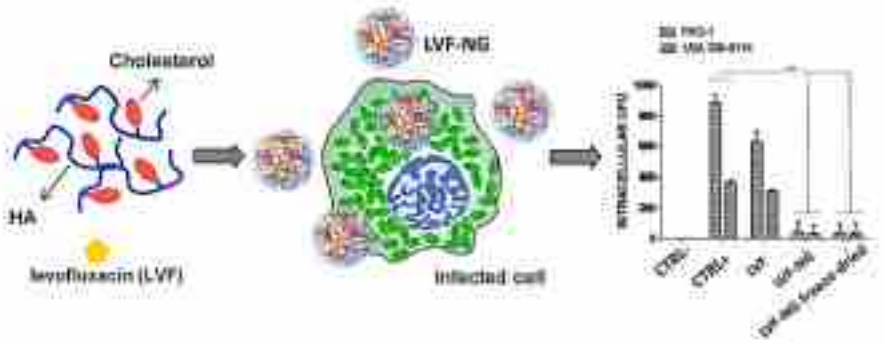

FIGURE 4 Schematic illustration of LVF-NGs for targeting intracellular infections (Montanari et al., 2014)

with no change in extracellular activity. Furthermore, unlike their former study, this study investigated biosafety and drug release studies, which are critical in nanoantibiotics characterization. Further in vivo studies are required in order to provide a step forward toward reaching the clinical stage. Another antibiotic azithromycin (AZ) was explored in a study by P. D. Khodzińska, Rahanjam, et al. (2019) where they evaluated and compared HA-NGs and coated poly(lactic-co-glycolic acid) NPs (T-PLGA NPs) in a head-to-head comparison to determine the relative benefits and drawbacks of each as promising delivery system (Figure 5). The microfluidic technique was used to prepare the HA-NGs, followed by AZ loading. Compared to T-PLGA NPs, AZ-loaded NGs were larger in size and had a higher EE %; nevertheless, both had a diameter of less than 200 nm. The in vitro cytotoxicity assay revealed that loaded HA-NGs are relatively nontoxic to HepG2 and lung epithelial cells (Calu-3), but T-PLGA NPs exhibit some toxicity. Although both delivery systems enhanced the antibacterial and anti-virulence activity of AZ, AZ-loaded NGs enhanced the penetration of AZ into biofilms and also eliminated preformed biofilms more effectively than T-PLGA NPs (S. N. Khodzińska, Wan, et al., 2019). Nevertheless, this study lacked in vitro drug release and in vivo antibacterial studies which may add further biological validation to such promising nanosystem. A recent study by Yuda Liu et al. (2021) further expanded the performance of HA-NGs in antibacterial delivery. They reported novel targeted "on-demand" delivery of composite nanosystems based on the triple controlled release of inclusion composites (IC), polymeric NPs, and HA-NGs. The ultimate objective of this investigation was to efficiently eliminate *S. aureus*. In this regard, enrofloxacin was incorporated into IC and then dispersed into poloxamer 188 coating NGs formulated by ionic complexation between chitosan (CS) and HA. Nanosystems with mean EE%, sizes, and PDI of 95.4%, 118.8 nm, and 0.26, respectively, were prepared. By incorporating IC into the HA-NGs, the nanosystem gained multifunctional characteristics by releasing enrofloxacin in a dual pH/HAase-responsive manner at the infection site, therefore reducing premature release of the drug. Furthermore, the composite nanosystems were able to be absorbed onto the surface of *S. aureus*, resulting in increased antibacterial activity (Liu et al., 2021). Unlike the above HA-NGs, this is the first stimuli-responsive HA-NGs encapsulated with an antibacterial drug. This study established that by cleverly integrating IC with HA-NGs stabilized with poloxamer 188, the developed composite nanosystems may reduce premature drug release and improve targeting to *S. aureus*. Therefore, this study may serve as a fruitful approach to tackle the treatment difficulties associated with *S. aureus* as well as other bacterial infections. In conclusion, the studies described in this paragraph could lay the ground for expanding the use of HA-NGs to enhance antibiotics delivery due to their ability to enhance intracellular antibacterial activity, alter the fate of several antibiotics, provide on-site antibiotic release, and, most importantly, eliminate side effects associated with loaded antibiotics.

Antimicrobial peptides are molecules that have been identified as among the most promising therapeutic candidates for the treatment of bacterial infections. However, these agents showed low stability and bioavailability as well as a high toxicity profile (Teixeira et al., 2020). Hyaluronic acid-based nanogels have been studied recently as a promising nanoplatform for the delivery of antimicrobial peptides and peptidomimetics (P. D. Khodzińska, Rahanjam, et al., 2019; S. N. Khodzińska et al., 2018; Silva et al., 2016). To this end, Silva et al. (2016) reported HA-NGs loaded with LLKKK18

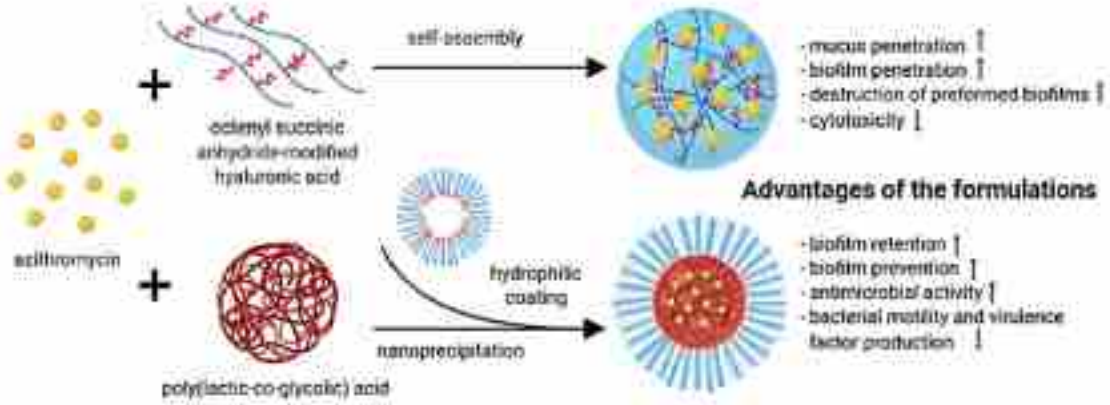

FIGURE 5 Head-to-head comparison of HA-NGs and coated poly (lactic-co-glycolic acid) NPs for AZ delivery (Khodzińska, Rahanjam, et al., 2019)

peptide to cure pulmonary mycobacterial infections (Figure 6). HA-NGs were prepared via cross-linking of HA with a thiolated alkyl chain and produced NGs with a large diameter (533 nm), small PDI (0.1), and high EE% (70%). The biocompatibility of the loaded NGs in bone marrow-derived macrophages (BMMΦ) was evaluated using two distinct assays. Both assays revealed that loaded NGs had no harmful impact on BMMΦ at concentrations up to 100 μM, which is more than 20-fold the toxic concentration of free peptide. Furthermore, activated macrophages overexpress the CD44 receptor, allowing infected macrophages to successfully uptake loaded HA-NGs, resulting in selective targeting of LLKKK18 to mycobacteria that reside in intracellular compartments. In vitro incubation of macrophages with LLKKK18-loaded NGs reduced *Mycobacterium avium* and *Mycobacterium tuberculosis* intracellular levels. Notably, in vivo studies with LLKKK18-loaded NGs demonstrated a substantial reduction in infection levels in mice infected with *M. avium* or *M. tuberculosis* (Silva et al., 2016). This study established a strong in vitro–in vivo correlation, thereby validating the potential of LLKKK18-loaded HA-NGs to eliminate mycobacteria efficiently. Moreover, HA-NGs enhanced stability and minimized cytotoxicity, while potentiating peptides targeting the main sites of infection. Continuing the research study into the delivery of antimicrobial peptides and peptidomimetics, Kłodzińska and his group developed HA-NGs by conjugating HA with octenyl succinic anhydride. In their first study, they explored the ability of the HA-NGs to enhance the antibacterial activity and biosafety of antimicrobial peptidomimetics (lysine-based α-peptide/β-peptoid). This was the first reported biopolymer NGs incorporating antimicrobial peptidomimetics. The NGs were prepared using the microfluidic chip technique. Design of Experiments (DoE) was used to assess the optimal parameters for preparation of the NGs; accordingly, 12 formulations were prepared (F1–F12). F10 was the most encouraging in this study with size, zeta potential (ZP), and EE% of 175 nm, −16 mV, and 88%, respectively. The HA-NGs encapsulating the peptidomimetic LBP-3 exhibited no hemolysis and reduced LBP-3 cytotoxicity in hepatocytes (HepG2 cells) when compared to free peptidomimetic, whereas the MIC and minimum biofilm inhibitory concentration (MBIC) values of LBP-3 against *P. aeruginosa* remained unchanged. Only F10 exhibited the potential to delay the regrowth of *P. aeruginosa* (Kłodzińska et al., 2018). Despite the significant enhancements, this study lacked investigations into morphology, the peptidomimetic release from the NGs, and in vivo studies, which would have further validated the ability of HA-NGs to effectively deliver LBP-3 and other peptidomimetics. Another peptide-loaded HA-NG was formulated by the same group, this time focusing mainly on improving peptide biosafety. Kłodzińska et al. (2019) evaluated the ability of HA-NGs to encapsulate the antibiofilm peptide DJK-5 with the overall goal of improving the in vivo biosafety of DJK-5s (Figure 7). For this purpose, NGs with sizes ranging from 174 to 194 nm encapsulating 33%–40% of DJK-5 were prepared. This EE% was relatively low compared to their prior LBP-loaded HA-NGs, where the EE% reached 80%. The in vitro release studies showed that 80% of the loaded peptide was released within 5 h. The in vivo biosafety of DJK-5 and DJK-loaded NGs was evaluated using a *P. aeruginosa* abscess model following both IV and subcutaneous administration. Encapsulation of DJK-5 in HA-NG reduced its toxicity by 2-fold following IV administration, and by 4-fold after subcutaneous injections, compared to the free peptide, without compromising the anti-abscess efficacy of DJK-5 (P. D. Kłodzińska, Rahanjam, et al., 2019). In comparison to their previous study, all essential physicochemical and biological characterization stages (in vitro and in vivo) were carried out perfectly in this study, hence supporting the use of HA-NGs to improve the safety of antibacterial and anti-biofilm peptides. Taken together, the findings of these studies support the application of HA-NGs to enhance antimicrobial peptides and peptidomimetics delivery owing to their ability to improve antibiofilm activity, antibiotic localization on-site, and to eliminate the

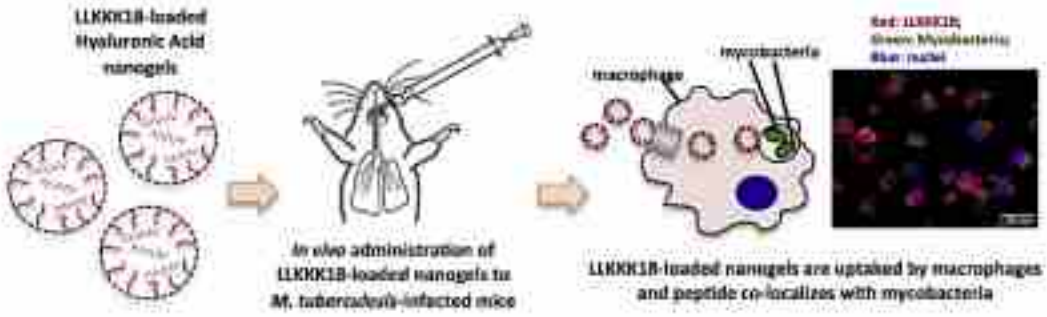

FIGURE 6 Schematic illustration of LLKKK18-loaded HA-NGs targeting intracellular mycobacteria (Silva et al., 2016)

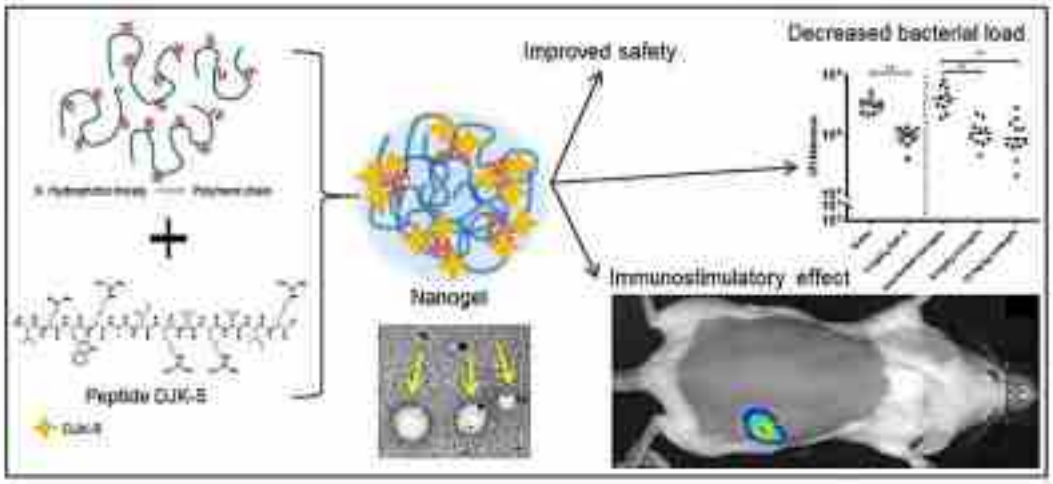

FIGURE 7 Schematic representation of antibiofilm peptide, DJK-5, loaded into HA-NGs (Khdair ieka, Rabanjam, et al., 2019)

cytotoxicity of loaded drugs. Finally, various tailored HA-NGs and formulation conditions can be explored to determine the most appropriate delivery system for peptide and peptidomimetics and allow their efficient use in the clinic.

In addition to the above-mentioned applications of HA-NGs, HA-NGs have been also formulated without drug loading. Since *S. aureus* is able to persist within keratinocytes and phagocytic cells being protected from both the immune system and a variety of antibacterials, to overcome these obstacles, nano-formulations that enable targeted therapies against intracellular *S. aureus* might be developed. In this regard, Montanari et al. (2020) formulated blank HA-NGs (with no drug) to investigate the biodistribution and intracellular localization of HA-NGs (compared to HA) following intravenous (IV) injections (in mice) and topical administrations (in ex vivo human skin). All HA and NGs used in this study were labeled using rhodamine B isothiocyanate without loading of any drug. Following IV injection, HA accumulated considerably in the skin, which corroborates the findings of Pedrosa et al. (2017), who showed that HA-NGs exhibited high accumulation in the skin but with a blood clearance rate slower than HA (Pedrosa et al., 2017). Furthermore, after topical administration in an ex vivo human skin model, neither HA nor its NGs penetrated the intact skin. In contrast, in both barrier-disrupted skin and mechanically produced wounds, HA was taken up by dermis cells in a higher percentage than HA-NGs; however, in both cases, the uptake is mediated by the CD44 receptor. Then, using human dermal fibroblasts and murine macrophages, they investigate the intracellular fate of HA and its NGs in dermal cells. Interestingly, the data obtained suggest the potential of both HA and HA-NGs to accumulate in dermal cell lysosomes, which is in accordance with their previous work (Montanari et al., 2018, 2020).

From all the papers discussed in this subsection, the loaded molecule, molecular weight of HA, cross-linked hydrophobic moiety, targeted bacteria, and in vitro/in vivo status information were extracted and then presented in Table 3. So far, only four types of hydrophobic moieties have been used to formulate HA-NGs. Therefore, in the future, other hydrophobic moieties such as methacrylate molecules, fatty acids, acetic anhydride, as well as active antibacterial compounds, could be investigated. In summary, the findings presented in this subsection confirm the potential of HA-NGs as a promising nanosystem for antibacterial delivery, with the capability to offer selective targeting while also improving bioavailability, penetration, and antibacterial activity. Moreover, HA-NGs provide controlled release behavior and reduce the toxicity of loaded compounds.

3.2 | Hyaluronic acid-ion complex NPs

Owing to its anionic nature, HA tends to form ion complex NPs with cationic small molecules or polymers through polyelectrolyte complexation, which is based on the ability of polyelectrolytes to cross-link in the presence

TABLE 6 | Summary of HA-NCs for antibacterial delivery

Antibacterial agents	Molecular weight of HA (kDa)	Cross-linked hydrophobic moiety	Targeted bacteria	Key characterization methods	Model of efficacy/in vivo status	References
Levofloxacin	200	Cholesterol	*S. aureus* and *P. aeruginosa*	Size and PDI EE% Stability studies	*In vitro* (MIC and intracellular *Staphylococcus aureus*-infected cell model)	(Mumuni et al., 2014)
Gentamicin or levofloxacin	200	Cholesterol	*S. aureus*	Size, PDI and ZP EE% and DLC% MTT assay	*In vitro* (MIC, MBC, intracellular HeLa cell infection model, cellular uptake studies)	(Mumuni et al., 2018)
Azithromycin	50	Octenyl succinic anhydride	*P. aeruginosa*	Size, PDI and ZP EE% MTT assay	*In vitro* (MIC, antibiofilm, motility assay)	(S. N. Rnjak-Kovacina, Wise, et al., 2015)
Erythromycin	Not mentioned	Chitosan	*S. aureus*	Size, PDI and ZP EE% and DLC% SEM DSC, XDR and FTIR	*In vitro* (Zone of inhibition, MIC and TEA)	(Viseu Lis et al., 2021)
LLECK18 peptide	7.46	11-amino-1-undecanethiol	*M. avium* and *M. tuberculosis*	Size, PDI and ZP EE % MTT assay	*In vivo* (Mice infected with *M. avium* or *M. tuberculosis*)	(Silva et al., 2016)
Peptidomimetic (1,2H-3)	30	Octenyl succinic anhydride	*P. aeruginosa*	Size, PDI and ZP EE% and DLC% MTT and lysozyme assays	*In vitro* (MIC, MBC and TEA)	(S. N. Rnjak-Kovacina et al., 2018)
IDR-5 peptide	30	Octenyl succinic anhydride	*P. aeruginosa*	Size, PDI and ZP TEM EE % circular dichroism	*In vivo* (Murine abscess model)	(Khodabakhsh, Khorsand, et al., 2019)
No drug	200	Cholesterol	*S. aureus*	-	*In vivo* and *ex vivo* wound model	(Mumuni et al., 2020)

Abbreviations: HAC, drug loading capacity %; DSC, differential scanning calorimetry; EE%, entrapment efficiency %; FTIR, Fourier transform infrared; PDI, polydispersity index; SEM, scanning electron microscopy; TEM, transmission electron microscopy; XDR, x-ray diffraction; ZP, zeta potential.

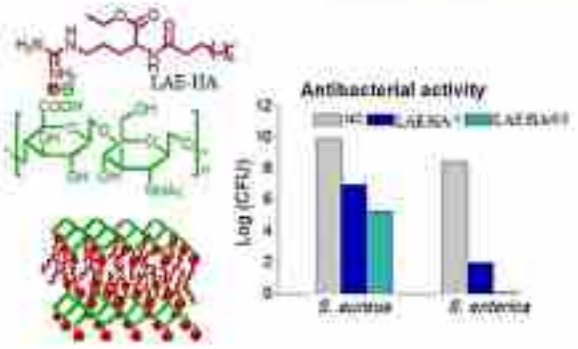

FIGURE 8 Scheme illustrating the ionic complexation of LAE-HA and its antibacterial activity (Gamarra et al., 2018)

of counter ions. This is due to the fact that coupling of complementary ionic building blocks could result in molecular configurations capable of self-assembling into well-organized nanostructures (S. N. Khodzinska & Nielsen, 2021).

To date, two such nanosystems have been reported in the literature for potential applications in the prevention as well as therapy of bacterial infections. Electrostatic assembly of HA with an arginine-based compound, called ethyl-α-N-lauroyl-L-arginate hydrochloride (LAE), to build antimicrobial nanofilms with potential application in food preservation and designing of antiseptic medical devices has been reported by Gamarra et al. (2018) (Figure 8). Thin films prepared from HA-LAE by casting exhibited a smectic-like structure based on an ordered arrangement of LAE and HA layers with a nanometric periodicity of 3.8–3.9 nm. In such systems, HA acts as a matrix for holding and regulating the antimicrobial release from LAE, therefore reducing its potential toxicity and prolonging its activity time compared to the neat LAE. Thereafter, the rate of LAE release from the nanofilm was studied at two pH levels (5.5 and 7.4). Within 4–8 h of incubation, the dissociation equilibrium was reached. At that time, the concentration of LAE was much greater at pH 7.4 than at pH 5.5, and the quantity of free LAE accumulated significantly increased with the LAE: HA ratio in the nanofilm. The antibacterial activity of LAE-HA at pH 7.4 was explored using the gram-positive (*L. monocytogenes* and *S. aureus*) and gram-negative (*S. enterica* and *E. coli*) bacteria. The results indicated significant bactericide activity against both gram-positive and gram-negative bacteria, with the highest activity observed against *S. enterica*. Although further in vitro biocompatibility and in vivo antibacterial studies are required to support their hypothesis, the findings of this research demonstrate that HA has the potential to form arginine-based nanofilms with inherent antibacterial activity as an alternative antiseptic and preservation agent.

Current TB therapies yield low drug loading and/or accumulation in the lung alveoli. Therefore, Mukhtar et al. (2020) developed dry powder inhalers containing CS/thiolated CS (TC) in conjugation with HA as an innovative drug delivery strategy that will allow the antibacterial agent to penetrate deeper lung tissues. The ionic gelation approach was used to produce CS-HA and TC-HA NPs, which were subsequently loaded with isoniazid (INH). Several formulations were developed using DoE, and the average particle size of optimized formulations was 300.2 nm and 342.1 nm with EE% of 90.23% and 92.58% for CS-HA and TC-HA NPs, respectively. The NPs carried a cationic ZP, making them favorable to target the negatively charged surface of macrophages. Additionally, incorporating HA into NPs enables targeting of macrophage CD44 surface receptors, therefore activating a synergistic strategy. Later the in vitro drug release of both NPs, a controlled release pattern was revealed over time, with approximately more than 50% of INH released from both. The MTT cell viability assay was carried out on adenocarcinoma human alveolar basal epithelial (A549) cells. Isoniazid-loaded NPs were found to be biocompatible with the A549 cell line and had no cytotoxicity at concentrations ranging from 0.1 to 0.5 mg/ml. Moreover, the in vitro drug accumulation followed by Andersen Cascade measurement was promising and aligned with the in silico particle deposition model for TB. Both formulations exhibited a greater amount of particle accumulation in the alveolar area, which was considered the site of action. Collectively, the results of this study proposed a novel HA-NC that actively delivers anti-TB medication to the site of action while also improving

the pulmonary drug deposition, however, antibacterial studies are still required to confirm the antibacterial effects of this nanosystem (Mukhtar et al., 2020).

The above-mentioned data demonstrates that the complexation of cationic molecules with HA for targeting bacteria can lead to controlled drug release and consequent inhibition of bacterial growth in infected areas (Gamarra et al., 2018; Mukhtar et al., 2020).

3.3 | Hyaluronic acid-polymersomes

In recent decades, polymersomes have garnered remarkable attention for antibacterial delivery owing to their colloidal stability, flexible membrane characteristics, and capacity to encapsulate or integrate a wide variety of drugs and molecules. Polymersomes are defined as self-assembling nano-vesicles composed of amphiphilic block copolymers. Along with its application in antibacterial delivery, polymersomes are also efficiently utilized to encapsulate therapeutic molecules such as anti-inflammatory, anticancer, antifungal, as well as DNA and RNA fragments either in the aqueous core or integrated into their membrane (J. S. Lee & Feijen, 2012; A. K. Sharma et al., 2020).

The application of HA-based polymersomes as diagnostic tools is recognized as a popular area of research (Manouni & Leroux, 2020). In this regard, Huss et al. (2015) developed smart enzyme-sensitive polymersomes to detect pathogenic bacteria such as *S. aureus* in wounds and burn environments. They describe a novel HAase-responsive amphiphilic block copolymer system based on HA and polycaprolactone (PCL). These polymersomes were constructed using an inversed solvent-shift technique using chloroform and water followed by loading with various fluorescent dyes and antibacterial agents, resulting in HA-PCL assemblies varying in size from 50 to 400 nm, depending on the loaded molecules. The polymersomes, as demonstrated by two different imaging microscopes, are vesicular in nature. In the presence of HAase, the in vitro release of the loaded molecule was studied using the dynamic light scattering technique; a reduction in diameter was observed as the reaction time increased, indicating that the polymersomes were successfully degraded by HAase. Additionally, when loaded with a fluorogenic dye, fluorescence spectroscopy revealed a spontaneous light-up in the presence of HAase and chymotrypsin. However, the degradation of the HA-PCL vesicles was studied using bovine HAase instead of bacterial HAase, which are different. This work supports the potential of HA-PCL polymersomes as a smart indicator system for identifying harmful bacteria in wounds. This approach may be exploited to produce innovative detective and therapeutic HA-polymersomes targeting various HAase-producing bacteria (Huss et al., 2015).

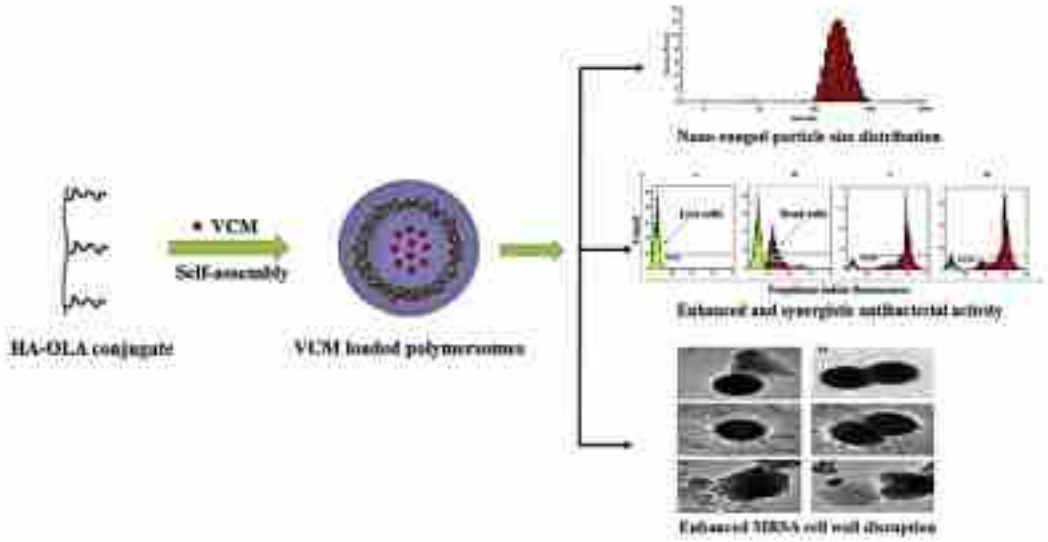

FIGURE 9 Scheme illustrating formulation of HA-OLA polymersomes to eradicate MRSA infection (Waiwekar et al., 2019).

In addition to the above-mentioned application in infection diagnosis, HA-polymersomes have been recently explored for antibacterial delivery. For this purpose, our research group developed novel HA-oleylamine (HA-OLA) polymersomes to enhance the antibacterial activity of vancomycin (VCM) against MRSA (Figure 9). Following the synthesis of novel HA-OLA, the biosafety of the conjugates was confirmed using the MTT assay on three different human cell lines: embryonic kidney cells, cervix adenocarcinoma cells, and human breast adenocarcinoma cells. A probe ultrasonication technique was used to prepare the polymersomes, which were subsequently loaded with VCM. The optimized VCM-loaded HA-OLA polymersomes (VCM-PS6) had an average diameter of less than 250 nm and an EE% of 43.12%. These polymersomes showed slow and sustained release of VCM over 3 days. The in vitro MIC studies against MRSA showed that VCM-PS6 had fourfold the activity of bare VCM. Furthermore, the synergistic action of VCM and HA-OLA against MRSA was reported. Additionally, when samples were treated at an MIC of 1.95 g/ml, flow cytometry demonstrated that VCM-PS6 resulted in 1.8 fold more dead MRSA cells than free VCM. A bacterial membrane rupture test revealed that VCM-loaded polymersomes were more effective in disrupting MRSA membranes than free VCM. These findings suggest that VCM-PS6 was more effective against MRSA than free VCM in all antibacterial tests. In summary, these findings confirm that HA-OLA polymersomes have the potential to be promising antibacterial nanosystems to tackle resistant bacterial strains (Walvekar et al., 2019).

Of the HA-NPs studied, and to the best of our knowledge, only the abovementioned polymersomes have been designed, constructed, and studied for their potential in antibacterial therapy. These polymersomes have considerable therapeutic and diagnostic potential for bacterial infections, which can be significantly increased by mimicking the natural substrate of B-HAase, thus enabling the self-regulated release of antimicrobials. Accordingly, there is a gap in research for designing innovative multifunctional HA-based polymersomes for dual detection and treatment of HAase-producing microorganisms.

3.4 | Other hyaluronic acid-based nanocarriers

In addition to all the HA-NPs mentioned above, others have been reported to either eradicate or prevent bacterial infections. These include HA-based micelles, nanocapsules, nanoplexes, nanofibers (NFs), and nanofilms (Baier et al., 2013; Gao et al., 2014; Hussein et al., 2020; Montanari et al., 2016).

Nanometer-sized HA systems can selectively deliver antibacterial drugs into infection sites via interaction with overexpressed CD44 receptors in certain cells, such as macrophages, which allow effective and enhanced localization of loaded antibacterial drugs in the site of infection. For this purpose, two studies have reported HA-NPs for targeted delivery of antibacterial agents, namely rifampicin (RIF) and tannic acid (TA), to eradicate intracellular bacterial infections (Gao et al., 2014; Montanari et al., 2016). Gao et al. (2014) presented a TB-targeted drug delivery system based on HA functionalized micelles loaded with RIF, a drug widely used for the treatment of TB. Tocopherol succinate was grafted onto HA to generate a hydrophobic moiety enabling self-assembly. They synthesized an HA-tocopherol succinate conjugate (HA-TS), which self-assembled into HA-micelles with average particle diameter ranging from 212 to 294.6 nm. The RIF was incorporated with high drug loading capacity exceeding 30%. The in vitro release studies conducted in two different environments (PBS at pH 7.4 and acetate buffer at pH 5.2) revealed the sustained release of RIF at both pH levels; however, a slower release rate of RIF was observed in acidic media compared to the release rate at physiologic pH. The in vitro biocompatibility on murine alveolar macrophage (MH-S cells) was examined using the MTT assay. The results showed that the loaded micelles exhibited slightly higher cytotoxicity to MH-S cells compared to free RIF within the first 2 days, while no apparent cytotoxicity was observed for blank HA-TS micelles with concentrations between 25 and 250 μg/ml. As expected, the loaded micelles were more efficiently taken up by MH-S cells than the free drug. This uptake occurred via phagocytosis and CD44-mediated endocytosis, and it was time- and dose-dependent. Additionally, the HA-TS micelles may promote the release of pro-inflammatory cytokines, which could improve the antibacterial action of RIF. In another study, Montanari et al. (2016) designed and synthesized HA-aminophenyl (HA-APBA) conjugated NPs with a pH-cleavable linkage for smart delivery of TA to intracellular infection sites. A reaction between HA-APBA and TA yielded NPs with a size smaller than 400 nm, which was dependent on the molecular weight of HA. The boronate ester bond made the NPs stable at physiological pH, while hydrolyzing in an acidic environment allowed TA release within endosomal compartments. The presence of HA enhanced the selectivity of these NPs toward bacteria that colonize within macrophages. Therefore, RAW 246.7 macrophages were used as the model to assess the cytotoxicity of the NPs. The results indicated that HA-APBA alone exhibited slight cytotoxicity. TA significantly reduced cell viability at 56 μg/ml only when combined with AA, but neither AA nor TA appeared to have any

impact when used alone. The loaded NPs exhibited similar toxicity to the TA-AA combination. Finally, three bacterial models were employed in the antibacterial study: *S. aureus*, MRSA, and *E. coli*. Both the loaded NPs and TA had no significant action against *E. coli*, while activity against sensitive and resistant *S. aureus* were significantly greater. Interestingly, the NPs demonstrated nearly comparable antibacterial activity to the TA/ascorbic acid combination, confirming that the boronate complexation retains the reduced (catechol) form of TA and that the NPs indeed release this active form of TA in an acidic medium (Montanari et al., 2016). The outcomes of these two studies confirm the potential of HA-NPs to eradicate intracellular bacteria; however, in vivo antibacterial studies of both nanocarriers are required to validate their theory.

Hyaluronic acid-NPs can also act as carriers for the purpose of wound dressing and tissues regeneration. Wound dressing has been widely studied in order to develop an "optimal" technique that promotes rapid recovery while minimizing scarring. For this reason, HA-NPs, with their diverse physicochemical properties, are a promising research domain for wound dressing and healing (Prajapati & Maheriya, 2019). In this regard, Baier et al. (2013) developed novel HA-based nanocapsules encapsulating an antibacterial agent that cleaves specifically in the presence of HAase. The inverse miniemulsion approach was used to prepare stable cross-linked HA-based nanocapsules loaded with polyhexamide (PH). The obtained nanocapsules had diameters of 360–380 nm and a negative surface. Furthermore, the release of the entrapped PH was quantified by measuring the absorbance of the model dye that was released in response to HAase. As expected, control nanocapsules composed of starch derivative or only PH as a shell material did not exhibit any enzyme-responsive release. The in vitro antibacterial studies in the presence of *S. aureus* and *E. coli* revealed that both the PH containing HA-based (HA-PH-NCs) and the PH-based nanocapsules (PH-NCs) had antibacterial activity. Additionally, these nanocapsules were found to be bactericidal against both *S. aureus* and *E. coli*. However, the MIC for *S. aureus* was lower, reaching 62.5 μg/ml for both nanocapsules, while their activity against *E. coli* was significantly reduced with MIC values of 250 and 125 μg/ml for HA-PH-NCs and PH-NCs, respectively. This is explained by the capacity of *S. aureus* to generate and release HAase, which cleaves HA and promotes bacterial dissemination (Baier et al., 2013). Using another strategy for wound healing, Hussein et al. (2020) reported novel L-arginine-loaded HA-based NFs as a bioactive wound dressing with inherent wound healing properties. To address the poor mechanical properties of HA-based NFs, they strengthened them by including cellulose nanocrystals (CNC) as a bio-composite, which were then loaded with L-arginine. An electrospinning technique was used to fabricate the HA-based NFs. Thereafter, HA-based NFs showed round-shaped nanoparticles with an average size of 120 nm. It was observed that this size fell to 60 nm after incorporation of the CNC, then increased again to 100 nm after incorporation of L-arginine. This result was in accordance with Raoul et al., who observed that the size of L-arginine-loaded lignin NFs increased from ~20–50 nm to ~100–250 nm (Raoul et al., 2018). The loaded HA-CNC NFs (PVA/HA/CNCs/L-arginine NFs) showed slow-release behavior, which led to a sustained elevation in the level of arginine in plasma, thus reducing its adverse effects. Interestingly, the slow release of arginine was found to be a trigger for nitric oxide (NO) signaling, thus accelerating wound closure. Using normal human skin melanocyte (HFB-4) and lung fibroblast (WI38) cell lines, in vitro bio-evaluation of NFs revealed that PVA/HA/CNCs/L-arginine NFs displayed favorable hemocompatibility, elevated protein adsorption, and excellent proliferation and adhesive capability on HFB-4 cells. Regarding the antibacterial studies, PVA/HA/CNCs/L-arginine demonstrated acceptable antibacterial action, particularly against *Klebsiella pneumonia*, a common acute pathogen that causes skin infection (Hussein et al., 2020). Overall, the data presented in this paragraph confirms that such functionalization (using HA) can represent a robust technique for developing multifunctional HA-nanosystems for wound dressing and infection control.

Infections associated with biomedical devices contribute significantly to the growing problem of nosocomial infections, imposing a considerable societal and economic impact (Khan et al., 2017). Therefore, a HA-nanofilm was developed to reduce this biobunden. Hernandez-Montelongo et al. (2016) described the optimal fabrication of layer-by-layer HA-CS nanofilms (HA-CS) as an antibacterial coating technique for preventing nosocomial infections from biomedical devices. Hyaluronic acid created a soft, well-hydrated, nontoxic coating for this nanosystem, whereas CS demonstrated antibacterial properties. The optimization of HA-CS nanofilm synthesis was based on altering the pH values of the biopolymer stem solutions and, as a result, the degree of ionization. Moreover, by increasing the number of HA-CS bilayers, the surface density of amino groups, which is associated with antibacterial activity, was enhanced. The antibacterial activity of HA-CS nanofilms was then investigated against *S. aureus* and *P. aeruginosa* using the spread plate counting method. The HA-nanofilms demonstrated promising results against *S. aureus*, which was highly sensitive to the surface of nanofilms fabricated at various pH values compared to the control sample (silicon substrate). This sensitivity was attributed to the free ammonium group of CS on the top HA-CS layer of the nanofilms. However, when *P. aeruginosa* cultures were cultured for 4 h at pH 4.5 and pH 3, the HA-CS nanofilms had no significant antibacterial action, even though the bacteria were grown at slightly lower rates when compared to the control. Thus, HA-CS

nanofilm in the optimized conditions of synthesis shown here are an excellent alternative as antibacterial surfaces against *S. aureus*. Nevertheless, their use against *P. aeruginosa* would require the addition of antimicrobial agent, such as bioactive peptides, silver nanoparticles, and other suitable biocides (Hernandez-Montelongo et al., 2016).

The outcomes of all the studies mentioned in this section validate the potential application of HA as a promising polymer to formulate HA-NPs for preventing and eradicating bacterial infections. These NPs can enhance the localization of antibacterial agents by providing smart targeted antibacterial therapy, lowering adverse effects of loaded drugs, and regulating the release of the loaded antibacterial agents.

4 | HYALURONIC ACID-COATED NANOCARRIERS

The surface of nanocarriers can be functionalized with a variety of polymers depending on the surface characteristics of nanocarriers (Almalik et al., 2017; Frank et al., 2020; Muddineti et al., 2015). Coating nanocarriers with HA may improve their biological characteristics and biocompatibility, boost their antibacterial activity, and enable controlled site-specific drug release. Additionally, coating with HA can facilitate the ability of nanocarriers to evade immune cell detection and uptake by the reticuloendothelial system, while also significantly improving target recognition and localization. Therefore, HA-coated nanocarriers have been widely applied for targeted drug delivery in the treatment and diagnosis of cancer. However, the use of HA to coat antibacterial-loaded NPs is still in its infancy (Arora et al., 2016; K. Kim et al., 2019; Osman et al., 2021; Sakurai & Harashima, 2019). In this section, we discuss and critically elaborate on the antibacterial nanocarriers that have been surface-modified using HA, which are summarized in Table 2. We have systematically categorized these nanocarriers according to the function of the HA layer into (i) CD44 targeting nanocarriers; (ii) HAase-responsive nanocarriers; and (iii) others.

4.1 | Hyaluronic acid-coated nanocarriers targeting CD44 receptors

The primary receptor for HA, which is CD44, is overexpressed in a subset of cells, such as the majority of cancer cells and activated inflammatory cells (including macrophages). This can boost the selectivity of HA-NPs through CD44-mediated uptake, allowing HA to serve as a homing device (C. Chen et al., 2018; J. H. Kim et al., 2018; Pandey et al., 2017). Among the several HA-coated nanocarriers, inorganic NPs are gaining considerable interest for antibacterial delivery due to their high stability, simplicity of functionalization, and inertness. Apart from improving the targeting of these nanocarriers, HA also regulates and controls drug release and increases the colloidal stability (Y. Chen, Chen, & Shi, 2014; Ivanova et al., 2018; Ran et al., 2017; Sekhon & Kamboj, 2010).

Macrophages, the predominant site of intracellular infection, shield intracellular bacteria from the immune cells, therefore limiting the action of antibiotics. These macrophages express CD44 receptors. Thus, modifying nanocarriers with HA enables the development of therapeutic NPs that may actively target these macrophages, enhancing the release and localization of the loaded antibiotics (Jordan et al., 2015; Matthiolakis et al., 2015; Sánchez et al., 2020). To this end, X. Zhang et al. (2019) and Liu et al. (2020) designed pH-responsive HA-coated metal-organic frameworks (MOFs) loaded with antibiotics for targeted elimination of intracellular bacteria. Zeolitic imidazolate framework-8 (ZIF-8) was chosen as an appropriate MOF owing to its acceptable stability, minimal cytotoxicity, and acid sensitivity, which facilitates drug release at the site of infection. The antibiotics were loaded into the ZIF-8 formed by the self-assembly of the zinc ion and organic bond via an aqueous phase self-assembly approach. Then, HA was added to decorate the surface of the nanocarrier via the coordination effect between its carboxylic acid groups and Zn^{2+} in ZIF-8. In both studies, the nanocarriers can be taken up by cells via an HA-mediated pathway owing to CD44 receptors on the macrophage surface (Liu et al., 2020; X. Zhang et al., 2019). X. Zhang et al. encapsulated tetracycline in HA-coated ZIF-8 to create tetracycline-loaded HA-ZIF-8 (TZH) as shown in (Figure 10a). The in vitro drug release study was carried out at pH 5.5 and 7.4. As expected, both tetracycline and Zn^{2+} were released rapidly from TZH at pH 5.5 compared to the physiological pH. Both in vitro and in vivo antibacterial results demonstrated that ZIF-8 and tetracycline encapsulated in TZH had a synergistic effect, with an intracellular bacterial eradication rate exceeding 99% at a safe low dose, which was significantly greater than the effect of equal amounts of antibacterial agents alone. Similarly, Liu et al. loaded their HA-coated ZIF-8 (HA-ZIF8) with VCM, and the formed nanocarrier was abbreviated as ZVH (Figure 10b). The release studies were carried out in PBS solutions at pH values of 5.5, 6.5, and 7.4. The results indicated that a larger amount of VCM was released at pH 5.5 than at the other two pH levels. The MTT assay on RAW 264.7 cells displayed slight dose-dependent cytotoxicity; nevertheless, the formulation was biocompatible at

TABLE 2 Hyaluronic acid-coated nanocarriers tested for their antibacterial activity

Nanocarrier	Cargo	Size (nm)	Targeted bacteria	Malignancy-like stimuli	Therapy strategy	Proof of efficacy studies	References
TZH	Tetracycline	300	*S. aureus* *Salmonella typhi*	Acidic environment	Chemotherapy	In vivo	(K. Zhang et al., 2016)
ZVH	Vancomycin	180	MRSA	Acidic environment	Chemotherapy	In vivo	(Ying‐in Liu et al., 2020)
GNR/AgNCs@HA	AgNPs	200	*S. aureus* *E. coli*	H_2O_2 from glycolysis	Chemotherapy	In vivo	(Tinglu Li et al., 2021)
HA‐PAni/Ag@	Ag^0	138	MDR‐AB	Neutrophilic	Chemotherapy, Photothermal	In vivo	(Yiting et al., 2020)
MSN‐Lys‐HA‐PDMA	Amoxicillin Lysozyme	175	*S. aureus*	B‐HAse	Chemotherapy	In vivo	(Wu et al., 2015)
AuNP‐HA@MMSNs	Vancomycin	240	*S. aureus*	B‐HAse	Diagnosis, Chemotherapy	In vitro	(Xu et al., 2019)
GO‐HA‐AgNPs	Ag^0	-	*S. aureus*	B‐HAse	Chemotherapy Photothermal	In vivo	(Ran et al., 2017)
AuAgBiuglHA‐Myr2	Ataluru acid, Ciprofloxacin	206	*S. aureus* *P. aeruginosa*	B‐HAse	Chemotherapy, Photothermal	In vivo	(Yanan Liu et al., 2019)
HA‐AgNPs	Ag^0	-	*S. aureus* *E. coli*	Neutrophilic	Chemotherapy	In vitro	(Abdel‐Mohsen et al., 2015)
HA/AC NPs	Antimicrobials	50	*E. coli* *S. aureus*	Neutrophilic	Chemotherapy	In vitro	(Jiménez et al., 2018)

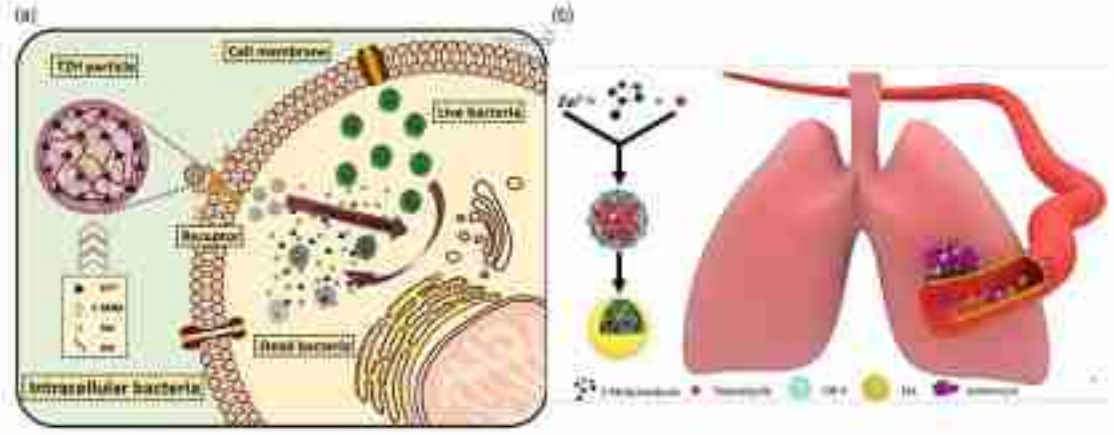

FIGURE 10 Schematic illustration of (a) tetracycline-loaded HA-ZIF8 and (b) VCM-loaded HA-ZIF8 targeting intracellular bacteria (Liu et al., 2020; X. Zhang et al., 2019)

concentrations below 60 μg/ml. Both in vitro and in vivo antibacterial studies confirmed the superiority of VCM loaded in the HA-ZIF8 compared to the same dose of bare VCM. These results confirmed that TZH and ZVH are unique biosafe nanoplatforms that are able to selectively deliver antibiotics to pathogenic sites and achieve responsive and controllable release, thus improving the therapeutic effect against resistant infections and providing a new platform for further overcoming antibiotic resistance (Liu et al., 2020; X. Zhang et al., 2019). Li et al. (2021) reported another HA-ZIF8, wherein they elaborated the use of HA-coated MOFs to deliver silver NPs (AgNPs) rather than conventional antibacterial agents. In this nanosystem, ZIF-8 accompanied by glucose oxidase was loaded with silver nanocubes and subsequently coated with HA to enhance their biocompatibility and capability to target CD44. Interestingly, this nanosystem can function as a pool for releasing silver ions (Ag^+) and tiny Ag NPs (5 nm) from large silver nanocubes (30 nm) in response to bacterial microenvironments. The nanocomposite formed, termed GOD/Ag@ZIF-HA, had significant antibacterial activity against the studied bacteria with an MIC value of less than 10 μg/ml; this is concomitant with the controlled release profile of Ag^+ and the small size of AgNPs in the presence of bacteria. Additionally, at the MIC concentration, GOD/Ag@ZIF-HA inhibited the growth of tested bacteria completely (Li et al., 2021). Even though biocompatibility studies are still outstanding for this research, this study revealed a promising Ag nanoplatform with both size-switchable and selective targeting ability.

While all the above-mentioned studies investigated MOFs, a recent study expanded the pool and explored HA-coated nanocages. Yang et al. (2020) presented gold-silver hybrid nanocages coated with antimicrobial peptide and HA (HA-P(Au/Ag)). This study aimed to treat pneumonia by eradicating multidrug-resistant bacteria-Acinetobacter baumannii (MDR-AB). These HA-P(Au/Ags were biosafe with negligible cytotoxicity and hemolytic effects. The functionalization of the surface of the nanocages with HA facilitates the adhesion of HA-P(Au/Ag) to the bacteria, enabling the loaded antibacterial agents to penetrate and kill the bacteria. Thus, in vitro antibacterial tests revealed that the MIC and MBC values of uncoated nanocages were reduced to 5 and 12 μg/ml, respectively, after coating with HA and the peptide. Furthermore, combining photothermal therapy with the coated nanocages further potentiates their antibacterial activity and entirely eradicates MDR-AB. Similarly, the in vivo antibacterial studies using a pneumonia mice model revealed that treatment with HA-P(Au/Ag) dramatically improved the survival rate of tested mice while restoring the normal structure of the alveoli. This study proved that HA-P(Au/Ag) in combination with photothermal treatment is a viable approach for potentially overcoming MDR-AB multiple mechanisms (Yang et al., 2020).

Collectively, these findings elucidate that surface coating of nanocarriers with HA for targeting CD44 receptors on the surface of phagocytic cells can improve their uptake and internalization, resulting in targeted drug release and subsequent eradication of bacteria within infected macrophages.

4.2 | Hyaluronic acid-coated nanocarriers for hyaluronidase responsiveness

Bacterial infection sites are characterized by acidic pH as well as the presence of numerous virulent enzymes, including B-HAase. Therefore, exploiting these enzymes for diagnostics, drug targeting, and drug release is remarkably promising

(Devnarain et al., 2021). Since HA can be easily degraded by B-HAase, HA has been widely employed as a targeting and capping agent. As previously reported, many species of bacteria, including *S. aureus*, *Clostridium difficile*, and others, were capable of generating HAase (Baier et al., 2013; Hynes & Walton, 2000). Hence, by taking advantage of this phenomenon, HA (as a coating agent) can be used to detect and/or eradicate these bacteria (Wu et al., 2015; Xu et al., 2019).

In recent years, mesoporous silica nanoparticles (MSNs) have been introduced as a promising drug delivery system. Mesoporous silica nanoparticles have essential parts of nanomedicines owing to their chemical stability, large encapsulation capacity, favorable biosafety, ease of preparation and modification, and tunable pore size (Castillo & Vallet-Regí, 2021). Thus, coating MSNs with HA could efficiently provide anti-adhesion properties in physiological fluids, as well as on-demand drug release in response to B-HAase (Wu et al., 2015; Xu et al., 2019). In this regard, Wu et al. (2015) explored the potential of layer-by-layer coated MSNs to release encapsulated amoxicillin in response to the HAase of *S. aureus*. In this study, amoxicillin, an example of a broad-spectrum antibiotic, was encapsulated into MSNs and subsequently coated with antimicrobial lysozyme, followed by a second layer of HA, and then a third layer of modified cationic polyglycerol methacrylate (Figure 11). The prepared NPs, abbreviated as MSN-Lys-HA-PGMA, had a diameter of 174 nm and a drug encapsulation capacity of 8.5%. The presence of the HA layer enables enzyme-responsive release behavior in the presence of B-HAase, which leads to the enzymolysis of MSN-Lys-HA-PGMA, followed by the release of lysozyme and the loaded amoxicillin at the site of action. The biosafety evaluation of MSN-Lys-HA-PGMA was carried out using the CCK-8 assay and hemolysis studies. Both attested to the biocompatibility of the coated nanosystem. In vitro antibacterial action was assessed by determining MIC, zone of inhibition, and bacterial cell viability. These studies showed that MSN-Lys-HA-PGMA had higher antibacterial activity than the equal dose of the loaded antibacterial agents alone. However, their efficacy against gram-negative bacteria was lower due to the presence of the lipopolysaccharide layers, which may inhibit the synergistic action of the lysozyme. Furthermore, the in vivo antibacterial test confirmed the superior activity of the MSN-Lys-HA-PGMA against with a 99.9% inhibition rate, which was consistent with the in vitro findings (Wu et al., 2015).

Magnetic MSN, in contrast to the nonmagnetic MSN discussed above, enables integrated diagnosis and treatment of infection owing to its excellent magnetic property. As a step toward this direction, Xu et al. (2019) reported on-demand magnetic MSNs for the detection and treatment of *S. aureus*. In this study, magnetic MSNs were loaded with VCM, and

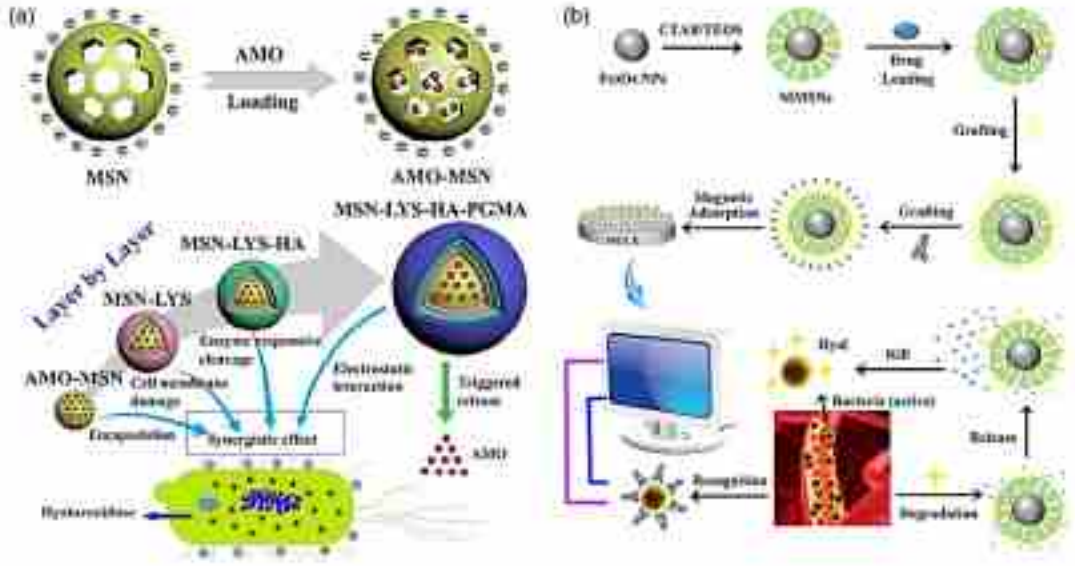

FIGURE 11 Schematic representation of (a) layer-by-layer coating of MSN-Lys-HA-PGMA and the possible antibacterial mechanism for each layer. (b) Synthesis of an "on-demand" integrated Alg@S-HA@MMSNs for diagnosis and treatment toward *S. aureus* (Wu et al., 2015; Xu et al., 2019)

then coated with sulfonated HA, followed by functionalization of the surface of magnetic MSNs (Abᵩ@S-HA@MMSNs) with *S. aureus* antibodies by chemical reaction. Here, sulfonated-HA, instead of bare HA, was chosen owing to superior anticoagulant and release behavior. The prepared Abᵩ@S-HA@MMSNs were spherical with a size of 240 nm and a maximum VCM loading capacity of 10.7%; thereafter these NPs were functionalized on the surface of magnetic glassy carbon electrode (MGCE). Therefore, since these NPs have both HA (which exerts anticoagulant action) and *S. aureus* antibodies, they can be directly applied to detect the amount of pathogenic *S. aureus* in whole blood. In addition, with the increased amount of *S. aureus* arriving at the MGCE, the coat of Abᵩ@S-HA@MMSNs was degraded by B-HAase leading to the release of the encapsulated VCM and ultimately, the effective eradication of *S. aureus*. At a concentration below 500 μg/ml, Abᵩ@S-HA@MMSNs were hemocompatible with a hemolysis rate of less than 5%. Owing to the on-demand controlled release of VCM, the antibacterial studies (in vitro) showed significant bacteriostatic action with a rate reaching 98% against *S. aureus* (Xu et al., 2019). Therefore, the finding presented in this paragraph displayed that such integrated nanosystems can be promising multifunctional platforms for achieving accurate detection and efficient eradication of *S. aureus* bloodstream infections.

Recently, multifunctional nanomedicines derived from a combination of chemo and photothermal treatments have garnered considerable interest due to their cooperatively enhanced bactericidal activity (Huo et al., 2021; Wei et al., 2020). In this regard, Ran et al. (2017) presented an HAase-triggered photothermal nanoplatform for the eradication of bacteria based on AgNPs and graphene oxide (GO). First, The AgNPs were coated with HA to form nanocomposites with a size of 30 nm; subsequently, these NPs were integrated with GO to form GO-HA-AgNPs. Due to the presence of the HA layer, the nanocomposites exhibited low toxicity to host cells. Furthermore, the release behavior of HAase-responsive AgNPs enabled AgNPs to be protected by the HA layer without affecting host cells and offer controlled release in the presence of bacteria. After HA was degraded, the sheetlike GO could accumulate on the surface of bacteria via physical interactions, and upon illumination of NIR light, the GO-based sheet locally raised the temperature, resulting in significant bacteriostatic and bactericidal actions thus resulting in synergistic therapy. This hypothesis was confirmed by performing both in vitro and in vivo antibacterial studies, which showed that GO-HA-AgNPs had greater antibacterial activity compared to AgNPs (Ran et al., 2017). Two years later, another HAase-responsive nanocomposite, AA@Ru@HA-MoS2, with a synergistic chemo-photothermal property was reported by Liu et al. (2019) to treat bacterial infections. In this study, HA-coated mesoporous ruthenium nanoparticles (MRNs) were used as nanocarriers, ascorbic acid was loaded as a prodrug, and then ciprofloxacin-molybdenum disulfide was integrated as a catalyst at the outer surface. The formulated nanocomposites were pompon-like with a diameter of 206 nm. When AA@Ru@HA-MoS2 reached the infection site, B-HAase degraded the HA layer, releasing ascorbic acid and subsequently generating hydroxyl radicals in situ through molybdenum disulfide catalysis. Additionally, by exploiting the excellent photothermal properties of MRNs, a combination of chemo- and photo-thermal antibacterial therapy could be accomplished. A set of in vitro antibacterial studies on two bacterial models, namely *S. aureus* and *P. aeruginosa*, indicated that AA@Ru@HA-MoS2 not only had bactericidal activity, but also significant antibiofilm activity. The same finding was also obtained in the in vivo antibacterial experiment. Furthermore, the mouse infection model showed faster wound healing activity and excellent short and long-term biosafety profiles. Overall, these studies indicate that HA-coated antibacterial nanocarriers could further enhance the synergy of chemo-photothermal treatments. Such functionalization represents a robust strategy for designing enzyme-responsive multifunctional nanomedicines to improve targeted antibacterial delivery.

In summary, as HA is made up of enzyme-degradable disaccharide units, it is considered an ideal candidate for the fabrication of nanocarriers with an HAase-responsive crown. These HAase-responsive NPs hold great potential for more precise detection and more effective therapy of bacterial infections.

4.3 | Other hyaluronic acid-coated nanocarriers

In addition to the aforementioned rationales for coating various antibacterial nanocarriers with HA, HA can also be used as a coating material to reduce the toxicity of metallic NPs as well as an antiadhesive agent to prevent adsorption of biomolecules on the surface of nanocarriers (Abdel-Mohsen et al., 2013; Ivanova et al., 2018).

The application of colloidal Ag-based materials has been rising owing to their potent antimicrobial action. Therefore, AgNPs have been used in several areas, including manufacturing cosmetics, medical devices, and pharmaceutical products (Kraisch & Knoke, 2011; X.-F. Zhang, Liu, et al., 2016). However, due to its toxicity, these applications are limited. Silver NPs have been widely studied to reach biocompatible and environmentally friendly products by capping

AgNPs with various bioactive polymers (Mohamed Fahmy et al., 2019). Thus, coating AgNPs with HA could be a promising strategy for biomedical applications. In this regard, Abdel-Mohsen et al. (2013) designed and prepared AgNPs-capped with HA fibers (HA-AgNPs) as a potential wound dressing material. Silver NPs with diameters of 10 and 40 nm were prepared, then coated with HA fibers. In this study, HA served as a capping agent for Ag^+ as well as stabilizing agent during and after the synthesis of AgNPs. Several experiments were conducted to investigate the characterization, biocompatibility and cell viability, thermal profiles, and antibacterial activity of HA-AgNPs. Using mouse fibroblast 3T3 cells, the MTT assay indicated that HA, HA fibers, and HA-AgNPs were nontoxic to the cell line. Moreover, HA-AgNPs showed potent in vitro antibacterial activity against *S. aureus* and *E. coli*. This work showed that modification of AgNPs with HA can minimize their cellular toxicity. Further in vivo evaluation is necessary; however, AgNPs embedded in HA fibers can be employed for a variety of biomedical applications, most notably wound healing and dressing (Abdel-Mohsen et al., 2013).

Hyaluronic acid has been widely employed for surface engineering of nanomaterials to enhance their stability and functionalities for biomedical applications. One of the primary obstacles that face the optimized nanoformulations when administered in vivo is the biofouling effect. Biofouling is defined as nonspecific interactions between biomolecules and the engineered nanocarriers leading to in situ changes in their pharmacokinetics, pharmacodynamics, and toxicity. Among the polysaccharides studied as anti-biofouling agents, HA is the most employed polysaccharide. Its antifouling actions appeared to be promising in terms of inhibiting nonspecific protein adsorption and enhancing nanocarrier stability in complex serum-containing media (Lemarchand et al., 2004; Li et al., 2017; Mosalab et al., 2019). Ivanova et al. (2018) accomplished this goal by coating biomimetic polymeric NPs with several bilayers of biocompatible and antifouling HA and antibacterial aminocellulose. After five cycles of layer-by-layer coating technique, polyelectrolyte-coated NPs (HA-AC NPs) with a size below 50 nm were formed. The surface charge of the nanosystems is governed by its outermost layer. All coated NPs were shown to be biosafe when tested on human fibroblast cells. A series of in vitro antibacterial studies against *E. coli and S. aureus* were conducted. The results indicated that the coated NPs were capable of eradicating planktonic bacteria and inhibiting biofilm formation. For an exposure period of less than 1 h, the NPs with aminocellulose as the outermost layer demonstrated high antibacterial efficacy against gram-positive and gram-negative bacteria. On the other hand, when HA was used as the outermost layer of NPs, a significant increase in antibiofilm activity was found against tested bacteria (including *E. coli*). Although the exact antibiofilm mechanism of HA-terminated NPs is not fully understood, it has been justified by the contribution of the HA layer (as anti-biofouling) to the improved colloidal stability of the nanocarrier in tryptic soy growth media and consequently enhanced efficacy of NPs toward gram-negative strains. This work demonstrated the anti-biofouling property of HA in protecting nanocarriers from nonspecific interactions with serum proteins (Ivanova et al., 2018). However, further experiments (in vivo) should be pursued to study the potential of these NPs for treatment of infectious diseases.

Overall, surface functionalization with HA endows nanoparticles with bacterial targeting ability, enhances the colloidal stability and biosafety, protects the NPs from biofouling effects, and even serves as a gatekeeper to control the drug release. Table 2 summarizes all HA-coated nanocarriers that have been used to date for antibacterial delivery. The table provides comprehensive information such as the size of the nanosystem, bacteria species, antibacterial agents(s), release triggering strategy, mode of therapy, and mode of study.

5 | HYALURONIC ACID-DRUG CONJUGATES

Hyaluronic acid is a large biocompatible hydrophilic polymer of repeating sugar units that can be covalently attached to various drugs (Arora et al., 2016; Prajapati & Maheriya, 2019). In 1991, the concept of drug conjugation to HA was introduced for the first time (Drobnik, 1991). In antibacterial delivery, direct conjugation of HA to various drugs could yield novel nanosystems with promising antibacterial effects (Arshad, Tahish, Kiani, et al., 2021; Lu et al., 2020; Qiu et al., 2019). Such straightforward yet effective nanoformulations can be employed to enhance therapeutic efficacy against intracellular pathogens, as many inflammatory cells overexpress HA-targeted receptors (CD44). Furthermore, the covalent bonds between HA and the conjugated antibiotics can be tailored so they are not easily broken in the blood, but they are disrupted by hydrolysis and/or enzymatic degradation once they reach the target, releasing the drug. Thus, providing merits in terms of prolonging circulation time, increasing drug stability and solubility, and controlling release behavior (S. N. Kłodzińska & Nielsen, 2021).

Instead of conjugating macromolecular hydrophobic polymers, small lipophilic drug molecules can be grafted onto the N-acetyl, hydroxyl, or carboxyl groups of HA. The synthesized HA-drug conjugates can be self-assembled into

nanomicelles; thus, the conjugated drugs can be safely delivered to their destination (B. Chen, Miller, & Dhal, 2014). Even though antibiotics are powerful agents against pathogenic bacteria, more than 70% of them are ineffective against intracellular pathogens (Butler & Cooper, 2011). Accordingly, to combat these threatening infections, there is a dire need to invent novel antibacterial agents that can penetrate inside mammalian macrophages and efficiently eliminate these pathogens. In this regard, two studies by Jinyou Duan research group have been reported. In both studies, HA-based micelles were constructed by conjugating lipophilic antibiotics with HA. Hyaluronic acid was used to maximize the uptake of the conjugated drug via a CD44-mediated mechanism leading to improved antibacterial action (Lu et al., 2020; Qiu et al., 2019). In the former study, Qiu et al. (2019) designed and synthesized pH-sensitive HA-based micelles containing HA-streptomycin conjugate and rapamycin, an autophagy activator (Figure 12). The novel self-assembled compound was synthesized by grafting streptomycin and decylamine on HA (via acid-labile bond) and subsequently loading with rapamycin via a spontaneous self-assembly approach. The prepared HA-based micelles had a hydrodynamic diameter of 179 nm with an EE% of 69.3%. At pH 5.5, the drug-HA bond was cleaved, releasing streptomycin and the loaded rapamycin at the infection site. Moreover, using RAW 264.7 and HK-2 cell lines, MTT assay validated the biocompatibility of blank and loaded micelles at concentrations below 400 μg/ml. The rapamycin-loaded HA-micelles demonstrated a high intracellular eradication rate against *Salmonella typhimurium* and *S. aureus*, even more than the equivalent mixture of streptomycin and rapamycin. As mentioned in literature, bare streptomycin cannot penetrate mammalian cells, thus exhibiting poor antibacterial action against intracellular microorganisms (Tulkens, 1991). Accordingly, conjugation of streptomycin with HA facilitates its uptake via CD44-mediated endocytosis. In addition, the rapamycin could further potentiate the action of the system via activation of autophagy (Qiu et al., 2019). In the subsequent study, Lu et al. (2020) synthesized NO-triggered micelles (HA-NO-LVF) by conjugating an HA chain and a lipophilic LVF followed by self-assembly in aqueous conditions. It is known that when macrophages become infected, they generate a large amount of NO. Thus, exploiting endogenous NO to cleave HA-conjugated nanocarriers increases the potential for not only responsive drug release but also for scavenging redundant NO radicals to reduce tissue injury. In that sense, the in vitro release study in the presence of NO demonstrated that the micelles

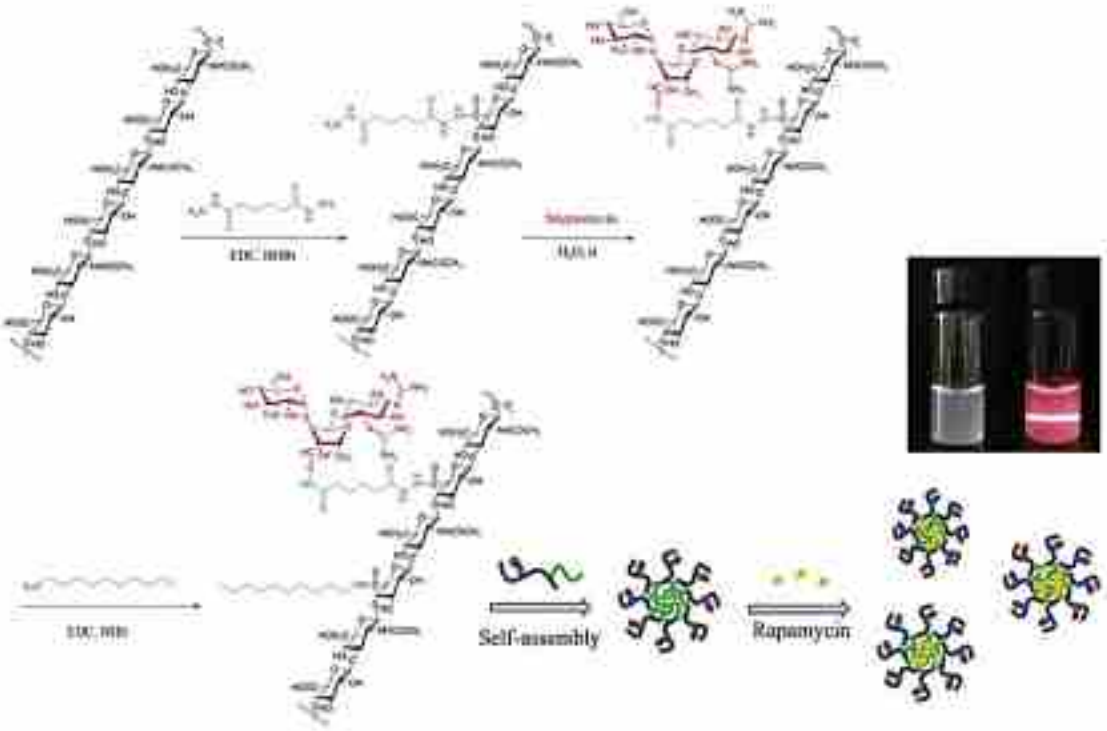

FIGURE 12 Schematic illustration of rapamycin-loaded HA-based micelles (Qiu et al., 2019)

were cleaved, releasing LVF in the pathogenic environment. Meanwhile, the NO-responsive HA-micelles retained hemocompatibility as well as biosafety profiles. Similar to their former study, HA-NO-LVF demonstrated significant antibacterial action against intracellular *S. aureus*, which could be due to CD44-mediated endocytosis of HA-NO-LVF and subsequent on-demand release of LVF, resulting in a higher eradication rate against intracellular bacteria. Moreover, in vivo evaluations acknowledged the ability of HA-NO-LVF to safely eliminate intracellular bacteria and reduce inflammatory mediators. In both studies, the assumption of CD44-mediated uptake of nanosystems was validated via performing a competitive inhibition assay. The findings of the assay revealed that when the CD44 receptors were occupied by HA, the intracellular uptake of the conjugated HA-micelles was dramatically reduced. Taken together, both studies proved the synergistic action of HA-mediated uptake and the bactericidal action of the antibiotic in eradicating intracellular pathogens, hence lowering the required doses of used antibiotics (Lu et al., 2020; Qiu et al., 2019).

Self-emulsifying drug delivery systems are isotropic mixtures of drugs, oil, surfactants, and co-surfactants that form oil-in-water (O/W) nanoemulsions upon contact with water and mild agitation. The formed nanoemulsions are thermodynamically stable with nanosized droplets, high solubilization ability for hydrophobic drugs, and enhanced biocompatibility and pharmacokinetic profiles (Dalal et al., 2021; Kazi et al., 2019). Due to the overexpression of CD44 receptors on intestinal inflammatory cells, HA is an ideal choice for the preparation of HA-based nanoemulsions targeting intestinal infections (Eriksson et al., 2003; Johnson & Ruffell, 2009). In this regard, Arshad, Tabish, Rizvi, et al. (2021) successfully conjugated ciprofloxacin to the HA chain via an amidation reaction. The synthesized conjugate was delivered as a self-nano emulsifying drug delivery system (HA-CIP-SNEDDS). The aim of this study was to improve ciprofloxacin mucopenetration, biopharmaceutical parameters, and hence intracellular antibacterial activity. The optimized nanoemulsion was found to be hemocompatible and biocompatible with a droplet size of 50 nm and maximum drug encapsulation efficiency of 85%. Moreover, at conditions mimicking the endosomal environment, HA-CIP-SNEDDS demonstrated superior and sustained release for 72 h in comparison to bare ciprofloxacin. As predicted, the fluorescence assay demonstrated that HA enhanced the internalization of ciprofloxacin by scavenger inflammatory cells, resulting in efficient targeting and eradication of *S. typhimurium*. Consequently, antibacterial studies showed that HA-CIP-SNEDDS had a strong bactericidal and antibiofilm activity against *S. typhimurium* compared to bare ciprofloxacin. When administered in vivo, HA-CIP-SNEDDS exhibited enhanced anti-salmonella activity, confirming the in vitro results. Therefore, this study showed that HA-CIP-SNEDDS seems to be a promising antibacterial agent against *S. typhimurium* with a strong targeting ability (Arshad, Tabish, Rizvi, et al., 2021).

These studies confirmed the potential use of HA as an antibacterial drug carrier to enhance targeted delivery and activity of conjugated antibiotics. This approach can significantly enhance antibiotic concentrations at infection sites, as well as cellular uptake and recognition of antibiotics, resulting in highly effective antibiotic targeted therapy.

6 | CONCLUSION AND FUTURE PERSPECTIVES

Polymer-based nanoantibiotics have been thoroughly explored to improve the efficacy of conventional antibiotics in various biomedical applications. Among all polymers used, HA has garnered considerable attention in the development of nanocarriers that can enhance the delivery of antibacterial agents to infection sites. In this review, we have highlighted and critically analyzed all reported nanosystems in literature that incorporate HA using different strategies for antibacterial applications such as treating, preventing, and/or diagnosing bacterial infections. After an extensive analytical search of various scientific databases, we have systematically categorized these HA-NPs according to their approach for application into HA-based nanocarriers, HA-capped NPs, and drug-conjugated HA-NPs. Therefore, HA and its conjugates are considered promising candidates for developing targeted nanocarriers of therapeutic or imaging agents for bacterial infections.

Based on the reported studies to date, we quantitatively analyzed and compared the various types of HA-based nanocarriers that have been employed for improving antibacterial properties (Figure 13). It is apparent that HA-based nanocarriers have been formulated and evaluated for their antibacterial potential, more than the other two strategies; and that the antibacterial activity of these nanocarriers has been tested against *S. aureus* and *E. coli*, more than other bacteria. This will aid future researchers in identifying the best strategy for preparing HA-NPs as well as the infectious microorganisms on which to focus.

Sites of bacterial infection have hallmarks not present in uninfected tissues; they often include cells overexpressing CD44 receptors and have unique microenvironments such as acidic pH and high levels of specific enzymes (including Ⅱ-HAase). Therefore, HA-NPs can enhance antibacterial delivery to eradicate intracellular infections such as TB,

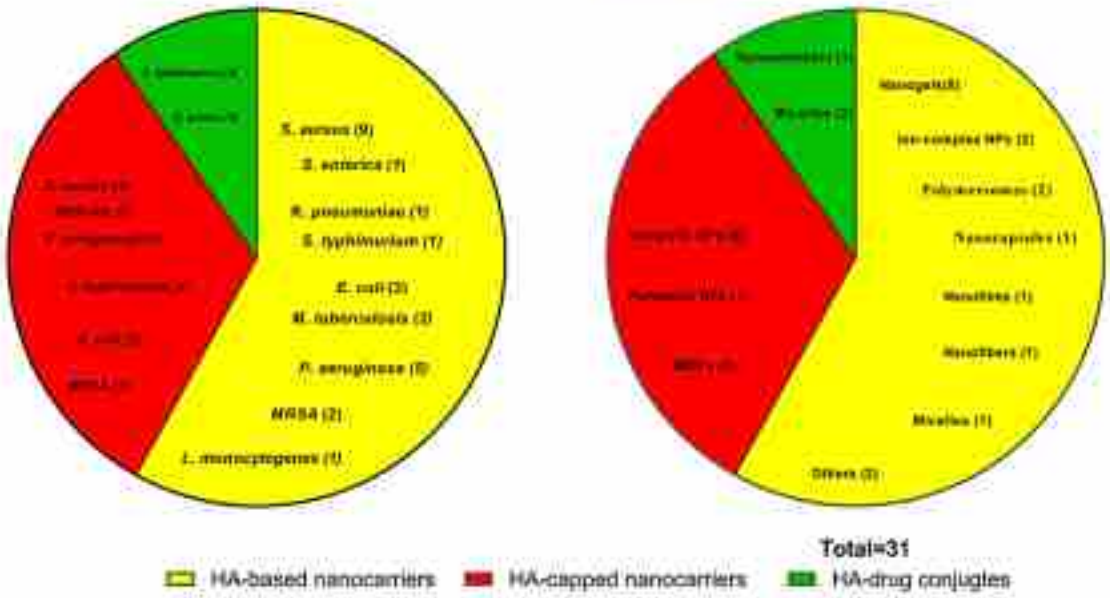

FIGURE 11 Hyaluronic acid-based nanoparticles (right) that have been developed for the detection and/or eradication of various bacteria (left) over the last two decades

typhoid, brucellosis, and others. Moreover, the polymeric nature of HA enables prolonged circulation of loaded (or conjugated) antibiotic(s) in the bloodstream, resulting in sustained release behavior. After reaching the targeted area, initial burst release of antibacterial agents and activation of their functions at the infection site may occur in response to B-HAase, thus enabling on-demand release of the loaded drug(s). In addition, surface functionalization using HA could increase the biocompatibility, intracellular uptake, and colloidal stability of inorganic nanoparticles. Therefore, this strategy has a bright future in advancing the field of inorganic nanomedicines drug delivery to treat and diagnose bacterial infections. On the other hand, HA-drug conjugates are considered as prodrugs synthesized by covalently attaching small antimicrobial drugs to HA. These linkages are not easily broken in the blood; however, they are breakable through acidic or enzymatic hydrolysis after reaching the target and releasing the drug. Therefore, such conjugates can serve as a targeting ligand for CD44 receptors on the surface of macrophages, allowing antibiotics to be safely delivered to eliminate intracellular infections.

While considerable efforts have been invested in proving the enhanced potential of HA-NPs for bacterial eradication and detection, these nanosystems are still in their laboratory research stages, and numerous further studies are necessary to obtain regulatory approval. The production, synthetic modification, and precise characterization and optimization of HA-NPs, as well as their biosafety and in vivo pharmacokinetics, should be carried out accurately according to clinical requirements. Moreover, more efforts are required to overcome obstacles associated with the process of scaling up these formulations into cost-effective products. Additional investigations, including in silico molecular dynamics and in vitro binding affinity calculations (using microscale thermophoresis), are required to fully understand the interactions between these nanocarriers and the targeted biomolecules. Furthermore, the in silico studies can help to determine the stability of the synthesized HA-NPs using virtual conditions that mimic experimental conditions.

Coating the surface of nanocarriers with HA is an effective strategy for enhancing antibacterial delivery as it provides anti-adhesion properties, colloidal stability, and selective targeting ability. In addition, the secretion of HAase by various bacteria can be exploited by creating multifunctional HA-coated NPs that can detect and treat HAase-secreting bacteria. These multifunctional nanocarriers have the potential to revolutionize the diagnosis and treatment of HAase-related infections. As a result, more research efforts should be focused on the surface modification of nanocarriers with HA. Furthermore, targeting bacterial virulence factors via mimicking cell signaling pathways may enhance antibacterial efficacy of loaded drugs and minimize their adverse effects and thereby, contribute to tackling the

pathogenesis of infection. Therefore, by synthesis of modified HA-NPs targeting B-HAase (as a virulent factor), it is possible to inhibit bacterial pathogenicity. However, up to the date of this review, no research has been done in order to develop HA-NPs with this biomimetic action, leaving huge research areas to be explored. Generally, formulating HA-drug conjugates is the simplest form in terms of preparation and validation; however, in antibacterial delivery, only three studies have been reported. Therefore, it is expected that the investigations particularly in the area of intracellular antibacterial delivery will be expanded, since HA can facilitate the internalization of conjugated antibiotics via CD44 receptors and provide "on-demand" release at the infection site. Based on the potential shown in this review, we envisage an explosion in the use of HA for transforming diagnosis and treatment of bacterial infections. Hyaluronic acid as a key excipient in nanomedicines has the potential to save lives and improve quality of life.

ACKNOWLEDGMENT

The authors acknowledge the University of KwaZulu-Natal (UKZN), University of Khartoum (UofK), the National Research Foundation of South Africa (NRF Grant No. 106040, 129326, 103664, and 116652), and the Medical Research Council (MRC) of South Africa for financial support.

CONFLICT OF INTEREST

The authors have declared no conflicts of interest for this article.

AUTHOR CONTRIBUTIONS

Mahir Mohammed: Conceptualization (lead); data curation (lead); formal analysis (lead); investigation (lead); methodology (lead); software (lead); validation (equal); visualization (lead); writing – original draft (lead); writing – review and editing (lead). **Nikita Devnarain:** Conceptualization (equal); data curation (equal); formal analysis (equal); methodology (equal); writing – review and editing (equal). **Eman Elhassan:** Data curation (supporting); methodology (supporting); writing – original draft (supporting); writing – review and editing (supporting). **Thirumala Govender:** Conceptualization (equal); funding acquisition (equal); supervision (equal); validation (equal); writing – review and editing (equal).

DATA AVAILABILITY STATEMENT

Data sharing is not applicable to this article as no new data were created or analyzed in this study.

ETHICS STATEMENT

Animal studies: No animal or human studies were carried out by the authors of this article.

ORCID

Mahir Mohammed https://orcid.org/0000-0002-8240-834X
Nikita Devnarain https://orcid.org/0000-0002-9538-4611
Eman Elhassan https://orcid.org/0000-0003-1238-2970
Thirumala Govender https://orcid.org/0000-0002-8968-4779

RELATED WIREs ARTICLES

Intrinsic stimuli-responsive nanocarriers for smart drug delivery of antibacterial agents: An in-depth review of the last two decades
Surface modification of nano-drug delivery systems for enhancing antibiotic delivery and activity
Inflammation-modulating nanoparticles for pneumonia therapy

REFERENCES

Abdel-Mohsen, A. M., Jirsova, R., Burgert, L., Abdel-Rahman, R. M., Hrkova, M., Šmejkalová, D., Kolář, M., Pekar, M., & Aly, A. S. (2013). Antibacterial activity and cell viability of hyaluronan fiber with silver nanoparticles. *Carbohydrate Polymers*, *92*(2), 1177–1187. https://doi.org/10.1016/j.carbpol.2012.09.098

Ahire, J. J., & Dicks, L. M. T. (2016). Antimicrobial hyaluronic acid-Cefoxitin sodium thin films produced by Electrospraying. *Current Microbiology*, *73*(2), 236–241. https://doi.org/10.1007/s00284-016-1057-1

Almalik, A., Benabdelkamel, H., Masood, A., Alanazi, I. O., Alradwan, I., Majrashi, M. A., Alfadda, A. A., Alghamdi, W. M., Alrabiah, H., Tirelli, N., & Alhasan, A. H. (2017). Hyaluronic acid coated chitosan nanoparticles reduced the immunogenicity of the formed protein Corona. *Scientific Reports*, *7*(1), 1–9. https://doi.org/10.1038/s41598-017-10836-7

Almalik, A., Karimi, S., Ouasti, S., Donno, R., Wandrey, C., Day, P. J., & Tirelli, N. (2013). Hyaluronic acid (HA) presentation as a tool to modulate and control the receptor-mediated uptake of HA-coated nanoparticles. *Biomaterials*, *34*(21), 5369–5380. https://doi.org/10.1016/j.biomaterials.2013.03.065

Arora, D., Sharma, N., Sharma, V., Abrol, V., Shankar, R., & Jaglan, S. (2016). An update on polysaccharide-based nanomaterials for antimicrobial applications. *Applied Microbiology and Biotechnology*, *100*(6), 2603–2615. https://doi.org/10.1007/s00253-016-7313-0

Arshad, R., Tabish, T. A., Kiani, M. H., Ibrahim, I. M., Shahzad, G., Rahdar, A., Kang, M., & Pandey, S. (2021). A hyaluronic acid functionalized self-nano-emulsifying drug delivery system (Snedds) for enhancement in ciprofloxacin targeted delivery against intracellular infection. *Nanomaterials*, *11*(5), 1086. https://doi.org/10.3390/nano11051086

Arshad, R., Tabish, T. A., Kesharwani, A. A., ul Hassan, M. R., Hussain, I., Hussain, S. S., & Shahnaz, G. (2021). Development of poly-L-lysine multi-functionalized mucus-penetrating self-emulsifying drug delivery system (SEDDS) for improved solubilization and targeted delivery of ciprofloxacin against intracellular salmonella typhi. *Journal of Molecular Liquids*, *333*, 115972. https://doi.org/10.1016/j.molliq.2021.115972

Balet, G., Cavallaro, A., Vasilev, K., Mailänder, V., Mayavanshi, A., & Landfester, K. (2015). Enzyme responsive hyaluronic acid nanocapsules containing polyhexanide and their exposure to bacteria to prevent infection. *Biomacromolecules*, *14*(4), 1105–1112. https://doi.org/10.1021/bm302003m

Bloom, D. E., & Cadarette, D. (2019). Infectious disease threats in the twenty-first century: Strengthening the global response. *Frontiers in Immunology*, *10*(MAR), 549. https://doi.org/10.3389/fimmu.2019.00549

Butler, M. S., & Cooper, M. A. (2011). Antibiotics in the clinical pipeline in 2011. *Journal of Antibiotics*, *64*(6), 413–425. https://doi.org/10.1038/ja.2011.44

Campani, E., Paghetta, F., Giustini, F., Della Pepa, C., Dotto, P., & Serpe, L. (2019). Recent developments in antibacterial therapy and therapeutic nanoparticles. *Molecules*, *24*, 1–15. https://doi.org/10.3390/molecules24101949

Castillo, R. R., & Vallet-Regí, M. (2021). Recent advances toward the use of Mesoporous silica nanoparticles for the treatment of bacterial infections. *International Journal of Nanomedicine*, *16*, 4409–4430. https://doi.org/10.2147/IJN.S273064

Chen, R., Millar, R. J., & Dhal, P. K. (2014). Hyaluronic acid-based drug conjugates: State-of-the-art and perspectives. *Journal of Biomedical Nanotechnology*, *10*(1), 4–16. https://doi.org/10.1166/JBN.2014.1781

Chen, C., Zhao, S., Karnad, A., & Freeman, J. W. (2018). The biology and role of CD44 in cancer progression: Therapeutic implications. *Journal of Hematology & Oncology*, *11*(1), 1–23. https://doi.org/10.1186/S13045-018-0605-5

Chen, Y., Chen, H., & Shi, J. (2014). Inorganic nanoparticle-based drug codelivery nanosystems to overcome the multidrug resistance of cancer cells. *Molecular Pharmaceutics*, *11*(8), 2495–2510. https://doi.org/10.1021/mp400599w

Choi, K. Y., Saravanakumar, G., Park, J. H., & Park, K. (2012). Hyaluronic acid-based nanocarriers for intracellular targeting: Interfacial interactions with proteins in cancer. *Colloids and Surfaces B: Biointerfaces*, *99*, 82–94. https://doi.org/10.1016/j.colsurfb.2011.10.039

Dahlal, L., Allaf, A. W., & El-Zein, H. (2021). Formulation and in vitro evaluation of self-nanoemulsifying liquisolid tablets of furosemide. *Scientific Reports*, *11*(1), 1–10. https://doi.org/10.1038/s41598-020-79940-3

Dermesrain, N., Osman, N., Fasiku, V. O., Makhathini, S., Salih, M., Ibrahim, H. H., & Govender, T. (2021). Intrinsic stimuli-responsive nanocarriers for smart drug delivery of antibacterial agents—An in-depth review of the last two decades. *WIREs Nanomedicine and Nanobiotechnology*, *13*(1), 1–38. https://doi.org/10.1002/wnan.1664

Desai, F., Arpicco, S., Stella, B., & Fattal, E. (2016). Hyaluronic acid for anticancer drug and nucleic acid delivery. *Advanced Drug Delivery Reviews*, *97*, 204–236. https://doi.org/10.1016/j.addr.2015.11.011

Drago, L., Cappelletti, L., De Vecchi, E., Pignataro, L., Torretta, S., & Mattina, R. (2014). Antiadhesive and antibiofilm activity of hyaluronic acid against bacteria responsible for respiratory tract infections. *APMIS (Acta Pathologica, Microbiologica et Immunologica Scandinavica)*, *122*(10), 1013–1019. https://doi.org/10.1111/apm.12254

Dreborg, S. (1991). Hyaluronan in drug delivery. *Advanced Drug Delivery Reviews*, *7*(2), 295–308. https://doi.org/10.1016/0169-409X(91)90008-Z

Eriksson, E., Doss, L., Rothfuchs, A. G., Heldin, P., Wigzell, H., & Rottenberg, M. E. (2003). CD44-regulated intracellular proliferation of listeria monocytogenes. *Infection and Immunity*, *71*(7), 4102–4111. https://doi.org/10.1128/IAI.71.7.4102-4111.2003

Farrell, J. M., Zhao, C. Y., Tarquinio, K. M., & Brown, S. P. (2021). Causes and consequences of COVID-19-associated bacterial infections. *Frontiers in Microbiology*, *0*, 1911. https://doi.org/10.3389/FMICB.2021.682571

Frank, L. A., Onzi, G. R., Morawski, A. S., Pohlmann, A. R., Guterres, S. S., & Contri, R. V. (2020). Chitosan as a coating material for nanoparticles intended for biomedical applications. *Reactive and Functional Polymers*, *147*, 104459. https://doi.org/10.1016/J.REACTFUNCTPOLYM.2019.104459

Gamarra, A., Missaglia, B., Urpi, L., Morató, J., & Muñoz-Guerra, S. (2018). Ionic coupling of hyaluronic acid with ethyl N-lauroyl L-arginate (LAE): Structure, properties and biocide activity of complexes. *Carbohydrate Polymers*, *197*, 109–116. https://doi.org/10.1016/j.carbpol.2018.05.057

Gao, Y., Sarkar, M. E., Chan, S. D., Rea, W., & Lilienberg, R. (2014). Hyaluronic acid-peripheral succinate-based self-assembling micelles for targeted delivery of rifampicin to alveolar macrophages. *Journal of Biomedical Nanotechnology*, *10*(8), 1312–1329. https://doi.org/10.1166/jbn.2014.2004

Guo, Y., Song, G., Sun, M., Wang, J., & Wang, Y. (2020). Prevalence and therapies of antibiotic-resistance in Staphylococcus aureus. *Frontiers in Cellular and Infection Microbiology*, *10*, 107. https://doi.org/10.3389/fcimb.2020.00107

Gupta, A., Mumtaz, S., Li, C. H., Hussain, I., & Rotello, V. M. (2019). Combatting antibiotic-resistant bacteria using nanomaterials. *Chemical Society Reviews*, *48*(2), 415–427. https://doi.org/10.1039/c7cs00748e

Haus, S., Hain, N., Rauch, M., Hambsch-Wang, S., Wang, T., Jiang, X., & Schlatterer, H. (2015). Enzyme degradable Polymersomes from hyaluronic acid-block-poly(ε-caprolactone) copolymers for the detection of enzymes of pathogenic bacteria. *Biomacromolecules*, *16*(3), 832–841. https://doi.org/10.1021/bm501728b

Han, H. S., Thambi, T., Choi, K. Y., Son, S., Ko, H., Lee, M. C., Jo, D. G., Chae, Y. S., Kang, Y. M., Lee, J. Y., & Park, J. H. (2015). Bioreducible shell-cross-linked hyaluronic acid nanoparticles for tumor-targeted drug delivery. *Biomacromolecules*, *16*(3), 847–856. https://doi.org/10.1021/bm501775x

Hernández-Montelongo, J., Lucchesi, E. G., González, I., Macedo, W. A. A., Nascimento, V. F., Moraes, A. M., Beppu, M. M., & Cotta, M. A. (2016). Hyaluronan/chitosan nanofilms assembled layer-by-layer and their antibacterial effect: A study using Staphylococcus aureus and Pseudomonas aeruginosa. *Colloids and Surfaces B: Biointerfaces*, *141*, 499–506. https://doi.org/10.1016/j.colsurfb.2016.02.028

Hou, J., Jia, Q., Huang, H., Zhang, J., Li, P., Deng, X., & Huang, W. (2021). Emerging photothermal-derived multimodal synergistic therapy in combating bacterial infections. *Chemical Society Reviews*, *50*(13), 8762–8789. https://doi.org/10.1039/D1CS00074H

Hussein, Y., El-Fakharany, E. M., Kamoun, E. A., Loutfy, S. A., Amin, R., Taha, T. H., Salim, S. A., & Amer, M. (2020). Electrospun PVA/hyaluronic acid/L-arginine nanofibers for wound healing applications: Nanofibers optimization and in vitro bioevaluation. *International Journal of Biological Macromolecules*, *164*, 867–876. https://doi.org/10.1016/j.ijbiomac.2020.07.126

Hynes, W. L., & Walton, S. L. (2000). Hyaluronidases of gram-positive bacteria. *FEMS Microbiology Letters*, *183*(2), 201–207. https://doi.org/10.1111/j.1574-6968.2000.tb08958.x

Ibrahim, U. H., Devnarain, N., & Govender, T. (2021). Biomimetic strategies for enhancing synthesis and delivery of antibacterial nanosystems. *International Journal of Pharmaceutics*, *598*, 120276. https://doi.org/10.1016/j.ijpharm.2021.120276

Itano, N., & Kimata, K. (2002). Mammalian hyaluronan synthases. *IUBMB Life*, *54*(4), 195–199. https://doi.org/10.1080/15216540214929

Ivanova, A., Ivanova, E., Hoyo, J., Heinze, T., Sanchez-Gomez, S., & Tzanov, T. (2018). Layer-by-layer decorated nanoparticles with tunable antibacterial and Antibiofilm properties against both gram-positive and gram-negative bacteria. *ACS Applied Materials and Interfaces*, *10*(4), 3314–3323. https://doi.org/10.1021/acsami.7b16568

Johnson, P., & Ruffell, B. (2009). CD44 and its role in inflammation and inflammatory diseases. *Inflammation & Allergy Drug Targets*, *8*(3), 208–220. https://doi.org/10.2174/187152809788680994

Jordan, A. R., Racine, R. R., Hennig, M. J. P., & Lokeshwar, V. B. (2015). The role of CD44 in disease pathophysiology and targeted treatment. *Frontiers in Immunology*, *6*(April), 182. https://doi.org/10.3389/fimmu.2015.00182

Kalhapure, R. S., Suleman, N., Mocktar, C., Seedat, N., & Govender, T. (2015). Nanoengineered drug delivery systems for enhancing antibiotic therapy. *Journal of Pharmaceutical Sciences*, *104*(3), 872–905. https://doi.org/10.1002/jps.24298

Kazi, M., Al-Swairi, M., Ahmad, A., Raish, M., Alanazi, F. K., Badran, M. M., Khan, A. A., Alanazi, A. M., & Hussain, M. D. (2019). Evaluation of self-nanoemulsifying drug delivery systems (SNEDDS) for poorly water-soluble Talinolol: Preparation, in vitro and in vivo assessment. *Frontiers in Pharmacology*, *10*(May), 459. https://doi.org/10.3389/FPHAR.2019.00459

Khan, H. A., Baig, F. K., & Mehboob, R. (2017). Nosocomial infections: Epidemiology, prevention, control and surveillance. *Asian Pacific Journal of Tropical Biomedicine*, *7*(5), 478–482. https://doi.org/10.1016/S2221169.2017.01.039

Khunmanee, S., Jeong, Y., & Park, H. (2017). Crosslinking method of hyaluronic-based hydrogel for biomedical applications. *Journal of Tissue Engineering*, *8*, 2041731417726464. https://doi.org/10.1177/2041731417726464

Kim, J. H., Moon, M. J., Kim, D. Y., Heo, S. H., & Jeong, Y. Y. (2018). Hyaluronic acid-based nanomaterials for cancer therapy. *Polymers*, *10*(10), 1–15. https://doi.org/10.3390/polym10101133

Kim, E., Choi, H., Choi, E. S., Park, M. H., & Ryu, J. H. (2019). Hyaluronic acid-coated nanomedicine for targeted cancer therapy. *Pharmaceutics*, *11*(7), 1–22. https://doi.org/10.3390/pharmaceutics11070301

Kłodzińska, P. D., Bahrenfels, N., Rades, T., Hinrichsen, K. E. W., & Nielsen, H. M. (2019). Hyaluronic acid-based nanogels improve in vivo compatibility of the anti-biofilm peptide DJK-5. *Nanomedicine: Nanotechnology, Biology, and Medicine*, *20*(6), 102022. https://doi.org/10.1016/j.nano.2019.102022

Kłodzińska, S. N., Moldrheim, N., Pranzyk, E., Hansen, P. R., Damborg, P., & Nielsen, H. M. (2018). Biopolymer nanogels improve antibacterial activity and safety profile of a novel lysine-based α-peptide/β-peptoid peptidomimetic. *European Journal of Pharmaceutics and Biopharmaceutics*, *128*(March), 1–9. https://doi.org/10.1016/j.ejpb.2018.03.012

Kłodzińska, S. N., & Nielsen, H. M. (2021). Hyaluronic acid-based nanosystems for drug delivery applications. In H. Ben, C. M. Hussain, & S. Saha (Eds.), *Biopolymer-based nanomaterials in drug delivery and biomedical applications* (pp. 231–260). Academic Press. https://doi.org/10.1016/b978-0-12-820874-8.00021-x

Kłodzińska, S. N., Wan, F., Jensen, H., Sternberg, C., Rades, T., & Nielsen, H. M. (2019). Utilizing nanoparticles for improving anti-biofilm effects of azithromycin: A head-to-head comparison of modified hyaluronic acid nanogels and coated poly (lactic-co-glycolic acid) nanoparticles. *Journal of Colloid and Interface Science*, *555*, 395–406. https://doi.org/10.1016/j.jcis.2019.08.006

Knetsch, M. L. W., & Koole, L. H. (2011). New strategies in the development of antimicrobial coatings: The example of increasing usage of silver and silver nanoparticles. *Polymers*, *3*(1), 340–366. https://doi.org/10.3390/PO3010340

Kolar, S. L., Kyme, P., Tseng, C. W., Soliman, A., Kaplan, A., Liang, J., Nizet, V., Jiang, D., Muneli, E., Ardell, M., Underhill, D. M., & Liu, G. Y. (2015). Group B streptococcus evades host immunity by degrading Hyaluronan. *Cell Host & Microbe*, *18*(6), 694–704. https://doi.org/10.1016/j.chom.2015.11.001

Lapčík, L., Lapčík, L., De Smedt, S., Demeester, J., & Chabreček, P. (1998). Hyaluronan: Preparation, structure, properties, and applications. *Chemical Reviews*, *98*(8), 2663–2704. https://doi.org/10.1021/cr941199z

Lee, J. S., & Feijen, J. (2012). Polymersomes for drug delivery: Design, formation and characterization. *Journal of Controlled Release*, *161*(2), 473–483. https://doi.org/10.1016/j.jconrel.2011.10.005

Lee, N. Y., Ko, W. C., & Hsueh, P. R. (2019). Nanoparticles in the treatment of infections caused by multidrug-resistant organisms. *Frontiers in Pharmacology*, *10*, 1153. https://doi.org/10.3389/fphar.2019.01153

Lemarchand, C., Gref, R., & Couvreur, P. (2004). Polysaccharide-decorated nanoparticles. *European Journal of Pharmaceutics and Biopharmaceutics*, *58*(2), 327–341. https://doi.org/10.1016/j.ejpb.2004.02.016

Li, Y., Gao, Z., Zhang, Y., Chen, F., An, P., Wu, H., Yan, C., & Sun, B. (2021). MOF-shielded and glucose-responsive ultrasmall silver nanofactory for highly-efficient anticancer and antibacterial therapy. *Chemical Engineering Journal*, *418*(November 2020), 127610. https://doi.org/10.1016/j.cej.2020.127610

Li, Y., Xia, Y., Fleischer, C. C., Huang, J., Liu, R., Yang, L., & Mao, H. (2017). Impact of anti-biofouling surface coatings on the properties of nanomaterials and their biomedical applications. *Journal of Materials Chemistry B*, *6*(1), 9–24. https://doi.org/10.1039/c7tb01695f

Liu, L., Liu, Y., Li, J., Du, G., & Chen, J. (2011). Microbial production of hyaluronic acid: Current state, challenges, and perspectives. *Microbial Cell Factories*, *10*, 99. https://doi.org/10.1186/1475-2859-10-99

Liu, T., Chen, D., Zhang, A., Xiao, M., Li, Z., Luo, W., Pan, Y., Qu, W., & Xie, S. (2021). Composite inclusion complexes containing hyaluronic acid/chitosan nanosystems for dual responsive enrofloxacin release. *Carbohydrate Polymers*, *252*(July 2020), 117162. https://doi.org/10.1016/j.carbpol.2020.117162

Liu, Y., Li, Z., Zuo, S., Lu, C., Xiao, Y., Bai, H., Zhang, X., Ma, H., Zhang, X., & Duan, J. (2020). Hyaluronic acid-coated ZIF-8 for the treatment of pneumonia caused by methicillin-resistant *Staphylococcus aureus*. *International Journal of Biological Macromolecules*, *155*, 103–109. https://doi.org/10.1016/j.ijbiomac.2020.03.187

Liu, Y., Liu, A., Liu, J., Chen, X., Zhu, X., Gong, Y., Yuan, G., Chen, L., & Liu, J. (2019). Enzyme-responsive Mesoporous ruthenium for combined chemo-Photothermal therapy of drug-resistant bacteria. *ACS Applied Materials and Interfaces*, *11*(30), 26980–26986. https://doi.org/10.1021/acsami.9b07906

Lu, C., Xiao, Y., Liu, Y., Sun, F., Qiu, Y., Ma, H., & Duan, J. (2020). Hyaluronic acid-based levofloxacin nanomicelles for nitric oxide-triggered drug delivery to treat bacterial infections. *Carbohydrate Polymers*, *229*(June 2019), 115479. https://doi.org/10.1016/j.carbpol.2019.115479

Matsuoka, S., & Lacroix, J.-C. (2020). Twenty-five years of polymersomes: Lost in translation? *Materials Horizons*, *7*(5), 1297–1309. https://doi.org/10.1039/C9MH01869D

Matthiolakis, G., Milani, L., Singh, A., Azmi, M. M. (2013). Hyaluronic acid targeting of CD44 for cancer therapy: From receptor biology to nanomedicine. *Journal of Drug Targeting*, *23*(7–8), 605–618. https://doi.org/10.3109/1061186X.2013.852072

McArthur, D. B. (2019). Emerging infectious diseases. *Nursing Clinics of North America*, *54*(2), 297–311. https://doi.org/10.1016/j.cnur.2019.02.006

Misra, R., Acharya, S., & Sahoo, S. K. (2010). Cancer nanotechnology: Application of nanotechnology in cancer therapy. *Drug Discovery Today*, *15*(19–20), 842–850. https://doi.org/10.1016/j.drudis.2010.08.006

Mohamed Fahmy, H., Mahmoud Mosleh, A., Abd Elghany, A., Shams-Eldin, E., Serea, E. S. A., Ashour Ali, S., & Esmail Shalan, A. (2019). Coated silver nanoparticles: Synthesis, cytotoxicity, and optical properties. *RSC Advances*, *9*(35), 20118–20136. https://doi.org/10.1039/C9RA02969A

Montanari, E., D'Arrigo, G., Di Meo, C., Virga, A., Coviello, T., Passariello, C., & Matricardi, P. (2014). Chasing bacteria within the cells using levofloxacin-loaded hyaluronic acid nanohydrogels. *European Journal of Pharmaceutics and Biopharmaceutics*, *87*(3), 518–523. https://doi.org/10.1016/j.ejpb.2014.03.003

Montanari, E., Gennari, A., Pellecia, M., Guzzini, C., Lalfana, E., Matricardi, P., Mellais, A. J., & Timili, N. (2016). Hyaluronan/tannic acid nanoparticles via catechol/Boronate Complexation as a smart antibacterial system. *Macromolecular Bioscience*, *16*(12), 1819–1823. https://doi.org/10.1002/mabi.201600351

Montanari, E., Mancini, P., Galli, F., Varani, M., Santino, I., Coviello, T., Mosca, L., Matricardi, P., Rancan, F., & Di Meo, C. (2020). Biodistribution and intracellular localization of hyaluronan and its nanogels. A strategy to target intracellular *S. aureus* in persistent skin infections. *Journal of Controlled Release*, *328*(June), 1–12. https://doi.org/10.1016/j.jconrel.2020.06.007

Montanari, E., Oates, A., Di Meo, C., Meade, J., Cerrone, R., Francisco, A., Devine, D., Coviello, T., Mancini, F., Mosca, L., & Matricardi, P. (2016). Hyaluronan-based Nanohydrogels for targeting intracellular *S. aureus* in human keratinocytes. *Advanced Healthcare Materials*, *7*(12), 1–12. https://doi.org/10.1002/adhm.201701403

Mosalab, T., Farr, D. C., Kiehl, M. J., & Houston, T. A. (2019). Carbohydrate-based nanocarriers and their application to target macrophages and deliver antimicrobial agents. *Advanced Drug Delivery Reviews*, *153*–*152*, 94–120. https://doi.org/10.1016/j.addr.2019.09.002

Muddineti, O. S., Ghosh, B., & Biswas, S. (2015). Current trends in using polymer coated gold nanoparticles for cancer therapy. *International Journal of Pharmaceutics*, *484*(1–2), 252–267. https://doi.org/10.1016/J.IJPHARM.2015.02.038

Mukhtar, M., Pellagi, E., Csóka, I., Benko, B., Farkas, A., Zsenhan, M., Bustán, K., Kókai, D., & Ambrus, R. (2020). Aerodynamic properties and in silico deposition of isoniazid loaded chitosan/thiolated chitosan and hyaluronic acid hybrid nanoplex DPIs as a potential TB treatment. *International Journal of Biological Macromolecules*, *165*(Pt B), 3007–3019. https://doi.org/10.1016/j.ijbiomac.2020.10.192

Muzammal, S., Hayat, S., Fakhar-e-Alam, M., Aslam, B., Siddiqui, M. H., Nisar, M. A., Saqalein, M., Atif, M., Sarwar, A., Khurshid, A., Amin, N., & Wang, Z. (2018). Nanoantibiotics: Future nanotechnologies to combat antibiotic resistance. *Frontiers in Bioscience - Elite*, *10*(2), 352–374. https://doi.org/10.2741/e827

Necas, J., Bartosikova, L., Brauner, P., & Kolar, J. (2008). Hyaluronic acid (hyaluronan): A review. *Veterinarni Medicina*, *53*(8), 397–411. doi: 10.17221/1930-VETMED

Nguyen, H. M., & Graber, C. J. (2009). Limitations of antibiotic options for invasive infections caused by methicillin-resistant Staphylococcus aureus: Is combination therapy the answer? *Journal of Antimicrobial Chemotherapy*, *65*(1), 24–36. https://doi.org/10.1093/jac/dkp377

Osman, N., Devnarain, N., Omolo, C. A., Fasiku, V., Jaglal, Y., & Govender, T. (2021). Surface modification of nano-drug delivery systems for enhancing antibiotic delivery and activity. *WIREs Nanomedicine and Nanobiotechnology*, *14*(1), e1756. https://doi.org/10.1002/WNAN.1756

Özkahraman, B., Tamahkar, E., İdil, N., Kılıç Süloğlu, A., & Perçin, İ. (2021). Evaluation of hyaluronic acid nanoparticle embedded chitosan–gelatin hydrogels for antibiotic release. *Drug Development Research*, *82*(2), 241–250. https://doi.org/10.1002/ddr.21747

Pandey, S., Mahtab, A., Rai, N., Rawat, P., Ahmad, F. J., & Talegaonkar, S. (2017). Emerging role of CD44 receptor as a potential target in disease diagnosis: A patent review. *Recent Patents on Inflammation & Allergy Drug Discovery*, *11*(2), 77–91. https://doi.org/10.2174/1872213x13666170907111839

Parn, A., Machaj, L., & Goyender, T. (2021). Advances in sepsis diagnosis and management: A paradigm shift towards nanotechnology. *Journal of Biomedical Science*, *28*(1), 1–30. https://doi.org/10.1186/s12929-020-00702-6

Pedrosa, S. S., Pereira, P., Correia, A., & Gama, F. M. (2017). Targetability of hyaluronic acid nanogel to cancer cells: In vitro and in vivo studies. *European Journal of Pharmaceutical Sciences*, *104*, 103–113. https://doi.org/10.1016/j.ejps.2017.03.045

Pirnazar, P., Wolinsky, L., Nachnani, S., Haake, S., Pilloni, A., & Bernard, G. W. (1999). Bacteriostatic effects of hyaluronic acid. *Journal of Periodontology*, *70*(4), 370–374. https://doi.org/10.1902/jop.1999.70.4.370

Prajapati, V. D., & Maheriya, P. M. (2019). Hyaluronic acid as potential carrier in biomedical and drug delivery applications. In S. Maiti & S. Jana (Eds.), *Functional Polysaccharides for Biomedical Applications* (pp. 215–265). Elsevier. https://doi.org/10.1016/B978-0-08-102555-8.00007-8

Qiu, Y., Lu, C., Chen, P., Sun, P., Wang, D., Wang, Z., Hou, C., Ma, H., & Duan, J. (2019). Synergistic clearance of intracellular pathogens by hyaluronan-streptomycin micelles encapsulated with rapamycin. *Carbohydrate Polymers*, *210*(January), 364–371. https://doi.org/10.1016/j.carbpol.2019.01.068

Ran, X., Du, Y., Wang, Z., Wang, H., Pu, P., Ran, J., & Qu, X. (2017). Hyaluronic acid-templated Ag nanoparticles/graphene oxide composites for synergistic therapy of bacteria infection. *ACS Applied Materials and Interfaces*, *9*(23), 19717–19724. https://doi.org/10.1021/acsami.7b05594

Ran, N. V., Rhie, J. G., Um, W., Ek, P. K., Nguyen, V. Q., Oh, B. H., Kim, W., & Park, J. H. (2020). Hyaluronic acid nanoparticles as nanomedicine for treatment of inflammatory diseases. *Pharmaceutics*, *12*(10), 1–16. https://doi.org/10.3390/pharmaceutics12100931

Rezaei, F., Minaiyan, M., & Taheri, A. (2018). A novel lignin-based nanofibrous dressing containing arginine for wound-healing applications. *Drug Delivery and Translational Research*, *8*(1), 111–122. https://doi.org/10.1007/s13346-017-0441-0

Sakuma, Y., & Hanashima, H. (2019). Hyaluronan-modified nanoparticles for tumor-targeting. *Expert Opinion on Drug Delivery*, *16*(9), 915–936. https://doi.org/10.1080/17425247.2019.1643115

Sánchez, A., Mejía, S. P., & Orozco, J. (2020). Recent advances in polymeric nanoparticle-encapsulated drugs against intracellular infections. *Molecules*, *25*(16), 3760. https://doi.org/10.3390/molecules25163760

Schanté, C. E., Zuber, G., Herlin, C., & Vandamme, T. F. (2011). Chemical modifications of hyaluronic acid for the synthesis of derivatives for a broad range of biomedical applications. *Carbohydrate Polymers*, *85*(3), 469–489. https://doi.org/10.1016/j.carbpol.2011.03.019

Sekhon, B. S., & Kamboj, S. R. (2010). Inorganic nanomedicine-part 2. *Nanomedicine: Nanotechnology, Biology, and Medicine*, *6*(5), 612–618. https://doi.org/10.1016/j.nano.2010.04.003

Shafran, N., Shafran, I., Ben-Zvi, H., Sofer, S., Sheena, L., Krause, I., Shlomai, A., Goldberg, E., & Sklan, E. H. (2021). Secondary bacterial infection in COVID-19 patients is a stronger predictor for death compared to influenza patients. *Scientific Reports*, *11*(1), 1–8. https://doi.org/10.1038/s41598-021-92220-0

Sharma, A., Kumar Arya, D., Dua, M., Chhatwal, G. S., & Johri, A. K. (2012). Nano-technology for targeted drug delivery to combat antibiotic resistance. *Expert Opinion on Drug Delivery*, *9*(11), 1325–1332. https://doi.org/10.1517/17425247.2012.717927

Sharma, A. K., Pradhan, P., Aljabali, A. A., Mishra, V., Gandhi, H., Kumar, S., Mutreja, S., Chellappan, D. K., Tambuwala, M. M., Dua, K., & Kapoor, D. N. (2020). Emerging era of "omes": Polymersomes as versatile drug delivery carrier for cancer diagnostics and therapy. *Drug Delivery and Translational Research*, *10*(5), 1171–1190. https://doi.org/10.1007/s13346-020-00769-2

Silva, J. P., Gonçalves, C., Costa, C., Sousa, J., Silva-Gomes, R., Castro, A. G., Pedrosa, J., Appelberg, R., & Gama, F. M. (2016). Delivery of LLKKK18 loaded into self-assembling hyaluronic acid nanogel for tuberculosis treatment. *Journal of Controlled Release*, *235*, 112–124. https://doi.org/10.1016/j.jconrel.2016.05.064

Singer, A. C., Kirchhelle, C., & Roberts, A. P. (2020). (Inter)nationalising the antibiotic research and development pipeline. *The Lancet Infectious Diseases*, *20*(2), 56–62. https://doi.org/10.1016/S1473-3099(19)30552-3

Singh, R., Dwivedi, S. P., Gaharwar, U. S., Meena, R., Rajamani, P., & Prasad, T. (2020). Recent updates on drug resistance in mycobacterium tuberculosis. *Journal of Applied Microbiology*, *128*(6), 1547–1567. https://doi.org/10.1111/jam.14478

Soares, S., Sousa, J., Pais, A., & Vitorino, C. (2018). Nanomedicine: Principles, properties, and regulatory issues. *Frontiers in Chemistry*, *6*, 360. https://doi.org/10.3389/fchem.2018.00360

Teixeira, M. C., Carbone, C., Sousa, M. C., Espina, M., Garcia, M. L., Sanchez-Lopez, E., & Souto, E. B. (2020). Nanomedicines for the delivery of antimicrobial peptides (amps). *Nanomaterials*, *10*(3), 1–23. https://doi.org/10.3390/nano10030560

Tiwari, S., & Bahadur, P. (2019). Modified hyaluronic acid based materials for biomedical applications. *International Journal of Biological Macromolecules*, *121*, 556–571. https://doi.org/10.1016/j.ijbiomac.2018.10.049

Tulkens, P. M. (1991). Intracellular distribution and activity of antibiotics. *European Journal of Clinical Microbiology & Infectious Diseases*, *10*(2), 100–106. https://doi.org/10.1007/BF01964420

Vouga, M., & Greub, G. (2016). Emerging bacterial pathogens: The past and beyond. *Clinical Microbiology and Infection*, *22*(1), 12–21. https://doi.org/10.1016/j.cmi.2015.10.019

Wahyudur, F., Gunnimani, R., Salih, M., Mukhariniu, S., Muckiar, C., & Govender, T. (2019). Self-assembled oleylamine grafted hyaluronic acid polymersomes for delivery of vancomycin against methicillin resistant Staphylococcus aureus (MRSA). *Colloids and Surfaces B: Biointerfaces*, *182*(May), 110388. https://doi.org/10.1016/j.colsurfb.2019.110388

Wang, D. E., Bahimi, M., & Filgueira, C. S. (2021). Nanotechnology applications for cardiovascular disease treatment: Current and future perspectives. *Nanomedicine: Nanotechnology, Biology and Medicine*, *34*, 102387. https://doi.org/10.1016/j.nano.2021.102387

Wei, G., Yang, G., Wang, Y., Jiang, H., Fu, Y., Yue, G., & Ju, R. (2020). Phototherapy-based combination strategies for bacterial infection treatment. *Theranostics*, *10*(26), 12241–12262. https://doi.org/10.7150/THNO.52729

World Health Organization [WHO]. (2020b, October 13). *Antimicrobial Resistance*. WHO. Retrieved from: https://www.who.int/news-room/fact-sheets/detail/antimicrobial-resistance

World Health Organization [WHO]. (2020b, December 9). *WHO—The top 10 causes of death*. 24 Maggio. Retrieved from: https://www.who.int/news-room/fact-sheets/detail/the-top-10-causes-of-death

Wu, Y., Long, Y., Li, Q. L., Han, S., Ma, J., Yang, Y. W., & Gao, H. (2017). Layer-by-layer (LBL) self-assembled biohybrid Nanomaterials for efficient antibacterial applications. *ACS Applied Materials and Interfaces*, *9*(31), 17235–17283. https://doi.org/10.1021/acsami.7b04218

Xiong, M. H., Bao, Y., Yang, X. Z., Zhu, Y. H., & Wang, J. (2014). Delivery of antibiotics with polymeric particles. *Advanced Drug Delivery Reviews*, *78*, 63–76. https://doi.org/10.1016/j.addr.2014.03.002

Xu, T., Li, J., Zhang, S., Jin, Y., & Wang, R. (2019). Integration of diagnosis and treatment in the detection and kill of Listeria in the whole blood. *Biosensors and Bioelectronics*, *142*(July), 111507. https://doi.org/10.1016/j.bios.2019.111507

Yang, J., Zhao, Y., Cao, J., Gong, C., Yao, J., Zhang, N., & Zhao, Y. (2020). Hyaluronic acid and antimicrobial peptide-modified gold/silver hybrid nanocages to combat bacterial multidrug resistance. *International Journal of Pharmaceutics*, *586*(May), 119505. https://doi.org/10.1016/j.ijpharm.2020.119505

Yetisgin, A. A., Cetinel, S., Zuvin, M., & Kutlu, O. (2020). Therapeutic nanoparticles and their targeted delivery applications. *Molecules*, *25*(2193), 1–31. https://doi.org/10.3390/molecules25092193

Zhang, H., Zhai, Y., Wang, J., & Zhai, G. (2016). New progress and prospects: The application of nanogel in drug delivery. *Materials Science and Engineering C*, *60*, 560–568. https://doi.org/10.1016/j.msec.2015.11.041

Zhang, X., Liu, L., Huang, L., Zhang, W., Wang, R., Yue, T., Sun, J., Li, G., & Wang, J. (2019). The highly efficient elimination of intracellular bacteria via a metal organic framework (MOF)-based three-in-one delivery system. *Nanoscale*, *11*(19), 9468–9477. https://doi.org/10.1039/c9nr01284b

Zhang, X.-F., Liu, Z.-G., Shen, W., & Gurunathan, S. (2016). Silver nanoparticles: Synthesis, characterization, properties, applications, and therapeutic approaches. *International Journal of Molecular Sciences*, *17*(9), 1534. https://doi.org/10.3390/IJMS17091534

Zhu, J., Li, F., Wang, X., Yu, J., & Wu, D. (2018). Hyaluronic acid and polyethylene glycol hybrid hydrogel encapsulating Nanogel with hemostasis and sustainable antibacterial property for wound healing. *ACS Applied Materials and Interfaces*, *10*(16), 13304–13316. https://doi.org/10.1021/acsami.7b19027

How to cite this article: Mohammad, M., Devnarain, N., Elhassan, E., & Govender, T. (2022). Exploring the applications of hyaluronic acid-based nanoparticles for diagnosis and treatment of bacterial infections. *WIREs Nanomedicine and Nanobiotechnology*, *14*(4), e1799. https://doi.org/10.1002/wnan.1799